STRUCTURE, REACTIONS, AND PARTIAL SYNTHESES OF INDOLE DERIVATIVES

LOW YUN YEE

FACULTY OF SCIENCE
UNIVERSITY OF MALAYA
KUALA LUMPUR

2013

STRUCTURE, REACTIONS, AND PARTIAL SYNTHESES OF INDOLE DERIVATIVES

LOW YUN YEE

A THESIS SUBMITTED IN FULFILMENT OF THE REQUIREMENTS FOR THE DEGREE OF DOCTOR OF PHILOSOPHY

DEPARTMENT OF CHEMISTRY
FACULTY OF SCIENCE
UNIVERSITY OF MALAYA
KUALA LUMPUR

2013

ABSTRACT

Two new alkaloids of the mersinine type, mersiphyllines A (**37**) and B (**38**), were isolated from the polar fraction of the alkaloid extract of *K. singapurensis* following repeated fractionation *via* gel-permeation chromatography. The structures of these alkaloids were elucidated based on NMR spectroscopy, formation of an alkaloid-borane complex **40**, as well as X-ray diffraction analysis.

Concise partial syntheses of several new indole alkaloids isolated from *Tabernaemontana*, *Alstonia*, and *Leuconotis* species were carried out. These include, lirofoline A (**44**) from ibogaine (**46**), alstolucine A (**91**) from alstolucine B (**94**), and (–)-eburnamaline (**96**) from (+)-eburnamonine (**98**).

Some transformations of the ring-opened *Aspidosperma* alkaloid, leuconolam (**54**) were investigated, *inter alia*, its reactions with base leading to enolate-mediated ring closure to yield the epimeric pentacylic meloscine-like compounds (**74** and **76**), its reaction with acids leading to transannular closure to the pentacyclic, doubly spirocyclic, 6,7-dehydroleuconoxine (**63**), or to the tetracyclic amino lactam-lactone (**78**). Bromination ($Br_2/CHCl_3$) of leuconolam (**54**) was shown to proceed *via* a two-step sequence involving the intermediacy of 6,7-dehydroleuconoxine (**63**). Other reactions investigated include enolate-mediated α-oxygenation, hydroboration, and reaction with trifluoroacetic acid. These studies led to concise semisynthesis of leuconoxine (**56**), and the new leuconoxine alkaloids, leuconodines A (**67**) and F (**72**). The results from these reactions also led to the realization that the original assignment of *epi*-leuconolam as **55** was incorrect. This was confirmed upon carrying out an X-ray diffraction analysis, which showed that '*epi*-leuconolam (**55**)' is in actual fact 6,7-dehydroleuconoxine (**63**).

The original stereochemical/configurational assignments of the alkaloids scholaricine (**114a**) and alstoumerine (**118a**) were reinvestigated (NMR, derivatization,

X-ray diffraction analysis) and the structures revised accordingly (to **114b** and **118b**, respectively). The revised structure of alstoumerine (**118b**) was necessary for the structure elucidation of the new bisindole, lumutinine C (**116**).

X-ray diffraction analyses were carried out for the macroline-macroline bisindole alkaloids, perhentinine (**104**) (*via* formation of the dimethyl diiodide salt of the ring *E*-cyclized hemiketal form, **104b**) and macralstonine (**105**), and the results were then applied to support the configurational assignment of C-20 in the new *Alstonia* bisindoles, perhentidines A–C (**101**–**103**).

Andransinine (**119**) (in all probability an artifact derived from the alkaloid andranginine (**120**) during isolation of alkaloids from *A. angustiloba* and *K. pauciflora*), was found to exhibit polymorphism in the solid state, forming crystals with different crystal systems and space groups in different solvent systems. In addition, it undergoes spontaneous resolution when crystallized in ethyl acetate, forming racemic conglomerate crystals.

X-ray diffraction analyses of a number of new indole and bisindole alkaloids isolated from various plants of the genus *Alstonia*, *Kopsia*, *Leuconotis*, and *Tabernaemontana* were carried out. These include: the bisindole alkaloids, leuconoline (**124**) from *L. griffithii*, and lumusidines A (**125**) and B (**126**) (*via* its dimethyl diiodide salts, **125a** and **126a**) from *A. macrophylla*, the novel indole alkaloids voatinggine (**128**) and tabertinggine (**129**) from *T. corymbosa*, grandilodines A (**135**) and B (**136**) from *K. grandifolia*, and leuconodines B (**68**) and E (**71**) from *L. griffithii*.

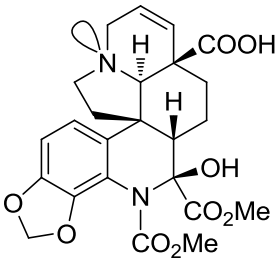

37 mersiphylline A

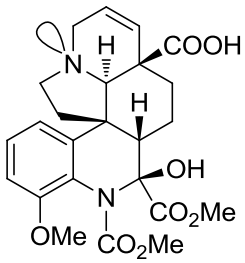

38 mersiphylline B

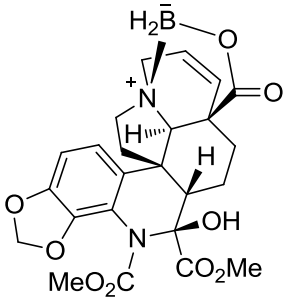

40

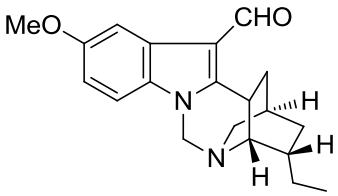

44 lirofoline A

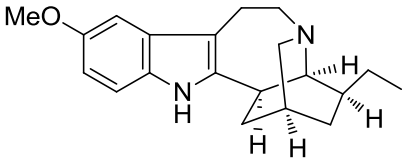

46 ibogaine

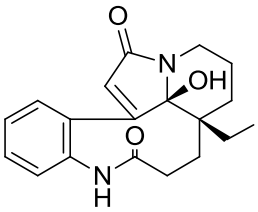

54 leuconolam

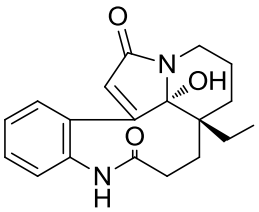

'**55** *epi*-leuconolam'

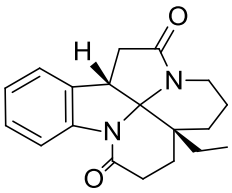

56 leuconoxine

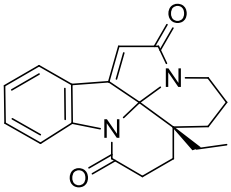

63 6,7-dehydroleuconoxine

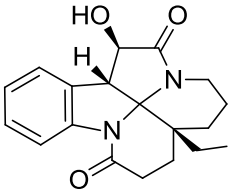

67 leuconodine A

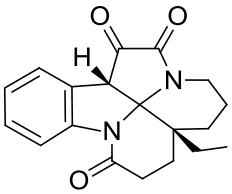

72 leuconodine F

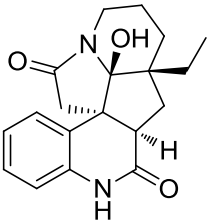

74

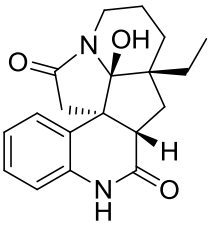

76

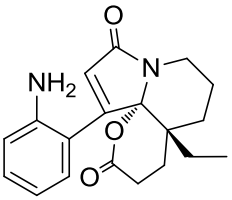

78

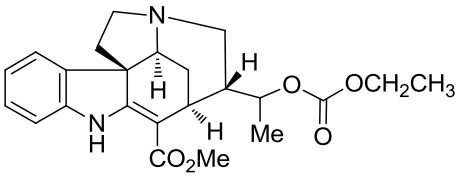

91 alstolucine A

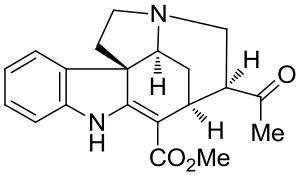

94 alstolucine B

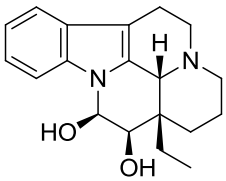

96 (–)-eburnamaline

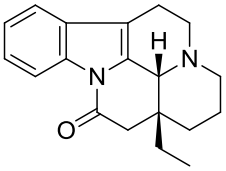

98 (+)-eburnamonine

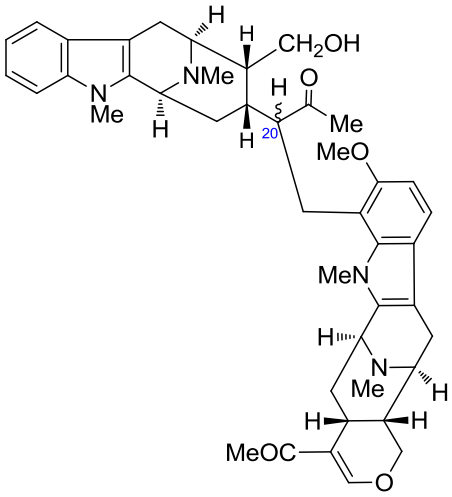

101 perhentidine A (20*S*)
102 perhentidine B (20*R*)

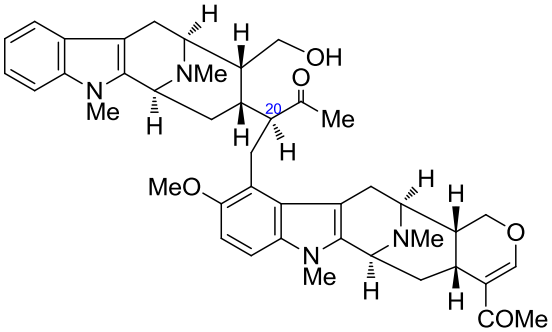

103 perhentidine C (20*S*)

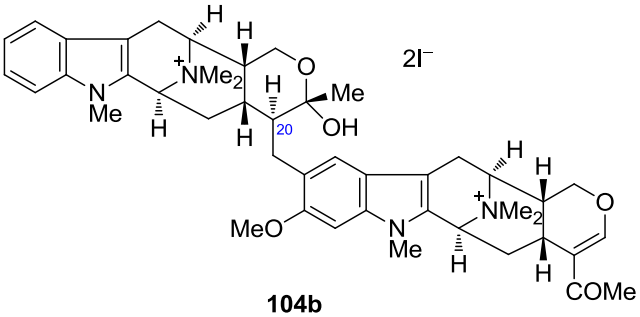

104b

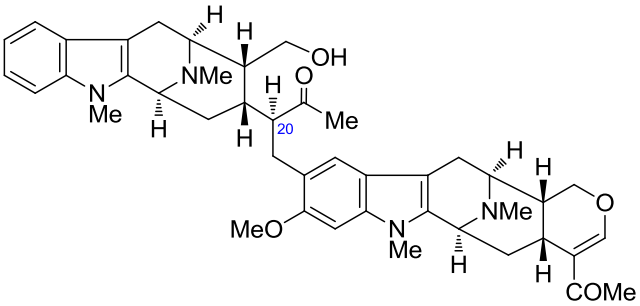

104 perhentinine (20*S*)

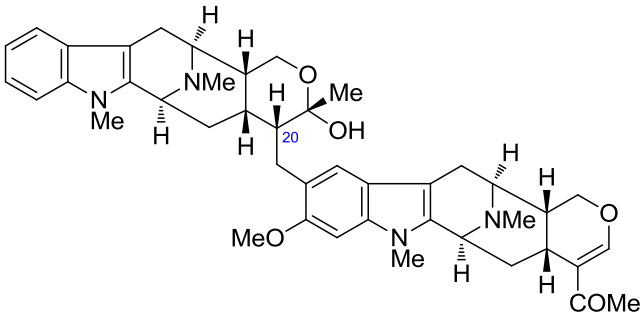

105 macralstonine (20*R*)

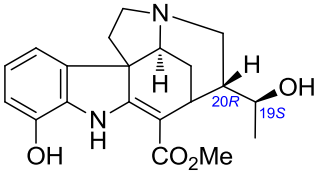

114a scholaricine
(previous assignment)

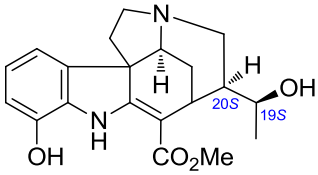

114b scholaricine
(revised)

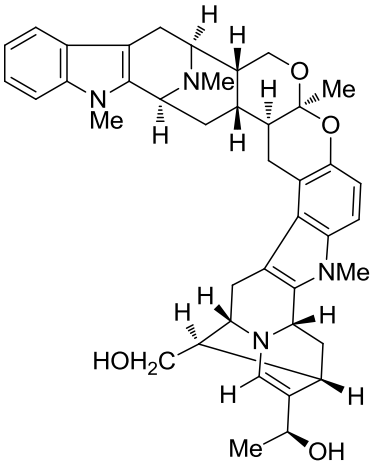

116 lumutinine C

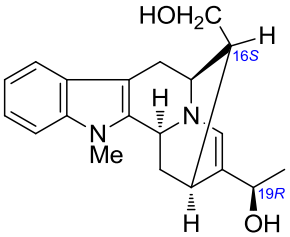

118a alstoumerine
(previous assignment)

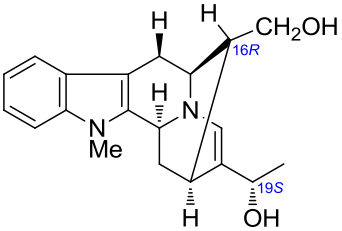

118b alstoumerine
(revised)

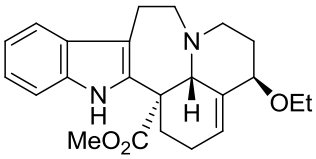

119 andransinine

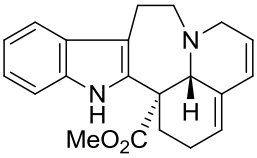

120 andranginine

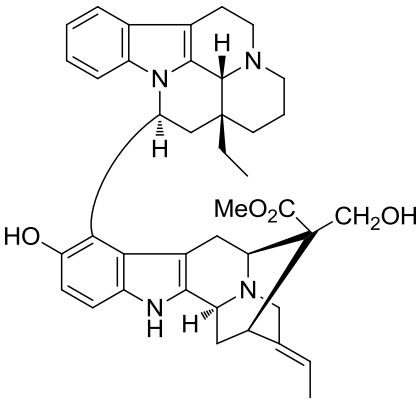

124 leuconoline

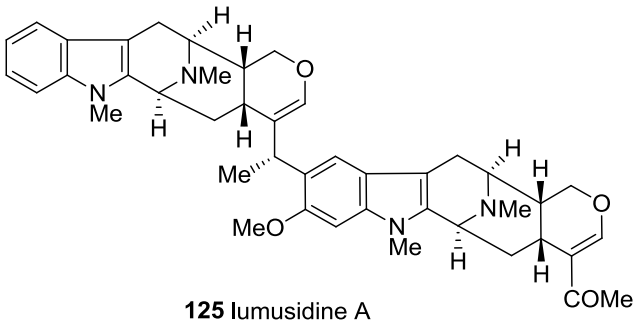

125 Iumusidine A

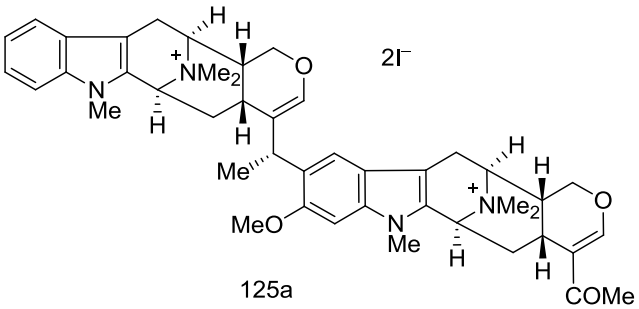

125a

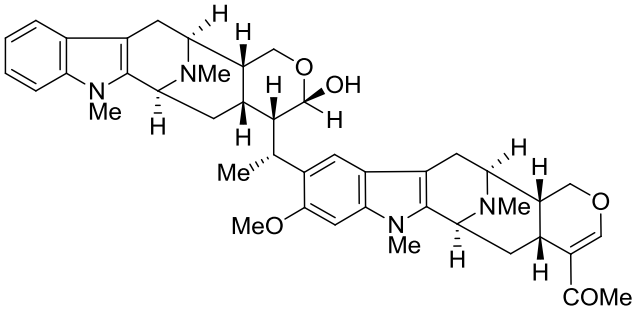

126 Iumusidine B

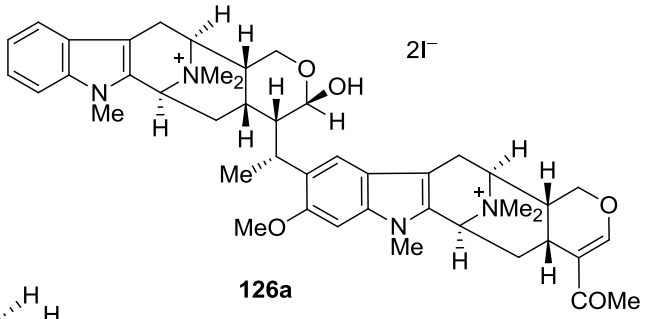

126a

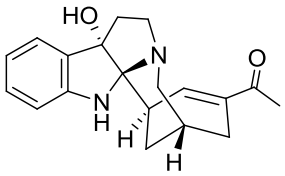

128 voatinggine

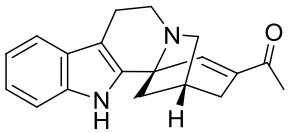

129 tabertinggine

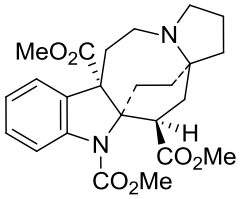

135 grandilodine A

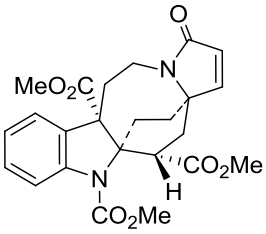

136 grandilodine B

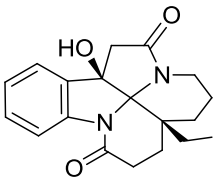

68 Ieuconodine B

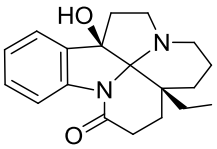

71 Ieuconodine E

ABSTRAK

(BAHASA MALAYSIA VERSION)

Dua alkaloid baru jenis mersinine, mersiphylline A (**37**) dan B (**38**), telah diasingkan daripada fraksi kutub ekstrak alkaloid *K. singapurensis*, berikutan fraksi berulangan menggunakan kromatografi gel penjerapan. Struktur alkaloid yang dinyatakan dikenalpasti menggunakan teknik spekstroskopi NMR, pembentukan kompleks alkaloid-borane **40**, serta analisis pembelauan sinar-X.

Sintesis separa untuk beberapa alkaloid indola yang diasing daripada spesis *Tabernaemontana*, *Alstonia*, and *Leuconotis* telah dijalankan. Ini termasuk lirofoline A (**44**) daripada ibogaine (**46**), alstolucine A (**91**) daripada alstolucine B (**94**), dan (–)-eburnamaline (**96**) daripada (+)-eburnamonine (**98**).

Beberapa transformasi alkaloid *Aspidosperma*, leuconolam (**54**) telah disiasat. Ini termasuk, tindak balas dengan alkali secara perantaraan enolat, yang membawa kepada penutupan gelang kepada sebatian jenis meloscine (**74** and **76**), tindak balas dengan asid menghasilkan sebatian gandaan dua spirosiklik, 6,7-dehydroleuconoxine (**63**) secara penutupan 'transannular', atau kepada sebatian tetrasiklik amino laktam-lakton (**78**). Pembrominan ($Br_2/CHCl_3$) leuconolam (**54**) menunjukkan bahawa tindakbalas ini berlaku dalam dua langkah, yang melibatkan 6,7-dehydroleuconoxine (**63**) sebagai perantaraan. Tindak balas yang lain termasuk pengoksigenan-α dengan perantaraan enolat, penghidroboranan, dan tindak balas dengan TFA. Tindakbalas yang dinyatakan telah membawa kepada sintesis separa leuconoxine (**56**), dan alkaloid leuconoxin yang baru, leuconodine A (**67**) and F (**72**). Keputusan daripada penyelidikan ini juga membawa kepada kesedaran bahawa penentuan asal untuk struktur *epi*-leuconolam sebagai **55** adalah salah. Keputusan ini disahkan dengan menjalankan

analisis pembelauan sinar-X, yang menunjukkan bahawa '*epi*-leuconolam (**55**)' sebenarnya adalah 6,7-dehydroleuconoxine (**63**).

Stereokimia/konfigurasi asal untuk alkaloid scholaricine (**114a**) dan alstoumerine (**118a**) telah disiasat semula (NMR, penyediaan terbitan, analisis pembelauan sinar-X) dan struktur yang dinyatakan telah dikemaskini dengan sewajarnya (kepada **114b** dan **118b**). Struktur alstoumerine (**118b**) yang telah dikemaskini adalah amat penting dalam penentuan struktur alkaloid bisindola yang baru, lumutinine C (**116**).

Analisis pembelauan sinar-X telah dijalankan untuk alkaloid macroline-macroline, perhentinine (**104**) (melalui pembentukan garam dimetil diiodida gelang *E*-tertutup bentuk hemiketal, **104b**) dan macralstonine (**105**). Keputusan yang diperolehi daripada analisis yang dinyatakan telah digunakan untuk membantu dalam penentuan konfigurasi C-20 untuk alkaloid bisindola yang baru daripada *Alstonia*, perhentidine A–C (**101**–**103**).

Andransinine (**119**) (kebarangkalian merupakan artifak yang berasal daripada alkaloid andranginine (**119**) semasa proses pengasingan alkaloid daripada *A. angustiloba* dan *L. griffithii*), didapati mempamerkan sifat 'polymorphism' dalam keadaan pepejal, membentuk hablur dengan sistem hablur serta kumpulan ruangan yang berbeza dalam pelarut yang berlainan. Tambahan pula, ia akan menjalani resolusi secara spontan semasa penghabluran di dalam etil asetat, menghasilkan hablur racemic konglomerat.

Analisis pembelauan sinar-X untuk beberapa alkaloid indola dan bisindola baru yang diasingkan daripada pelbagai tumbuhan dengan genus *Alstonia*, *Kopsia*, *Leuconotis*, dan *Tabernaemontana* telah dilakukan. Ini termasuk: alkaloid bisindola, leuconoline (**124**) daripada *L. griffithii*, dan lumusidine A (**126**) dan B (**126**) (melalui pembentukan garam dimetil diiodida, **125a** dan **126a**) daripada *A. macrophylla*, alkaloid

indola istimewa, voatinggine (**128**) dan tabertinggine (**129**) daripada *T. corymbosa*, grandilodine A (**135**) and B (**136**) daripada *K. grandifolia*, dan leuconodine B (**68**) dan E (**71**) daripada *L. griffithii*.

ACKNOWLEDGEMENTS

Firstly, it is my pleasure to express my deepest gratitude to my supervisor, Professor Dr. Kam Toh Seok for all his guidance, invaluable advice, and dedication throughout this research. His patience and support will forever be remembered. I would also like to convey my appreciation to my co-supervisor Professor Dr. Richard Wong Chee Seng for his help and support. I would like to specially acknowledge Professor Dr. Ward T. Robinson (Visiting Professor, 2008–2009) for introducing me to the world of X-ray crystallography.

My deepest appreciation also goes to Dr Lim Kuan Hon for all his help in numerous aspects of laboratory practice and NMR studies, and Dr Subramaniam Gurusamy for his preliminary work on the mersinine alkaloids.

Many thanks to my colleagues in Lab C-100, Lim Siew Huah, Tan Shin Jowl, Gan Chew Yan, Nge Choy Eng, Hong Fong Jiao, Ku Wai Foong and Yap Wai Sum, for their invaluable support and advice throughout this project.

My heartfelt gratitude also goes to my parents, my brothers, and my loved one for their constant support, encouragement, and patience throughout this research.

Financial support from the University of Malaya and the Ministry of Higher Education, Malaysia, is gratefully acknowledged.

TABLE OF CONTENTS

LIST OF FIGURES

LIST OF TABLES

CHAPTER ONE

General Introduction to the Alkaloids

Alkaloids have a wide distribution in the plant kingdom. More than 20% of all plant species produce alkaloids.[1] Among the plant kingdom which produce alkaloids includes angiosperma, aspidosperma, gymnosperms, club mosses (*Lycopodium*), horsetails (*Equisetum*), mosses, and algae.[2–7] Alkaloids also occur in microorganisms (bacteria, fungi), many marine animals (sponges, slugs, worms, bryozoa), arthropods, amphibians (toads, frogs, salamanders), and also in a few birds, and mammals.[2–9] As of 2001, a total of 26,900 alkaloids have been isolated from various sources.[10] Among notable alkaloids include reserpine, an antihypertensive alkaloid from *Rauwolfia serpentina*, vinblastine, an antitumor alkaloid from *Catharanthus roseus*, morphine from *Papaver somniferum*, which exhibits nacrotic effects, atropine from *Atropa belladonna*, which acts as muscle relaxant, cocaine from the leaves of cocoa plant, which is a local anesthetic and a potent central nervous system stimulant, and strychnine, a nerve stimulant from *Strychnos nux-vomica*.[11]

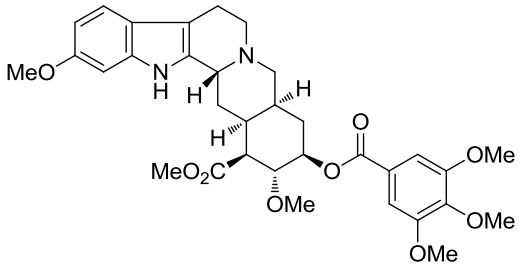

(–)-reserpine

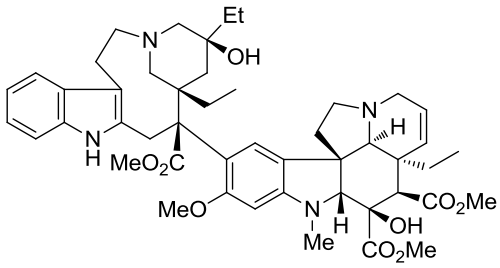

(–)-vinblastine

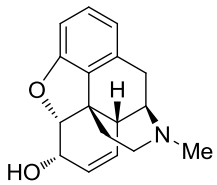

(–)-morphine

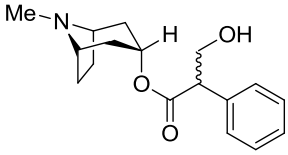

(±)-atropine

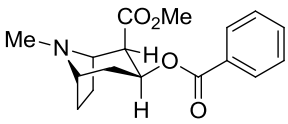

(–)-cocaine

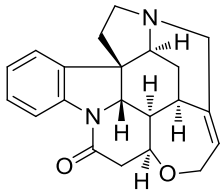

(–)-strychnine

1.1 Definition of Alkaloid

In 1819, a German pharmacist Carl F. W. Meissner introduces the term alkaloid. This term is usually applied to basic, nitrogen-containing compounds of plant origin. The first modern definition of alkaloid is by Winterstein and Trier who described these compounds as basic nitrogen containing compounds of either plant or animal origin.[12] Alkaloids were defined as compounds meeting additional four qualifications as follows:

i. Nitrogen is present as part of the heterocyclic ring system
ii. The compound occurrence is restricted to plant kingdom
iii. The compound has complex molecular structure
iv. The compound manifests significant physiological activity

Several nitrogenous compounds from plants or from other living organisms which do not confer to the above mentioned criteria are termed 'pseudoalkaloids'. This type of classifications which separates nitrogeneous compounds into true alkaloid and pseudoalkaloid based on biogenesis is very arbitrary.

In 1983, Pelletier suggested a simple general definition of an alkaloid: "An alkaloid is a cyclic compound containing nitrogen in a negative oxidation state which is of limited distribution in living organisms."[13] This definition encompasses compounds with nitrogen as part of a heterocyclic system as well as those with extracyclic bond nitrogen such as colchicines or capsaicin. However, compounds such as amino acids, amino sugars, peptides, nucleic acids, porphyrind, and vitamins or simple widely wimple widely distributed plant bases such as methyl amine, trimethylamine, β-phenylethyl amine derivatives, and other straight chain alkyl amines such as hordenine and ephedrine are not considered alkaloids because their nitrogen is not involved in the heterocyclic ring.[1] More recently, Hesse has defined alkaloids as nitrogen containing organic substances of natural origin with a greater or lesser degree of basic character.[14]

1.3 Classification of Alkaloids

Five distinct alkaloid classes were put forward according to the position of the N-atom in the main structural element:[14]

i. Heterocyclic alkaloids

ii. Alkaloids with exocyclic N-atoms and aliphatic amines (*e.g.*, cassaine, capsaicine)

iii. Putrescine, spermidine, and spermine alkaloids (*e.g.*, paucine, inandenin-12-one, chaenorhin)

iv. Peptide alkaloids (*e.g.*, integerrine, mucronine A)

v. Terpene and steroid alkaloids (*e.g.*, aconitine, conessine)

Among the five classes, the heterocyclic alkaloids constitute the largest group. These can be further divided into 15 subclasses based on the carbon-nitrogen skeleton as shown below:[14]

a. Pyrrolidine
b. Indole
c. Piperidine
d. Tropane
e. Imidazole
f. Isoquinoline
g. Quinoline
h. Quinazoline
i. Pyridine
j. Pyrrolizidine
k. Indolizidine
l. Quinolizidine
m. Pyrazine
n. Pteridine
o. Purine bases

Alkaloid class	Basic ring system	Example
Pyrrolidine	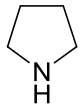	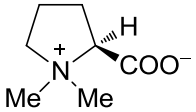 (–)-stachydrine
Piperidine	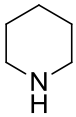	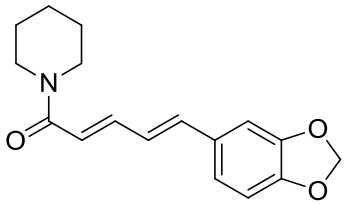 piperine
Pyridine		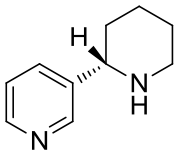 (–)-anabasine
Indole	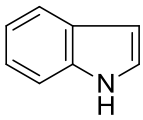	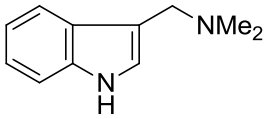 gramine
Tropane	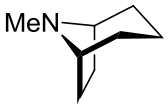	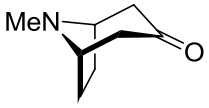 tropinone
Quinoline	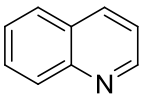	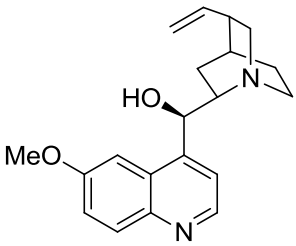 quinine
Isoquinoline	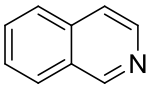	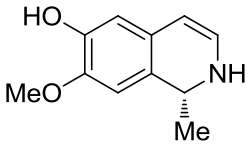 (+)-salsoline

Alkaloid class	Basic ring system	Example
Quinazoline	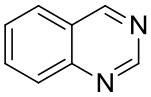	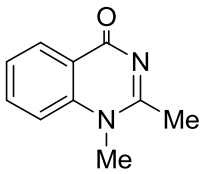 glomerine
Imidazole	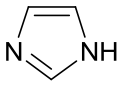	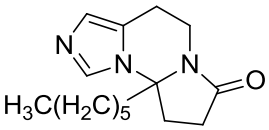 glochidine
Quinolizidine	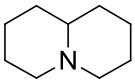	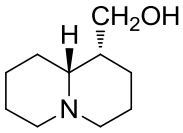 (–)-lupinine
Pyrrolizidine	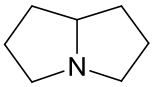	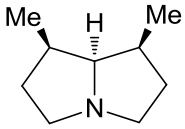 (–)-retronecanol
Indolizidine	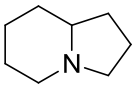	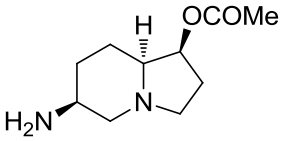 (–)-slaframine
Pyrazine	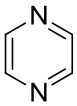	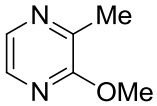 2-methoxy-3-methylpyrazine
Pteridine	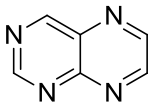	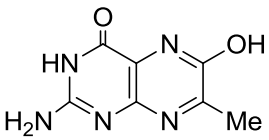 chrysopterin
Purine bases	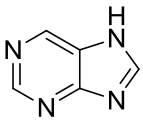	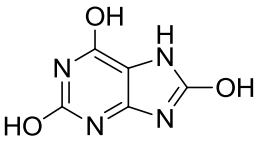 uric acid

1.4 Indole Alkaloids

Indole alkaloids constitute an important class of natural products, and include a large number of pharmacologically important substances, such as the antitumour alkaloids, vinblastine and vincristine, the antihypertensive alkaloid, reserpine, the hallucinatory alkaloid, lysergic acid, and the cardio-arrhythmic alkaloid, ajmalicine.[15] They are defined as natural products containing an indole nucleus or an oxidized, reduced, or substituted equivalent of it. The number of indole alkaloids of known structure amounts to approximately 5191 (2001).[10] This figure includes both those compounds that incorporate the actual indole chromophore and those containing its derivatives, namely, dihydroindole, indolenine, α-methyleneindoline, pseudoindoxyl, and oxindole. Also members of this group are alkaloids in which the nucleus incorporates an additional benzene or pyridine ring, for instance, carbazole or β- and γ-carbolines and their derivatives.

1.5 Structural Classes of the Monoterpenoid Indole Alkaloids

To further subclass the indole alkaloids, criteria such as structural and biogenetic pathways are applied. They can be divided into two main categories. First category comprises the simple indole alkaloids which do not present a structural uniformity, possessing only the indole nucleus or a direct derivative of it as a common feature (*e.g.*, harmane, **1**).

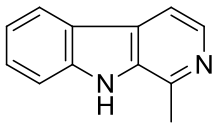

1 harmane

The indole bases of the second category contain two structural units, *viz.*, tryptamine (**2**) (or tryptophan, **3**) with the indole nucleus, and a C_9 or C_{10} monoterpene moiety derived from secologanin (**4**).

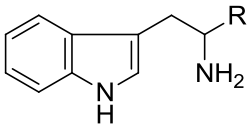

2 R = H
3 R = COOH

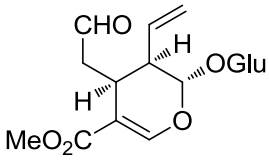

4 secologanin

The majority of the indole alkaloids from plants of the Apocynaceae belong to this category and can be classified into nine main types depending on the structural characteristic of their skeletons (Scheme 1.1).[16–18]

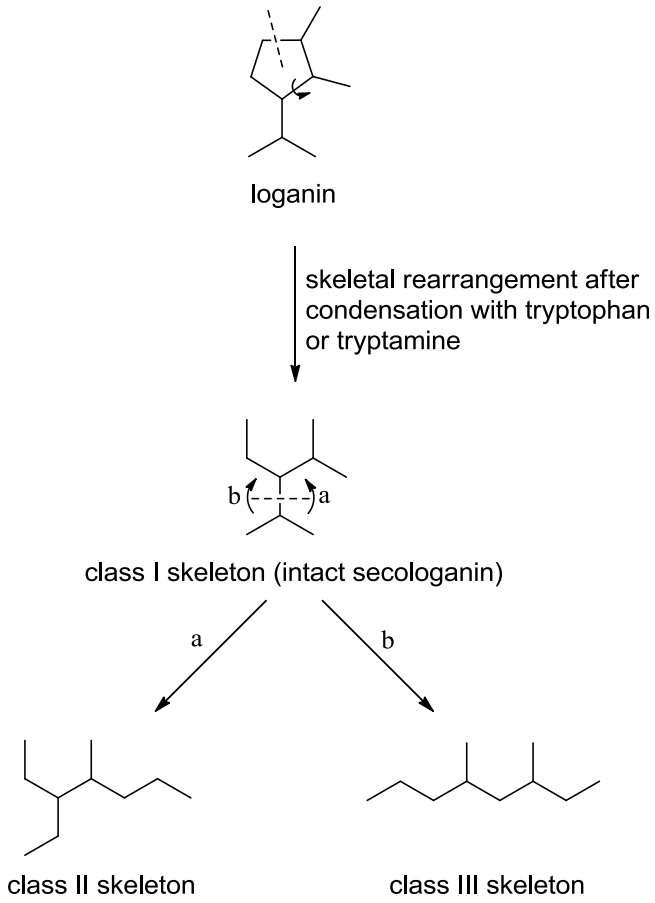

Scheme 1.1. The three major skeletal classes from loganin

Following Hesse,[16–18] eight main types have been defined: vincosan, vallesiachotaman, corynanthean, strychnan, aspidospermatan (all belonging to the class I skeleton with an intact secologanin), plumeran, eburnan (belonging to the class II skeleton, corresponding to a rearranged secologanin), and ibogan (belonging to the class III skeleton, corresponding to a further rearranged monoterpene). A ninth type, tacaman (with class III skeleton) was added by Verpoorte and Van Beek to account for the isolation of a few tacamines.[19–20] The nine main skeletal types are given in Table 1.1.

Table 1.1. Classification of indole alkaloids

Alkaloid Type	Example	Skeleton
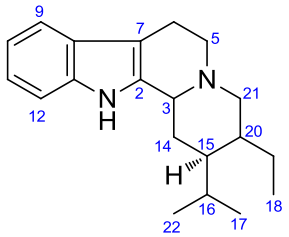 C-type	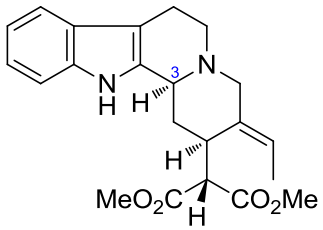 isositsirikine	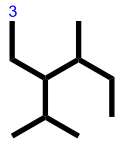 class I
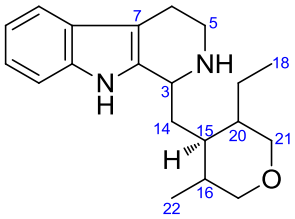 C-type	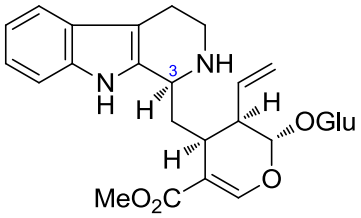 strictosidine	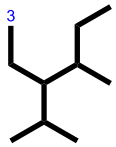 class I
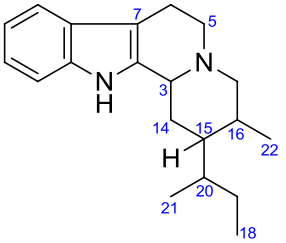 V-type	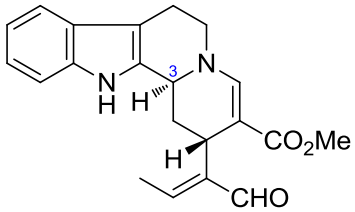 vallesiachotamine	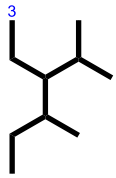 class I
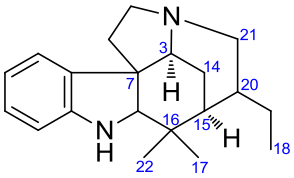 S-type	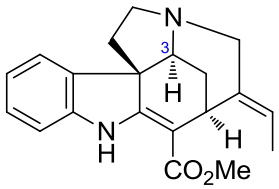 akuammicine	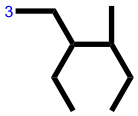 class I

Table 1.1, continued. Classification of indole alkaloids

Alkaloid Type	Example	Skeleton
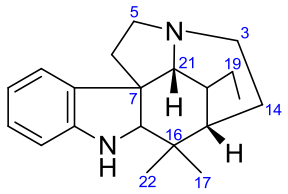 A-type	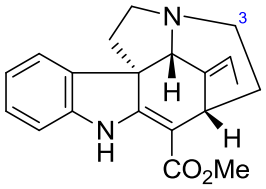 condylocarpine	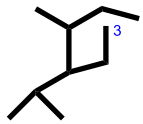 class I
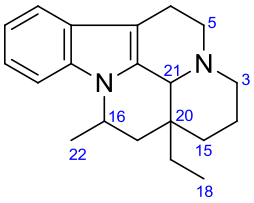 E-type	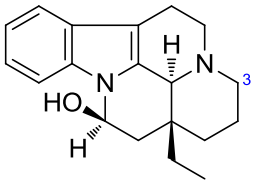 (–)-eburnamine	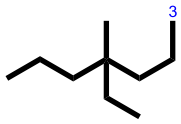 class II
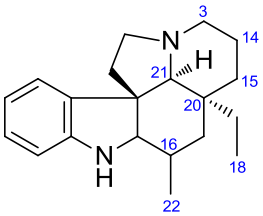 P-type	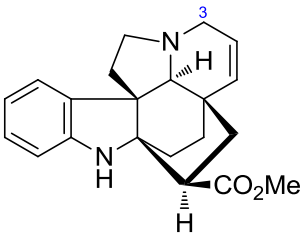 venalstonine	 class II
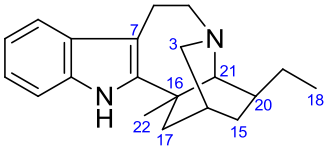 J-Type	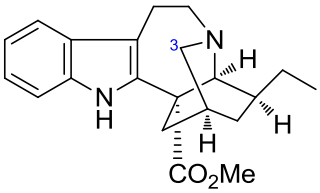 catharanthine	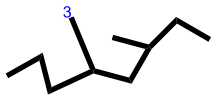 class III
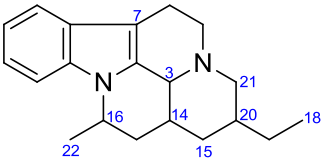 Tacaman-type	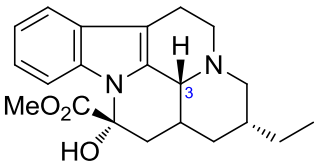 tacamine	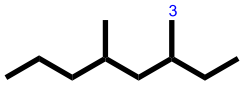 class III

1.6 Biogenesis of the Monoterpenoid Indole Alkaloids

The biogenesis of indole alkaloids is shown in Scheme 1.2. Although there are more than 1000 known structural types of indole alkaloids, they are nevertheless all derived from a common intermediate, namely, strictosidine (**8**). Wenkert, Scott, and others[21,22] suggested that **8** is transformed to geissoschizine (**9**), ajmalicine (**10**) and preakuammicine (**11**), and eventually to stemmadenine (**13**), whose isomerization and collapse *via* enamine **14** provides didehydrosecodine (**15**), from which the *Aspidosperma*, *Iboga*, and *Vinca/Eburnea* alkaloids are in turn derived.

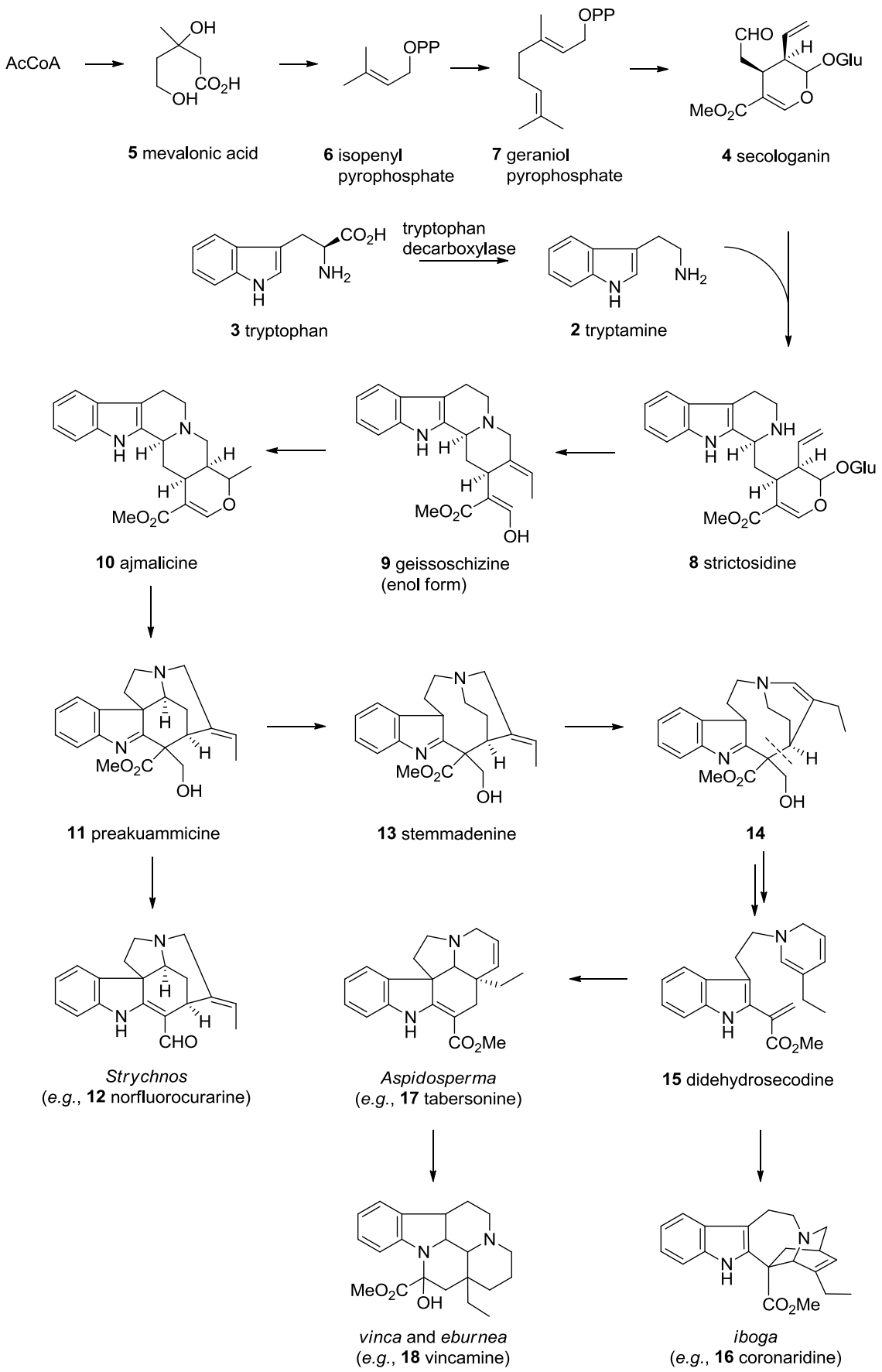

Scheme 1.2. Biogenesis of indole alkaloids.

1.7 Objectives

The objectives of the present research include the following:

i) Structure elucidation of selected alkaloids with difficult stereochemical issues (*e.g.*, the mersiphyllines from *Kopsia singapurensis*)

ii) Investigations of reactions of selected alkaloids (*e.g.*, leuconolam from *Leuconotis* species)

iii) Implementation of viable partial syntheses of selected alkaloids (*e.g.*, lirofoline A from *Tabernaemontana corymbosa*)

iv) Structure elucidation of several indole alkaloids *via* partial synthesis (*e.g.*, alstolucine A from *Alstonia spatulata* and (–)-eburnamaline from *Leuconotis griffithii*)

v) Reinvestigation of the stereochemical assignment of several indole alkaloids (*e.g.*, scholaricine and alstoumerine from *Alstonia* species)

vi) Determination of absolute configuration of several bisindole alkaloids *via* chemical transformations and X-ray diffraction analyses (*e.g.*, perhentinine, macralstonine, and perhentidines A – C from *Alstonia* species)

vii) X-ray diffraction analyses of a number of new indole and bisindole alkaloids (from *Alstonia*, *Kopsia*, *Leuconotis*, and *Tabernaemontana* species).

CHAPTER TWO

Mersiphyllines A and B, Two New Pentacyclic Alkaloids of the Mersinine Group. Determination of Relative Configuration at a Quaternary Center *via* Formation of an Alkaloid–Borane Complex

2.1 Introduction

The alkaloids of the mersinine group represent a novel subclass of the monoterpenoid indole alkaloids.[23–26] To date these alkaloids have been found exclusively and for the first time in only one species, a variant of the Malayan *Kopsia singapurensis*.[25] These alkaloids are characterized by a novel pentacyclic skeleton incorporating a quinolinic chromophore, and from a biogenetic viewpoint can be considered to have arisen from an aspidofractinine precursor **19** *via* formation of an aziridinium intermediate **20**, followed in succession by aziridinium ring opening and reduction as shown in Scheme 2.1.[23]

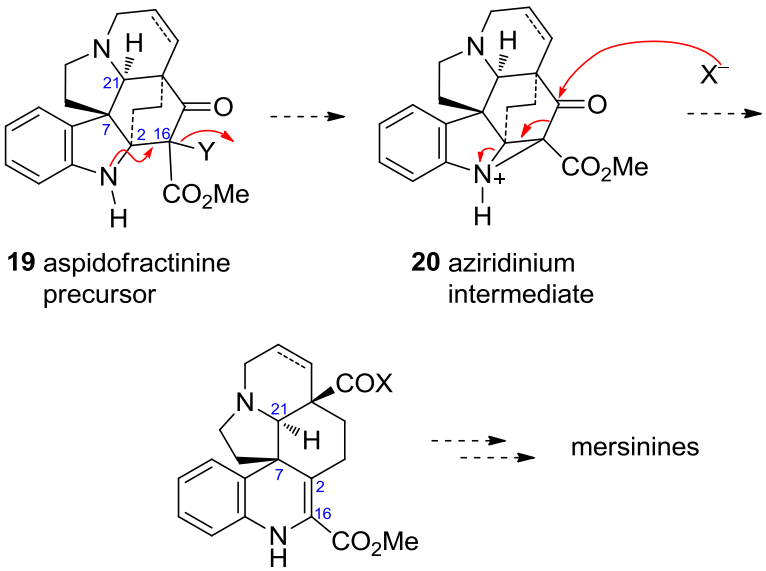

Scheme 2.1

There are a total of 16 mersinine-type alkaloids, representing variations in aromatic substitution, functional groups, and stereochemistry.[25] The mersinine alkaloids can be divided into two broad stereochemical groups, *viz.*, those with *cis*-D/E ring junction stereochemistry and a C-20–$\beta$$CO_2Me$ group (*e.g.*, mersinines A (**21**) and B (**22**)), and those with *trans*-D/E ring junction stereochemistry and a C-20–$\alpha$$CO_2Me$ group (*e.g.*, mersinine C (**23**)).[25] The relative configurations at C-2, C-7, and C-21 are all *R*, based on extensive NOE experiments,[23,24] as well as an X-ray diffraction study of mersinine A (**21**).[27]

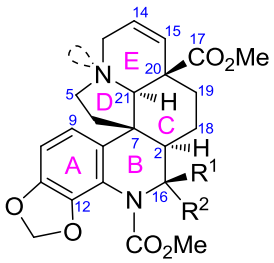

21 mersinine A $R^1 = CO_2Me$, $R^2 = OH$
22 mersinine B $R^1 = OH$, $R^2 = CO_2Me$

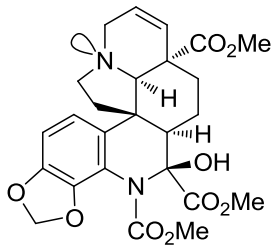

23 mersinine C

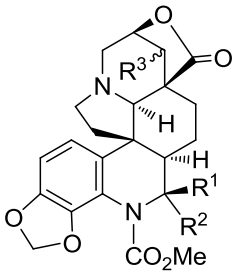

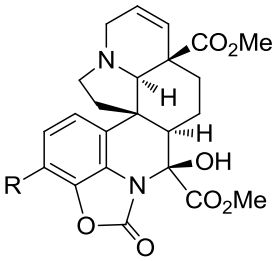

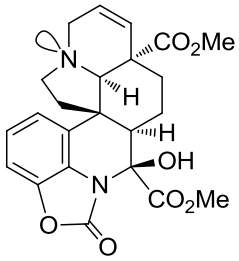

24 mersiloscine $R^1 = OH$, $R^2 = CO_2Me$, $R^3 = \alpha$-OH
25 mersiloscine A $R^1 = CO_2Me$, $R^2 = OH$, $R^3 = \alpha$-OH
26 mersiloscine B $R^1 = OH$, $R^2 = CO_2Me$, $R^3 = \beta$-OH

27 mersifoline A R = H
28 mersifoline B R = OMe

29 mersifoline C

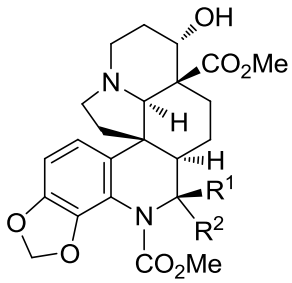

30 mersidasine A $R^1 = CO_2Me$, $R^2 = OH$
31 mersidasine B $R^1 = OH$, $R^2 = CO_2Me$

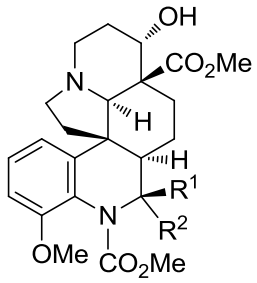

32 mersidasine C $R^1 = CO_2Me$, $R^2 = OH$
33 mersidasine D $R^1 = OH$, $R^2 = CO_2Me$

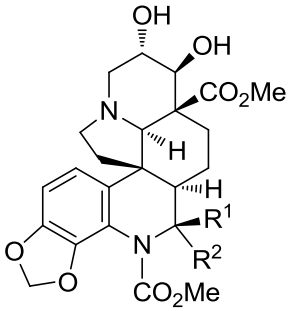

34 mersidasine E

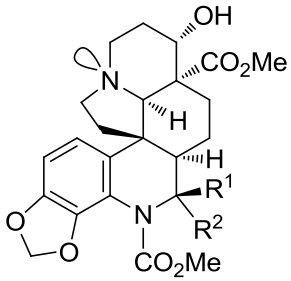

35 mersidasine F $R^1 = CO_2Me$, $R^2 = OH$
36 mersidasine G $R^1 = OH$, $R^2 = CO_2Me$

2.2 Results and Discussion

Two additional alkaloids, mersiphyllines A (**37**) and B (**38**), were obtained from the leaf extract of *K. singapurensis*.[28] These polar alkaloids proved difficult to purify as they resisted resolution by conventional chromatography, as well as HPLC. Eventually, mersiphyllines A and B were successfully separated by repeated passage through Sephadex G-75, with MeOH as the eluent (gel permeation chromatography). The separation process was very time consuming and laborious and yielded only 0.5 mg of **37** and 0.2 mg of **38** in each separation. Many repeated separations were performed in order to obtain sufficient amounts for further spectroscopic analysis and chemical transformations.

Mersiphylline A (**37**) was initially obtained as a light yellowish oil, and subsequently, as colorless block crystals from EtOH, mp 184–186 ^{o}C, $[\alpha]^{25}_{D}$ –59 (*c*

0.43, $CHCl_3$). The UV spectrum (219, 245, and 287 nm) was similar to those of the other mersinine alkaloids,[24] while the IR spectrum showed bands at 3463, 1746, and 1717 cm^{-1}, due to OH, ester/acid and carbamate functionalities, respectively. The EIMS showed an $[M]^+$ at *m/z* 486, which analyzed for $C_{24}H_{26}N_2O_9$, differing from mersinines A–C (**21**–**23**) by 14 mass units. The ^{13}C NMR data (Table 2.1) accounted for all 24 carbon resonances, and confirmed the presence of a carbamate (δ_C 154.4) and two carboxyl functions (δ_C 170.8 and 175.4, attributable to ester and/or acid groups), in addition to a low-field quaternary resonance (δ_C 87.3) due to C-16, which is α to both a nitrogen and an oxygen atom. The ^1H NMR data (Table 2.1) showed signals due to two adjacent aromatic hydrogens (AB doublets at δ_H 6.65, 6.74), two olefinic hydrogens (δ_H 5.86), a methylenedioxy function (δ_H 6.01, 6.02), two singlets due to carbamate and ester methoxy groups (δ_H 3.77, 3.81), and two broad OH singlets, δ_H 5.25 and 16.35, which undergo exchange with D_2O. The COSY and HMQC data showed the presence of NCH_2CH_2, $NCH_2CH{=}CH$, $CHCH_2CH_2$ partial structures, as well as an isolated aminomethine corresponding to H-21. These, and the HMBC data (three-bond correlations from H-2 to C-8, C-6, C-16; H-5 to C-7; H-9 to C-7; H-15 to C-17; H-19 to C-2, C-17; H-21 to C-3, C-15, C-17, C-19) (Figure 2.1) indicated that **37** has the same carbon skeleton as the mersinines (*e.g.*, mersinines A–C, **21**–**23**).[23–25]

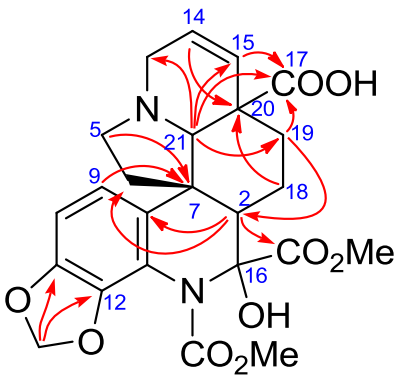

Figure 2.1. Selected HMBCs of **37**.

However, instead of the presence of the two characteristic methyl ester groups, one at C-16 and the other at C-20, as is the case in the other mersinine alkaloids,[24] the ^{1}H NMR data showed the presence of only one ester function, and two OH signals (one strongly deshielded), although two carboxyl functionalities associated with ester and/or acid functions were present (δ_C 170.8 and 175.4). One of the two carbonyl resonances must therefore be due to an acid group. In the HMBC spectrum, the ester methyl hydrogens at δ_H 3.77 showed a clear three-bond correlation to the carbonyl resonance at δ_C 170.8, indicating that this carbonyl (C-22) is associated with the methyl ester function. On the other hand, clear three-bond correlations were observed from H-21 and H-19 to the carbonyl carbon at δ_C 175.4 (C-17) indicating that this carbonyl is associated with the acid group attached to C-20. In both mersiphylline A (**37**) and mersiphylline B (**38**) (which differs from mersiphylline A (**37**) only in the aromatic substitution, *i.e.*, 12-OMe instead of 11,12-methylenedioxy, Table 2.1), the EIMS showed, in addition to the $[M]^+$ peaks, strong fragment peaks due to M–CO_2 and M–COOH (*m*/*z* 442 and 441, respectively, in the case of **37**, and *m*/*z* 428 and 427, respectively, in the case of **38**), while the acid functionality in **37** can be readily esterified with $TMSCHN_2$ in MeOH/$PhCH_3$ (replacement of low field acid signal at δ_C 16.35 by a methyl ester signal at δ_H 3.71 in the methyl ester product), providing additional proof for the presence of the carboxylic acid function in **37**. The ^{1}H NMR spectra of mersiphyllines A (**37**) and B (**38**) are shown in Figures 2.2 and 2.3, respectively.

Table 2.1. ^{1}H (400 MHz) and ^{13}C (100 MHz) NMR data (δ) of compounds **37**, **38**, and **40**

Position	**37**[a]		**38**[a]		**40**[b]	
	δ_C	δ_H	δ_C	δ_H	δ_C	δ_H
2	48.0	2.60 m	48.5	2.66 m	46.7	2.66 dd (12.6, 6.6)
3α	52.7	3.89 m	52.9	4.14 br d (16)	66.1	4.24 ddd (16, 4, 1)
3β		3.51 br d (16)		3.59 br d (16)		3.75 m
5α	50.2	3.37 m	51.1	3.80 m	59.7	3.46 dd (10, 6)
5β		2.60 m		2.72 m		2.85 ddd (13, 10, 5)
6α	39.0	2.08 dd (13, 4.5)	38.8	2.14 dd (13, 4.5)	37.3	1.99 dd (13, 5)
6β		2.78 td (13, 6)		2.84 td (13, 6)		3.29 td (13, 6)
7	44.7	–	44.5	–	43.6	–
8	129.0	–	136.3	–	129.1	–
9	117.2	6.74 d (8.2)	116.2	6.90 d (8)	115.7	6.44 d (8.6)
10	103.9	6.65 d (8.2)	125.0	7.17 t (8)	104.0	6.66 d (8.6)
11	147.8	–	111.7	6.94 d (8)	148.2	–
12	139.8	–	152.6	–	140.4	–
13	119.3	–	125.7	–	119.5	–
14	127.1	5.86 m	126.9	5.89 m	127.1	5.99 m
15	133.4	5.86 m	133.3	5.89 m	132.1	5.89 ddd (9.5, 2.4, 1)
16	87.3	–	87.4	–	87.4	–
17	175.4	–	175.9	–	169.4	–
18α	20.4	0.84 m	20.4	0.75 s	20.6	0.79 m
18β		1.45 m		1.44 m		1.43 m
19α	23.9	0.84 m	24.2	0.82 m	24.8	0.79 m
19β		2.84 m		2.74 m		2.46 m
20	44.1	–	44.7	–	43.2	–
21	70.7	3.35 s	70.4	3.49 s	73.4	3.85 m
22	170.8	–	170.6	–	170.5	–
12-O<u>Me</u>	–	–	56.6	3.88 s	–	–
22-O<u>Me</u>	53.0	3.77 s	53.1	3.75 s	53.1	3.74 s
*N*CO$_2$<u>Me</u>	53.3	3.81 s	53.1	3.75 s	53.2	3.79 s
N<u>C</u>O$_2$Me	154.4	–	155.9	–	154.5	–
OCH$_2$O	101.6	6.01 d (1.3)	–	–	102.1	6.02 d (1.2)
		6.02 d (1.3)				6.03 d (1.2)
16-OH	–	5.25 br s	–	5.32 br s	–	5.36 br s
17-OH	–	16.35 s	–	15.27 br s	–	–

[a]$CDCl_3$; [b]CD_2Cl_2; assignments based on COSY, HMQC, and HMBC.

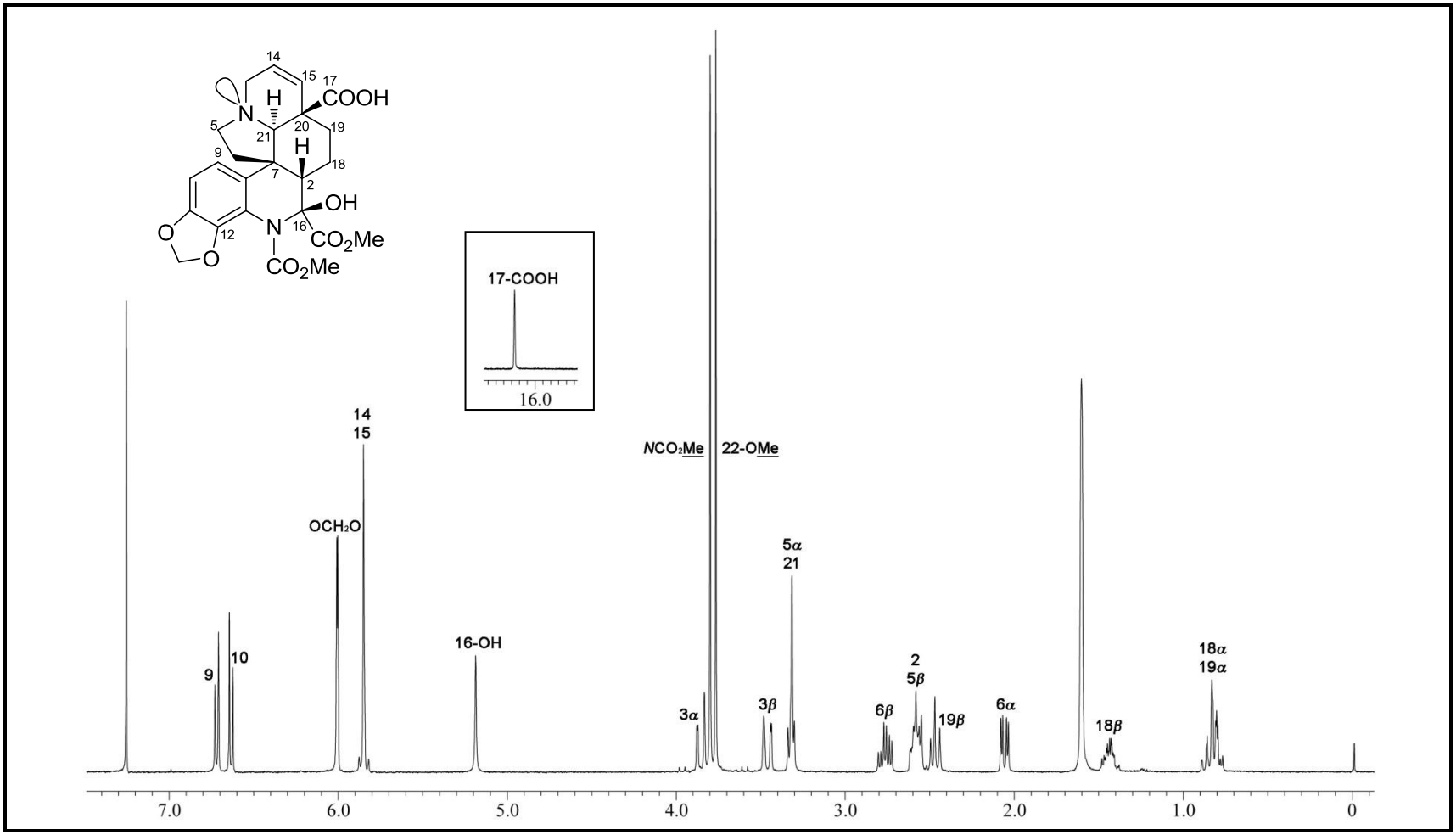

Figure 2.2. ^{1}H NMR spectrum ($CDCl_3$, 400 MHz) of mersiphylline A (**37**).

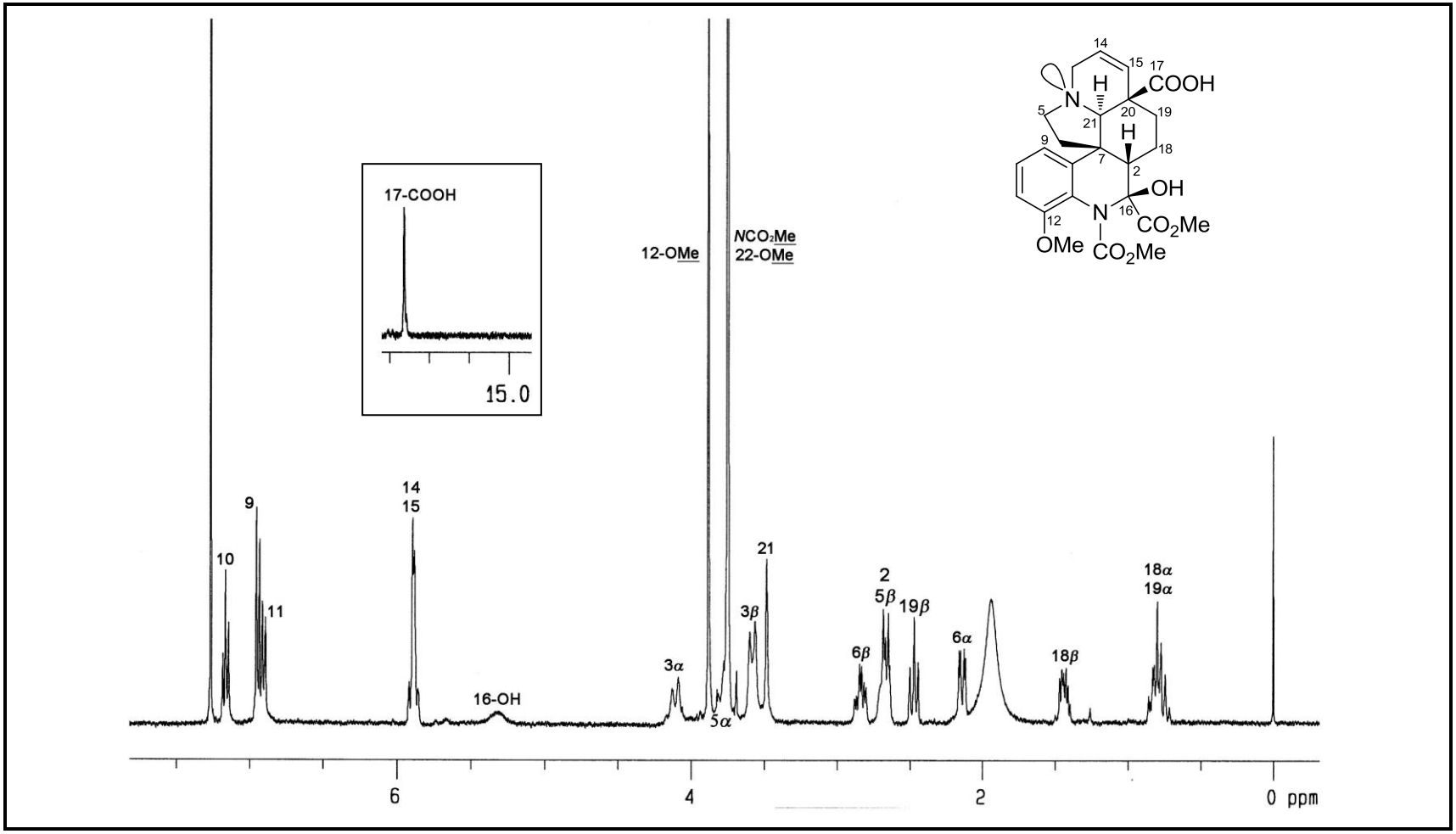

Figure 2.3. ^{1}H NMR spectrum ($CDCl_3$, 400 MHz) of mersiphylline B (**38**).

The reciprocal NOEs observed for H-9/H-21 and H-19α/H-21 (Figure 2.4), permitted assignment of the relative configurations at C-7 and C-21, which were similar to those in mersinines A (**21**) and B (**22**).[23,24] The configuration at the quaternary C-16 was deduced to be similar to that in **22**, *i.e.*, *S*, from the characteristic C-16–OH shift of δ_H 5.25 and the C-2 shift of δ_C 48.0.[23] The presence of Wenkert-Bohlmann bands[29] in the IR has been previously invoked to signify the presence of a *trans*-D/E ring junction, with a β-oriented *N*-4 lone pair, in mersinine C (**23**), mersifoline C (**29**), mersidasine F (**35**) and mersidasine G (**36**).[24,25] This conclusion was also supported by the NOE enhancement observed for H-3α, H-5α, and H-9 on irradiation of H-21. In the case of **37** and **38**, although Wenkert-Bohlmann bands were not detected (possibly due to intramolecular H-bonding involving the *N*-4 lone pair, *vide infra*), these NOEs were also observed, suggesting the presence of a *trans*-C/D junction. Irradiation of H-2 resulted in enhancement of H-6β, H-18β, and 16-OH, while irradiation of H-18β resulted in enhancement of H-2 (Figure 2.4). These observations indicated a β-orientation for H-2 (2*S*), and represents a significant departure from the previous mersinine alkaloids, where the orientation of H-2 is α (2*R*) as indicated by the observed H-2/H-21 or H-6β/H-18β NOEs. This may also be reflected to some extent by the noticeable departure in the ^{1}H (H-6α, H-18α, H-19α) and ^{13}C (C-6) NMR data compared to those of the mersinines (*vide supra*).

The remaining issue concerns the relative configuration at the carboxyl bearing quaternary center, C-20. In this instance the observed NOEs were insufficient to unambiguously assign the configuration.

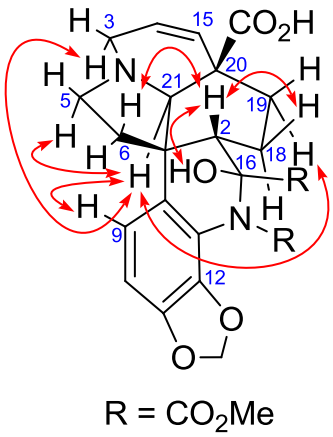

Figure 2.4. Selected NOEs of **37**.

An early indication that the orientation of the acid group is β was from the observation of the deshielded, low-field, acid-H signal at δ_C 16.35, suggesting intramolecular H-bonding to *N*-4 (with its β-oriented lone pair in view of the *trans*-D/E fusion mentioned earlier).

In the event, a second line of evidence was obtained which provided cogent proof of 20*R* configuration. In an attempt to reduce the acid group, alkaloid **37** was treated with BH_3.THF.[30–32] Instead of the alcohol **39**, an unexpected alkaloid-borane complex **40** was obtained (Scheme 2.2), as deduced from the data.

The mass-spectral data clearly showed boron incorporation ($[M]^+$, *m*/*z* 498), while the IR spectrum showed the characteristic B–H stretching frequencies at 2431, 2376, and 2285 cm^{-1} (Figure 2.5).[33] The ^1H and ^{13}C NMR data (Table 2.1) of the complex **40** were essentially similar to those of **37**, except for loss of the low field acid signal in ^1H NMR data, and the distinct downfield shifts of the C-3, C-5, and C-21 signals in the ^{13}C NMR data (and the corresponding H-3, H-5, and H-21 signals in the ^1H NMR data), an effect somewhat reminiscent of that shown by alkaloid *N*-oxide derivatives, suggesting that *N*-4 has been rendered electron-deficient.

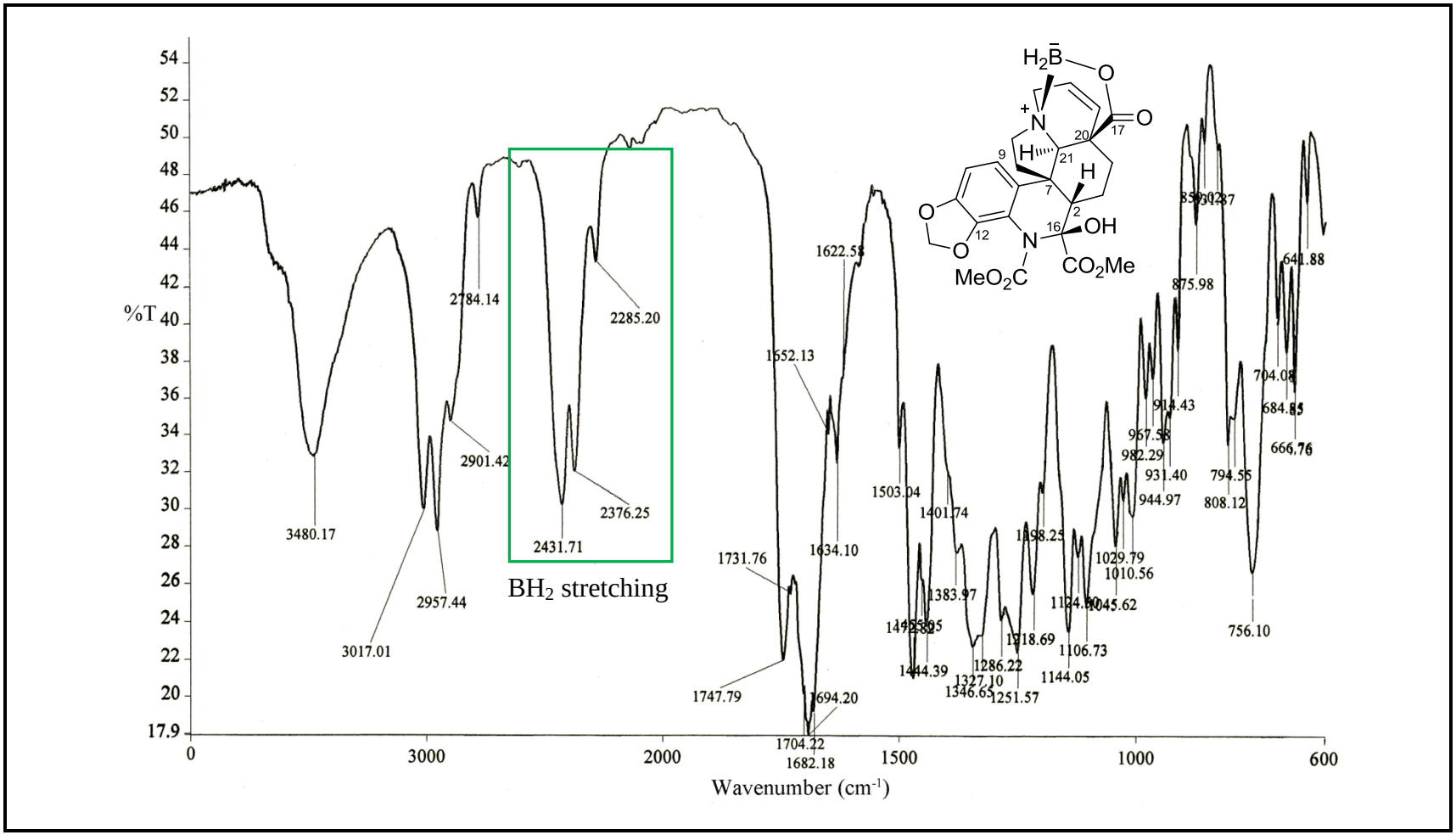

Figure 2.5. IR spectrum (neat) of mersiphylline A-borane complex **40**.

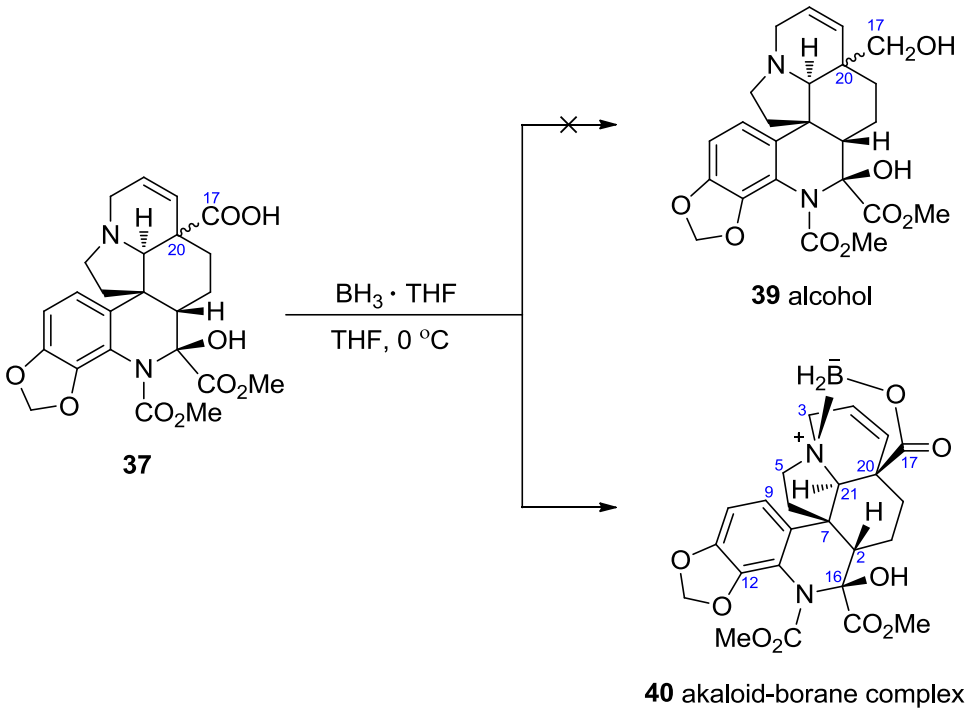

Scheme 2.2

A likely formulation for the alkaloid-borane complex **40** is one in which BH_2 has been incorporated into the molecule *via* formation of an O=CO–boron, as well as a dative *N*-4→B bond, linked at the carboxyl oxygen and at *N*-4, respectively, as shown in **40**. Such a structure would be compatible with the MS, IR, and NMR data (the B–H hydrogens were not observed in the ^{1}H NMR spectrum due to broadening[34,35]). Additional confirmation was obtained by accurate mass measurements of both the $C_{24}H_{27}N_2O_9{}^{11}B$ ($[M]^+$) as well as the $C_{24}H_{26}N_2O_9{}^{10}B$ ($[M - H]^+$) peaks in HREIMS, which were in excellent agreement with the proposed constitution of the complex.

The formation of the alkaloid-borane complex **40** is presumably *via* the proposed pathway shown in Scheme 2.3. Reaction of the alkaloid with BH_3.THF gives in the first instance, the acid-borane complex **41**, which on loss of H_2, followed by intramolecular interception by *N*-4 of the resulting organoborane intermediate **42**, furnishes the alkaloid-borane complex **40** (This unexpected diversion accounts for the exclusive formation of **40** at the expense of the alcohol **39**, normally formed *via* the

intermediacy of trialkoxyboroxine **43** and its subsequent hydrolysis to **39**[31,36,37]) (Scheme 2.3).

The formation of the alkaloid-borane complex **40** is only possible if the C-20 carboxylic acid function has a *β*-orientation (20*R*) (C-20–COOH and *N*-4 lone pair *syn*). The alkaloid-borane complex **40** also showed a better resolved ^{1}H NMR spectrum with less overlap compared to that of mersiphylline A (**37**) allowing for better NOE data to be obtained (Table 2.1). The ^{1}H NMR spectrum of **40** is shown in Figure 2.6. Attempts to obtain a ^{11}B NMR on the alkaloid-borane complex **40** was unsuccessful due to insufficient amount of material available (the formation of the alkaloid-borane complex is also reversible, if left in solution in $CDCl_3$ or EtOH over a prolonged period).

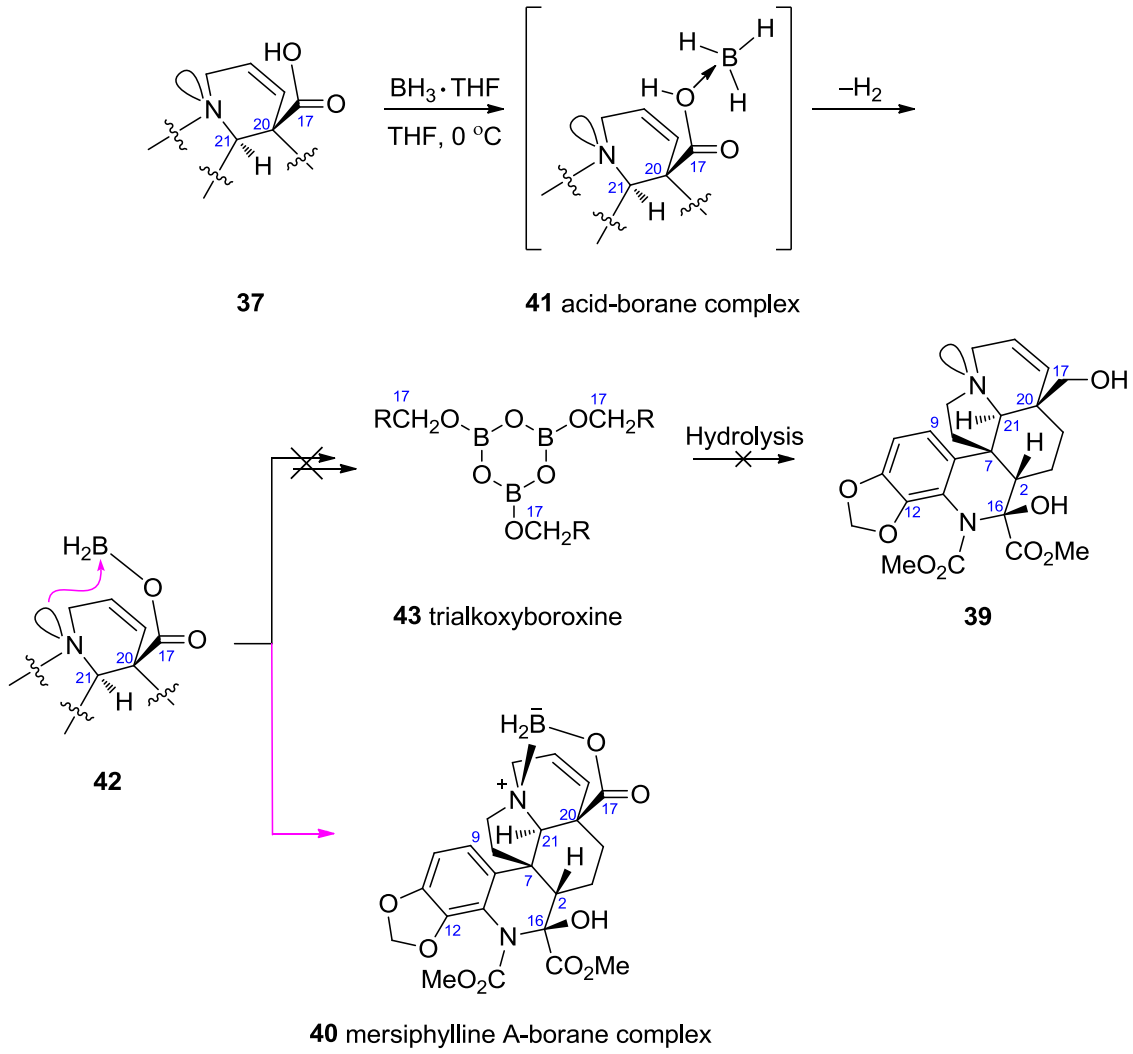

Scheme 2.3

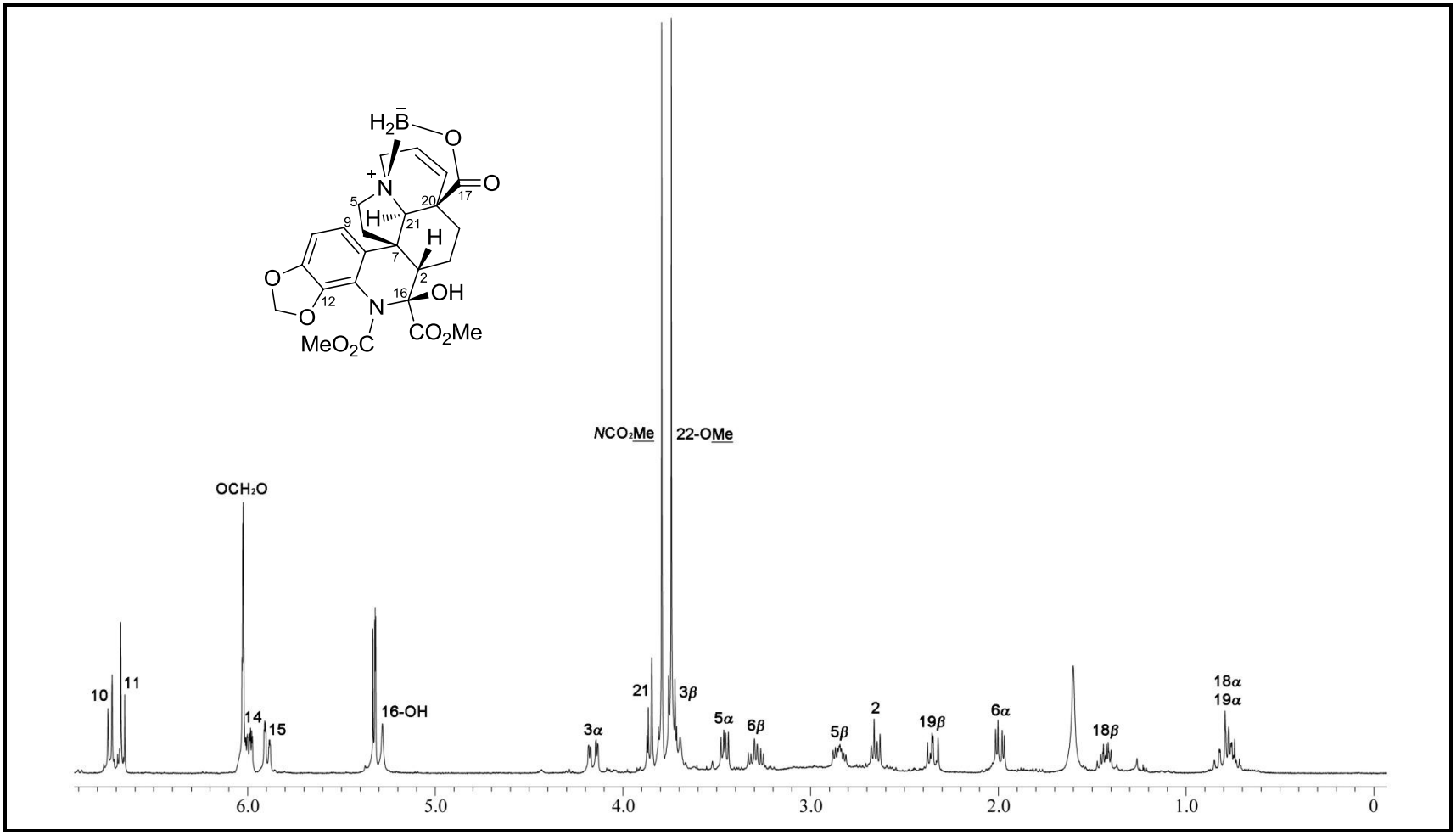

Figure 2.6. ^{1}H NMR spectrum (CD_2Cl_2, 400 MHz) of mersiphylline A-borane complex **40**.

Finally, to obtain support for the above deduction, as well as to secure unambiguous proof of the structure, X-ray diffraction analysis was carried out for **37** (Figure 2.7) which provided confirmation of the structure and relative configuration deduced from all the above observations.

Suitable crystals of **37** were obtained by slow evaporation in EtOH. The structure and relative configuration of **37** is shown in Figure 2.7. From the X-ray crystal structure, it can be seen that **37** exists as a zwitterion [(*N*-4–H)$^{+}$(C-17–OO)$^{-}$] in the solid state. It can also be seen that **37** co-crystallizes with the solvent used during crystallization. Hydrogen bonding between the EtOH molecule with C-17–OO^{-} can also be seen from the crystal structure.

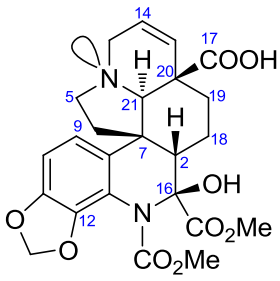

37 mersiphylline A

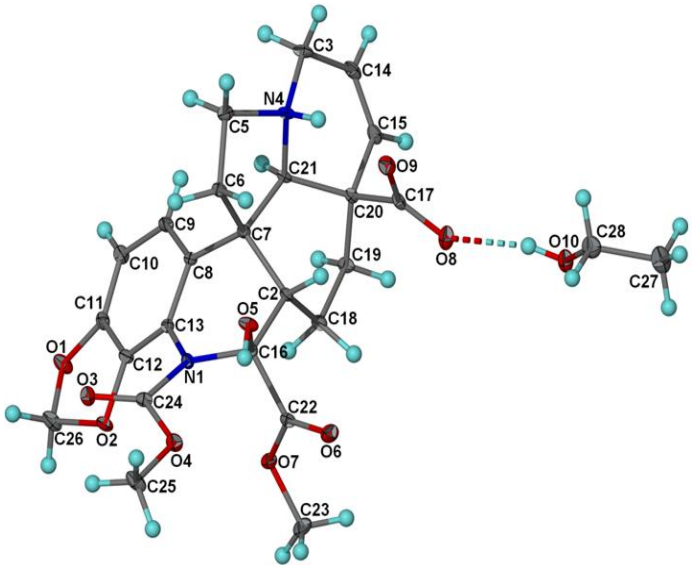

Figure 2.7. X-ray crystal structure of **37**.

With the structure of mersiphylline A (**37**) thus established, the structure of mersiphylline B (**38**) follows readily from the spectroscopic data.

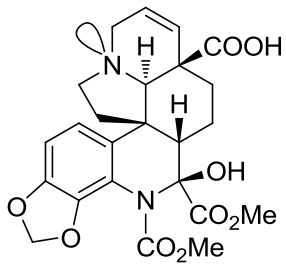

37 mersiphylline A

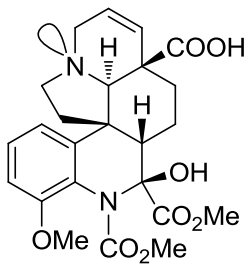

38 mersiphylline B

2.3 Conclusion

Mersiphyllines A (**37**) and B (**38**) represent yet another addition to the mersinine group of alkaloids, constituting a new and distinct stereochemical group, with a *trans* D/E ring junction stereochemistry, a *β*-oriented carboxylic acid functionality linked to the quaternary C-20 (20*R*), and a *β*-oriented hydrogen at C-2 (2*S*). Although several examples of related organoborane complexes exist in the literature, such as the condylocarpine-BH_3 adduct,[38] various simple cyclic borane derivatives of amino acids,[33] and the chiral oxazaborolidines (or CBS reagent),[34] the present example nevertheless represents the first instance where the formation of an alkaloid-borane complex has been invoked to underpin a difficult stereochemical assignment at a quaternary stereogenic center in an alkaloid.

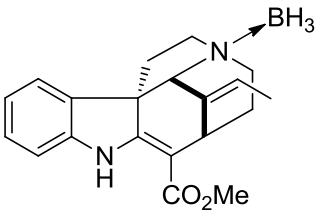

condylocarpine-BH_3

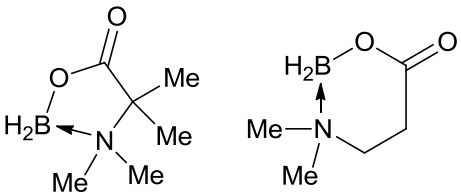

cyclic borane derivatives of amino acids

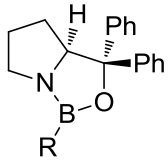

CBS reagent

CHAPTER THREE

A Biomimetic Partial Synthesis of Lirofoline A

3.1 Introduction

Lirofolines A (**44**) and B (**45**) were new alkaloids recently isolated from two *Tabernaemontana* species.[39] Both **44** and **45** were isolated from the stem-bark extract of *T. corymbosa*, while **45** was also isolated from the stem-bark extract of *T. divaricata* (single flower variety) (isolation and structure by K. H. Lim and H. S. Pang).

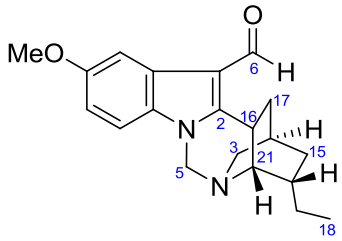

44 lirofoline A

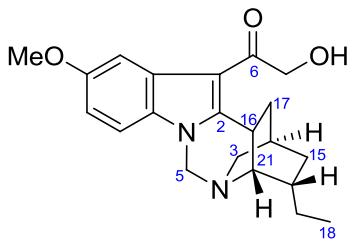

45 lirofoline B

The lirofolines are characterized by a novel pentacyclic skeleton, previously unencountered as a natural product. After the structures were solved by the application of spectroscopic methods, a search in the literature indicated that the basic ring system has been encountered previously as unwanted minor side products in reactions in the ibogaine and catharanthine series (chemical transformations of ibogaine (**46**) to voacangine (**47**)[40] (Scheme 3.1) and coupling of catharanthine (**48**) and its derivatives with vindoline[41] (Scheme 3.2)).

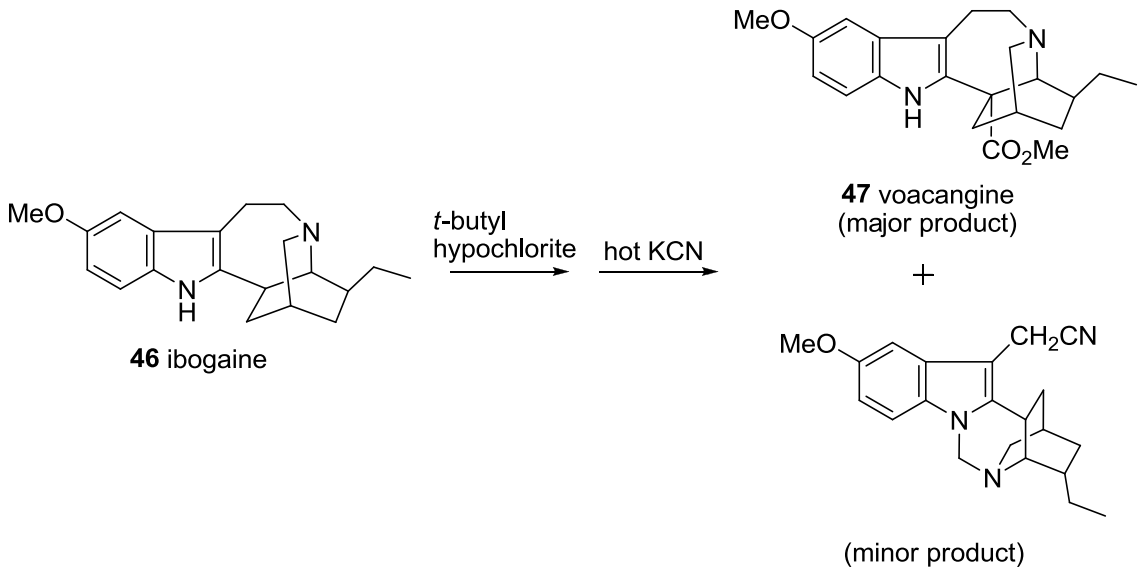

Scheme 3.1

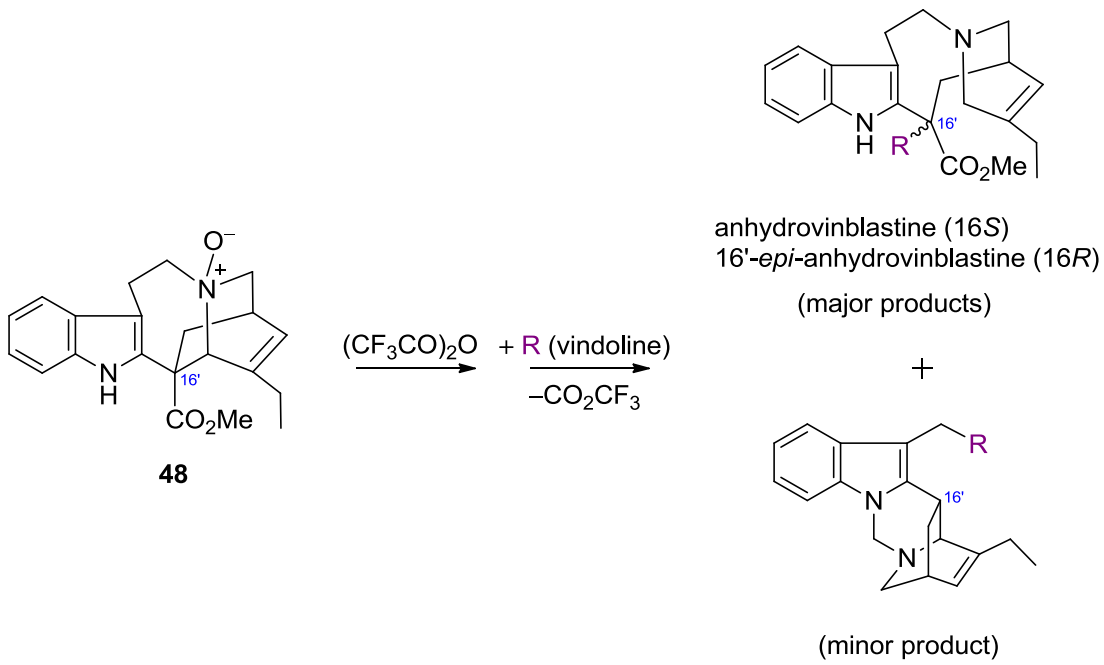

Scheme 3.2

The ^{1}H and ^{13}C NMR data of lirofolines A (**44**) and B (**45**) are summarized in Table 3.1, while the ^{1}H NMR spectra of **44** and **45** are shown in Figures 3.1 and 3.2, respectively.

Table 3.1. ^{1}H and ^{13}C NMR data (δ) of lirofolines A (**44**) and B (**45**)[a]

Position	**44**		**45**	
	δ_C	δ_H	δ_C	δ_H
2	153.7	–	152.6	–
3α	53.5	2.72 dt (10, 3)	53.5	2.67 dt (10, 2.5)
3β		3.27 dt (10, 3)		3.27 dt (10, 2.5)
5α	67.1	4.88 d (12)	67.2	4.92 d (12)
5β		4.94 d (12)		4.98 d (12)
6	182.9	10.1 (s)	192.5	–
7	111.8	–	108.0	–
8	127.0	–	126.8	–
9	103.1	7.74 br d (2.4)	103.9	7.36 d (2)
10	156.8	–	156.6	–
11	112.8	6.88 dd (8.8, 2.4)	111.6	6.90 dd (8.5, 2)
12	109.8	7.12 d (8.8)	110.0	7.17 d (8.5)
13	129.9	–	129.8	–
14	25.5	1.81 m	25.4	1.81 m
15α	31.1	1.90 dddd (12.5, 10, 4, 2)	31.2	1.91 dddd (13, 10, 4, 2.5)
15β		1.20 ddt (12.5, 6.8, 2)		1.18 ddt (13, 7.5, 2)
16	29.7	3.55 br dt (12, 2)	31.8	3.67 dt (12, 2)
17α	33.4	1.70 m	32.4	1.58 m
17β		2.20 br t (12)		2.29 tdd (12, 2.5, 2)
18	11.7	0.96 t (7.3)	11.7	0.96 t (7.5)
19	27.4	1.59 m	27.3	1.60 m
		1.59 m		1.60 m
20	37.8	1.72 m	37.7	1.73 dq (10, 7.5)
21	51.8	2.85 br s	51.9	2.82 br s
22	–	–	67.0	4.73 dd (17, 4)
				4.78 dd (17, 4)
10-O<u>Me</u>	55.8	3.89 s	55.9	3.90 s
22-OH	–	–	–	4.15 br s

[a]$CDCl_3$, 400 and 100 MHz, respectively; assignments based on COSY, HMQC, and HMBC.

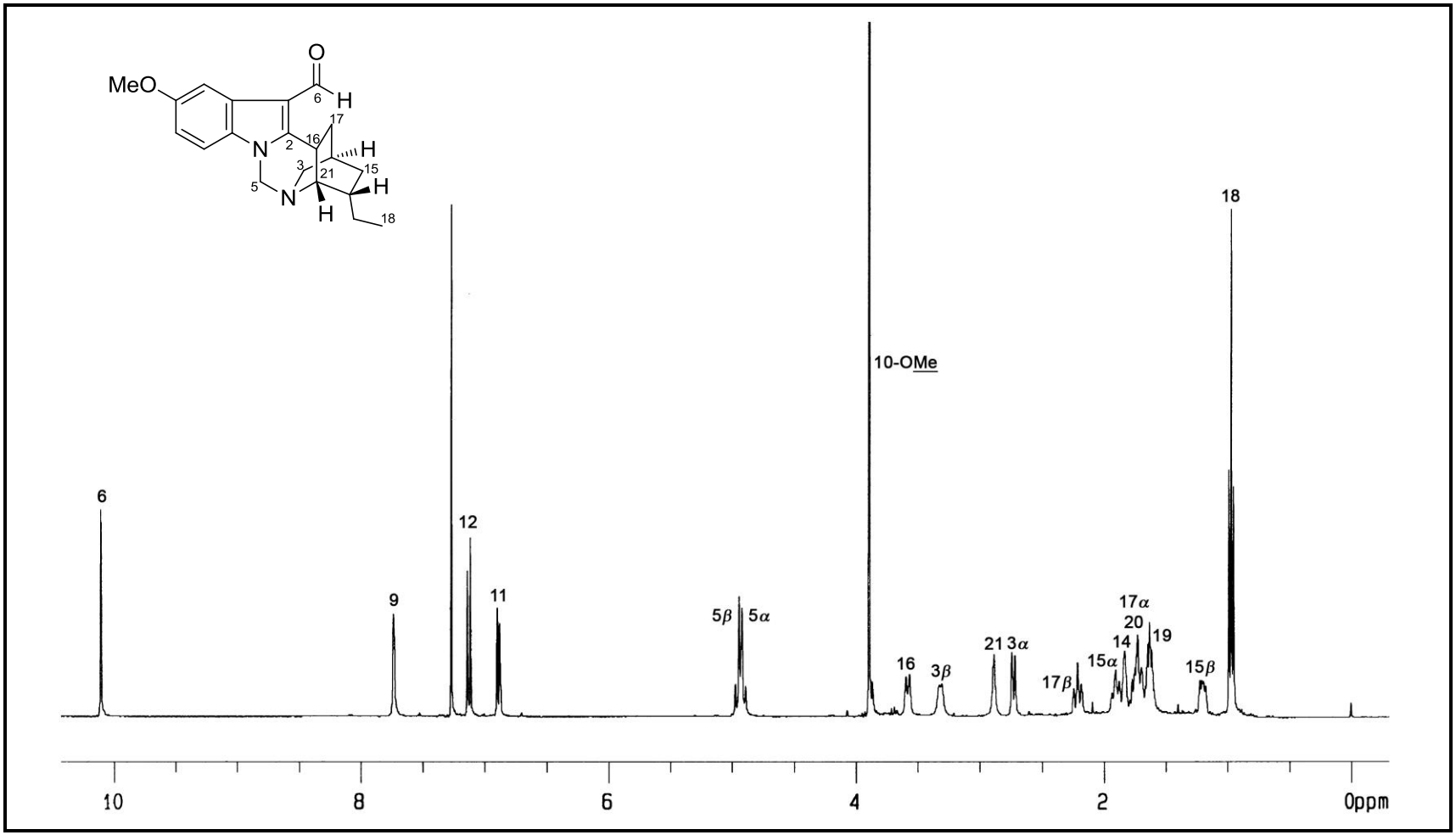

Figure 3.1. ^{1}H NMR spectrum ($CDCl_3$, 400 MHz) of natural lirofoline A (**44**).[42]

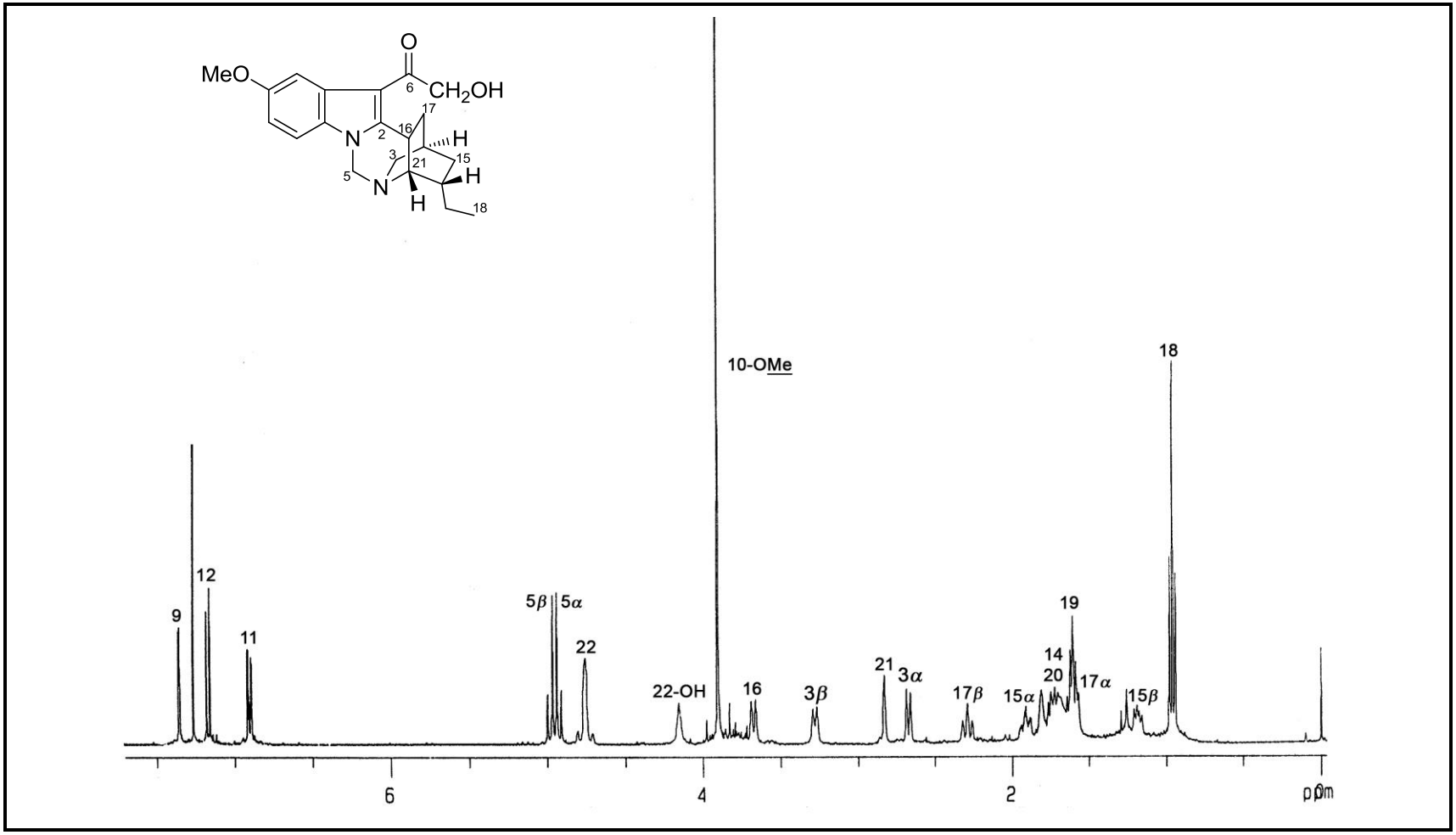

Figure 3.2. ^{1}H NMR spectrum ($CDCl_3$, 400 MHz) of lirofoline B (**45**).[43]

3.2 Results and Discussion

Based on the previous observations (*vide supra*), it follows that the ring system of the lirofolines in all probability arises from similar precursors and in like fashion, *viz.*, *via* scission of the C-5–C-6 bond of an oxidized derivative to the iminium ion intermediate **49**, followed by intramolecular bond formation between C-5 and *N*-1 (Scheme 3.3).

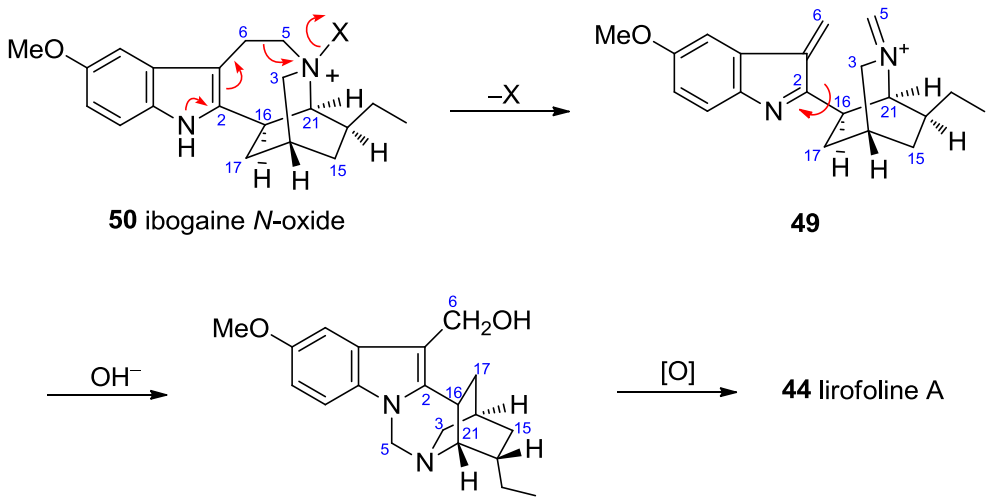

Scheme 3.3

Based on this supposition, and with limited, but sufficient amounts of the requisite precursor (ibogaine (**46**), *ca.* 50 mg) available from our ongoing work in alkaloid chemistry, we decided to carry out such a biomimetic conversion of ibogaine (**46**) to lirofoline A (**44**) under Polonovski conditions.

The ^{1}H and ^{13}C NMR data of ibogaine (**46**) are summarized in Table 3.2, while the ^{1}H NMR spectrum of **46** is shown in Figure 3.3.

The first step in the Polonovski approach to this biomimetic transformation involved oxidation of ibogaine (**46**) to its *N*-oxide **50**, using *m*-chloroperbenzoic acid (*m*-CPBA) in CH_2Cl_2 at –30 ^{o}C to give 74% of **50** (Scheme 3.4).

Ibogaine *N*-oxide (**50**) was obtained as a colorless oil, with $[\alpha]^{25}_{D}$ +71 (*c* 0.16, $CHCl_3$). The UV spectrum (210, 224, 280, 297, and 307 nm) showed absorption maxima characteristic of an indole chromophore, while the IR spectrum showed the presence of an *N*H (3149 cm^{-1}) function. The HRESIMS of **50** showed an $[M + H]^+$ at *m/z* 327.2080, which is consistent with the molecular formula $C_{20}H_{26}N_2O_2 + H$ (16 mass units higher than that of **46**). The ^1H NMR data showed characteristic downfield shifts for H-3, H-5, and H-21, while the same downfield shifts were observed for C-3, C-5, and C-21 in ^{13}C NMR data, when compared with those of ibogaine (**46**). The ^1H and ^{13}C NMR data of **50** are summarized in Table 3.2, while the ^1H NMR spectrum of **50** is shown in Figure 3.4.

With ibogaine *N*-oxide (**50**) to hand, a Polonovski transformation was carried out. Ibogaine *N*-oxide (**50**) on treatment with acetic anhydride (10 equiv in 50 ml CH_2Cl_2, added dropwise at –10 ^oC for 30 min), followed by hydrolysis (NaOH) gave a single major product **51** in 70% yield. High dilution used in this reaction was necessary to obtain optimum yields for this reaction based on our previous work on related Polonovski transformations.[44]

In the presence of acetic anhydride, cleavage of the C-5–C-6 bond takes place, leading to the iminium ion **52**. The iminium ion **52** then undergoes a concerted conjugate addition by acetate anion, followed by intramolecular bond formation between C-5 and *N*-1 to give **53**. Basic hydrolysis with 10% NaOH during work up leads to the alcohol **51**. Attempted purification and characterization of the alcohol **51** was not successful due to its facile decomposition during chromatography, upon exposure to air, and in $CDCl_3$.

Table 3.2. ^{1}H and ^{13}C NMR data (δ) of ibogaine (**46**) and ibogaine *N*-oxide (**50**)[a]

Position	**46**		**50**	
	δ_C	δ_H	δ_C	δ_H
2	142.9	–	139.8	–
3	49.9	2.97 dt (9, 3)	70.3	3.54 br d (12)
		3.07 dt (9, 2)		3.79 br d (12)
5	54.2	3.14 m	76.9	3.71 br d (11.5)
		3.37 m		3.93 m
6	20.7	2.61 m	21.1	3.08 m
		3.32 m		2.94 m
7	109.1	–	107.2	–
8	129.7	–	128.1	–
9	100.3	6.93 d (2)	100.0	6.82 d (2)
10	153.9	–	153.9	–
11	110.8	6.77 dd (8.5, 2)	111.8	6.78 dd (8.7, 2.3)
12	110.6	7.13 d (8.5)	111.5	7.19 d (8.7)
13	130.1	–	130.3	–
14	26.5	1.84 m	26.1	2.17 m
15	32.1	1.20 ddt (13, 5, 2.5)	31.6	1.49 m
		1.79 m		2.26 m
16	41.5	2.88 ddd (11, 4, 1.5)	37.0	3.24 m
17	34.2	1.64 ddd (13, 6.5, 4)	30.4	1.82 m
		2.03 ddt (13, 11, 2.5)		1.97 m
18	11.9	0.89 t (7)	13.0	0.93 t (7.8)
19	27.8	1.47 m	31.2	2.10 m
		1.54 m		
20	41.9	1.54 m	43.1	1.69 m
21	57.5	2.84 br s	72.4	3.49 br s
*N*H	–	7.54 br s	–	9.71 br s
10-O<u>Me</u>	56.0	3.85 s	56.1	3.83 s

[a]$CDCl_3$, 400 and 100 MHz, respectively; assignments based on COSY, HMQC, and HMBC.

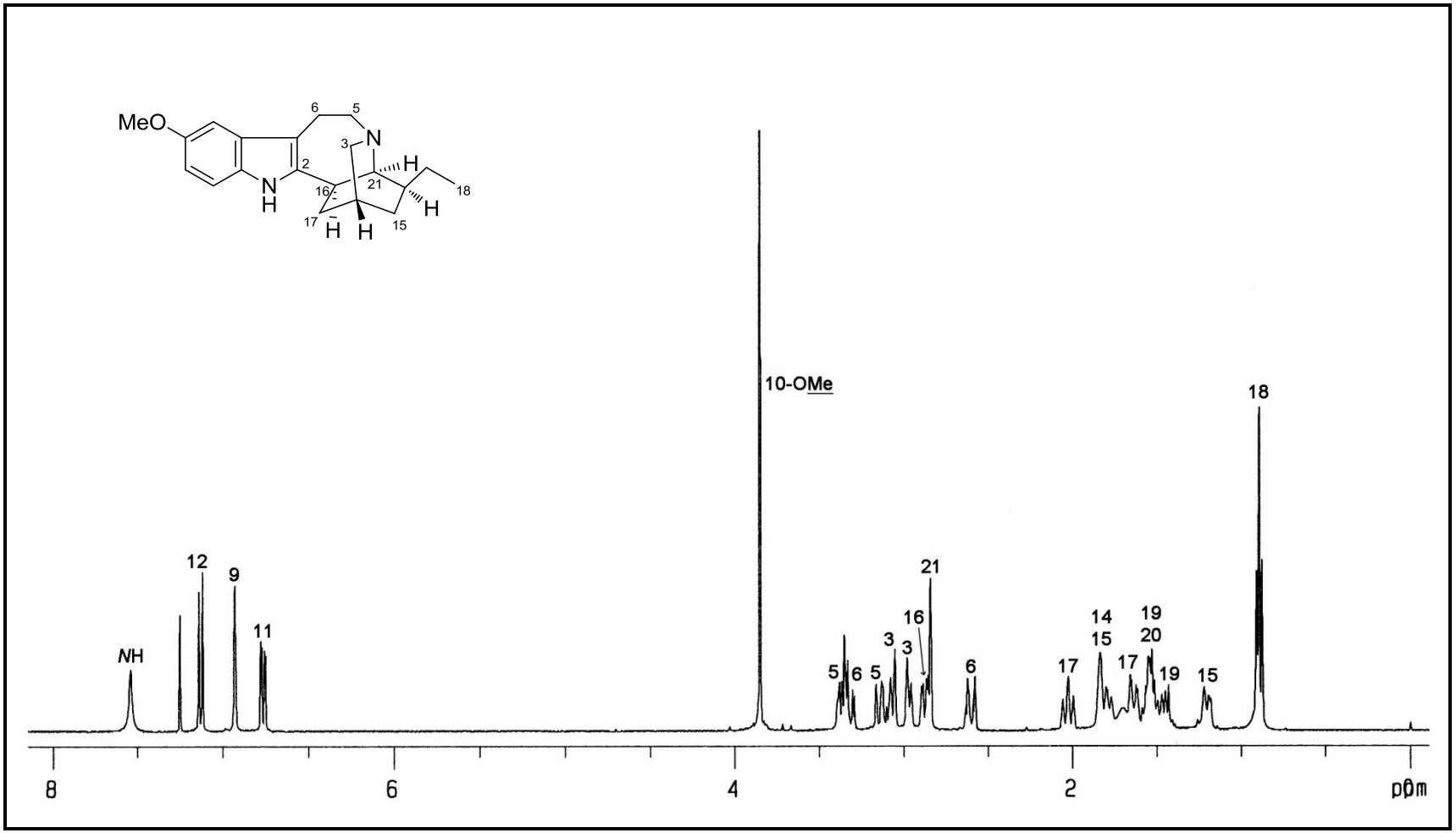

Figure 3.3. ^{1}H NMR spectrum ($CDCl_3$, 400 MHz) of ibogaine (**46**).

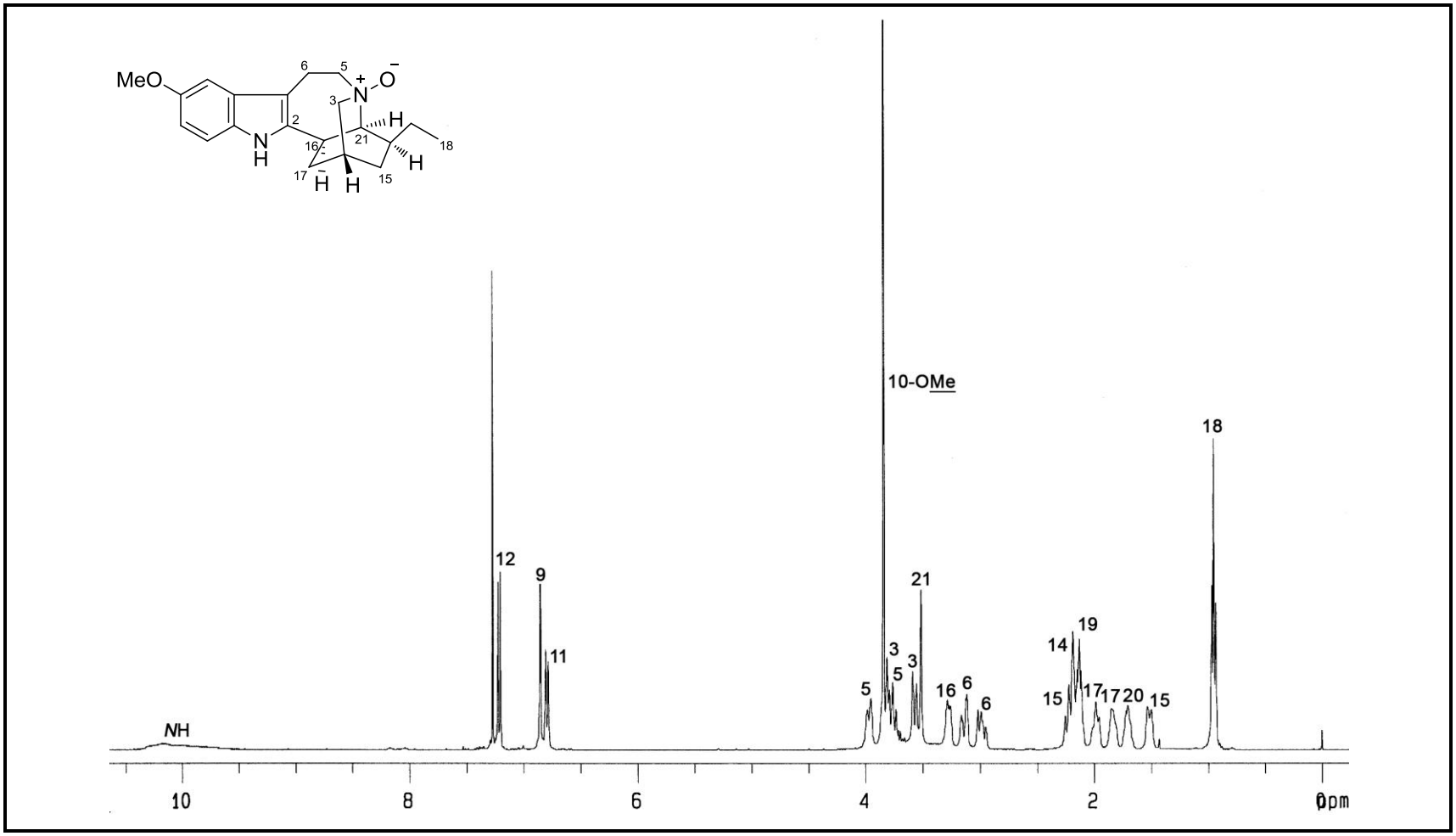

Figure 3.4. ^{1}H NMR spectrum ($CDCl_3$, 400 MHz) of ibogaine *N*-oxide (**50**).

To reduce decomposition, the crude product mixture was quickly filtered through a short pad of silica gel followed immediately by the oxidation step. Only a ^{1}H NMR spectrum was obtained due to the tendency of alcohol **51** to decompose in $CDCl_3$. In the ^{1}H NMR spectrum (Figure 3.5), the characteristic pair of AB doublets due to H-5, which are observed downfield at δ_H 4.88 and 4.78 (J = 11.4 Hz), provided firm evidence for the formation of the lirofoline skeleton. Recovery of alcohol **51** after the NMR experiment was not successful due to its rapid decomposition.

The next step involves oxidation of the alcohol **51** to an aldehyde. The first choice oxidation reagent Dess-Martin periodinane,[45] however, did not give any significant product. Alcohol **51** was successfully oxidized with tetra-*n*-propylammonium perruthenate (TPAP, 5 mol %) in the presence of excess *N*-methylmorpholine *N*-oxide (NMO, 20 equiv) and 4 Å molecular sieves (Ley oxidation)[46] to give lirofoline A (**44**) in 30% yield (Scheme 3.4).

The spectroscopic data (^{1}H and ^{13}C NMR, IR, UV) and other properties ($[\alpha]_D$ and R_f of TLC in different solvent systems) of semisynthetic **44** were indistinguishable from those of the natural **44**. The ^{1}H NMR spectrum of semisynthetic **44** is shown in Figure 3.6.

Further attempts to further transform lirofoline A (**44**) to lirofoline B (**45**) could not be carried out due to the limited amount of **44** available.

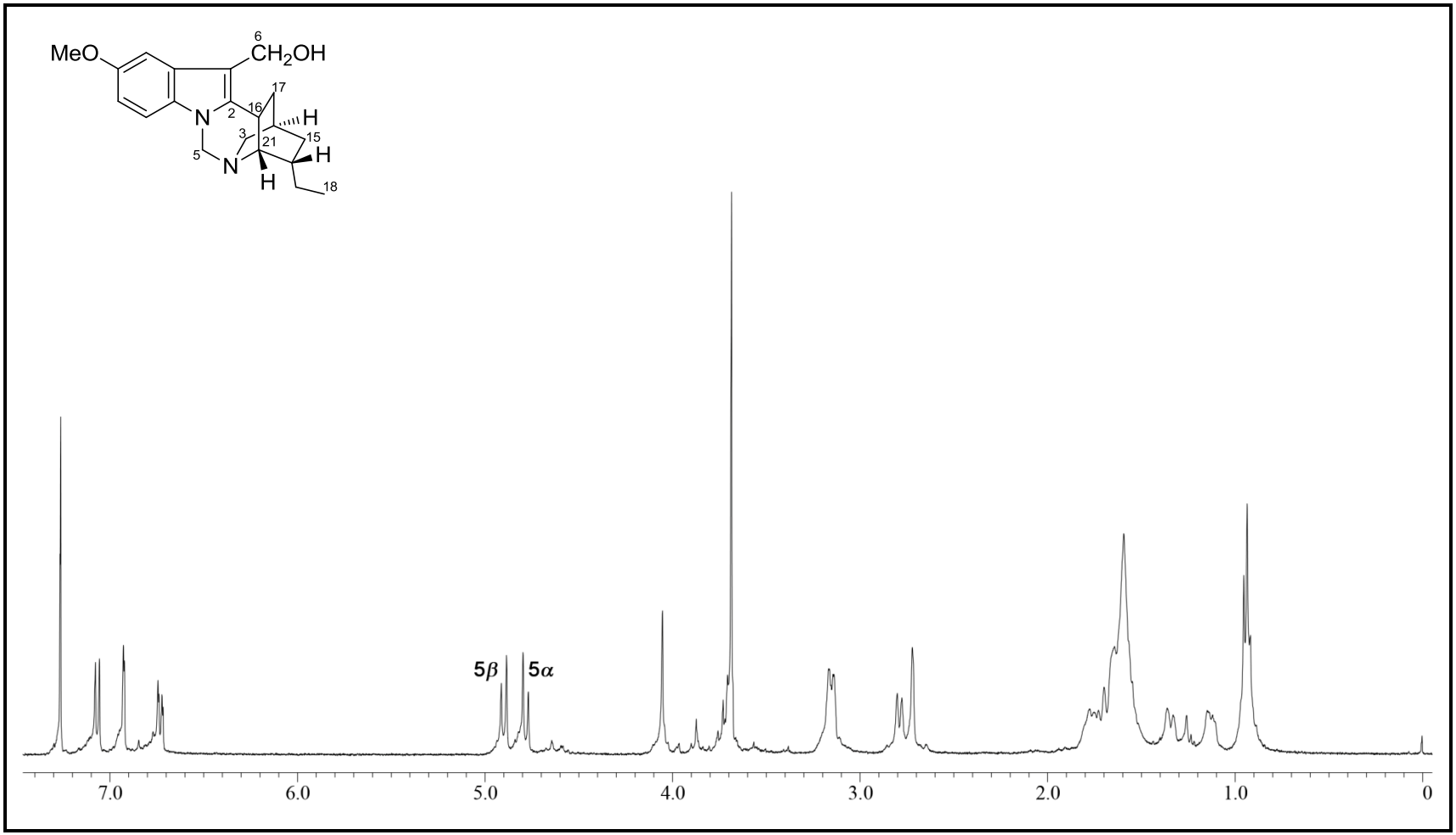

Figure 3.5. ^{1}H NMR spectrum ($CDCl_3$, 400 MHz) of alcohol **51**.

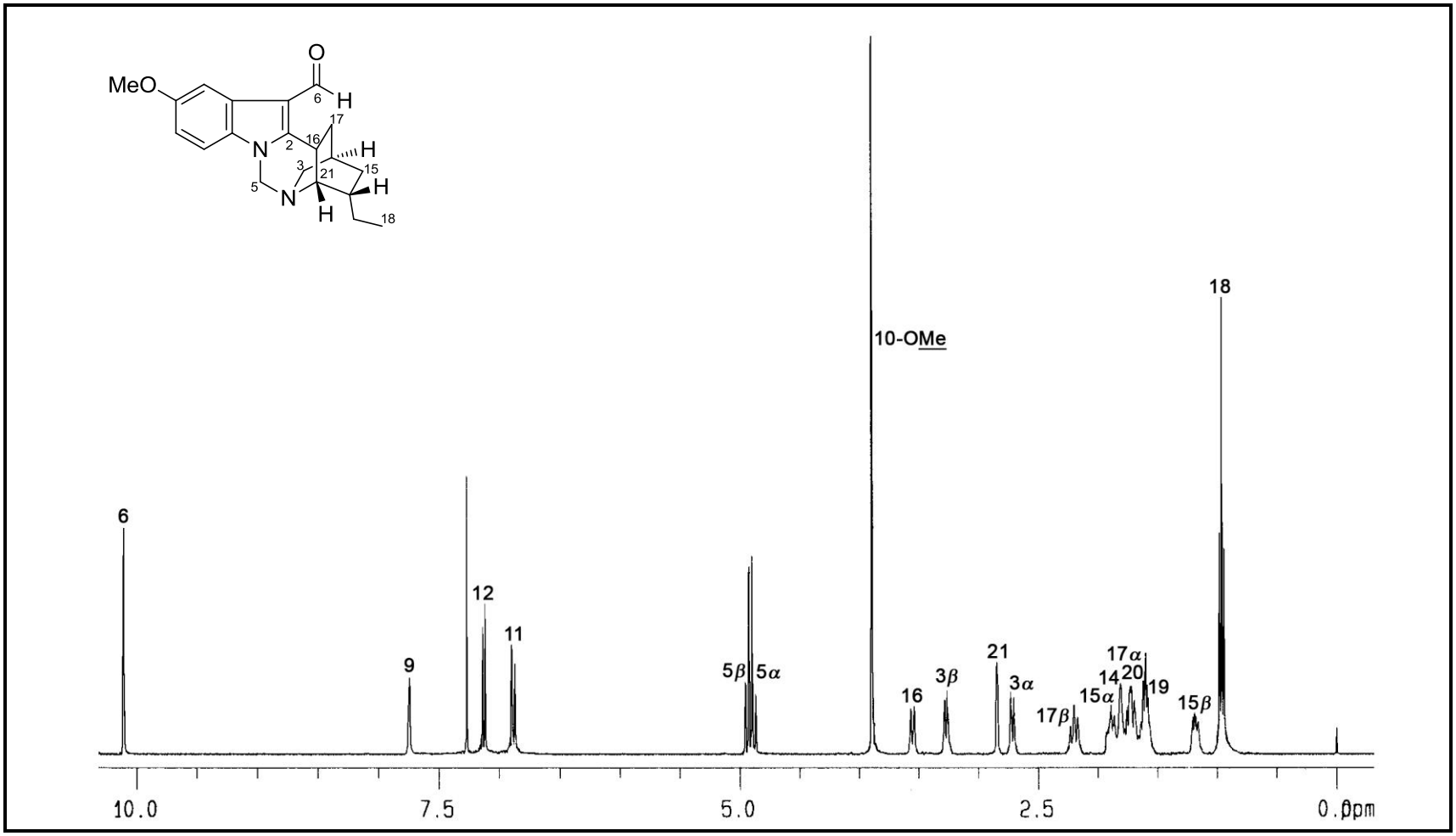

Figure 3.6. ^{1}H NMR spectrum ($CDCl_3$, 400 MHz) of semisynthetic lirofoline A (**44**).

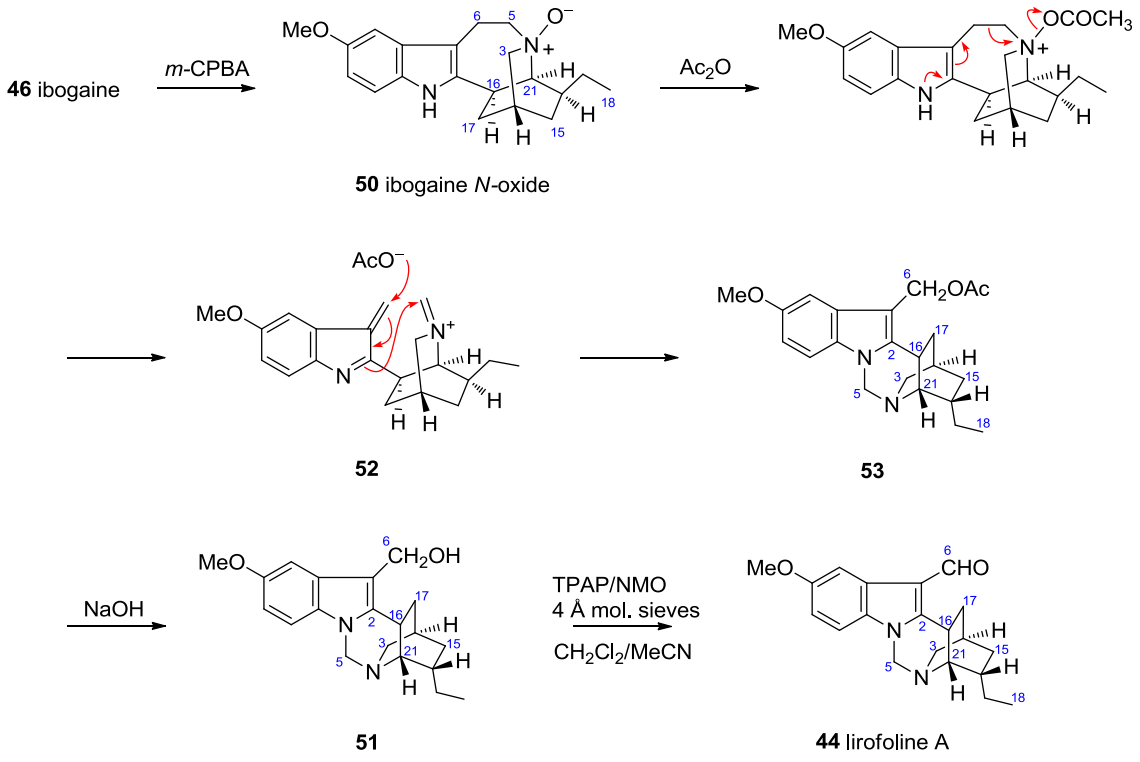

Scheme 3.4

3.3 Conclusion

A biomimetic partial synthesis of lirofoline A (**44**) has been achieved from ibogaine (**46**) under Polonovski conditions. Despite the above transformation, the possibility that the lirofolines isolated from the natural sources could be artifacts was rendered unlikely by the observation that repeated extractions of fresh material of *T. divaricata* consistently provided **45**, while **44** was isolated from an entirely different *Tabernaemontana* species (*T. corymbosa*). Furthermore, subjecting the putative precursor of the lirofolines, ibogaine (**46**) or its *N*-oxide **50**, to reaction under the conditions of the extraction, resulted only in recovery of the intact starting materials, with no evidence of any transformation into either **44** or **45**.[39]

CHAPTER FOUR

Transformations of Leuconolam and Partial Synthesis of Some Leuconoxine-type Alkaloids

4.1 Introduction

The ring-opened *Aspidosperma* alkaloid, leuconolam (**54**) and its C-21 epimer, *epi*-leuconolam (**55**) were first isolated from the bark extract of *Leuconotis griffithii*.[47–49] Subsequently the related diazaspiro pentacyclic alkaloid leuconoxine (**56**) was reported from the Indonesian *L. eugenefolia*.[50] Since then, closely related alkaloids were also found in other genus such as *Kopsia*.[25] These alkaloids include rhazinilam (**57**),[51] rhazinal (**58**),[52] rhazinicine (**59**),[53] and arboloscine (**60**).[54]

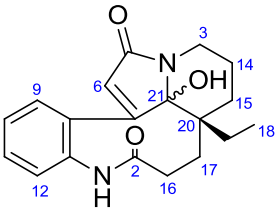

54 leuconolam 21β-OH
55 *epi*-leuconolam 21α-OH

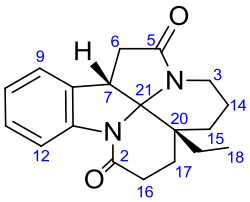

56 leuconoxine

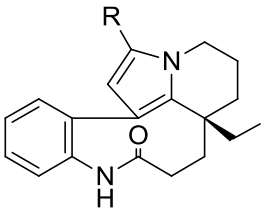

57 rhazinilam R = H
58 rhazinal R = CHO

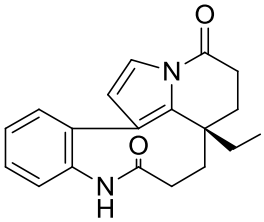

59 rhazinicine

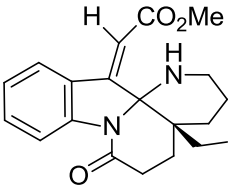

60 arboloscine

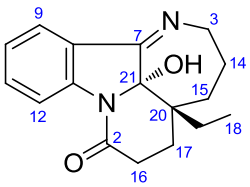

61 mersicarpine

Another new indole alkaloid recently reported from *Kopsia* (*K. singapurensis*) was mersicarpine (**61**), which is characterized by a novel tetracyclic carbon skeleton, containing a seven-membered imine ring.[55] The structure of **61** represents a departure from the rhazinilam-leuconolam group of alkaloids which coexists with **54** in the stem-bark extract of the plant. From a biogenetic viewpoint, it appears to have lost the two-carbon tryptamine bridge corresponding to C-5 and C-6, normally present in the other monoterpenoid indole alkaloids. In addition, the presence of the lactam-containing ring D suggested an affinity to leuconoxine (**56**), although a further rearrangement appears to have occurred leading to loss of the two-carbon chain and formation of the seven-membered imine-containing ring C. Since the initial report of the isolation and structure elucidation of **61**, several total syntheses have also been subsequently reported which have provided confirmation of the proposed structure.[56] A possible biogenetic pathway from a leuconolam precursor was also presented in the initial report, in which the key step was the formation of a benzylic carbocation **62** from a dehydroleuconoxine precursor, **63**, followed by a 1,2-alkyl shift leading to the iminium ion intermediate **64** (Scheme 4.1).[55] It was noted that the halogenated marine alkaloids, chartellamides A and B (**65** and **66**) from the marine bryozoan *Chartelle papyraceae*,[57] possess a structure displaying a remarkable resemblance to the 6-5-7 ring system of **61** and in addition incorporate a β-lactam unit corresponding to that present in the proposed intermediate **64**, providing additional support for the proposed pathway.

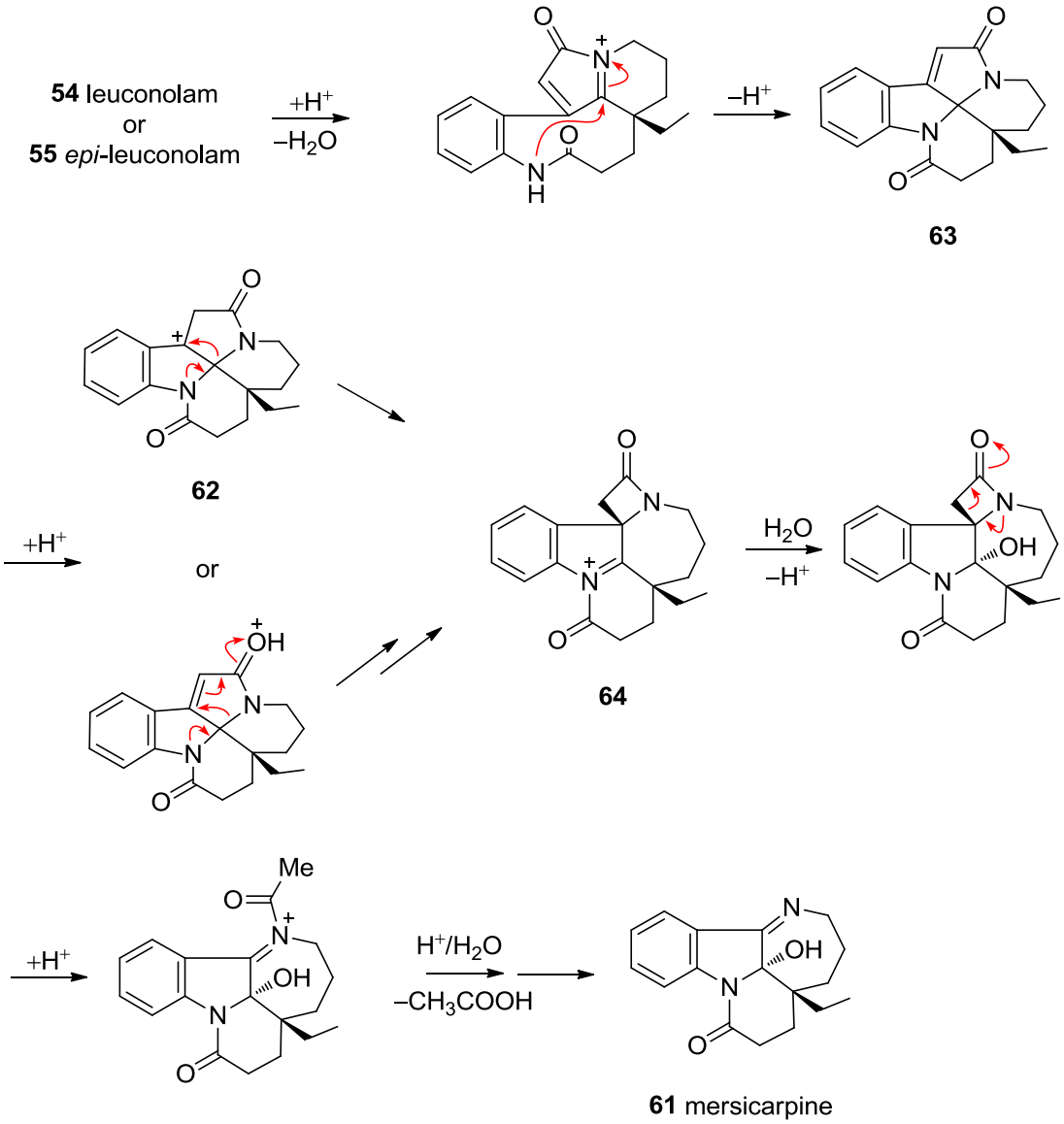

Scheme 4.1

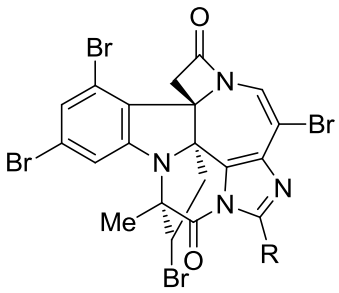

65 chartellamide A R = H
66 chartellamide B R = Br

Recently, six new leuconoxine-type alkaloids, leuconodines A–F (**67**–**72**), and a nor-rhazinilam derivative, *nor*-rhazinicine (**73**), were isolated from the stem-bark extract of *L. griffithii*,[58] representing the latest additions to this group of *Aspidosperma* alkaloids.

The availability of leuconolam (**54**) (one of the major alkaloids in *L. griffithii*), presented the opportunity to explore its chemistry, in particular to attempt various transformations aimed at transannular cyclization to leuconoxine (**56**) and its congeners.

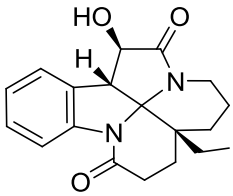

67 leuconodine A

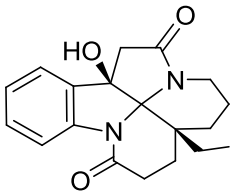

68 leuconodine B

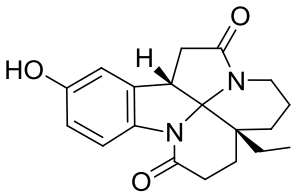

69 leuconodine C

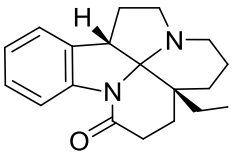

70 leuconodine D

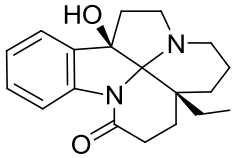

71 leuconodine E

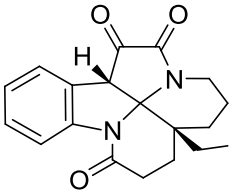

72 leuconodine F

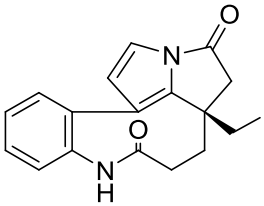

73 *nor*-rhazinicine

4.2 Results and Discussion

4.2.1 Base-induced transformations

In an earlier report,[49] treatment of leuconolam (**54**) with KOH in EtOH/MeOH gave the cyclized product **74** (the optical antipode of the 21-hydroxy derivative of (+)-meloscine **75**)[59] as the sole product in high yield. At the time of this report, no evidence was presented to support the stereochemical assignments. We decided to reinvestigate this transformation.

When the reaction was repeated by the use of stronger bases, such as NaOMe/MeOH or NaHMDS/THF, the reaction did not proceed, and led only to the recovery of starting material. When the reaction was repeated using the original conditions employed in the earlier report (KOH in EtOH/MeOH for 6 h), two products **74** and **76** were formed, with the former obtained as the major product (12 and 3%, respectively). The reaction was also accompanied by recovery of unreacted **54** (20%) (The original report claimed formation of a single product, **74**, with a yield of 80%.[49] We were not able to reproduce the reported yield.).

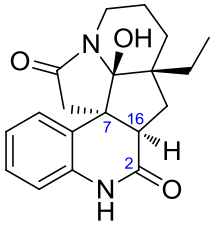

74

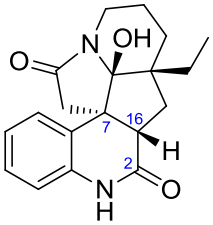

76

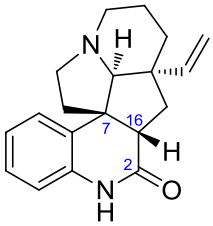

75 (+)-meloscine

The major product **74** was obtained as a colorless oil, and subsequently as colorless block crystals (mp 266–268 ^{o}C) from CCl_4/MeOH, with $[\alpha]^{25}_{D} = -198$ (*c* 0.06, $CHCl_3$). The UV spectrum showed absorption maxima at 210, 253, and 287 nm, indicating the presence of a dihydroquinolone chromophore,[59] while the IR spectrum showed the presence of OH (3226 cm^{-1}) and lactam carbonyl functions (1667 cm^{-1}). The ESIMS of **74** showed an $[M + H]^+$ at *m/z* 327, and HRESIMS measurements gave the molecular formula as $C_{19}H_{22}N_2O_3$ + H. The ^{1}H and ^{13}C NMR data of **74** are similar to those reported earlier.[49] The attachment of C-16 to C-7 was supported by the observed three-bond correlation from H-16 to C-6 in the HMBC spectrum. The orientation of H-16 was assigned as β from the observed NOE enhancement between H-6α and H-16 (Figure 4.1). The ^{1}H and ^{13}C NMR data of **74** are summarized in Table 4.1, while the ^{1}H NMR spectrum of **74** is shown in Figure 4.2.

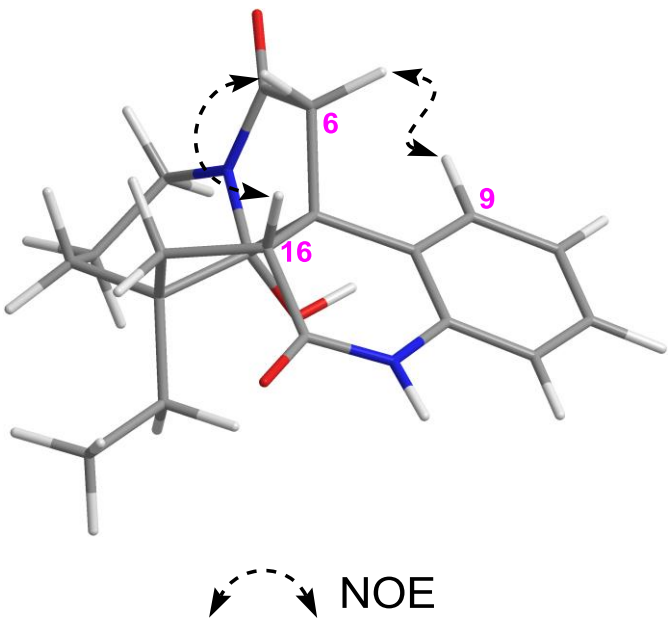

Figure 4.1. Selected NOEs of **75**.

Table 4.1. ^{1}H and ^{13}C NMR data (δ) of compounds **74** and **76**[a]

Position	**74**		**76**	
	δ_C	δ_H	δ_C	δ_H
2	170.5	–	170.7	–
3	37.2	2.94 m	36.6	3.08 m
		4.23 dt (13, 7.5)		4.03 dt (13, 7.5)
5	171.0	–	171.1	–
6β	50.0	2.69 d (17.7)	41.5	2.35 d (18)
6α		3.03 d (17.7)		2.75 d (18)
7	50.6	–	50.0	–
8	122.0	–	133.0	–
9	129.1	7.39 dd (8, 1.5)	123.9	6.85 br d (7.8)
10	123.8	7.23 td (8, 1.5)	123.6	7.19 td (7.8, 1.5)
11	129.0	7.10 td (8, 1.5)	127.9	7.01 td (7.8, 1.5)
12	116.1	6.76 dd (8, 1.5)	117.0	7.69 d (7.8)
13	136.0	–	137.2	–
14	19.6	1.59 m	17.7	1.66 m
		1.59 m		1.66 m
15	28.0	1.44 m	30.0	1.20 td (14.5, 6.8)
		1.81 dt (14.5, 4.5)		1.82 dt (14.5, 4.5)
16	51.9	2.91 m	46.3	3.07 dd (13.7, 5.5)
17	32.2	2.20 ddd (14, 10.5, 2)	30.4	1.56 m
		2.32 dd (14, 2.5)		2.17 dd (13.7, 5)
18	7.4	0.67 t (7.6)	8.8	0.89 t (7.3)
19	26.3	0.96 dq (14, 7.6)	24.0	1.41 m
		1.08 dq (14, 7.6)		1.59 m
20	46.7	–	50.3	–
21	100.8	–	99.2	–
*N*H	–	8.41 br s	–	7.65 br s
21-OH	–	2.38 br s	–	2.90 br s

[a]$CDCl_3$, 400 and 100 MHz, respectively; assignments based on COSY, HMQC, and HMBC.

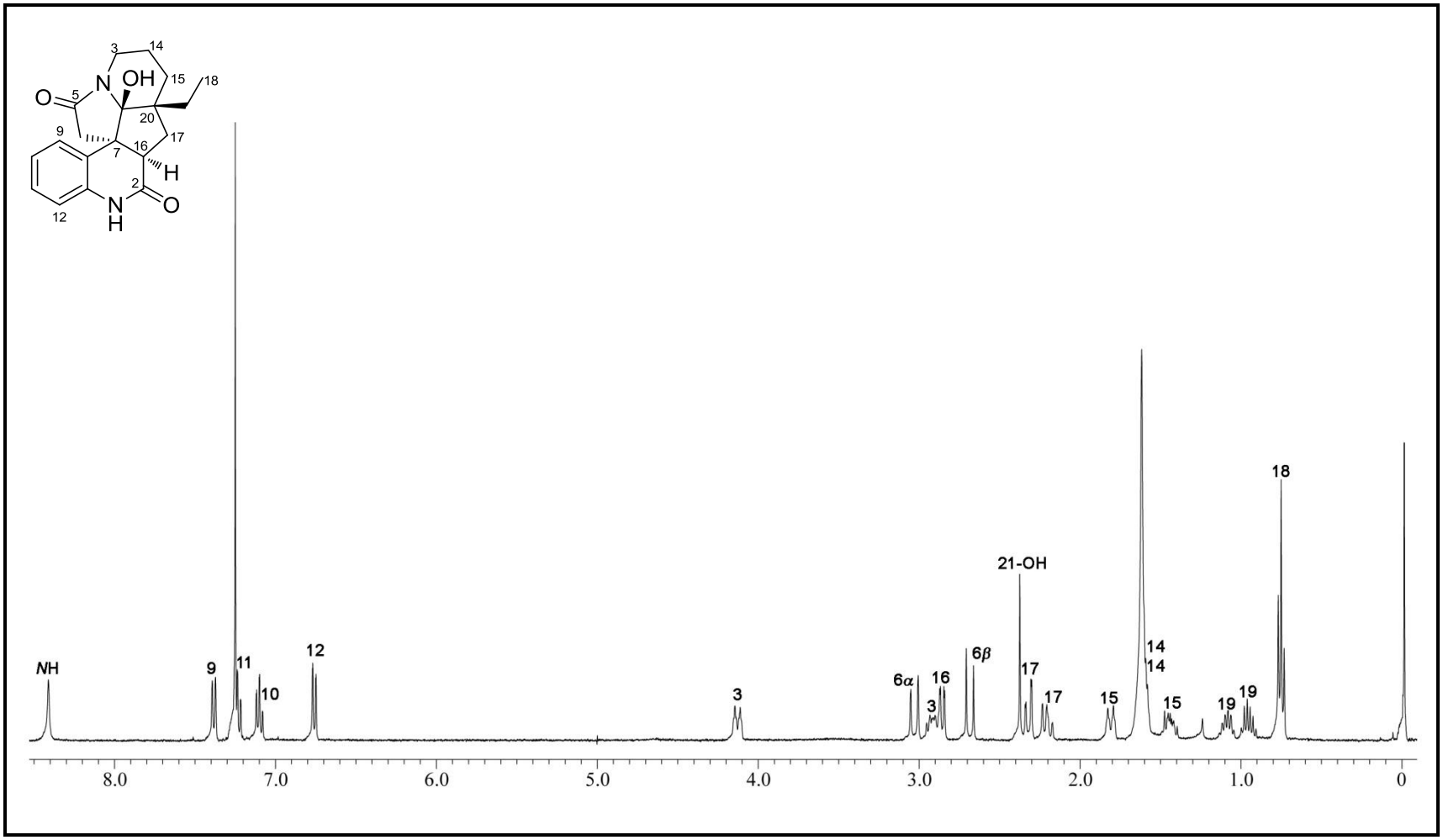

Figure 4.2. ^{1}H NMR spectrum ($CDCl_3$, 400 MHz) of compound **74**.

The minor product **76** was obtained as a colorless oil, and subsequently as colorless block crystals (mp 250–252 ^{o}C) from CH_2Cl_2/hexanes, with $[\alpha]^{25}_{D}$ = –150 (*c* 0.01, $CHCl_3$). The UV (210, 251, 306 nm) and IR data (3322, 1712, 1667 cm^{-1}) were similar to those of **74** indicating the presence of similar chromophores and functionalities. The ESIMS of **76** showed an $[M + H]^+$ at *m/z* 327, and HRESIMS measurements gave the molecular formula as $C_{19}H_{22}N_2O_3$ + H. As in the case of **74**, a three-bond correlation from H-16 to C-6 was also observed. A major difference in the NMR data of **76** compared with the previous compound **74**, was the notable absence of NOE between H-6α and H-16, which suggested that in **76**, the orientation of H-16 is β. The ^{1}H and ^{13}C NMR data of **76** are summarized in Table 4.1, while the ^{1}H NMR spectrum of **76** is shown in Figure 4.3.

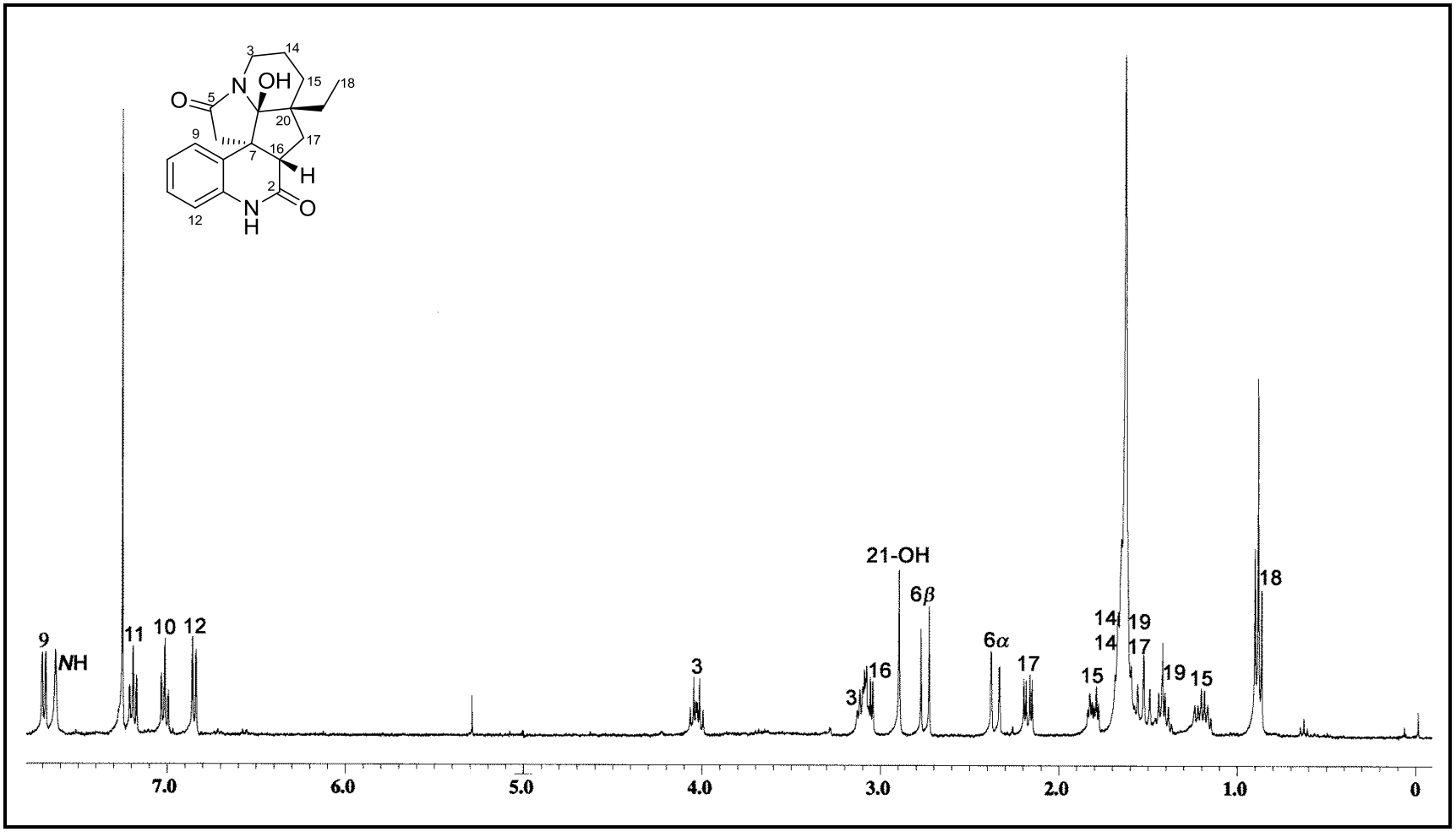

Figure 4.3. ^{1}H NMR spectrum ($CDCl_3$, 400 MHz) of compound **76**.

Since suitable crystals of both **74** and **76** were obtained, X-ray diffraction analyses were carried out which confirmed the structures and relative configurations assigned based on the NMR data (Figure 4.4).

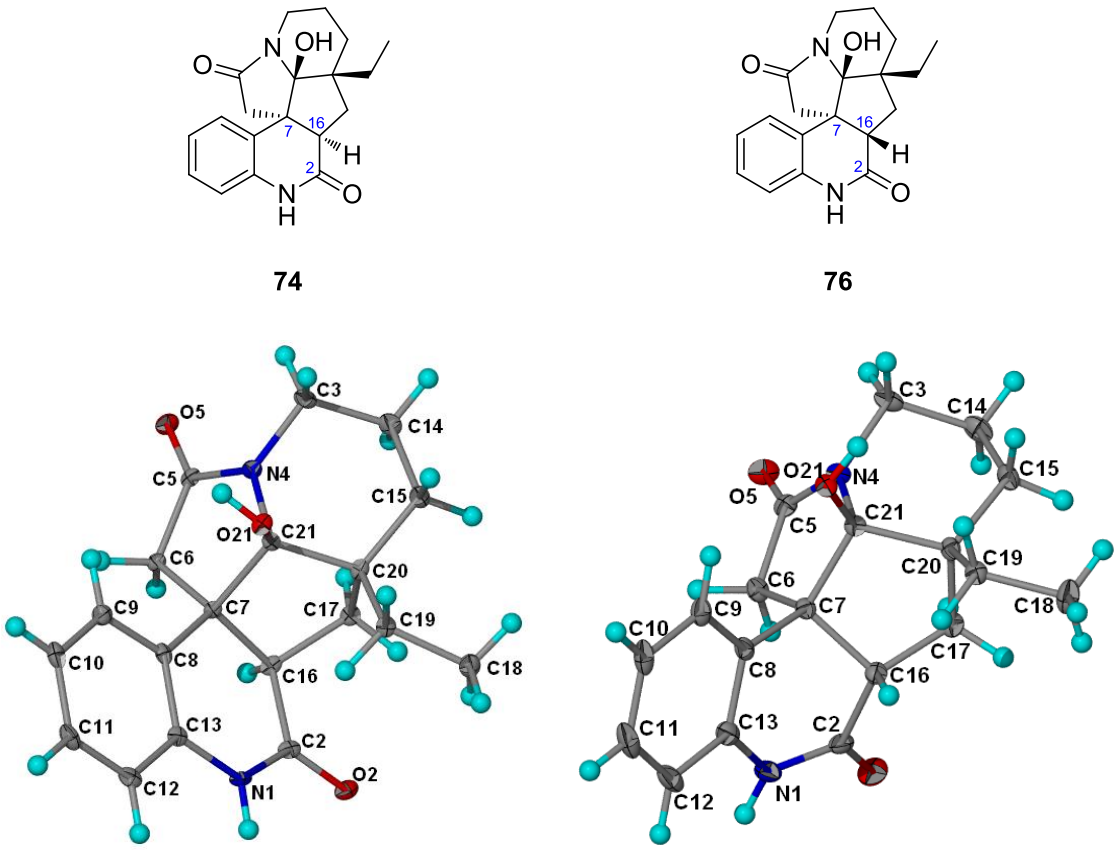

Figure 4.4. Left: X-ray crystal structure of **74**. Right: X-ray crystal structure of **76**.

The formation of **74** and **76** can be rationalized based on an intramolecular Michael addition from the presumably more stable *E*-enolate which approaches from the α-face to form the major product **74**, while the minor product **76** resulted from attack by the presumably less stable *Z*-enolate (Scheme 4.2).

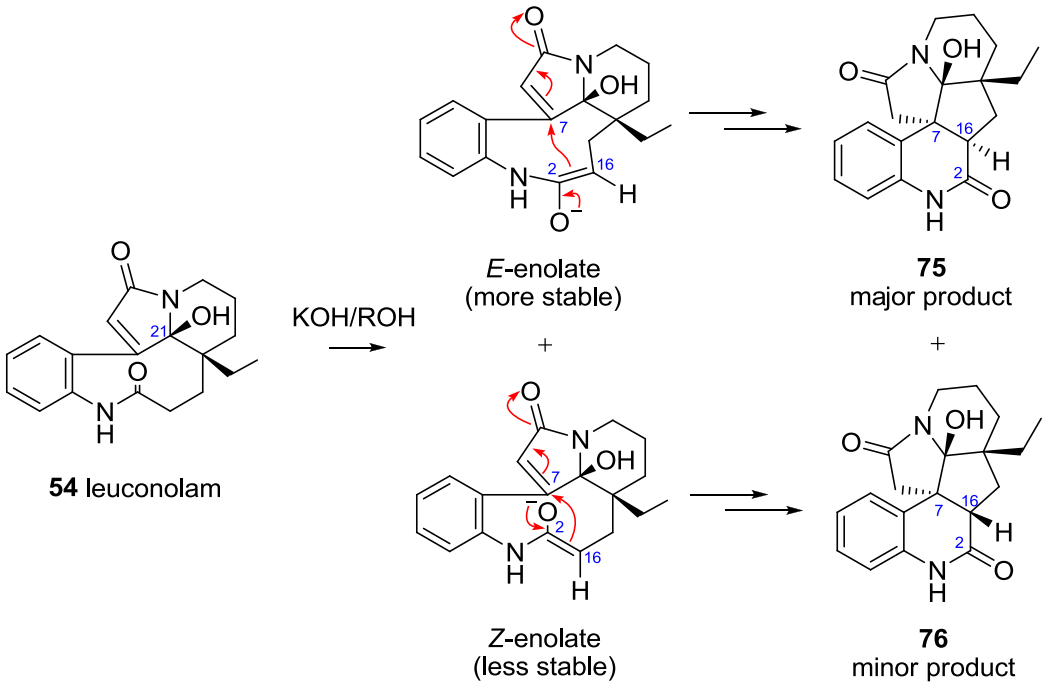

Scheme 4.2

4.2.2 Acid-induced transformations

It was initially envisaged that treatment of leuconolam (**54**) with acid should result in a facile transannular closure to give a dehydroleuconoxine derivative **63** which could serve as a possible starting compound for further elaboration to leuconoxine (**56**) and its recently discovered congeners (leuconodines) or to mersicarpine (**61**) (Scheme 4.3).

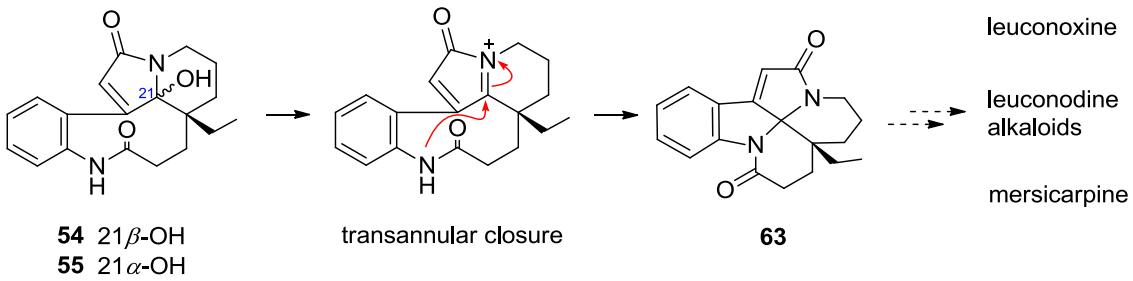

Scheme 4.3

Treatment of leuconolam (**54**) with aqueous HCl (5%) did not result in any reaction, leading only to recovery of starting material. When the same reaction was carried in a two-phase medium in the presence of a phase-transfer catalyst (tetraethylammonium chloride, TEACl), both *epi*-leuconolam (**55**) (45%) and leuconolam (**54**) (35%) were obtained. Careful examination of the product mixture revealed the formation of a minor product (compound A), with a yield of 1.5%. Repeating the two-phase experiment (5% HCl/CH_2Cl_2, TEACl) with *epi*-leuconolam (**55**), resulted in the isolation of leuconolam (**54**) (15%) and *epi*-leuconolam (**55**) (84%).

When leuconolam (**54**) was treated with 10-camphorsulfonic acid (CSA) in anhydrous CH_2Cl_2, *epi*-leuconolam (**55**) was obtained in yield of 62%, accompanied by 2% of the previously noted minor product (compound A). Similar treatment of **54** with CSA in anhydrous MeOH resulted in the formation of *O*-methylleuconolam (**77**)[49] in 94% yield, accompanied by 2% of compound A. Treatment of **54** with conc. HCl (few drops) in anhydrous MeOH gave only **77** with a reduced yield of 63%. Treatment of **54** with *p*-toluenesulfonic acid (PTSA) in anhydrous MeOH also yielded the *O*-methyl derivative **77** as the major product (94%) with compound A detected as the minor product (1%).

When leuconolam (**54**) was treated with PTSA in anhydrous CH_2Cl_2, an inversion in the product distribution was noted, with compound A obtained as the major product (42%), and *epi*-leuconolam (**55**) as the minor product (5%). These results are summarized in Table 4.2. The ^{1}H and ^{13}C NMR data of *O*-methylleuconolam (**77**) are summarized in Table 4.3, while the ^{1}H NMR spectrum of **77** is shown in Figure 4.5.

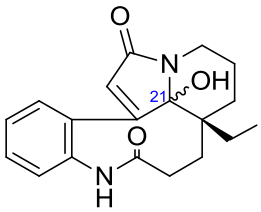

54 leuconolam 21β-OH
55 *epi*-leuconolam 21α-OH

Compound A

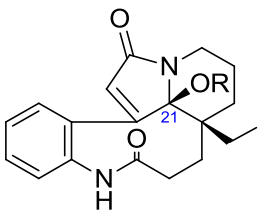

77 *O*-methylleuconolam R = Me

Table 4.2. Summary of reactions of leuconolam (**54**) with acids

Entry	Starting material	Reaction conditions	Products			
			54	**55**	Compound A	**77**
1	**54**	5% HCl, rt, 8 h	No reaction			
2	**54**	5% HCl/CH_2Cl_2 + TEACl, rt, 14 h[a]	35%	47%	1.5%	–
3	**54**	HCl/MeOH, rt, 12 h	4%	–	–	63%
4	**54**	CSA/CH_2Cl_2, rt, 14 h[a]	10%	62%	2%	–
5	**54**	CSA/CH_2Cl_2, rt, 11 h (4 equiv MeOH added)	–	19%	–	54%
6	**54**	CSA/MeOH, rt, 14 h	4%	–	2%	94%
7	**54**	PTSA/MeOH, rt, 14 h	4%	–	0.8%	94%
8	**54**	PTSA/CH_2Cl_2, rt, 14 h	3%	5%	42%	–
9	**55**	5% HCl/CH_2Cl_2 + TEACl, rt, 12 h[a]	15%	84%	–	–
10	**55**	CSA/CH_2Cl_2, rt, 15 h	No reaction[b]			
11	**55**	PTSA/CH_2Cl_2, rt, 10 h	–	1%	70%	–
12	**77**	PTSA/CH_2Cl_2, rt, 10 h	No reaction[c]			

[a]Prolonged reaction time leads to reduced overall yields; [b]traces of **54** and compound A detected from TLC; [c]traces of **54** and **55** detected from TLC.

Table 4.3. ^{1}H and ^{13}C NMR data (δ) of *O*-methylleuconolam (**77**)[a]

Position	δ_C	δ_H
2	178.6	–
3	35.9	2.61 td (12.5, 4)
		4.18 td (12.5, 4)
5	166.8	–
6	131.9	6.33
7	151.0	–
8	133.1	–
9	126.7	7.26 ddd (7.5, 1, 0.5)
10	127.0	7.34 m
11	129.9	7.41 m
12	128.6	7.42 m
13	135.7	–
14	19.6	1.49 m
15	32.5	1.50 m
		2.05 ddd (15, 5, 2)
16	28.0	2.17 td (15, 6)
		1.50 m
17	26.2	1.75 m
		1.50 m
18	7.3	0.55 t (7.5)
19	24.1	1.28 dq (13.6, 7.5)
		1.54 m
20	45.5	–
21	97.4	–
*N*H	–	8.25 br s
21-OMe	49.9	3.15 s

[a]$CDCl_3$, 400 and 100 MHz, respectively; assignments based on COSY, HMQC, and comparison with literature.

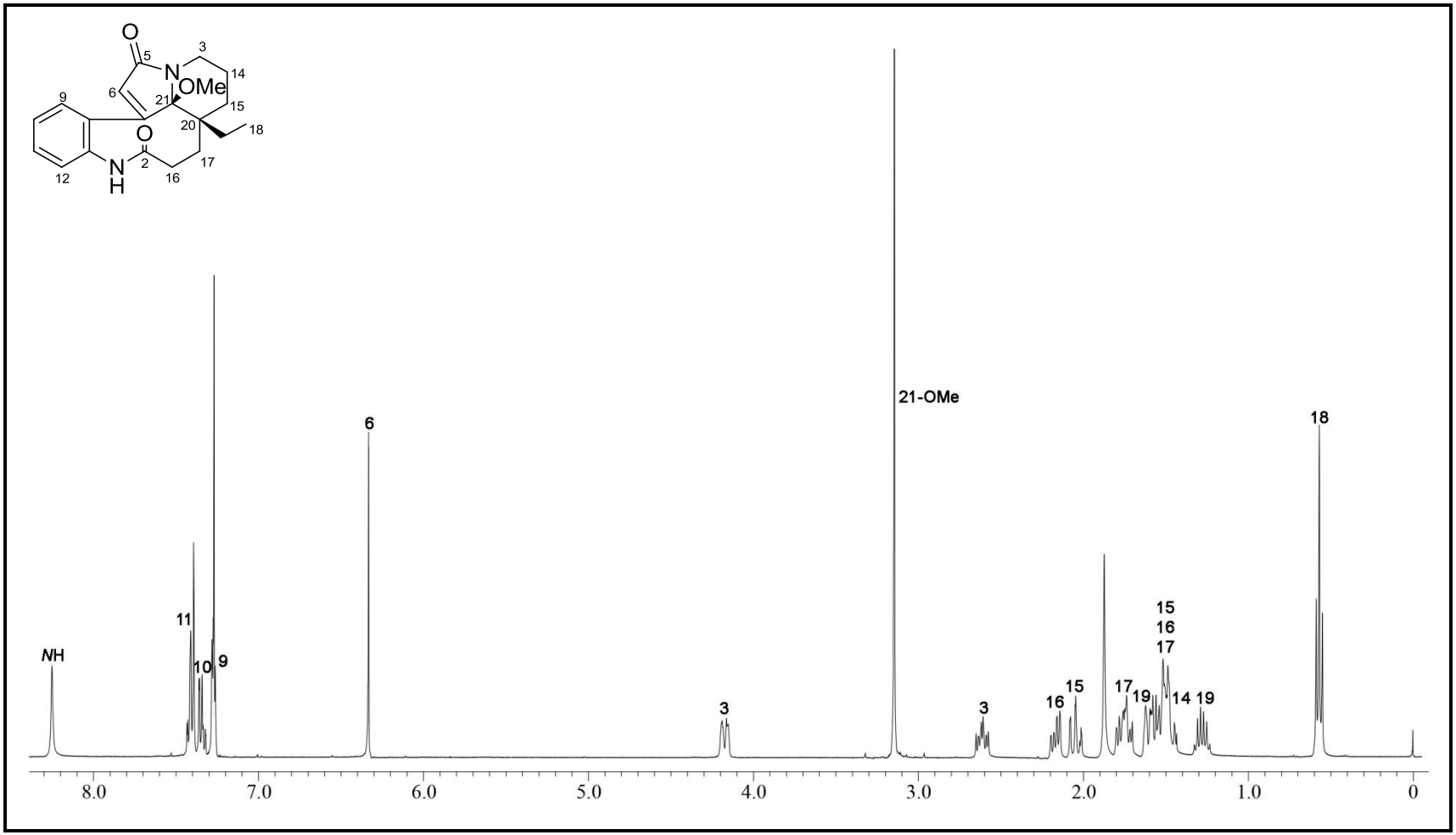

Figure 4.5. ^{1}H NMR spectrum ($CDCl_3$, 400 MHz) of *O*-methylleuconolam (**77**).

The results of the reaction of leuconolam (**54**) with acid, as summarized in Table 4.2 presented some puzzling features. The formation of *epi*-leuconolam (**54**) and leuconolam (**54**) when leuconolam (**54**) or *epi*-leuconolam (**55**) was treated with aqueous acid under two-phase conditions (entries 2 and 9, Table 4.2) suggested the possibility that the products obtained derived from reversible formation of the *N*-4–C-21 iminium ion, followed by nucleophilic capture by water to give a mixture of **55** and **54**, with **55** (*epi*-leuconolam) predominating in both instances. This would appear to suggest that **55** is the thermodynamically more stable product under such conditions. When the acid-induced reaction was carried out in MeOH (entries 3, 6, and 7, Table 4.2) in the presence of either HCl, CSA, or PTSA, virtually quantitative conversion to *O*-methylleuconolam (**77**, 21β-OMe) was observed, suggesting efficient trapping of the iminium ion from the β-face by MeOH. The exclusive formation of the C-21 β-oriented methyl ether product is puzzling, especially since the α-OH epimer (*epi*-leuconolam, **55**) appeared to be the thermodynamically preferred product. Another discrepancy was noted when comparing entries 4 and 10, Table 4.2. The reaction of leuconolam (**54**) with CSA in CH_2Cl_2 gave *epi*-leuconolam (**55**) as the major product, but when *epi*-leuconolam (**55**) was exposed to the same conditions, no reaction occurred (*cf.* entries 2 and 9, Table 4.2). Other inconsistencies were subsequently noted for the hydrogenation and bromination reactions of leuconolam (**54**) and *epi*-leuconolam (**55**). For instance, while *epi*-leuconolam (**55**) was smoothly hydrogenated, leuconolam (**55**) was by comparison unreactive, whereas in the case of the bromination reaction, both **54** and **55** apparently reacted to give the same bromine addition product. Furthermore debromination (Zn/AcOH) of the bromine addition product apparently yielded *epi*-leuconolam (**55**). These puzzling and apparently inconsistent results led us to reevaluate the earlier structure elucidation for leuconolam (**54**) and *epi*-leuconolam (**55**).

Leuconolam (**54**) was first reported from the Malayan *Leuconotis* species, *L. griffithii* and *L. eugenefolia*.[47,49] The structure was confirmed by an X-ray diffraction analysis which showed that the *N*-1–C-2 lactam, as well as the C-6–C-7 double bond, were out of plane with benzene ring, therefore minimizing conjugation.[47] The hydroxyl group attached to C-21 was shown to be β-oriented, while the ethyl side chain attached to C-20 was *syn* to the C-21 hydroxyl group.

Epi-leuconolam was first isolated as a minor alkaloid from *L. griffithii* and *L. eugenefolia*.[47,49] It has subsequently been detected as a minor alkaloid in *Kopsia griffithii*.[60] The structure was assigned as the C-21 epimer of leuconolam (*i.e.*, **55**) based on EIMS and NMR data. In the initial report, the EIMS (measured on a Kratos MS 3074 Mass Spectrometer) apparently showed an $[M]^+$ at *m/z* 326, which was also the base peak, and which analyzed for $C_{19}H_{22}N_2O_3$ by HREIMS, indicating an isomeric relationship with leuconolam (**54**).[47,49] This was confirmed by a subsequent independent EIMS measurement (on a VG ProSpec Mass Spectrometer) which also showed the $[M]^+$ as a base peak at *m/z* 326, and which also analyzed for $C_{19}H_{22}N_2O_3$.[60] In both instances, a strong $[M - H_2O]^+$ peak at *m/z* 308 was also detected. The ^{1}H NMR spectrum showed features, which in many ways indicated the alkaloid's isomeric relationship with leuconolam (**54**). A sharp singlet at δ_H 6.02 ppm showed the presence of an isolated olefinic proton corresponding to H-6, while the triplet centered at δ_H 0.76 ppm indicated the presence of an ethyl side chain. A notable difference observed in the ^{1}H NMR spectrum of *epi*-leuconolam when compared with that of **54** however, was the absence of the characteristic indolic *N*H and C-21–OH signals (Table 4.4). The ^{13}C NMR spectrum of *epi*-leuconolam accounted for all the 19 carbons and showed a close similarity to the spectrum of leuconolam (**54**), except for small differences in the chemical shifts (Table 4.5).[47,49]

It was also demonstrated by the original investigators that *epi*-leuconolam (**55**) was likely an artifact due to the presence of acid, as extraction carried out under neutral or basic conditions did not result in the isolation of this compound, whereas extraction under acidic conditions resulted in its isolation.[47,49] In our hands, although leuconolam (**54**) was obtained as the major compound, *epi*-leuconolam was invariably also detected, albeit as a minor alkaloid, since brief exposure to traces of acid could not be avoided under the conditions used for the isolation and purification.

Since the structure of **54** rested firmly on an X-ray diffraction analysis (which we have repeated, Figure 4.6), we decided to reinvestigate the structure of *epi*-leuconolam using a natural sample from our concurrent work in alkaloid chemistry (natural sample courtesy of C. Y. Gan[58]).

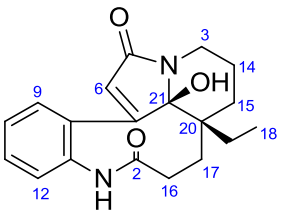

54 leuconolam

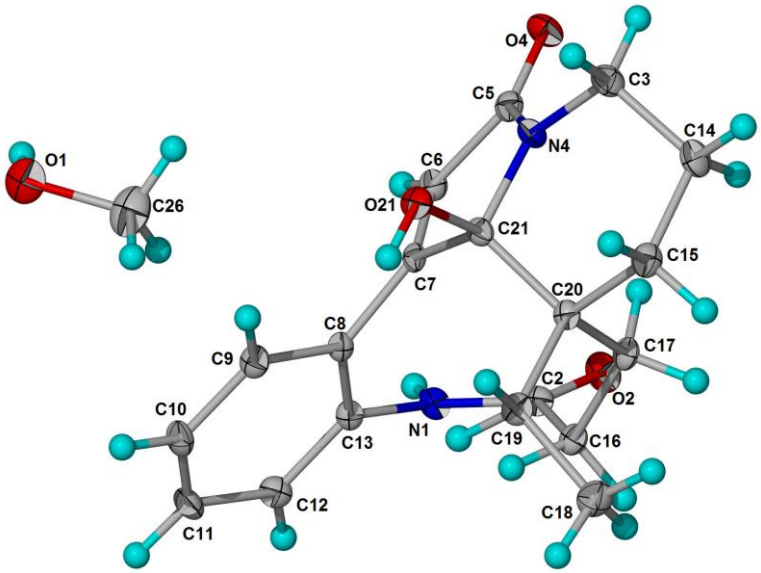

Figure 4.6. X-ray crystal structure of **54**.

LC-ESIMS analysis of *epi*-leuconolam gave an $[M + H]^+$ peak at *m/z* 309, which indicated a molecular ion (*m/z* 308), 18 mass units less than that obtained previously by EIMS. HRESIMS gave the formula $C_{19}H_{20}N_2O_2 + H$. The measurement was repeated by GC-EIMS, which also gave the molecular ion at *m/z* 308 (instead of the previously observed *m/z* 326 peak detected by direct probe EIMS). Banwell and co-workers have

also reported syntheses of rhazinal (**58**),[61] rhazinilam (**57**), leuconolam (**54**), and *epi*-leuconolam.[62] The latter two compounds were obtained by oxidation of rhazinilam (**57**) (excess PCC, 18 ^{o}C, 4 Å molecular sieves), followed by aqueous workup (EtOAc/MeOH/H_2O) of the reaction product mixture.[62] The EIMS of the synthetic *epi*-leuconolam showed a base peak at *m/z* 308, with the *m/z* 326 ion detected as a very weak peak (< 1%).

In the original report, it was noted that the IR spectrum of *epi*-leuconolam showed a strong broad absorption at 3400 cm^{-1} attributed to *N*H and OH.[47,49] We have recorded the IR spectrum of *epi*-leuconolam and leuconolam (**54**) (Figure 4.7). It can be seen that while the IR spectrum of leuconolam (**54**) showed a broad absorption at *ca*. 3260 cm^{-1}, *epi*-leuconolam did not show any significant absorption in the 3400 cm^{-1} region (the same result was obtained by Banwell and co-workers[62]). In addition, the UV spectra of leuconolam (**54**) (207, 220, 287 nm) and *epi*-leuconolam (203, 252, 350 nm) were markedly different indicating the presence of different chromophores (Figure 4.8).

The ^{1}H and ^{13}C NMR data for *epi*-leuconolam have been reported on a number of occasions and were each time in agreement with those of the original report.[47,49,60,62] We have also carried out additional 2-D NMR experiments (COSY, HMQC, HMBC) for *epi*-leuconolam, which indicated the presence of similar correlations as those in leuconolam (**54**).

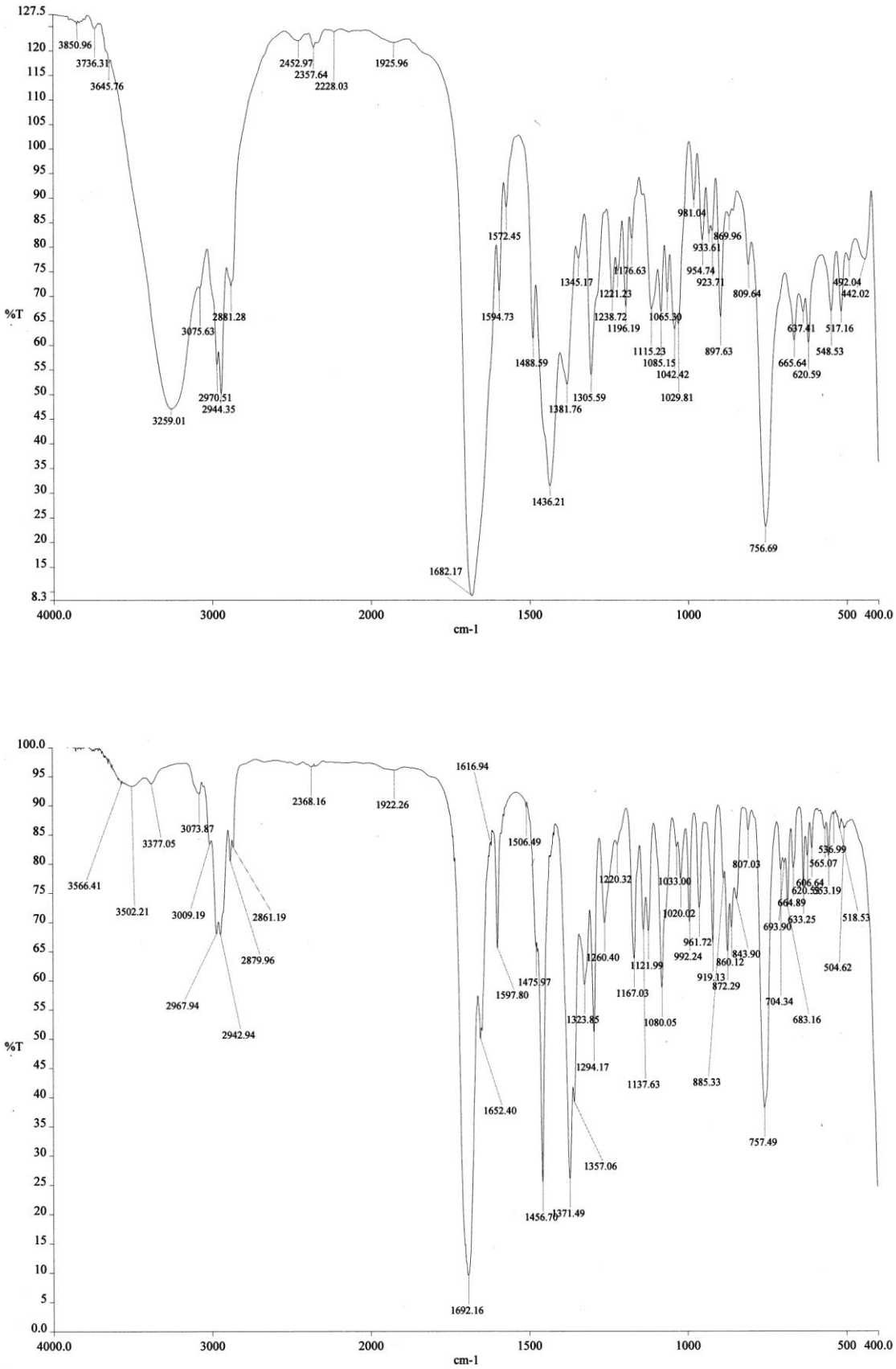

Figure 4.7. Top: IR spectrum of leuconolam (**54**). Bottom: IR spectrum of '*epi*-leuconolam'.

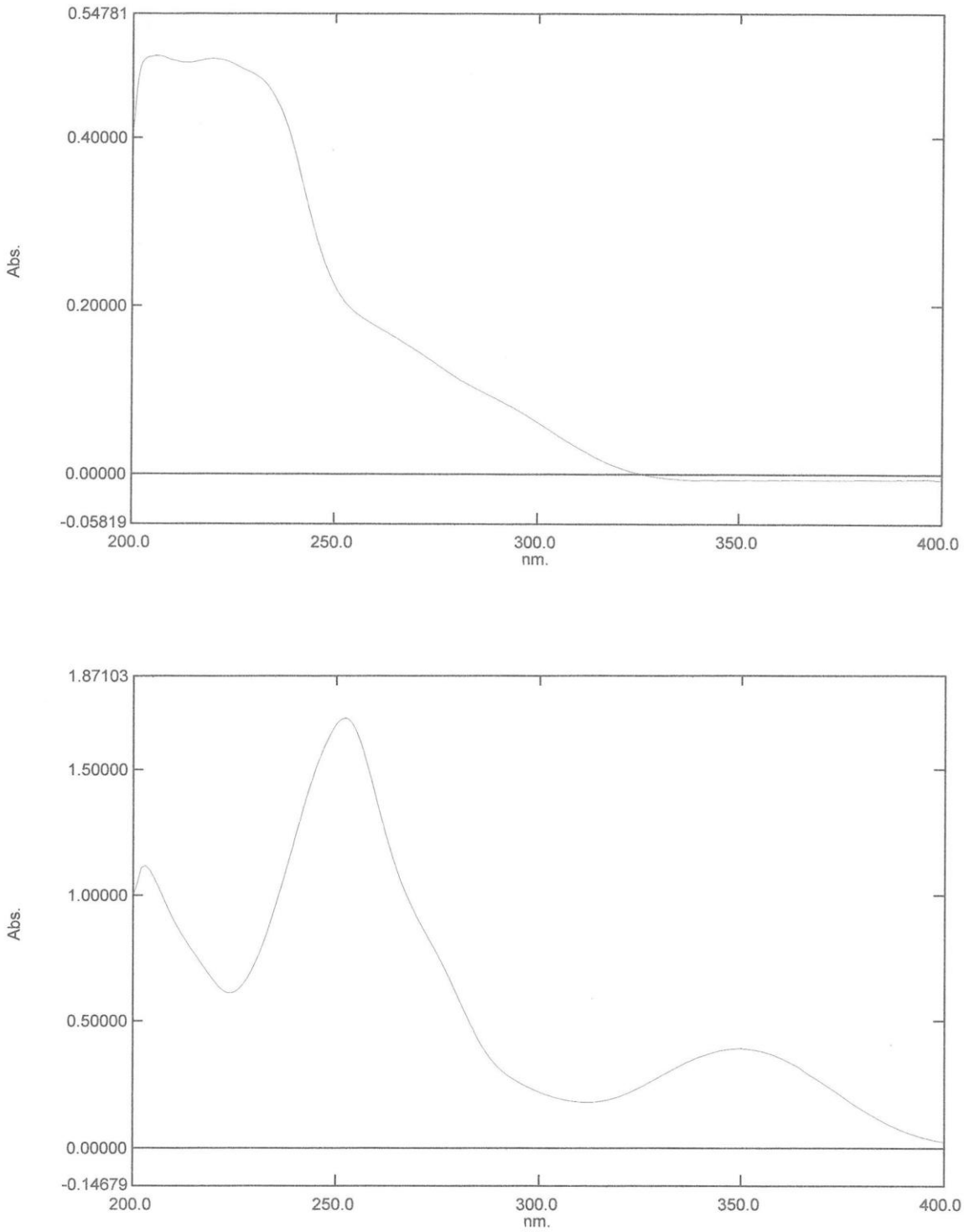

Figure 4.8. Top: UV spectrum of leuconolam (**54**). Bottom: UV spectrum of '*epi*-leuconolam'.

In view of the above results, we decided to undertake X-ray diffraction analysis of the alkaloid which has to date been assigned as *epi*-leuconolam (**55**) (natural sample, suitable crystals were obtained from CH_2Cl_2/hexanes solution). The X-ray diffraction analysis revealed that the alkaloid previously assigned as '*epi*-leuconolam (**55**)' is in actual fact 6,7-dehydroleuconoxine (**63**) (Figure 4.9).

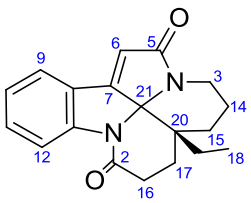

63 6,7-dehydroleuconoxine

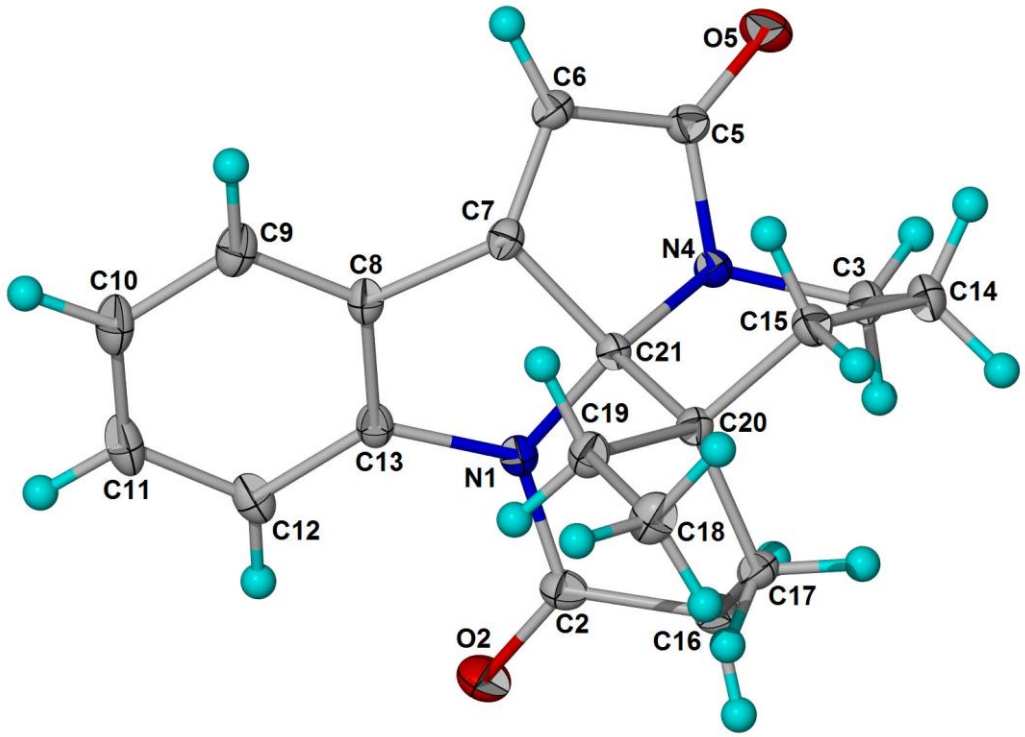

Figure 4.9. X-ray crystal structure of **63**.

The previously observed molecular ion at *m/z* 326 in EIMS was in all probability an artifact due to facile cleavage of the initially formed molecular ion followed by equally facile capture by water present as a contaminant in the sample, as shown in Scheme 4.4. The presence of water also accounts for the observation of the broad absorption at 3400 cm^{-1} in the IR spectrum which was attributed to the presence of *N*H/OH groups, while the revised structure, 6,7-dehydroleuconoxine (**63**), is now compatible with the UV spectrum.

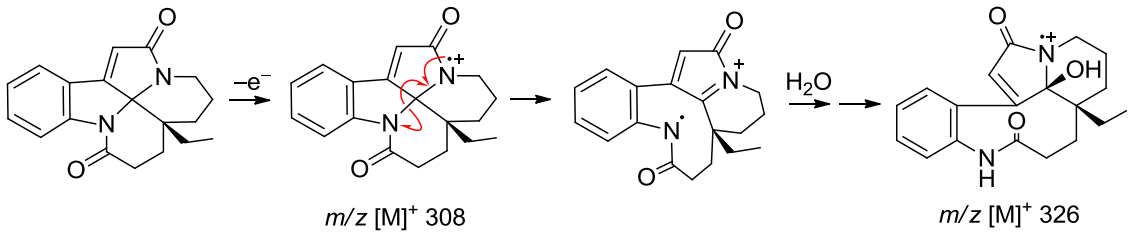

Scheme 4.4

The revised structure also accounted for Banwell's transformation of rhazinilam (**57**) to leuconolam (**54**) and '*epi*-leuconolam' (or 6,7-dehydroleuconoxine (**63**)),[62] since the use of excess PCC, followed by the aqueous workup, resulted in an acidic medium which triggered the transannular closure of leuconolam (**54**) to 6,7-dehydroleuconoxine (**63**).

The ^{1}H and ^{13}C NMR data of leuconolam (**54**), '*epi*-leuconolam' reported by Goh *et al.*,[49] Banwell *et al.*,[62] and from the present study (natural), and of semisynthetic 6,7-dehydroleuconoxine (**63**) from the current study, are summarized in Tables 4.4 and 4.5, respectively. The ^{1}H NMR spectra of leuconolam (**54**), '*epi*-leuconolam' (natural, present study), and semisynthetic 6,7-dehydroleuconoxine (**63**) (present study), are shown in Figures 4.10, 4.11, and 4.12, respectively.

Table 4.4. Comparison of ^{1}H NMR data (δ) of leuconolam (**54**), '*epi*-leuconolam', and 6,7-dhydroleuconoxine (**63**) in $CDCl_3$

Position	leuconolam (**54**)		'*epi*-leuconolam'			6,7-dehydroleuconoxine (**63**)
	Goh *et al.*[a,49]	Present study[b]	Goh *et al.*[a,49]	Banwell *et al.*[c,62]	Present study (natural)[d,58]	Present study (semisynthetic)[b]
3	2.96 dt (12, 4)	2.94 td (12.5, 4.5)	3.07 dt (10, 4.4)	3.27 – 3.00 m	3.22 ddd (15, 9.6, 6)	3.22 ddd (15, 9.5, 6)
	3.98 dd (12, 4)	3.98 dd (12.5, 4.5)	4.44 dt (10, 4.4)	4.50 m	4.46 ddd (15, 12, 4)	4.46 ddd (15, 12, 4)
6	5.79 s	5.77 s	6.20 s	6.21 s	6.22 s	6.22 s
9	7.20 dd (6, 2)	7.18 dd (7.5, 1.5)	7.45 br d (8.5)	7.45 d (7.8)	7.46 ddd (7.5, 1, 0.6)	7.46 dd (7.5, 1)
10	7.33 m	7.36 td (7.5, 1.5)	7.12 t (8.5)	7.11 t (7.8)	7.12 td (7.5, 1)	7.12 td (7.5, 1)
11	7.33 m	7.33 td (7.5, 1.5)	7.33 t (8.5)	7.33 t (7.8)	7.33 td (7.5, 1)	7.33 td (7.5, 1)
12	7.92 dd (6, 2)	7.91 dd (7.5, 1.5)	8.16 br d (8.5)	8.16 d (7.8)	8.16 ddd (7.5, 1, 0.6)	8.15 dd (7.5, 1)
14	1.65 – 1.37 m	1.48 m	1.30 – 1.79 m	1.85 – 0.75 m	1.79 m	1.80 m
	1.65 – 1.37 m	1.48 m	1.30 – 1.79 m	1.85 – 0.75 m	2.04 m	2.05 m
15	1.65 – 1.37 m	1.57 m	1.30 – 1.79 m	1.85 – 0.75 m	1.10 td (14, 7)	1.10 td (14, 7)
	1.79 dt (12.5, 5)	1.79 td (13.5, 4.5)	1.30 – 1.79 m	1.85 – 0.75 m	1.66 ddd (14, 6, 1.5)	1.66 ddd (14, 6, 1.5)
16	2.00 t (12.5)	1.99 td (14, 1.7)	2.66 dd (5.5, 2.5)	2.62 m	2.62 ddd (15, 5, 2)	2.63 ddd (15, 5, 2)
	2.14 dd (12.5, 6)	2.12 dd (14, 7.3)	3.16 dd (5.5, 2.5)	3.27–3.00 m	3.09 td (15, 6)	3.09 dd (15, 6)
17	1.65 – 1.37 m	1.40 br t (14.5)	2.03 – 2.13 dd (5.5, 2.5)	2.05 m	1.71 td (15, 5)	1.71 td (15, 5)
	1.65 – 1.37 m	1.60 td (14.5, 7.3)	2.03 – 2.13 dd (5.5, 2.5)	2.05 m	2.09 ddd (15, 6, 2)	2.11 dd (15, 6, 2)
18	0.55 t (8)	0.55 t (7.5)	0.73 t (7)	0.75 t (7.2)	0.76 t (7.4)	0.76 t (7.4)
19	1.65 – 1.37 m	1.23 dq (13.6, 7.5)	1.30 – 1.79 m	1.85–0.75 m	1.35 dq (13.6, 7.4)	1.35 dq (13.6, 7.4)
	1.65 – 1.37 m	1.60 m	1.30 – 1.79 m	1.85–0.75 m	1.45 dq (13.6, 7.4)	1.46 dq (13.6, 7.4)
*N*H	7.89 br s	7.71 br s	Not observed	Not observed	Not observed	Not observed
21-OH	5.13 br s	4.99 br s	Not observed	Not observed	Not observed	Not observed

[a]270 MHz; [b]600 MHz; [c]300 MHz; [d]400 MHz; [b,d]assignments based on COSY, HMQC, and HMBC.

Table 4.5. Comparison of ^{13}C NMR data (δ) of leuconolam (**54**), '*epi*-leuconolam', and 6,7-dehydroleuconoxine (**63**) in $CDCl_3$

Position	leuconolam (**54**)		'*epi*-leuconolam'			6,7-dehydroleuconoxine (**63**)
	Goh *et al.*[a,49]	Present study[b]	Goh *et al.*[a,49]	Banwell *et al.*[c,62]	Present study (natural)[d,58]	Present study (semisynthetic)[b]
2	178.3	177.8	176.1	175.8	176.1	176.3
3	35.6	35.3	37.0	37.0	37.0	37.2
5	166.8	166.5	173.5	173.2	173.5	173.8
6	128.3	128.1	118.2	118.1	118.2	118.4
7	156.1	155.6	164.2	164.1	164.2	164.5
8	133.5	133.1	123.5	123.4	123.5	123.7
9	126.5	129.3	121.6	124.2	121.6	121.8
10	126.9	126.3	124.3	121.4	124.3	124.6
11	129.7	129.4	131.6	131.4	131.6	131.8
12	129.6	126.6	115.9	115.8	115.9	116.2
13	135.3	135.0	148.6	148.6	148.6	148.9
14	20.0	19.7	16.8	16.8	16.8	17.0
15	32.4	24.5	26.0	26.1	26.0	26.3
16	28.0	32.1	33.1	34.1	33.1	34.4
17	25.7	25.4	30.4	30.4	30.4	30.7
18	7.3	6.9	8.3	8.2	8.3	8.5
19	24.4	27.3	34.1	33.0	34.1	33.4
20	45.2	44.9	44.6	44.5	44.6	44.8
21	93.8	93.6	93.7	93.6	93.7	93.9

[a]68 MHz; [b]150 MHz; [c]75 MHz; [d]100 MHz; [b,d]assignments based on COSY, HMQC, and HMBC.

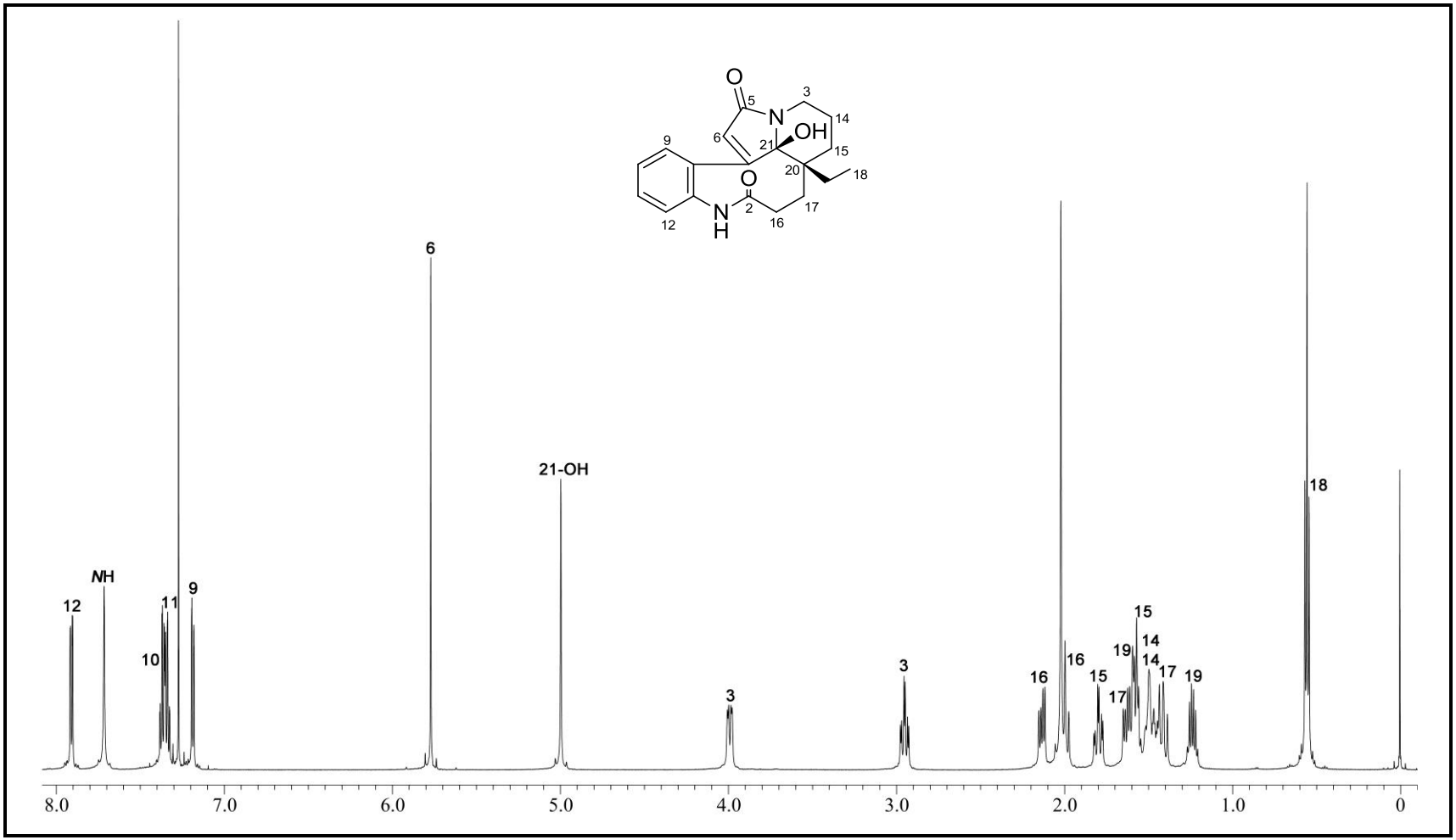

Figure 4.10. ^{1}H NMR spectrum ($CDCl_3$, 600 MHz) of leuconolam (**54**).

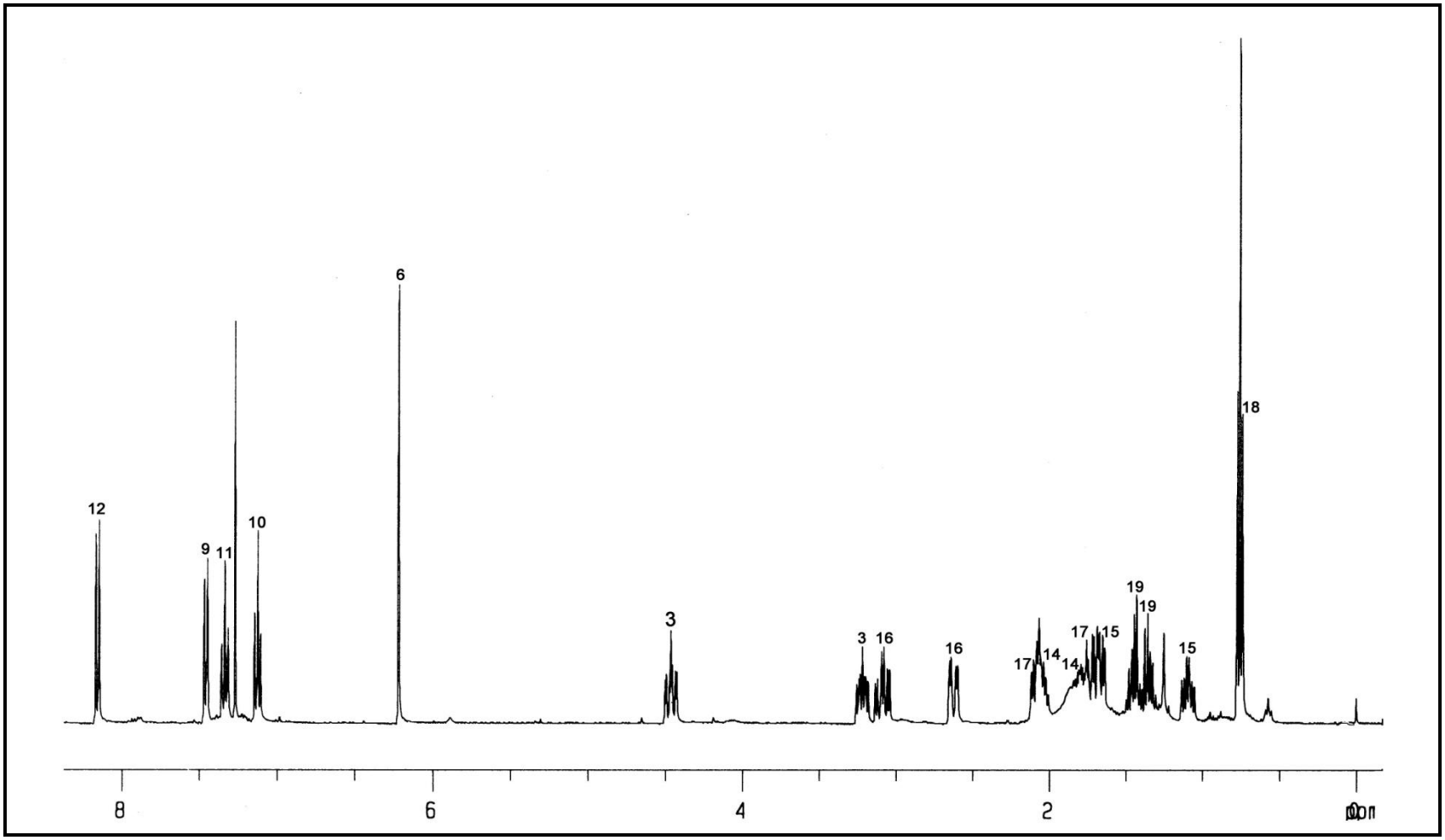

Figure 4.11. ^{1}H NMR spectrum ($CDCl_3$, 400 MHz) of '*epi*-leuconolam' (natural, present study).[58]

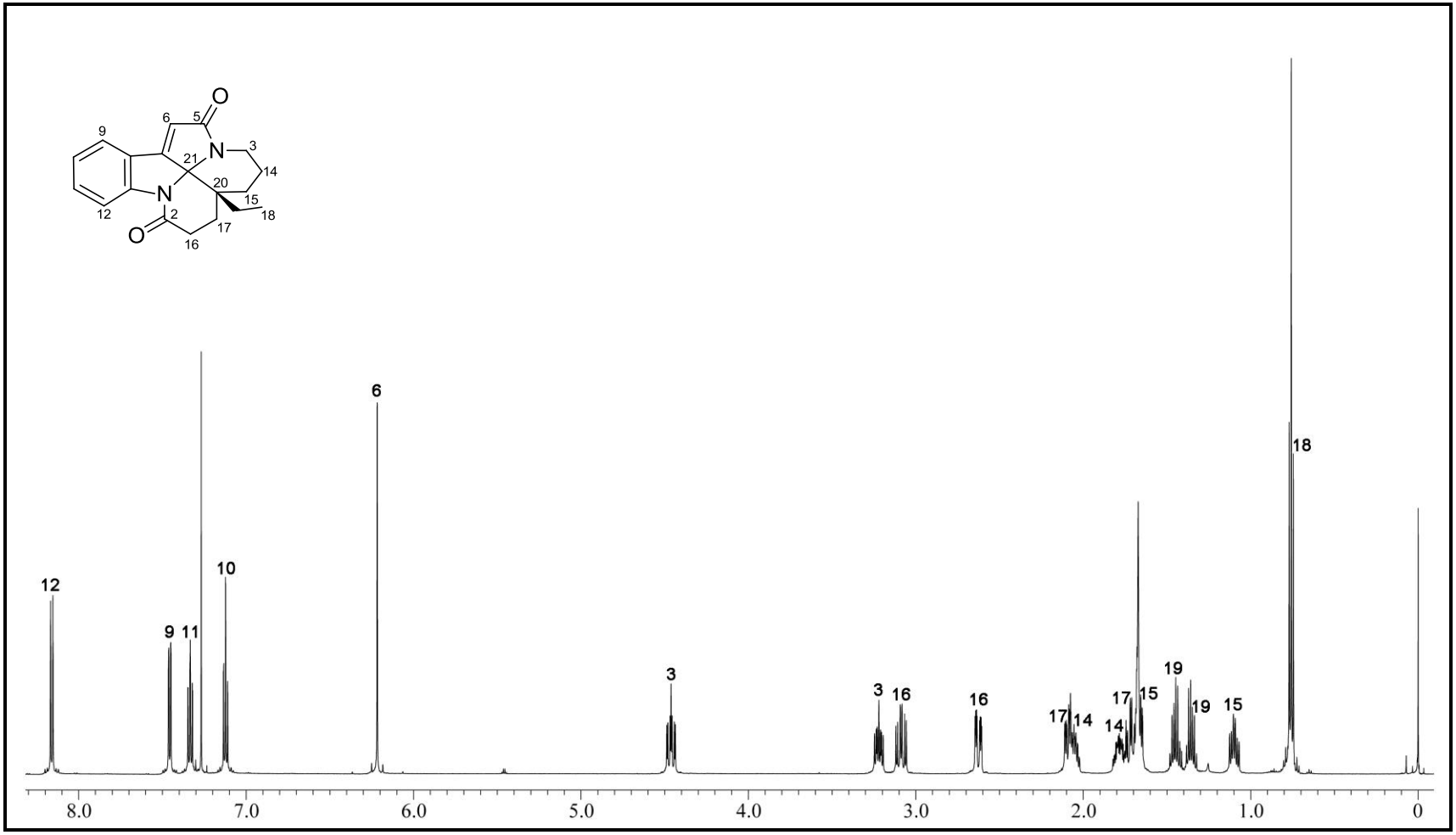

Figure 4.12. ^{1}H NMR spectrum ($CDCl_3$, 600 MHz) of semisynthetic 6,7-dehydroleuconoxine (**63**).

With the problem regarding the misassigned structure of '*epi*-leuconolam' resolved, the next issue to be addressed is the structure of compound A, obtained in the acid-induced transformations of leuconolam (**54**).

Compound A was obtained as a yellowish oil and subsequently as yellowish block crystals from CH_2Cl_2/hexanes (mp 179–182 ^oC) with $[\alpha]^{25}_D$ = +116 (*c* 0.52, $CHCl_3$). The UV spectrum showed absorption maxima at 212, 240, and 340 nm, while the IR spectrum showed the presence of NH_2 (3483 and 3397 cm^{-1}) and carbonyl functions (1743 and 1709 cm^{-1}). The EIMS of compound A showed an $[M]^+$ at *m/z* 326, while HREIMS measurements gave the molecular formula $C_{19}H_{22}N_2O_3$ (DBE 10).

The ^{13}C NMR data (Table 4.6) accounted for all 19 carbon resonances, and confirmed the presence two carbonyl functions at δ_C 166.8 (lactam carbonyl) and 170.6 (lactone carbonyl), in addition to a low-field quaternary resonance (δ_C 102.1) due to C-21, which is α to both a nitrogen and an oxygen atom.

The ^1H NMR data (Table 4.6) showed signals due to four adjacent aromatic hydrogens (δ_H 6.65, 6.66, 6.96, and 7.09) corresponding to an *ortho*-disubstituted aromatic moiety, one olefinic proton (δ_H 6.14), and a broad two-H singlet due to an amino group NH_2 (δ_H 3.94, exchangeable with D_2O). The COSY and HMQC data showed the presence of $NCH_2CH_2CH_2$, $C{=}OCH_2CH_2$, and CH_2CH_3 partial structures, as well as an isolated vinylic hydrogen, corresponding to H-6 (Figure 4.13).

Comparison of the NMR data of compound A (Table 4.6) with those of the starting leuconolam (**54**) (Tables 4.4 and 4.5) indicated that the *N*-4–C-5–C-6, *N*-4–C-3–C-14–C-15, C-16–C-17–C=O partial structures, as well as the C-20 ethyl side chain have remained intact. The attachment of C-5 and C-3 to *N*-4 was supported by the

observed correlations from H-6 and H-3 to C-21 (low-field quaternary resonance at δ_C 102.1) indicated the connection of C-21 to *N*-4. The observed three-bond correlations from H-15 to C-17, C-19, and C-21, indicated attachment of C-15, C-17, and C-19 to the quaternary C-20, as well as the attachment of C-20 to C-21. It remains to complete the assembly of the molecule by cleavage of the *N*-1 amide function to a free primary amine and attachment of the carboxyl oxygen to C-21, to reveal the amino lactam-lactone as shown in **78**.

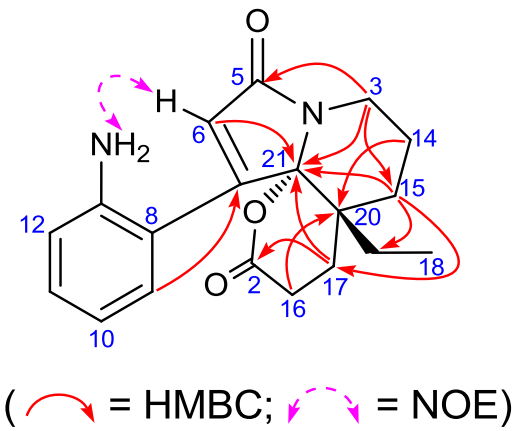

Figure 4.13. Selected HMBCs and NOE of **78**.

The ^{1}H and ^{13}C NMR data of compound **78** are summarized in Table 4.6, while the ^{1}H NMR spectrum of compound **78** is shown in Figure 4.14.

Table 4.6. ^{1}H and ^{13}C NMR data (δ) of compound **78**[a]

Position	δ_C	δ_H
2	170.6	–
3	35.9	2.82 ddd (13, 4, 2)
		4.09 ddd (13, 11, 4)
5	166.8	–
6	121.9	6.14 s
7	155.7	–
8	118.0	–
9	128.9	6.96 dd (8, 1.5)
10	118.4	6.65 td (8, 1.5)
11	130.8	7.09 td (8, 1.5)
12	116.6	6.65 dd (8, 1.5)
13	144.1	–
14	19.8	1.58 m
15	25.5	1.53 m
		1.43 m
16	26.3	2.20 ddd (19, 10, 1.2)
		2.44 ddd (19, 6, 1.5)
17	25.6	1.28 m
		1.45 m
18	7.1	0.68 t (7.6)
19	25.0	1.26 m
		1.51 m
20	37.9	–
21	102.1	–
*N*H$_2$	–	3.94 br s

[a]CD_2Cl_2, 400 and 100 MHz, respectively; assignments based on COSY, HMQC, and HMBC.

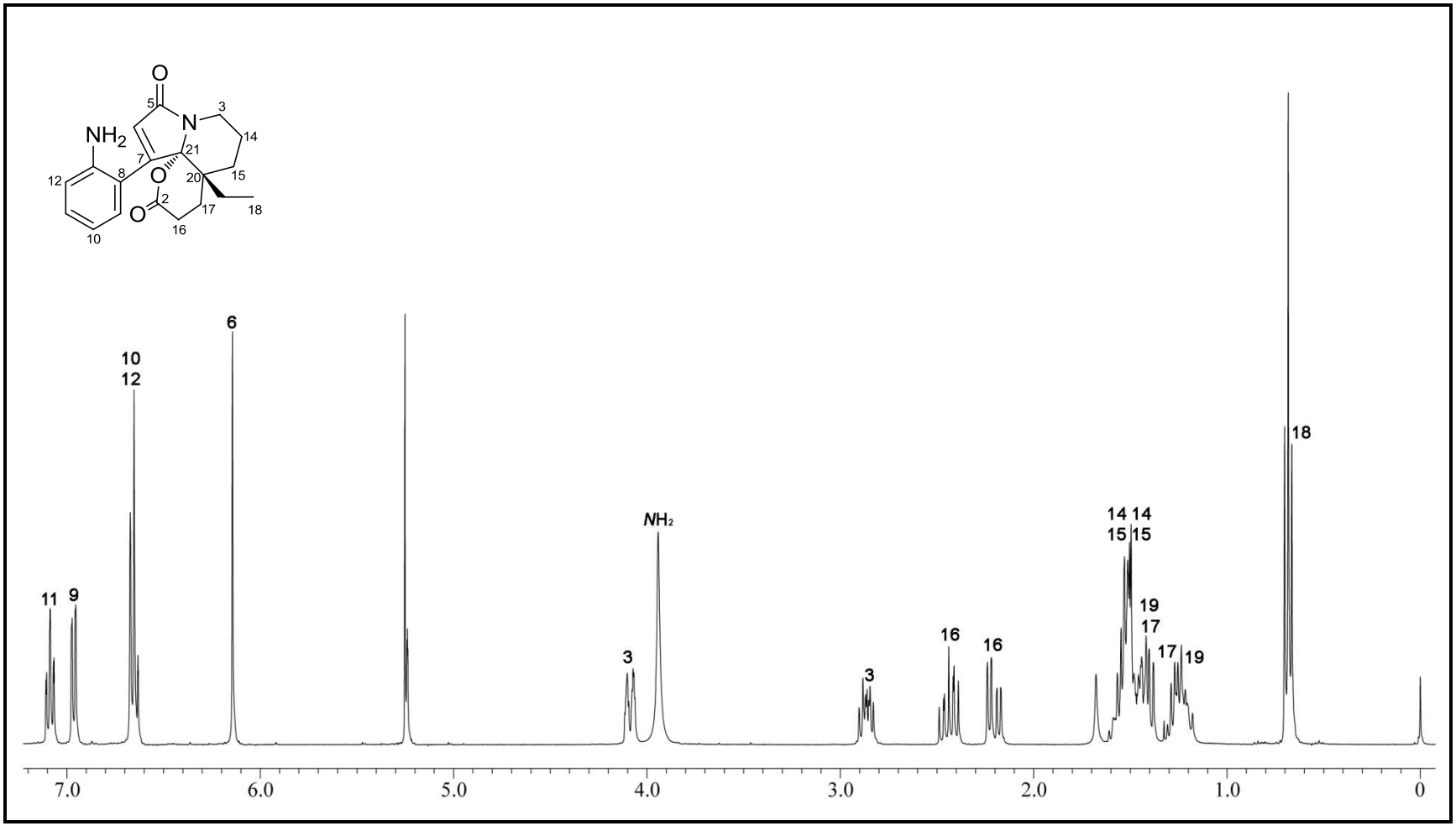

Figure 4.14. ^{1}H NMR spectrum (CD_2Cl_2, 400 MHz) of amino lactam-lactone **78**.

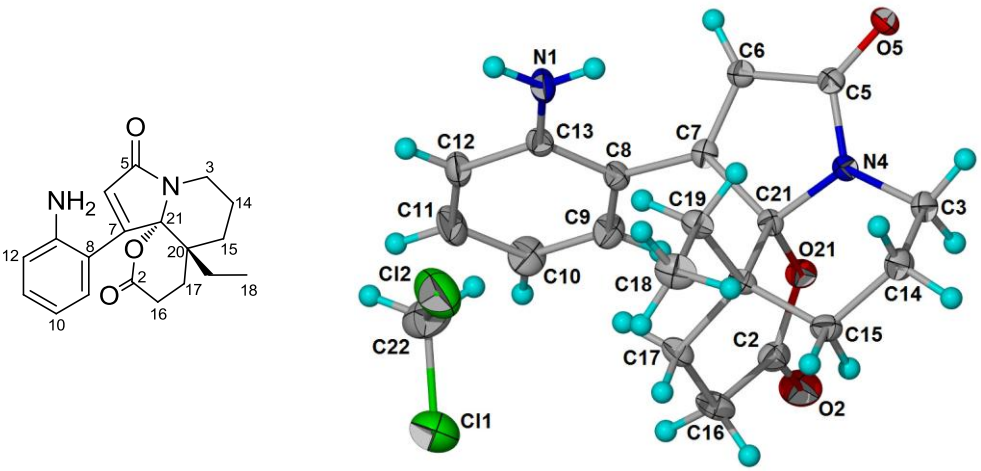

Figure 4.15. X-ray crystal structure of **78**
[Flack parameter,[63] x = –0.06(0.06);
Hooft parameter,[64] y = –0.02(0.03)].

In order to provide firm proof of the proposed structure, X-ray diffraction analysis was carried out which confirmed the structure proposed and yielded the absolute configuration, as shown in Figure 4.15 (since compound **78** co-crystallized with the solvent (CH_2Cl_2) used during crystallization, the presence of heavy atoms in the crystal lattice facilitated the determination of the absolute configuration of **78** despite the use of Mo K_α radiation).

The crystal structure showed that the NH$_2$ group is oriented away from the lactone moiety and proximate to the vinylic H-6 (Figure 4.15), which is also supported by the observed reciprocal NOE observed between NH$_2$ and H-6 (Figure 4.14).

With the structure of 6,7-dehydroleuconoxine (**63**) (previously misassigned as *epi*-leuconolam, **55**) and that of compound A (**78**) firmly established, the results of the reaction of leuconolam (**54**) (and 6,7-dehydroleuconoxine (**63**)) with acid (Table 4.7) become intelligible.

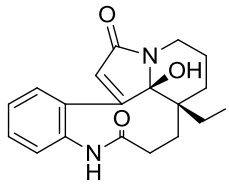

54 leuconolam

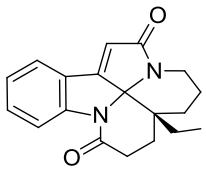

63 6,7-dehydroleuconoxine

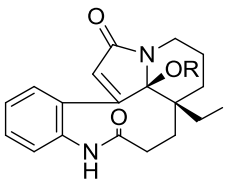

77 *O*-methylleuconolam R = Me

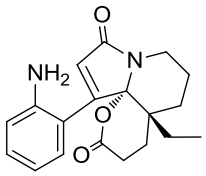

78

Table 4.7. Summary of reactions of leuconolam (**54**) with acids (updated)

Entry	Starting material	Reaction conditions	Products			
			54	**63**	**78**	**77**
1	**54**	5% HCl, rt, 8 h	No reaction			
2	**54**	5% HCl/CH_2Cl_2 + TEACl, rt, 14 h[a]	35%	45%	1.5%	–
3	**54**	HCl/MeOH, rt, 12 h	4%	–	–	63%
4	**54**	CSA/CH_2Cl_2, rt, 14 h[a]	10%	62%	2%	
5	**54**	CSA/CH_2Cl_2, rt, 11 h (4 equiv MeOH added)	–	19%	–	54%
6	**54**	CSA/MeOH, rt, 14 h	4%	–	2%	94%
7	**54**	PTSA/MeOH, rt, 14 h	4%	–	0.8%	94%
8	**54**	PTSA/CH_2Cl_2, rt, 14 h	3%	5%	42%	–
9	**63**	5% HCl/CH_2Cl_2 + TEACl, rt, 12 h[a]	15%	84%	–	–
10	**63**	CSA/CH_2Cl_2, rt, 15 h	No reaction[b]			
11	**63**	PTSA/CH_2Cl_2, rt, 10 h	–	1%	70%	–
12	**77**	PTSA/CH_2Cl_2, rt, 10 h	No reaction[c]			

[a]Prolonged reaction time leads to reduced overall yields; [b]traces of **54** and **78** detected from TLC; [c]traces of **54** and **63** detected from TLC.

The formation of 6,7-dehydroleuconoxine (**63**) with recovered leuconolam (**54**), when leuconolam (**54**) was treated with aqueous acid under two-phase conditions (entry 2, Table 4.7) in all probability derives from reversible formation of the *N*-4–C-21 iminium ion **79**, followed by transannular cyclization to the doubly spirocyclic dehydroleuconoxine (**63**) (Scheme 4.5). The reversible nature of this reaction is indicated by the formation of **54** with recovered **63**, when **63** was subjected to the same reaction conditions (entry 9, Table 4.7). When the acid-induced reaction was carried out in the polar, protic, nucleophilic MeOH (entries 3, 6, and 7, Table 4.7) in the presence of either HCl, CSA, or PTSA, virtually quantitative conversion to *O*-methylleuconolam (**77**) was observed, suggesting efficient trapping of the iminium ion from the *β*-face by the larger and more nucleophilic MeOH. With the larger and more nucleophilic MeOH, approach from the less hindered convex *β*-face is overwhelmingly favored (Figure 4.16), and the nucleophilic addition step is virtually irreversible, the *O*-methylleuconolam (**77**) once formed is stable under the reaction conditions (**77** does not react when exposed to acid, entry 12, Table 4.7).

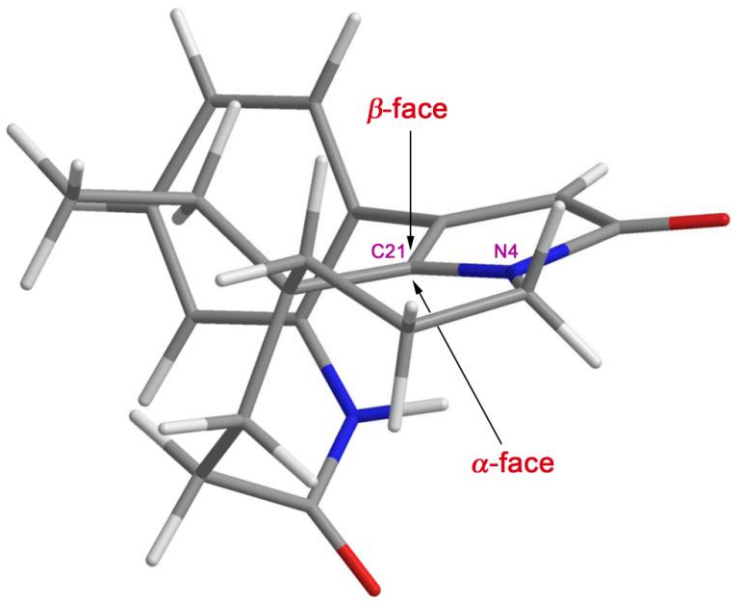

Figure 4.16. Iminium ion **79**.

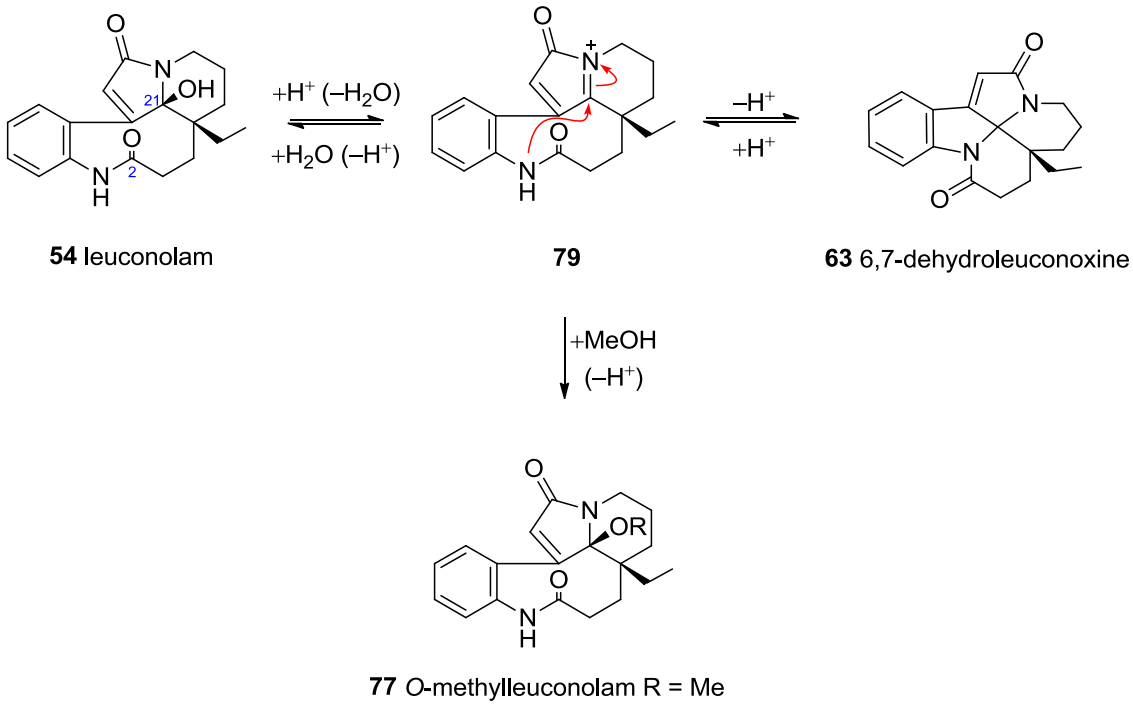

Scheme 4.5

When the reaction was carried out in PTSA/CH_2Cl_2, a change in the product distribution was observed with the amino lactam-lactone **78**, obtained as the major product (42%) and 6,7-dehydroleuconoxine (**63**) as the minor product (5%). TLC monitoring of the progress of reaction showed that the amino lactam-lactone **78** was formed, subsequent to the formation of **63**, suggesting that **78** originated from the first-formed **63**. Further confirmation was provided by the observation that treatment of **63** with PTSA/CH_2Cl_2, resulted in the formation of the lactam-lactone **78** as the major product in 70% yield (entry 11, Table 4.7).

A possible pathway for the formation of **78** from **63** is shown in Scheme 4.6 involving protonation of *N*-1, fragmentation to the iminium ion **79**, intramolecular attack by the lactam carbonyl oxygen, followed by cleavage to yield **78**. This pathway is rendered less likely on geometric grounds as examination of models showed that the key intermediate **80** is too strained to exist and therefore unlikely to form.

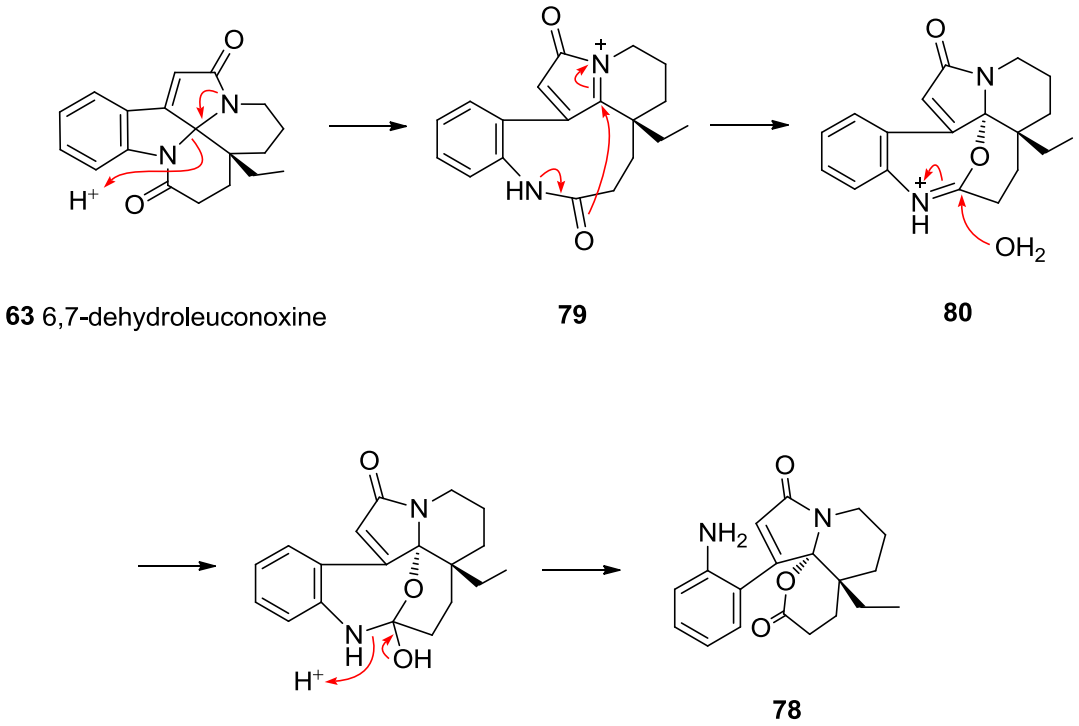

Scheme 4.6

An alternative pathway is shown in Scheme 4.7, which involves the formation of a transient *epi*-leuconolam intermediate (**55**), followed in succession by protonation of the C-2 lactam carbonyl and nucleophilic addition of the appositely oriented C-21-αOH on the C-2 carbonyl function, leading eventually to *N*-1–C-2 cleavage to yield compound **78**.

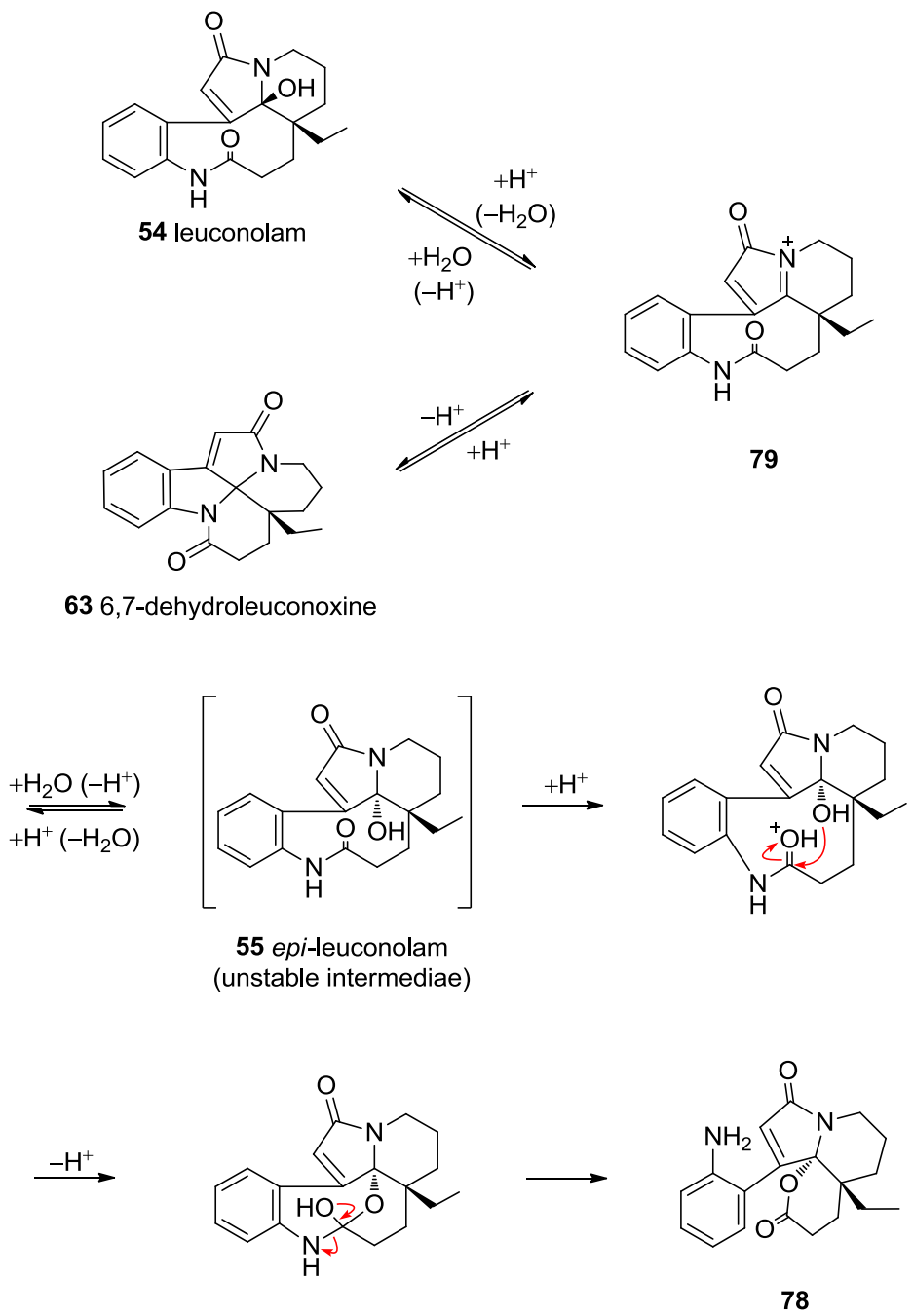

Scheme 4.7

A third possible pathway is shown in Scheme 4.8, involving acidic hydrolysis of the *N*-1 lactam, followed in succession by fragmentation to the iminium ion **81**, and finally, facile intramolecular capture of the iminium ion **81** by the carboxylic acid group, leading eventually to the amino lactam-lactone product **78**. The fact that the starting dehydroleuconoxine **63** is comparatively more strained than the product **78** (as shown

by examination of models) constitutes additional support for the proposed amide hydrolysis under relatively mild conditions.

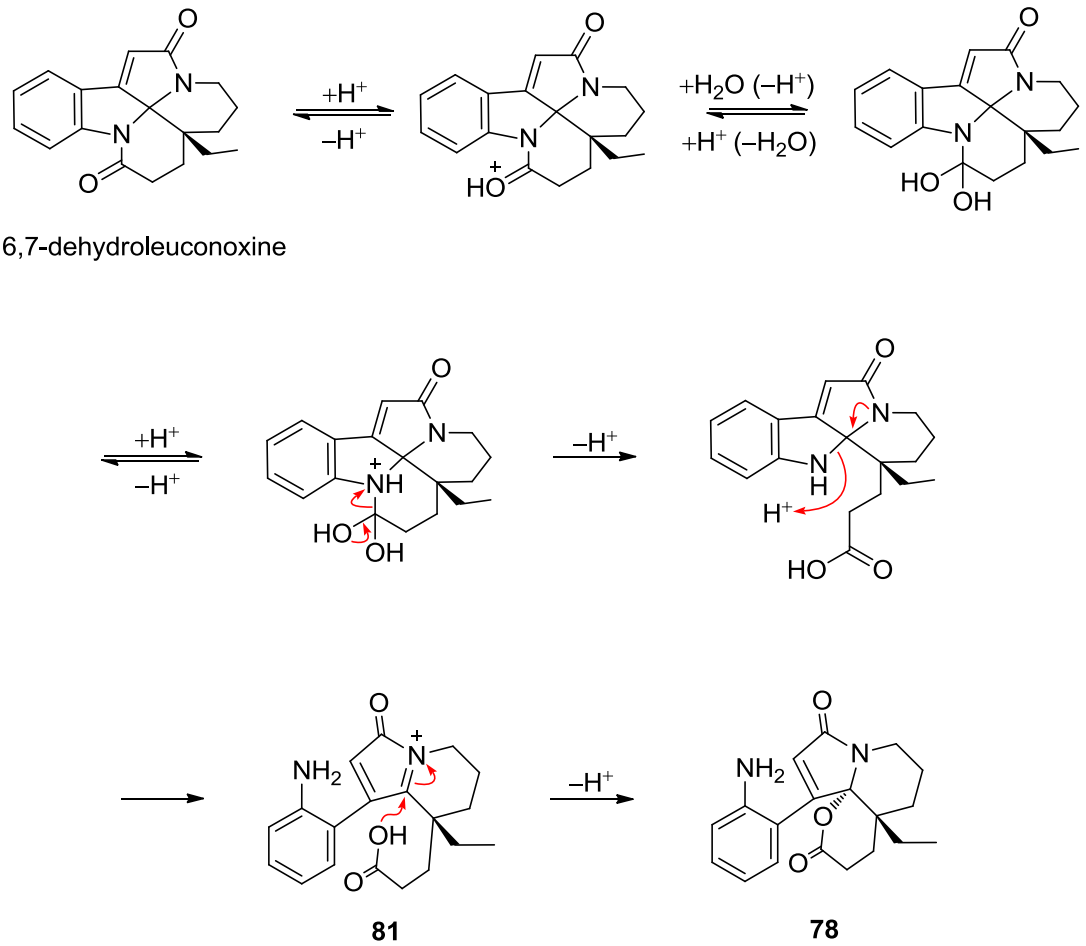

Scheme 4.8

In view of the facile acid-induced transannular cyclization of leuconolam (**54**) to 6,7-dehydroleuconoxine (**63**), a two-step sequence involving cyclization followed by hydrogenation yielded leuconoxine (**56**) in *ca.* 55% overall yield from leuconolam (**54**). This transformation represents a partial synthesis of leuconoxine (**56**) from leuconolam (**54**) (Scheme 4.9) (leuconoxine (**56**) was previously obtained by bioconversion of rhazinilam (**57**) with *Beauveria bassiana* LMA (ATCC 7159), but with very low yield (0.6%)[65]). The ^{1}H and ^{13}C NMR data of **56** are summarized in Table 4.8. The ^{1}H NMR

spectrum of natural **56** and semisynthetic **56** are shown in Figures 4.17 and 4.18, respectively.

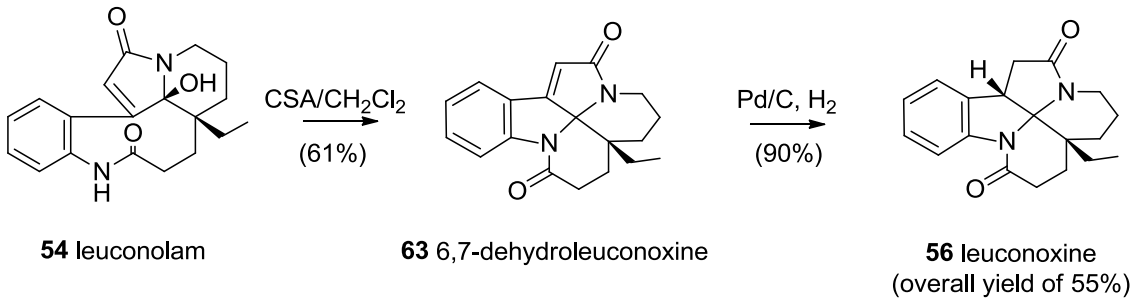

Scheme 4.9

During the course of the present study, an alkaloid corresponding to 6,7-dehydroleuconoxine (**63**) (NMR data identical to '*epi*-leuconolam' or 6,7-dehydroleuconoxine) was reported as a minor alkaloid from the stem-bark extract of *Melodinus henryi*.[66] In view of the above, the possibility that this alkaloid is an artifact due to the action of traces of acid on leuconolam (**54**) which may have been present cannot be discounted.

Table 4.8. ^{1}H and ^{13}C NMR data (δ) of leuconoxine (**56**)[a]

Position	δ_C	δ_H
2	172.9	–
3	36.8	2.80 m
		3.95 ddt (13, 4.4, 2.3)
5	170.8	–
6	37.6	2.68 d (17)
		2.87 dd (17, 7.3)
7	41.9	3.82 d (7.3)
8	135.4	–
9	123.8	7.17 dd (7.6, 1)
10	125.5	7.14 td (7.6, 1)
11	128.0	7.25 td (7.6, 1)
12	120.1	7.77 dd (7.6, 1)
13	142.1	–
14	20.1	1.60 m
		1.60 m
15	26.2	1.60 m
		1.97 ddd (14, 12, 5)
16	29.4	2.49 ddd (19, 6, 1.4)
		2.78 ddd (19, 14, 6.5)
17	26.6	1.60 m
		1.86 ddd (14, 6.5, 1.4)
18	7.3	0.93 t (7.4)
19	26.9	1.37 dq (13.4, 7.4)
		1.78 dq (13.4, 7.4)
20	38.1	–
21	92.5	–

[a]$CDCl_3$, 400 and 100 MHz, respectively; assignments based on COSY, HMQC, and comparison with literature.

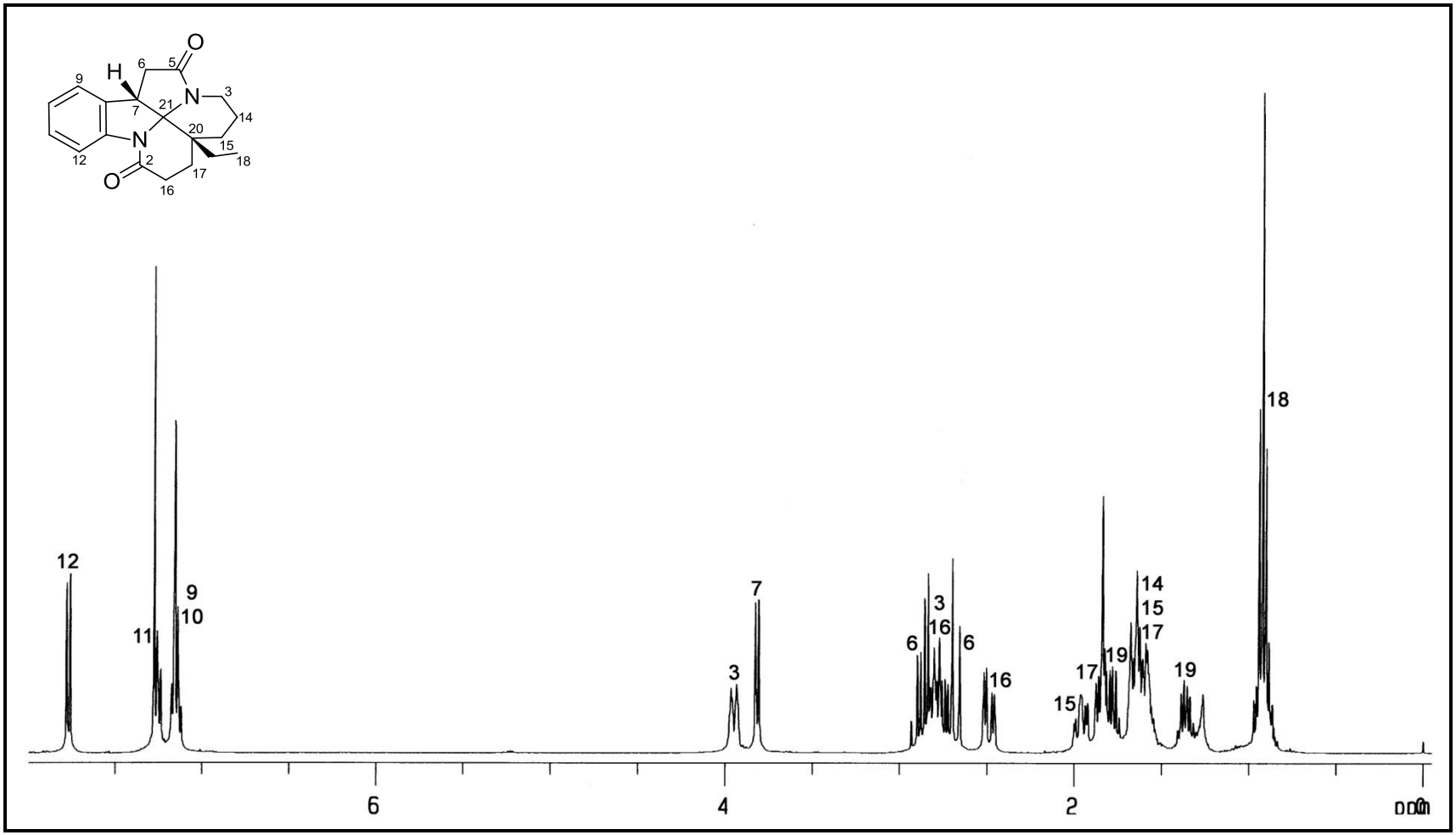

Figure 4.17. ^{1}H NMR spectrum ($CDCl_3$, 400 MHz) of natural leuconoxine (**56**).[58]

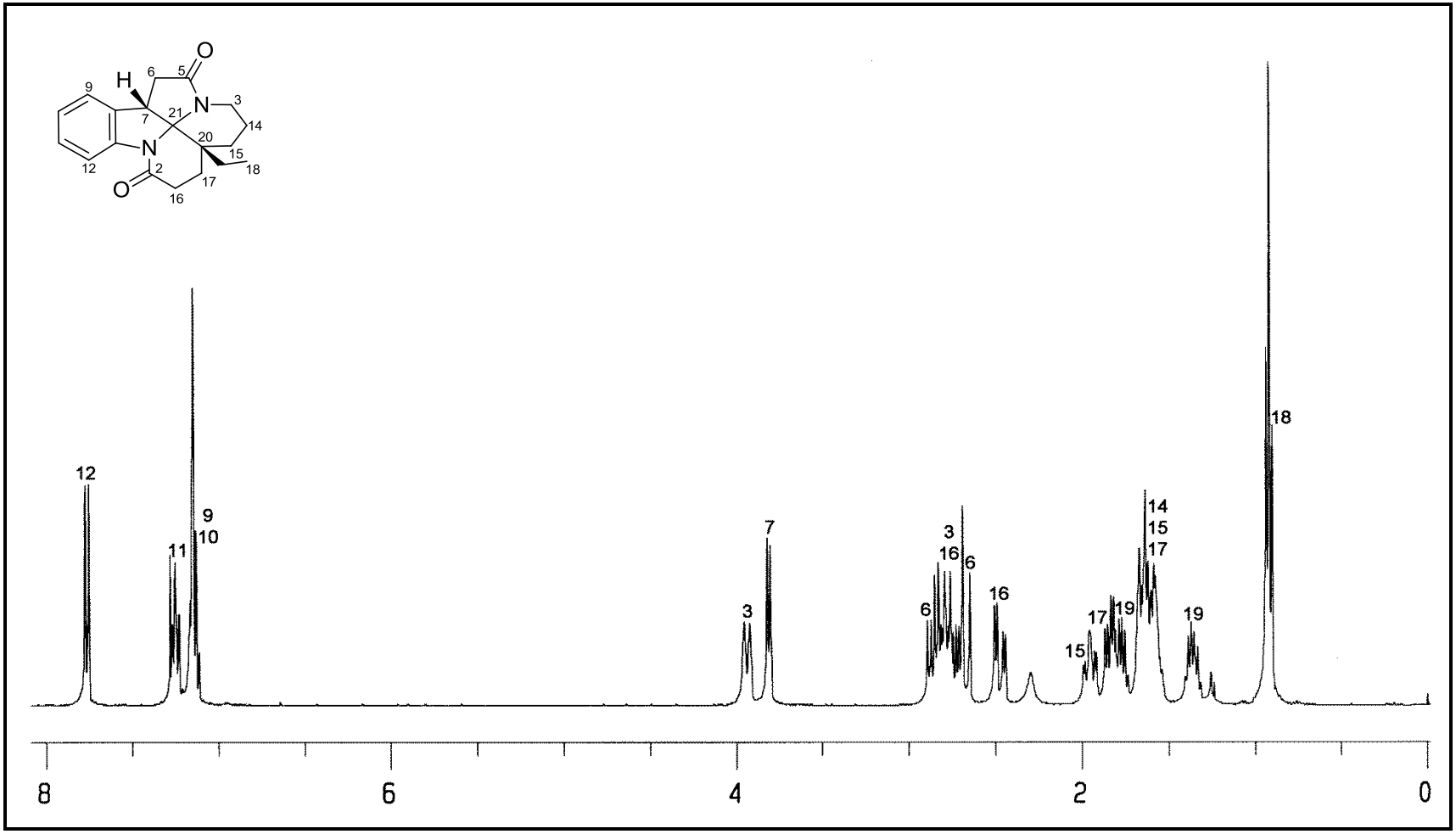

Figure 4.18. ^{1}H NMR spectrum ($CDCl_3$, 400 MHz) of semisynthetic leuconoxine (**56**).

4.2.3 Bromination of leuconolam

Treatment of leuconolam (**54**) with Br_2 in $CHCl_3$ gave the dibromoleuconoxine derivative, 6*β*,7*β*-dibromoleuconoxine (**82**) as the sole product in about 90% yield.[49]

6*β*,7*β*-Dibromoleuconoxine (**82**) was obtained as a white amorphous solid (mp 98–102 ^{o}C), with $[\alpha]^{25}_{D} = -38$ (*c* 0.62, $CHCl_3$). The UV spectrum showed absorption maxima at 208, 227, and 292 nm, while the IR spectrum showed the presence of two lactam carbonyls at 1691 and 1709 cm^{-1}. The ESIMS of **82** showed an $[M + H]^+$ peak at *m/z* 467, and HRESIMS measurements gave the molecular formula $C_{19}H_{21}N_2O_2{}^{79}Br_2$ + H. The ^{1}H and ^{13}C NMR data of **82** were similar to those of **82** previously reported by Goh *et al*.[49] The configuration of the 6,7-dibromoleuconoxine was assigned as 6*β*,7*β*-dibromoleuconoxine (**82**) by analogy to leuconoxine and its congeners, where H or OH substituents attached to C-7 in the diazaspiro leuconoxine skeleton has to be *β*-oriented (7*α*-substituted analogs are highly strained and none are known). In addition, the observed NOE between H-6 and H-9 is only possible if H-6 has the *α*-configuration. The ^{1}H and ^{13}C NMR data of **82** are summarized in Table 4.9, while the ^{1}H NMR spectrum of **82** is shown in Figure 4.19.

Table 4.9. ^{1}H and ^{13}C NMR data (δ) of 6β,7β-dibromoleuconoxine (**82**)[a]

Position	δ_C	δ_H
2	172.4	–
3	38.7	2.73 m
		4.08 ddd (13.5, 4, 2)
5	164.3	–
6	50.6	5.17 s
7	63.7	–
8	136.9	–
9	126.5	7.33 m
10	123.8	7.24 dt (7.2 , 1)
11	130.4	7.36 m
12	120.9	7.80 dd (7.2, 1)
13	139.2	–
14	19.6	1.56 m
		1.60 m
15	24.5	1.62 m
		2.75 m
16	29.4	2.64 m
		2.82 m
17	25.5	2.03 m
		2.23 m
18	7.0	0.94 t (7)
19	28.0	1.73 m
		1.98 m
20	39.2	–
21	100.5	–

[a]$CDCl_3$, 400 and 100 MHz, respectively; assignments based on COSY, HMQC, and comparison with literature.

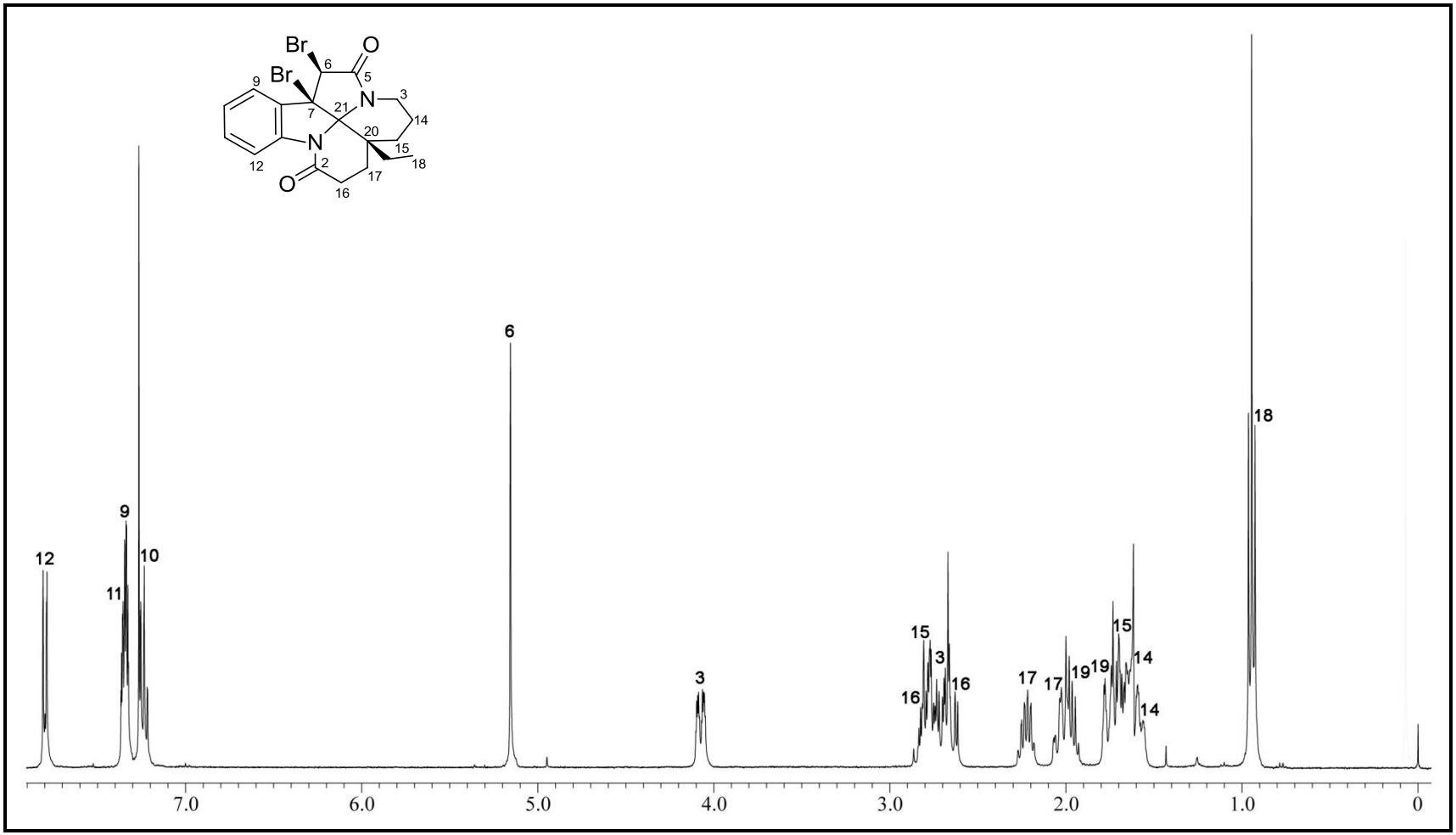

Figure 4.19. ^{1}H NMR spectrum ($CDCl_3$, 400 MHz) of 6*β*,7*β*-dibromoleuconoxine (**82**).

Monitoring of the progress of the bromination reaction by TLC indicated that two products, in addition to the starting leuconolam (**54**), were detected at a very early stage of the reaction. These were 6*β*,7*β*-dibromoleuconoxine (**82**) and 6,7-dehydroleuconoxine (**63**). This observation suggested a two-step sequence involving transannular cyclization to **63**, followed by bromine addition to furnish **82** (Scheme 4.10). This was supported by the observation that treatment of 6,7-dehydroleuconoxine (**63**) with $Br_2/CHCl_3$ proceeded smoothly to yield the same dibromoleuconoxine product, **82**. Reaction monitoring by TLC showed only the presence of 6,7-dehydroleuconoxine (**63**) and the dibromoleuconoxine addition product, **82**. Furthermore debromination of the dibromo addition product led smoothly to 6,7-dehydroleuconoxine (**63**) (Scheme 4.10).

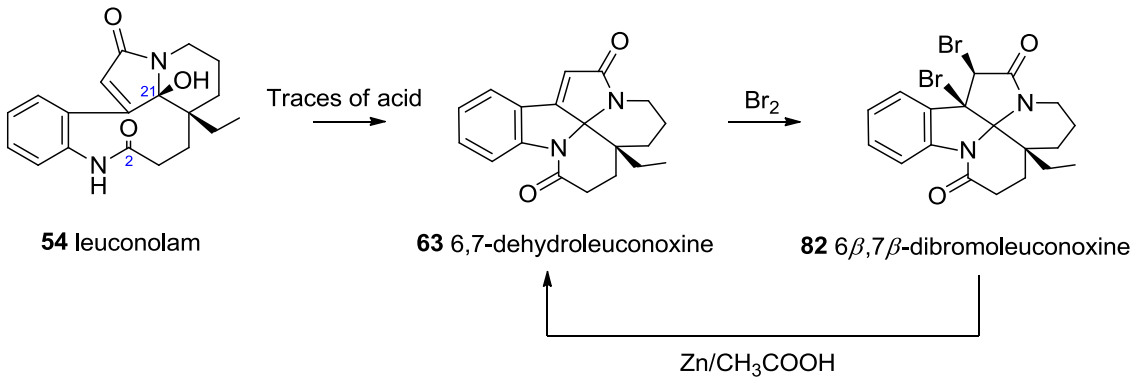

Scheme 4.10

The bromination of alkenes is a well-known reaction, which usually yields *trans*-dibromo products as a consequence of *anti*-addition of bromine. The generally accepted mechanism invokes the intermediacy of a bromonium ion intermediate **83** (Table 4.11). In this instance however, a *cis*-dibromo addition product was clearly obtained as the sole product. Deviations from *trans* selectivity (usually giving rise to *cis*/*trans* mixtures of addition products) have nevertheless been previously observed (*e.g.*, in acenaphthylene).[67] Deviations from *trans* selectivity are explained by the

intermediacy of non-bridged cationic species such as the β-bromocarbenium ion **84**,[68] or more recently by the intermediacy of the tribromide adduct **85** (Scheme 4.11).[69]

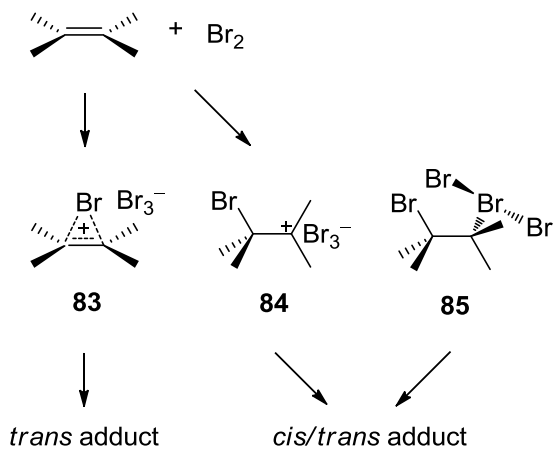

Scheme 4.11

The formation of exclusively *cis*-dibromo addition product in the present instance can be explained by acid-catalyzed epimerization of the *trans* addition product (formed either with exclusive *trans* selectivity *via* the bromonium ion **84**, or, from *cis*/*trans* mixtures formed *via* intermediacy of the β-bromocarbenium ion **84**, or the tribromide adduct **85**) (Scheme 4.12).

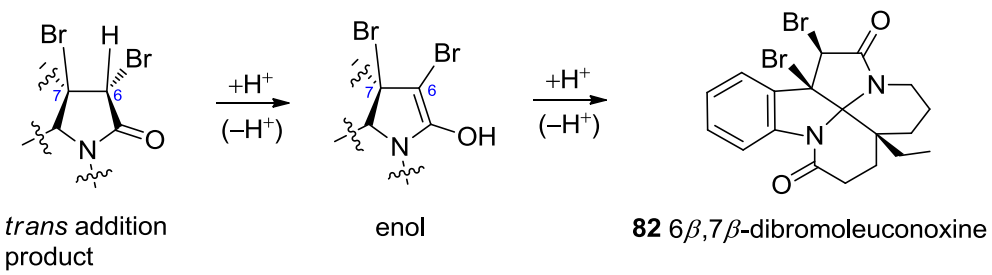

Scheme 4.12

4.2.4 Reaction with BH_3

It was at first envisaged that a hydroboration reaction on dehydroleuconoxine (**63**) might lead to 6-hydroxyleuconoxine (or leuconodine A (**67**)), a new leuconoxine type alkaloid from *L. griffithii*.[58] However, when **63** was treated with $BH_3.SMe_2$ (5 equiv) in THF at rt,[32,70,71] a complex mixture of products was obtained from which two leuconoxine-type derivatives arising from reduction of the C-2 lactam carbonyl *viz.*, **86** (completely reduced product, 37%) and **87** (partially reduced product, 6%) were successfully isolated (Scheme 4.13).

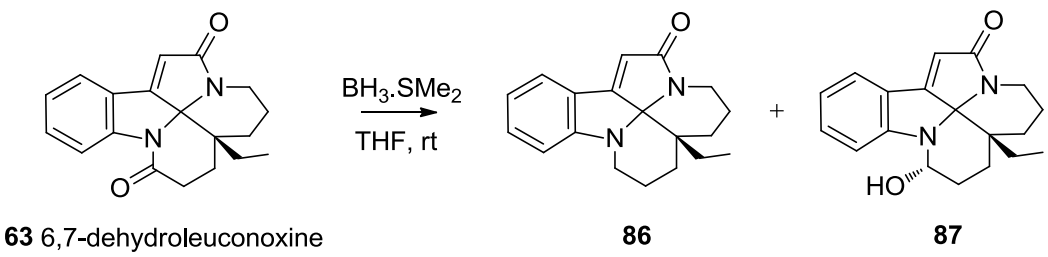

Scheme 4.13

Compound **86** was obtained as a yellowish oil, and subsequently as yellowish needles from MeOH (mp 128–132 ^{o}C), with $[\alpha]^{25}_{D}$ = +584 (*c* 0.35, $CHCl_3$). The UV spectrum showed absorption maxima at 209, 246, and 388 nm, while the IR spectrum showed a conjugated lactam carbonyl at 1641 and 1682 cm^{-1}. The ESIMS of **86** showed an $[M + H]^+$ at *m/z* 295, in agreement with the molecular formula $C_{19}H_{22}N_2O$ + H. A notable difference in the ^{1}H NMR spectrum of **86** when compared with that of 6,7-dehydroleuconoxine (**63**) was the presence of additional two proton signals due to a methylene group adjacent to a heteroatom at δ_H 3.55, 3.81, attributable to H-2 (based on HMQC). Also, the characteristic C-2 lactam carbonyl signal observed in the ^{13}C NMR spectrum of **63** was now replaced by a signal at δ_C 40.8 attributed to C-2 in **86**. These

observations clearly indicated deoxygenation at C-2 of **86**. The ^{1}H and ^{13}C NMR data of **86** are summarized in Table 4.10, while the ^{1}H NMR spectrum of **86** is shown in Figure 4.20.

Compound **87** was obtained as a fluorescent yellowish oil, and subsequently as a fluorescent yellowish rods (mp 198–200 ^{o}C), with $[\alpha]^{25}_{D}$ = +667 (*c* 0.33, $CHCl_3$). The UV spectrum showed absorption maxima at 209, 245, and 394 nm, while the IR spectrum showed an OH band at 3343 cm^{-1} and a lactam carbonyl at 1666 cm^{-1}. The ESIMS of **87** showed an $[M + H]^+$ at *m/z* 311, in agreement with the molecular formula $C_{19}H_{22}N_2O_2$ + H. Notable differences in the ^{1}H NMR spectrum of **87** when compared with that of 6,7-dehydroleuconoxine (**63**) were the presence of a low field proton signal at δ_H 5.52 due to H-2, and a broad OH signal at δ_H 4.02. The ^{13}C NMR spectrum showed the absence of the characteristic C-2 lactam signal, while displaying an additional resonance at δ_C 76.1, attributed to C-2. These observations indicated that the C-2 carbonyl in **63** has been reduced to an OH in **87**. The C-2 configuration was assigned as *S*, based on the observed NOE between C-2 and C-12. of The ^{1}H and ^{13}C NMR data of **87** are summarized in Table 4.10, while the ^{1}H NMR spectrum of **87** is shown in Figure 4.21.

Table 4.10. ^{1}H and ^{13}C NMR data (δ) of compounds **86** and **87**[a]

Position	**86**		**87**	
	δ_C	δ_H	δ_C	δ_H
2	40.8	3.55 ddd (15.4, 11, 7.8)	76.1	5.52 br s
		3.81 dd (15.4, 7.8)		
3	39.0	3.05 ddd (13.5, 4.5, 2)	35.8	3.67 ddd (14, 4, 2)
		4.31 ddd (13, 11, 4.5)		3.99 ddd (14, 11, 4)
5	173.7	–	177.1	–
6	116.9	6.16 s	117.3	5.67 s
7	166.1	–	166.1	–
8	122.5	–	120.0	–
9	122.4	7.36 dd (7.5, 1)	122.7	6.99 dd (7.8, 1)
10	119.7	6.83 td (7.5, 1)	119.3	6.68 br t (7.8)
11	131.3	7.24 td (7.5, 1)	131.3	7.15 td (8.2, 1)
12	109.7	6.75 dd (7.5, 1)	108.2	6.60 br d (8.2)
13	157.0	–	153.7	–
14	20.1	1.56 m	18.1	1.54 m
		1.56 m		1.84 m
15	27.4	1.69 m	24.0	0.87 m
		2.00 m		1.73 m
16	17.0	1.69 m	23.8	1.73 m
		2.00 m		1.81 m
17	25.4	1.15 m	21.5	1.31 m
		1.53 m		2.36 td (14.5, 4)
18	8.3	0.67 t (7.6)	8.3	0.55 t (7.4)
19	29.6	1.14 dq (13.2, 7.6)	29.6	0.97 dq (13.1, 7.4)
		1.38 dq (13.2, 7.6)		1.27 dq (13.1, 7.4)
20	41.4	–	42.3	–
21	94.5	–	94.7	–
OH	–	–	–	4.02 br s

[a]$CDCl_3$, 400 and 100 MHz, respectively; assignments based on COSY, HMQC, and HMBC.

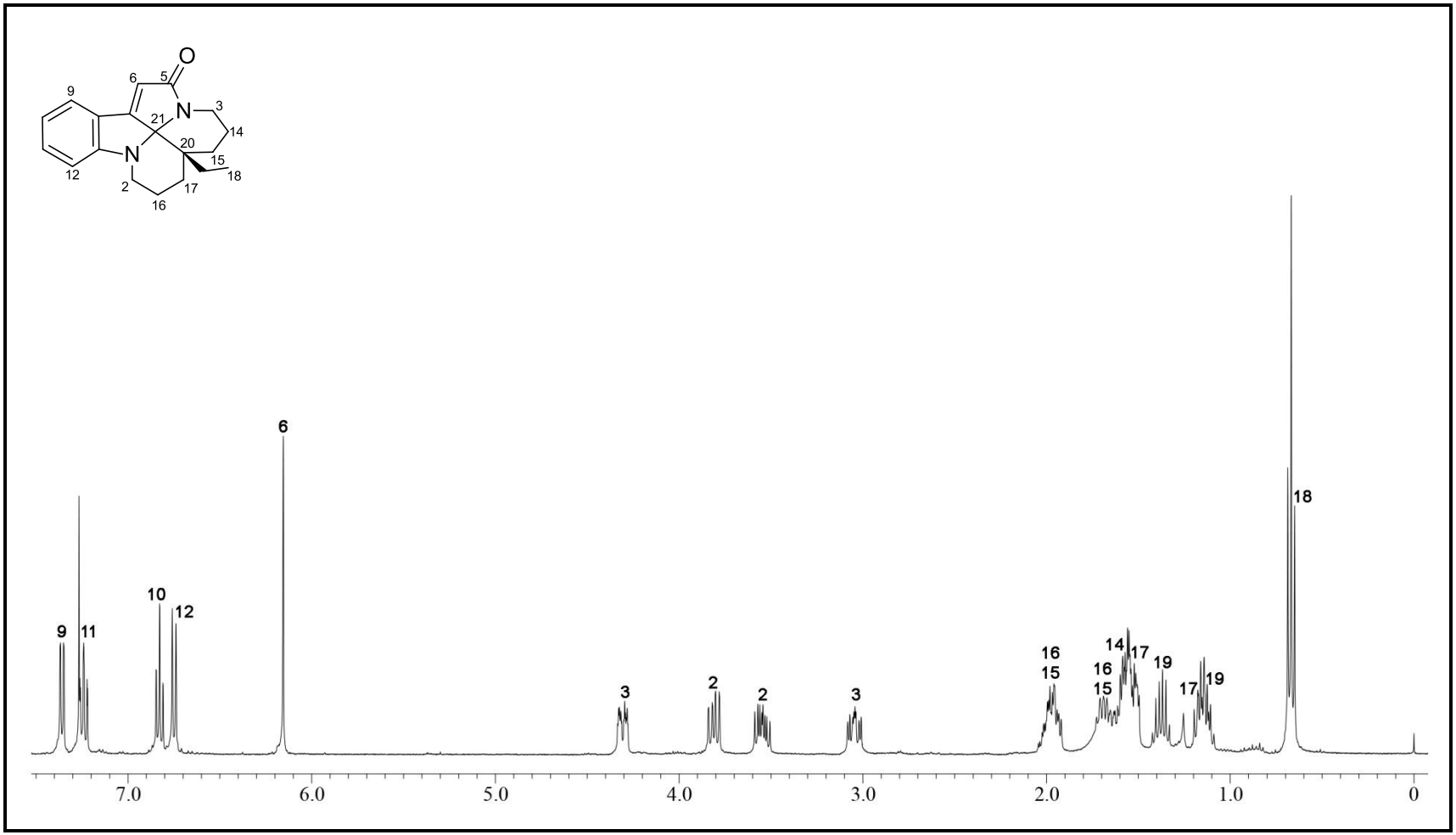

Figure 4.20. ^{1}H NMR spectrum ($CDCl_3$, 400 MHz) of compound **86**.

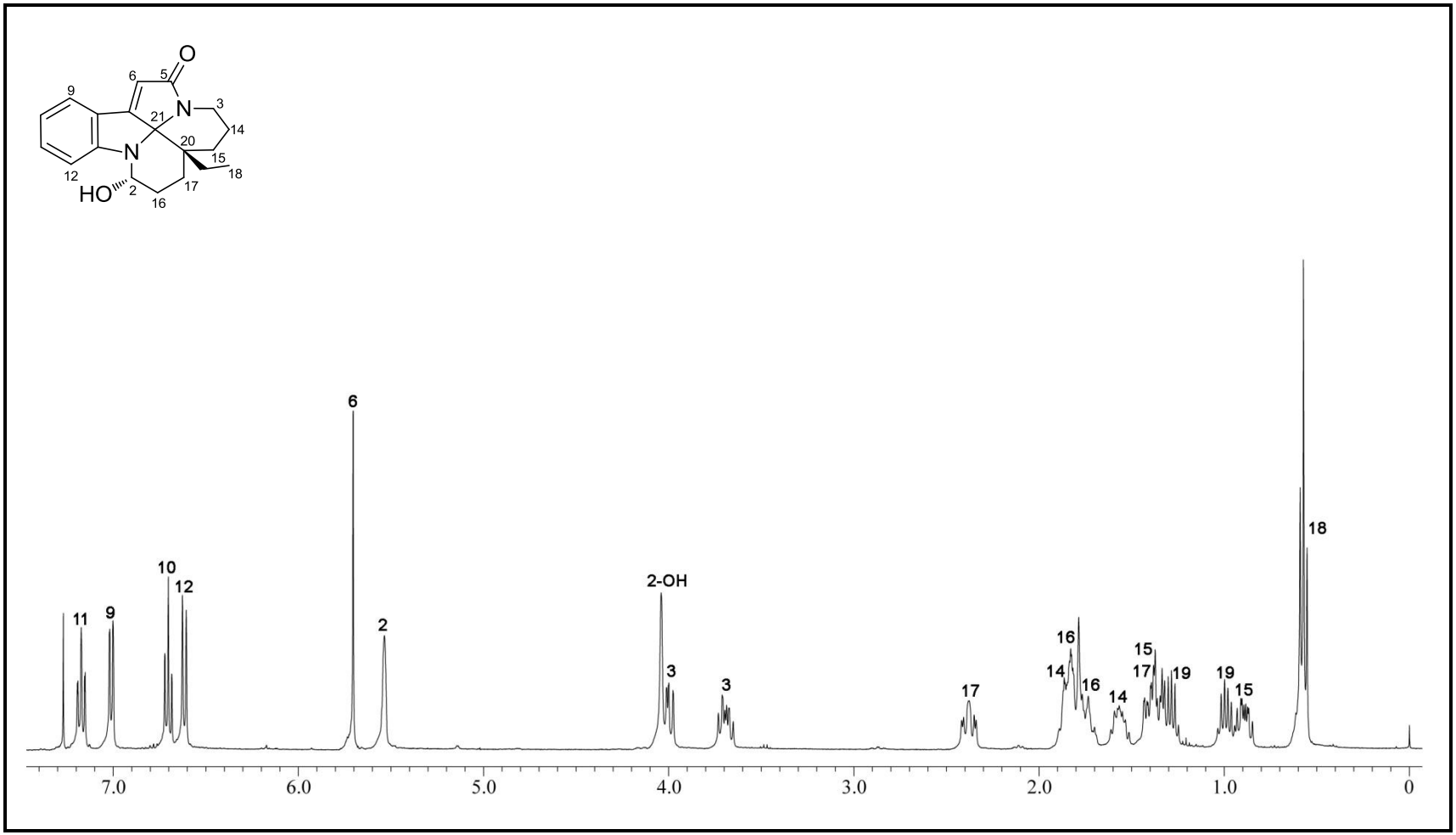

Figure 4.21. ^{1}H NMR spectrum ($CDCl_3$, 400 MHz) of compound **87**.

Since suitable crystals of compounds **86** and **87** were obtained, X-ray diffraction analyses were carried out, confirming the gross structures proposed by NMR data. The X-ray crystal structures of compounds **86** and **87** are shown in Figures 4.22 and 4.23, respectively.

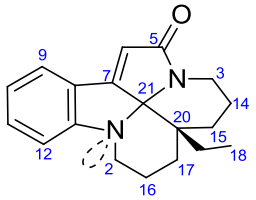

86

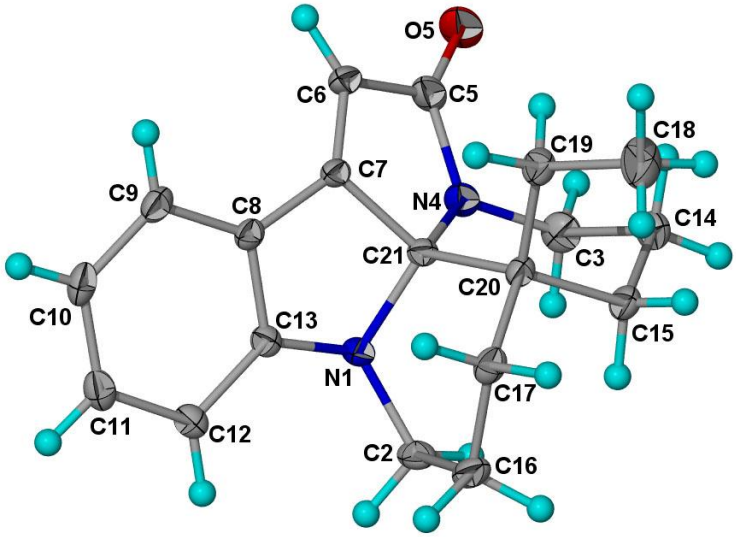

Figure 4.22. X-ray crystal structure of **86**.

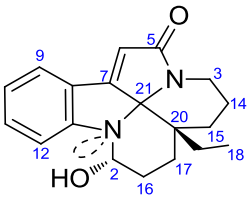

87

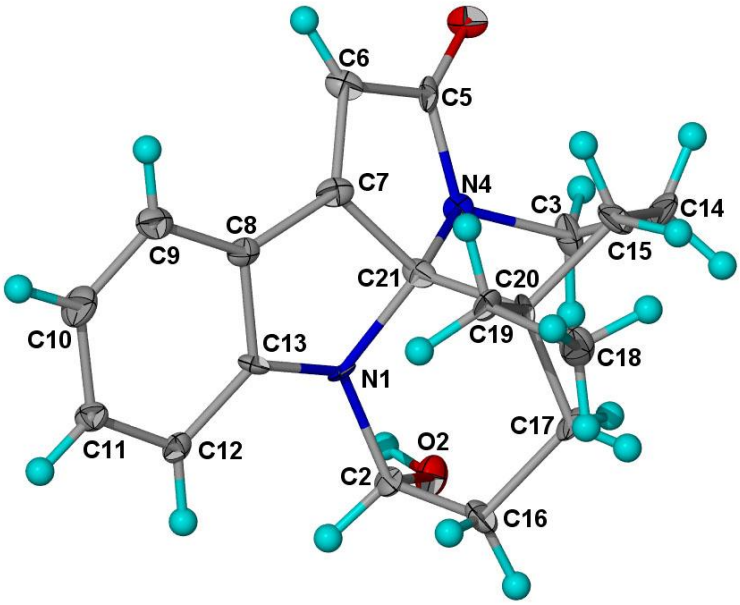

Figure 4.23. X-ray crystal structure of **87**.

A possible mechanism for the formation of compounds **86** and **87** is shown in Scheme 4.14. Since boranes are electron-deficient species, they behave as Lewis acids.[71,72] Reduction proceeds with an electrophilic attack on the C-2 lactam carbonyl to form complex **88**. After a hydride transfer, an alkaloid-borane complex **89** was generated, followed in succession by elimination and reduction to give **86**. Alternatively, the presence of traces of water in the system will result in quenching of the alkaloid-borane complex **89** to give compound **87**.

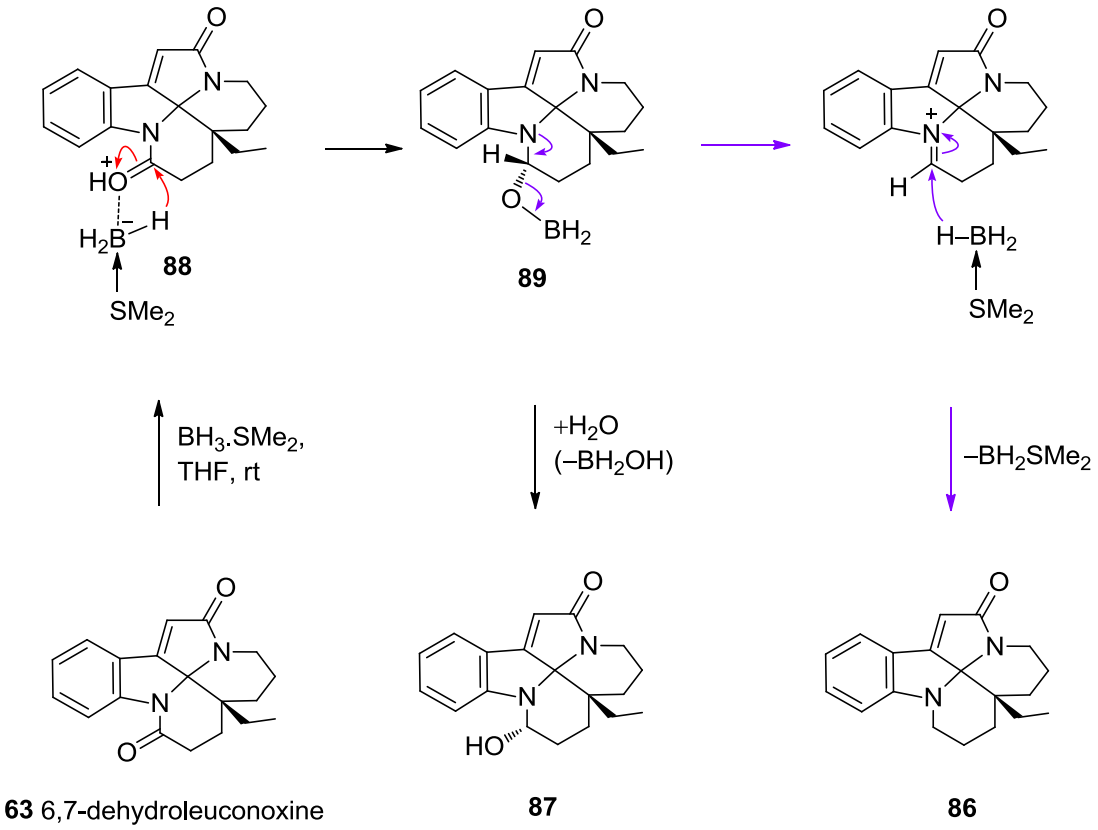

Scheme 4.14

4.2.5 Partial syntheses of leuconodines A and B

Since hydroboration of **63** did not furnish leuconodine A (**67**), a direct α-oxygenation of leuconoxine (**56**) at C-6, *via* enolate mediated oxidation was next attempted.

It turned out however, that treatment of leuconoxine (**56**) with lithium diisopropylamide (LDA) in THF at 0 ^{o}C, followed by oxidation of the lactam enolate with O_2,[73] gave compound **90** as the sole product (21%), accompanied by a significant amount of unreacted **56** (69%).

The enolate mediated oxidation occurred at C-16 instead of at C-6, possibly due to the formation of the more stable 6-membered enolate (Scheme 4.15).

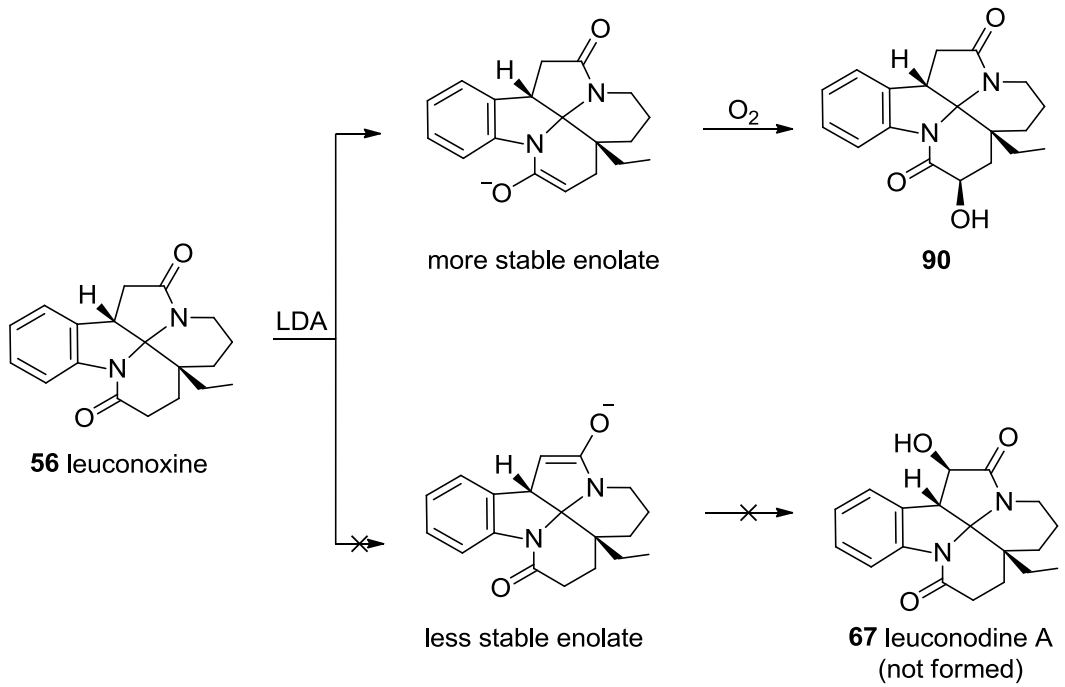

Scheme 4.15

Compound **90** was obtained as a colorless oil, and subsequently as colorless needles from CH_2Cl_2/hexanes (mp 184–186) with $[\alpha]^{25}_D = -29$ (*c* 0.16, $CHCl_3$). The UV spectrum showed absorption maxima at 210, 241, and 374 nm, while the IR spectrum showed the presence of an OH (3417 cm^{-1}) and carbonyl functions (1691 cm^{-1}, broad). The ESIMS of **90** showed an $[M + H]^+$ peak at *m/z* 327, in agreement with the molecular formula $C_{19}H_{22}N_2O_3$ + H. Notable differences in the ^{1}H NMR spectrum of **90** when compared with that of **56** include the downfield shift of H-16 from δ_H 2.78 and 2.49 in **56** to δ_H 4.45 in **90** and the presence of an OH peak at δ_H 3.28 (exchangeable with D_2O) in **90**. The ^{13}C NMR data showed that the resonance due to C-16 had shifted downfield (δ_C 64.9), when compared to that of **56**. These results strongly suggested that oxidation had occurred at C-16. The relative configuration at C-16 was assigned as *R*, based on the observed NOE between H-16 and H-15α. The ^{1}H and ^{13}C NMR data of **90** are summarized in Table 4.11, while the ^{1}H NMR spectrum of **90** is shown in Figure 4.24.

Table 4.11. ^{1}H and ^{13}C NMR data (δ) of compound **90**[a]

Position	δ_C	δ_H
2	175.0	–
3	36.8	2.69 ddd (13.5, 4.5, 1.5)
		3.81 m
5	171.0	–
6	37.4	2.56 d (17)
		2.77 dd (17, 7.8)
7	42.4	3.83 d (7.8)
8	135.3	–
9	124.0	7.22 m
10	126.3	7.13 m
11	128.0	7.21 m
12	120.9	7.60 br d (7.8)
13	140.9	–
14	20.0	1.51 m
		1.56 m
15	28.1	1.66 m
		1.82 ddd (14.5, 11, 4)
16	64.9	4.45 dd (13, 6)
17	35.9	1.50 m
		2.26 dd (13, 6)
18	7.5	0.88 t (7.3)
19	29.3	1.38 dq (14.5, 7.1)
		1.66 m
20	38.9	–
21	93.7	–
16-OH	–	Not observed

[a]$CDCl_3$, 400 and 100 MHz, respectively; assignments based on COSY, HMQC, and HMBC.

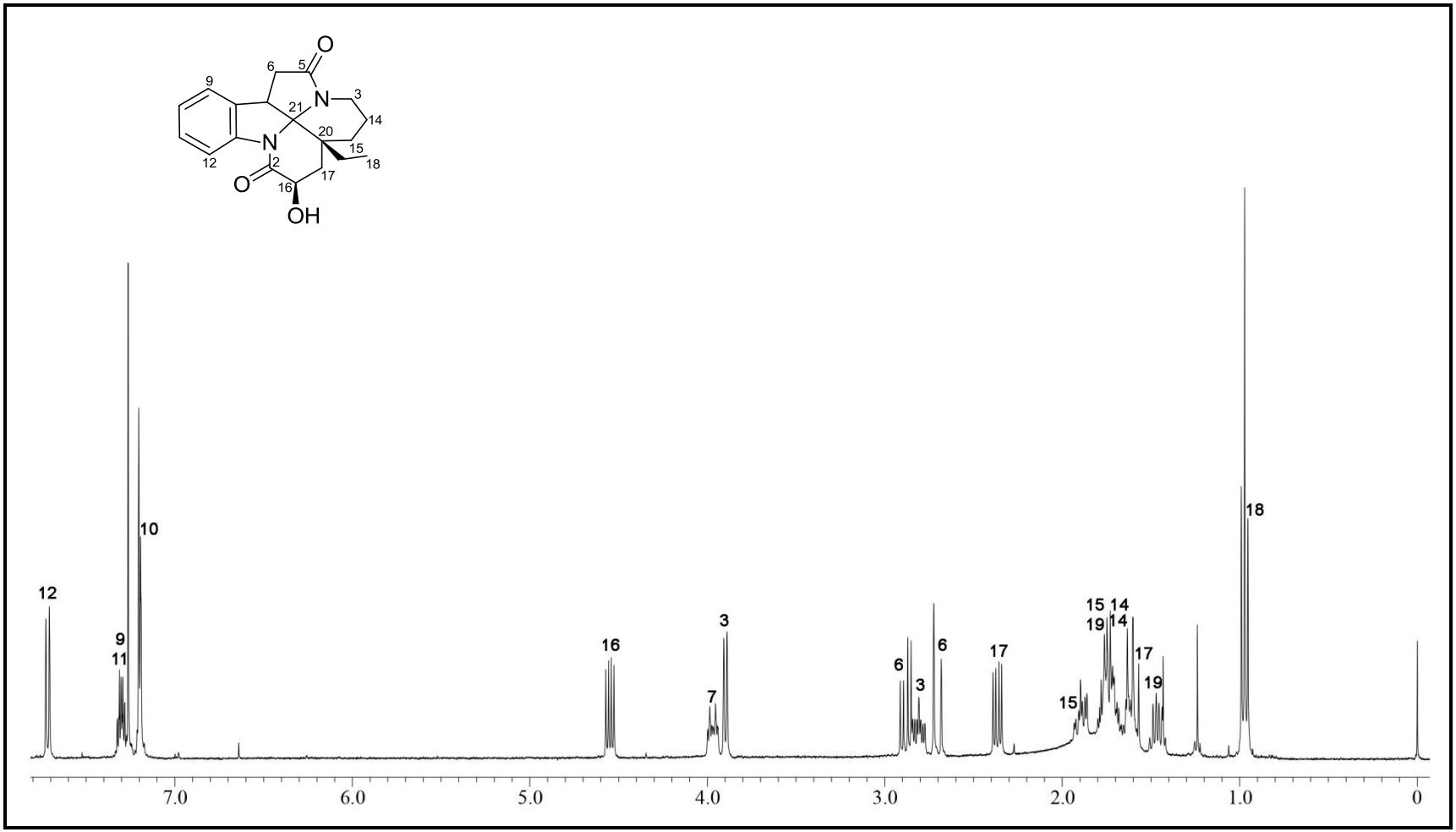

Figure 4.24. ^{1}H NMR spectrum ($CDCl_3$, 400 MHz) of compound **90**.

Since suitable crystals of **90** were obtained from CH_2Cl_2/hexanes, an X-ray diffraction analysis was carried out, which confirmed the above observations, as well as yielding the relative configuration (Figure 4.25).

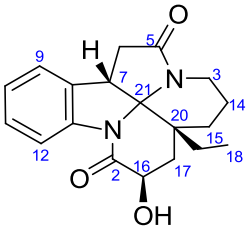

90

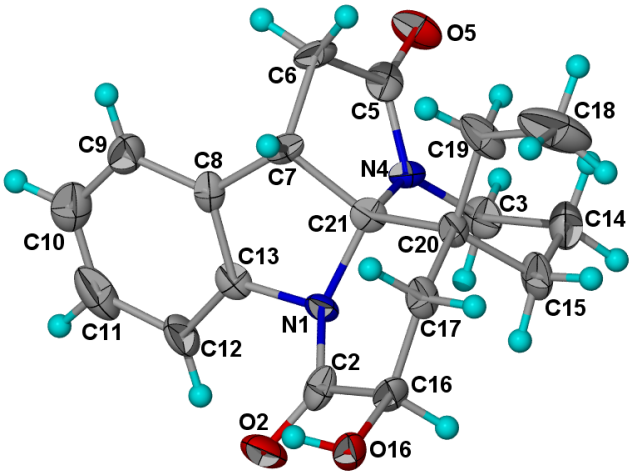

Figure 4.25. X-ray crystal structure of **90**.

Leuconodine A (**67**) was eventually obtained by treatment of leuconolam (**54**) with excess trifluoroacetic acid (TFA). Treatment of leuconolam (**54**) with TFA (2 equiv) resulted in transannular cyclization to 6,7-dehydroleuconoxine (**63**) (Scheme 4.16). The use of excess TFA (20 equiv) gave a mixture of two products, *viz.*, **63** (30% yield) and leuconodine A (**67**) (25% yield) (Scheme 4.16).

The formation of **63** and **67** in the presence of excess TFA is rationalized in Scheme 4.17. In the presence of excess TFA, conjugate addition by the TFA anion to the conjugated iminium ion **79**, competes with transannular cyclization to **63**, leading eventually to leuconodine A (**67**). Dess-Martin periodinane (DMP) oxidation of leuconodine A (**67**) gave another newly found leuconoxine alkaloid, leuconodine F (**72**) (76% yield) (Scheme 4.17).

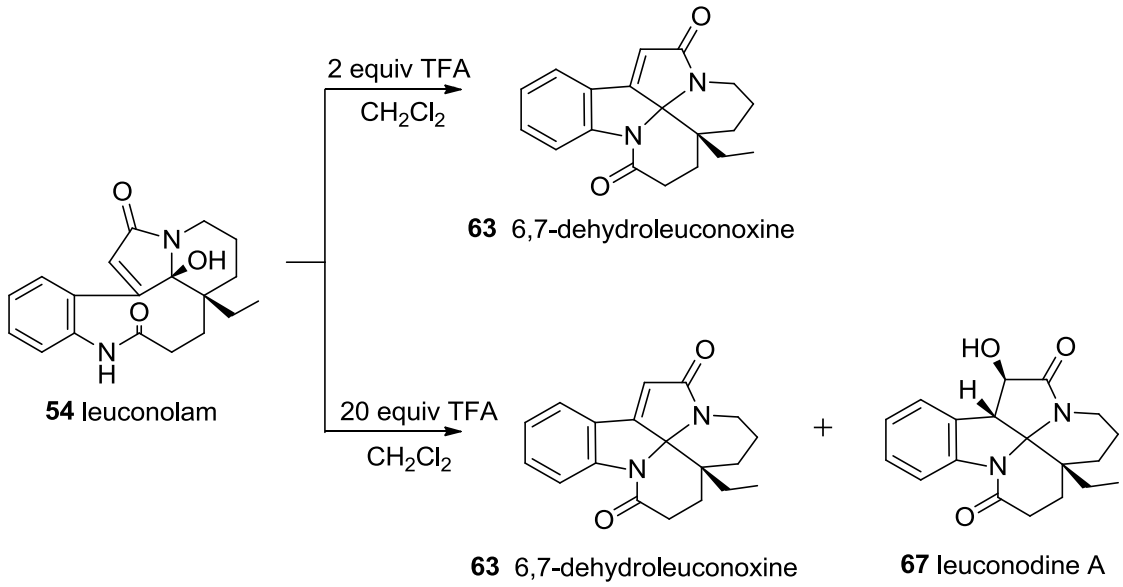

Scheme 4.16

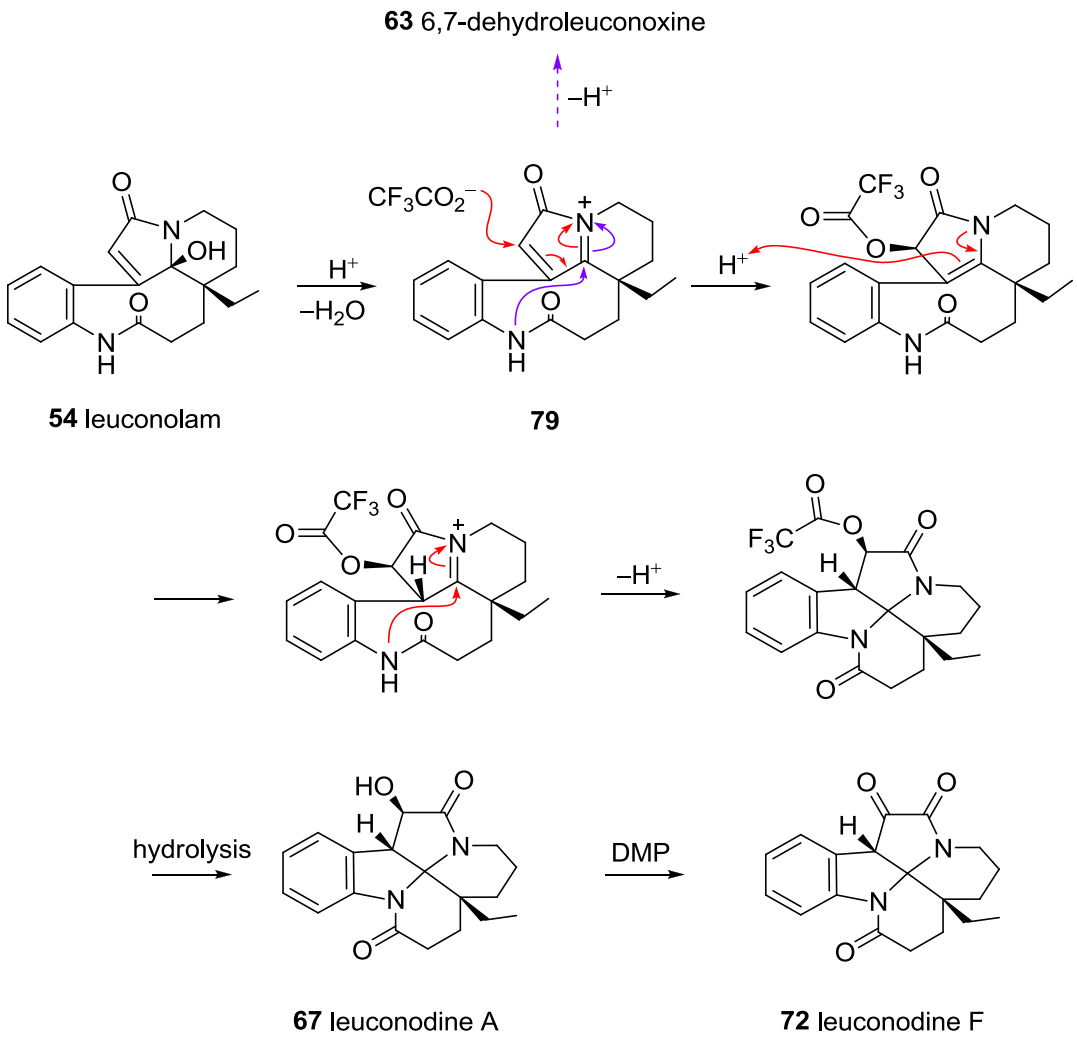

Scheme 4.17

Leuconodine A (**67**) was obtained as a colorless oil, and subsequently as colorless block crystals from EtOH/CH_2Cl_2 (mp 134–137 ^oC) with $[\alpha]^{25}_D = -19$ (*c* 0.21, $CHCl_3$). The UV spectrum showed absorption maxima at 209, 241, and 277 nm, while the IR spectrum showed the presence of OH (3357 cm^{-1}) and C=O (1676 cm^{-1}, lactam) functionalities. The EIMS of **67** showed an $[M]^+$ at *m/z* 326, while HREIMS measurements gave the molecular formula as $C_{19}H_{22}N_2O_3$. The ^{13}C NMR data (Table 4.12) showed a total of 19 carbon resonances, in agreement with the molecular formula. The ^1H and ^{13}C NMR spectra of **67** were somewhat similar to those of the known alkaloid, leuconoxine (**56**). The ^1H NMR spectrum of **67** showed a broad OH singlet at δ_H 5.11 (exchangeable with D_2O), while the ^{13}C NMR spectrum of alkaloid **67** indicated the absence of the resonance at δ_C 37.6, which was replaced by a lower field resonance at δ_C 75.1 (an indication of oxygenation). The methine singlets at δ_H 3.90 and 4.51 were assigned to H-7 and H-6, respectively, based on the observed three-bond correlations from H-7 to C-5 and C-9, and from H-6 to C-8 and C-21. The HMQC spectrum showed a H-C correlation between the methine singlet at δ_H 4.51 and the carbon resonance at δ_C 75.1, suggesting that oxygenation had occurred at C-6. The relative configuration of C-7 in **67** was deduced to be *S*, by analogy to leuconoxine (**56**) and its congeners, where any substituents attached to C-7 in the diazaspiro leuconoxine skeleton have to be *β*-oriented. The C-6 configuration was assigned as *R*, based on the small coupling constant observed between H-6 and H-7 ($J \sim 0$ Hz), *i.e.*, dihedral angle ~ 90°, as well as from the observed reciprocal NOEs between H-6 and H-9. The ^1H and ^{13}C NMR data of **67** are summarized in Table 4.12, while the ^1H NMR spectrum of natural **67**[58] and semisynthetic **67** are shown in Figures 4.26 and 4.27, respectively.

Table 4.12. ^{1}H and ^{13}C NMR data (δ) of leuconodines A (**67**) and F (**72**)[a]

Position	**67**		**72**	
	δ_C	δ_H	δ_C	δ_H
2	173.1	–	172.2	–
3	36.8	2.89 ddd (13, 11, 4)	37.8	3.10 ddd (13, 11, 4)
		3.99 ddd (13, 5, 2)		4.11 ddt (13, 5, 2.3)
5	172.0	–	157.5	–
6	75.1	4.51 s	192.5	–
7	49.6	3.90 s	53.4	4.23 s
8	132.1	–	126.2	–
9	124.5	7.27 dd (7.8, 1)	125.1	7.22 dd (7.6, 1)
10	125.4	7.13 td (7.8, 1)	125.9	7.16 td (7.6, 1)
11	128.3	7.25 td (7.8, 1)	129.9	7.37 td (7.6, 1)
12	119.6	7.87 dd (7.8, 1)	121.0	7.82 dd (7.6, 1)
13	141.9	–	142.6	–
14	19.4	1.70 m	20.1	1.71 m
		1.70 m		1.71 m
15	27.3	1.64 m	26.3	1.71 m
		1.92 m		2.05 m
16	30.2	2.53 ddd (19, 6, 1.4)	29.5	2.59 ddd (19, 6, 1.4)
		2.78 ddd (19, 14, 6.5)		2.86 ddd (19, 14, 6.5)
17	27.5	1.60 m	26.6	1.66 td (14, 6)
		1.94 m		1.98 ddd (14, 6.5, 1.4)
18	7.7	0.90 t (7.3)	7.3	0.92 t (7.4)
19	28.5	1.49 dq (13, 7.3)	27.7	1.23 dq (13, 7.4)
		1.96 m		1.49 dq (13, 7.4)
20	36.7	–	37.6	–
21	93.5	–	88.0	–
6-OH	–	not observed[b]	–	–

[a]$CDCl_3$, 400 and 100 MHz, respectively; [b]6-OH was observed at δ_H 5.11 as a broad singlet in natural **67**;[58] assignments based on COSY, HMQC, and HMBC.

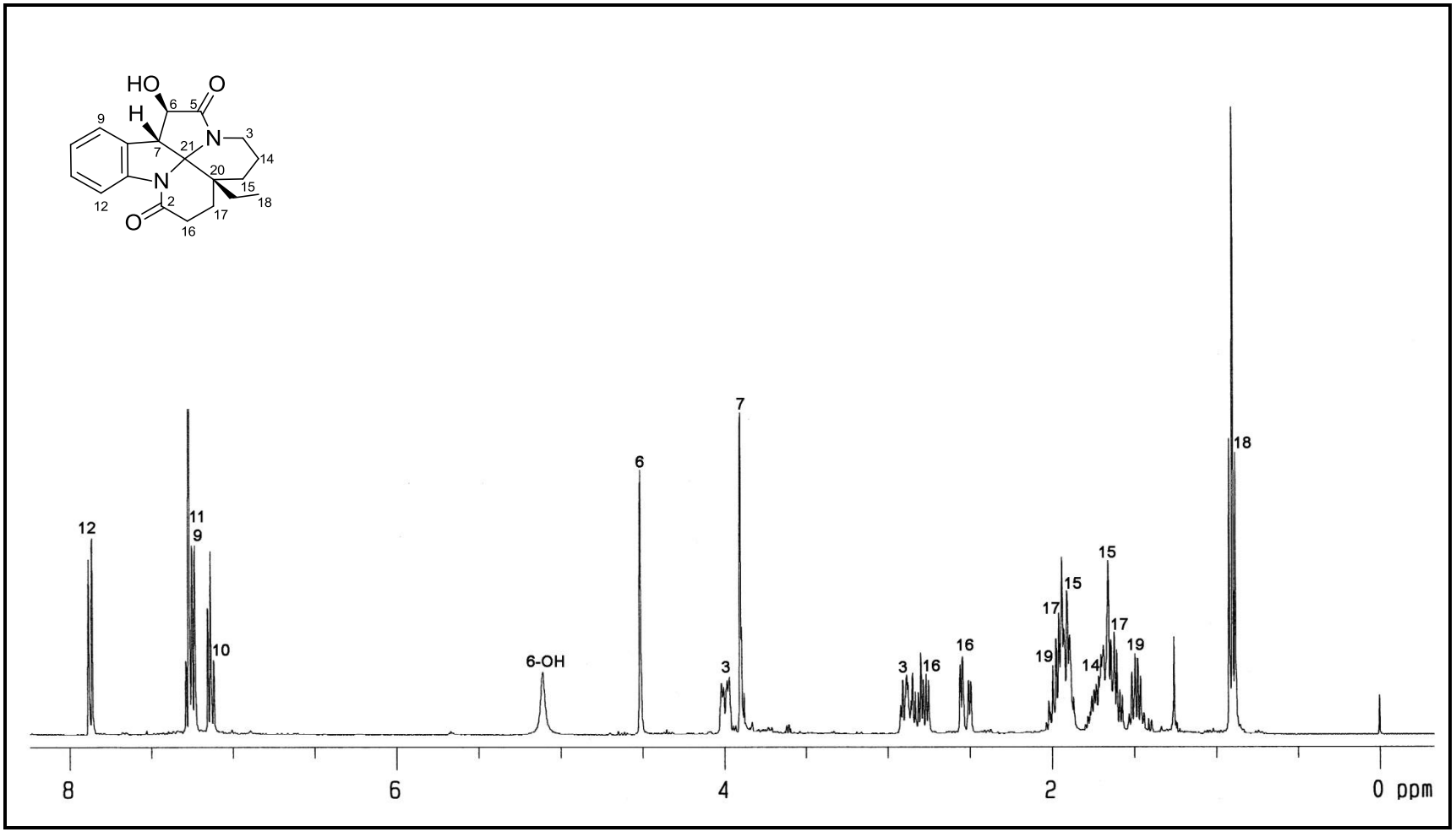

Figure 4.26. ^{1}H NMR spectrum ($CDCl_3$, 400 MHz) of natural leuconodine A (**67**).[58]

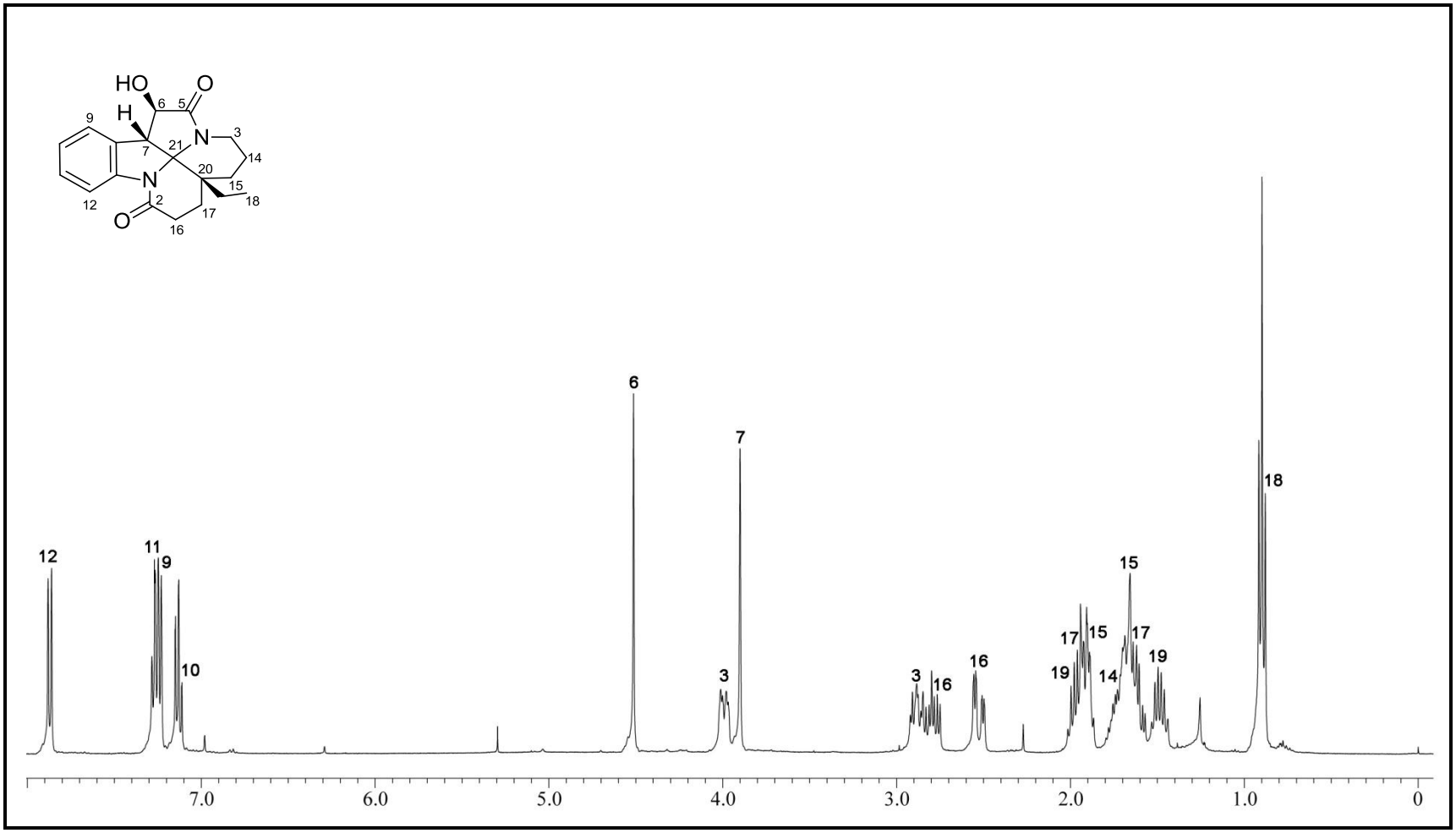

Figure 4.27. ^{1}H NMR spectrum ($CDCl_3$, 400 MHz) of semisynthetic leuconodine A (**67**).

Since suitable crystals of compound **67** were obtained from EtOH/CH_2Cl_2, an X-ray diffraction analysis was carried out (Figure 4.28), confirming all of the above observations. It can be seen that **67** co-crystallized with the solvent molecule used during crystallization (EtOH). The EtOH molecule formed a hydrogen bond with the C-5 lactam carbonyl.

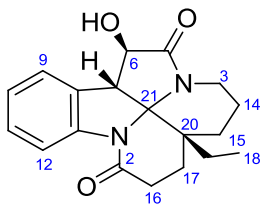

67 Ieuconodine A

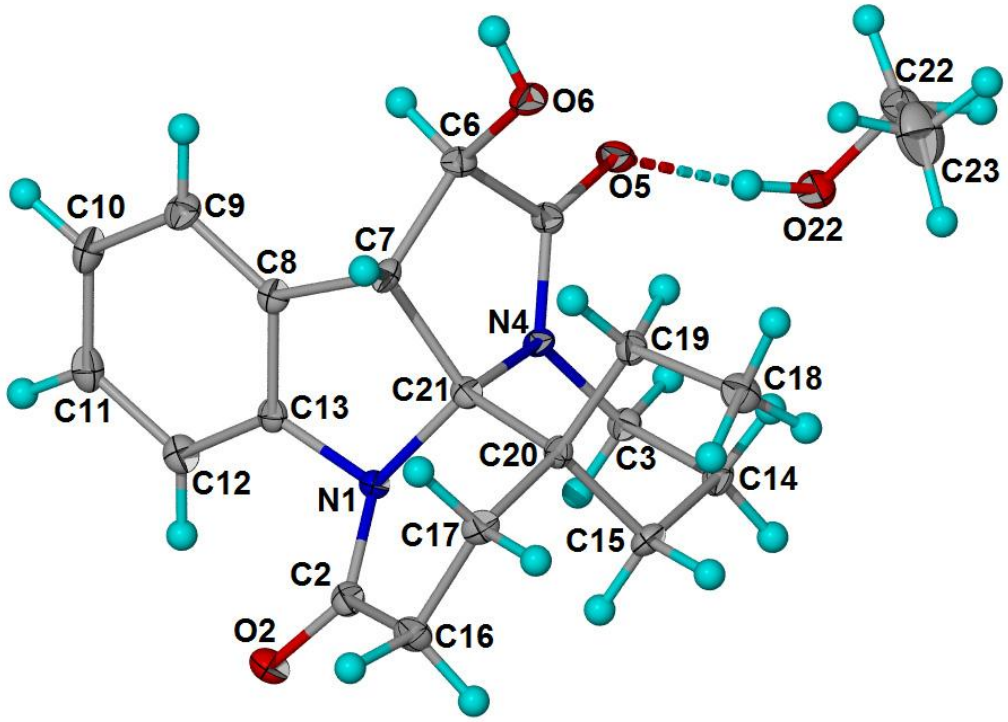

Figure 4.28. X-ray crystal structure of **67**.

Leuconodine F (**72**) was obtained as a colorless oil, and subsequently as colorless block crystals from MeOH (mp 246–250 ^{o}C) with $[\alpha]^{25}_{D}$ = +94 (*c* 0.05, $CHCl_3$). The UV spectrum displayed absorption maxima at 203, 232, 254, and 350 nm, while the IR spectrum showed, in addition to the lactam carbonyl functions (1689 cm^{-1}, broad), a band at 1715 cm^{-1} due to a ketone. The presence of the ketone carbonyl function was also indicated by the carbon resonance at δ_C 192.5 in the ^{13}C NMR spectrum. The EIMS of **72** showed an $[M + H]^+$ at *m/z* 325, while HREIMS measurements gave the molecular formula as $C_{19}H_{20}N_2O_3$ + H, differing from leuconoxine (**56**) by 14 mass units, suggesting **72** to be an oxo-derivative of leuconoxine (**56**). The ^{1}H and ^{13}C NMR data were generally similar to those of leuconoxine (**56**), except for the absence of the signals due to H-6. The signal due to H-7 was now observed as a singlet at δ_H 4.23 indicating that H-7 was unusually deshielded as a result of its proximity to the ketone carbonyl function. This confirmed the location of the ketone function at C-6. The ^{1}H and ^{13}C NMR data of **72** are summarized in Table 4.12, while the ^{1}H NMR spectrum of natural **72**[58] and semisynthetic **72** are shown in Figures 4.29 and 4.30, respectively.

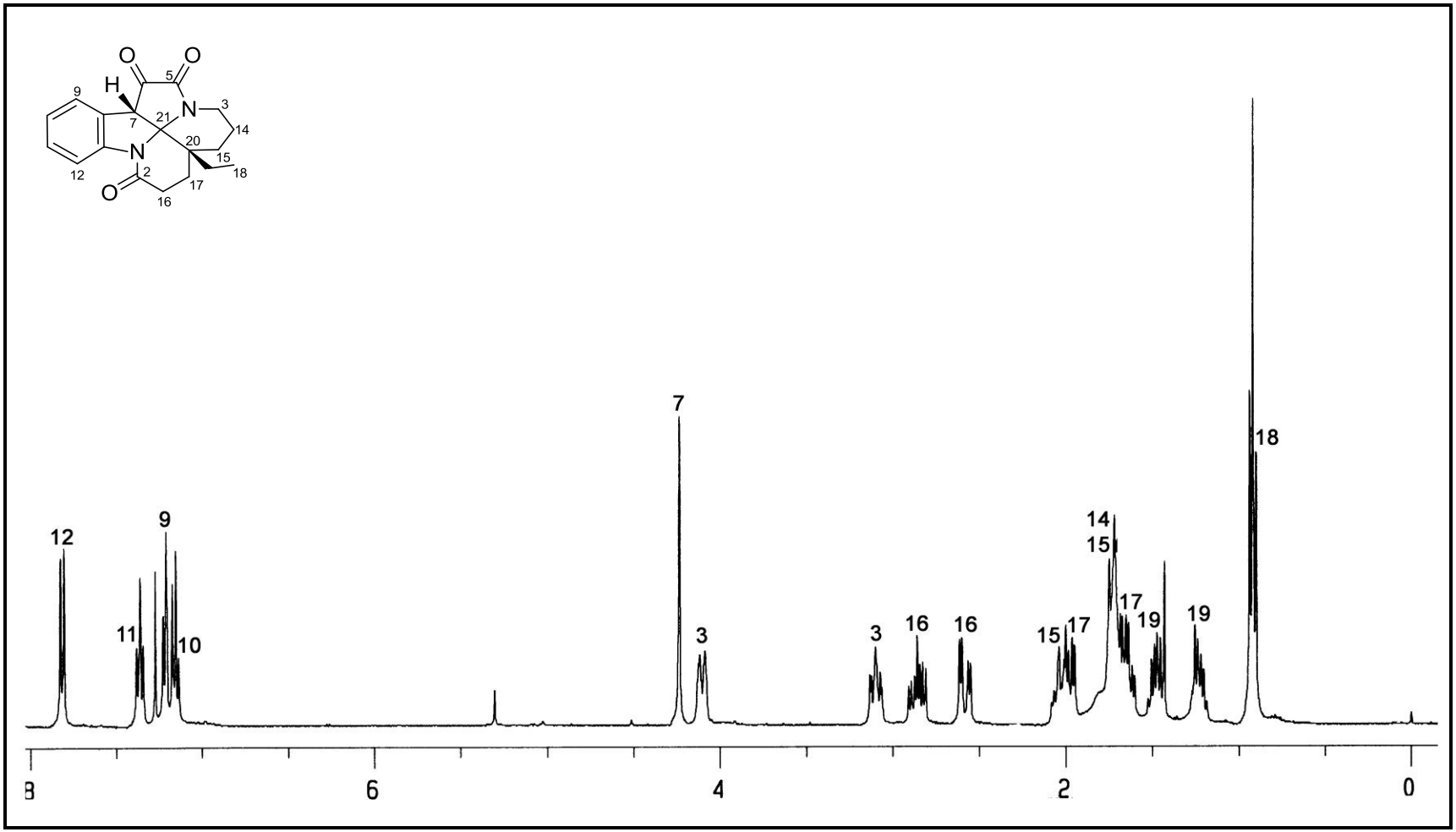

Figure 4.29. ^{1}H NMR spectrum ($CDCl_3$, 400 MHz) of natural leuconodine F (**72**).[58]

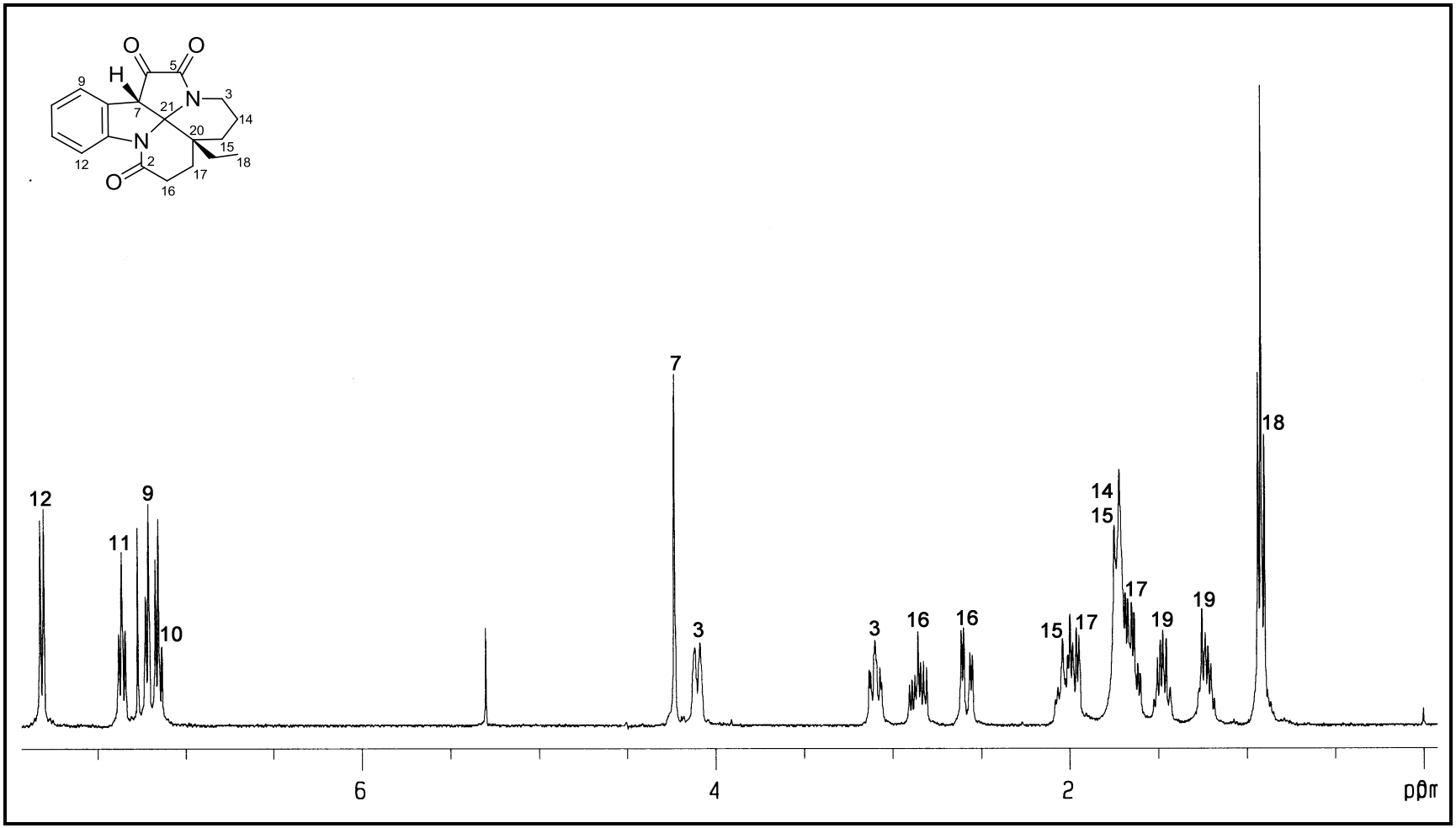

Figure 4.30. ^{1}H NMR spectrum ($CDCl_3$, 400 MHz) of semisynthetic leuconodine F (**72**).

Since suitable crystals of compound **72** were obtained from CH_2Cl_2/hexanes, an X-ray diffraction analysis was carried out (Figure 4.31), confirming all of the above observations.

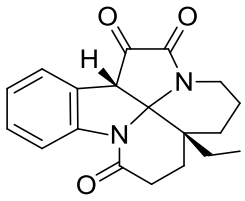

72 leuconodine F

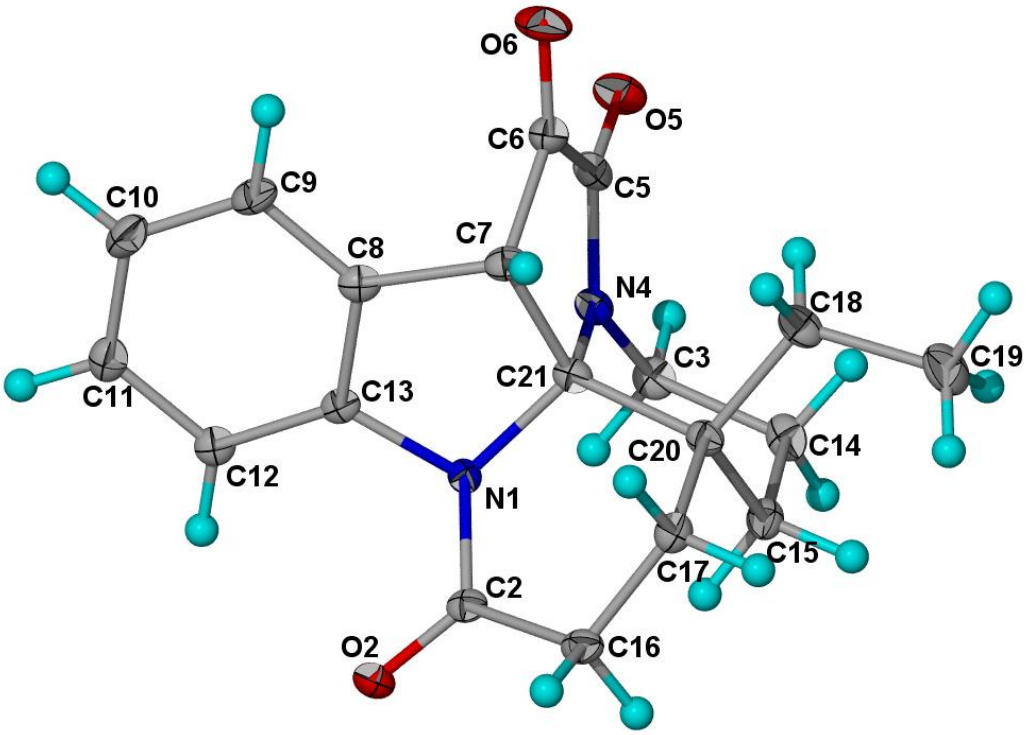

Figure 4.31. X-ray crystal structure of **72**.

4.3 Conclusion

Several reactions of the ring-opened *Aspidosperma* alkaloid, leuconolam (**54**), were investigated. The based-induced reaction of leuconolam (**54**) resulted in enolate-mediated transannular closure to give two epimeric pentacyclic meloscine-like products (**74** and **76**), while the acid-induced reactions (HCl in two-phase medium, CSA in CH_2Cl_2) resulted in transannular closure to give 6,7-dehydroleuconoxine (**63**). A two-step sequence from leuconolam (**54**), comprising acid-induced closure, followed by catalytic hydrogenation, provided a concise semisynthesis of leuconoxine (**56**). When the acid-induced reaction of leuconolam (**54**) (or 6,7-dehydroleuconoxine (**63**)) was carried out with PTSA in CH_2Cl_2, the product was the amino lactam-lactone **78**, while the acid-induced reactions in the presence of MeOH as solvent furnished *O*-methylleuconolam (**77**) as the sole product in high yields. The original assignment of the structure of *epi*-leuconolam (**55**) was revised to 6,7-dehydroleuconoxine (**63**) based on X-ray diffraction analysis. Bromination ($Br_2/CHCl_3$) of leuconolam (**54**) proceeds in two steps *via* intermediacy of 6,7-dehydroleuconoxine (**63**) to furnish the 6*β*,7*β*-dibromoleuconoxine adduct (**82**). Concise semisynthesis of the new leuconoxine-type alkaloids, leuconodines A and F (**67** and **72**, respectively), was achieved by treatment of leuconolam (**54**) with excess TFA (which gave leuconodine A (**67**) as the minor product), followed by oxidation of **67** to leuconodine F (**72**).

CHAPTER FIVE

Partial Syntheses of the New Strychnan Alkaloid, Alstolucine A, and the New Eburnane Alkaloid, (–)-Eburnamaline

5.1 Alstolucine A

5.1.1 Introduction

Alstolucine A (**91**) is a new strychnan-type alkaloid obtained from the leaf extract of *Alstonia spatulata* (isolation and structure by S. J. Tan).[74]

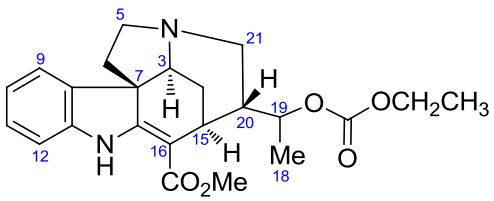

91 alstolucine A

Alstolucine A (**91**) was obtained as a light yellowish oil, with $[\alpha]^{25}_{D}$ –438 (*c* 0.12, $CHCl_3$). The UV spectrum showed absorption maxima at 230, 298, and 328 nm, characteristic of a *β*-anilinoacrylate chromophore.[75] The IR spectrum (thin film) showed a broadened band at 3378 cm^{-1} due to the indolic *N*H function, another band at 1742 cm^{-1} due to a carbonate group (–OCO_2–), and a band at 1683 cm^{-1} due to an *α,β*-unsaturated ester function. The ESIMS of **91** showed an $[M + H]^+$ peak at *m/z* 413, and HRESIMS measurements yielded the molecular formula $C_{23}H_{29}N_2O_5$ + H (DBE 11).

The ^{13}C NMR data (Table 5.1) showed all 23 carbon resonances, comprising three methyl, five methylene, eight methine, and seven quaternary carbons. The

presence of conjugated ester and carbonate functionalities were supported by the observed quaternary carbon signals at δ_C 167.9 and 155.0, respectively, while the signals due to the two olefinic quaternary carbons at δ_C 167.9 (C-2) and 103.6 (C-16) were consistent with the presence of the β-anilinoacrylate moiety. Two downfield signals at δ_C 76.5 and 63.8 were associated with the presence of oxymethine and oxymethylene moieties, respectively.

The ^{1}H NMR data (Table 5.1) showed the presence of an unsubstituted aromatic moiety, an indolic *N*H as a broad singlet at δ_H 8.92, an oxymethine at δ_H 4.76, an oxymethylene at δ_H 4.21, and three methyl groups. The highest field methyl at δ_H 1.33 (t, J = 7.0 Hz) was associated with the oxymethylene at δ_H 4.21, constituting part of an ethoxy moiety, while the methyl at δ_H 1.34 (d, J = 6.0 Hz) was adjacent to the oxymethine at δ_H 4.76 (m) as shown by the COSY spectrum. The remaining methyl at δ_H 3.77 (s) was associated with the conjugated methyl ester function.

The COSY, HMQC, and HMBC data revealed the structure of alstolucine A (**91**). The relative configuration at the various centers were established from the observed NOEs as well as analysis of the vicinal coupling constants, except for the carbon bearing the carbonate group at C-19, for which the NOE data proved inconclusive. A partial synthesis of **91** was therefore carried out, and the results obtained were used to establish the configuration at C-19. The ^{1}H and ^{13}C NMR data of alkaloid **91** are summarized in Table 5.1, while ^{1}H NMR spectrum of alkaloid **91** is shown in Figure 5.1.

An ideal starting material that bears a close resemblance to alstolucine A (**91**) would be the known alkaloid, *N*(4)-demethylalstogustine (**92**)[76] or its C-19 epimer (**93**).[77] Acylation of either **92** or **93** should lead to **91** (Scheme 5.1), which would then allow confirmation of the C-19 configuration of **91**. However, since both **92** and **93** were not available, another choice of starting material was indicated.

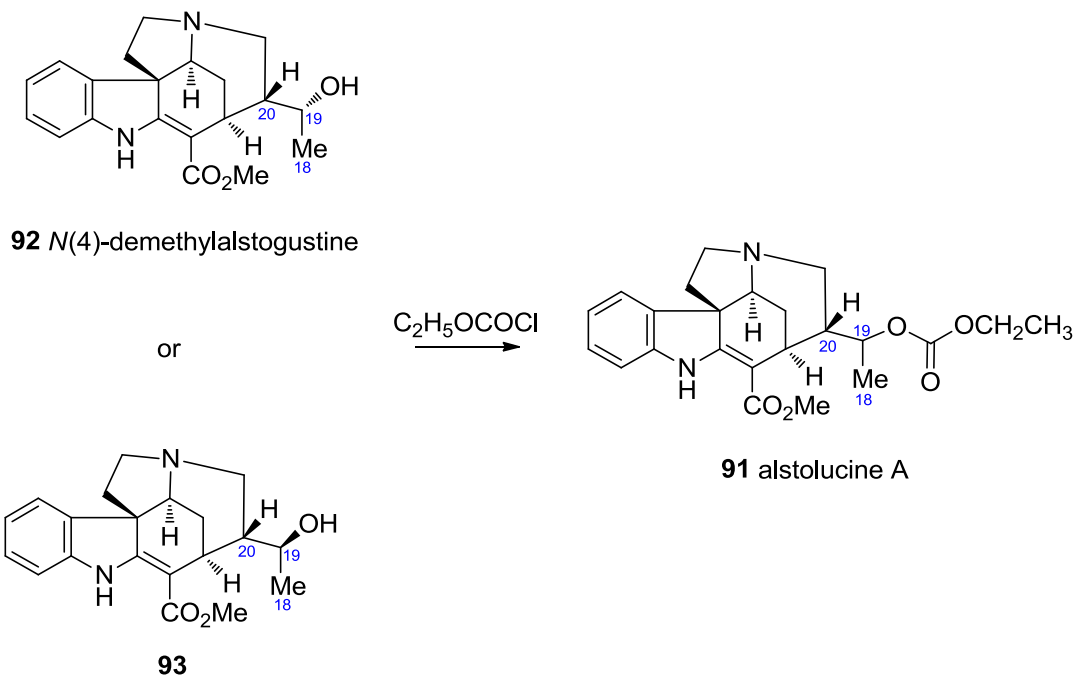

Scheme 5.1

An alternative starting material for the partial synthesis of alstolucine A (**91**) is alstolucine B (**94**),[74] a new alkaloid isolated from the same study. An advantage of using **94** as starting compound is that the structure and relative configuration of **94** can be established by NMR and X-ray diffraction analysis. The ^{1}H and ^{13}C NMR data of alkaloid **94** are summarized in Table 5.1, while the ^{1}H NMR spectrum of alkaloid **94** is shown in Figure 5.2. The X-ray crystal structure of **94** is shown in Figure 5.3.

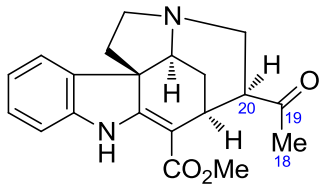

94 alstolucine B

Table 5.1. ^{1}H and ^{13}C NMR data (δ) of alstolucines A (**91**) and B (**94**)[a]

Position	**91**		**94**	
	δ_C	δ_H	δ_C	δ_H
2	167.9	–	172.2	–
3	58.9	4.04 m	60.6	3.87 br t (3.0)
5β	53.5	3.00 m	54.0	2.87 m
5α		3.20 ddd (11.4, 8.7, 6.6)		3.05 m
6α	45.6	2.00 m	43.4	1.83 m
6β		2.29 ddd (12.0, 8.0, 6.5)		3.04 m
7	58.1	–	56.7	–
8	135.3	–	135.4	–
9	120.8	7.20 br d (7.5)	119.6	7.15 br d (8.0)
10	120.9	6.90 br t (7.5)	121.1	6.90 td (8.0, 1.0)
11	127.8	7.14 td (7.5, 1)	127.6	7.11 td (8.0, 1.0)
12	109.6	6.82 br d (7.5)	109.7	6.80 br d (8.0)
13	144.1	–	144.2	–
14*R*	27.4	1.18 dt (13.6, 2.6)	31.7	1.47 dt (13.0, 3.0)
14*S*		2.24 dt (13.6, 3.5)		2.12 dt (13.0, 3.0)
15	27.0	3.09 m	30.8	3.47 m
16	103.6	–	96.5	–
18	17.2	1.34 d (6.0)	29.2	2.30 s
19	76.5	4.76 m	208.5	–
20	41.2	2.11 m	50.0	2.87 m
21α	47.6	2.67 dd (14.0, 6.0)	45.6	2.64 t (12.0)
21β		3.03 dd (14.0, 11.8)		2.83 dd (12.0, 4.0)
22	155.0	–	–	–
23	63.8	4.21 m	–	–
		4.21 m		
24	14.3	1.33 t (7.0)	–	3.68 s
CO_2<u>Me</u>	51.0	3.77 s	50.9	8.93 br s
<u>C</u>O_2Me	167.9	–	167.2	3.90 s
*N*H	–	8.92 br s	–	4.15 br s

[a]$CDCl_3$, 400 and 100 MHz, respectively; assignments based on COSY, HMQC, and HMBC.

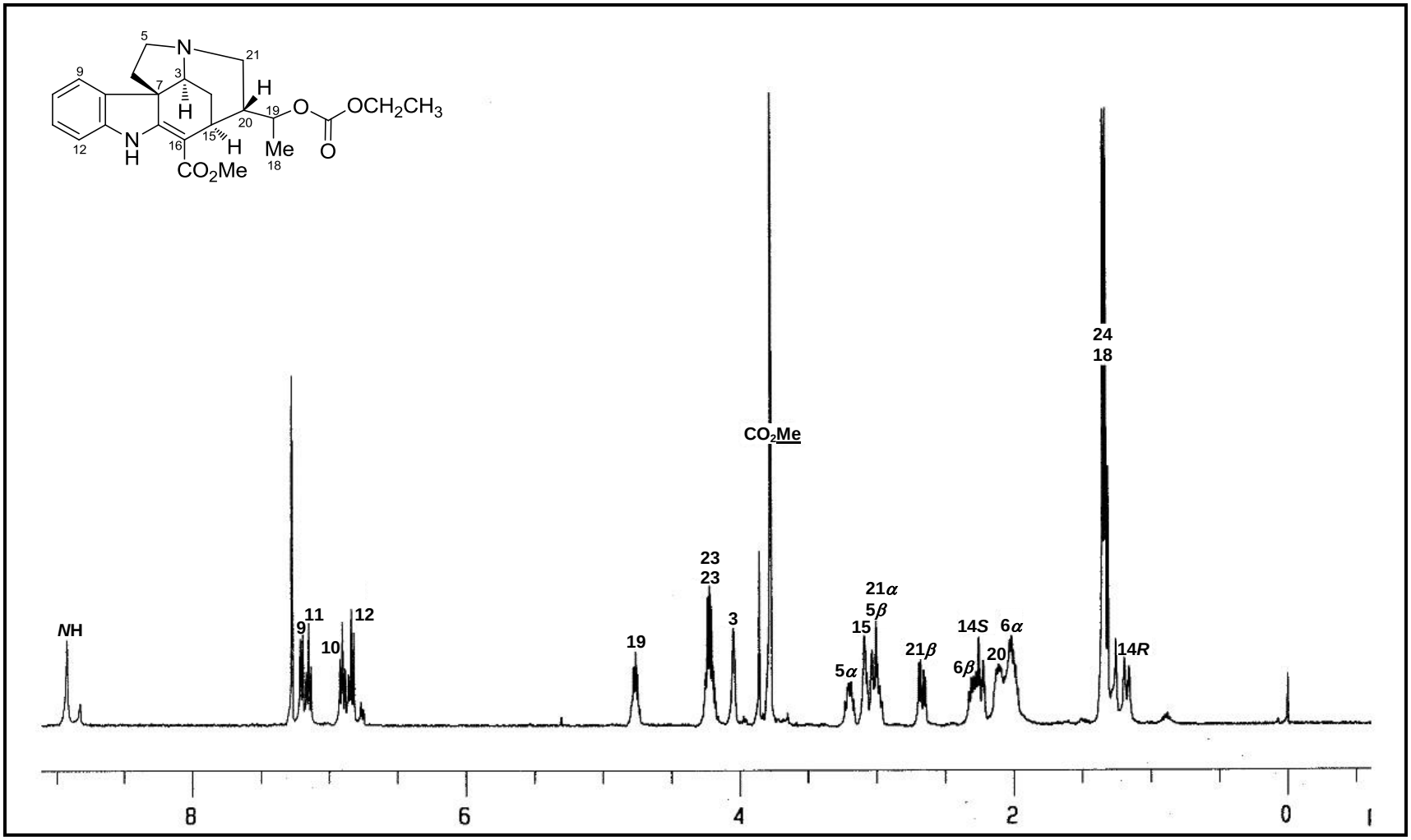

Figure 5.1. ^{1}H NMR spectrum ($CDCl_3$, 400 MHz) of natural alstolucine A (**91**).[78]

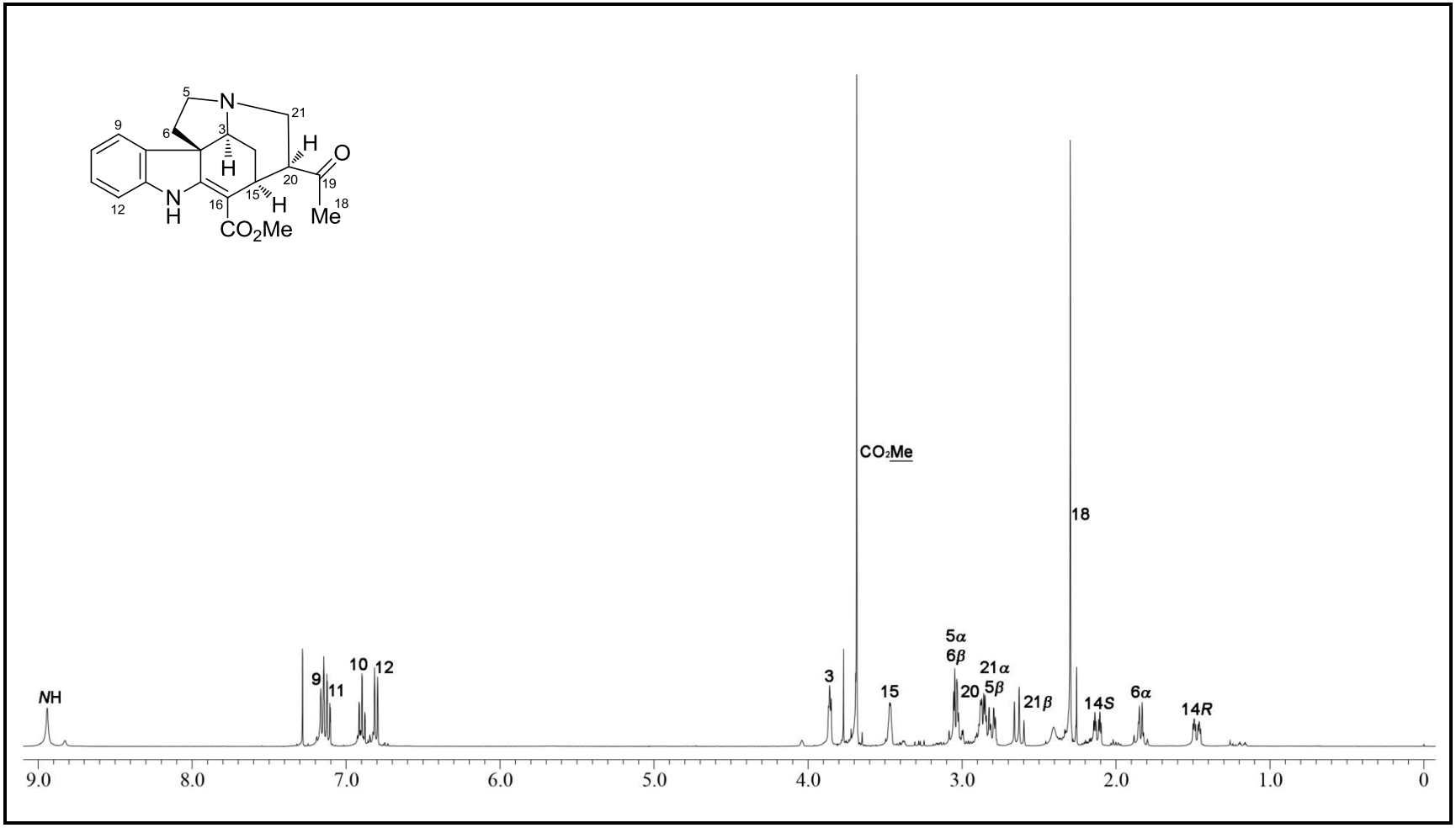

Figure 5.2. ^{1}H NMR spectrum ($CDCl_3$, 400 MHz) of alstolucine B (**94**).[78]

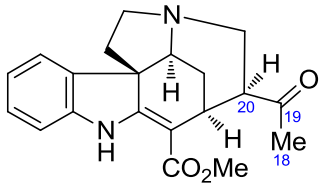

94 alstolucine B

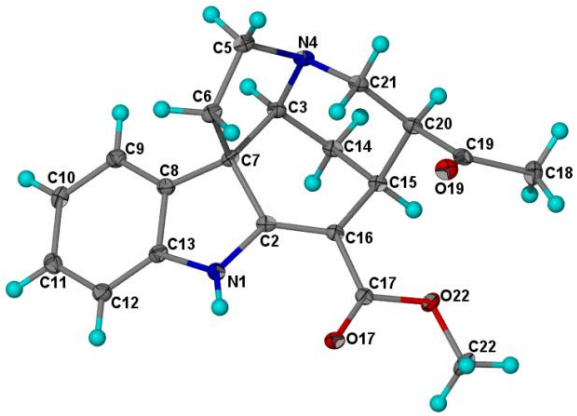

Figure 5.3. X-ray crystal structure of **94**.

In the event, the C-20 configuration of alstolucine B (**94**) as revealed by the X-ray diffraction analysis is 20*R*, which is opposite to that of alstolucine A (**91**, 20*S*). The first step in the transformation therefore requires epimerization of **94** to the C-20 epimer **95**, followed in succession by reduction to **92** (or **93**), and acylation to **91** (Scheme 5.2).

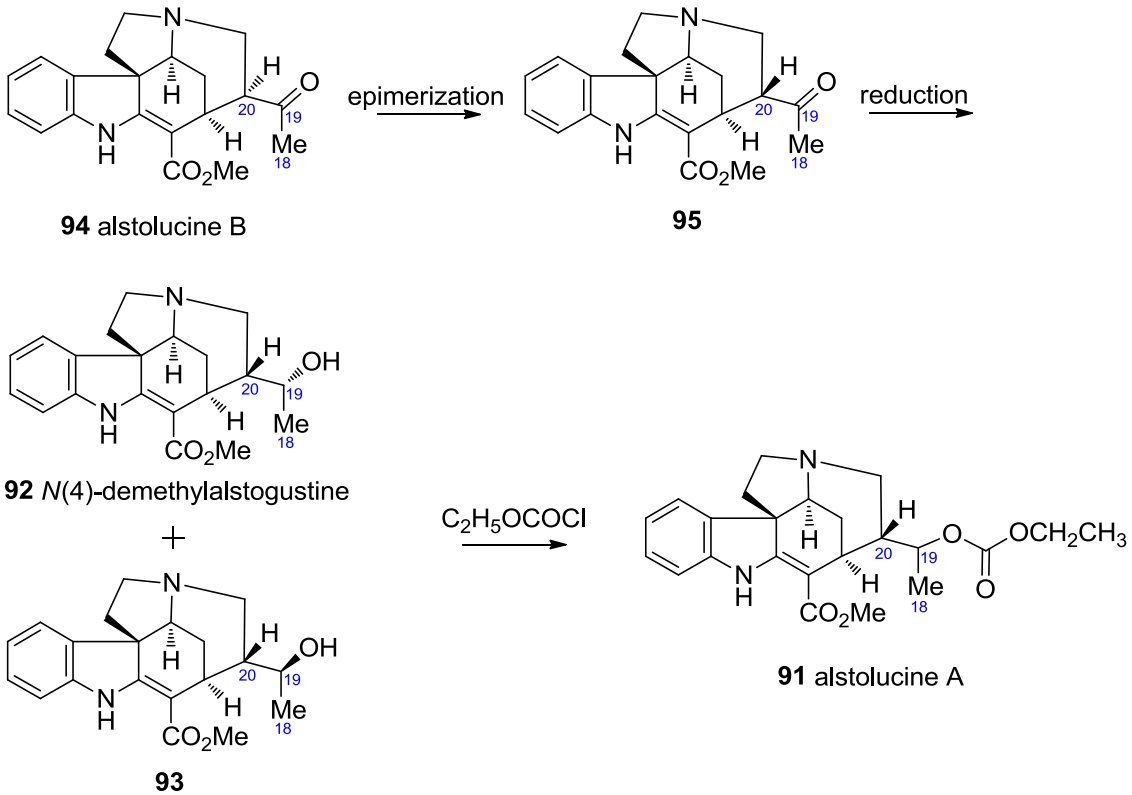

Scheme 5.2

5.1.2 Results and discussion

The partial synthesis was therefore carried out as outlined in Scheme 5.2. In the first step, treatment of alstolucine B (**94**) with NaOMe/MeOH (0 ^{o}C, 3 h) gave a 2:1 mixture of **94** and its C-20 epimer, **95** (Scheme 5.3).

Compound **95** was obtained as a light yellowish oil, with $[\alpha]^{25}_{D}$ −371 (*c* 0.35, $CHCl_3$). The UV spectrum showed absorption maxima at 229, 297, and 328 nm, while the IR spectrum (thin film) showed bands at 3378 (*N*H), 1704 (C=O), and 1678 (α,β-unsaturated ester) cm^{-1}. The ESIMS of **95** showed an $[M + H]^+$ at *m/z* 339, and HRESIMS measurements yielded the molecular formula $C_{20}H_{22}N_2O_3$. The ^{1}H and ^{13}C NMR data of **95** were identical to those of alstolucine B (**94**), except for differences in the chemical shift of H-20 in the ^{1}H NMR spectrum, and differences in the shifts of C-19, C-20, and C-21 in the ^{13}C NMR spectrum. Compound **95** is therefore the C-20 epimer of alstolucine B (**94**). The ^{1}H and ^{13}C NMR data of **95** are summarized in Table 5.2, while the ^{1}H NMR spectrum of **95** is shown in Figure 5.4.

Reduction of **95** with $NaBH_4$ in MeOH (0 ^{o}C, 1 h) gave two products: the major product (85%) was identical to *N*(4)-demethylalstogustine (**92**),[76] while the minor product (10%) was the corresponding C-19 epimer **93** (Scheme 5.3).[77]

The $[\alpha]_D$, UV, IR, MS, ^{1}H and ^{13} C NMR data of *N*(4)-demethylalstogustine (**92**) and its C-19 epimer **93** are identical to those reported in the literature.[76,77] The ^{1}H and ^{13}C NMR data of **92** and **93** are summarized in Table 5.2, while the ^{1}H NMR spectra of **92** and **93** are shown in Figures 5.5 and 5.6, respectively.

Subsequent treatment of *N*(4)-demethylalstogustine (**92**) with ethyl chloroformate and triethylamine in CH_2Cl_2 (5 equiv in 5 ml CH_2Cl_2, rt, 30 min) gave, after silica gel chromatography, an acylated derivative which was identical ($[\alpha]_D$, ^{1}H

and ^{13}C NMR, MS) with alstolucine A (**91**) (Scheme 5.3). The ^{1}H NMR spectrum of semisynthetic **91** is shown in Figure 5.7.

Table 5.2. ^{1}H and ^{13}C NMR data (δ) of compounds **92**, **93,** and **95**[a]

Position	**92**		**93**		**95**	
	δ_C	δ_H	δ_C	δ_H	δ_C	δ_H
2	167.6	–	168.1	–	168.7	–
3	59.1	4.07 m	59.2	4.04 m	58.6	4.05 m
5β	53.9	3.05 ddd (11, 6, 4.5)	53.8	2.99 ddd (11, 6.7, 4)	53.1	2.96 ddd (11.0, 6.4, 5.5)
5α		3.24 ddd (11, 9, 6)		3.18 ddd (11, 9, 6.7)		3.16 dt (11.0, 7.0)
6α	46.7	2.02 ddd (12.4, 6, 5)	45.9	1.98 ddd (12.8, 6, 4)	45.2	2.01 ddd (12.5, 6.5, 5.5)
6β		2.32 m		2.39 ddd (12, 9, 7)		2.34 ddd (12.5, 7.5, 6.7)
7	58.6	–	58.2	–	58.3	–
8	135.7	–	135.6	–	135.0	–
9	120.9	7.20 br d (7.5)	120.8	7.20 br d (7.5)	120.8	7.19 br d (7.7)
10	121.2	6.91 br t (7.5)	121.1	6.91 br t (7.5)	121.2	6.91 td (7.7, 1.0)
11	128.0	7.16 br t (7.5)	127.9	7.15 br t (7.5)	128.0	7.15 td (7.7)
12	109.7	6.85 br d (7.5)	109.7	6.83 br d (7.5)	109.8	6.84 br d (7.7)
13	143.8		144.1		144.2	
14*R*	27.4	1.22 dt (13.7, 2.3)	27.6	1.19 dt (13.6, 2.7)	26.6	1.19 dt (13.7, 2.4)
14*S*		2.29 m		2.23 dt (13.6, 3.4)		2.18 dt (13.7, 3.3)
15	29.3	3.00 m	27.8	2.95 m	27.4	3.38 m
16	102.9	–	103.4	–	102.6	–
18	20.3	1.16 d (6.2)	20.2	1.26 d (6.2)	29.4	2.26 s
19	71.1	3.62 m	69.9	3.80 m	210.0	
20	45.5	1.83 m	43.4	2.03 m	49.5	3.02 ddd (10.0, 6.0, 2.8)
21α	48.4	2.66 dd (14, 6)	47.4	2.71dd (14, 6)	47.0	2.81 dd (14.0, 6.0)
21β		2.94 t (14)		3.09 dd (14, 11)		3.28 dd (14.0, 10.0)
CO_2<u>Me</u>	51.5	3.82 s	51.3	3.80 s	51.2	3.77 s
<u>C</u>O_2Me	167.9	–	168.1	–	168.0	–
*N*H	–	8.52 br s	–	8.65 br s	–	8.82 br s

[a]$CDCl_3$, 400 and 100 MHz, respectively; assignments based on COSY, HMQC, and HMBC.

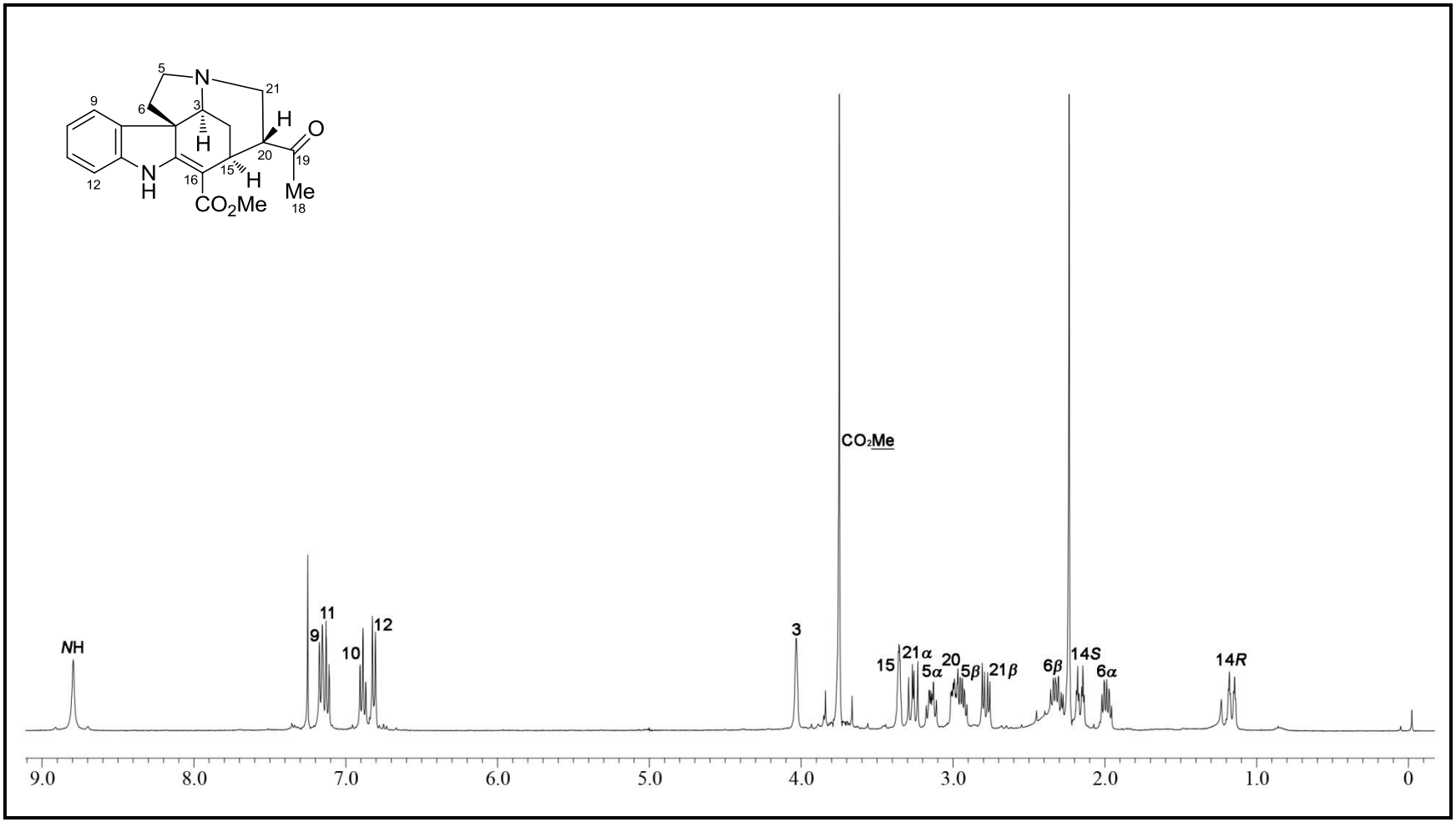

Figure 5.4. ^{1}H NMR spectrum ($CDCl_3$, 400 MHz) of compound **95**.

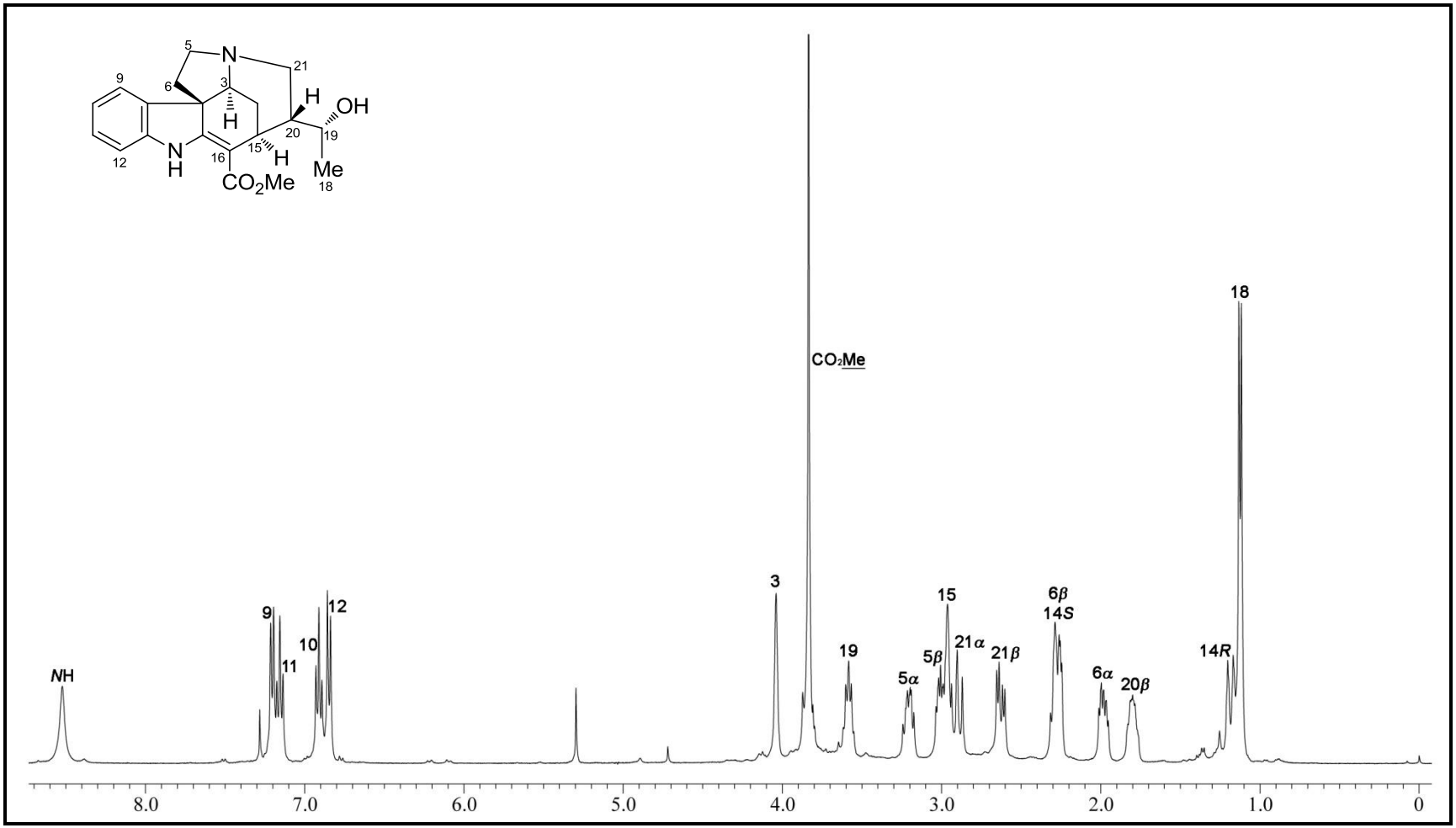

Figure 5.5. ^{1}H NMR spectrum ($CDCl_3$, 400 MHz) of *N*(4)-demethylalstogustine (**92**).

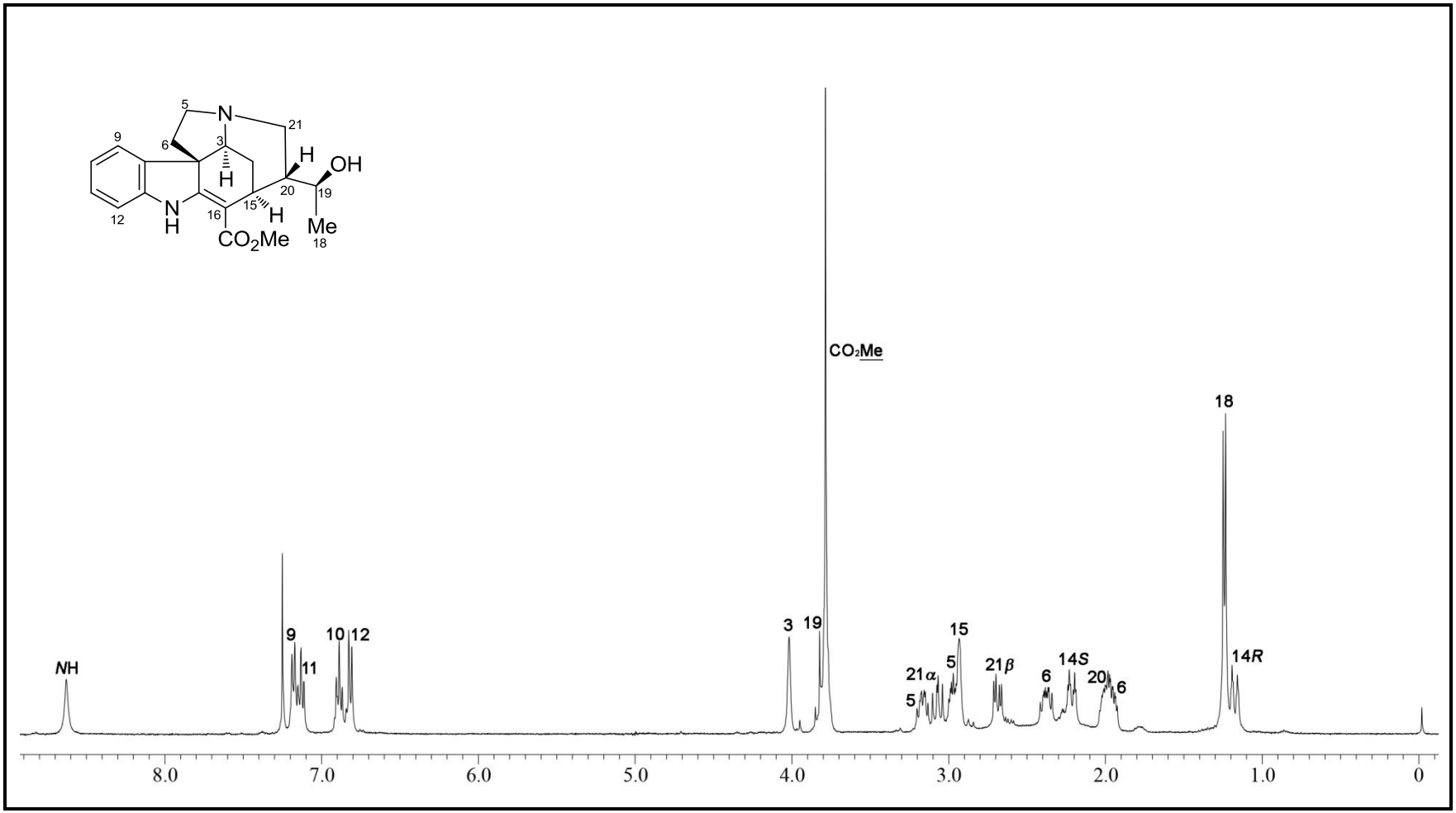

Figure 5.6. ^{1}H NMR spectrum ($CDCl_3$, 400 MHz) of 19-*epi*-*N*(4)-demethylalstogustine (**93**).

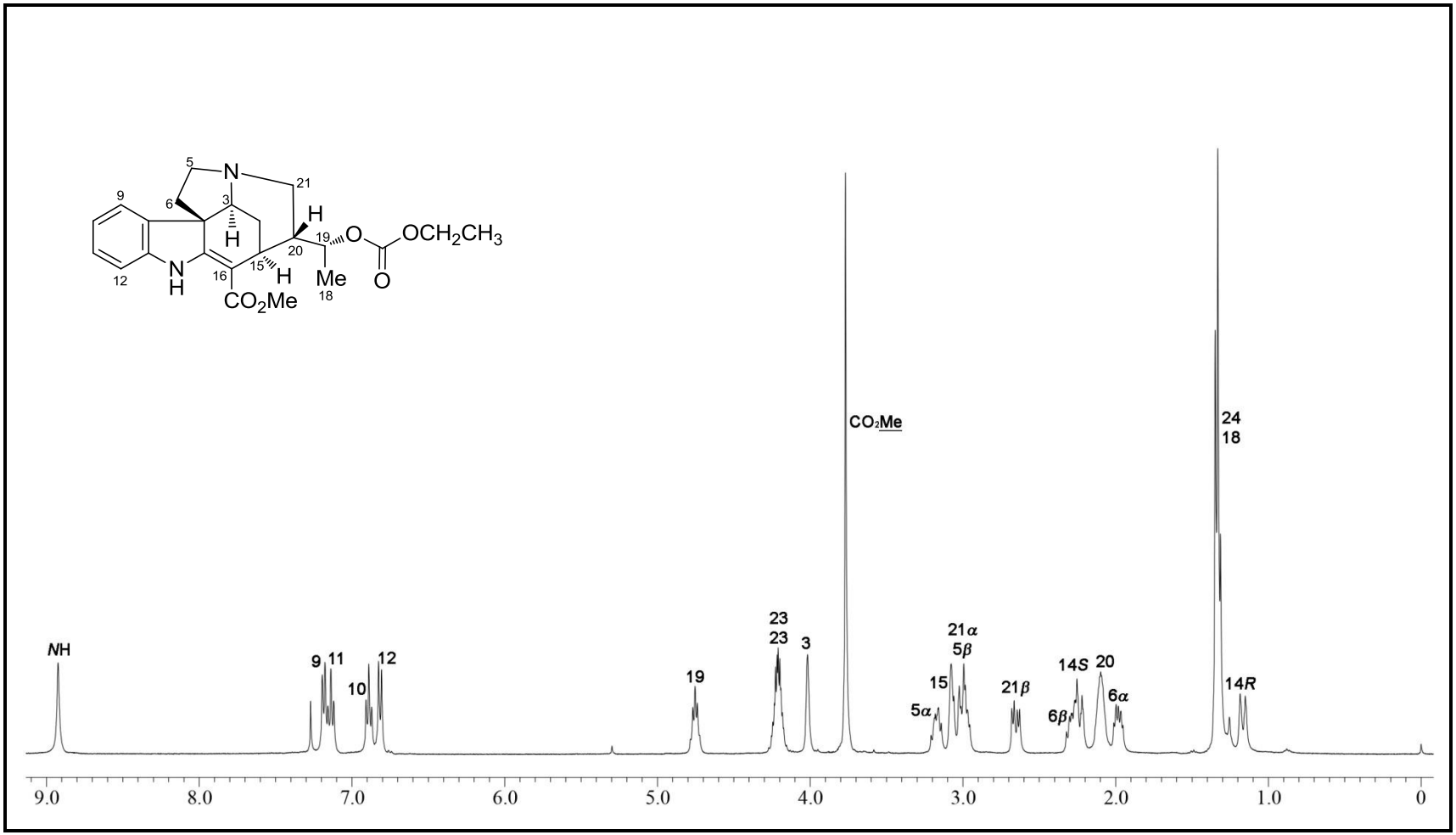

Figure 5.7. ^{1}H NMR spectrum ($CDCl_3$, 400 MHz) of semisynthetic alstolucine A (**91**).

5.1.3 Conclusion

A partial synthesis of alstolucine A (**91**) was successfully carried out. The C-19 configuration of **91** was found to be 19*R*, based on chemical correlation with *N*(4)-demethylalstogustine (**92**),[76,77] whose configuration was established by X-ray diffraction.[79]

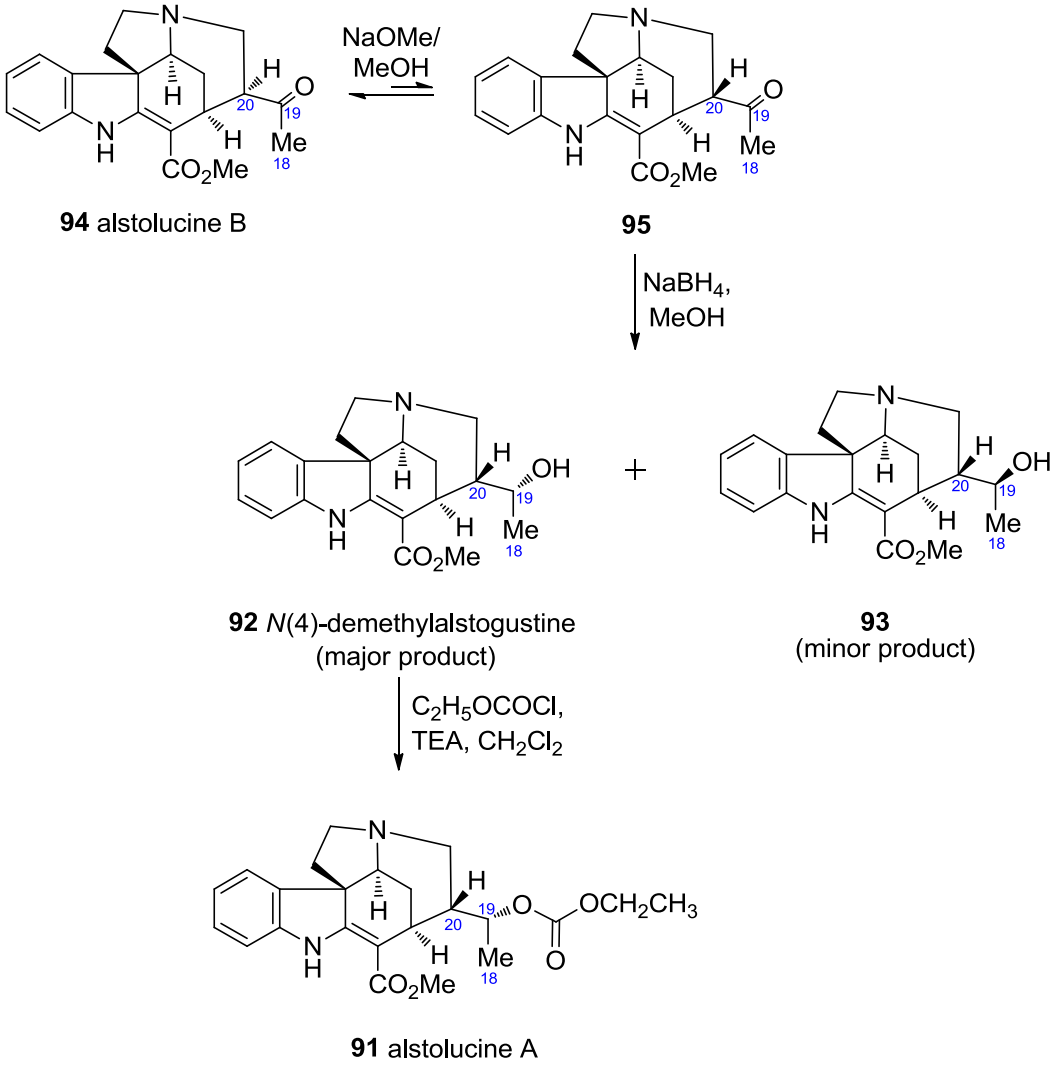

Scheme 5.3

5.2 (–)-Eburnamaline

5.2.1 Introduction

The alkaloid (–)-eburnamaline (**96**) was obtained as a minor alkaloid from *Leuconotis griffithii* (isolation and structure by C. Y. Gan).[80] It bears some similarity to the known alkaloid, (–)-eburnamine (**97**),[49,81,82] but with an additional β-OH group on C-17.

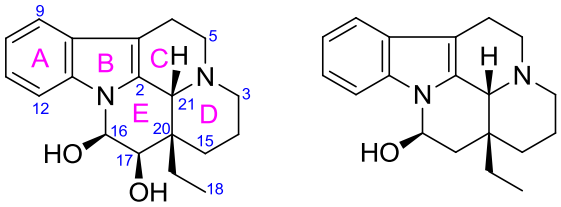

96 (–)-eburnamaline **97** (–)-eburnamine

(–)-Eburnamaline (**96**) was obtained as a light yellowish oil, with $[\alpha]^{25}_{D}$ –49 (*c* 0.21, $CHCl_3$). The UV spectrum (230 and 280 nm) showed the presence of an indole chromophore, while the IR spectrum indicated the presence of hydroxyl groups at 3370 cm^{-1}. The EIMS of **96** showed an $[M]^+$ at *m/z* 312, with a prominent fragment peak due to loss of H_2O at *m/z* 294, while the HREIMS showed an $[M]^+$ at 312.1827, which analyzed for $C_{19}H_{24}N_2O_2$ (DBE 9, 16 mass units higher than (–)-eburnamine (**97**)). The NMR data of **96** (Table 5.3) showed a close resemblance to those of **97**,[49,81,82] except for some notable differences associated with changes involving ring E. First, compared with **97**, a doublet was observed at δ_H 3.90 (δ_C 71.7) which indicated the presence of an oxymethine. This doublet coupled to the other oxymethine hydrogen (H-16) which required it to be vicinal to C-16. Alkaloid **96** is therefore the 17-hydroxy congener of

97. This conclusion is consistent with the loss of the H-17 signals seen in **97**, and the presence of a CHCH fragment in **96**, in place of the $CHCH_2$ fragment seen in the COSY spectrum of **97**.

The configuration at C-16 in the 16-hydroxysubstituted eburnan alkaloids can be deduced from the presence or absence of paramagnetic deshielding exerted by the oxygen of the C-16–OH substituent.[83–86] The relative configuration at the hydroxy-substituted C-17 was deduced to be *R* (β–OH) based on the following evidence. First, the reciprocal NOEs observed for H-16/H-17, H-17/H-15β, and H-17/H-18 are only consistent with a β-oriented C-17–OH (H-17α). Second, the observed $J_{16\text{-}17}$ of 3 Hz is in agreement with an equatorially-disposed H-17 (an axial or β-oriented H-17 would result in H-17 and H-16 being *trans*-diaxial). Third, the resonances for H-21 and H-19 were shifted downfield (δ_H 4.02; 1.79, 2.30) when compared to those of (–)-eburnamine (**97**) (δ_H 3.48; 1.27, 1.89), as a result of paramagnetic deshielding exerted by the proximate oxygen of the β-oriented C-17–OH (Figure 5.8). The ^{1}H and ^{13}C NMR data for alkaloid **96** are summarized in Table 5.3, while ^{1}H NMR spectrum of alkaloid **96** is shown in Figure 5.9.

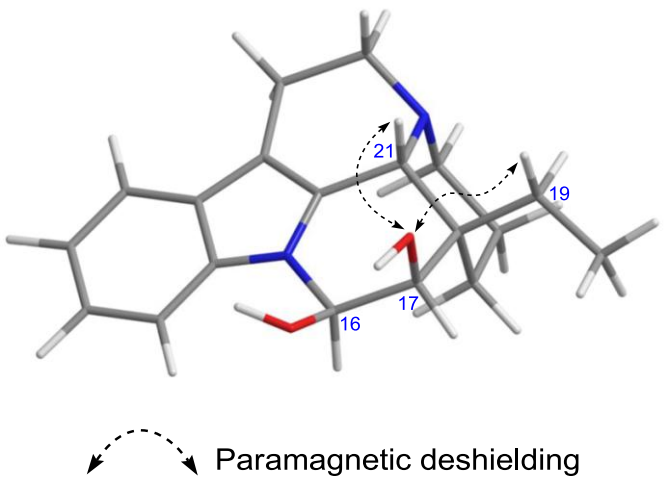

Figure 5.8. Paramagnetic deshielding exerted by C-17–OH.

The *cis*-diol configuration at C-16 and C-17 for alkaloid **96** is a rather uncommon structural feature and as such, further proof is required to further substantiate the *cis*-diol configuration assigned. To this end a partial synthesis of **96** was carried out in order to obtain additional support for this uncommon structural feature. In addition, with more of **96** available from partial synthesis, suitable crystals can be obtained for X-ray diffraction analysis.

A concise route to **96** is one based on (+)-eburnamonine (**98**)[87] as the starting compound (^{1}H and ^{13}C NMR data of alkaloid **98** are summarized in Table 5.3, while the ^{1}H NMR spectrum of alkaloid **98** is shown in Figure 5.10). As shown in Scheme 5.4, oxidation of **98** to 17-hydroxyeburnamonine (**99**), followed by reduction of the lactam should furnish alkaloid **96**.

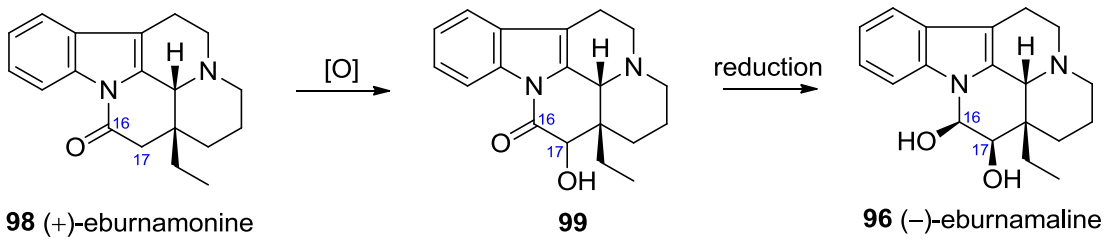

Scheme 5.4

Table 5.3. ^{1}H and ^{13}C NMR data (δ) of (–)-eburnamaline (**96**) and (+)-eburnamonine (**98**)[a]

Position	**96**		**98**	
	δ_C	δ_H	δ_C	δ_H
2	131.5	–	132.0	–
3	44.8	2.35 m	44.2	2.41 m
		2.53 br d (13)		2.53 m
5	50.9	3.14 ddd (14, 12, 6)	50.5	3.20 ddd (14, 11, 6)
		3.22 dd (14, 6)		3.32 dd (14, 6)
6	16.7	2.42 ddd (16, 6, 2)	16.4	2.41 m
		2.88 dddd (16, 12, 6, 2)		2.88 m
7	105.6	–	112.4	–
8	128.7	–	130.0	–
9	118.0	7.45 dd (7, 1)	117.9	7.42 dd (7, 2)
10	120.2	7.13 td (7, 1)	123.7	7.27 td (7, 2)
11	121.3	7.17 td (7, 1)	124.2	7.31 td (7, 2)
12	112.3	7.79 dd (7, 1)	116.1	8.37 dd (7, 2)
13	137.2	–	134.0	–
14	20.0	1.29 m	20.5	1.37 br d (13)
		1.70 dt (13, 3.6)		1.74 br qt (13, 3)
15	21.9	0.66 td (13, 3.6)	26.8	1.01 td (13.5, 3)
		1.37 br d (13)		1.48 br d (13.5)
16	77.0	5.54 d (3)	119.7	–
17	71.7	3.90 d (3)	116.7	2.56 d (17)
				2.65 d (17)
18	6.9	0.89 t (7.7)	9.0	0.92 t (7)
19	22.9	1.79 dq (14.5, 7.7)	27.5	1.63 dq (14, 7)
		2.30 dq (14.5, 7.7)		2.03 dq (14, 7)
20	40.8	–	37.3	–
21	55.8	4.02 br s	55.8	3.92 s

[a]$CDCl_3$, 400 and 100 MHz, respectively; assignments based on COSY, HMQC, and HMBC.

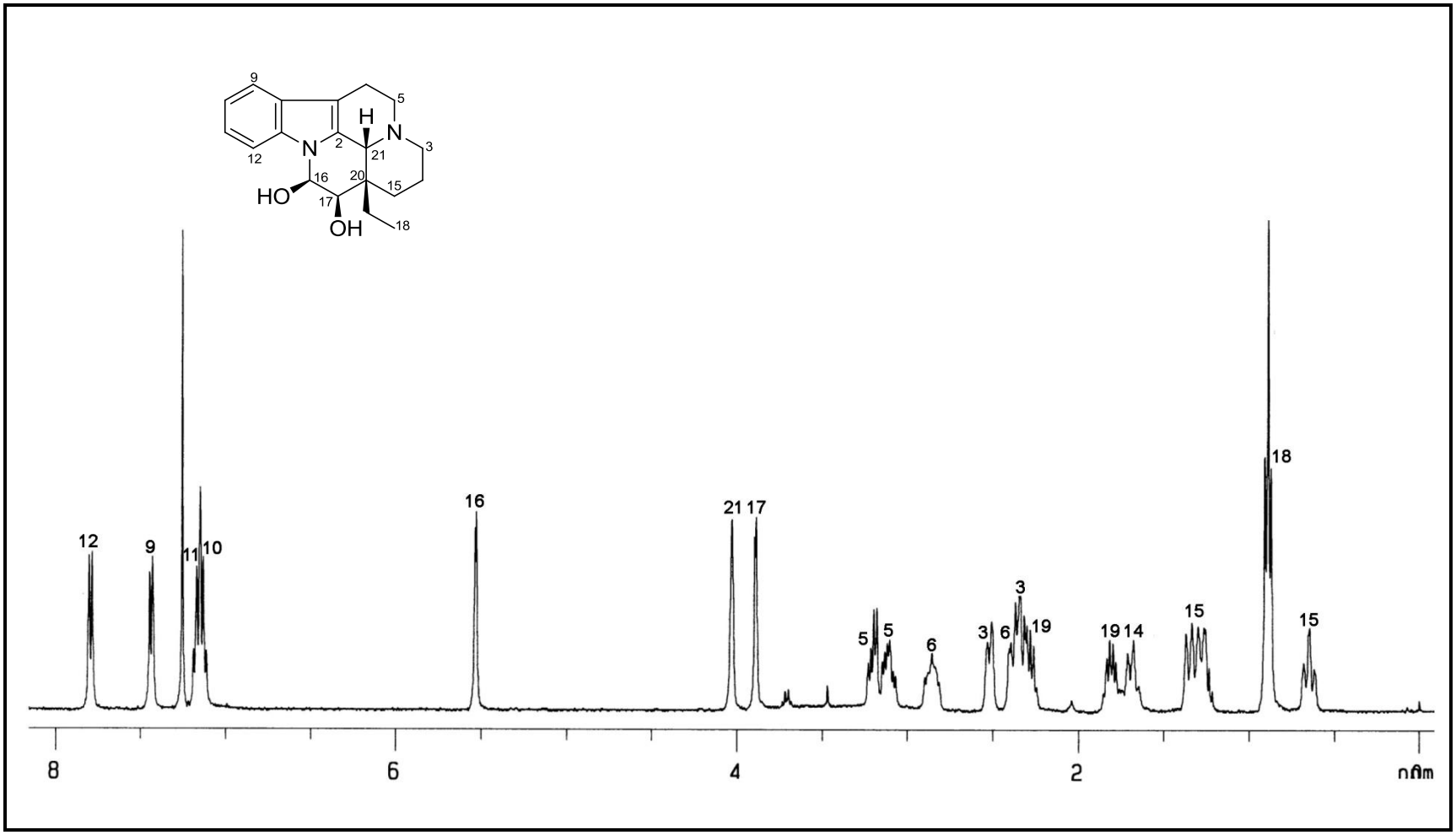

Figure 5.9. ^{1}H NMR spectrum ($CDCl_3$, 400 MHz) of natural (–)-eburnamaline (**96**).[58]

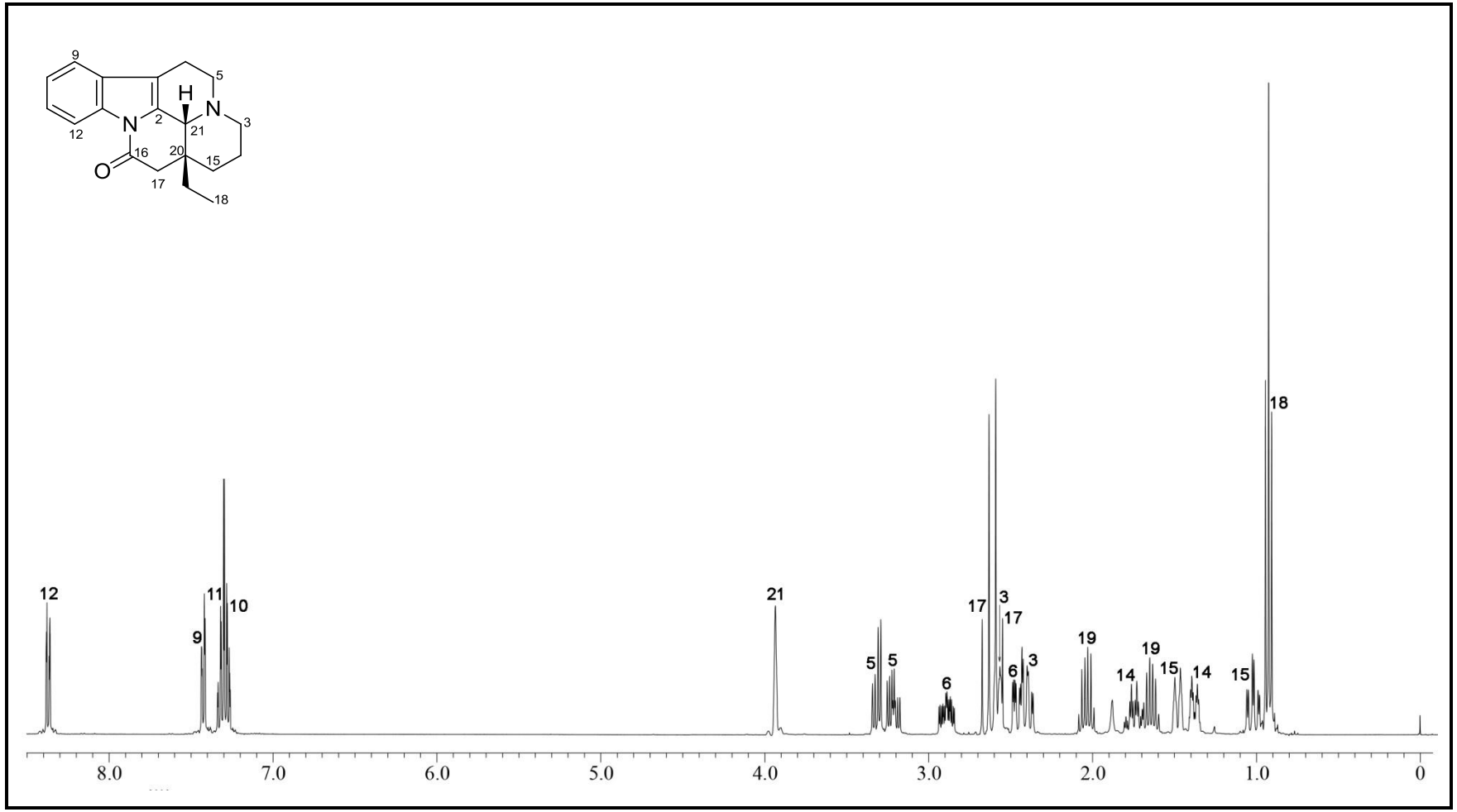

Figure 5.10. ^{1}H NMR spectrum ($CDCl_3$, 400 MHz) of (+)-eburnamonine (**98**).

5.2.2 Results and discussion

The partial synthesis was carried out based on the proposed route outlined in Scheme 5.4. The first step involved an α-oxygenation of **98** at the adjacent C-17 of (+)-eburnamonine (**98**) *via* enolate-mediated oxidation.

Treatment of **98** with LDA in THF at 0 ^{o}C, followed by oxidation of the lactam enolate with O_2,[69] gave the desired (+)-17β-hydroxyeburnamonine (**99**) as the sole product (26%), accompanied by recovery of unreacted **98** (60%). The high recovery of **98** may be due to quenching of the lactam enolate by water present in the oxygen gas. Attempts to improve the yield by prior drying of the oxygen gas *via* passage through $CaCl_2$ or activated SiO_2, did not result in significant improvement of the yields. A significant improvement in the yield (83%) was achieved with the use of (+)-camphorsulfonyl oxaziridine in place of gaseous oxygen in the enolate oxidation.[88] (Scheme 5.5).

(+)-17β-Hydroxyeburnamonine (**99**) was obtained as a light yellowish oil, with $[\alpha]^{25}_{D}$ +126 (*c* 0.62, $CHCl_3$). The UV spectrum (229 and 282 nm) showed the presence of an indole chromophore, while the IR spectrum indicated the presence of an OH and carbonyl group at 3382 and 1703 cm^{-1}, respectively. The HRESIMS showed an $[M + H]^+$ at 311.1760, which analyzed for $C_{19}H_{22}N_2O_2$ + H (16 mass units higher than **98**). The ^{1}H and ^{13}C NMR data (Table 5.4) were generally similar with those of **98**, except for the downfield shifts of H-17 and C-17 to δ_H 4.15 and δ_C 75.1, respectively, and the presence of an OH (δ_H 4.78) in the ^{1}H NMR spectrum. The assignment of the configuration at C-17 in **99** was based on the observed downfield shift of the H-21 and H-19 signals (compared to **98**)[82,87] as a result of paramagnetic deshielding by the β-oriented C-17–OH, as well as from the observed H-17/H-15β, H-18 NOEs. The ^{1}H and

^{13}C NMR data of compound **99** are summarized in Table 5.4, while ^{1}H NMR spectrum of **99** is shown in Figure 5.11.

Treatment of **99** in the presence of $LiAlH_4$ in THF under reflux gave two epimeric products, **96** (54%) and **100** (39%) (Scheme 5.5).[82] The major product showed $[\alpha]_D$, TLC R_f, ESIMS, and ^{1}H and ^{13}C NMR data which were identical with those of **96**. The ^{1}H NMR spectrum of semisynthetic **96** is shown in Figure 5.12.

The minor product **100** was obtained as white amorphous solid, and subsequently as colorless crystals from CH_2Cl_2 (mp 190–193 ^{o}C) with $[\alpha]^{25}_{D}$ –44 (*c* 0.62, MeOH). The UV spectrum (229 and 281 nm) showed the presence of an indole chromophore, while the IR spectrum indicated the presence of OH groups at 3448 cm^{-1}. The HRESIMS of **100** gave $[M + H]^{+}$ at 313.1915, corresponding to the formula $C_{19}H_{24}N_2O_2$ + H, which was similar to that of **96**. Compound **100** was assigned as the 16α-OH epimer of **99** based on the observed downfield shift of H-15 compared to those of **96** due to paramagnetic deshielding, as well as the virtual absence of the H-16–H-17 vicinal coupling ($J_{16\beta\text{-}17\alpha} \approx 0$), in agreement with the required H-16–H-17 dihedral angle of *ca.* 90° in **100**. The ^{1}H and ^{13}C NMR data for compound **100** are summarized in Table 5.4, while the ^{1}H NMR spectrum of compound **100** is shown in Figure 5.13.

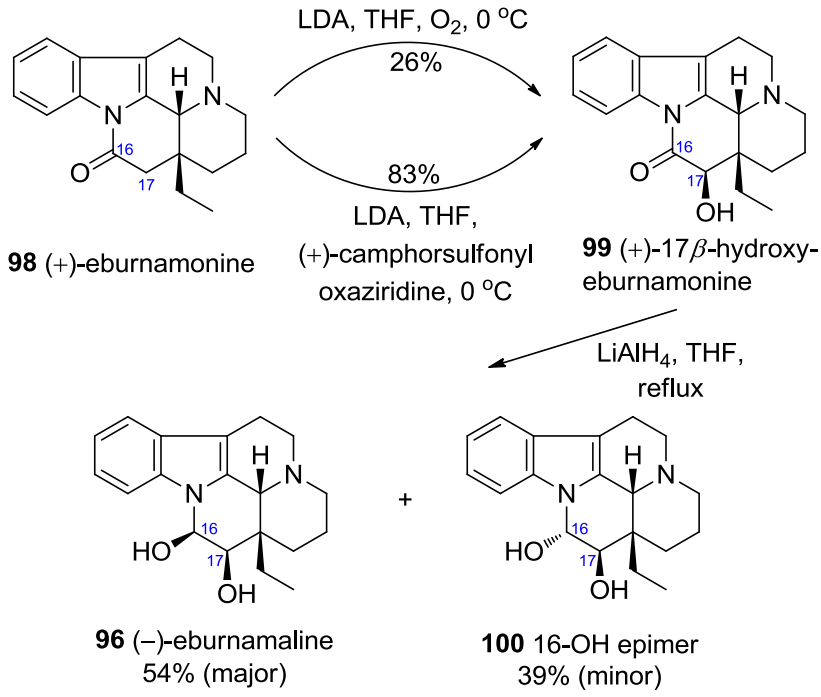

Scheme 5.5

Table 5.4. ^{1}H and ^{13}C NMR data (δ) of compounds **99** and **100**[a]

Position	**99**		**100**[b]	
	δ_C	δ_H	δ_C	δ_H
2	131.6	–	130.5	–
3	44.7	2.35 m	45.2	2.55 m
		2.62 br d (11)		2.55 m
5	50.3	3.26 m	51.5	3.23 dd (14, 6)
		3.30 m		3.14 m
6	16.6	2.40 dd (16, 6)	16.6	2.85 m
		2.83 dddd (16, 14, 6, 2)		2.66 m
7	113.0	–	105.5	–
8	130.5	–	129.1	–
9	118.4	7.40 dd (7, 1)	110.2	7.34 br d (7.5)
10	124.2	7.26 m	121.4	7.20 td (7.5)
11	124.4	7.29 m	120.3	7.16 td (7.5)
12	116.4	8.29 dd (7, 1)	118.7	7.47 br d (7.5)
13	134.6	–	135.4	–
14	20.2	1.37 br d (13.5)	20.4	1.33 m
		1.77 dt (13.5, 3.5)		1.33 m
15	23.0	1.51 br d (13.7)	22.3	1.47 td (14, 3.5)
		0.70 td (13.7, 3.5)		1.37 m
16	169.0	4.78 br s	79.9	5.74 br s
17	75.1	4.15 s	73.4	3.84 br s
		–		
18	7.1	0.89 t (7.4)	7.1	0.92 t (7.3)
19	21.2	1.96 dq (14.6, 7.4)	23.1	2.29 dq (14.5, 7.3)
		2.22 dq (14.6, 7.4)		1.71 dq (14.5, 7.3)
20	41.9	–	39.0	–
21	55.6	4.17 br s	56.4	4.04 br s
16-OH	–	–	–	Not observed
17-OH	–	4.78 br s	–	Not observed

[a]$CDCl_3$, 400 and 100 MHz, respectively; [b]low solubility in $CDCl_3$; assignments based on COSY, HMQC, and HMBC.

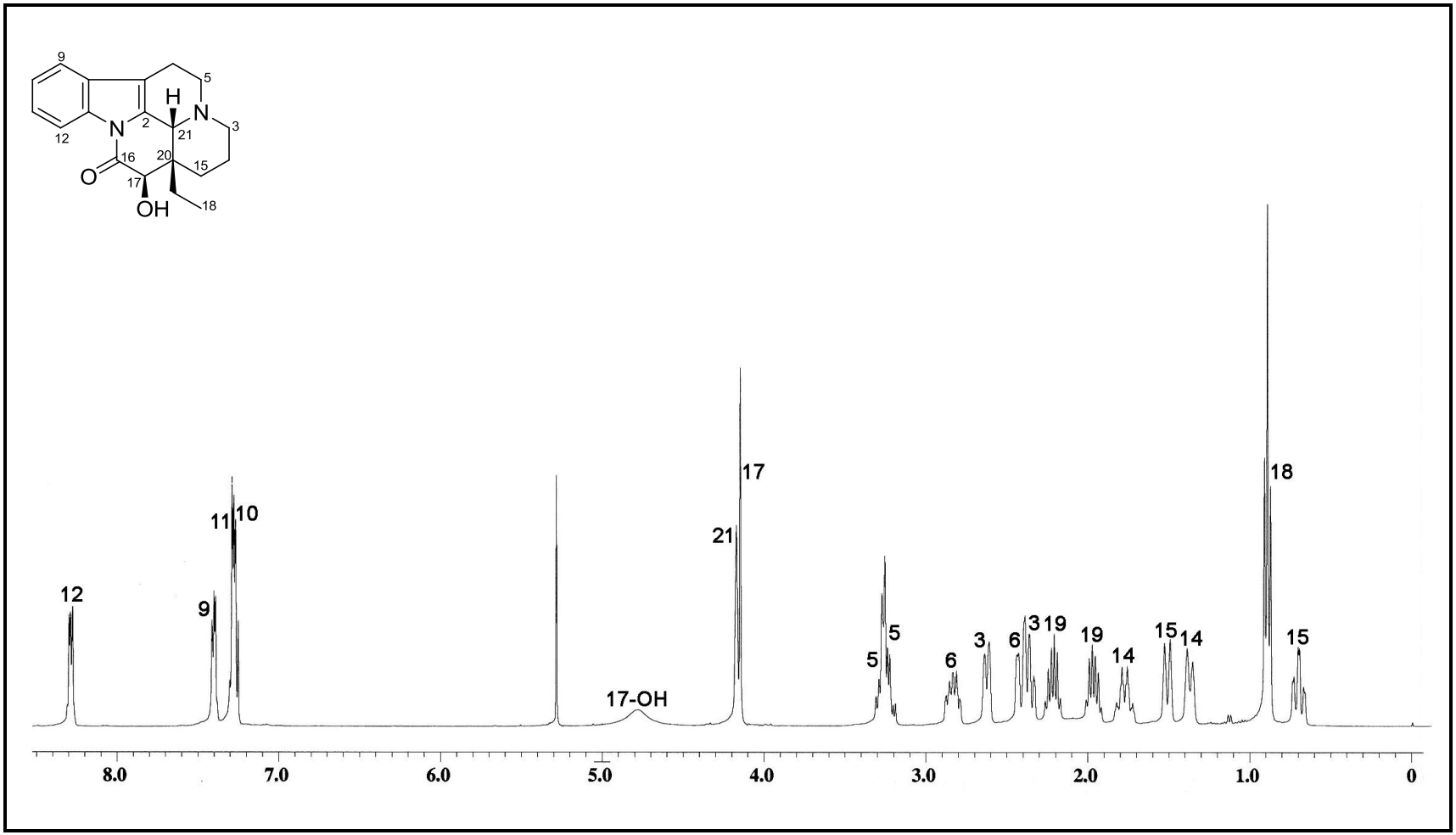

Figure 5.11. ^{1}H NMR spectrum ($CDCl_3$, 400 MHz) of (+)-17*β*-hydroxyeburnamonine (**99**).

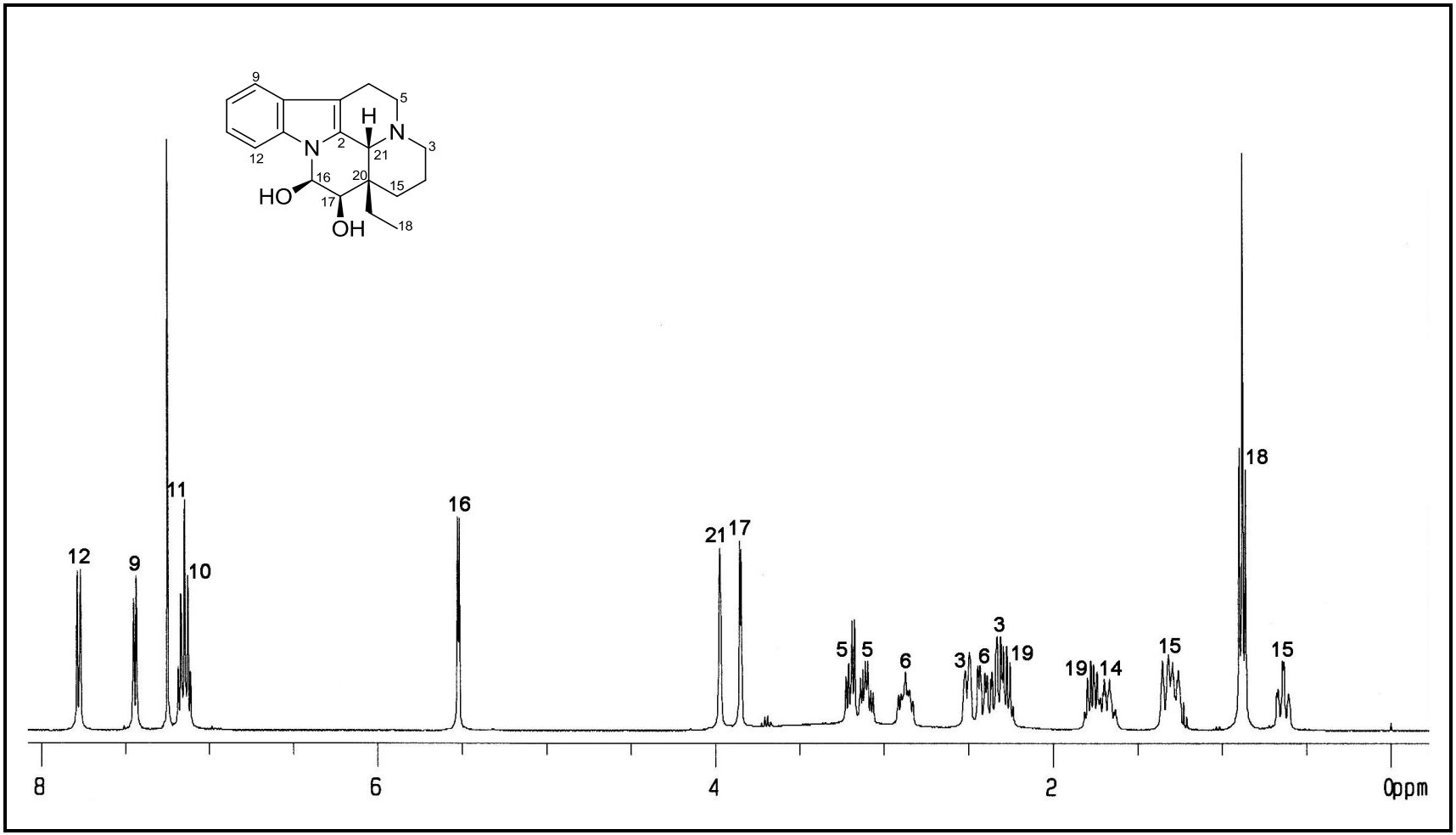

Figure 5.12. ^{1}H NMR spectrum ($CDCl_3$, 400 MHz) of semisynthetic (–)-eburnamaline (**96**).

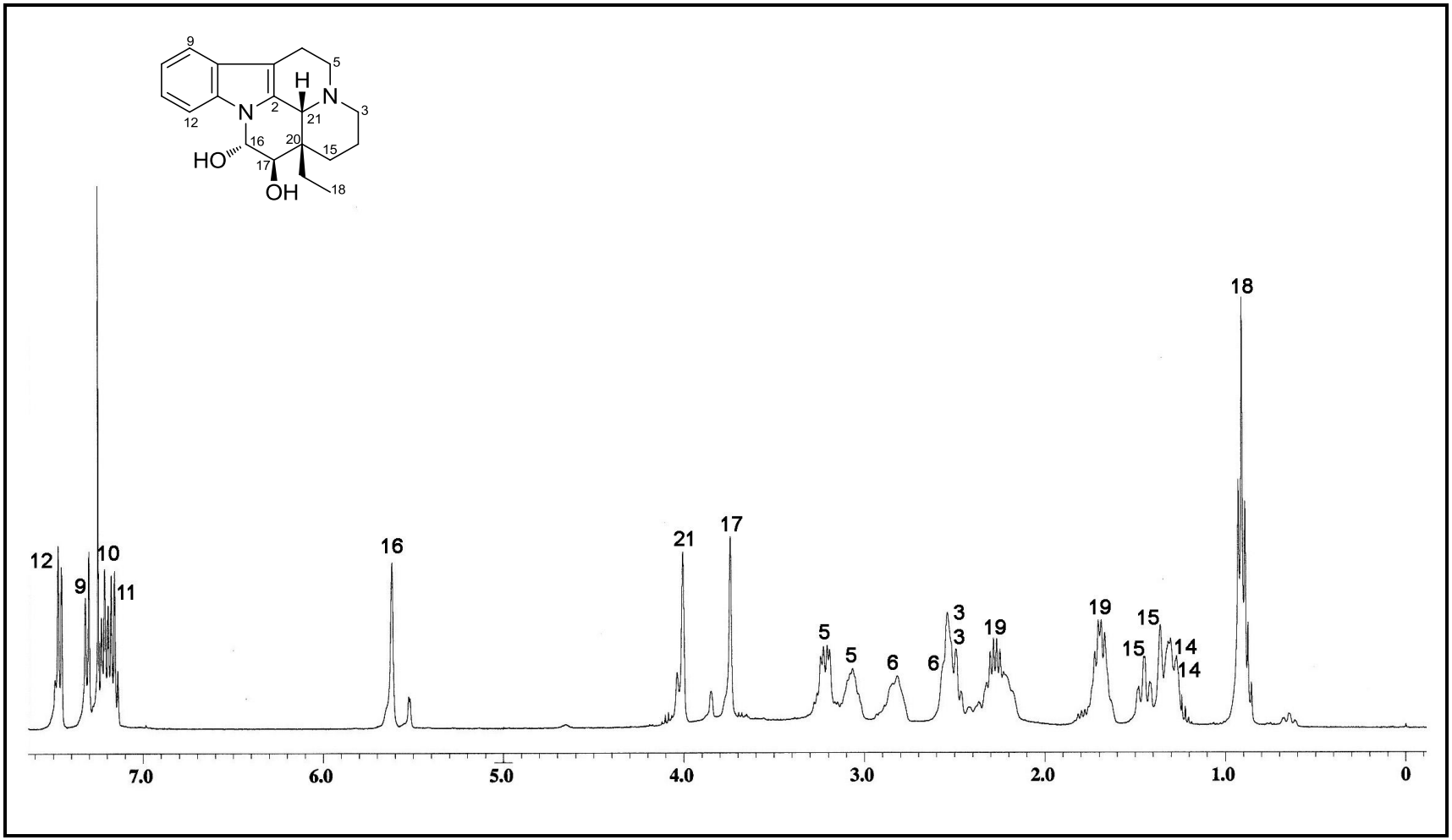

Figure 5.13. ^{1}H NMR spectrum ($CDCl_3$, 400 MHz) of compound **100**.

As a sufficient amount of (–)-eburnamaline (**96**) was made available, attempts were made to obtain suitable crystals for X-ray analysis, but to no avail. However, the 16α-OH epimeric compound **100** crystallized readily in CH_2Cl_2, and therefore an X-ray diffraction analysis was carried out which yielded the absolute configuration of compound **100** (Figure 5.14). The absolute configuration at C-16 and C-17 of compound **100** were found to be 16*S* and 17*R*, respectively. With the absolute configuration of the 16α-OH epimer **100** determined, the absolute configuration of C-16 and C-17 of (–)-eburnamaline (**96**) could be readily deduced as 16*R* and 17*R*, respectively.

Compound **100** was first obtained as white amorphous solid, and subsequently as colorless needles from slow evaporation from CH_2Cl_2 solution. The crystal structure obtained showed that **100** co-crystallized with the solvent. The presence of heavy atoms (CH_2Cl_2) in the unit cell enabled measurement of the Flack parameter,[63] which in turn permitted the determination of the absolute configuration (Figure 5.14).

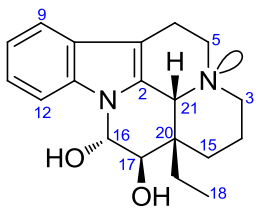

100

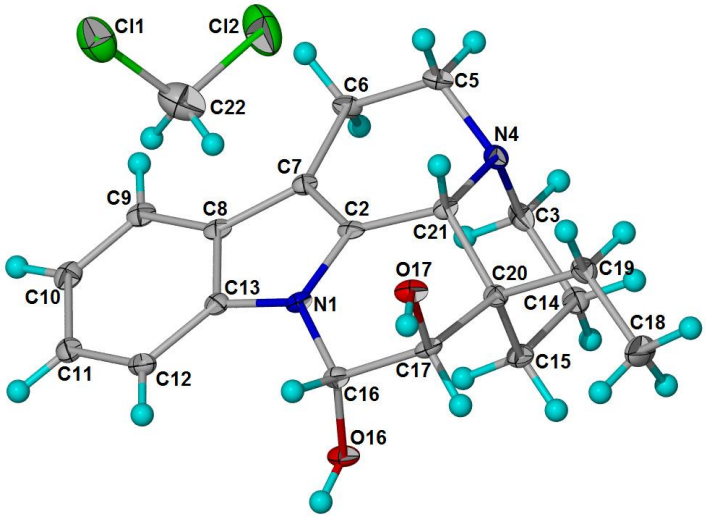

Figure 5.14. X-ray crystal structure of **100**

[Flack parameter: x = –0.06(0.06)].

5.2.3 Conclusion

The partial synthesis of (–)-eburnamaline (**96**) was achieved *via* a concise two-step oxidation-reduction sequence from (+)-eburnamonine (**98**). The absolute configuration of (–)-eburnamaline (**96**) was determined *via* correlation with its C-16 epimer **100**, for which crystal data was available from an X-ray diffraction analysis.

CHAPTER SIX

Absolute Configuration of Perhentinine and Macralstonine and Determination of C-20 Configuration in the New *Alstonia* Bisindoles, Perhentidines A–C

6.1 Introduction

Perhentidines A–C (**101**–**103**) are new bisindole alkaloids from the stem-bark extract of *Alstonia macrophylla* and *Alstonia angustifolia* (isolation and structure by S. H. Lim and S. J. Tan).[89]

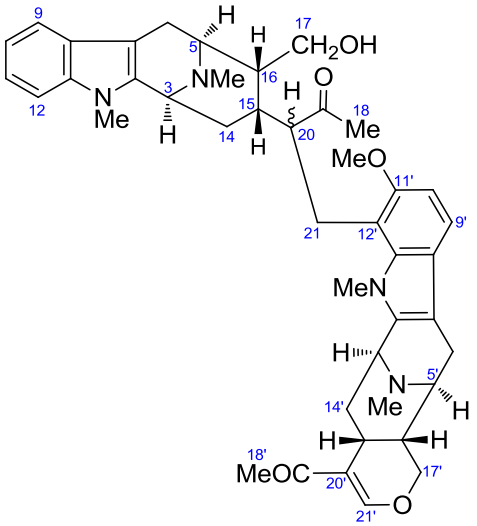

101 perhentidine A (C-20 *R* or *S*)
102 perhentidine B (C-20 opposite of **101**)

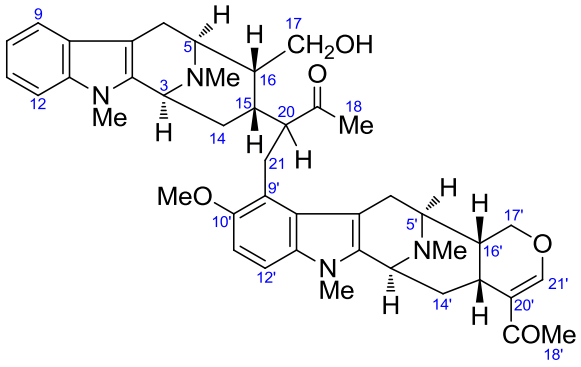

103 perhentidine C

Examination of the ^{1}H and ^{13}C NMR data of alkaloids **101**–**103** (Tables 6.1 and 6.2), indicated that these bisindoles are constituted from the union of macroline units, with the upper half corresponding to an *E-seco*-macroline (or alstomicine) moiety, and the lower half corresponding to a type B macroline (12-substituted alstophylline or 9-substituted-10-methoxyalstonerine). The ^{1}H and ^{13}C NMR data of alkaloids **101**–**103**

are shown in Tables 6.1 and 6.2, while the ^{1}H NMR spectra of alkaloids **101**–**103** are shown in Figures 6.1–6.3.

Table 6.1. ^{1}H NMR data (δ) of perhentidines A–C (**101–103**)[a]

Position	**101**	**102**	**103**
3	4.14 m	3.98 m	4.14 m
5	3.48 d (7.6)	3.63 m	3.45 m
6β	2.57 d (17)	2.58 d (17)	2.56 d (17)
6α	3.29 m	3.37 dd (17, 7)	3.29 dd (17, 7)
9	7.56 d (7.5)	7.56 d (8)	7.56 d (7.5)
10	7.16 t (7.5)	7.14 m	7.16 t (7.5)
11	7.26 m	7.22 m	7.24 m
12	7.36 d (7.5)	7.32 d (8)	7.34 d (7.5)
14β	2.01 m	1.48 m	2.04 m
14α	2.46 m	2.26 m	2.50 m
15	2.27 m	2.11 m	2.21 m
16	1.66 m	1.88 m	1.60 m
17a	3.88 dd (11, 2)	4.09 m	3.83 dd (11, 2)
17b	3.91 dd (11, 2)	4.49 d (12)	3.90 m
18	1.55 s	1.40 s	1.30 s
20	3.26 m	3.55 m	3.42 m
21a	2.92 dd (13, 10.5)	3.05 m	2.60 t (12)
21b	3.26 m	3.17 m	3.23 dd (12, 4)
N_1Me	3.69 s	3.57 s	3.69 s
N_4Me	2.36[b] s	2.36 s	2.37 s
3'	3.80 m	3.72 m	3.77 m
5'	3.05 d (7)	3.01 m	2.87 d (7)
6'α	2.40 m	2.34 m	2.26 d (17)
6'β	3.23 dd (17, 7)	3.20 m	3.18 dd (17, 7)
9'	7.22 d (8.6)	7.20 d (8.6)	–
10'	6.75 d (8.6)	6.76 d (8.6)	–
11'	–	–	6.83 d (9)
12'	–	–	7.07 d (9)
14'α	1.75 td (12, 4)	1.70 td (12.5, 3.5)	1.75 m
14'β	2.01 m	1.99 m	2.04 m
15'	2.50 m	2.51 m	2.50 m
16'	1.84 m	1.82 m	1.75 m
17'α	4.14 m	4.12 m	4.08 dd (11, 4)
17'β	4.39 t (11)	4.37 t (11)	4.32 t (11)
18'	2.06 s	2.05 s	2.06 s
21'	7.49 s	7.48 s	7.49 s
N_1Me'	3.58 s	3.53 s	3.53 s
N_4Me'	2.37[b] s	2.24 s	2.24 s
10'-OMe	–	–	3.89 s
11'-OMe	3.83 s	3.94 s	–

[a]$CDCl_3$, 400MHz; [b]assignments are interchangeable; assignments based on COSY, HSQC, and HMBC.

Table 6.2. ^{13}C NMR data (δ) of perhentidines A–C (**101–103**)[a]

Position	**101**	**102**	**103**
2	132.8	132.9	133.1
3	53.2	53.2	53.3
5	59.5	59.6	59.3
6	22.1	22.5	22.1
7	106.1	106.1	106.2
8	126.4	126.5	126.5
9	118.4	118.2	118.3
10	118.9	118.9	118.8
11	121.0	121.1	120.8
12	108.8	109.2	108.8
13	137.1	137.4	137.1
14	32.2	32.7	32.0
15	31.5	32.4	31.7
16	42.6	42.2	42.7
17	66.8	66.1	66.7
18	31.8	34.4	32.6
19	212.9	214.7	213.3
20	55.5	52.7	53.9
21	26.0	26.3	28.8
N_1Me	29.1	29.1	28.9[c]
N_4Me	41.3[b]	41.4	41.3
2'	133.5	133.7	133.9
3'	53.9	53.9	53.9
5'	54.6	54.7	54.4
6'	22.5	22.77	25.2
7'	105.8	105.3	105.3
8'	122.9	123.3	126.2
9'	116.0	115.9	118.0
10'	104.8	104.3	151.2
11'	153.6	153.9	106.4
12'	110.9	110.2	107.1
13'	136.3	136.2	133.0
14'	32.2	32.1	32.3
15'	22.7	22.85	22.7
16'	38.4	38.6	38.3
17'	67.6	67.8	67.6
18'	24.9	25.1	25.0
19'	195.2	195.6	195.5
20'	121.0	121.2	121.0
21'	157.2	157.5	157.5
N_1Me'	32.3	32.5	29.0[c]
N_4Me'	41.9[b]	41.8	41.6
10'-OMe	–	–	56.9
11'-OMe	56.7	56.7	–

[a]$CDCl_3$, 100 MHz; [b,c]assignments are interchangeable; assignments based on COSY, HSQC, and HMBC.

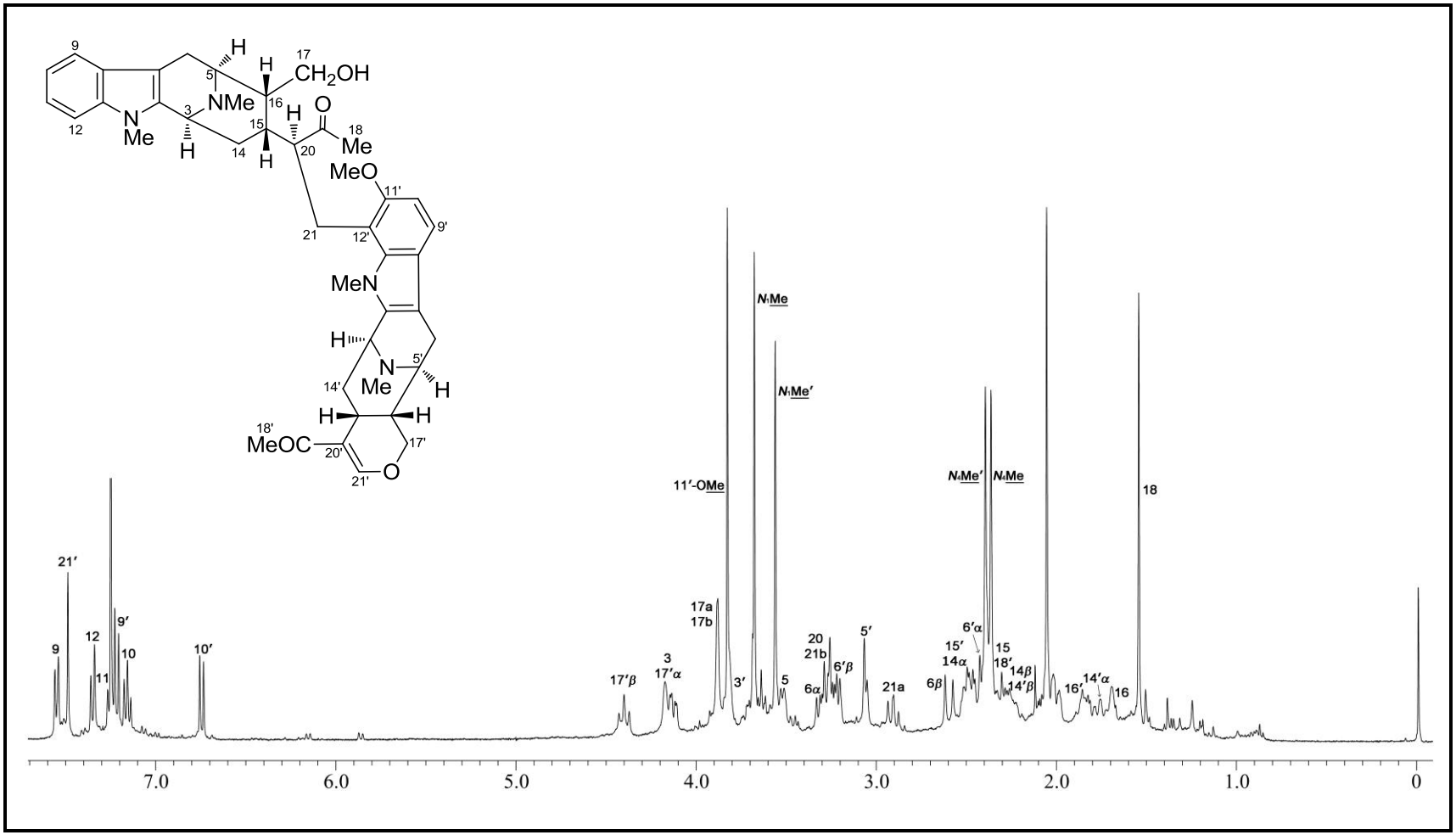

Figure 6.1. ^{1}H NMR spectrum ($CDCl_3$, 400 MHz) of perhentidine A (**101**).

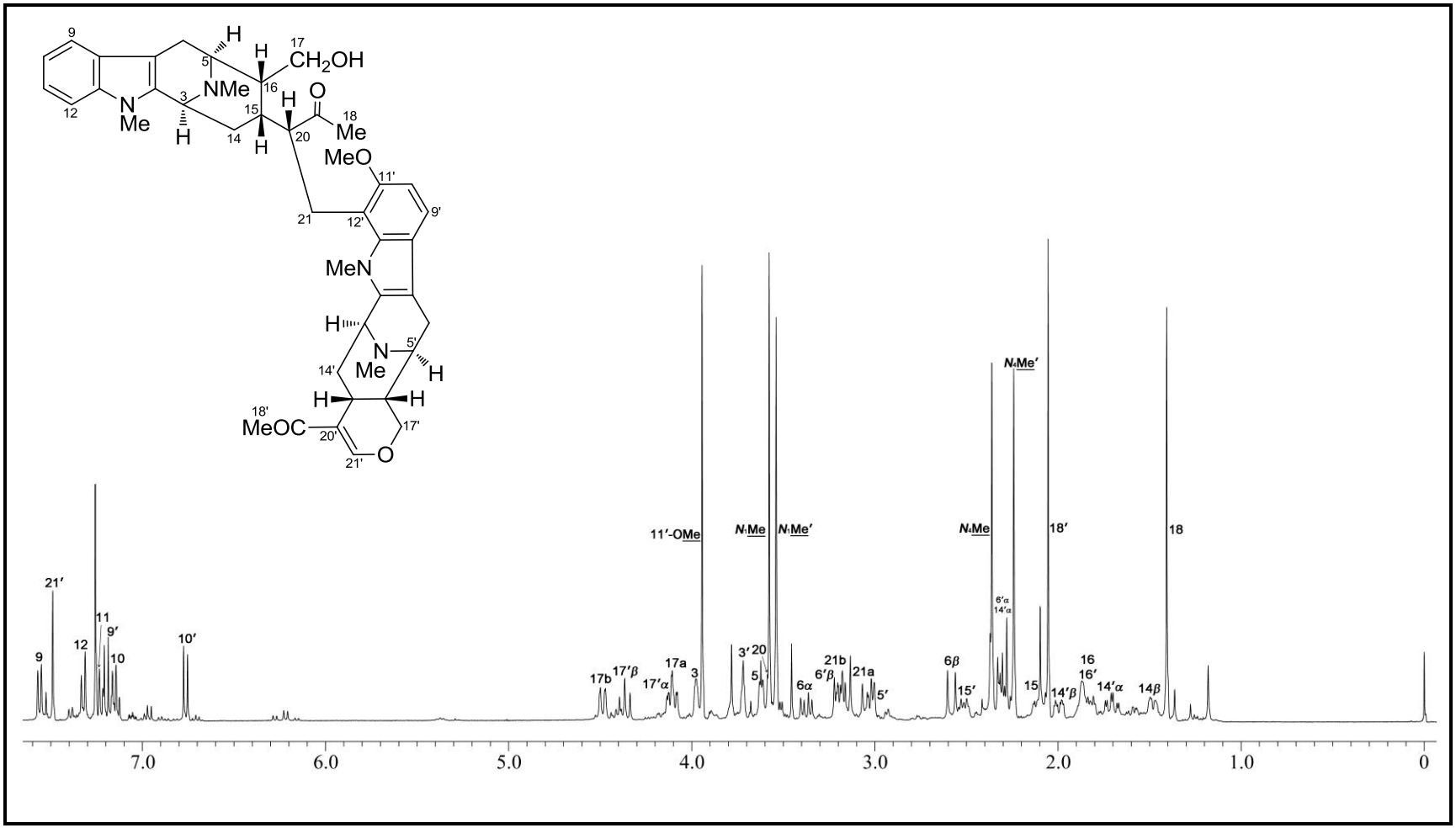

Figure 6.2. ^{1}H NMR spectrum ($CDCl_3$, 400 MHz) of perhentidine B (**102**).

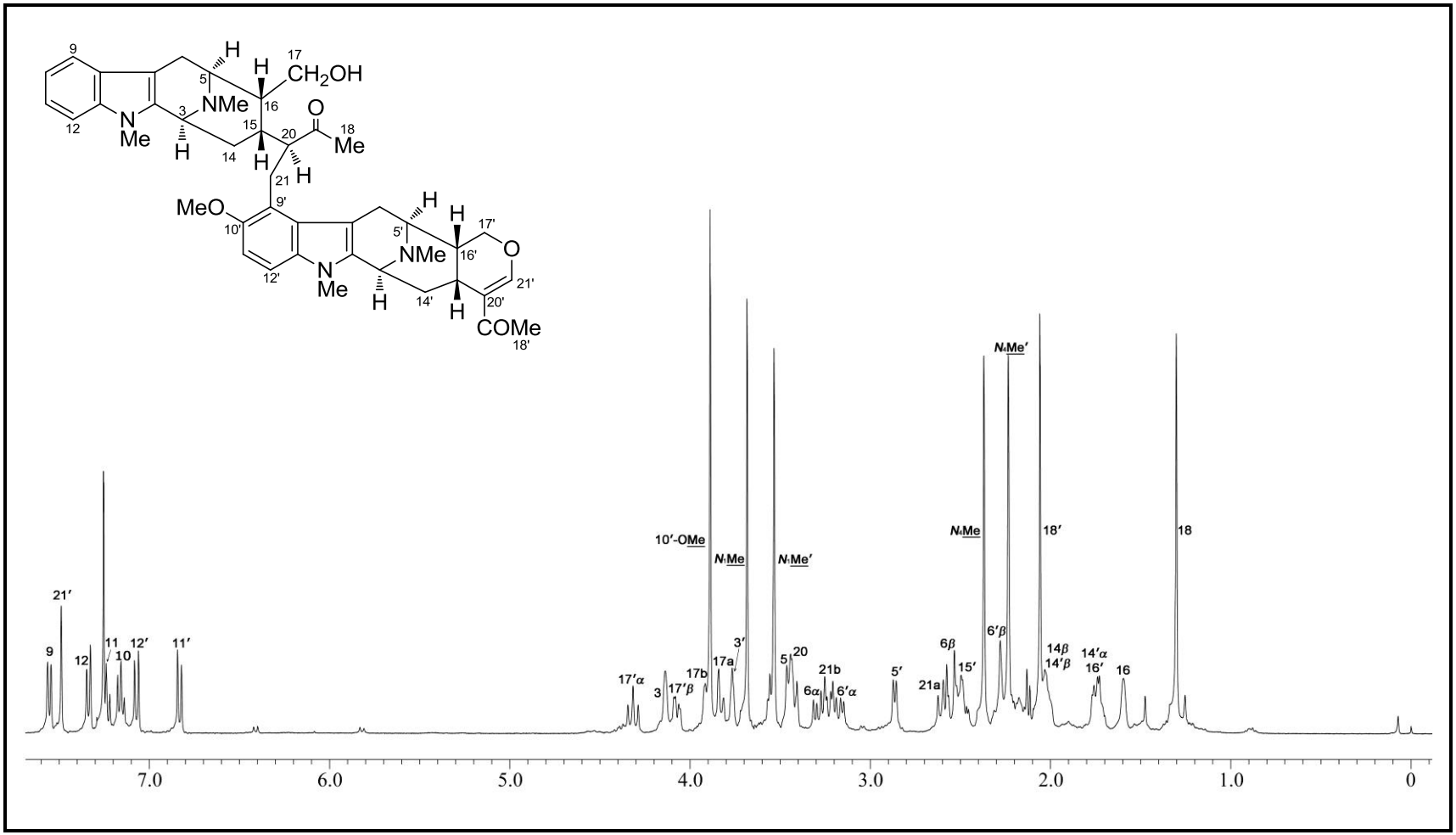

Figure 6.3. ^{1}H NMR spectrum ($CDCl_3$, 400 MHz) of perhentidine C (**103**).

Although the gross structures could be established from the NMR data, including the relative configurations at the stereogenic centers, the relative configuration at C-20 for these alkaloids could not be determined directly (except for perhentidine C (**103**)), as the combined NMR data (including NOESY) were insufficient for establishing the configuration (the signals of H-20 in both perhentidines A and B were observed as multiplets, while the signal of one of the C-21 hydrogens in perhentidine A (**101**), and of both the C-21 hydrogens in perhentidine B (**102**) were also observed as multiplets). Since the perhentidines are regioisomers of the previously isolated *Alstonia* bisindoles, perhentinine (**104**)[90] and the *E-seco* form (**106**) of macralstonine (**105**),[91–95] determination of the C-20 configuration of these bisindole alkaloids, **104** and **105** would be useful in facilitating the assignment of C-20 configuration in the regioisomeric perhentidines. Establishment of the configuration at C-20 for both **104** and **105** was therefore carried out by X-ray diffraction analysis, and the results obtained were used to facilitate the assignment of the C-20 configuration of the perhentidines.

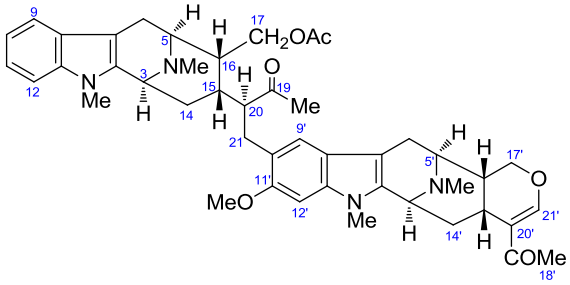

104 perhentinine (20*S*)

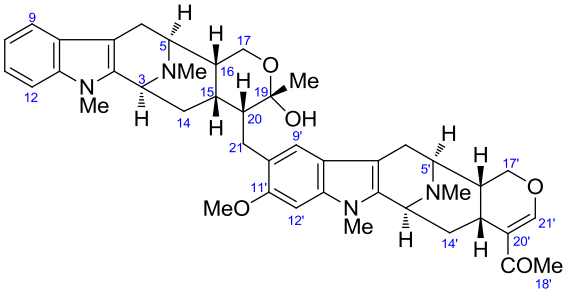

105 macralstonine (20*R*)

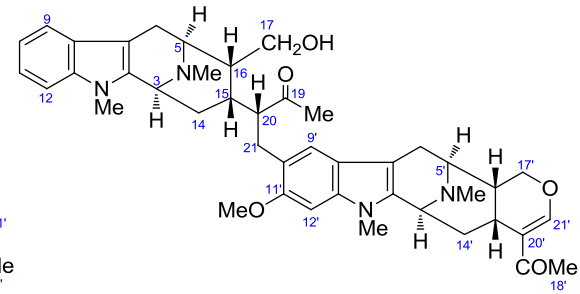

106 *E-seco*-macralstonine (20*R*)

6.2 Determination of the Configuration at C-20 of Perhentinine and Macralstonine

6.2.1 Perhentinine

The bisindole alkaloid perhentinine (**104**) was first isolated from the bark extract of *A. macrophylla* by Y. M. Choo in 2004.[90] The structure was established based on interpretation of the spectral data (NMR, MS, UV, and IR) which indicated constitution from the union of an *E-seco*-macroline (or alstomicine) moiety and a 12-substituted alstophylline, the connection between the two moieties being mediated by a methylene bridge. The data were however insufficient to establish the configuration at C-20.

Since NOE data were of little assistance as the H-20 and H-21 signals in perhentinine were observed as multiplets, the *O*-acetyl derivative **104a** was prepared, in anticipation of an improved resolution of the H-10 and H-21 signals. Fortuitously, the H-20 and H-21 signals of the *O*-acetyl derivative were clearly resolved, and analysis of the coupling constants ($J_{20\text{-}21a}$ = 11.0, $J_{20\text{-}21b}$ = 3.5 Hz; H-20 and H-21a *trans*-diaxial) and the observed NOEs (H-21a/H-15; H-21b/H-14*β*, H-20; 18-Me/H-17, H-20) allowed assignment of the configuration at C-20 as *S* (Figure 6.4).

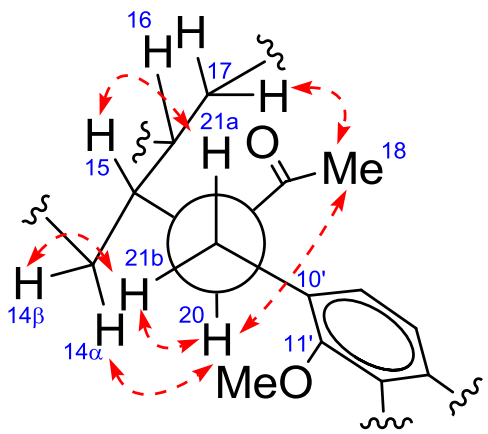

Figure 6.4. Selected NOEs of **104a**.

The ^{1}H and ^{13}C NMR data of **104** and **104a** are summarized in Tables 6.3 and 6.4, respectively, while the ^{1}H NMR spectra of **104** and **104a** are shown in Figures 6.5 and 6.6, respectively.

Table 6.3. ^{1}H NMR data (δ) of perhentinine (**104**) and *O*-acetylperhentinine (**104a**)[a]

Position	**104**[b]	**104a**[c]	Position	**104**[b]	**104a**[c]
3	4.09 dd (4, 2)	4.00 m	3'	3.79 t (3)	3.80 br s
5	3.46 d (7)	3.26 m	5'	2.99 d (7)	3.02 d (7)
6β	2.54 m	2.44 d (17)	6'α	2.28 m	2.54 m
6α	3.32 m	3.14 dd (17, 7)	6'β	3.08 m	3.14 dd (16.5, 7)
9	7.52 d (8)	7.54 br d (7.5)	9'	6.90 s	6.87 s
10	7.13 td (8, 1)	7.13 td (7.5, 1)	12′	6.69 s	6.69 s
11	7.22 td (8, 1)	7.22 td (7.5, 1)	14'α	1.75 td (12, 3)	1.75 m
12	7.32 d (8)	7.32 br d (7.5)	14'β	2.04 m	2.06 m
14β	1.98 m	1.86 m	15'	2.54 m	2.53 dt (11.5, 6)
14α	2.41 m	1.86 m	16'	1.84 dt (11, 4)	1.88 m
15	2.14 m	2.14 m	17'β	4.13 ddd (11, 4, 1)	4.14 dd (11, 2)
16	1.57 m	1.88 m	17'α	4.37 t (11)	4.41 t (11)
17a	3.95 dd (11, 3)	4.28 dd (11, 3.5)	18'	2.05 s	2.07 s
17b	4.01 dd (11, 2)	4.58 t (11)	21'	7.51 s	7.51 s
18	1.72 s	1.71 s	N_1Me'	3.55 s	3.57 s
20	3.32 m	3.08 td (11, 3.5)	N_4Me'	2.25 s	2.30 s
21a	2.41 m	2.31 m	11'-OMe	3.87 s	3.88 s
21b	3.08 m	2.97 dd (13.5, 3.5)			
N_1Me	3.65 s	3.64 s			
N_4Me	2.34 s	2.28 s			
OCOMe	–	2.06 s			

[a]$CDCl_3$; [b]400 MHz; [c]600 MHz; assignments based on COSY, HSQC, and HMBC.

Table 6.4. ^{13}C NMR data (δ) of perhentinine (**104**) and *O*-acetylperhentinine (**104a**)[a]

Position	**104**[b]	**104a**[c]	Position	**104**[b]	**104a**[c]
2	132.9	133.8	2'	131.1	131.5
3	53.1	53.5	3'	53.7	53.8
5	59.2	54.2	5'	54.7	54.7
6	22.6	21.8	6'	22.0	22.8
7	105.9	106.8	7'	105.4	105.6
8	126.3	126.6	8'	120.1	119.2
9	118.2	118.3	9'	118.7	119.4
10	119.0	118.7	10'	119.1	118.7
11	120.9	120.7	11'	153.6	153.7
12	108.7	108.8	12'	91.3	91.4
13	137.0	137.0	13'	136.5	136.7
14	32.3	30.3	14'	32.4	32.4
15	31.5	31.3	15'	22.8	22.9
16	43.1	43.6	16'	38.3	38.4
17	66.5	63.5	17'	67.7	67.8
18	31.1	31.7	18'	24.9	25.4
19	213.2	213.1	19'	195.4	195.6
20	54.5	54.1	20'	120.8	121.1
21	32.0	33.2	21'	157.4	157.7
N_1Me	29.0	29.2	N_1Me'	28.9	29.0
N_4Me	41.7	42.1	N_4Me'	41.2	41.9
OCOMe	–	21.1	11'-OMe	55.5	55.6
OCOMe	–	171.4			

[a]$CDCl_3$; [b]100 MHz; [c]150 MHz; assignments based on COSY, HSQC, and HMBC.

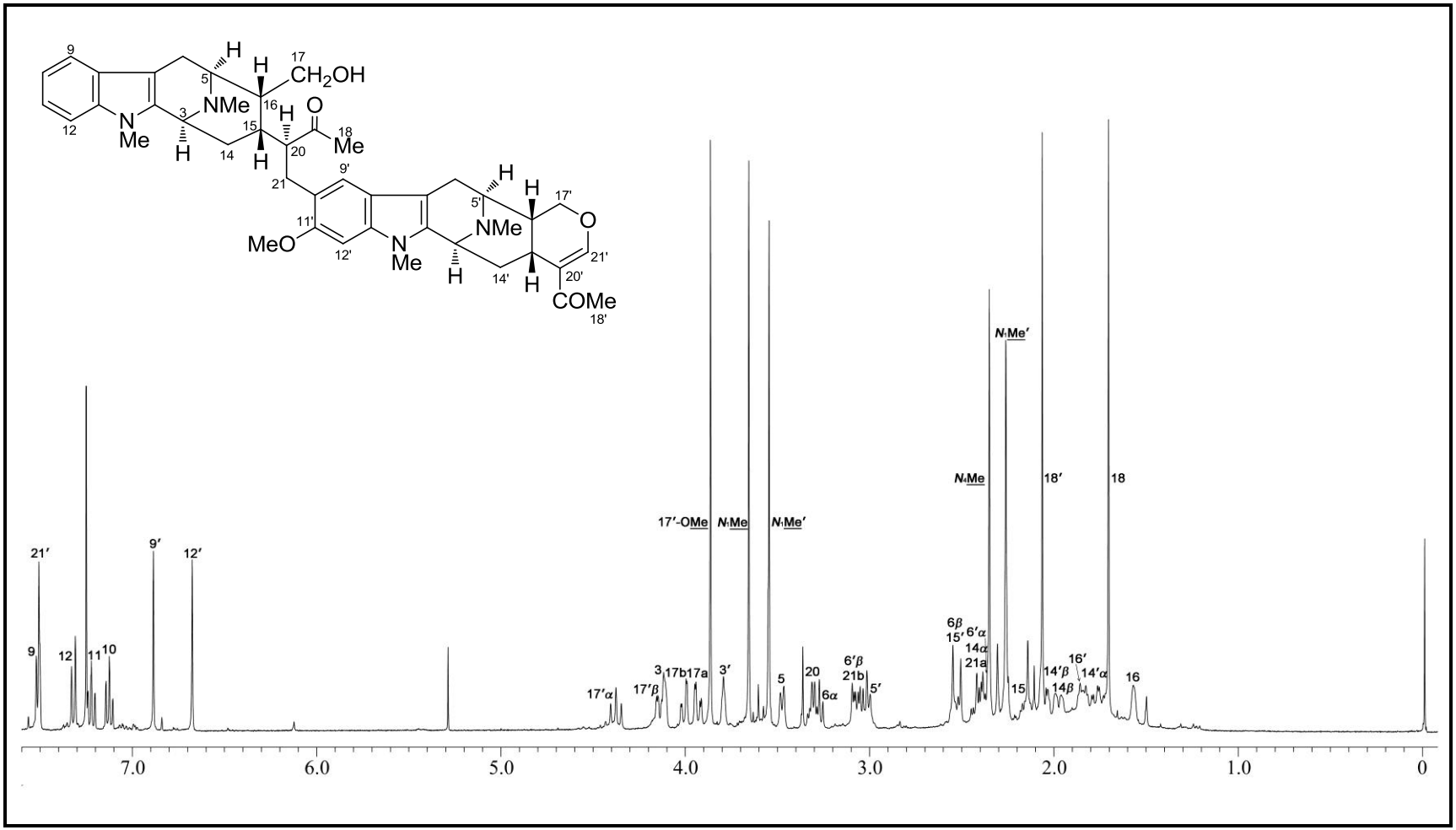

Figure 6.5. ^{1}H NMR spectrum ($CDCl_3$, 400 MHz) of perhentinine (**104**).

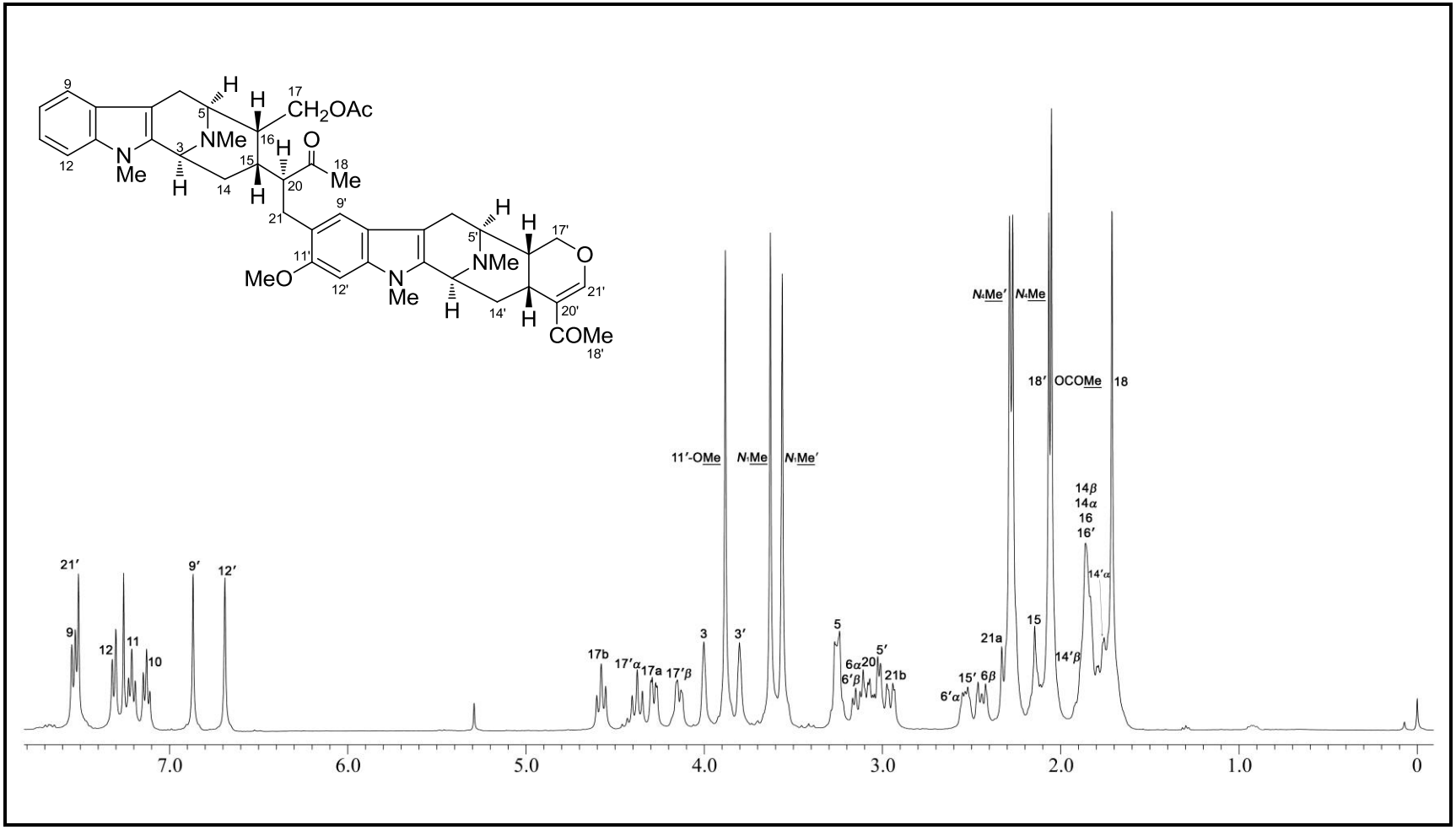

Figure 6.6. ^{1}H NMR spectrum ($CDCl_3$, 600 MHz) of *O*-acetylperhentinine (**104a**).

Additional confirmation by X-ray diffraction analysis was next attempted. However, attempts to obtain suitable crystals of perhentinine (**104**) were singularly unsuccessful. Eventually, it was found that treatment of **104** with excess MeI provided suitable crystals (recrystallized from hot MeOH), which, upon X-ray diffraction analysis, revealed the formation of the dimethyl diiodide salt of the ring-E cyclized (hemiketal) form of perhentinine **104b** (Figure 6.7), from which the absolute configuration at C-20 of the precursor *E-seco*-compound, perhentinine (**104**), could be established as 20*S*.

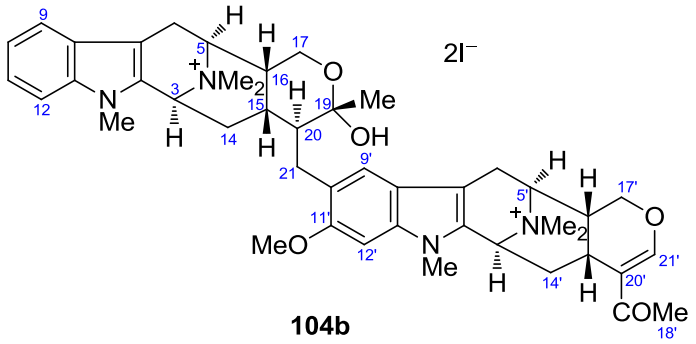

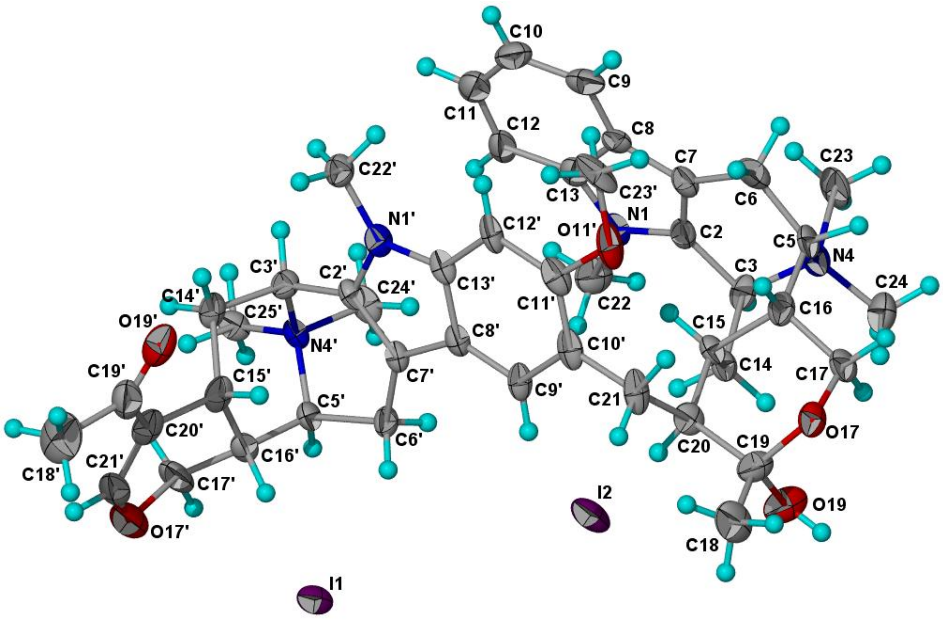

Figure 6.7. X-ray crystal structure of **104b**

[Flack parameter:[63] x = 0.04(0.03), Hooft parameter:[64] y = 0.022(0.07)].

6.2.2 Macralstonine

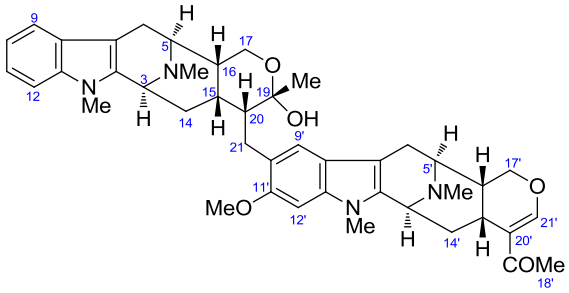

105 macralstonine (20*R*)

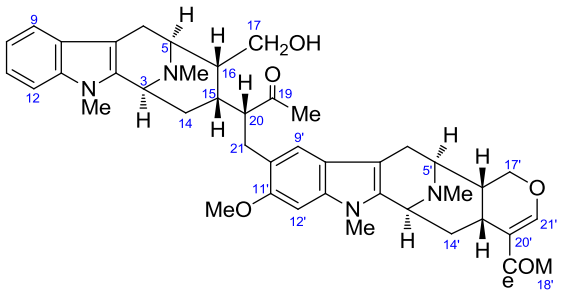

106 *E-seco*-macralstonine (20*R*)

Macralstonine (**105**) was first isolated by Sharp from the bark extract of *A. macrophylla*,[91] and subsequently investigated in detail by Hesse and Schmid,[92] who observed that macralstonine exists as an equilibrium mixture of acyclic (ketone, **106**) and cyclized (hemiketal, **105**) forms in $CHCl_3$ solution. We have confirmed this by analysis of high-field NMR data (600 MHz) of macralstonine. Thus, in $CDCl_3$ solution, the ratio of acyclic to cyclized form was 2.32:1, while in CD_2Cl_2, it was 1.14:1, and in THF-d_8, it was detected only as the cyclized hemiketal form **105**, albeit with poor solubility in this solvent. The two forms were readily distinguishable with the use of 2-D NMR methods. (The ^{1}H and ^{13}C NMR data of **105** and **106** (in $CDCl_3$ and THF) are summarized in Tables 6.5 and 6.6, respectively, while the ^{1}H NMR spectra of **105** and **106** in $CDCl_3$, CD_2Cl_2, and THF are shown in Figures 6.8, 6.9, and 6.10, respectively).

The *E-seco*-macralstonine (**106**) could be trapped by conversion to its *O*-acetyl derivative **106a**,[92] in which case the NMR data of the pure *O*-acetyl-*E-seco*-macralstonine could be determined (The ^{1}H and ^{13}C NMR data of **106a** are summarized in Tables 6.5 and 6.6, respectively, while the ^{1}H NMR spectrum of **106a** is shown in Figure 6.11).

Table 6.5. ^{1}H NMR data (δ) of compounds **105**, **106**, and **106a**[a]

Position	**105**[a]	**106**[a]	**105**[b]	**106a**[a]
3	3.95 m	4.00 m	3.91 m	3.90 m
5	2.93 d (6)	3.59 m	2.84 d (7)	3.43 d (6)
6*a*	2.13 m	2.56 d (17)	2.20 d (16.2)	2.49 d (17)
6*b*	2.63 dd (17, 10)	3.35 dd (17, 7.5)	2.76 dd (16.2, 7)	3.33 dd (17, 7)
9	7.33 (7.5)	7.51 d (7.5)	7.22 d (7.5)	7.53 d (7.5)
10	7.00 m	7.12 t (7.5)	6.84 t (7.5)	7.12 td (7.5, 1)
11	7.09 m	7.21 t (7.5)	7.01 t (7.5)	7.19 td (7.5, 1)
12	7.09 m	7.30 d (7.5)	7.10 d (7.5)	7.29 d (7.5)
14*a*	1.87 m	1.44 d (12)	1.83 m	1.28 d (12)
14*b*	2.86 td (13, 3.5)	2.35 m	2.92 td (12.5, 4)	1.89 m
15	1.77 m	2.01 m	1.62 m	2.03 m
16	1.77 m	1.90 m	1.63 m	2.23 m
17a	3.49 m	4.12 dd (12, 3)	3.27 td (11.5, 5)	4.59 m
17b	4.52 t (11.5)	4.43 d (12)	4.49 t (11.5)	4.59 m
18	1.51 s	1.68 s	1.40 s	1.59 s
20	1.91 m	3.39 td (11, 4)	1.74 m	3.06 td (11, 4)
21a	2.43 m	2.39 m	2.42 dd (13.5, 10.5)	2.37 m
21b	3.06 dd (14, 3.5)	3.00 m	2.99 dd (13.5, 3.5)	3.15 m
N_1Me	3.47 s	3.56 s	3.45 s	3.55 s
N_4Me	2.28 s	2.38 s	2.21 s	2.31 s
OCOMe	–	–	–	2.15 s
3'	3.75 m	3.79 m	3.78 m	3.81 m
5'	3.00 m	3.00 m	3.03 d (7)	3.03 m
6'*a*	2.33 m	2.35 m	2.26 d (16.2)	2.39 m
6'*b*	3.00 m	3.17 dd (16.5, 7)	3.09 dd (16.2, 7)	3.17 m
9'	6.74 s	6.90 s	6.72 s	6.90 s
12'	6.40 s	6.69 s	6.42 s	6.69 s
14'*a*	1.76 m	1.77 m	1.69 m	1.78 m
14'*b*	2.01 m	2.01 m	1.99 m	2.07 m
15'	2.60 m	2.60 m	2.47 m	2.59 m
16'	1.87 m	1.87 m	1.83 m	1.89 m
17'*a*	4.19 dd (11, 3)	4.14 dd (12, 3)	4.14 dd (11.5, 3)	4.14 d (11)
17'*b*	4.38 m	4.38 t (12)	4.37 t (11.5)	4.39 t (11)
18'	2.07 s	2.09 s	1.98 s	2.09 s
21'	7.52 s	7.53 s	7.57 s	7.54 s
N_1Me'	3.50 s	3.59 s	3.51 s	3.57 s
N_4Me'	2.13 s	2.24 s	2.13 s	2.26 s
11'-OMe	3.92 s	3.65 s	3.59 s	3.91 s

[a]600MHz; [b]$CDCl_3$; [c]THF-d_8; assignments based on COSY, HSQC, and HMBC.

Table 6.6. ^{13}C NMR data (δ) of compounds **105**, **106**, and **106a**[a]

Position	**105**[b]	**106**[b]	**105**[c]	**106a**[b]
2	133.3	132.6	134.4	133.4
3	54.0	53.1	54.7	53.2
5	55.5	59.6	56.7	53.6
6	22.7	22.4	23.3	22.1
7	106.5	105.9	106.7	106.6
8	126.45	126.36	127.3	126.5
9	117.9	118.0	117.9	118.0
10	118.4	118.9	118.6	118.7
11	120.2	121.0	120.4	120.8
12	108.5	109.0	109.0	109.0
13	136.8	137.2	137.7	137.2
14	26.9	33.0	27.4	31.5
15	25.9	32.3	26.6	31.5
16	44.0	42.1	45.5	41.9
17	61.4	66.2	61.5	62.6
18	29.5	33.9	29.1	32.7
19	99.0	214.5	98.5	213.9
20	45.6	53.8	46.9	53.9
21	28.8	32.49	29.6	31.8
N_1Me	29.07	29.14	28.7	29.1
N_4Me	41.69	41.4	41.7	42.1
OCOMe	–	–	–	21.3
OCOMe	–	–	–	171.4
2'	131.2	131.5	131.7	131.3
3'	53.76	53.8	54.4	53.9
5'	54.7	54.7	55.4	54.7
6'	22.5	22.8	22.9	22.9
7'	105.1	105.6	105.7	105.5
8'	119.7	119.1	120.6	120.1
9'	118.8	119.5	119.3	119.4
10'	120.1	120.2	121.9	119.0
11'	153.9	153.8	154.8	153.9
12'	91.4	91.2	91.9	91.3
13'	136.1	136.6	137.1	136.7
14'	32.4	32.47	33.3	32.4
15'	22.9	22.9	23.6	22.8
16'	38.5	38.4	39.5	38.4
17'	67.87	67.85	68.2	67.8
18'	25.0	25.1	24.6	25.1
19'	195.5	195.8	193.9	195.7
20'	121.2	121.2	121.9	121.1
21'	157.4	157.7	157.3	157.6
N_1Me'	28.7	29.04	28.6	29.0
N_4Me'	41.77	41.74	42.1	41.9
11'-OMe	55.3	55.6	55.1	55.5

[a]150 MHz; [b]$CDCl_3$; [c]THF-d_8; assignments based on COSY, HSQC, and HMBC.

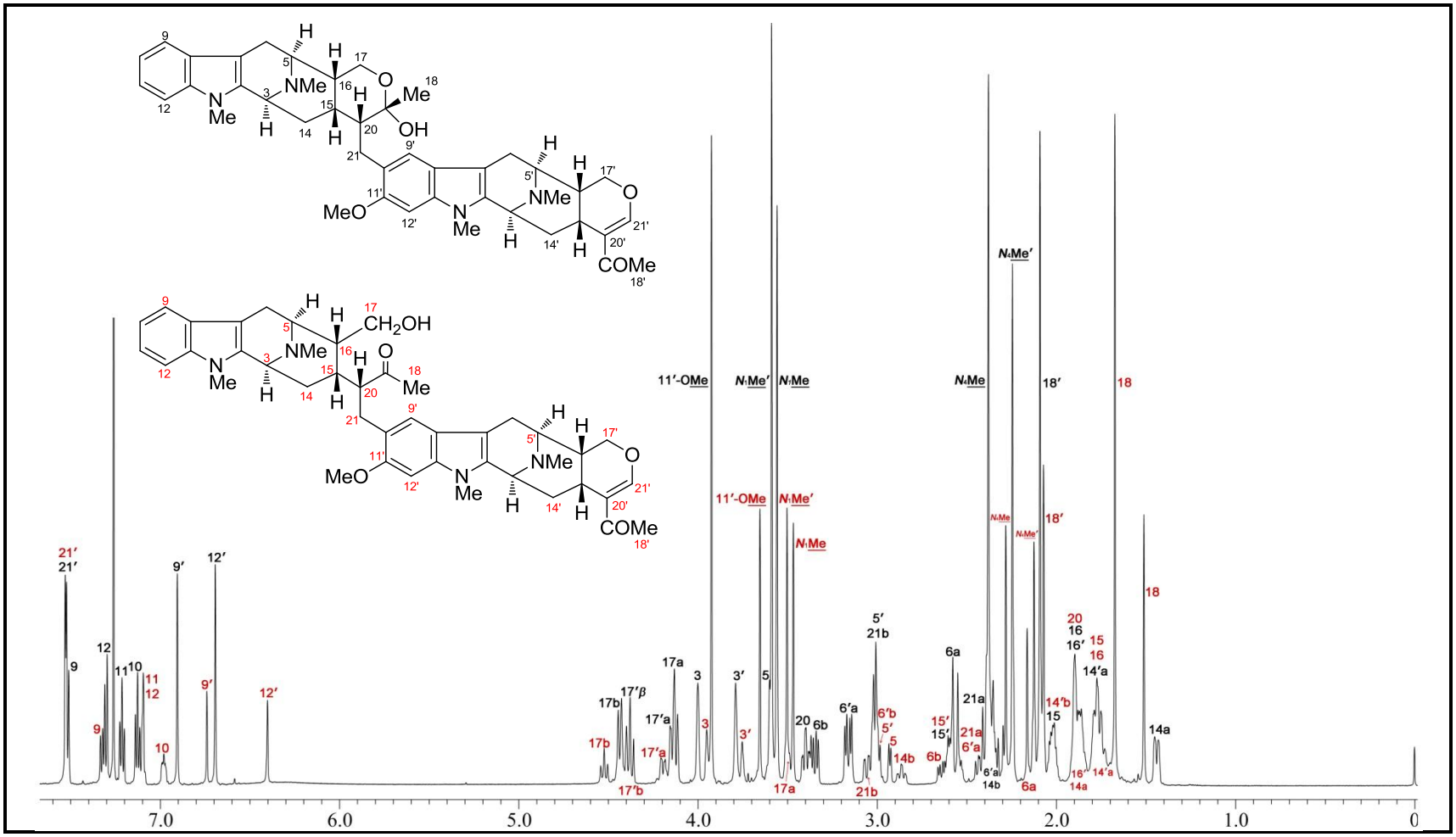

Figure 6.8. ^{1}H NMR spectrum ($CDCl_3$, 600 MHz) of macralstonine (**105**) and *E-seco*-macralstonine (**106**).

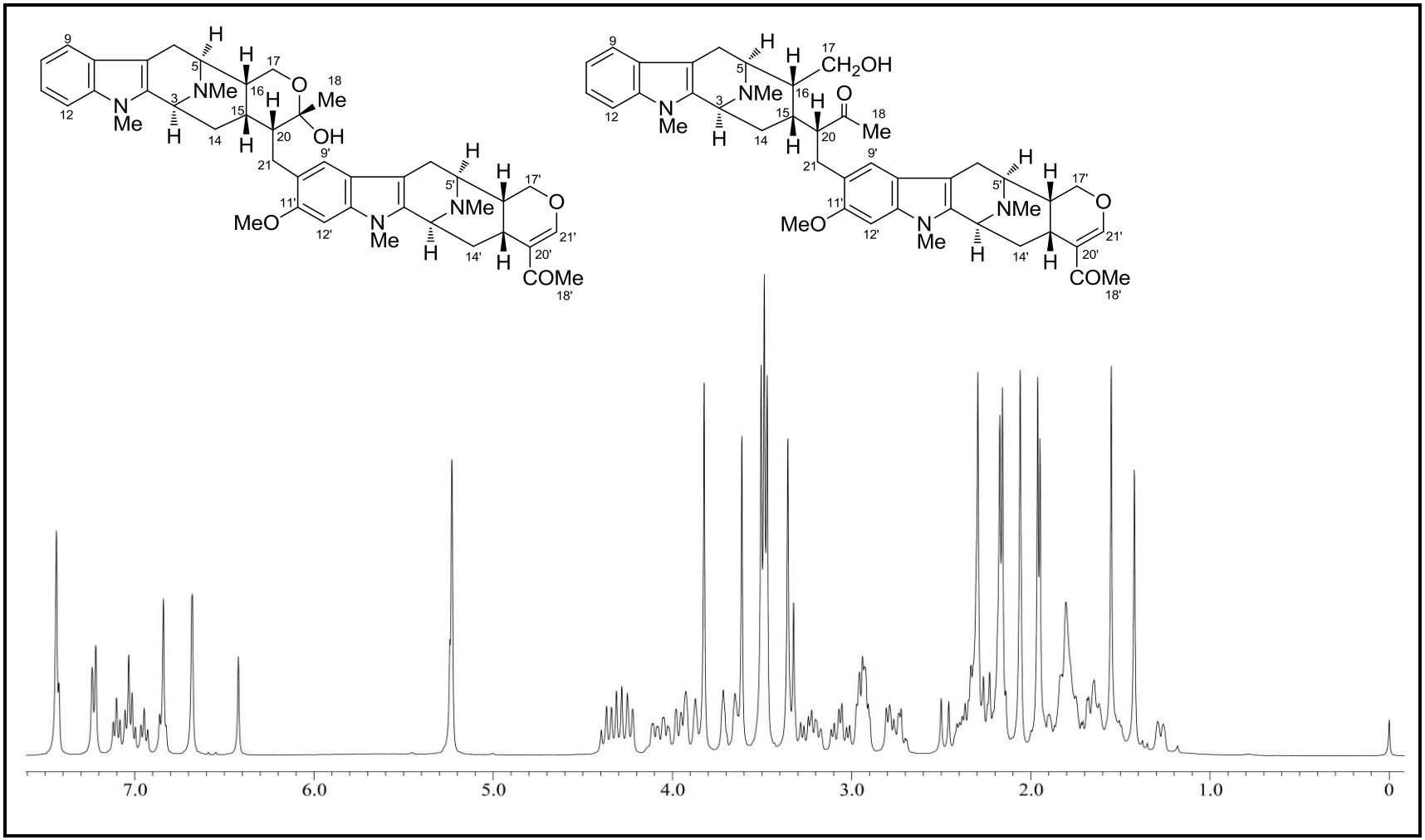

Figure 6.9. ^{1}H NMR spectrum (CD_2Cl_2, 400 MHz) of macralstonine (**105**) and *E-seco*-macralstonine (**106**).

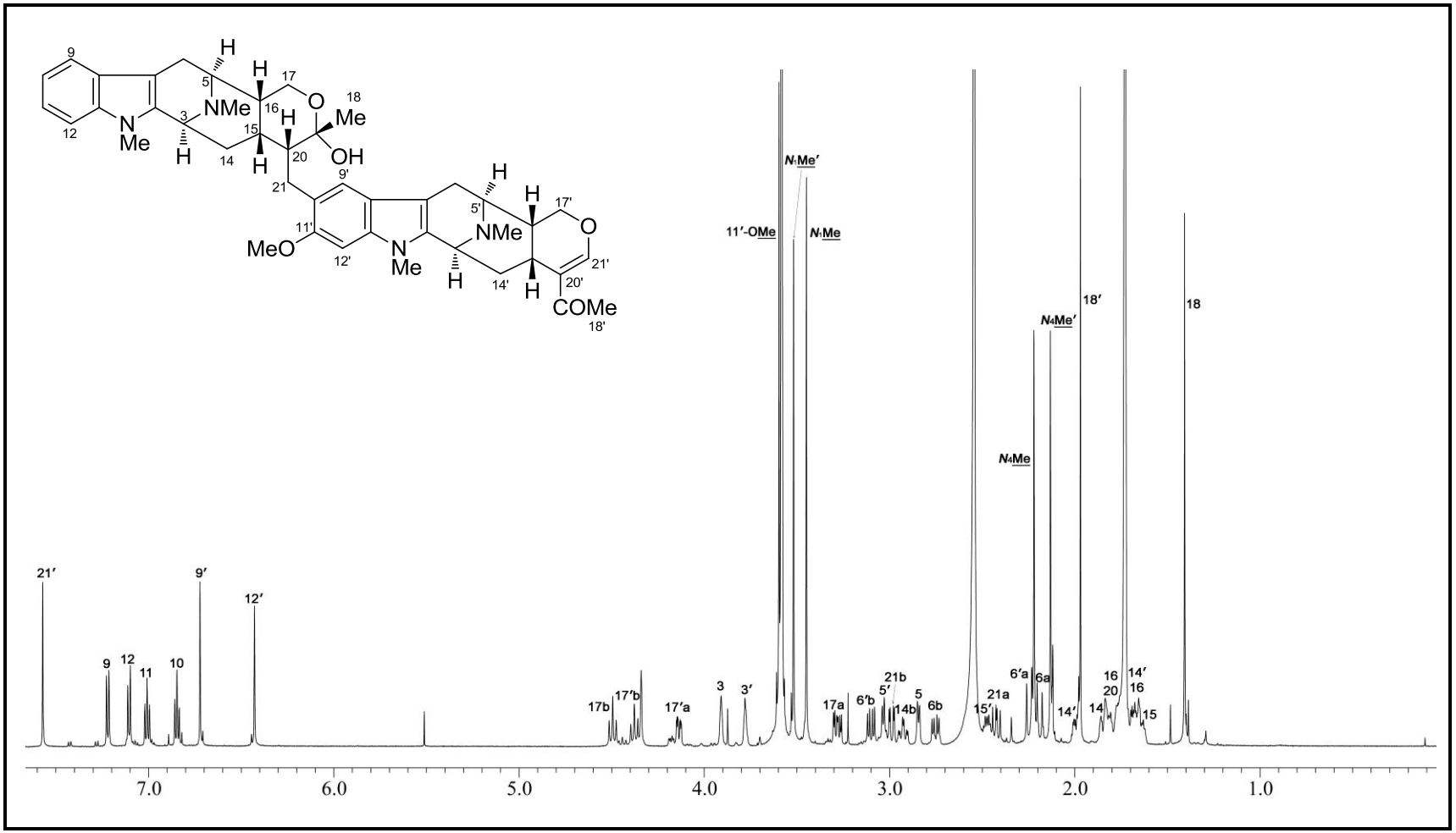

Figure 6.10. ^{1}H NMR spectrum (THF-d_8, 600 MHz) of macralstonine (**105**).

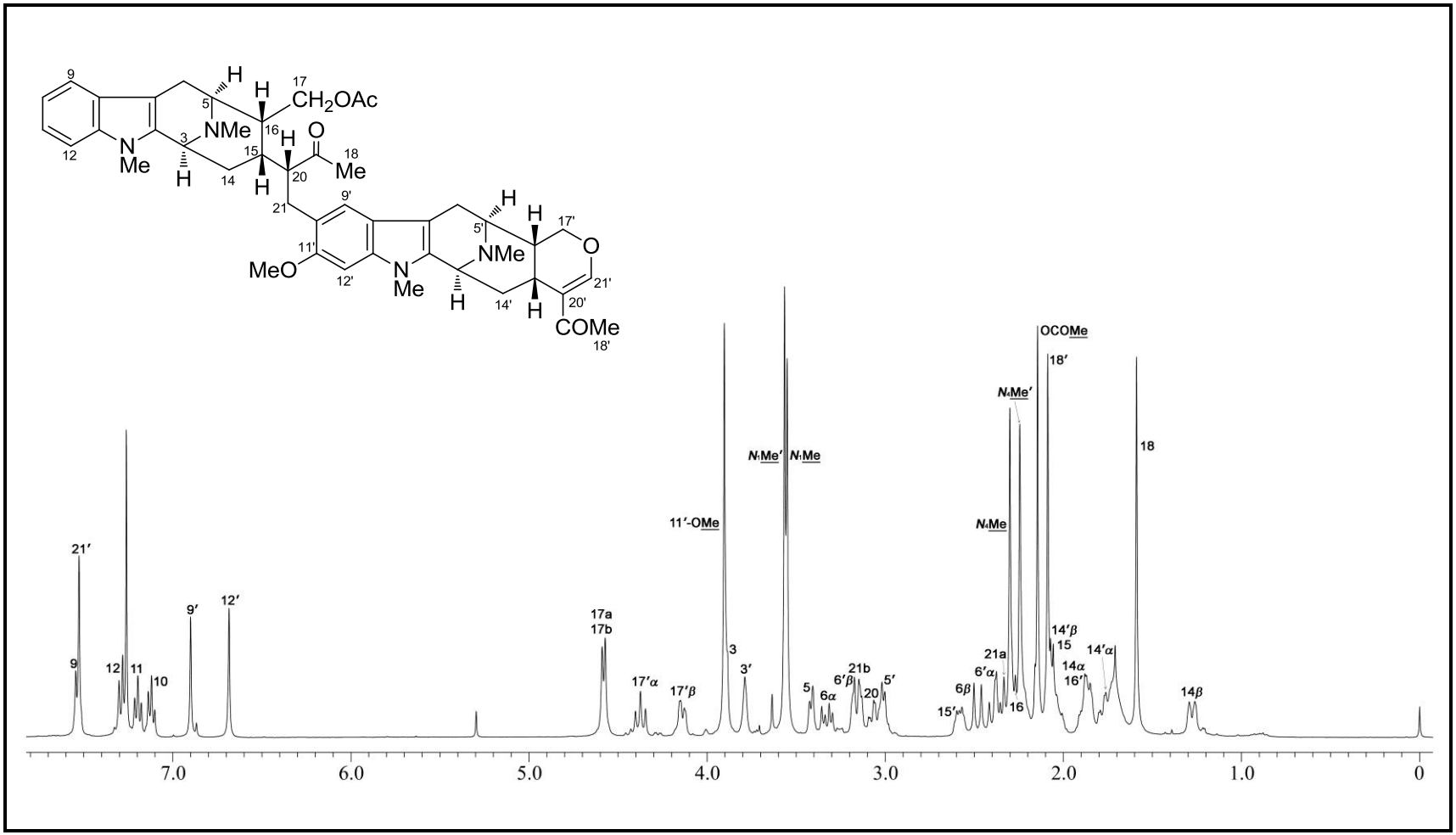

Figure 6.11. ^{1}H NMR spectrum ($CDCl_3$, 600 MHz) of *O*-acetyl-*E*-*seco*-macralstonine (**106a**).

The relative configuration at C-20 in the *O*-methyl congener of macralstonine, **107**, isolated from the Thai *A. macrophylla* was established as 20*R* based on its NOESY spectrum.[93,95] In the case of macralstonine (**105**), however, NOE was not feasible due to the observation of H-20 and H-21 as multiplets.

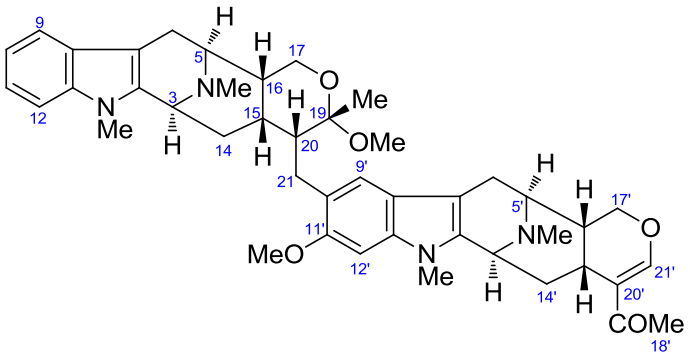

107 *O*-methylmacralstonine

In the case of the *O*-acetyl-*E*-*seco*-macralstonine derivative **106a**, H-20 was clearly seen as a triplet of doublets ($J_{20\text{-}21a}$ = 11.0, $J_{20\text{-}21b}$ = 4.0 Hz; H-20 and H-21a *trans*-diaxial) at δ_H 3.06 and this, coupled with the observed NOEs (H-20/H-14α, H-18; H-21a/H-15, H-9'; H-21b/H-16, H-17, H-9'), allowed assignment of the C-20 configuration as *R* (Figure 6.12).

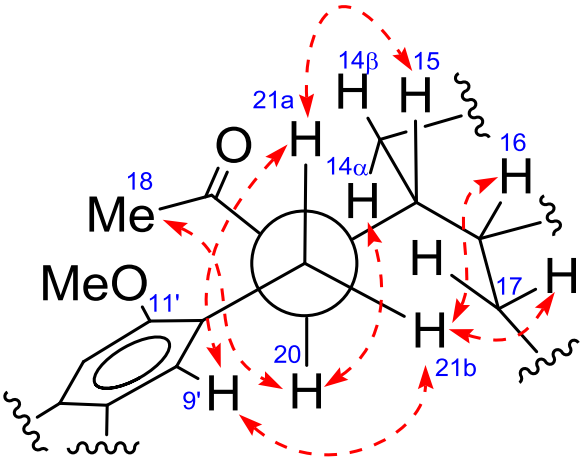

Figure 6.12. Selected NOEs of **106a**.

In the event, macralstonine crystallized as the cyclized hemiketal form (**105**) from CH_2Cl_2/MeOH solution. X-ray analysis was therefore carried out and confirmed the 20*R* absolute configuration (Figure 6.13).

The X-ray crystal structure of **105** also showed that it existed as the cyclized form in the solid state. Repeating the X-ray diffraction experiment using different crystals yielded the same outcome as the first experiment.

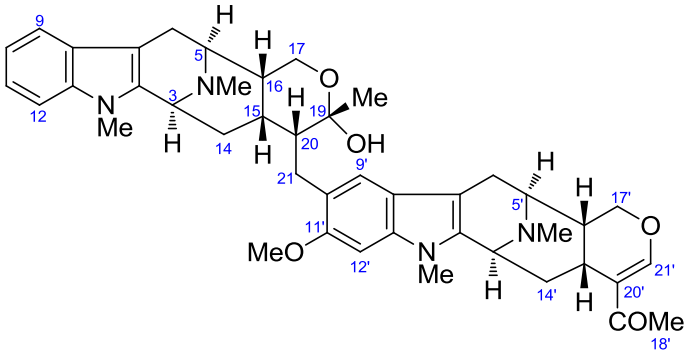

105 macralstonine (20*R*)

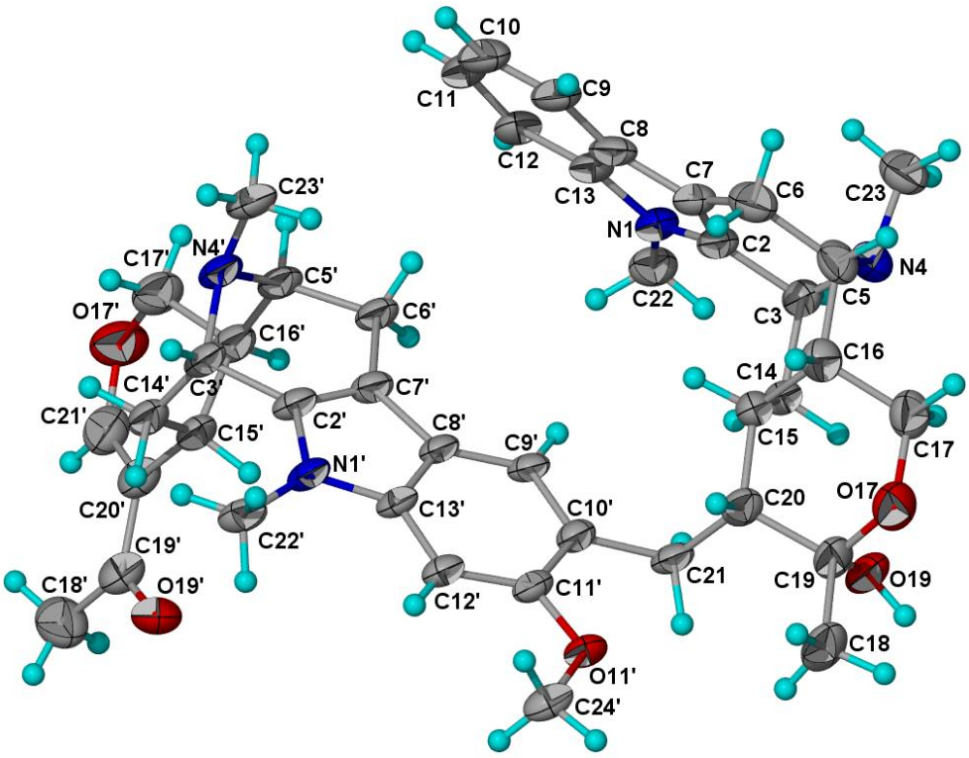

Figure 6.13. X-ray crystal structure of **105**

[Flack parameter:[63] $x = -0.1(0.4)$; Hooft parameter:[64] $y = -0.30(0.14)$].

With the C-20 configuration of both perhentinine and macralstonine determined *via* their acetate derivatives (**104a** and **106a**), the same approach can be used for the determination of the C-20 configuration in the perhentidines.

6.3 Determination of the Configuration at C-20 of Perhentidines A–C

The gross structures of the perhentidines A–C (**101**–**103**) were established *via* extensive application of 2D NMR techniques, including determination of the relative configurations at the various stereogenic centers, with the exception of the configuration at C-20.[89]

Examination of the ^{1}H NMR data of perhentidines A (**101**) and B (**102**) showed that the signals of H-20 in both alkaloids were observed as multiplets (Table 6.1). Furthermore, the signal of one of the C-21 hydrogens in perhentidine A (**101**), and of both the C-21 hydrogens in perhentidine B (**102**), were also observed as multiplets. Acetylation of alkaloids **101** and **102** yielded the *O*-acetyl derivatives **101a** and **102a**, in which the signals for H-20 and H-21 of both the compounds were clearly resolved (Table 6.7). The signal due to H-20 in *O*-acetylperhentidine A (**101a**) was seen as a triplet of doublets at δ_H 2.99 with J = 10.7 and 3.8 Hz (*i.e.*, $J_{20\text{-}21a} = J_{15\text{-}20}$ = 10.7 Hz, $J_{20\text{-}21b}$ = 3.8 Hz). The signal of one of the hydrogens on C-21 was observed as a doublet of doublets at δ_H 2.83 ($J_{21a\text{-}21b}$ = 14 Hz, $J_{20\text{-}21a}$ = 10.7 Hz). The large coupling constant of 10.7 Hz due to the coupling between H-20 and H-21a, suggested that the conformation adopted about the C-20–C-21 bond was one that places the two vicinal hydrogens at C-20 and C-21 *anti* (*trans*-diaxial) to one another. The preferred *anti* conformation was likely due to the presence of three bulky groups, two on C-20, and one on C-21, which resulted in steric hindrance to free rotation about the C-20–C-21 bond. The observation that H-20 is *trans*-diaxial to H-21a, coupled with the observed NOE interactions

between H-21a and H-15; H-20 and H-14α, H-21b; H-21b and H-14; 18-Me and H-17, H-20 (Figure 6.14) allowed the configuration at C-20 in the acetate derivative **101a**, and therefore in perhentidine A (**101**) as well, to be assigned as 20*S*.

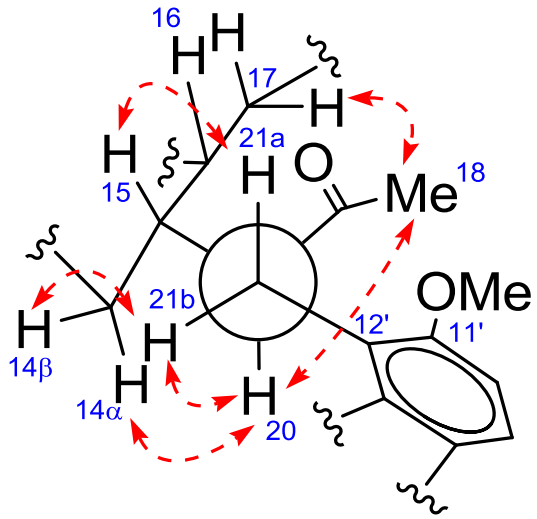

Figure 6.14. Selected NOEs of **101a**.

In the case of *O*-acetylperhentidine B (**102a**), the signal due to H-20 was also seen as a triplet of doublets at δ_H 3.23 with J = 11 and 5 Hz. The observed H-20–H-21a coupling of 11 Hz, indicated a *trans*-diaxial disposition of the two hydrogens, as in the case of *O*-acetylperhentidine A acetate (**101a**). In this instance however, the definitive NOEs, which allowed the assignment of the configuration at C-20, were different from those observed in **101a**. Thus, in the case of *O*-acetylperhentidine B (**102a**), NOEs were observed between H-20 and H-14, H-21b; H-21a and H-15; H-21b and H-16, H-17; H-18 and H-14, H-15, H-20 (Figure 6.15). These NOEs are consistent with the assignment of the C-20 configuration in **102a** (and therefore **102**) as 20*R*.

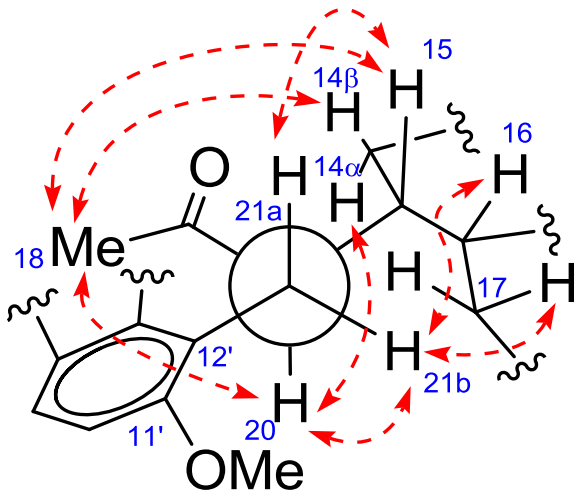

Figure 6.15. Selected NOEs of **102a**

The ^{1}H and ^{13}C NMR data of compounds **101a** and **102a** are summarized in Tables 6.7 and 6.8, respectively, while the ^{1}H NMR spectra of compounds **101a** and **102a** are shown in Figures 6.16 and 6.17, respectively.

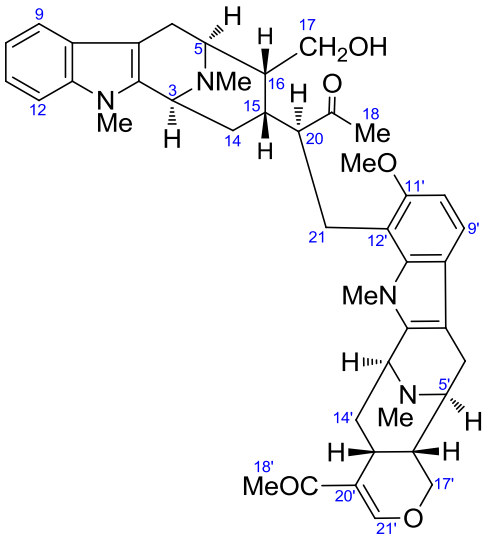

101 perhentidine A (20*S*)

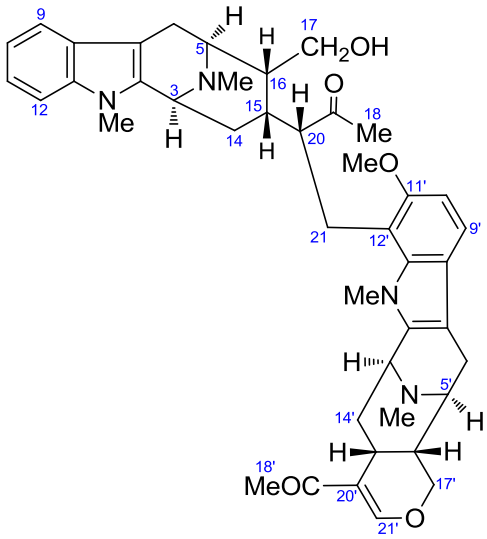

102 perhentidine B (20*R*)

Table 6.7. ^{1}H NMR data (δ) of compounds **101a**–**103a**[a]

Position	**101a**[b]	**102a**[b]	**103a**[c]
3	4.03 m	3.88 m	4.07 m
5	3.25 m	3.44 m	3.25 m
6β	2.50 m	2.52 m	2.48 m
6α	3.25 m	3.35 dd (17, 8)	3.25 m
9	7.57 d (8)	7.58 d (7.5)	7.58 br d (7.5)
10	7.15 t (8)	7.14 t (7.5)	7.16 td (7.5, 1)
11	7.23 t (8)	7.22 t (7.5)	7.23 td (7.5, 1)
12	7.34 d (8)	7.31 d (7.5)	7.33 br d (7.5)
14β	1.94 m	1.32 m	1.94 m
14α	1.94 m	1.81 m	1.94 m
15	2.25 m	2.14 m	2.21 m
16	1.94 m	2.21 m	1.87 m
17a	4.15 dd (11, 3.5)	4.63 m	4.22 dd (11, 4)
17b	4.53 dd (11, 9)	4.63 m	4.49 dd (11, 9)
18	1.59 s	1.30 s	1.34 s
20	2.99 td (10.7, 3.8)	3.23 td (11, 5)	3.15 m
21a	2.83 dd (14, 10.7)	3.04 m	2.48 m
21b	3.17 dd (14, 3.8)	3.32 dd (14, 5)	3.15 m
N_1Me	3.66 s	3.55 s	3.67 s
N_4Me	2.35 s	2.28 s	2.37 s
OCOMe	2.03 s	2.16 s	1.99 s
3'	3.79 m	3.72 m	3.81 m
5'	3.05 m	3.01 m	2.81 d (7)
6'α	2.40 d (16)	2.35 d (16)	2.26 d (16)
6'β	3.23 m	3.18 dd (16, 7)	3.11 m
9'	7.23 d (8.5)	7.19 d (8.5)	–
10'	6.76 d (8.5)	6.77 d (8.5)	–
11'	–	–	6.83 d (8.7)
12'	–	–	7.07 d (8.7)
14'α	1.74 m	1.71 td (12, 3.5)	1.75 m
14'β	1.98 m	1.99 m	2.08 m
15'	2.48 m	2.50 m	2.48 m
16'	1.84 m	1.82 m	1.69 m
17'α	4.13 dd (11.5, 3.5)	4.12 dd (11, 3)	4.09 m
17'β	4.39 t (11.5)	4.37 t (11)	4.31 t (11)
18'	2.06 s	2.06 s	2.06 s
21'	7.49 s	7.50 s	7.50 s
N_1Me'	3.48 s	3.52 s	3.53 s
N_4Me'	2.27 s	2.24 s	2.31 s
10'-OMe	–	–	3.88 s
11'-OMe	3.85	3.92 s	–

[a]$CDCl_3$, [b]600 MHz; [c]400 MHz; assignments based on COSY, HSQC, and HMBC.

Table 6.8. ^{13}C NMR data (δ) of compounds **101a–103a**[a]

Position	**101a**[b]	**102a**[b]	**103a**[c]
2	133.6	133.6	133.1
3	53.5	53.2	53.7
5	54.6	53.3	55.0[d]
6	21.7	22.1	21.8
7	107.0	106.7	107.1
8	126.7	126.7	126.8
9	118.4	118.0	118.5
10	118.8	118.6	118.7
11	120.7	120.7	120.7
12	108.8	109.1	108.9
13	137.0	137.2	137.2
14	30.3	31.3	30.1
15	30.8	31.6	31.2
16	43.0	42.0	43.3
17	63.7	62.6	64.0
18	32.2	34.1	32.9
19	212.8	214.1	213.1
20	54.8	52.4	53.2[d]
21	26.2	25.6	29.0
N_1Me	29.1	28.9	29.1[e]
N_4Me	41.9	41.9	41.6[f]
OCOMe	21.2	21.3	21.2
OCOMe	171.3	171.6	171.2
2'	133.8	133.6	133.8
3'	53.9	53.8	54.0
5'	54.6	54.6	54.4
6'	22.5	22.7	25.3
7'	105.8	105.2	105.3
8'	122.9	123.2	126.3
9'	116.1	115.8	118.0
10'	104.7	104.5	151.2
11'	153.5	153.8	106.5
12'	110.9	110.0	107.3
13'	136.3	136.1	133.1
14'	32.2	32.0	32.2
15'	22.7	22.8	22.8
16'	38.4	38.5	38.5
17′	67.7	67.7	67.5
18'	25.0	25.0	25.1
19'	195.3	195.5	195.7
20'	121.0	121.1	120.9
21'	157.2	157.4	157.8
N_1Me′	32.2	32.4	29.2[e]
N_4Me′	42.1	41.7	42.2[f]
10'-OMe	–	–	56.9
11'-OMe	56.6	56.6	–

[a]$CDCl_3$; [b]150 MHz; [c]100 MHz; [d–f]assignments are interchangeable; assignments based on COSY, HSQC, and HMBC.

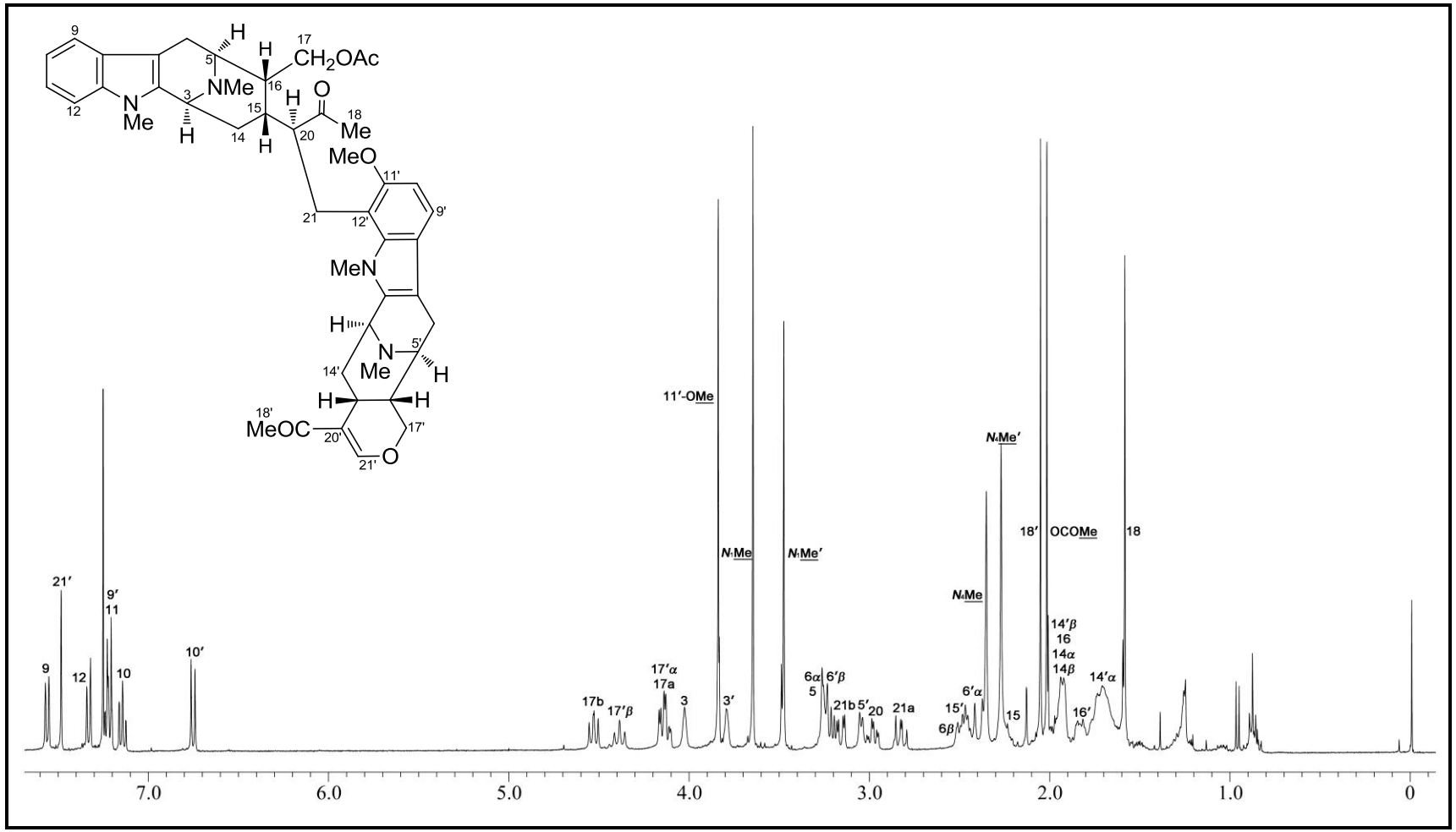

Figure 6.16. ^{1}H NMR spectrum ($CDCl_3$, 600 MHz) of *O*-acetylperhentidine A (**101a**).

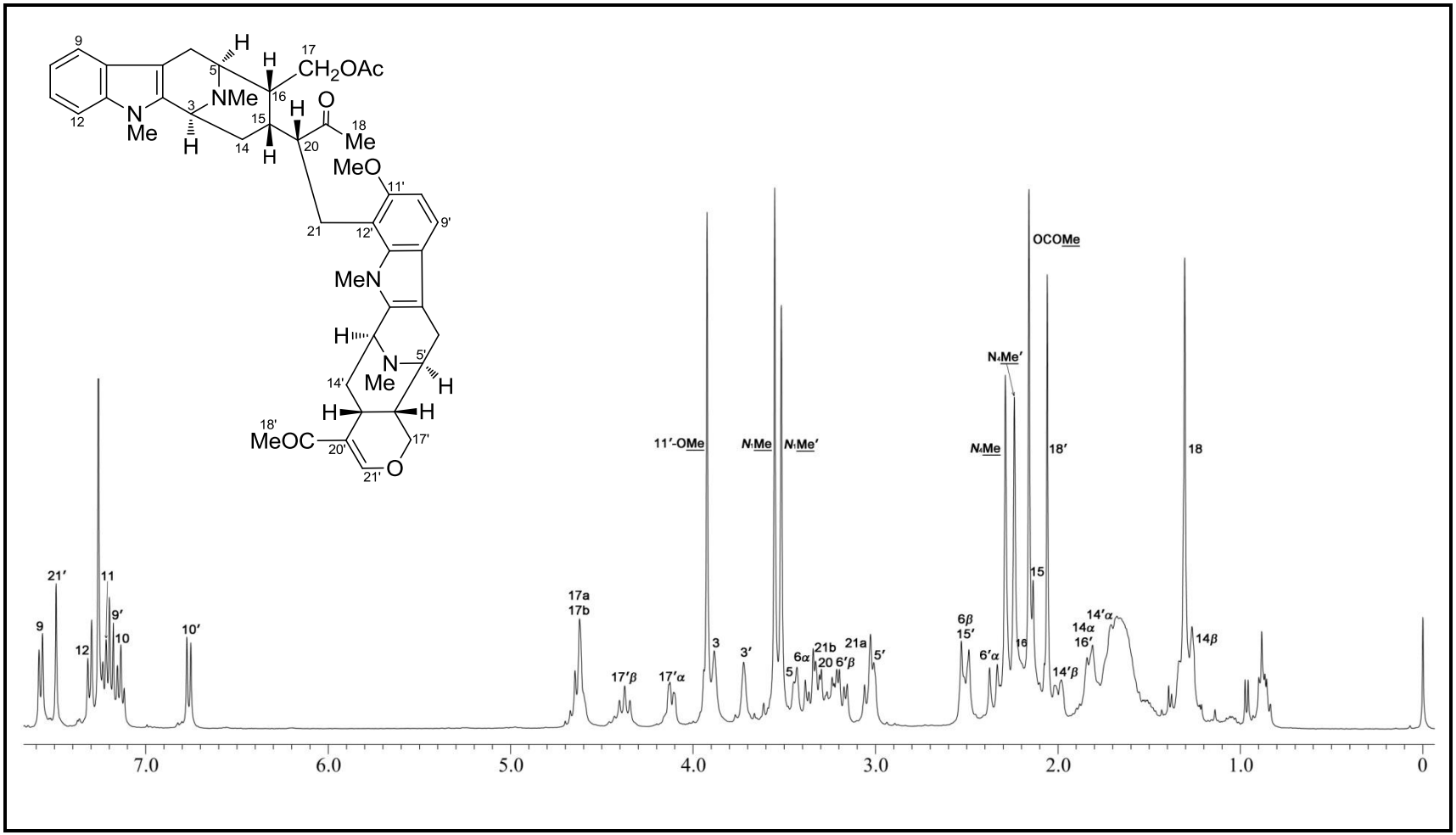

Figure 6.17. ^{1}H NMR spectrum ($CDCl_3$, 600 MHz) of *O*-acetylperhentidine B (**102a**).

In the case of perhentidine C (**103**), the relative configuration of C-20 in **103** can be deduced directly from analysis of the coupling constants and the observed NOEs of the parent compound. In the case of **103**, and unlike **101** and **102**, the H-21 resonances were well resolved in the ^{1}H NMR spectrum, whereas the resonances of H-20 and H-21 were multiplets in the *O*-acetyl derivative **103a** (Table 6.7). As before, the signal due to one of the hydrogens on C-21 was observed as a triplet at δ_H 2.60 ($J_{21a\text{-}21b} = J_{21a\text{-}20} = 12$ Hz) indicating a preferred conformation about the C-20–C-21 bond which places the two vicinal hydrogens *anti* (*trans*-diaxial) to one another due to steric hindrance caused by the presence of three bulky groups. This, coupled with the observed NOE interactions between H-21a and H-15, H-6'β; H-21b and H-14β; 18-Me and H-16, H-17, H-20 (Figure 6.18) allowed the configuration at C-20 to be assigned as 20*S*.

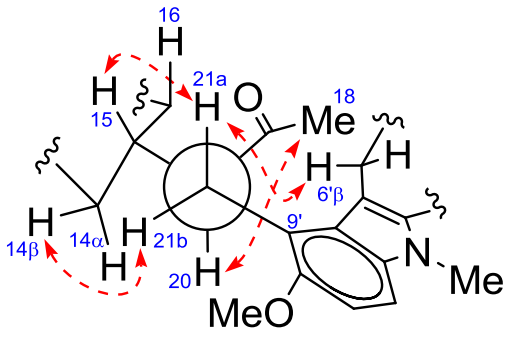

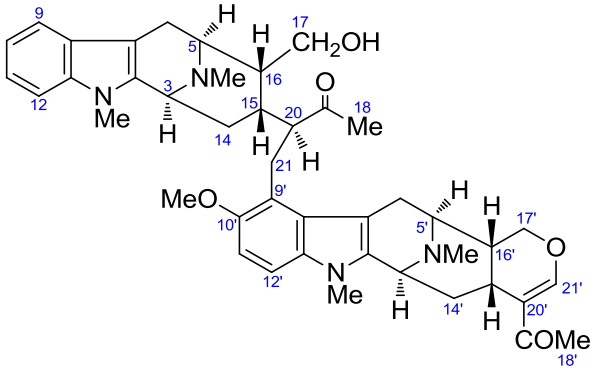

Figure 6.18. Selected NOEs of **103**.

103 perhentidine C (20*S*)

The ^{1}H and ^{13}C NMR data of **103a** are summarized in Tables 6.7 and 6.8, respectively, while the ^{1}H NMR spectrum of **103a** is shown in Figure 6.19.

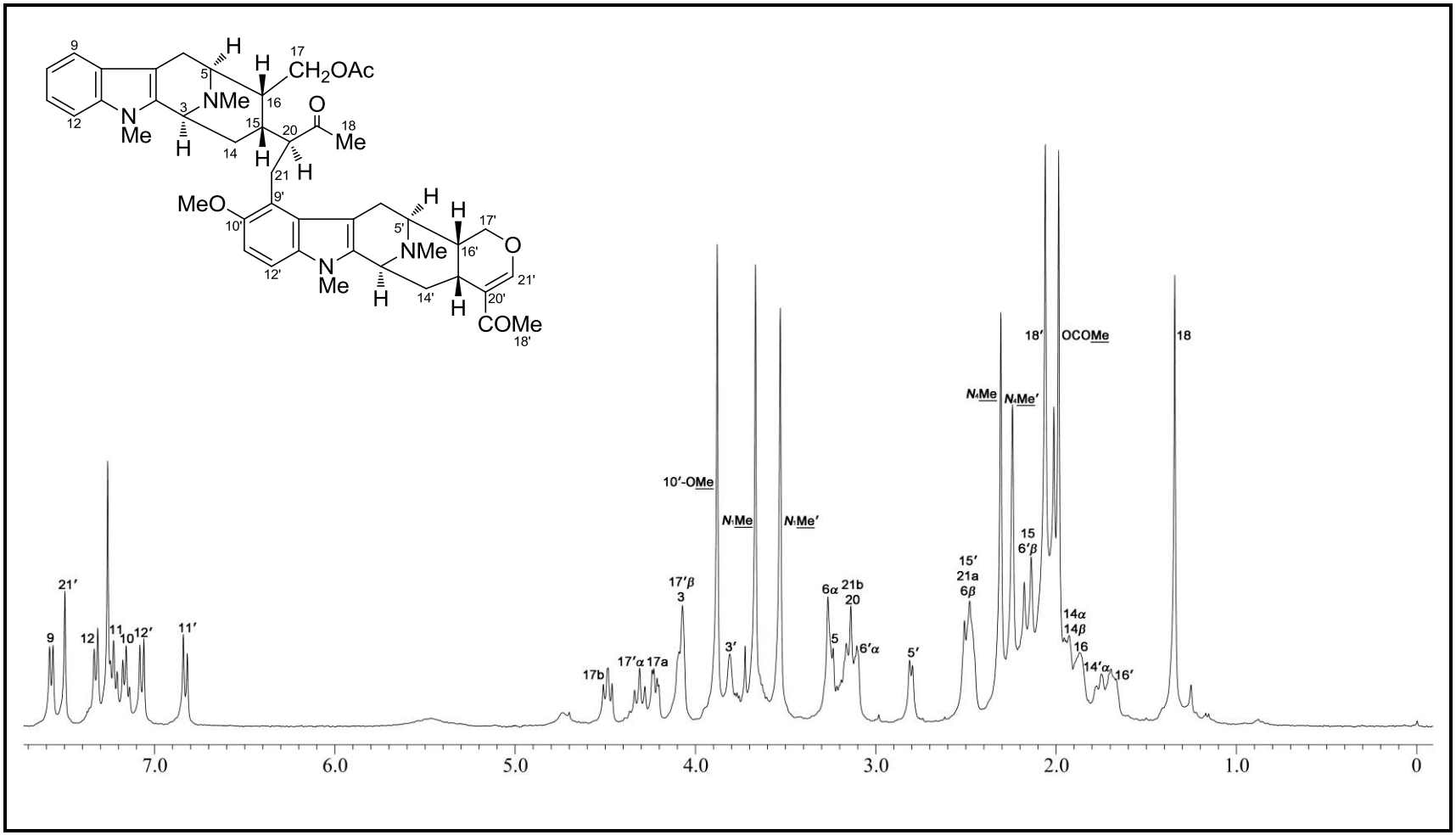

Figure 6.19. ^{1}H NMR spectrum ($CDCl_3$, 400 MHz) of *O*-acetylperhentidine C (**103a**).

6.4 Comparison of NMR Data between Alkaloids 101–104, and 106

Since we now have two bisindole alkaloids, *viz*., perhentinine (**104**) (and its cyclized hemiketal derivative in the form of its dimethyl diiodide salt, **104b**) and macralstonine (**105**) (and its ring-opened form as its acetate derivative, **106a**) that possess opposite C-20 configuration, and for which we have obtained X-ray crystal structure data, these two alkaloids can therefore serve as model compounds for comparison of the perhentidines.

It was observed that in the NMR spectra of the parent bisindoles (**101**–**104**, **106**), the signals of the C-17 oxymethylene hydrogens are well separated in the case of the 20*R* bisindoles, **102** and **106** ($\Delta\delta_H = \delta_{17b}-\delta_{17a}$ ~ 0.3–0.4 ppm), whereas these signals were very close in the 20*S* compounds, **101**, **103**, and **104** ($\Delta\delta_H = \delta_{17b}-\delta_{17a}$ ~ 0.02–0.07 ppm) (Figure 6.20). In the case of the *O*-acetyl derivatives (**101a**–**104a**, **106a**) however, this trend was reversed, and a clear distinction could be observed between the 20*S* and 20*R* series. Thus, the signals due to the C-17 oxymethylene hydrogens in the acetate derivatives of the 20*S* series (**101a**, **103a**, and **104a**) were observed as well separated AX doublet of doublets ($\Delta\delta_H = \delta_{17b}-\delta_{17a}$ ~ 0.3–0.4 ppm), while those in the *O*-acetyl derivatives of the 20*R* series (**102a** and **106a**) were invariably observed as overlapped multiplets ($\Delta\delta_H = \delta_{17b}-\delta_{17a}$ ~ 0 ppm) (Figure 6.20). This not only provided additional strong support for the assignment of the C-20 configurations in alkaloids **101**–**105** based on analysis of the NMR coupling constants and NOE data (*vide infra*), but in addition could serve as a potentially general method for the determination of the configuration at C-20 in related bisindoles with a similar constitution and branching of the monomeric units.

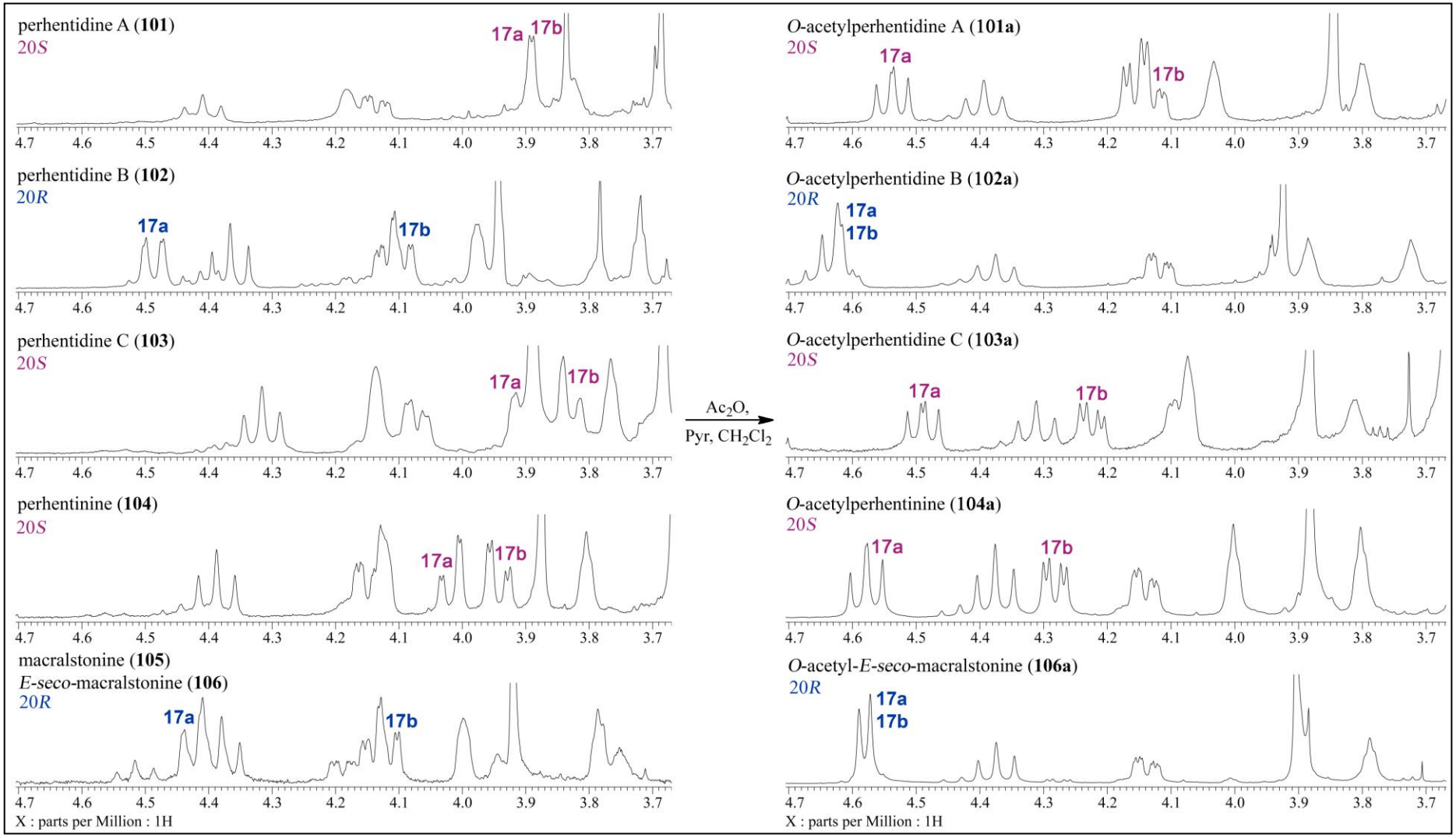

Figure 6.20. Partial ^{1}H NMR spectrum (400 MHz) of alkaloids **101–105** and **106**, and acetates **101a–104a** and **106a**.

6.5 Conclusion

In conclusion, we have established complete and firm structure assignment of the new macroline-macroline bisindoles perhentidines A (**101**), B (**102**), and C (**103**), including the determination of the configuration at C-20. We have also obtained X-ray confirmation (determination of absolute configuration) of the structures of the previously isolated bisindole alkaloids, perhentinine (**104**) and macralstonine (**105**), which has also facilitated the firm assignment of the structures of perhentidines A–C (**101**–**103**).

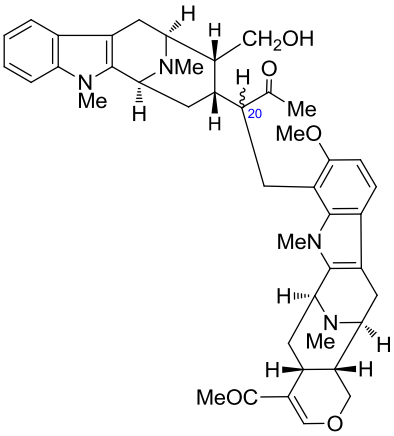

101 perhentidine A (20*S*)
102 perhentidine B (20*R*)

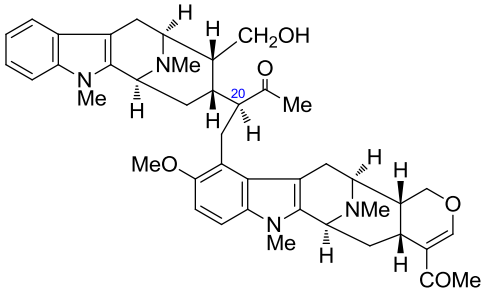

103 perhentidine C (20*S*)

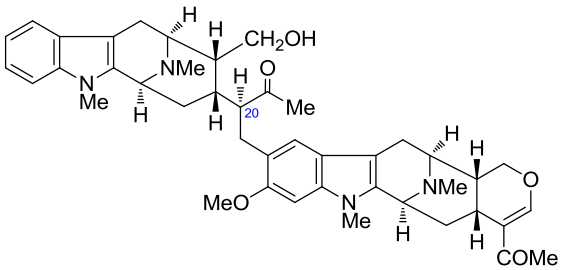

104 perhentinine (20*S*)

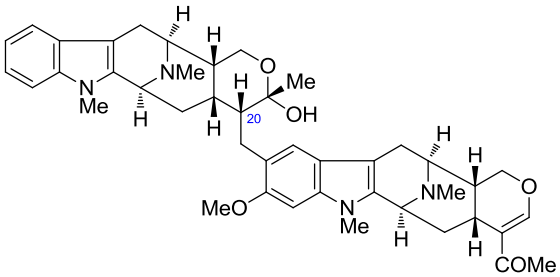

105 macralstonine (20*R*)

CHAPTER SEVEN

Reinvestigation of the Stereochemical Assignment of Scholaricine and Alstoumerine – Revision of Configurational Assignment of C-20 of Scholaricine and C-16 and C-19 of Alstoumerine

7.1 Scholaricine

In the course of the ongoing investigations of indole alkaloids (*e.g.*, see Chapter 5), the NMR data of many strychnan alkaloids were compared (**92**–**94**, **108–114**).[75,96–103] It emerged from such a comparison that the configuration at C-20 attributed to the alkaloid scholaricine (**114**) required re-examination. Specifically, the resonances of C-2, C-14, and C-16 in the akuammicine-type alkaloids with C-20*S* are characteristically observed at δ_C 172, 31, and 96, respectively, while those with C-20*R* are usually found at δ_C 168, 27, and 103, respectively (Table 7.1). An attempt was previously made to rationalize the C-14 and C-16 shifts on the basis of the γ-gauche effects.[77] However, this analysis can only be applied in cases where the piperidine ring adopts a chair conformation, which is not always the case for this group of alkaloids.

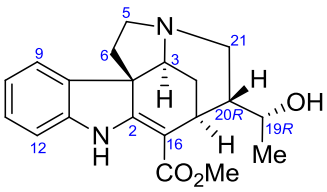

92 *N*(4)-demethylalstogustine

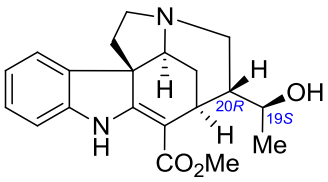

93 19-*epi*-*N*(4)-demethylalstogustine

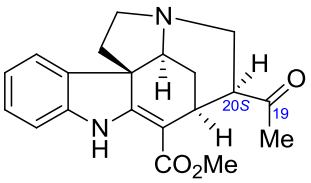

94 alstolucine B

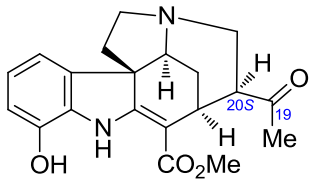

108 alstolucine D

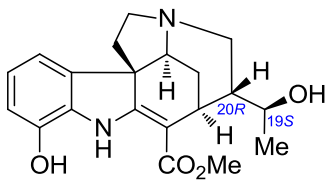

109 alstolucine E

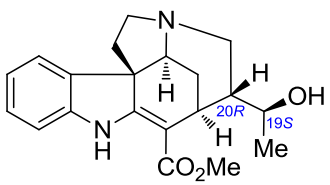

110 alstolucine F

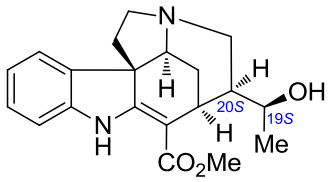

111 echitamidine

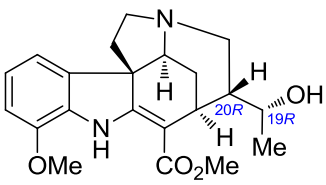

112 *N*(4)-demethyl-12-methoxyalstogustine

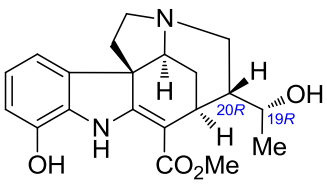

113 19-*epi*-scholaricine

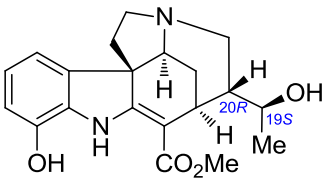

114 scholaricine (previous assignment)

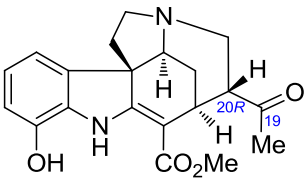

115

The indole alkaloid scholaricine (**114**) was first reported by Atta-ur-Rahman and co-workers from the leaf extract of *Alstonia scholaris*, but without any stereochemical assignments.[102] The configuration at C-20 was subsequently assigned as 20*R* by Yamauchi *et al.*[98] from the observation that the same ketone product **115**, was obtained from the oxidation of scholaricine (**114**) and 19-*epi*-scholaricine (**113**), following the method used by Hesse for the assignment of the C-19 and C-20 configurations of 19-*epi*-alstogustine.[79]

Comparison of the ^{13}C NMR data of scholaricine (**114**) showed resonances for C-2, C-14, and C-16 at δ_C 172.1, 30.8, and 96.3, respectively, which correspond to the C-20*S* series of these strychnan derivatives (Tables 7.1 and 7.2). The C-20*S* configuration was also supported by the observed H-21/H-5, H-6 and H-20/H-14*S* NOEs (axial H-20 in chair ring D). To secure unambiguous confirmation, an X-ray diffraction analysis was carried out (Figure 7.1) using a sample of **114** from our

previous study of another *Alstonia* species,[104] which confirmed the configuration (C-20*S*) deduced from the NMR data (^{13}C NMR and NOEs).

Scholaricine (**114**) was recrystallized by slow evaporation from EtOAc solution. From the crystal structure, an intramolecular hydrogen bond was observed between C-19–OH and the C-17 carbonyl oxygen (Figure 7.1).

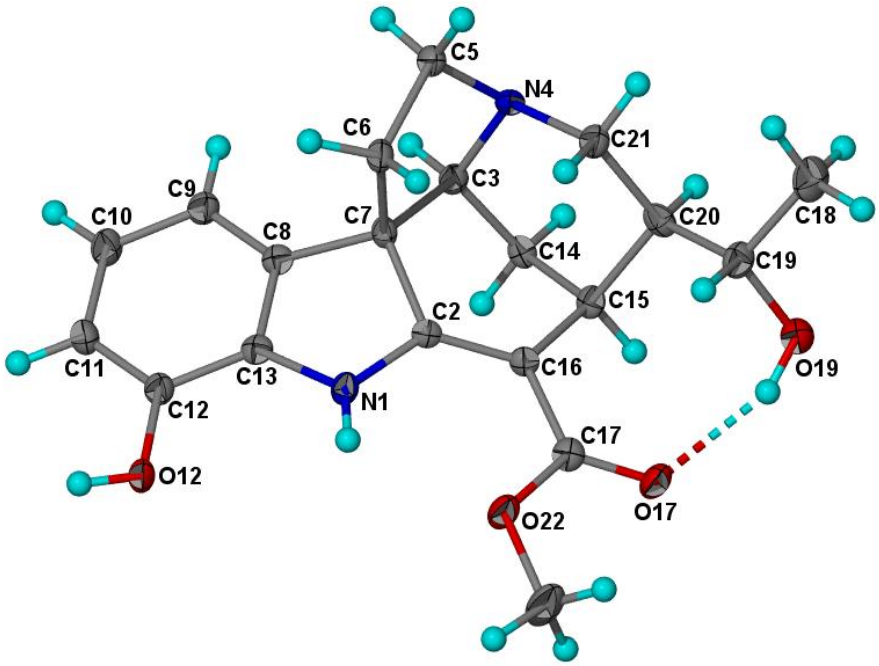

Figure 7.1. X-ray crystal structure of **114**.

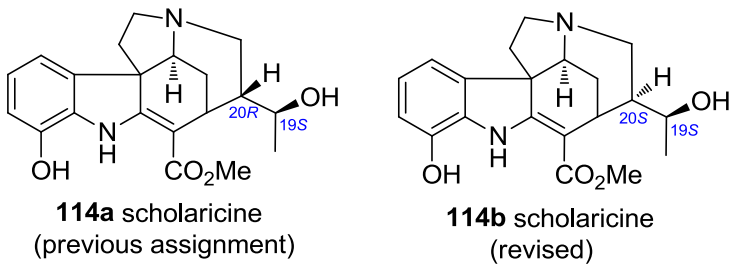

The ^{1}H and ^{13}C NMR data of alkaloid **114** (obtained from the current study) are summarized in Table 7.2, while the ^{1}H NMR spectrum of alkaloid **114** is shown in Figure 7.2.

Table 7.1. ^{13}C NMR data (δ) of compounds **92**–**94**, and **108**–**114** found in the literature[a]

Position	**92**[97] (20*R*)	**93**[99,100] (20*R*)	**94**[75] (20*S*)	**108**[75] (20*S*)	**109**[75] (20*R*)	**110**[75] (20*R*)	**111**[98,103] (20*S*)	**112**[77] (20*R*)	**113**[98] (20*R*)	**114**[102] (20*R*)[b]
2	167.6	168.1	172.2	171.8	168.5	168.7	172.6	167.1	168.5	172.2[c]
3	59.1	59.2	60.6	60.4	58.5	58.6	61.0	58.9	60.2	60.2
5	53.9	53.8	54.0	53.6	52.7	53.1	54.2	53.5	54.4	53.9
6	46.7	45.9	43.4	43.0	44.8	45.2	46.0	46.0	46.6	43.4
7	58.6	58.2	56.7	57.1	58.9	58.3	57.3	59.2	59.5	58.0
8	135.7	135.6	135.4	136.4	136.1	135.0	135.8	136.2	138.2	132.2
9	128.0	127.9	119.6	111.3	112.4	120.8	121.4	113.3	112.3	111.3
10	121.2	121.1	121.1	122.2	122.2	121.2	119.8	121.9	122.3	122.4
11	120.9	120.8	127.6	115.8	116.0	128.0	127.6	110.3	115.8	115.1
12	109.7	109.7	109.7	141.7	141.8	109.8	109.6	144.4	143.1	137.0
13	143.8	144.1	144.2	132.2	132.2	144.2	143.8	132.4	132.9	141.8
14	27.4	27.6	31.7	31.5	26.4	26.6	31.2	27.0	28.2	31.0
15	29.3	27.8	30.8	30.7	27.4	27.4	28.9	29.2	27.9	28.9
16	102.9	103.4	96.5	96.5	102.3	102.6	96.9	103.1	104.5	96.7
18	20.3	20.2	29.2	29.3	29.4	29.4	19.8	20.2	21.3	19.7
19	71.1	69.9	208.5	208.5	209.8	210.0	68.4	71.0	69.2	68.5
20	45.5	43.4	50.0	49.6	49.3	49.5	43.7	45.8	44.9	46.0
21	48.4	47.4	45.6	45.4	46.5	47.0	48.2	48.1	49.2	48.2
$CO_2\underline{Me}$	51.5	51.3	50.9	51.0	51.3	51.2	51.8	51.5	50.7	51.8
$\underline{C}O_2Me$	167.9	168.1	167.2	167.5	167.8	168.0	168.9	167.8	168.0	169.1[c]
12-O$\underline{Me}$	–	–	–	–	–	–	–	55.5	–	–

[a]$CDCl_3$; [b]previous configurational assignment; [c]the original assignments by Atta-ur-Rahman *et al*. for C-2 and $\underline{C}O_2Me$ were δ_C 169.1 and 172.2, respectively.[102]

Table 7.2. ^{1}H and ^{13}C NMR data (δ) of scholaricine (**114**) (current study)[a]

Position	δ_C	δ_H
2	172.1	–
3	60.7	3.91 t (3)
5β	53.7	2.89 m
5α		3.07 m
6α	43.1	1.90 dd (13, 6)
6β		2.89 m
7	57.4	–
8	136.7	–
9	110.9	6.69 dd (8, 1)
10	122.3	6.81 t (8)
11	115.6	6.76 br d (8)
12	142.0	–
13	131.9	–
14*R*	30.8	1.45 dt (13, 3)
14*S*		2.01 m
15	28.7	3.45 br d (3)
16	96.3	–
18	19.6	1.17 d (6)
19	68.4	3.29 dq (9, 6)
20	45.7	1.78 m
21β	47.9	2.01 m
21α		2.89 m
CO_2<u>Me</u>	51.9	3.88 s
<u>C</u>O_2Me	169.1	–
*N*H	–	8.59 br s

[a]$CDCl_3$, 400 MHz; assignments based on COSY and HMQC.

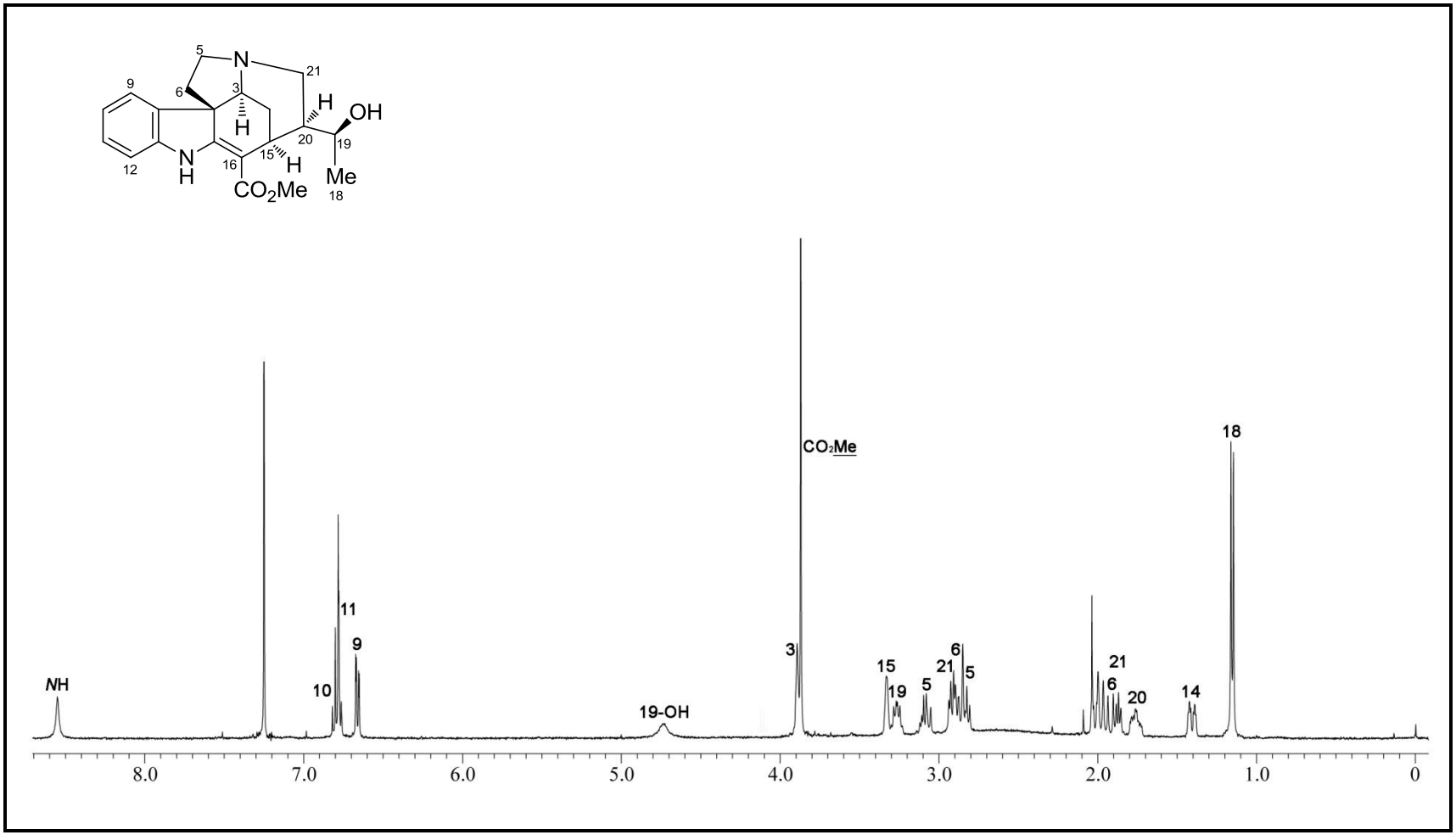

Figure 7.2. ^{1}H NMR spectrum ($CDCl_3$, 400 MHz) of scholaricine (**114**).

7.2 Alstoumerine

Lumutinine C (**116**) is a new bisindole alkaloid isolated from the stem-bark extract of *Alstonia macrophylla* (isolation and structure by S. H. Lim).[105] Lumutinine C (**116**) represents a ring A/F fused macroline-sarpagine type bisindole alkaloid.

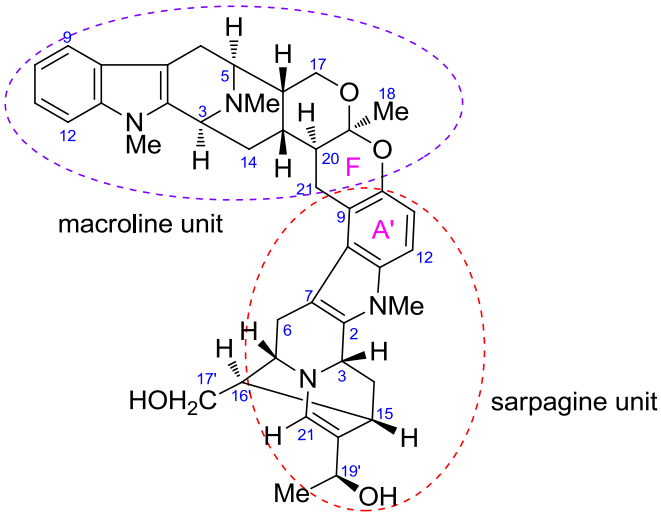

116 lumutinine C

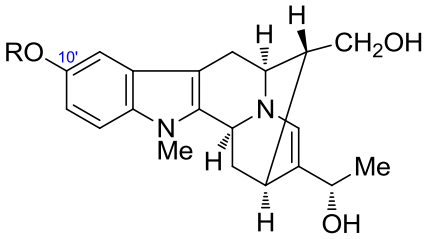

117 R = H or Me

After discounting the signals due to the upper macroline-derived half, the monomeric unit corresponding to the lower half was deduced from NMR spectroscopic data to comprise an alkaloid of the sarpagine type, specifically, a 10-hydroxy- or 10-methoxyalstoumerine (**117**). The ^{1}H and ^{13}C NMR data of lumutinine C (**116**) are summarized in Table 7.3, while the ^{1}H NMR spectrum of **116** is shown in Figure 7.3.

Table 7.3. ^{1}H and ^{13}C NMR data (δ) of lumutinine C (**116**)[a]

Position	δ_C	δ_H	Position	δ_C	δ_H
2	133.4	–	2'	139.3	–
3	54.0	3.74 m	3'	48.7	3.82 m
5	55.2	2.99 m	5'	56.4	2.87 m
6β	22.8	2.45 d (16)	6'α	27.9	2.71 m
6α		3.28 m	6'β		3.22 m
7	107.0	–	7'	102.1	–
8	126.4	–	8'	125.0	–
9	118.1	7.50 d (7.5)	9'	111.4	–
10	119.0	7.10 t (7.5)	10'	147.7	–
11	120.9	7.17 t (7.5)	11'	112.6	6.71 d (9)
12	108.9	7.25 d (7.5)	12'	107.7	7.01 d (9)
13	136.9	–	13'	132.4	–
14β	26.7	1.18 m	14'α	38.6	1.66 m
14α		2.35 td (13, 3)	14'β		1.89 m
15	30.4	1.87 m	15'	29.2	2.82 m
16	43.5	2.00 m	16'	45.0	1.55 m
17β	62.3	3.67 dd (11.5, 4)	17'α	64.5	3.42 m
17α		4.62 t (11.5)	17'β		3.61 dd (12, 3)
18	25.4	1.35 s	18'	22.5	1.34 d (6)
19	99.0	–	19'	67.3	4.46 q (6)
20	37.2	1.97 m	20'	149.3	–
21	26.8	2.75 m	21'	136.1	6.44 s
		3.25 m	N_1Me'	29.4	3.48 s
N_1Me	29.3	3.40 s			
N_4Me	41.8	2.26 s			

[a]$CDCl_3$, 400 and 100 MHz, respectively; assignments based on COSY, HMQC, and HMBC.

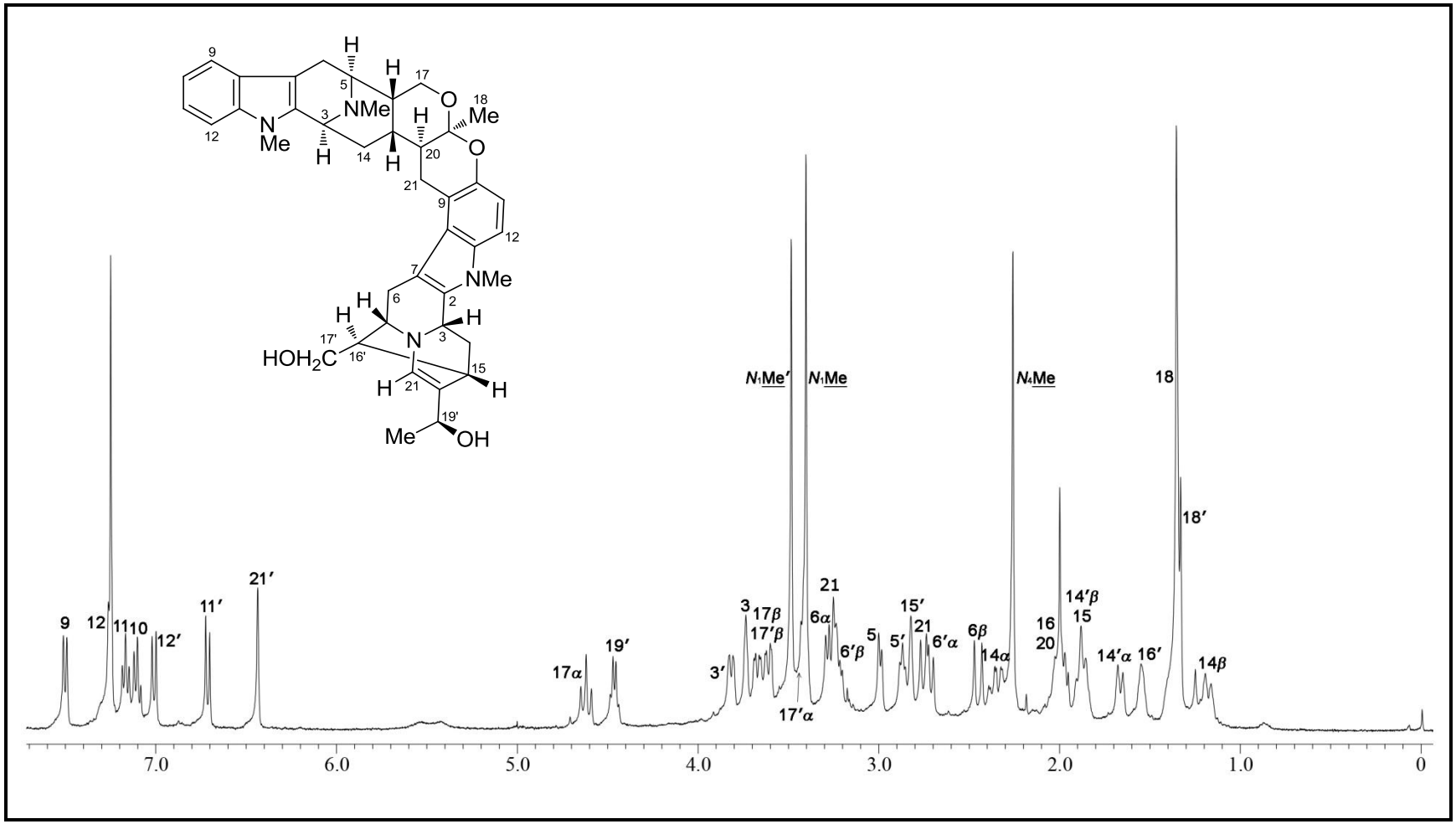

Figure 7.3. ^{1}H NMR spectrum ($CDCl_3$, 400 MHz) of lumutinine C (**116**).

Comparison of the NMR data with those reported for alstoumerine (**118a**)[106] showed a general agreement for the non-indole portion of the molecule, providing support for such a conclusion. Despite this, some inconsistencies were noted regarding the earlier structure elucidation of alstoumerine (**118a**).

Alstoumerine (**118**), a sarpagine-type alkaloid, was first reported by Atta-ur-Rahman and co-workers from the leaf extract of *A. macrophylla* collected in Sri Lanka.[106] The structure of **118a** was deduced based on NMR spectral data.

The configuration of the hydroxy-substituted C-19 was previously determined using Horeau's procedure[107] and was assigned as 19*R*, while the configuration of C-16 was assigned as 16*S* with the hydroxymethyl group pointing towards the indole moiety and H-16 pointing away from the indole moiety. This was despite the observation of the resonance due to H-16 at δ_H 1.63 and those for the C-17 oxymethylene hydrogens at δ_H 3.46 and 3.64. The resonances of H-16 and H-17 are of diagnostic significance for the determination of C-16 configuration in the sarpagine type alkaloids.[108–111] The observed resonance for H-16 upfield at δ_H 1.63 is indicative of shielding due to it being located within the shielding zone of the aromatic moiety, which in turn requires H-16 to be oriented towards the indole moiety with the hydroxymethyl group directed away from the indole unit. The original assignment of the C-16 configuration of alstoumerine (**118a**), therefore, requires amendment to 16*R* (**118b**). In the case of lumutinine C (**116**), the resonance due to H-16′ was observed at δ_H 1.55, while the resonance due to the C-17′ oxymethylene hydrogens were seen at δ_H 3.42 and 3.61. These values were similar to those in alstoumerine (**118**) and require H-16′ to be directed towards the indole moiety (16′*R*).

Since we were in possession of authentic alstoumerine (**118**) from our past and ongoing work in alkaloid chemistry,[109] a rigorous configurational assignment of alkaloid **118** was carried out. The ^{1}H and ^{13}C NMR data of alstoumerine (**118**) are

summarized in Table 7.4. The ^{1}H NMR spectrum of **118** is shown in Figure 7.4. In addition to the chemical shift considerations mentioned above, the 16*R* configuration of alstoumerine (**118b**) was further confirmed by NOE experiments, which showed strong NOE between H-16 and H-6β, requiring H-16 to be directed towards the indole moiety and hence proximate to H-6β.

Table 7.4. ^{1}H and ^{13}C NMR data (δ) of alstoumerine (**118**)[a]

Position	δ_C	δ_H
2	139.5	–
3α	48.6	3.83 dd (10, 2)
5α	56.2	3.03 t (6)
6	25.4	2.69 d (15)
7	102.5	–
8	127.3	–
9	118.1	7.48 br d (8)
10	118.9	7.10 td (8, 1)
11	121.0	7.19 td (8, 1)
12	108.7	7.28 br d (8)
13	137.4	–
14	38.8	1.61 m
15	29.6	2.78 br s
16	44.4	1.61 m
17	64.7	3.46 dd (12, 5)
		3.51 dd (12, 4)
18	22.5	0.36 d (7)
19	67.4	4.52 d (7)
20	149.1	–
21	136.4	6.54 d (1)
*N*Me	29.3	3.58 s

[a]$CDCl_3$, 400 and 100 MHz, respectively; assignments are based on COSY, HMQC, and HMBC.

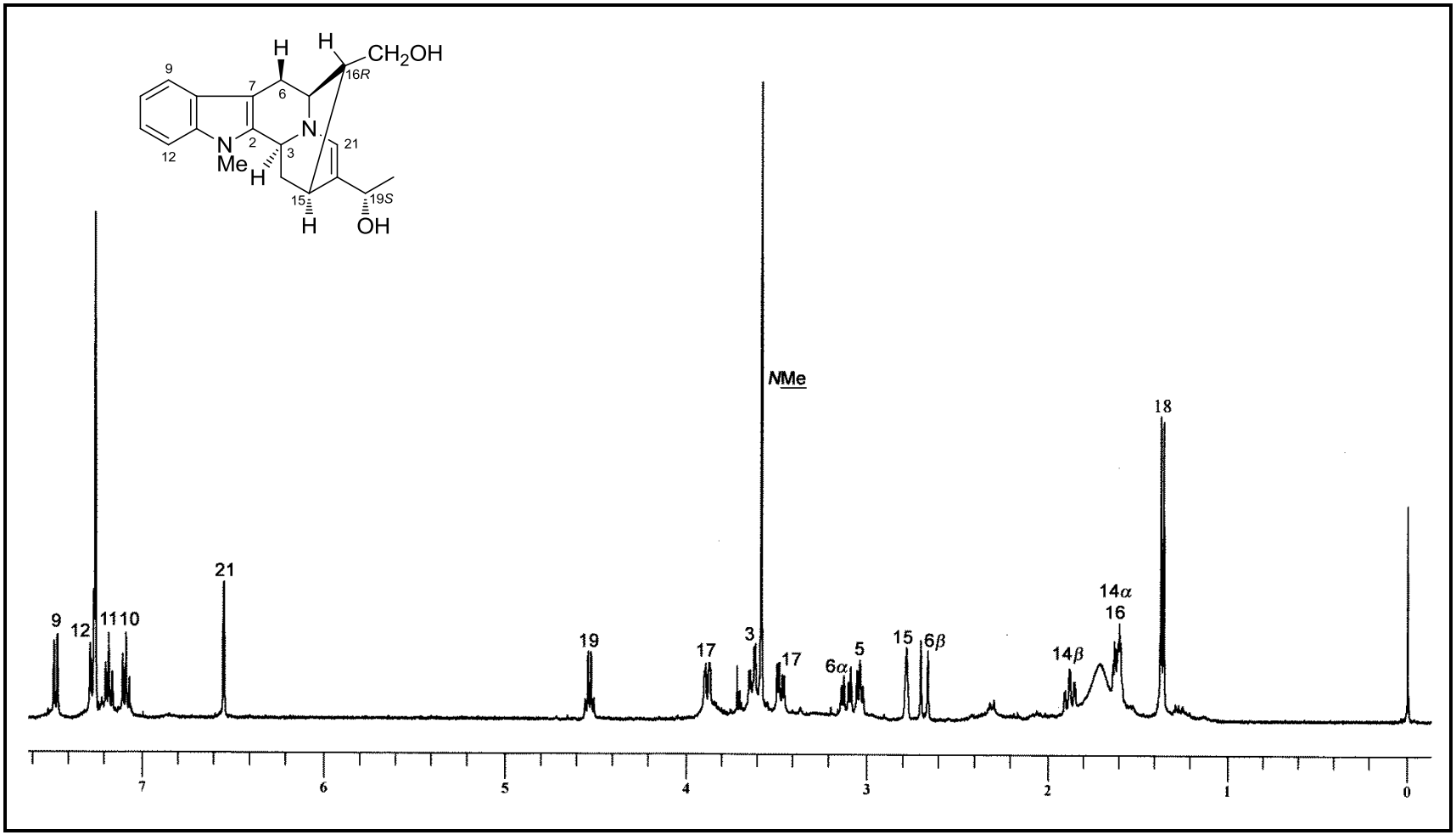

Figure 7.4. ^{1}H NMR spectrum ($CDCl_3$, 400 MHz) of alstoumerine (**118**).

The C-19 configuration was also reinvestigated, by repeating the determination using Horeau's procedure.[107] Alstoumerine (**118**) (1 equiv) was added to a solution of racemic 2-phenylbutyric anhydride (4 equiv) in anhydrous pyridine (1 ml). The resulting mixture was stirred for 20 h at rt. Water (3 ml) was then added and the mixture was allowed to stand for 30 min. The pH of the solution was adjusted to pH 9 by drop-wise addition of NaOH (0.1 M), after which the solution was extracted with CH_2Cl_2. The aqueous layer was acidified to pH 3 using 1.0 M HCl and extracted with CH_2Cl_2. Evaporation of the solvent from the organic phase gave the unreacted 2-phenylbutyric acid: $[\alpha]^{25}_{D}$ –3.1 (*c* 1.66, C_6H_6); $[\alpha]^{25}_{D}$ –3 (*c* 1.66, $CHCl_3$). The optical rotation of the unreacted 2-phenylbutyric acid was found to be negative (*R*), indicating the *S* configuration at C-19 in alstoumerine (**118b**). The determination was repeated several times to confirm that the correct result was obtained each time.

The present determination therefore yielded a result (19*S*), which was opposite to that of the previous report (19*R*).[106] In view of the two major discrepancies noted, an X-ray diffraction analysis was carried out (Figure 7.5), which confirmed the structure and absolute configuration of alstoumerine (**118b**).

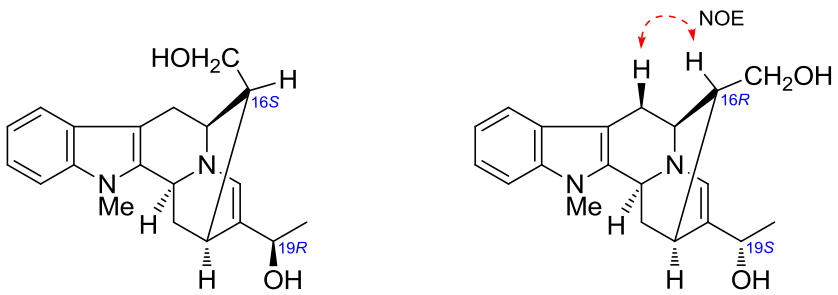

118a alstoumerine (previous assignment)

118b alstoumerine (revised)

Alstoumerine (**118b**) crystallized readily on standing in $CHCl_3$ solution. The presence of heavy atoms ($CHCl_3$) in the unit cell enabled measurement of the Flack[63]

parameter, which in turn permitted determination of the absolute configuration (Figure 7.5).

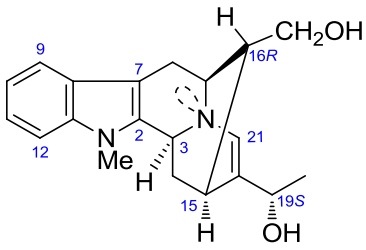

118b alstoumerine

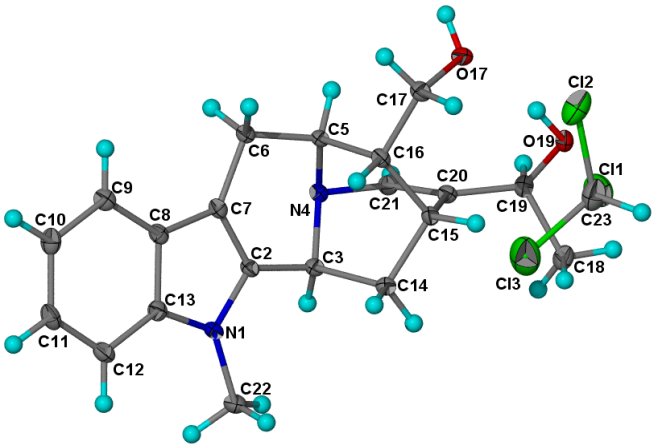

Figure 7.5. X-ray crystal structure of **118b** [Flack parameter,[63] x = 0.01(0.04); Hooft parameter,[64] y = 0.01(0.04)].

With the correct structure of alstoumerine (**118b**) unequivocally established, the structure of lumutinine C follows accordingly as shown in **116**.

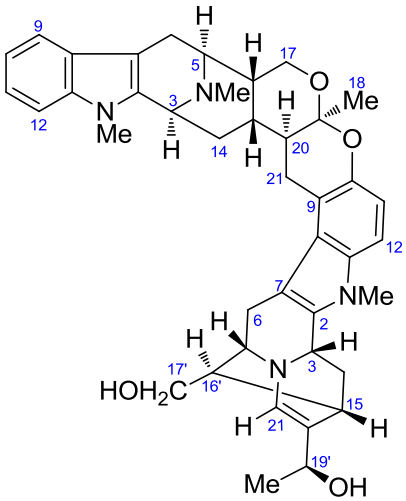

116 lumutinine C

CHAPTER EIGHT

Andransinine – An Example of Spontaneous Resolution of a Racemic Alkaloid Mixture

8.1 Introduction

8.1.1 Crystallization of racemates and enantiomers

Chirality is a concept well known to all chemists concerned in any way with structure. It has numerous implications ranging from those affecting physical properties of matter to those related to biological mechanisms. The terminology of several concepts regarding chirality will be defined in following paragraphs.[112]

The geometric property of a rigid object (or spatial arrangement of points or atoms) of being nonsuperposable on its mirror image is called chirality. A chiral object may exist in two enantiomorphic forms, which are mirror image of one another. Such forms lack inverse symmetry elements, that is, a center, a plane, and an improper mirror plane, a centre of inversion or a rotoinversion axis. Objects that possess one or more of these inverse symmetry elements are superposable on their mirror images; they are achiral. All objects necessarily belong to one of these categories; a hand, a spiral staircase, and a snail shell are all chiral, while a cube and a sphere are achiral.

According to Lord Kelvin, "two equal and similar right hands are homochirally similar. Equal and similar right and left hands are heretochirally similar".[113] All of the foregoing definitions remain valid at the molecular level; there are achiral, as well as chiral molecules. The latter exist in two enantiomeric forms. The term enantiomer is used to designate either a single molecule, a homochiral collection of molecules, or

even a heterochiral collection that contains an excess of one enantiomer and whose composition is defined by its enantiomeric purity, or the enantiomeric excess, ee.

The oldest known manifestation of molecular chirality is optical activity, or rotator power, the properties that are exhibited by the rotation of the plane of polarized light. Two enantiomers of a given compound have a rotator powers of equal absolute value, but of opposite sign, or sense. One is positive, or dextrorotatory, while the other is negative, or levorotatory. The absolute designations of sign are arbitrary inasmuch as they are wavelength, temperature, and solvent dependent, but the relative designations are always valid. That is, a given enantiomer may be (+) at one wavelength and (–) at another, while the other enantiomer will always have the opposite sign at the corresponding wavelength.

The expression optically active substance may signify a pure enantiomer or a mixture containing an excess of one of the two. The composition of a mixture of two enantiomers may be characterized by its optical purity, which may in turn be determined from the ratio of the optical rotation of the mixture to that of the pure enantiomer. The optical purity (experimental value) is generally equal to the enantiomeric purity, which reflects the real composition. A pure enantiomer is often called optically pure.

The absolute configuration is the spatial arrangement of the atoms of a physically identified chiral molecule entity (or group) and its stereochemical description (*e.g.*, *R* or *S*, *P* or *M*, *D* or *L*, *etc.*), whereas the absolute structure is the spatial arrangement of the atoms of a physically identified non-centrosymmetric crystal and its description by way of unit-cell dimensions, space group and representative coordinates of all atoms.

An equimolar mixture of two enantiomers whose physical state is unspecified or unknown is called racemate. It does not exhibit optical activity. The chemical name or formula of a racemate is distinguished from those of the enantiomers by the prefix (±).

The separation of the two enantiomers that constitute a racemate is called a resolution, or an optical resolution. When the separation is not complete, a mixture is obtained which is often called either a partially resolved racemate or a partially resolved enantiomer.

Crystalline racemates may belong to one of three different classes. In the first, the crystalline racemate is a conglomerate, that is, a mechanical mixture of crystals of the two pure enantiomers (racemic conglomerate). The process of its formation on crystallization of a racemate is called spontaneous resolution, since pure or nearly pure enantiomers can often be obtained from the conglomerate by sorting. One of the most famous examples is the separation of a racemic conglomerate of sodium ammonium tartarate salt by Pasteur.[114]

The second and most common type of crystalline racemate is that in which the two enantiomers are present in equal quantities in a well-defined arrangement within the crystal lattice. The resultant homogeneous solid phase corresponds to a true crystalline addition compound, which is called a racemic compound (also referred to as a 'true racemate').

The third possibility corresponds to the formation of a solid solution between the two enantiomers, coexisting in an unordered manner in the crystal lattice. The term pseudoracemate (or racemic solid solution) is used to designate this case.

8.1.2 Space groups

A crystallographic space group is the set of geometrical symmetry operations that take a three-dimensional periodic object into itself. The space groups in three dimensions are made from combinations of the 32 crystallographic point groups with the 14 Bravais lattices, each of the latter belonging to one of 7 lattice systems.[112,115] This

results in a space groups being some combination of the translational symmetry of a unit cell including lattice centering, the point group symmetry operations of reflections, rotation, and improper rotations (also called rota-inversion), and the screw axis and glide plane symmetry operations. The combination of all these symmetry operations results in a total of 230 unique space groups describing all possible crystal symmetries. All of the 230 space groups are collected in a book known as the International Tables for Crystallography. They are represented by the symmetry-elements diagram and general position diagram, notated with the Hermann-Mauguin symbols and other relevant information.[116]

This results in a space groups being some combination of the translational symmetry of a unit cell including lattice centering, the point group symmetry operations of reflections, rotation, and improper rotations (also called rota-inversion), and the screw axis and glide plane symmetry operations.

There are 230 ways of arranging objects repetitively in a three-dimensional network. These 230 space groups may be divided among the 32 crystal classes according to their symmetry. The 11 enantiomorphous crystal classes encompass 65 space groups which are devoid of inverse symmetry elements. Thus, an enantiomer (or enantiomerically pure compounds) may only crystallize in one of these 65 groups (*e.g.*, $P2_1$, $P2_12_12_1$, $C2$, and $P4_2$).[112]

While an enantiomer necessarily crystallizes in an enantiomorphous system, the inverse of this statement is not true. A racemate, in principle, may crystallize in any space groups, even in a chiral space groups; the optical activity of the crystal does not necessarily imply any optical activity of the molecules in the liquid state (a circular staircase may be built out of achiral blocks). In fact, in almost all cases, racemates crystallize in those space groups that possess elements of inverse symmetry (165 possibilities, *e.g.*, $P\bar{1}$, $P2_1$/c, $C2$/c, and Pna2_1).[112]

The Tables shown below represents the division of the 32 crystal classes according to property (Table 8.1),[117,118] and the relationship between the molecular properties, the nature of the solution, and the nature of possible crystals (Table 8.2).[117]

Table 8.1. Division of the 32 crystal classes according to property[117,118]

	Crystal characteristic		Flack classification	Crystal class
1	Centrosymmetric	Achiral	CA (Centrosymmetric Achiral)	$\bar{1}$, 2/m, mmm, 4/m, 4/mmm, $\bar{3}$, $\bar{3}$m, 6/m, 6/mmm, m$\bar{3}$, m$\bar{3}$m
2	Non- centrosymmetric	Achiral	NA (Non-centrosymmetric Achiral)	m, mm2, $\bar{4}$, 4mm, $\bar{4}$2m, 3m, $\bar{6}$, 6mm, $\bar{6}$2m, $\bar{4}$3m
3	Non- centrosymmetric	Chiral	NC (Non-centrosymmetric Chiral)	1, 2, 222, 4, 422, 3, 32, 6, 622, 23, 432

Table 8.2. Relationship between molecular properties, nature of the solution, and nature of possible crystals[117]

Solution	**Chiral molecul**							**Achiral Molecule**		
Molecular composition of the single crystal	Enantiopure chiral		Enantiomeric mixture					Homogeneous		
	Enantiopure chiral		Enantiopure chiral	Enantiomeric mixture				–	–	–
Crystal structure	Achiral	Non-centro-symmetric chiral	Conglomerate (collection of resolved crystals)	Inversion twinned	Non-centrosymmetric achiral	Racemic	Disordered solid solution	Non-centro-symmetric chiral	Non-centro-symmetric achiral	Centro-symmetric achiral
Flack classification		NC	NC	NC	NA	NA or CA				
Examples	Not known in nature	$P2_12_12_1$	$P6_1$ and $P6_5$	$P2_1$ (twinned)	Pc	$P2_1$ or $P2_1$/c	Any	$P3_121$	Pn	$P2_1$/c

8.1.3 X-ray radiation/source

Copper (Cu K_α, λ = 1.54184 Å) and molybdenum (Mo K_α, λ = 0.71073 Å) are the two most common sources used for X-ray diffraction experiments.[115]

Copper X-ray tubes produce a higher flux of incident photons (for the same power settings) and these are diffracted more efficiently than molybdenum radiation. Hence, copper radiation is particularly useful for small or otherwise weakly diffracting

crystals, especially if the absorption effects are moderate. For crystals with long unit cell dimensions, reflections are further apart when the longer-wavelength copper radiation is used, and this can minimize reflection overlap. If absolute configuration determination is needed, but the crystals do not contain elements heavier than silicone, then copper radiation is essential.

On the other hand, molybdenum radiation has less absorption effects, and this can be crucial if elements of a high atomic number are present. Molybdenum radiation allows the collection of data to a higher resolution, and is likely to cause fewer restrictions if low-temperature or other attachments are required.

The following illustrative examples on when to use Cu or Mo X-ray source[115]:

- a well-diffracting organic compound containing iodine:

  use Mo to minimize absorption

- a poorly diffracting organic compound (CHNO):

  use Cu to maximize diffracted intensity

- an organic compound (CHNO) with $b > 50$ Å:

  use Cu to minimize overlap

- absolute configuration of $C_{19}H_{22}N_2O_3$

  feasible only with Cu

- most metal complexes, *etc.*

  use Mo to minimize absorption

- high-resolution studies

  use Mo

The Chemistry Department, University of Malaya operates two X-ray diffractometers for small molecule crystallography studies. The first X-ray

diffractometer is the Bruker SMART APEX II, commissioned in December 2007, only has Mo K_α X-ray radiation. The second X-ray diffractometer, Agilent SuperNova Dual, comissioned more recently (April 2011) is a hybrid instrument with two different X-ray sources, Mo K_α and Cu K_α. The author has full access to the Bruker X-ray diffractometer, but only very limited access to the Agilent X-ray diffractometer.

8.1.4 Glossary of terms

Below is the glossary of terms which will be used in the subsequent chapter. Many of the definitions of terms given in this glossary are drawn from the IUPAC Basic Terminology of Stereochemistry,[118] which have been summarized and reworded by Flack *et al.*[119]

Absolute configuration: The spatial arrangement of the atoms of a physically identified chiral molecular entity (or group) and its stereochemical description (*e.g.*, (*R*) or (*S*), (*P*) or (*M*), or D or L, *etc*.).

Absolute structure: The spatial arrangement of the atoms of a physically identified non centrosymmetric crystal and its description by way of unit-cell dimensions, space group, and representative coordinates of all atoms.

Chiral: Having the property of chirality.

Chirality: The geometric property of a rigid object (or spatial arrangement of points or atoms) of being nonsuperposable by pure rotation and translation on its image formed by inversion through a point; the symmetry group of such an object contains no

symmetry operations of the second kind (inversion through a point, $\bar{1}$; reflection through a plane, m; roto-inversion, $\bar{N}$). When the object is superposable by pure rotation and translation on its inverted image, the object is described as being achiral; the symmetry group of such an object contains symmetry operations of the second kind. Barron[120] provides a more general definition of chirality: 'True chirality is exhibited by systems that exist in two distinct enantiomorphic states that are interconverted by space inversion but not by time reversal combined with any proper spatial rotation'.

Chirality sense: The property that distinguishes enantiomorphs. The specification of two enantiomorphic forms by reference to an oriented space, *e.g.*, of a screw, a right threaded one or a left threaded one. The expression opposite chirality is short for opposite chirality sense.

Enantiomer: One of a pair of chiral molecular entities of opposite chirality sense.

Enantiomerically pure/enantiopure: A sample in which all molecules have (within limits of detection) the same chirality sense.

Enantiomorph: One of a pair of chiral objects or models that are non-superposable mirror images of each other.

Flack parameter: The Flack parameter, x encodes the relative abundance of the 'strength' and sign of the measured resonant scattering signal measured in units of f'' (the imaginary component of the atomic scattering factor) in an inversion twin.[63] In short, by determining x for all data (usually found between 0 and 1), if the value is near 0 with a small standard uncertainty, the absolute structure given by the structure is

likely correct, and if the value is near 1, then the inverted structure is likely correct. If the value is near 0.5, the crystal may be racemic or twinned.

Hooft parameter: A new probabilistic procedure introduced in 2008, based on Bijvoet-pair intensity differences that can be used to establish the absolute structure.[64] Hooft parameter, *y* behaves like the Flack parameter,[63] in that it will have a value of 0 for the correct absolute structure model (with a small standard uncertainty), and 1 for the inverted model.

Inversion twin: An inversion twin consists of centrosymmetrically related crystalline domains. The symmetry operation relating domain structures in an inversion twin is that of a centre of symmetry. In an inversion twin, the crystal lattice (*i.e.*, the lattice translations after removing the atoms) is maintained throughout the whole volume of the sample, but the atoms and molecules take up either one spatial arrangement or the inverted one depending on the position within the crystal. A visual model of an inversion twin, applicable to chiral crystal structures, is to imagine the individual components of a racemic conglomerate being stuck together with their lattices being perfectly oriented. The inversion-twinned crystal is an oriented solid-state mixture of inverted structures. Inversion-twinned crystals do not form from an enantiopure sample of a substance.

Racemate: An equimolar mixture of a pair of enantiomers. It does not exhibit optical activity in solution. The chemical name or formula of a racemate is distinguished from those of the enantiomers by the prefix (±) or rac or by the symbols (*RS*) or (*SR*).

Racemic: Pertaining to a racemate.

Racemic compound: A crystalline racemate in which the two enantiomers are present in equal amounts in a well-defined arrangement within the lattice of a homogeneous crystalline addition compound.

Racemic conglomerate: An equimolar mechanical mixture of crystals, each one of which contains only one of the two enantiomers present in a racemate. The process of its formation on crystallization of a racemate is called spontaneous resolution, since pure or nearly pure enantiomers can often be obtained from the conglomerate by sorting.

Relative configuration: The configuration of any stereogenic centre with respect to any other stereogenic centre contained within the same molecular entity.

8.2 Andransinine

Andransinine (**119**) is an andranginine (**120**)[121,122] derivative recently isolated from the leaf extract of *Alstonia angustiloba*.[123]

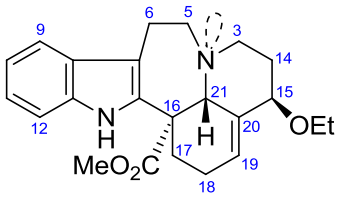

119 andransinine

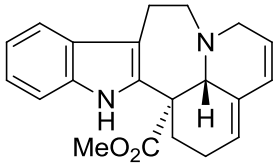

120 andranginine

Compound **119** was isolated as a light yellowish oil. The UV spectrum was characteristic of an indole chromophore with absorption maxima at 223 and 284 nm, while the IR spectrum indicated the presence of *N*H (3387 cm^{-1}) and ester carbonyl (1732 cm^{-1}) functions. In addition, the presence of Wenkert-Bohlmann bands were noted at 2740 and 2885 cm^{-1}. The ESIMS of **119** showed an $[M + H]^+$ *m/z* 381 and HRESIMS measurements yielded the molecular formula $C_{23}H_{28}N_2O_3$ (DBE 11). The ^{13}C NMR data (Table 8.3) showed 23 carbon resonances, comprising two methyl, seven methylene, six methine, and eight quaternary carbons. An ester carbonyl resonance was observed at δ_C 171.8, while olefinic resonances due to a trisubstituted double bond were observed at δ_C 126.0 and 134.0, in addition to the characteristic peaks due to the indole moiety. The ^1H NMR data (Table 8.3) showed the presence of an unsubstituted indole moiety from the presence of four aromatic resonances (δ_H 7.50, d, J = 8 Hz, H-9; 7.11, t, J = 8 Hz, H-10; 7.17, t, J = 8 Hz, H-11; 7.33, d, J = 8 Hz, H-12), an indolic *N*H as a broad singlet at δ_H 8.17, a methoxy group associated with a methyl ester function as a singlet at δ_H 3.63, a vinylic hydrogen at δ_H 5.74, and an ethoxy group (δ_H 3.19, m, 1H, CH_3CHHO; 3.33, m, 1H, CH_3CHHO; 1.11, t, J = 7 Hz, CH_3CH_2O). In addition, an

isolated aminomethine was observed as a singlet at δ_H 3.79 (δ_C 63.4). The ^{1}H and ^{13}C NMR data were similar to those of andranginine (**120**),[121] the difference in the present alkaloid being replacement of the C-14, C-15 double bond by an ethoxy substituent at C-15.

Andranginine (**120**) was previously isolated as an optically inactive alkaloid from *Craspidospermum* verticillatum,[121] and the relative configuration was established by X-ray diffraction analysis.[122] The observed NOE between H-21 and the hydrogens of the ethoxy group (H-22 and H-23) in **119** (Figure 8.1) indicated an α-oriented H-15 and permitted the assignment of the relative configuration at C-15 as *R*. The observed H-21/H-3β, H-6β and H-15/H-19 NOEs (Figure 8.1) were also in accord with the relative configuration of andransinine as depicted in **119**, as is the observed Wenkert-Bolmann bands in the IR spectrum, which is consistent with the *trans* disposition of H-21 and the *N*-4 lone pair.[29]

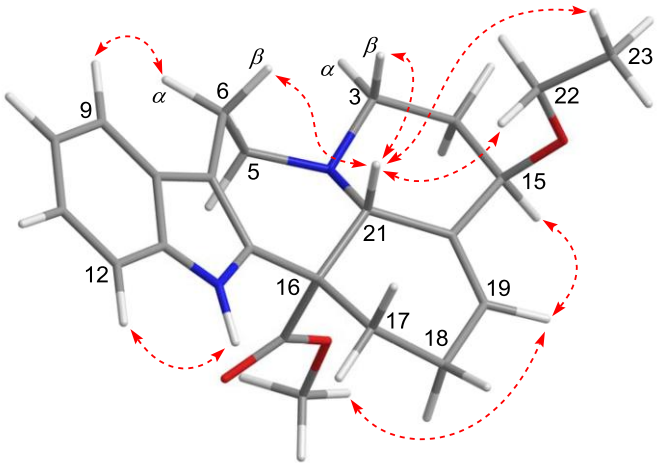

Figure 8.1. Selected NOEs of **119**.

Table 8.3. ^{1}H and ^{13}C NMR data (δ) of andransinine (**119**)[a]

Position	δ_C	δ_H
2	137.9	–
3α	50.0	2.80 m
3β		3.08 m
5a	57.0	3.17 m
5b		3.31 m
6α	18.6	2.76 m
6β		3.12 m
7	114.8	–
8	127.6	–
9	118.4	7.50 d (8)
10	121.9	7.11 t (8)
11	119.5	7.17 t (8)
12	110.8	7.33 d (8)
13	134.8	–
14a	32.4	1.95 br dd (14, 3)
14b		2.07 m
15	78.0	3.78 m
16	48.5	–
17a	32.4	2.07 m
17b		2.49 dd (13, 3)
18α	22.2	2.05 m
18β		2.20 m
19	126.0	5.74 d (5)
20	134.0	–
21	63.4	3.79 s
22	62.2	3.19 m
		3.33 m
23	15.4	1.11 t (7)
$CO_2\underline{Me}$	52.4	3.63 s
$\underline{C}O_2Me$	171.8	–
*N*H	–	8.17 br s

[a]$CDCl_3$, 400 and 100 MHz, respectively; assignments based on COSY, HMQC, and HMBC.

Since andransinine (**119**) crystallized readily from EtOAc to give good quality colorless block crystals (mp 212–214 °C), an X-ray diffraction analysis was carried out (Mo K_α radiation) which confirmed all of the observations above (Figure 8.2). The crystal system is monoclinic, with a space group of $P2_1$ (a chiral space group). The crystal data and structure refinement parameters of **119** are summarized in Table 8.4.

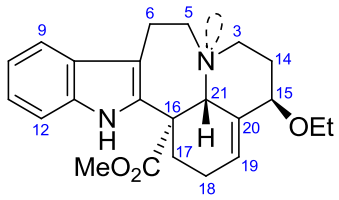

119 andransinine

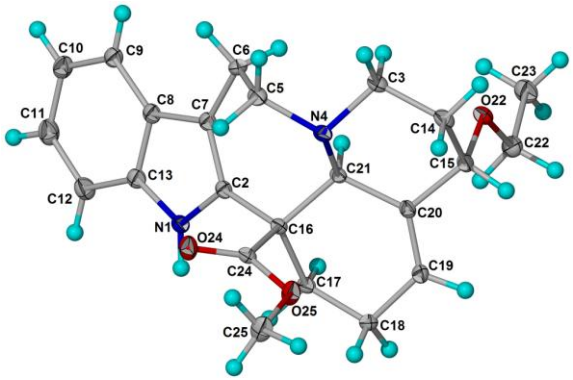

Figure 8.2. X-ray crystal structure of andransinine (**119**).

Table 8.4. Crystal data and structure refinement parameters of alkaloid **119**

Empirical formula	$C_{23}H_{28}N_2O_3$
Molecular formula	$C_{23}H_{28}N_2O_3$
Molecular weight, M_r	380.47
Melting point	212–214 °C
Temperature during diffraction experiment, T	100 K
X-ray source	Mo K_α
Crystal system	Monoclinic
Space group	$P2_1$
a	8.5064(2) Å
b	9.1496(2) Å
c	12.5255(2) Å
α	90.00°
β	96.0070(10)°
γ	90.00°
Volume, V	969.51(3) Å^3
No. of molecule per unit cell, Z	2
Density (calcd)	1.303 mg/mm^3
F(000)	408.0
Crystal size	0.44 × 0.21 × 0.17 mm
2θ range for data collection	3.26 to 54.98°
Index ranges	$-10 \le h \le 11$, $-11 \le k \le 11$, $-16 \le l \le 16$
Reflections collected	8915
Independent reflections	2366[R_{int} = 0.0211]
Data/restraints/parameters	2366/1/255
Goodness-of-fit on F^2	1.025
Final R indexes [$I \ge 2\sigma(I)$]	R_1 = 0.0302, wR_2 = 0.0759
Final R indexes [all data]	R_1 = 0.0321, wR_2 = 0.0774
Largest diff. peak/hole / e Å^{-3}	0.22/–0.18

From the crystal data shown above, it can be seen that compound **119** crystallized in a chiral space group (monoclinic, $P2_1$). Crystallization of **119** in a chiral space group was initially puzzling as it suggested the possibility that compound **119** is an enantiomerically pure compound. This is in contrast to the parent alkaloid, andranginine (**120**), which was obtained as an optically inactive racemate. The crystal system is monoclinic, with the observed space group of *P*2/c (centrosymmetric space group), which is consistent with a racemate.[112,115,117]

Compound **119** initially isolated from *A. angustiloba* also gave inconsistent results for the specific rotation with values of $[\alpha]^{25}_{D}$ varying from +11 to –8 (the compound was re-purified each time before measurement) which contributed to the initial confusion. Compound **119** (and a minor amount of the methoxy derivative **121**) was however, subsequently isolated as a racemate ($[\alpha]^{25}_{D} = 0$) from the bark extract of *Kopsia pauciflora*, which indicated that the earlier inconsistent values obtained for **119** from *A. angustiloba*, was likely a result of racemate contamination (which has been subsequently borne out by HPLC, *vide infra*).

The ^{1}H NMR spectrum of **119** obtained from *A. angustiloba* and *K. pauciflora* are shown in Figures 8.3 and 8.4, respectively.

Recrystallization of **119** (from *K. pauciflora*) from EtOAc gave similar colorless block crystals with similar melting points as that obtained previously (mp 212–214 °C). An X-ray diffraction analysis was carried out, and the results obtained indicated a similar crystal system (monoclinic, space group of $P2_1$) with the sample of **119** from *A. angustiloba*.

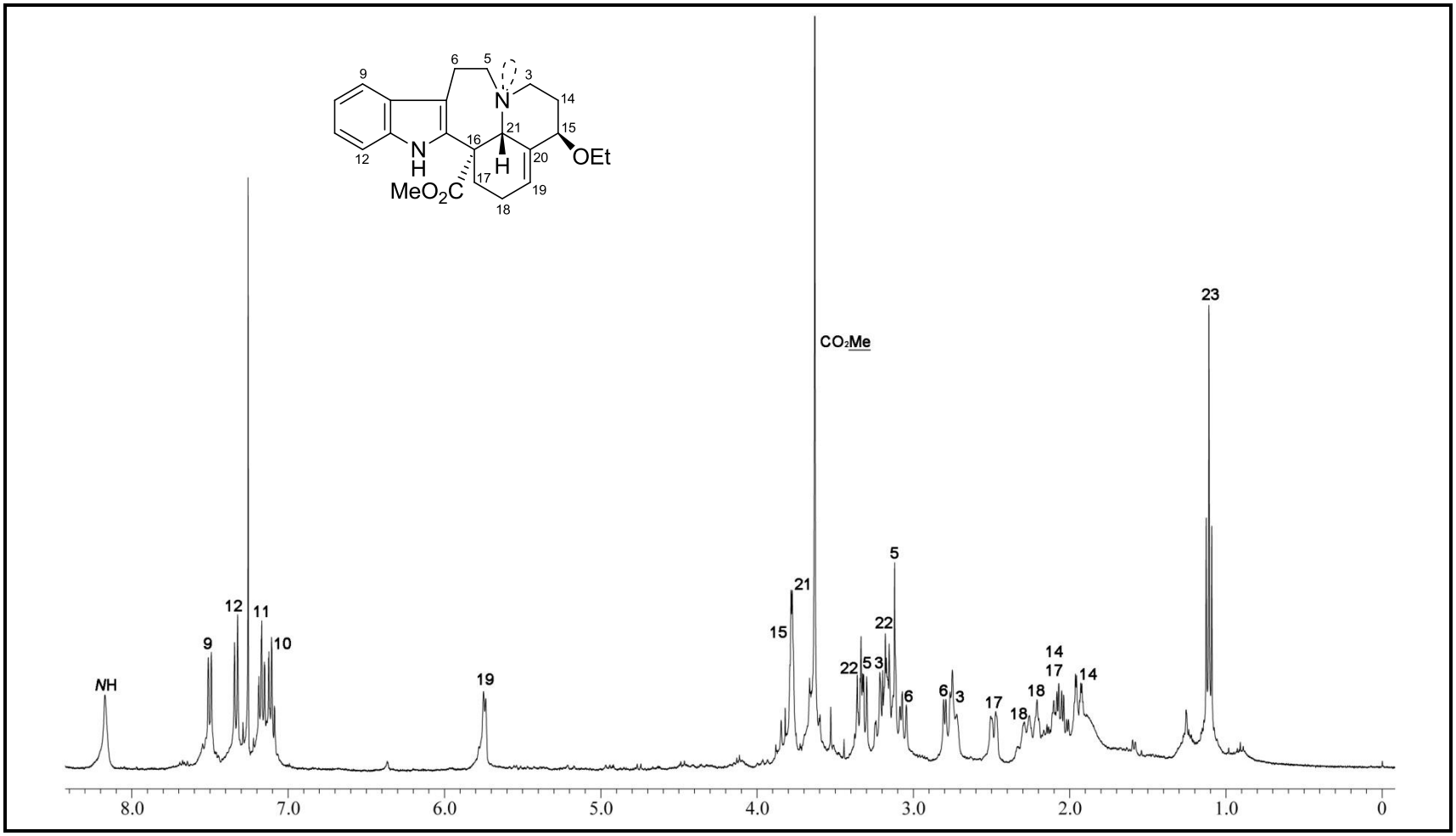

Figure 8.3. ^{1}H NMR spectrum ($CDCl_3$, 400 MHz) of (±)-andransinine (**119**) obtained from *A. angustiloba*.

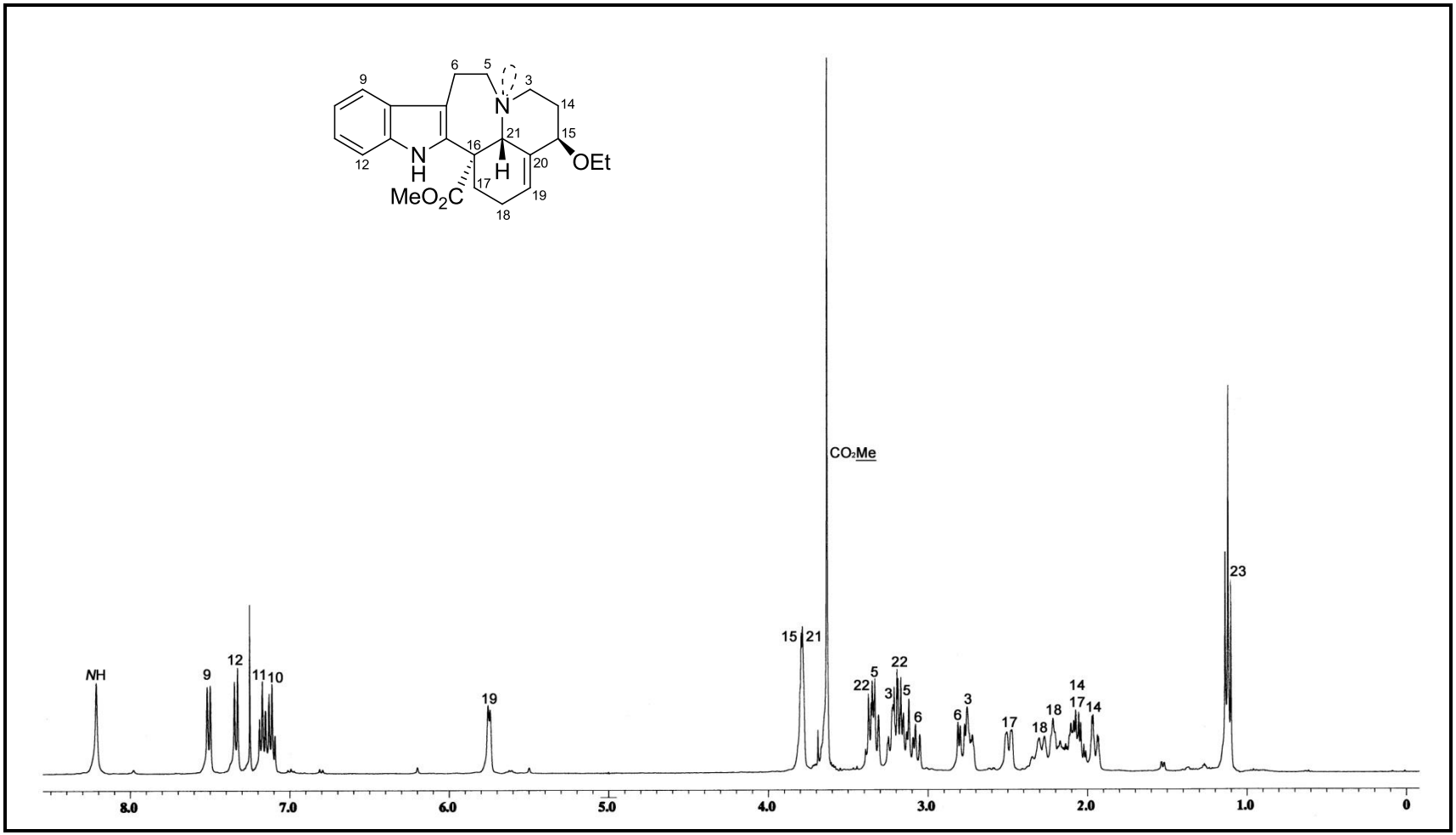

Figure 8.4. ^{1}H NMR spectrum ($CDCl_3$, 400 MHz) of (±)-andransinine (**119**) obtained from *K. pauciflora*.

A non-enzymatic pathway (involving a Diels-Alder cycloaddition of a secodine-type precursor as the key step) was presented to account for the isolation of racemic andranginine (**120**) from *Craspidospermum verticillatum* which was supported by the observation that thermolysis of the putative precursor, precondylocarpine acetate (**121**), at 100 ^{o}C in EtOAc solution, resulted in the formation of racemic **120**, while carrying out the thermolysis in MeOH led to the formation of the methoxy derivative, **122** (Scheme 8.1).[121] It is therefore likely that both andransinine (**119**) and **122** are artifacts, formed by a similar pathway since the precursor alkaloid, precondylocarpine (**121**) or its acetate **123** was present among the alkaloids isolated and denatured ethanol was used in the extraction of the plant materials (*K. pauciflora*).[58]

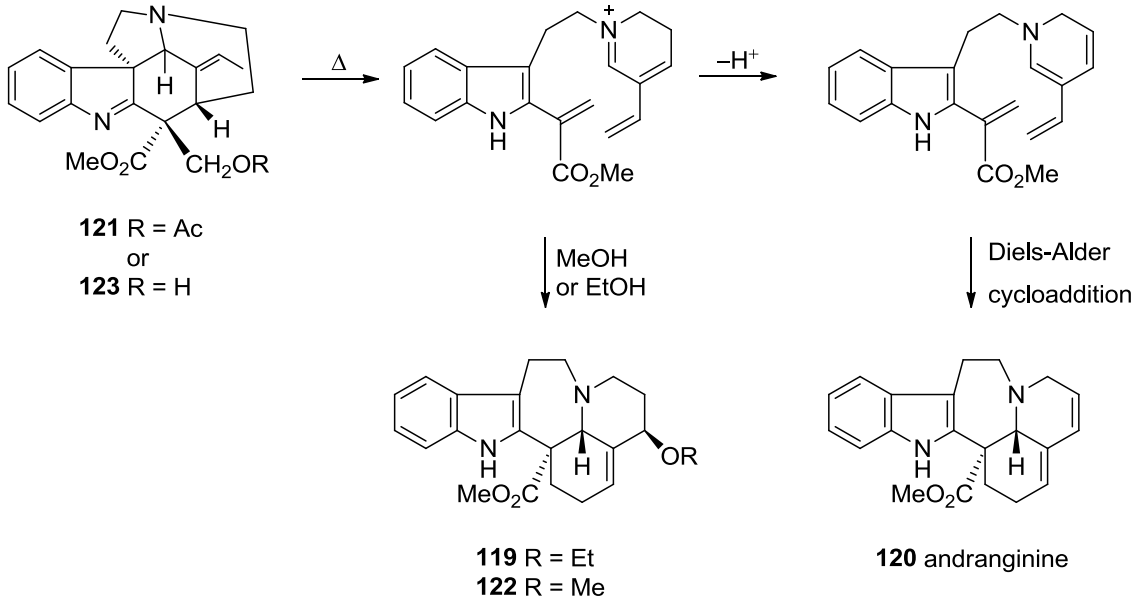

Scheme 8.1

Examination of all the diffraction evidence, unit cell (Figures 8.5, 8.6, and 8.7), space group (Table 8.4), and structure determination, showed the presence of only one enantiomer.

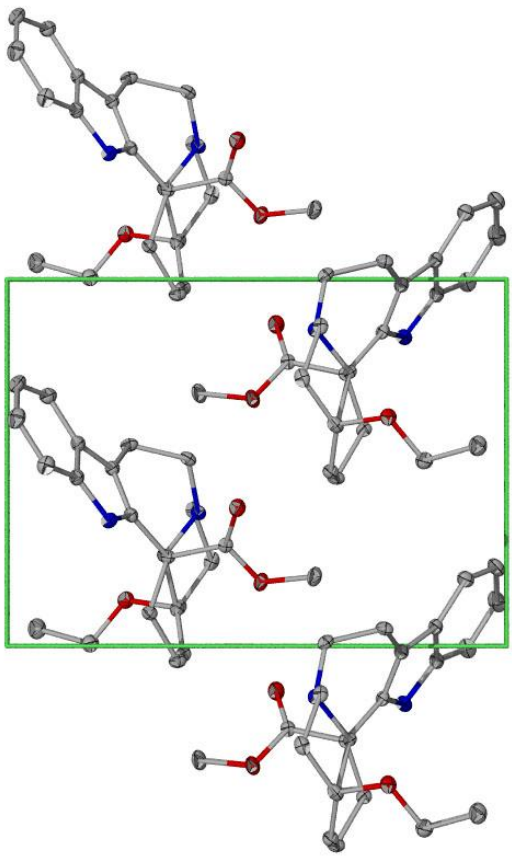

Figure 8.5. Packing diagram of **119** viewing down the *a*-axis.

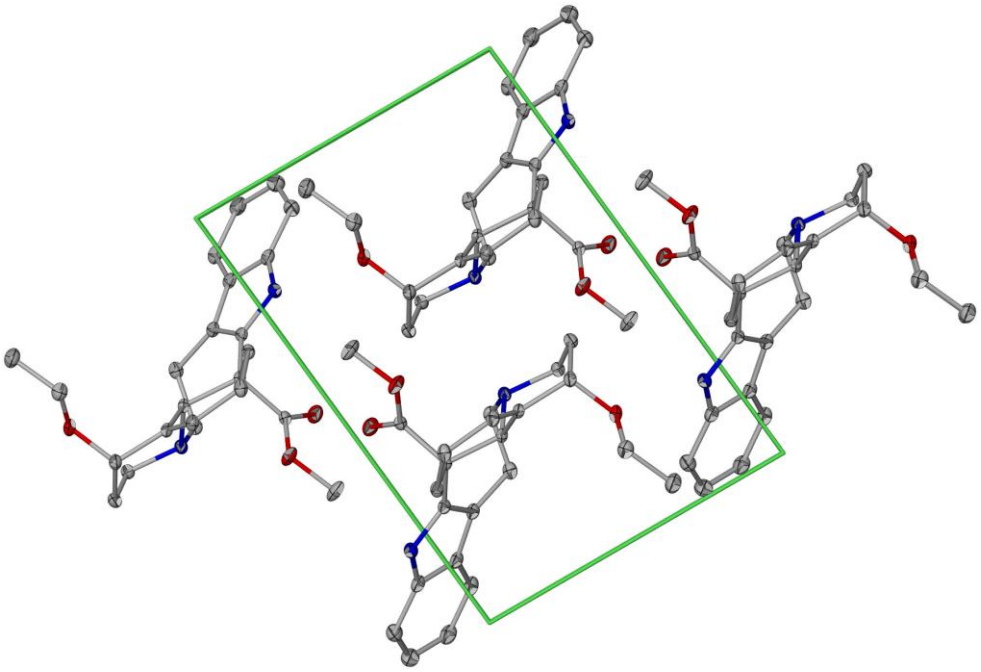

Figure 8.6. Packing diagram of **119** viewing down the *b*-axis.

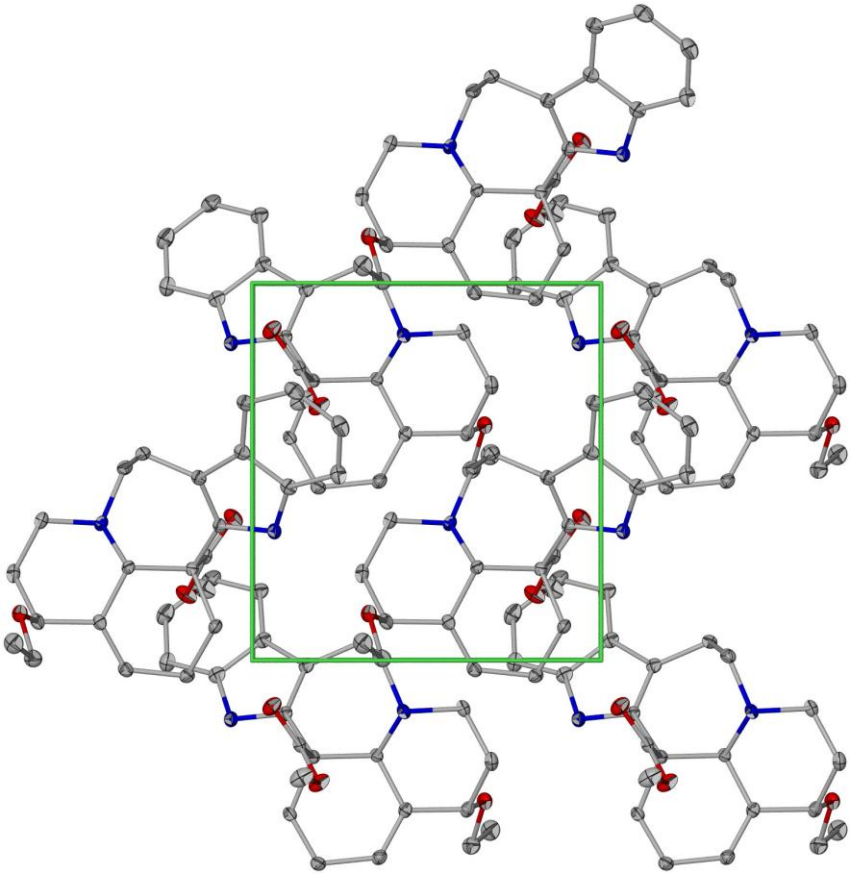

Figure 8.7. Packing diagram of **119** viewing down the *c*-axis.

Compound **119** was also subjected to crystallization in different solvent systems, such as CH_2Cl_2/hexanes and MeOH. Physical examination of these crystals under the microscope did not yield any useful information. However, from the melting point determination, it can be seen that the crystals obtained from the EtOAc solution had a higher melting point, when compared with those of crystals obtained from CH_2Cl_2/hexanes and MeOH (Table 8.5). This suggested the formation of a racemic conglomerate.[112,124] Crystals obtained from these solvents were then subjected to X-ray diffraction analyses. The physical data and X-ray diffraction analysis results are summarized in Table 8.5.

Table 8.5. Crystal data of andransinine (**119**)

	Crystals obtained from EtOAc solution	Crystals obtained from CH_2Cl_2/hexanes solution	Crystals obtained from MeOH solution
Physical appearance	Colorless block crystals (Figure 8.8)	Colorless needles (Figure 8.9)	Colorless lath crystals (Figure 8.10)
Melting point	212–214 °C	186–190 °C	204–206 °C
Crystal system	Monoclinic	Monoclinic	Orthorhombic
Unit cell dimension	a = 8.4914(10) Å b = 9.1548(11) Å c = 12.4788(15) Å $\alpha = \gamma = 90^o$, $\beta = 95.838(3)^o$	a = 39.082(4) Å b = 8.5880(11) Å c = 24.128(3) Å $\alpha = \gamma = 90^o$, $\beta = 105.802(7)^o$	a = 8.6828(2) Å b = 21.4082(4) Å c = 11.2277(2) Å $\alpha = \beta = \gamma = 90^o$
Space group	$P2_1$ (Non-centrosymmetric Chiral)	$C2/c$ (Centrosymmetric Achiral)	$Pna2_1$ (Non-centrosymmetric Achiral)
Molecular composition of the single crystal	Enantiopure chiral	Enantiomeric mixture	Enantiomeric mixture

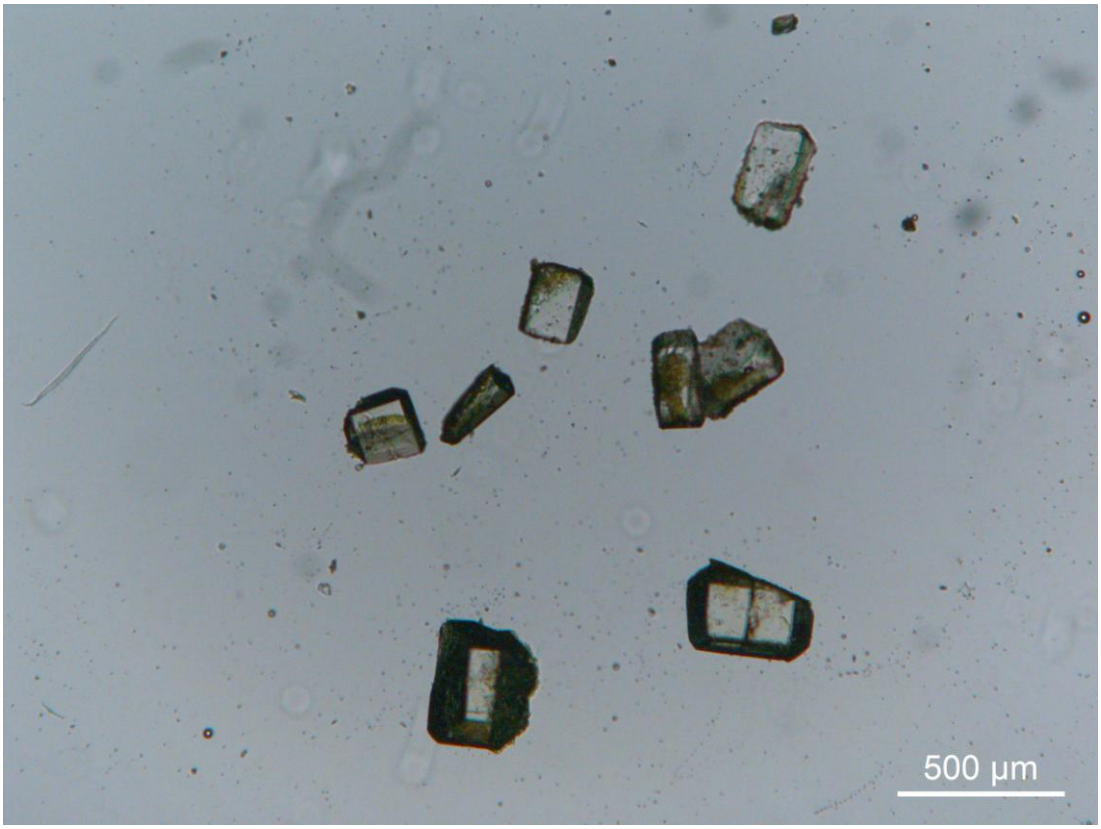

Figure 8.8. Andransinine (**119**) crystals obtained from EtOAc solution.

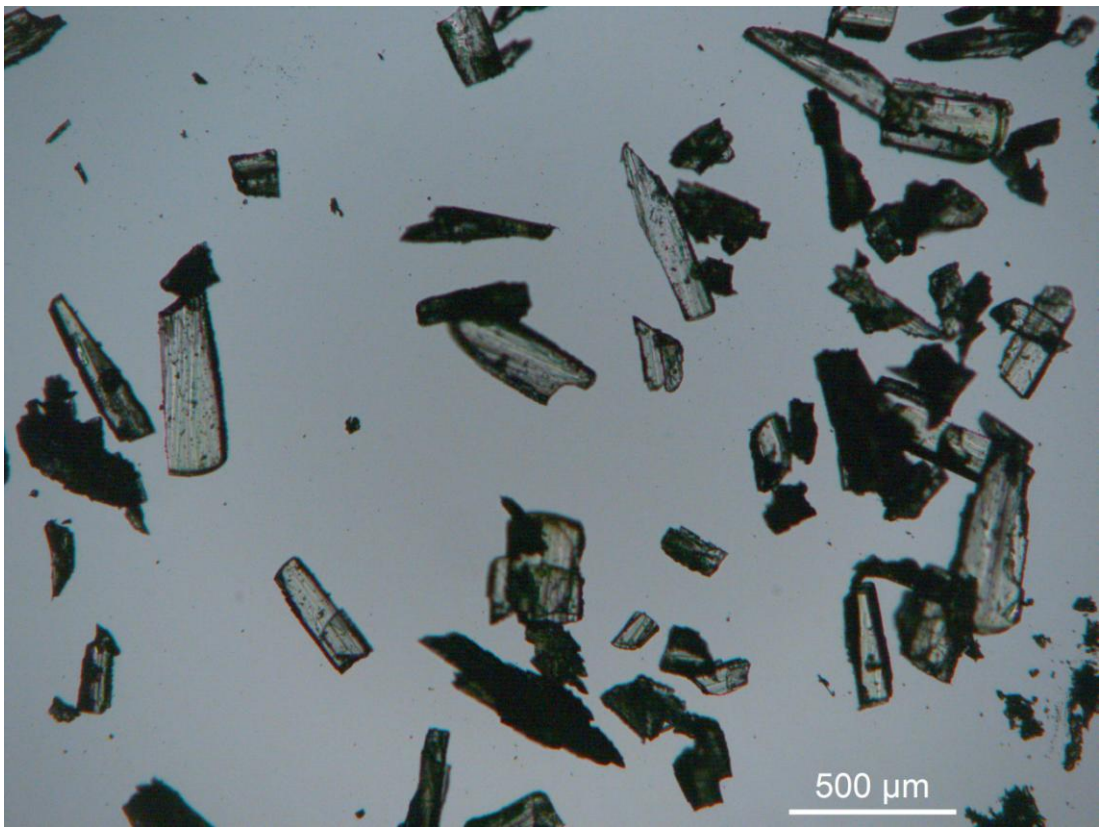

Figure 8.9. Andransinine (**119**) crystals obtained from CH_2Cl_2/hexanes solution.

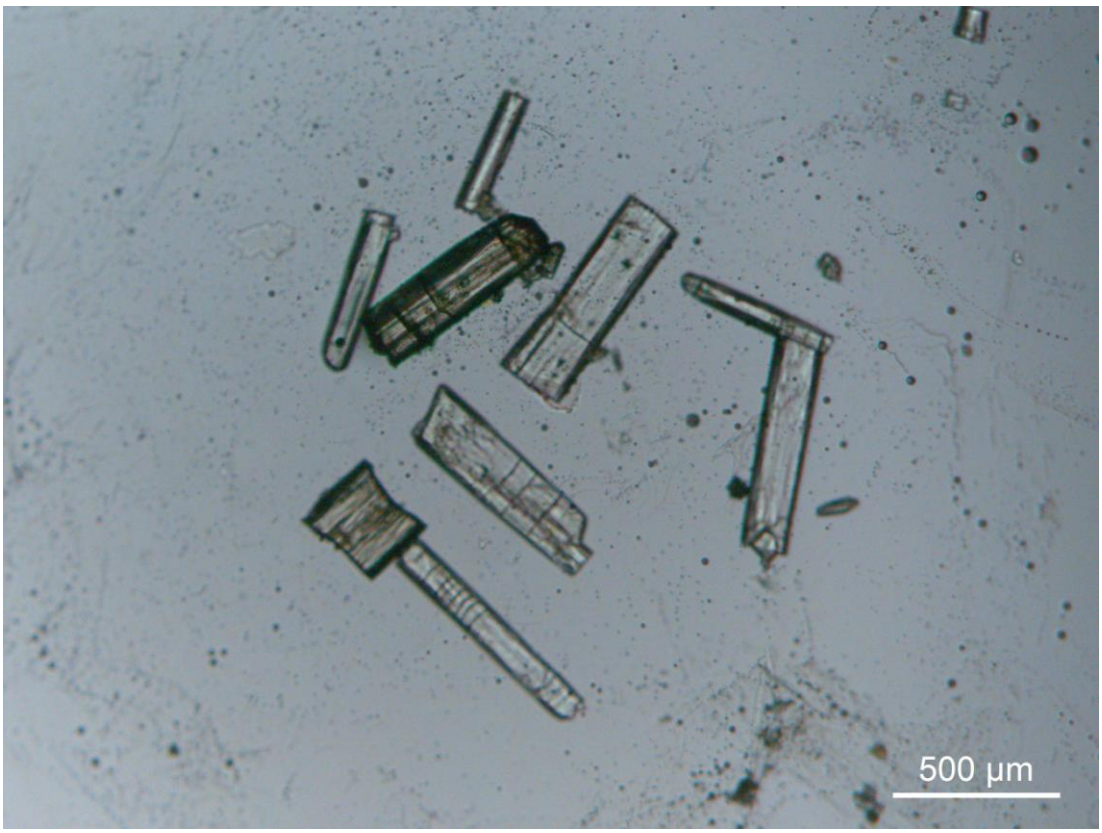

Figure 8.10. Andransinine (**119**) crystals obtained from MeOH solution.

From the X-ray data (Table 8.5), crystals obtained from EtOAc solution constitute a racemic conglomerate (an equimolar mechanical mixture of crystals, each one of which contains only one of the two enantiomers present in a racemate), while crystals from CH_2Cl_2/hexanes or MeOH solutions correspond to a racemic compound (or a crystalline racemate in which the two enantiomers are present in equal quantities in a well-defined arrangement within the crystal lattice).

Thus, it can be seen that **119** isolated from *A. angustiloba* and *K. pauciflora* are racemates, which spontaneously resolved to form racemic conglomerate crystals in EtOAc (Table 8.5), but formed racemic compound crystals when recrystallized using different solvent systems such as CH_2Cl_2/hexanes or MeOH. This can be clearly seen in the partial unit cell for both crystals obtained from CH_2Cl_2/hexanes and MeOH solutions (Figure 8.11).

Both batches of andransinine (**119**) were then subjected to chiral phase HPLC analysis,[125] using a Chiralpack AD-H column (4.6 x 150 mm; 5 μm; Daicel, Japan), with the solvent system of *n*-hexane/EtOH/diethylamine (DEA) (85:15:0.2) eluting in isocratic mode.

The HPLC chromatogram showed that both batches of andransinine (**119**) showed two major peaks (Figure 8.12) at retention time of *ca.* 3 and 7 min, which correspond to a pair of enantiomers. However, the HPLC chromatogram of **119** obtained from *Alstonia angustiloba* showed in addition to the presence of two major peaks, the presence of some minor peaks (Figure 8.12, Left). These minor peaks were not detected in the HPLC chromatogram of **119** obtained from *K. pauciflora* (Figure 8.12, Right). Thus, the presence of optical activity of **119** obtained from *A. angustiloba*, was likely a result of racemate contamination.

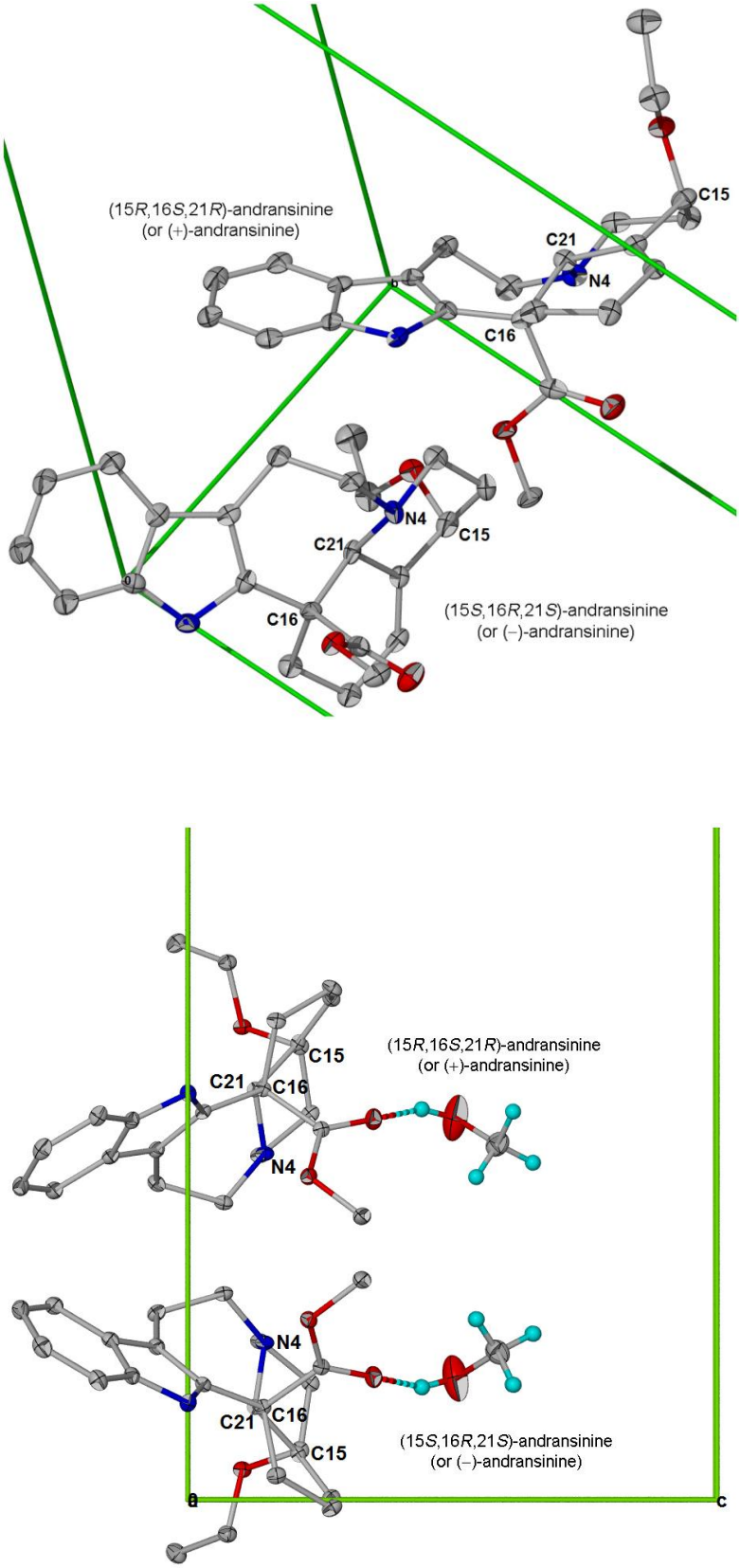

Figure 8.11. Top: Partial unit cell for crystals of **119**, obtained from CH_2Cl_2/hexanes solution. Bottom: Partial unit cell for crystals of **119**, obtained from MeOH solution. It can be seen that (±)-andransinine are present in both of the unit cell.

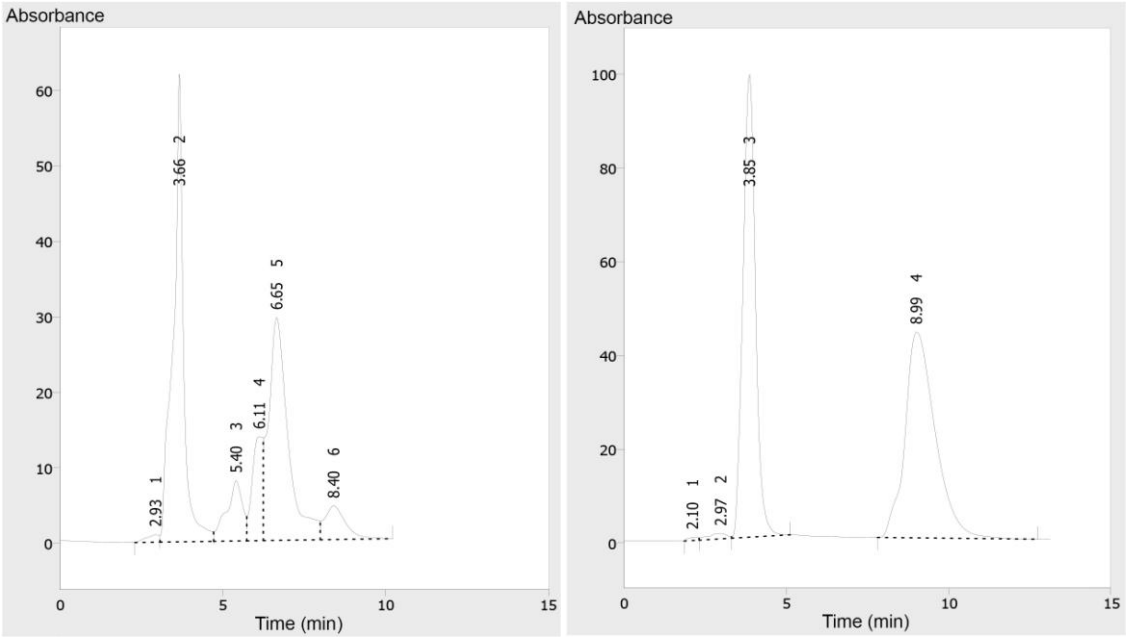

Figure 8.12. Left: HPLC chromatogram of (±)-andransinine (**119**) obtained from *A. angustiloba*. Right: HPLC chromatogram of (±)-andransinine (**119**) obtained from *K. pauciflora*. (Daicel Chiralpak AD-H (5 μm, 4.6 x 150 mm); mobile phase, *n*-hexane/EtOH/DEA = 85:15:0.2; flow rate: 0.8 ml/min).

Since (±)-andransinine (**119**) crystallized from EtOAc are racemic conglomerates, any of these crystals will yield an absolute configuration when the X-ray diffraction analysis is carried out using Cu K_α radiation. Accordingly, a suitably large crystal (*ca*. 0.43 x 0.35 x 0.28 mm) was picked from the EtOAc solution containing conglomerates of **119**. It was then cut in half (*ca.* 0.20 x 0.35 x 0.28 mm). This half crystal was then subjected to X-ray diffraction analysis using Cu K_α radiation. The absolute configuration of this crystal was determined to be (15*R*,16*S*,21*R*)-andransinine (Scheme 8.2).

The remaining half of the andransinine (**119**) crystal (*ca*. 0.23 x 0.35 x 0.28 mm) was dissolved in a minimum amount of EtOH and then subjected to chiral phase HPLC analysis (Scheme 8.2).

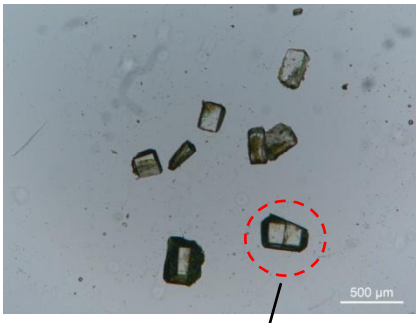

Racemic conglomerate crystals of **119**

One crystal was selected and cut into half

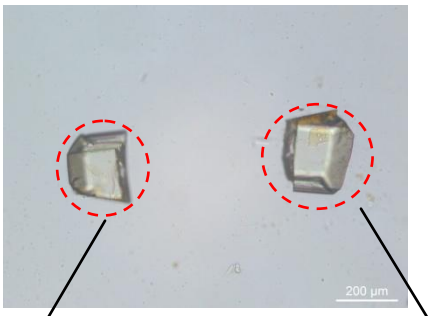

X-ray diffraction analysis (Cu K_α radiation)

Chiral phase HPLC analysis (Chiracel AD-H)

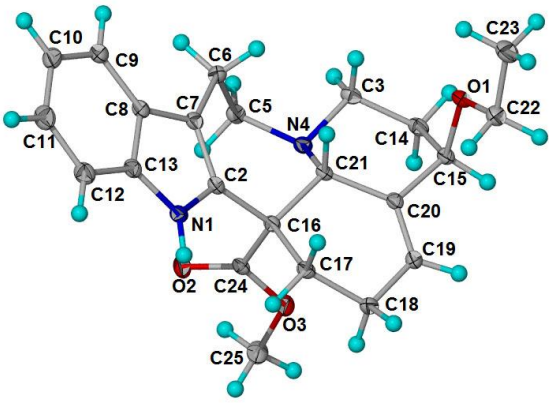

X-ray crystal structure of (15*R*,16*S*,21*R*)-andransinine (**119a**)
[Flack parameter,[63] $x = -0.15(0.12)$; Hooft parameter,[64] $y = -0.03(0.04)$].

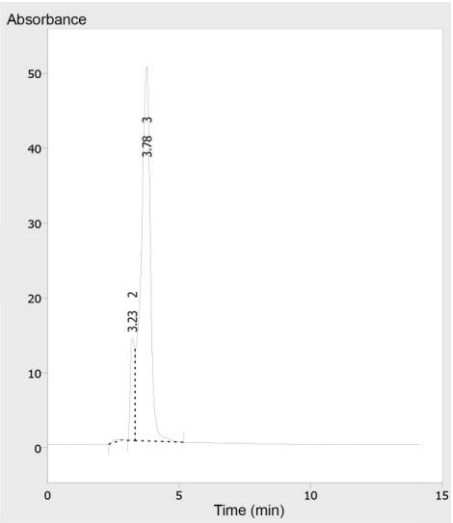

HPLC chromatogram of (15*R*,16*S*,21*R*)-andransinine (**119a**).

Scheme 8.2

It can be seen from the HPLC chromatogram that the retention time of the partially-dissolved crystal is *ca*. 3 min (Scheme 8.2), which corresponds to the first peak shown in the chromatogram in Figure 8.12. We can therefore conclude that the first peak in the HPLC chromatogram corresponds to (15*R*,16*S*,21*R*)-andransinine (**119a**), and the second peak (7 min) corresponds to (15*S*,16*R*,21*S*)-andransinine (**119b**) (Figure 8.12).

As attempts to obtain pure enantiomers from the conglomerate by mechanical sorting under the microscope was unsuccessful (lack of sufficient morphological differentiation), separation of both enantiomers was carried out using the same column and same solvent system as used previously in the analysis. Both enantiomers were successfully separated with >99% ee (Figure 8.13).

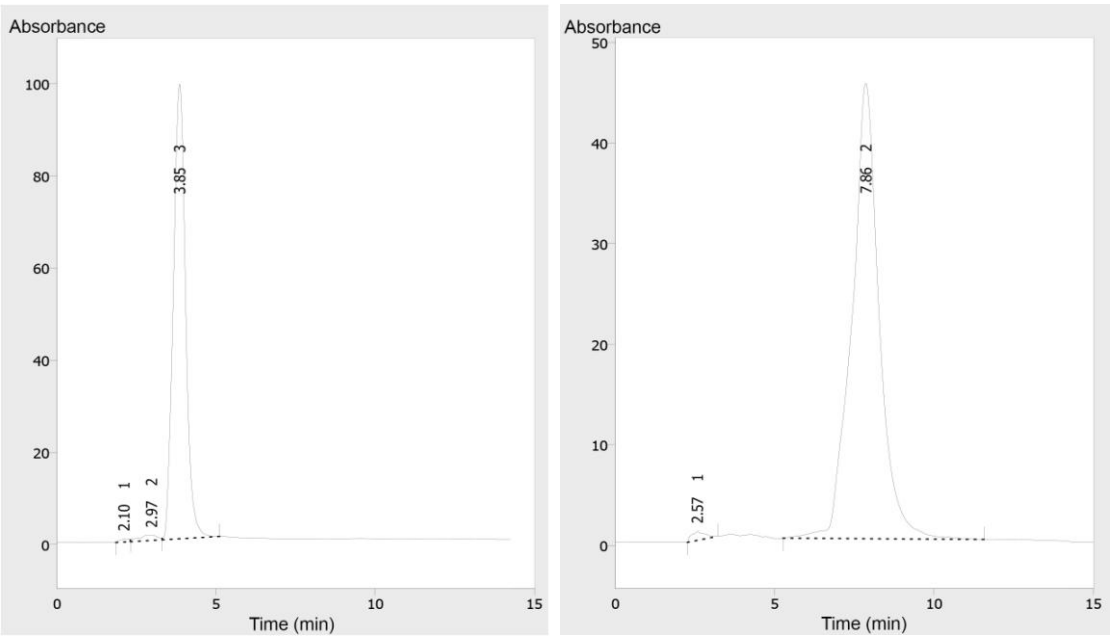

Figure 8.13. Left: HPLC chromatogram of (15*R*,16*S*,21*R*)-andransinine/(+)-andransinine (**119a**). Right: HPLC chromatogram of (15*S*,16*R*,21*S*)-andransinine/(–)-andransinine (**119b**). (Daicel Chiralpak AD-H (5 µm, 4.6 x 150 mm); mobile phase, *n*-hexane/EtOH/DEA = 85:15:0.2; flow rate: 0.8 ml/min).

The optical rotation for both enantiomers was determined. The specific rotation for (15*R*,16*S*,21*R*)-andransinine (**119a**) was found to be $[\alpha]^{25}_{D}$ +85 (*c* 0.10, $CHCl_3$), while that for (15*S*,16*R*,21*S*)-andransinine (**119b**) was found to be $[\alpha]^{25}_{D}$ –85 (*c* 0.07, $CHCl_3$). Both enantiomers were recrystallized and the crystals obtained were subjected to an X-ray diffraction analysis, using Cu K_α radiation. The absolute configuration for both enantiomers are shown in Figure 8.14.

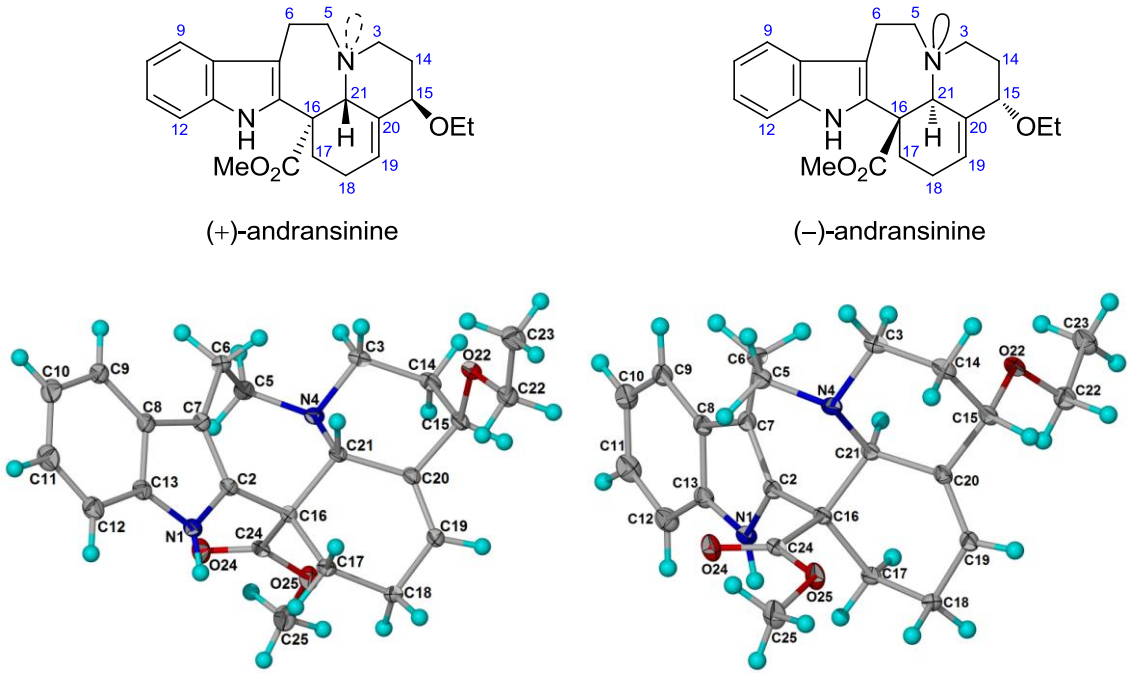

Figure 8.14. Left: X-ray crystal structure of (+)-andransinine (**119a**) [Flack parameter,[63] *x* = 0.10(0.12); Hooft parameter,[64] *y* = 0.07(0.08)]. Right: X-ray crystal structure of (–)-andransinine (**119b**) [Flack parameter,[63] *x* = –0.08(0.12); Hooft parameter,[64] *y* = 0.04(0.06)].

8.3 Conclusion

(±)-Andransinine (**119**), an artifact obtained during isolation of alkaloids from *A. angustilaoba* and *K. pauciflora*, was found to exhibit polymorphism in the solid state, forming crystals with different crystal systems and space groups in different solvent systems (Scheme 8.3). In addition, it undergoes spontaneous resolution when crystallized in EtOAc, forming racemic conglomerate crystals (Scheme 8.3). To the best of our knowledge this represents the first example encountered in alkaloids.

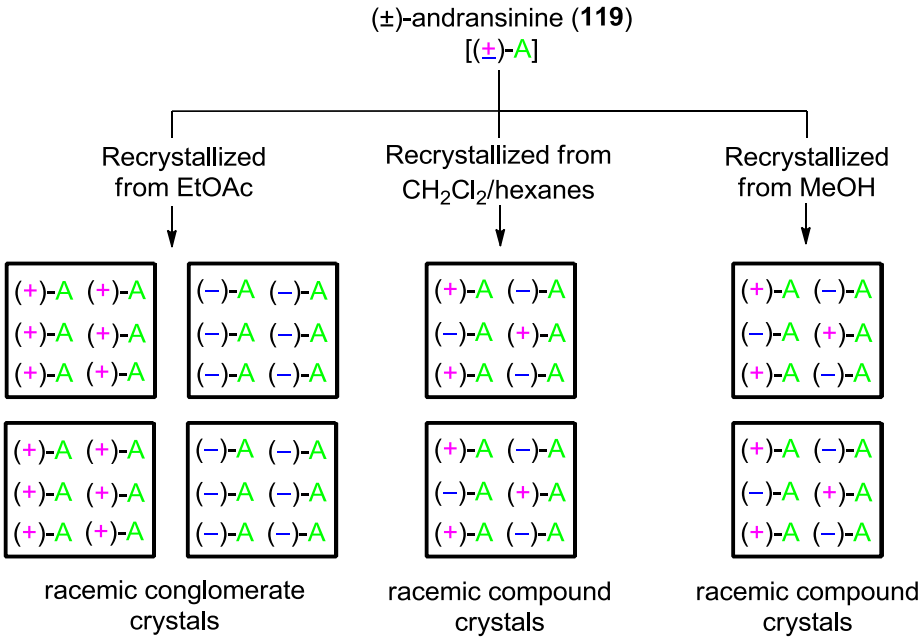

Scheme 8.3

Resolution of racemic (±)-andransinine (**119**) was carried out using chiral phase HPLC to afford the enantiomers, **119a** and **119b**, which were obtained with >99% ee. X-ray diffraction analysis yielded the absolute configuration of each enantiomer.

CHAPTER NINE

X-Ray Diffraction of New Indole and Bisindole Alkaloids

X-ray diffraction analyses were carried out on several new indole and bisindole alkaloids isolated from various plants in the family Apocynaceae. The author was responsible for crystallizing all of these alkaloids, carried out the diffraction experiments, and solved the structures.

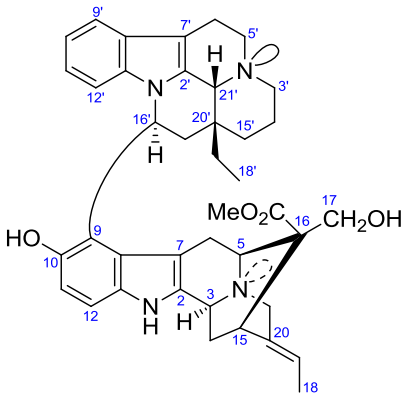

124 Ieuconoline

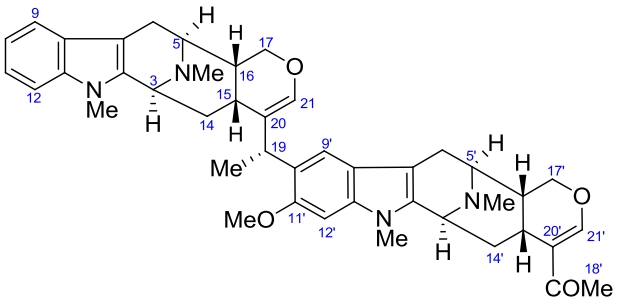

125 Iumusidine A

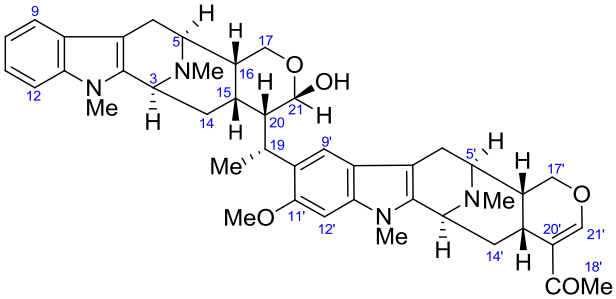

126 Iumusidine B

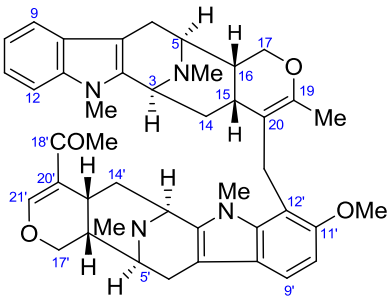

127 Iumusidine D

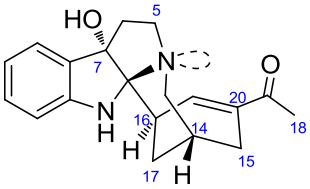

128 voatinggine

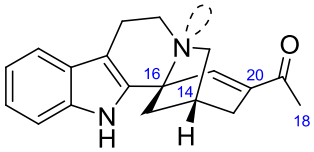

129 tabertinggine

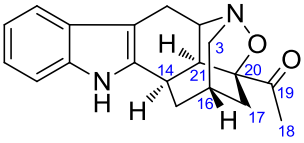

130

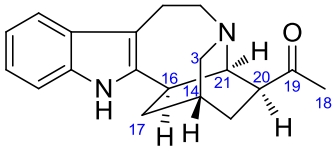

131

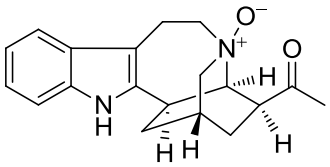

132

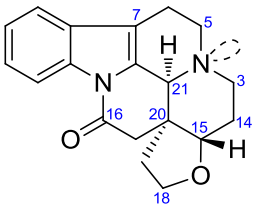

134

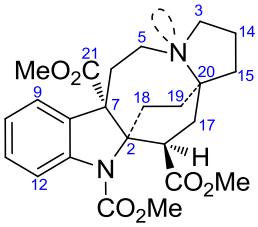

135 grandilodine A

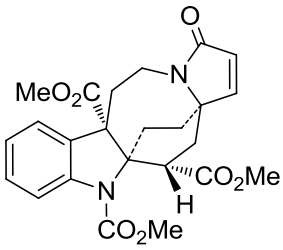

136 grandilodine B

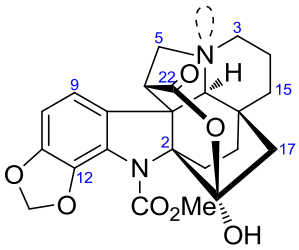

137

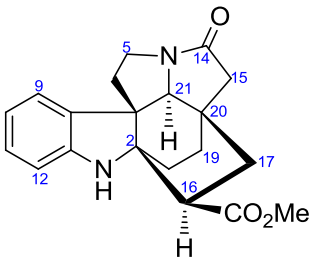

138

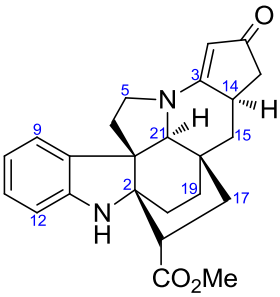

139

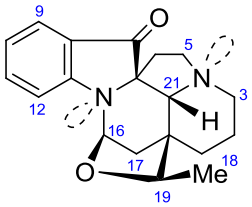

140

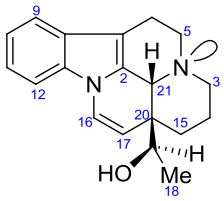

141

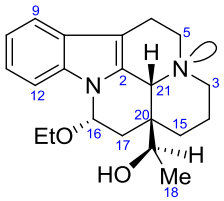

142

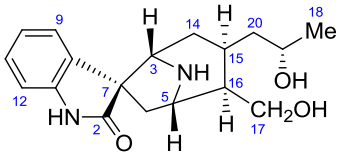

143 (7*S*)-*N*(1)-demethylalstonoxine B

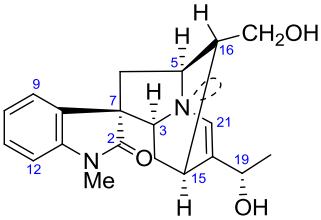

144 (7*S*)-alstoumerine oxindole

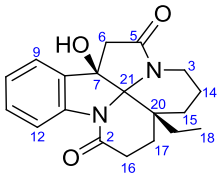

68 Ieuconodine B

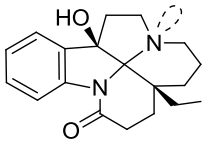

71 Ieuconodine E

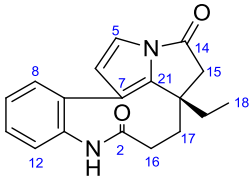

73 *nor*-rhazinicine

9.1 Bisindole Alkaloids

9.1.1 Leuconoline

The new eburnane-sarpagine type bisindole alkaloid, leuconoline (**124**), was obtained from the stem-bark extract of *Leuconotis griffithii*.[126] Suitable crystals of **124** were obtained from the slow evaporation of **124** in EtOAc solution. The structure of **124** is shown in Figure 9.1, while the crystal data and structure refinement parameters are summarized in Table 9.1.

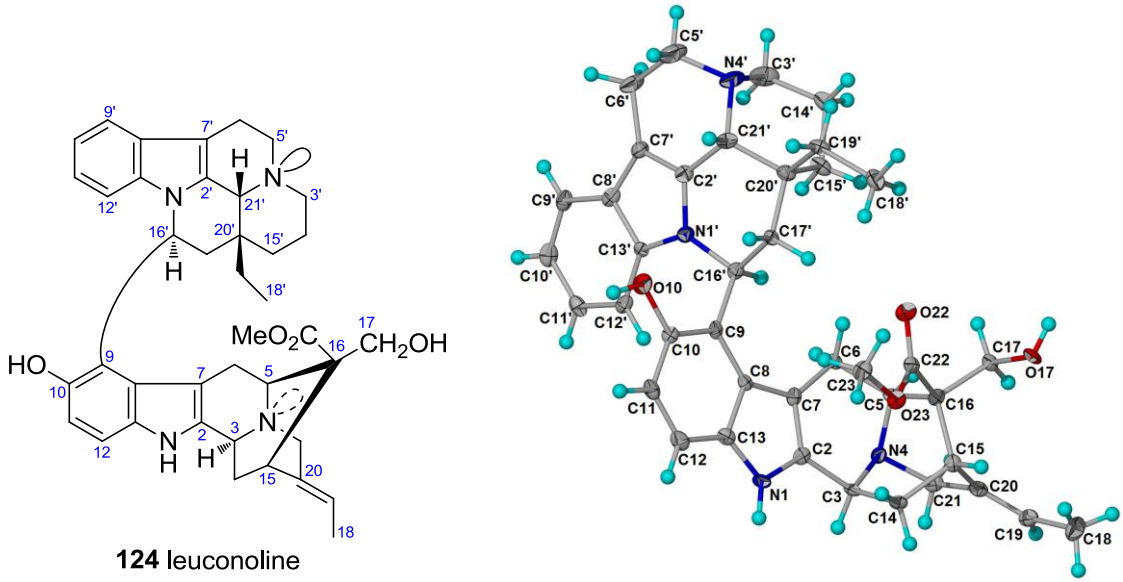

Figure 9.1. X-ray crystal structure of **124**.

Table 9.1. Crystal data and structure refinement parameters of leuconoline (**124**)

Empirical formula	$C_{40}H_{46}N_4O_4$
Molecular formula	$C_{40}H_{46}N_4O_4$
Molecular weight, M_r	646.81
Melting point	223–224 ^{o}C
Temperature during diffraction experiment, T	100 K
X-ray source	Mo K_α
Crystal system	Orthorhombic
Space group	$P2_12_12_1$
a	7.0778(2) Å
b	13.0650(4) Å
c	37.7977(12) Å
α	90.00°
β	90.00°
γ	90.00°
Volume, V	3495.21(18) Å^3
No. of molecule per unit cell, Z	4
Density (calcd)	1.229 mg/mm^3
F(000)	1384
Crystal size	0.37 × 0.08 × 0.05 mm
2θ range for data collection	4.32 to 49.5°
Index ranges	$-8 \leq h \leq 8$, $-15 \leq k \leq 15$, $-44 \leq l \leq 42$
Reflections collected	26153
Independent reflections	3428[R_{int} = 0.0728]
Data/restraints/parameters	3428/0/439
Goodness-of-fit on F^2	1.168
Final R indexes [$I \geq 2\sigma(I)$]	R_1 = 0.0644, wR_2 = 0.1358
Final R indexes [all data]	R_1 = 0.0716, wR_2 = 0.1387
Largest diff. peak/hole / e Å^{-3}	0.454/–0.237

9.1.2 Lumusidines A and B

Lumusidines A (**125**) and B (**126**) are new macroline-macroline type bisindole alkaloids isolated from the stem-bark extract of *Alstonia macrophylla*.[127] The structures and relative configurations of both alkaloids were successfully determined *via* NMR spectroscopy, except for C-19 (in the case of **125** and **126**) and C-20 (in the case of **125**).

Attempts to obtain suitable crystals for both bisindole alkaloids were unsuccessful. Eventually, conversion of lumusidines A (**125**) and B (**126**) to their dimethyl diiodide salts **125a** and **126a,** *via* treatment with iodomethane, followed by crystallization from hot MeOH, furnished suitable crystals. X-ray diffraction analyses of these crystals yielded the absolute configuration of the salts, **125a** and **126a**, which in turn yielded the absolute configuration of lumusidines A (**125**) and B (**126**). The structures and absolute configuration of the dimethyl diiodide salts **125a** and **126a** are shown in Figures 9.2 and 9.3, respectively.

The crystal data and structure refinement parameters of the dimethyl diiodide salt **125a** are summarized in Table 9.2, while the crystal data and structure refinement parameters of the dimethyl diiodide salt **126a** are summarized in Table 9.3.

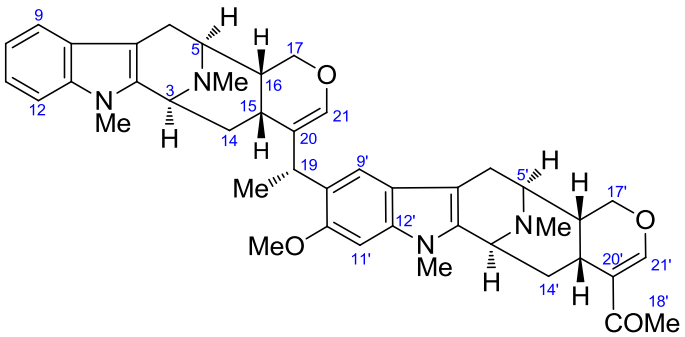

125 lumusidine A

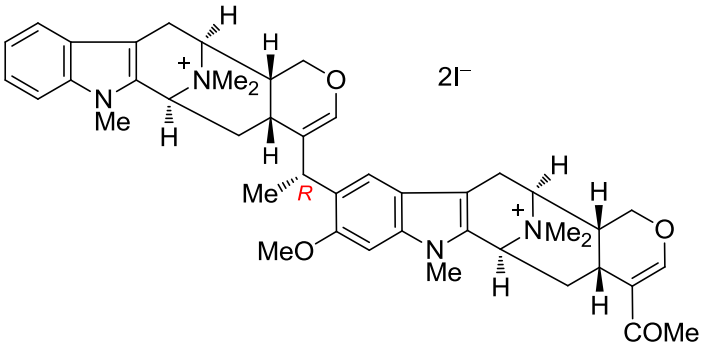

125a

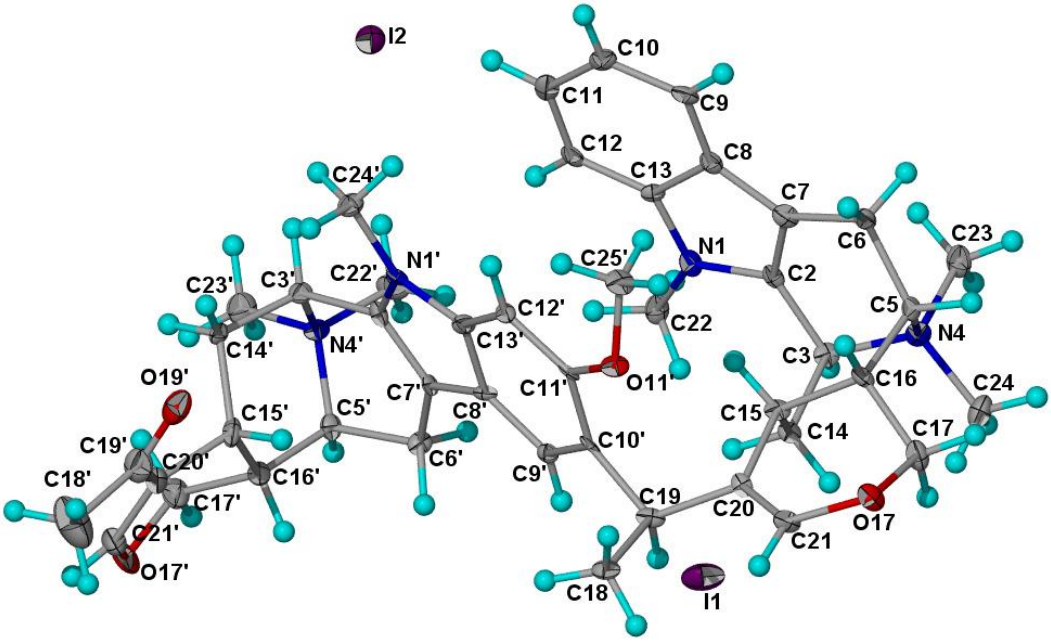

Figure 9.2. X-ray crystal structure of **125a**

[Flack parameter:[63] x = 0.01(0.03); Hooft parameter:[64] y = 0.010(0.015)].

Table 9.2. Crystal data and structure refinement parameters of compound **125a**

Empirical formula	$C_{45}H_{62}I_2N_4O_7$
Molecular formula	$C_{45}H_{56}N_4O_4^{2+}I_2^{2-}.3H_2O$
Molecular weight, M_r	1024.79
Melting point	> 198 °C dec
Temperature during diffraction experiment, T	100 K
X-ray source	Mo K_α
Crystal system	Monoclinic
Space group	$P2_1$
a	15.8916(2) Å
b	8.92620(10) Å
c	17.1572(3) Å
α	90.00°
β	112.2430(10)°
γ	90.00°
Volume, V	2252.67(5) Å^3
No. of molecule per unit cell, Z	2
Density (calcd)	1.511 mg/mm^3
F(000)	1044.0
Crystal size	0.18 × 0.12 × 0.10
2θ range for data collection	2.56 to 50°
Index ranges	$-18 \leq h \leq 18$, $-10 \leq k \leq 10$, $-20 \leq l \leq 20$
Reflections collected	17429
Independent reflections	7729[R_{int} = 0.0469]
Data/restraints/parameters	7729/10/550
Goodness-of-fit on F^2	1.030
Final R indexes [$I \geq 2\sigma(I)$]	R_1 = 0.0505, wR_2 = 0.1373
Final R indexes [all data]	R_1 = 0.0592, wR_2 = 0.1492
Largest diff. peak/hole / e Å^{-3}	3.90/–0.77
Flack parameter	0.01(0.03)
Hooft parameter	0.052(0.011)

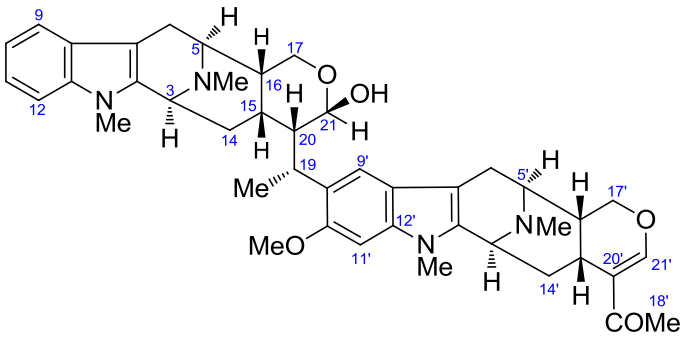

126 lumusidine B

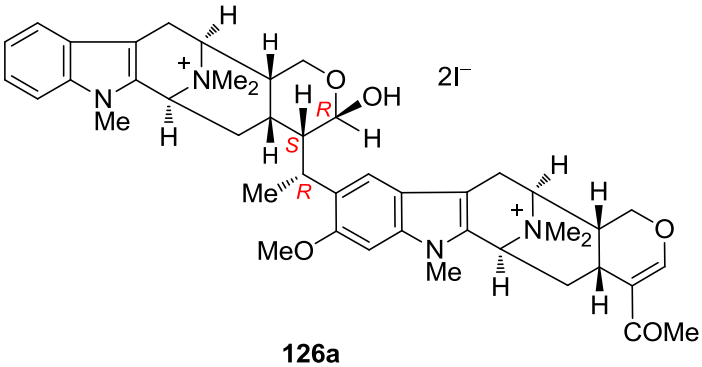

126a

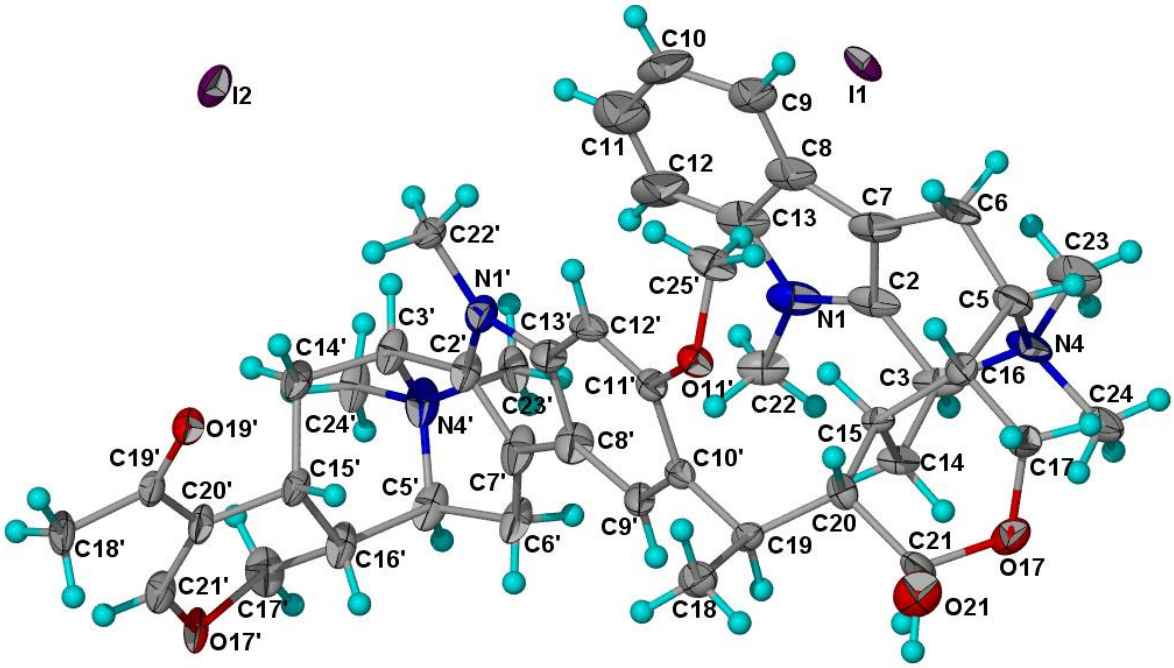

Figure 9.3. X-ray crystal structure of **126a**

[Flack parameter:[63] x = 0.01(0.03); Hooft parameter:[64] y = 0.052(0.011)].

Table 9.3. Crystal data and structure refinement parameters of compound **126a**

Empirical formula	$C_{45}H_{64}I_2N_4O_8$
Molecular formula	$C_{45}H_{58}N_4O_5^{2+}I_2^{2-}.3H_2O$
Molecular weight, M_r	1042.82
Melting point	230−234 °C
Temperature during diffraction experiment, T	100 K
X-ray source	Mo K_α
Crystal system	Monoclinic
Space group	$C2$
a	28.5993(5) Å
b	11.4265(2) Å
c	18.3052(4) Å
α	90.00°
β	127.1400(10)°
γ	90.00°
Volume, V	4768.59(16) Å^3
No. of molecule per unit cell, Z	2
Density (calcd)	0.404 mg/mm^3
F(000)	540.0
Crystal size	0.42 × 0.21 × 0.07 mm
2θ range for data collection	2.8 to 51°
Index ranges	$-34 \leq h \leq 34$, $-13 \leq k \leq 13$, $-22 \leq l \leq 22$
Reflections collected	19239
Independent reflections	8792[R_{int} = 0.0350]
Data/restraints/parameters	8792/1/600
Goodness-of-fit on F^2	1.338
Final R indexes [$I \geq 2\sigma(I)$]	R_1 = 0.0703, wR_2 = 0.1874
Final R indexes [all data]	R_1 = 0.0782, wR_2 = 0.1938
Largest diff. peak/hole / e Å^{-3}	1.82/–0.69
Flack parameter	0.05(0.03)
Hooft parameter	0.052(0.011)

9.1.3 Lumusidine D

Lumusidine D (**127**) was isolated from the stem-bark extract of *Alstonia macrophylla*.[127] Suitable crystals of **127** were obtained from the slow evaporation of **127** in CH_2Cl_2/hexanes solution. The structure and relative configuration of **127** are shown in Figure 9.4, while the crystal data and structure refinement parameters are summarized in Table 9.4.

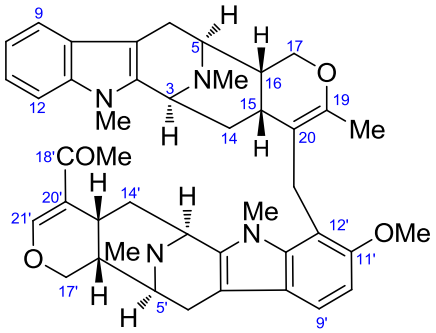

127 lumusidine D

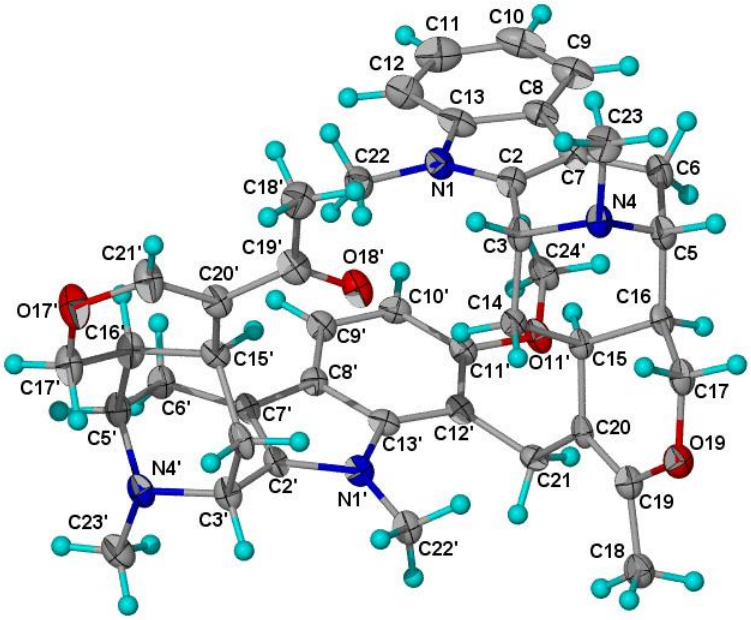

Figure 9.4. X-ray crystal structure of **127**.

Table 9.4. Crystal data and structure refinement parameters of lumusidine D (**127**)

Empirical formula	$C_{43}H_{50}N_4O_4$
Molecular formula	$C_{43}H_{50}N_4O_4$
Molecular weight, M_r	686.87
Melting point	> 270 ^{o}C dec
Temperature during diffraction experiment, T	100 K
X-ray radiation	Mo K_α
Crystal system	Orthorhombic
Space group	$P2_12_12_1$
a	9.8540(5) Å
b	14.1678(7) Å
c	25.6785(12) Å
α	90.00°
β	90.00°
γ	90.00°
Volume, V	3585.0(3) Å^3
No. of molecule per unit cell, Z	4
Density (calcd)	1.273 mg/mm^3
F(000)	1472.0
Crystal size	0.23 × 0.05 × 0.04 mm
2θ range for data collection	3.18 to 52.88°
Index ranges	$-12 \leq h \leq 12$, $-17 \leq k \leq 17$, $-32 \leq l \leq 32$
Reflections collected	31050
Independent reflections	4140[R_{int} = 0.1502]
Data/restraints/parameters	4140/0/467
Goodness-of-fit on F^2	1.069
Final R indexes [I>=2σ (I)]	R_1 = 0.0670, wR_2 = 0.1375
Final R indexes [all data]	R_1 = 0.1211, wR_2 = 0.1706
Largest diff. peak/hole / e Å^{-3}	0.38/–0.45

9.2 Indole Alkaloids

9.2.1 Indole alkaloids from *Tabernaemontana corymbosa*

9.2.1.1 Voatinggine and tabertinggine

Voatinggine (**128**) and tabertinggine (**129**) are new alkaloids which possess an unprecedented pentacyclic skeleton. Voatinggine (**128**) is characterized by a 5-6-6 ring system for the monoterpenoid portion, while tabertinggine (**129**) possess a 6-5-6 ring system fused to the indolic portion**.**

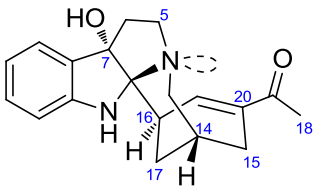

128 voatinggine

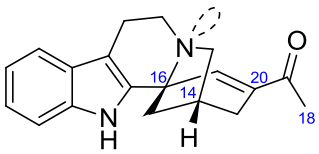

129 tabertinggine

Suitable crystals of voatinggine (**128**) were obtained from the slow evaporation of **128** in CH_2Cl_2/MeOH solution. The structure and absolute configuration of **128** are shown in Figure 9.5, while the crystal data and structure refinement parameters are summarized in Table 9.5.

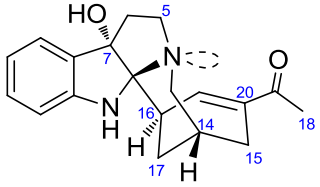

128 voatinggine

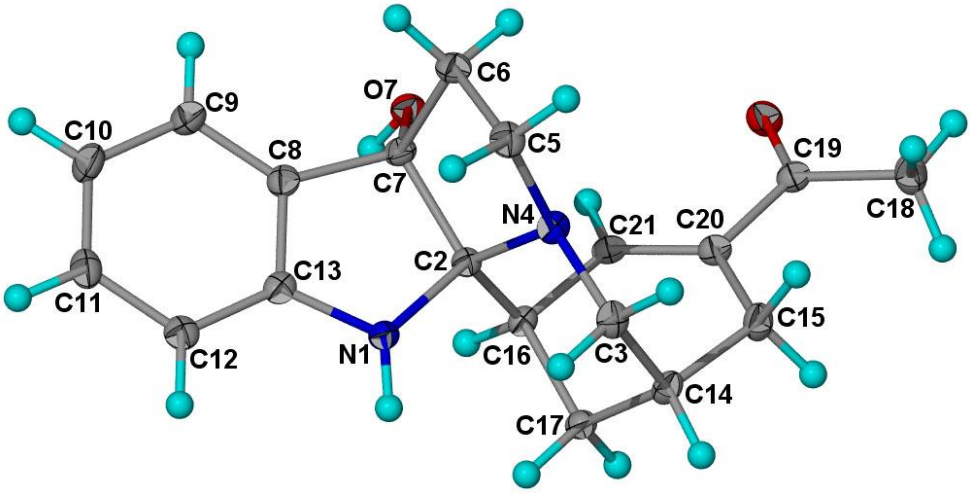

Figure 9.5. X-ray crystal structure of **128**

[Flack parameter:[63] $x = -0.17(0.19)$; Hooft parameter:[64] $y = -0.10(0.15)$].

Table 9.5. Crystal data and structure refinement parameters of voatinggine (**128**)

Empirical formula	$C_{19}H_{22}N_2O_2$
Molecular formula	$C_{19}H_{22}N_2O_2$
Molecular weight, M_r	310.39
Melting point	186–188 ^oC
Temperature during diffraction experiment, T	100 K
X-ray source	Cu K_α
Crystal system	Monoclinic
Space group	$P2_1$
a	9.6564(3) Å
b	8.3932(2) Å
c	9.8414(3) Å
α	90.00°
β	102.188(3)°
γ	90.00°
Volume, V	779.65(4) $Å^3$
No. of molecule per unit cell, Z	2
Density (calcd)	1.322 mg/mm^3
F(000)	332.0
Crystal size	0.35 × 0.17 × 0.14 mm
2θ range for data collection	9.2 to 148.44°
Index ranges	$-11 \leq h \leq 10$, $-10 \leq k \leq 10$, $-12 \leq l \leq 10$
Reflections collected	5115
Independent reflections	3066[R_{int} = 0.0160]
Data/restraints/parameters	3066/1/214
Goodness-of-fit on F^2	1.098
Final R indexes [$I \geq 2\sigma(I)$]	R_1 = 0.0373, wR_2 = 0.1061
Final R indexes [all data]	R_1 = 0.0376, wR_2 = 0.1064
Largest diff. peak/hole / e $Å^{-3}$	0.32/–0.20
Flack parameter, x	–0.17(0.19)
Hooft parameter, y	–0.10 (0.04)

Suitable crystals of tabertinggine (**129**) were obtained from the slow evaporation of **129** in $CHCl_3$/hexanes solution. The crystals obtained were very unstable when removed from the mother liquor, as the crystals will transform from colorless block crystals to white amorphous in matter of minutes when exposed to air. Thus, the crystallization of **129** had to be carried out prior to mounting the crystal onto the X-ray diffractometer. The structure and absolute configuration of **129** are shown in Figure 9.6, while the crystal data and structure refinement parameters are summarized in Table 9.6.

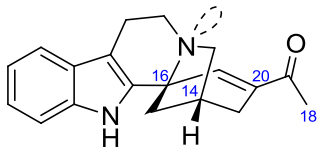

129 tabertinggine

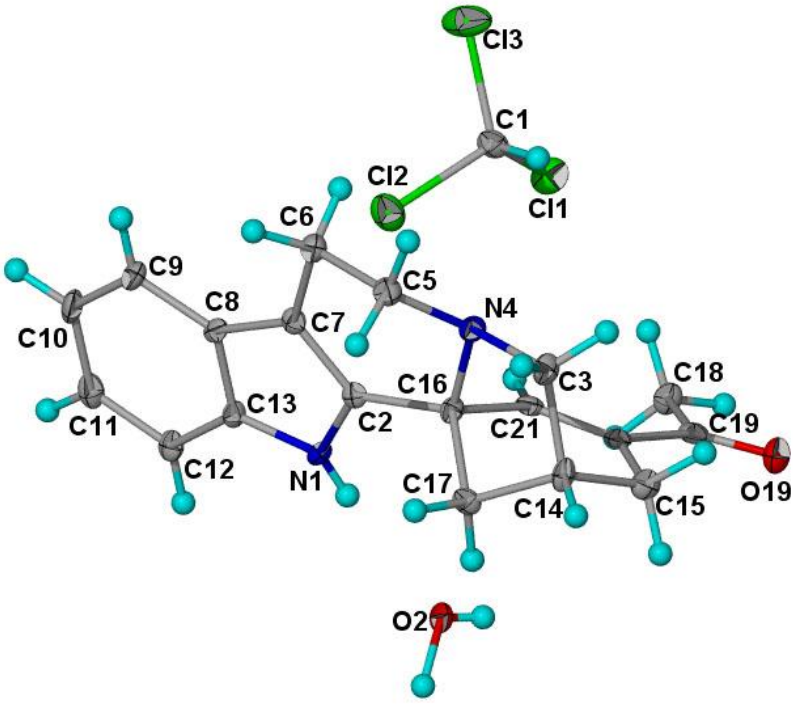

Figure 9.6. X-ray crystal structure of **129**

[Flack parameter:[63] x = –0.17(0.19); Hooft parameter:[64] y = –0.10(0.15)].

Table 9.6. Crystal data and structure refinement parameters of tabertinggine (**129**)

Empirical formula	$C_{20}H_{23}Cl_3N_2O_2$
Molecular formula	$C_{19}H_{20}N_2O.\ CHCl_3.\ H_2O$
Molecular weight, M_r	429.75
Melting point	186–188°C
Temperature during diffraction experiment, T	100 K
X-ray source	Mo K_α
Crystal system	Orthorhombic
Space group	$P2_12_12_1$
a	6.7462(2) Å
b	9.3007(3) Å
c	32.0517(9) Å
α	90.00°
β	90.00°
γ	90.00°
Volume, V	2011.06(10) Å^3
No. of molecule per unit cell, Z	4
Density (calcd)	1.419 mg/mm^3
F(000)	896.0
Crystal size	0.36 × 0.12 × 0.02 mm
2θ range for data collection	4.56 to 54.98°
Index ranges	$-8 \le h \le 8$, $-12 \le k \le 12$, $-41 \le l \le 41$
Reflections collected	18791
Independent reflections	4605[R_{int} = 0.1101]
Data/restraints/parameters	4605/0/257
Goodness-of-fit on F^2	0.951
Final R indexes [$I \ge 2\sigma(I)$]	R_1 = 0.0588, wR_2 = 0.1092
Final R indexes [all data]	R_1 = 0.0945, wR_2 = 0.1228
Largest diff. peak/hole / e Å^{-3}	0.29/–0.39
Flack parameter, x	0.05(0.09)
Hooft parameter, y	–0.10(0.04)

9.2.1.2 Alkaloid 130

Alkaloid **130** possesses a rare isoxazole in the ring system. Attempts to obtain suitable crystals for alkaloid **130** were unsuccessful. Eventually conversion of a small amount of alkaloid **130** (0.3 mg) to its methyl iodide salt **130a** *via* treatment with iodomethane, furnished suitable crystals on recrystallization from hot MeOH. X-ray diffraction analysis on these crystals yielded the absolute configuration of compound **130a**, which in turn yielded the absolute configuration of alkaloid **130**. The structure and absolute configuration of the methyl iodide salt **130a** are shown in Figure 9.7, while the crystal data and structure refinement parameters are summarized in Table 9.7.

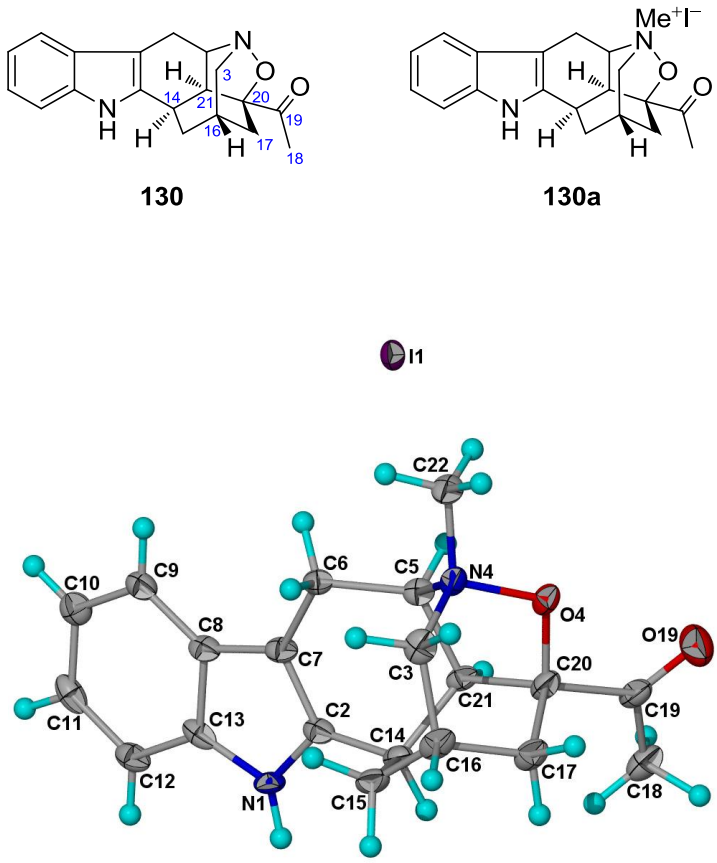

Figure 9.7. X-ray crystal structure of **130a**

[Flack parameter:[63] x = –0.00(0.03); Hooft parameter:[64] y = 0.005(0.0016)].

Table 9.7. Crystal data and structure refinement parameters of compound **130a**

Empirical formula	$C_{19}H_{22}N_2O_4I$
Molecular formula	$C_{19}H_{22}N_2O_4^+I^-$
Molecular weight, M_r	469.29
Melting point	214–218°C
Temperature during diffraction experiment, T	100 K
X-ray source	Mo K_α
Crystal system	Orthorhombic
Space group	$P2_12_12_1$
a	7.6879(8) Å
b	13.0251(14) Å
c	18.905(2) Å
α	90.00°
β	90.00°
γ	90.00°
Volume, V	1893.1(4) Å^3
No. of molecule per unit cell, Z	4
Density (calcd)	1.647 mg/mm^3
F(000)	940.0
Crystal size	0.20 × 0.20 × 0.02 mm
2θ range for data collection	3.8 to 52.72°
Index ranges	$-8 \leq h \leq 9$, $-8 \leq k \leq 16$, $-23 \leq l \leq 23$
Reflections collected	5892
Independent reflections	3636[R_{int} = 0.0519]
Data/restraints/parameters	3636/0/228
Goodness-of-fit on F^2	0.674
Final R indexes [$I \geq 2\sigma(I)$]	R_1 = 0.0422, wR_2 = 0.1050
Final R indexes [all data]	R_1 = 0.0586, wR_2 = 0.1160
Largest diff. peak/hole / e Å^{-3}	1.02/–0.93
Flack parameter, x	–0.00(0.03)
Hooft parameter , y	0.005(0.0016)

9.2.1.3 Alkaloids 131 and 132

Alkaloids **131** and its *N*-oxide derivative **132** are new iboga-type alkaloids. Alkaloid **131** is presumably the C-19 oxidation of the known alkaloid, (19*S*)-hydroxyibogamine (**133**).[128]

Suitable crystals of **131** were obtained from the slow evaporation of **131** in CH_2Cl_2/hexanes solution. The structure of **131** is shown in Figure 9.8, while the crystal data and structure refinement parameters are summarized in Table 9.8.

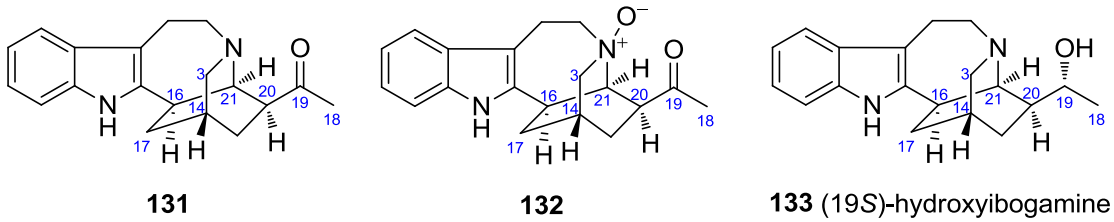

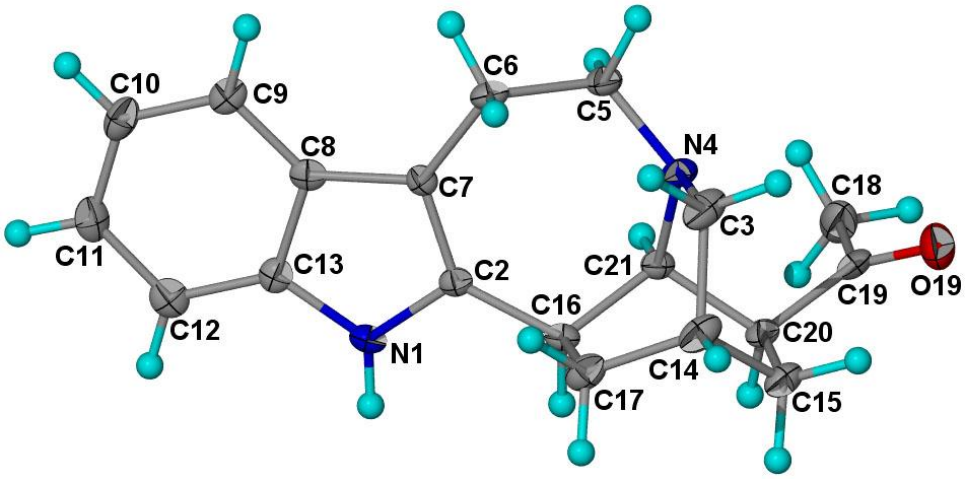

Figure 9.8. X-ray crystal structure of **131**.

Table 9.8. Crystal data and structure refinement parameters of alkaloid **131**

Empirical formula	$C_{19}H_{22}N_2O$
Molecular formula	$C_{19}H_{22}N_2O$
Molecular weight, M_r	294.39
Melting point	195–199 ^oC
Temperature during diffraction experiment, T	100 K
X-ray source	Mo $K\alpha$
Crystal system	Tetragonal
Space group	$P4_1$
a	10.1845(18) Å
b	10.1845(18) Å
c	14.613(3) Å
α	90.00°
β	90.00°
γ	90.00°
Volume, V	1515.7(5) $Å^3$
No. of molecule per unit cell, Z	4
Density (calcd)	1.290 mg/mm^3
$F(000)$	632.0
Crystal size	0.52 × 0.13 × 0.02 mm
2θ range for data collection	4 to 52.66°
Index ranges	$-12 \leq h \leq 12$, $-12 \leq k \leq 12$, $-11 \leq l \leq 17$
Reflections collected	8061
Independent reflections	1609[R_{int} = 0.0804]
Data/restraints/parameters	1609/1/200
Goodness-of-fit on F^2	0.877
Final R indexes [$I \geq 2\sigma(I)$]	R_1 = 0.0363, wR_2 = 0.0623
Final R indexes [all data]	R_1 = 0.0567, wR_2 = 0.0672
Largest diff. peak/hole / e $Å^{-3}$	0.16/–0.17

Suitable crystals of **132** were obtained from the slow evaporation of **132** in MeOH solution. The structure of **132** is shown in Figure 9.9, while the crystal data and structure refinement parameters are summarized in Table 9.9.

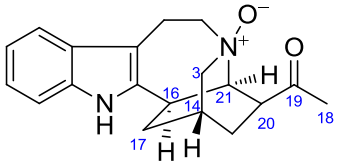

132

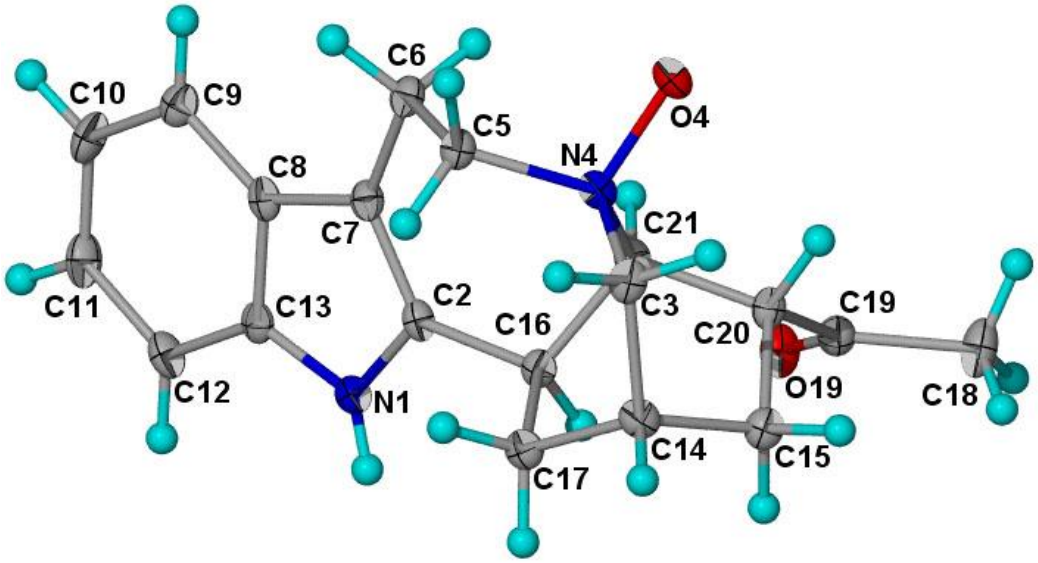

Figure 9.9. X-ray crystal structure of **132**.

Table 9.9. Crystal data and structure refinement parameters of alkaloid **132**

Empirical formula	$C_{20}H_{28}N_2O_4$
Molecular formula	$C_{19}H_{22}N_2O_2.CH_3OH.H_2O$
Molecular weight, M_r	360.44
Melting point	> 188 ^oC dec
Temperature during diffraction experiment, T	100 K
X-ray source	Mo K_α
Crystal system	Orthorhombic
Space group	$P2_12_12_1$
a	6.5750(4) Å
b	14.2730(8) Å
c	19.3071(10) Å
α	90.00°
β	90.00°
γ	90.00°
Volume, V	1811.87(18) $Å^3$
No. of molecule per unit cell, Z	4
Density (calcd)	1.321 mg/mm^3
$F(000)$	776.0
Crystal size	0.52 × 0.26 × 0.12 mm
2θ range for data collection	3.54 to 52.82°
Index ranges	$-8 \leq h \leq 8$, $-17 \leq k \leq 17$, $-23 \leq l \leq 24$
Reflections collected	13798
Independent reflections	3710[R_{int} = 0.0759]
Data/restraints/parameters	3710/0/250
Goodness-of-fit on F^2	1.018
Final R indexes [$I \geq 2\sigma(I)$]	R_1 = 0.0498, wR_2 = 0.1001
Final R indexes [all data]	R_1 = 0.0784, wR_2 = 0.1165
Largest diff. peak/hole / e $Å^{-3}$	0.22/–0.24

9.2.1.4 Alkaloid 134

Alkaloid **134** is a new eburnane alkaloid which possesses an additional ring having an ether bridge between C-15 and C-18. Suitable crystals of **134** were obtained from the slow evaporation of **134** in CH_2Cl_2/hexanes solution. The structure and absolute configuration of **134** are shown in Figure 9.10, while the crystal data and structure refinement parameters are summarized in Table 9.10.

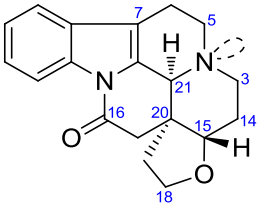

134

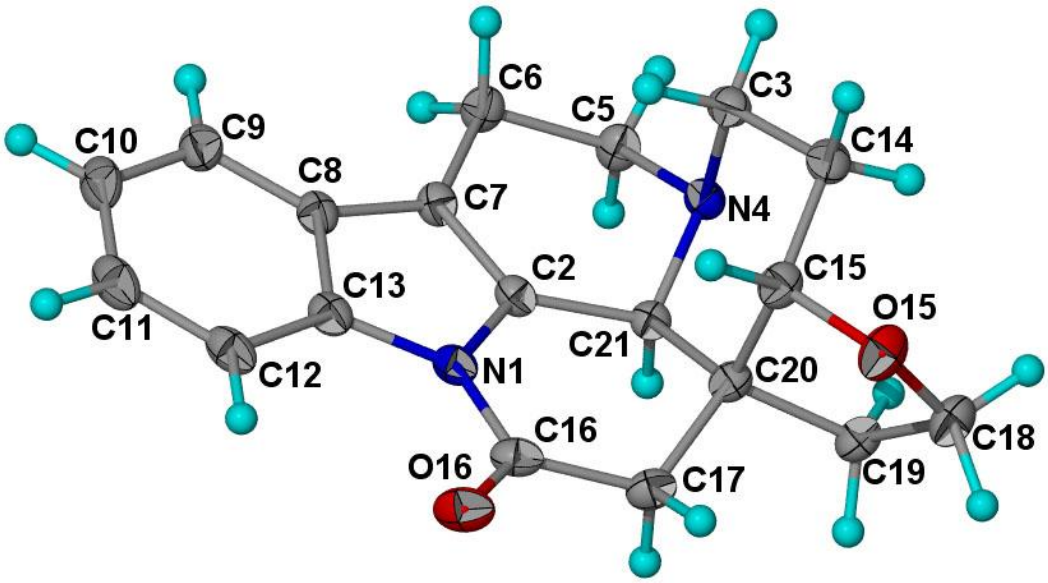

Figure 9.10. X-ray crystal structure of **134**

[Flack parameter:[63] x = –0.08(0.18); Hooft parameter:[64] y = –0.05(0.06)]

Table 9.10. Crystal data and structure refinement parameters of alkaloid **134**

Empirical formula	$C_{19}H_{20}N_2O_2$
Molecular formula	$C_{19}H_{20}N_2O_2$
Molecular weight, M_r	308.37
Melting point	> 252 ^{o}C dec
Temperature during diffraction experiment, T	100 K
X-ray source	Cu K_α
Crystal system	Orthorhombic
Space group	$P2_12_12_1$
a	11.73280(10) Å
b	13.07670(10) Å
c	19.2454(2) Å
α	90.00°
β	90.00°
γ	90.00°
Volume, V	2952.75(5) Å^3
No. of molecule per unit cell, Z	8
Density (calcd)	1.387 mg/mm^3
F(000)	1312.0
Crystal size	0.48 × 0.23 × 0.23 mm
2θ range for data collection	8.18 to 148.66°
Index ranges	$-14 \leq h \leq 14$, $-15 \leq k \leq 16$, $-23 \leq l \leq 22$
Reflections collected	10671
Independent reflections	5866[R_{int} = 0.0163]
Data/restraints/parameters	5866/0/415
Goodness-of-fit on F^2	1.071
Final R indexes [$I \geq 2\sigma(I)$]	R_1 = 0.0354, wR_2 = 0.0902
Final R indexes [all data]	R_1 = 0.0358, wR_2 = 0.0906
Largest diff. peak/hole / e Å^{-3}	0.30/–0.18
Flack parameter, x	–0.08(0.18)
Hooft parameter , y	–0.05(0.06)

9.2.2 Alkaloids from *Kopsia grandifolia*

9.2.2.1 Grandilodines A and B

The grandilodines A (**135**) and B (**136**) are new alkaloids isolated from the stem-bark extract of *Kopsia grandifolia*.[129]

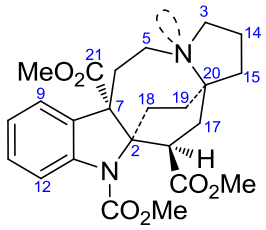

135 grandilodine A

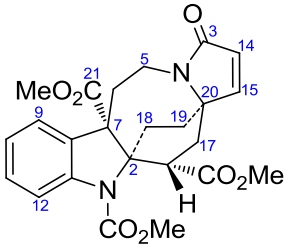

136 grandilodine B

Crystals of grandilodine A (**135**) were obtained from the slow evaporation of **135** in CH_2Cl_2/MeOH solution. The structure of **135** is shown in Figure 9.11, while the crystal data and structure refinement parameters are summarized in Table 9.11.

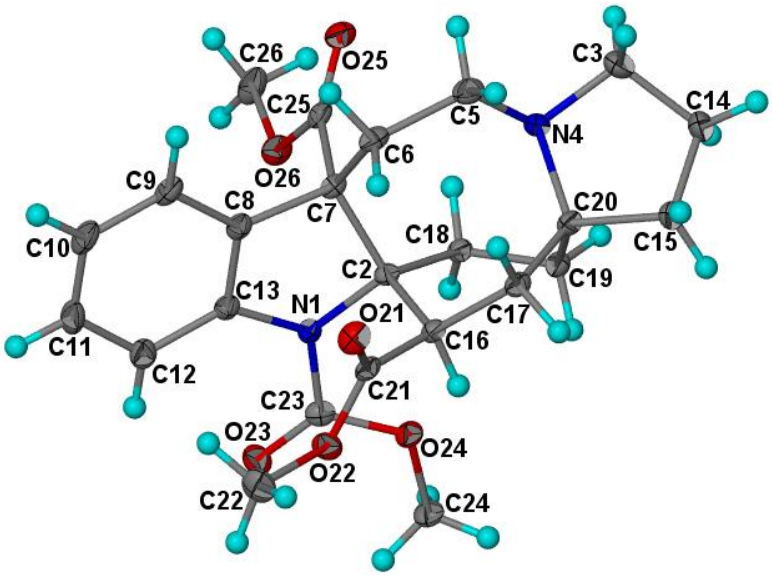

Figure 9.11. X-ray crystal structure of **135**.

Table 9.11. Crystal data and structure refinement parameters of grandilodine A (**135**)

Empirical formula	$C_{24}H_{30}N_2O_6$
Molecular formula	$C_{24}H_{30}N_2O_6$
Molecular weight, M_r	442.50
Melting point	120–122 ^{o}C
Temperature during diffraction experiment, T	100 K
X-ray source	Mo K_α
Crystal system	Orthorhombic
Space group	$P2_12_12_1$
a	8.0067(2) Å
b	11.2455(3) Å
c	24.1247(7) Å
α	90.00°
β	90.00°
γ	90.00°
Volume, V	2172.17(10) Å^3
No. of molecule per unit cell, Z	4
Density (calcd)	1.353 mg/mm^3
F(000)	944.0
Crystal size	0.61 × 0.20 × 0.15 mm
2θ range for data collection	4 to 55°
Index ranges	$-10 \leq h \leq 10$, $-14 \leq k \leq 14$, $-30 \leq l \leq 31$
Reflections collected	18782
Independent reflections	2846[R_{int} = 0.0671]
Data/restraints/parameters	2846/0/292
Goodness-of-fit on F^2	1.024
Final R indexes [$I \geq 2\sigma(I)$]	R_1 = 0.0401, wR_2 = 0.0910
Final R indexes [all data]	R_1 = 0.0516, wR_2 = 0.0969
Largest diff. peak/hole / e Å^{-3}	0.27/–0.27

Crystals of grandilodine B (**136**) were obtained from the slow evaporation of **135** in CH_2Cl_2/hexanes solution. The structure of **136** is shown in Figure 9.12, while the crystal data and structure refinement parameters are summarized in Table 9.12.

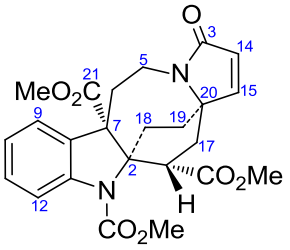

136 grandilodine B

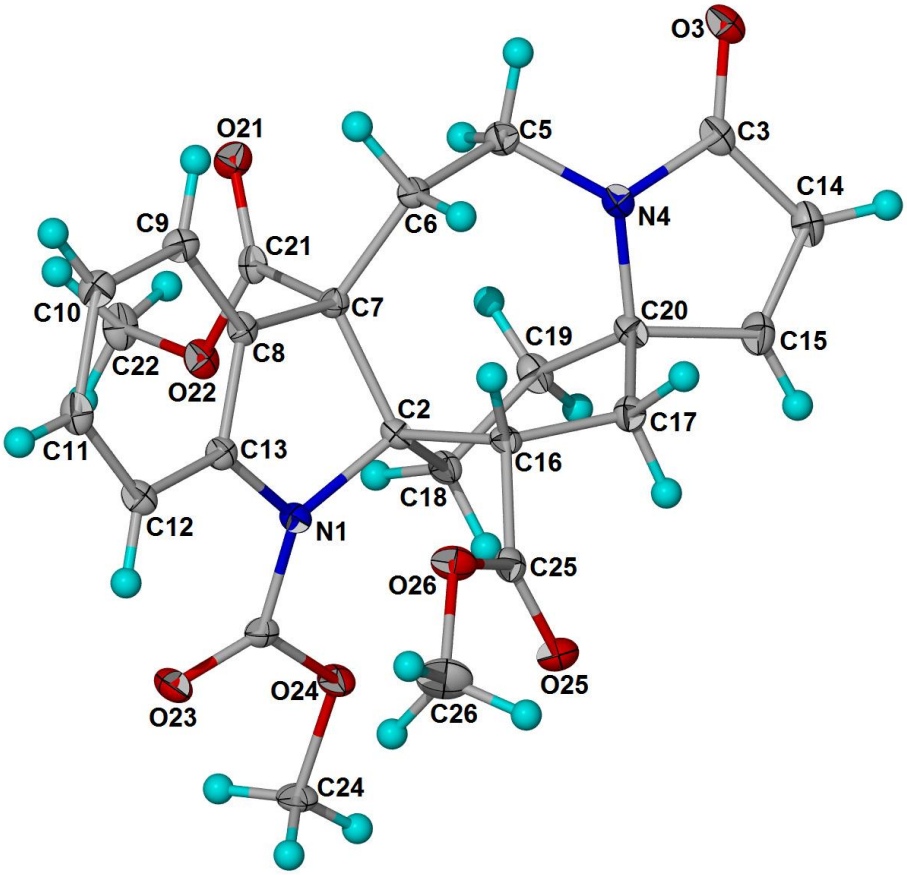

Figure 9.12. X-ray crystal structure of **136**.

Table 9.12. Crystal data and structure refinement parameters of grandilodine B (**136**)

Empirical formula	$C_{24}H_{26}N_2O_7$
Molecular formula	$C_{24}H_{26}N_2O_7$
Molecular weight, M_r	454.47
Melting point	204–206 ^oC
Temperature during diffraction experiment, T	100 K
X-ray source	Mo K_α
Crystal system	Monoclinic
Space group	$P2_1$
a	8.6505(2) Å
b	8.0985(2) Å
c	15.3926(4) Å
α	90.00°
β	90.057(2)°
γ	90.00°
Volume, V	1078.34(5) $Å^3$
No. of molecule per unit cell, Z	2
Density (calcd)	1.400 mg/mm^3
$F(000)$	480.0
Crystal size	0.47 × 0.28 × 0.08 mm
2θ range for data collection	2.64 to 55°
Index ranges	$-11 \leq h \leq 11$, $-10 \leq k \leq 10$, $-20 \leq l \leq 19$
Reflections collected	10203
Independent reflections	2655[R_{int} = 0.0497]
Data/restraints/parameters	2655/1/301
Goodness-of-fit on F^2	0.990
Final R indexes [$I \geq 2\sigma(I)$]	R_1 = 0.0335, wR_2 = 0.0759
Final R indexes [all data]	R_1 = 0.0404, wR_2 = 0.0790
Largest diff. peak/hole / e $Å^{-3}$	0.21/–0.20

9.2.2.2 Alkaloid 137

Crystals of the new alkaloid **137** were obtained from the slow evaporation of **137** in CH_2Cl_2/MeOH solution. The structure of **137** is shown in Figure 9.13, while the crystal data and structure refinement parameters are summarized in Table 9.13. From the crystal structure, an intramolecular hydrogen bond was observed between the C-16–OH and the amide carbonyl.

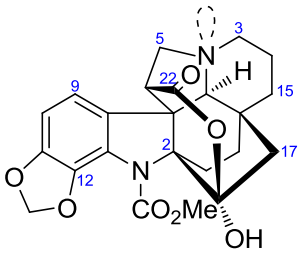

137

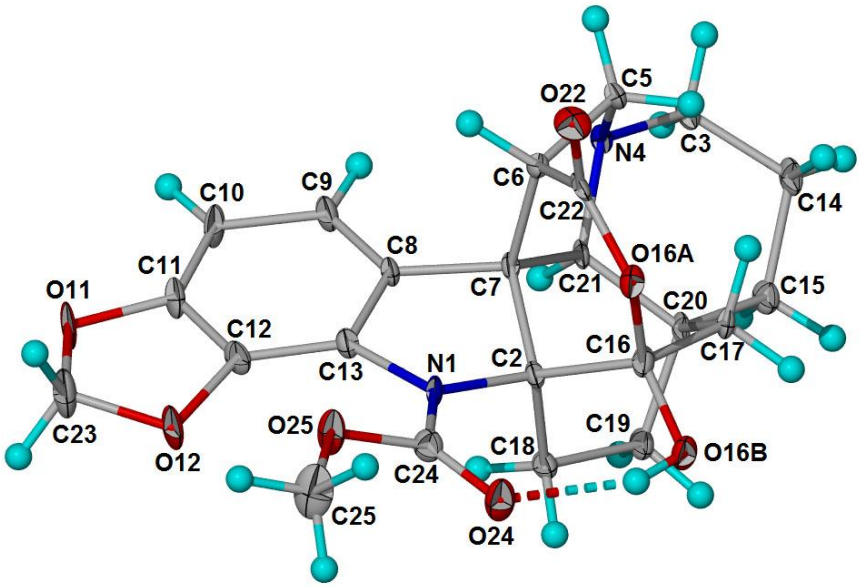

Figure 9.13. X-ray crystal structure of **137**.

Table 9.13. Crystal data and structure refinement parameters of alkaloid **137**

Empirical formula	$C_{23}H_{24}N_2O_7$
Molecular formula	$C_{23}H_{24}N_2O_7$
Molecular weight, M_r	440.44
Melting point	206–208 ^{o}C
Temperature during diffraction experiment, T	100 K
X-ray source	Mo K_α
Crystal system	Monoclinic
Space group	$P2_1$
a	9.9492(5) Å
b	8.2037(4) Å
c	13.0494(7) Å
α	90.00°
β	109.845(3)°
γ	90.00°
Volume, V	1001.84(9) Å^3
No. of molecule per unit cell, Z	2
Density (calcd)	1.460 mg/mm^3
F(000)	464.0
Crystal size	0.58 × 0.15 × 0.06
2θ range for data collection	3.32 to 55°
Index ranges	$-12 \leq h \leq 12$, $-10 \leq k \leq 10$, $-16 \leq l \leq 16$
Reflections collected	9224
Independent reflections	2462[R_{int} = 0.0536]
Data/restraints/parameters	2462/1/291
Goodness-of-fit on F^2	1.142
Final R indexes [$I \geq 2\sigma(I)$]	R_1 = 0.0504, wR_2 = 0.1186
Final R indexes [all data]	R_1 = 0.0588, wR_2 = 0.1220
Largest diff. peak/hole / e Å^{-3}	0.35/–0.32

9.2.2.3 Alkaloid 138

Alkaloid **138** is the first example of an aspidofractinine-type alkaloid which has lost one carbon in the piperidine ring D, resulting in five-membered lactam ring D.

Crystals of **138** were obtained from the slow evaporation of **138** in CH_2Cl_2/MeOH solution. It can be seen that **138** co-crystallized with the solvent used during crystallization (MeOH). The structure of **138** is shown in Figure 9.14, while the crystal data and structure refinement parameters are summarized in Table 9.14.

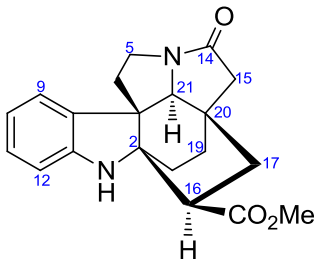

138

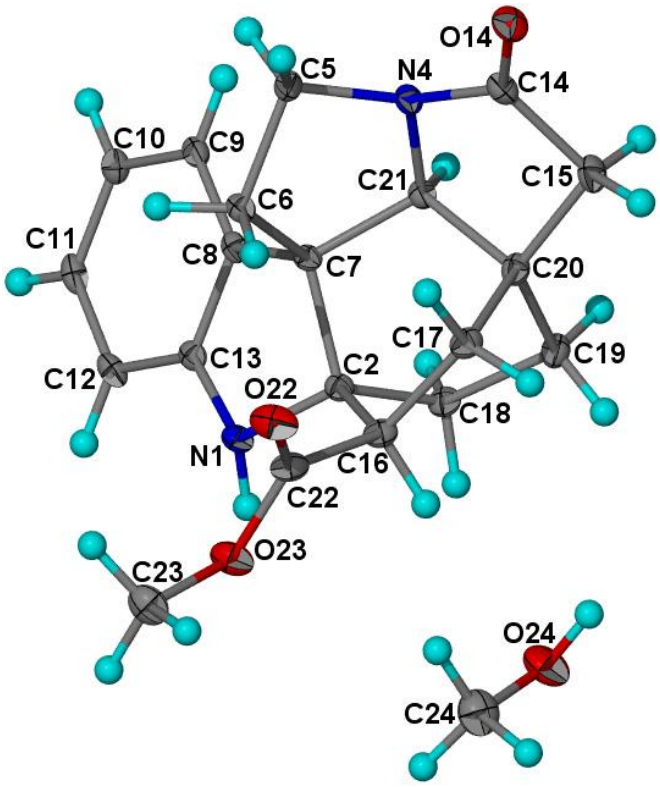

Figure 9.14. X-ray crystal structure of **138**.

Table 9.14. Crystal data and structure refinement parameters of alkaloid **138**

Empirical formula	$C_{21}H_{26}N_2O_4$
Molecular formula	$C_{20}H_{22}N_2O_3.CH_3OH$
Molecular weight, M_r	370.44
Melting point	180–182 ^oC
Temperature during diffraction experiment, T	100 K
X-ray source	Mo K_α
Crystal system	Orthorhombic
Space group	$P2_12_12_1$
a	6.7581(2) Å
b	11.4548(3) Å
c	23.3157(6) Å
α	90.00°
β	90.00°
γ	90.00°
Volume, V	1804.93(9) $Å^3$
No. of molecule per unit cell, Z	4
Density (calcd)	1.363 mg/mm^3
$F(000)$	792.0
Crystal size	0.58 × 0.25 × 0.13 mm
2θ range for data collection	3.5 to 54.96°
Index ranges	$-8 \leq h \leq 8$, $-14 \leq k \leq 14$, $-30 \leq l \leq 30$
Reflections collected	16954
Independent reflections	2385[R_{int} = 0.0513]
Data/restraints/parameters	2385/0/251
Goodness-of-fit on F^2	1.113
Final R indexes [$I \geq 2\sigma(I)$]	R_1 = 0.0332, wR_2 = 0.0856
Final R indexes [all data]	R_1 = 0.0399, wR_2 = 0.0993
Largest diff. peak/hole / e $Å^{-3}$	0.25/–0.25

9.2.2.4 Alkaloid 139

Alkaloid **139** is notable for having incorporated an additional five-membered ring fused to the piperidine ring D of an aspidofractinine carbon skeleton. Crystals of **139** were obtained from the slow evaporation of **139** in CH_2Cl_2/hexanes solution. It can also be seen that **139** co-crystallized with the solvent used during crystallization (CH_2Cl_2). The absolute structure of **139** is shown in Figure 9.15, while the crystal data and structure refinement parameters are summarized in Table 9.15.

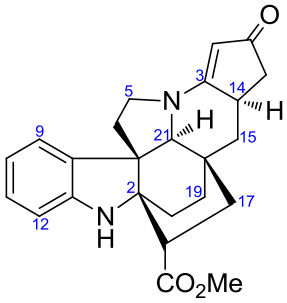

139

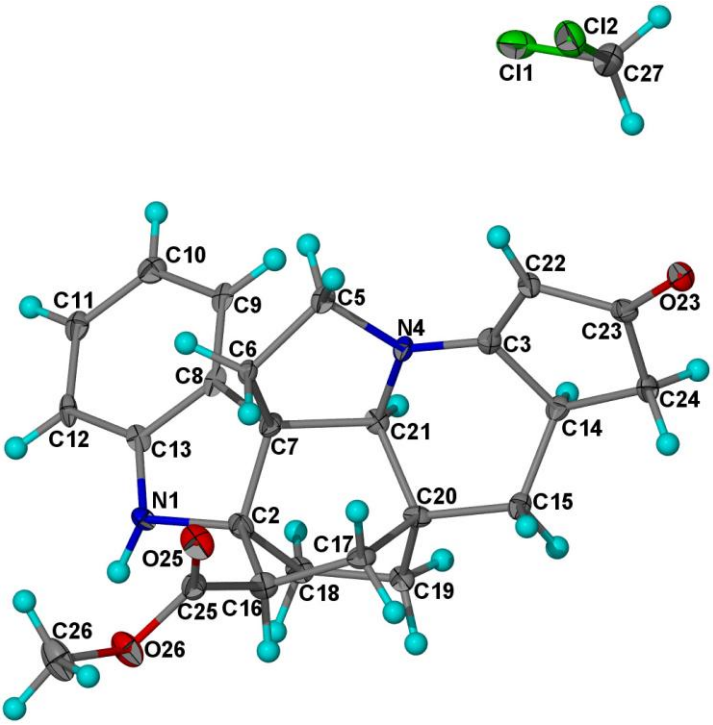

Figure 9.15. X-ray crystal structure of **139**

[Flack parameter:[63] x = –0.02(0.12); Hooft parameter:[64] y = –0.00(0.07)].

Table 9.15. Crystal data and structure refinement parameters of alkaloid **139**

Empirical formula	$C_{25}H_{28}Cl_2N_2O_3$
Molecular formula	$C_{24}H_{26}N_2O_3.CH_2Cl_2$
Molecular weight, M_r	475.39
Melting point	268–270 ^oC
Temperature during diffraction experiment, T	100 K
X-ray source	Mo K_α
Crystal system	Orthorhombic
Space group	$P2_12_12_1$
a	6.6620(4) Å
b	9.8110(5) Å
c	34.4440(18) Å
α	90.00°
β	90.00°
γ	90.00°
Volume, V	2251.3(2) $Å^3$
No. of molecule per unit cell, Z	4
Density (calcd)	1.403 mg/mm^3
F(000)	1000.0
Crystal size	0.42 × 0.04 × 0.02 mm
2θ range for data collection	2.36 to 52.76°
Index ranges	$-8 \leq h \leq 8$, $-12 \leq k \leq 12$, $-42 \leq l \leq 42$
Reflections collected	19611
Independent reflections	4609[R_{int} = 0.1662]
Data/restraints/parameters	4609/0/294
Goodness-of-fit on F^2	0.853
Final R indexes [$I \geq 2\sigma(I)$]	R_1 = 0.0600, wR_2 = 0.1277
Final R indexes [all data]	R_1 = 0.1258, wR_2 = 0.1664
Largest diff. peak/hole / e $Å^{-3}$	0.35/–0.35
Flack parameter	–0.02(0.12)
Hooft parameter	–0.00(0.07)

9.2.2.5 Alkaloid 140

Alkaloid **140** is a new alkaloid isolated from the stem-bark extract of *Kopsia grandifolia*. Suitable crystals of **140** were obtained from the slow evaporation of **140** in CH_2Cl_2/MeOH solution. The structure of **140** is shown in Figure 9.16, while the crystal data and structure refinement parameters, are summarized in Table 9.16.

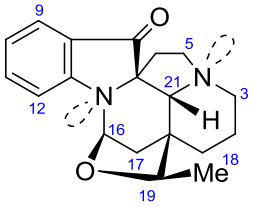

140

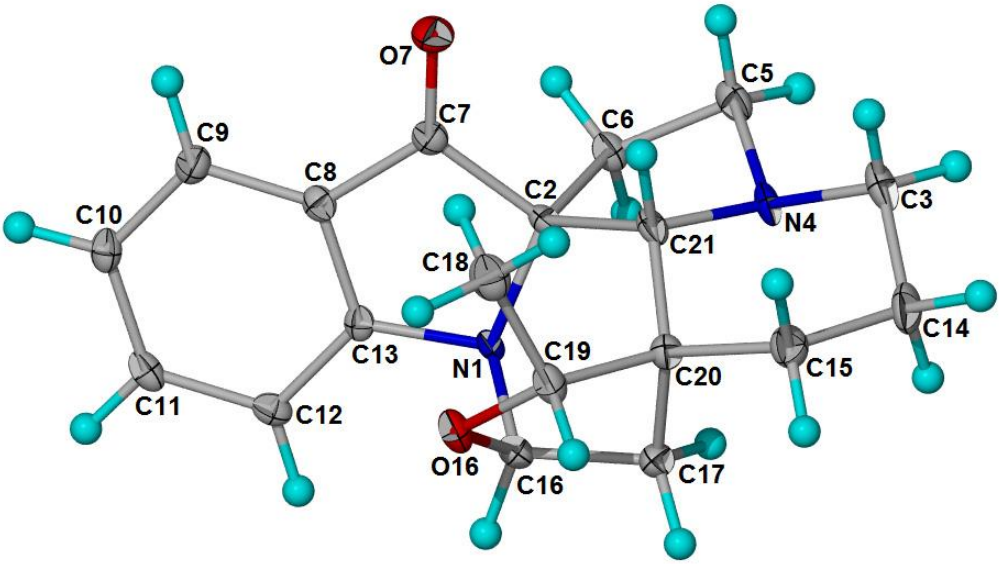

Figure 9.16. X-ray crystal structure of **140**.

Table 9.16. Crystal data and structure refinement parameters of alkaloid **140**

Empirical formula	$C_{19}H_{22}N_2O_2$
Molecular formula	$C_{19}H_{22}N_2O_2$
Molecular weight, M_r	310.39
Melting point	190–192 ^{o}C
Temperature during diffraction experiment, T	100 K
X-ray source	Mo K_α
Crystal system	Monoclinic
Space group	$P2_1$
a	14.2796(4) Å
b	7.9986(2) Å
c	15.7780(5) Å
α	90.00°
β	116.781(2)°
γ	90.00°
Volume, V	1608.81(8) Å^3
No. of molecule per unit cell, Z	4
Density (calcd)	1.281 mg/mm^3
F(000)	664.0
Crystal size	0.72 × 0.22 × 0.10 mm
2θ range for data collection	2.9 to 54.98°
Index ranges	$-18 \leq h \leq 18$, $-10 \leq k \leq 10$, $-20 \leq l \leq 20$
Reflections collected	15425
Independent reflections	3962[R_{int} = 0.0983]
Data/restraints/parameters	3962/1/417
Goodness-of-fit on F^2	0.957
Final R indexes [$I \geq 2\sigma(I)$]	R_1 = 0.0409, wR_2 = 0.0877
Final R indexes [all data]	R_1 = 0.0526, wR_2 = 0.0915
Largest diff. peak/hole / e Å^{-3}	0.25/–0.23

9.2.2.6 (19*R*)-Hydroxyeburnamenine

(19*R*)-Hydroxyeburnamenine (**141**) is a new eburnane alkaloid. Crystals of **141** were obtained from the slow evaporation of **141** in CH_2Cl_2/MeOH solution. The structure of **141** is shown in Figure 9.17, while the crystal data and structure refinement parameters are summarized in Table 9.17.

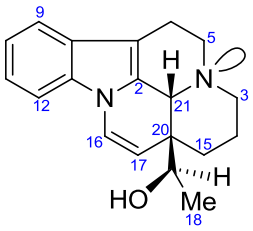

141

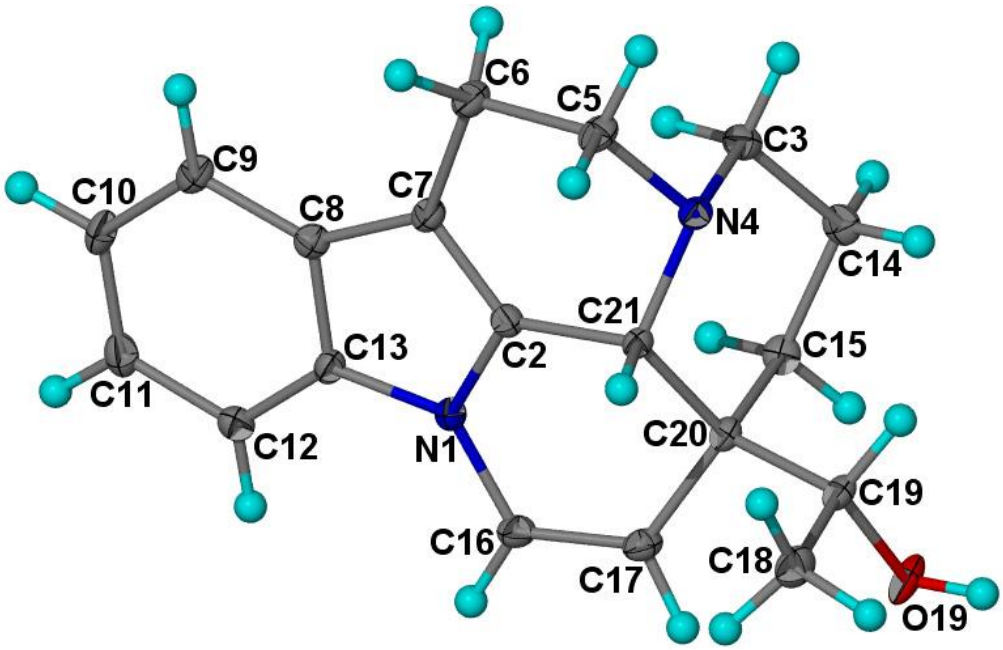

Figure 9.17. X-ray crystal structure of **141**.

Table 9.17. Crystal data and structure refinement parameters of (19*R*)-hydroxyeburnamenine (**141**)

Empirical formula	$C_{19}H_{22}N_2O$
Molecular formula	$C_{19}H_{22}N_2O$
Molecular weight, M_r	294.39
Melting point	162–164 ^{o}C
Temperature during diffraction experiment, T	100 K
X-ray source	Mo K_α
Crystal system	Monoclinic
Space group	$P2_1$
a	8.63910(10) Å
b	7.92600(10) Å
c	11.5438(2) Å
α	90.00°
β	98.4100(10)°
γ	90.00°
Volume, V	781.945(19) Å^3
No. of molecule per unit cell, Z	2
Density (calcd)	1.250 mg/mm^3
F(000)	316.0
Crystal size	0.34 × 0.16 × 0.15 mm
2θ range for data collection	3.56 to 55°
Index ranges	$-11 \leq h \leq 11$, $-10 \leq k \leq 10$, $-14 \leq l \leq 14$
Reflections collected	6701
Independent reflections	1920[R_{int} = 0.0384]
Data/restraints/parameters	1920/1/201
Goodness-of-fit on F^2	1.095
Final R indexes [$I \geq 2\sigma(I)$]	R_1 = 0.0373, wR_2 = 0.0852
Final R indexes [all data]	R_1 = 0.0451, wR_2 = 0.1035
Largest diff. peak/hole / e Å^{-3}	0.26/–0.20

9.2.2.7 Alkaloid 142

Alkaloid **142** may be an artifact of the alkaloid **141**, in view of the presence of an ethoxy group in the structure, and the use of EtOH during extraction.[130] Crystals of **142** were obtained from the slow evaporation of **142** in CH_2Cl_2/MeOH solution. The structure of **142** is shown in Figure 9.18, while the crystal data and structure refinement parameters are summarized in Table 9.18.

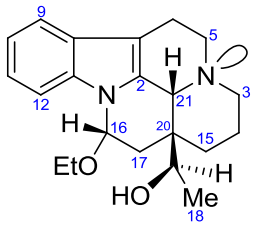

142

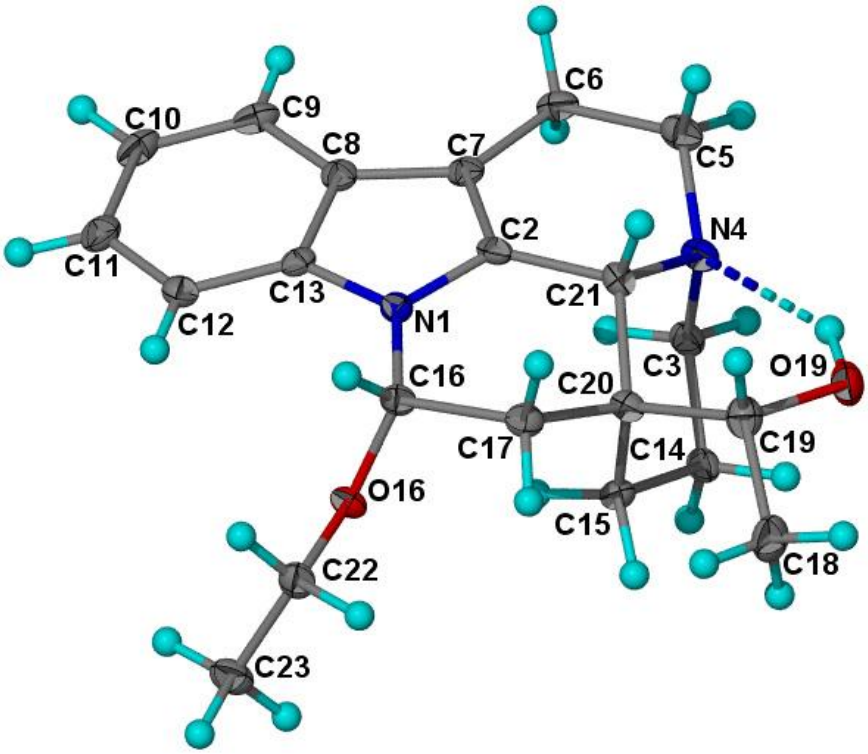

Figure 9.18. X-ray crystal structure of **142**.

Table 9.18. Crystal data and structure refinement parameters of alkaloid **142**

Empirical formula	$C_{21}H_{28}N_2O_2$
Molecular formula	$C_{21}H_{28}N_2O_2$
Molecular weight, M_r	340.45
Melting point	150–152 ^{o}C
Temperature during diffraction experiment, T	100 K
X-ray source	Mo K_α
Crystal system	Orthorhombic
Space group	$P2_12_12_1$
a	8.4666(3) Å
b	12.1895(4) Å
c	16.9938(6) Å
α	90.00°
β	90.00°
γ	90.00°
Volume, V	1753.82(10) Å^3
No. of molecule per unit cell, Z	4
Density (calcd)	1.289 mg/mm^3
F(000)	736.0
Crystal size	0.41 × 0.09 × 0.06 mm
2θ range for data collection	4.12 to 52.72°
Index ranges	$-10 \leq h \leq 10$, $-15 \leq k \leq 15$, $-21 \leq l \leq 21$
Reflections collected	15258
Independent reflections	2060[R_{int} = 0.1237]
Data/restraints/parameters	2060/0/229
Goodness-of-fit on F^2	1.038
Final R indexes [$I \geq 2\sigma(I)$]	R_1 = 0.0516, wR_2 = 0.0938
Final R indexes [all data]	R_1 = 0.0846, wR_2 = 0.1050
Largest diff. peak/hole / e Å^{-3}	0.20/–0.25

9.2.3 Alkaloids from *Alstonia angustifolia*

9.2.3.1 (7*S*)-*N*(1)-Demethylalstonoxine B (143)

(7*S*)-*N*(1)-Demethylalstonoxine B (**143**) is a new ring-opened macroline oxindole alkaloid isolated from the leaf extract of *Alstonia angustifolia*. The structure and relative configuration were established by 2D NMR techniques. The NMR data however, were insufficient to establish the stereochemistry of C-19 and for this purpose, an X-ray diffraction analysis was carried out. Suitable crystals of **143** were obtained from the slow evaporation of **143** in CH_2Cl_2/hexanes solution. From the crystal structure, it can be seen that alkaloid **143** co-crystallized with the solvent ($CHCl_3$). It can also be seen that an intramolecular hydrogen bond was formed between C-17–OH and *N*-4 lone pair (Figure 9.19). The crystal data and structure refinement parameters are summarized in Table 9.19.

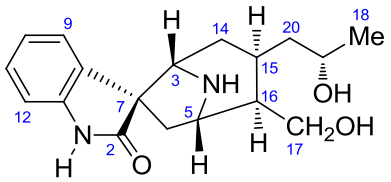

143 (7*S*)-*N*(1)-demethylalstonoxine B

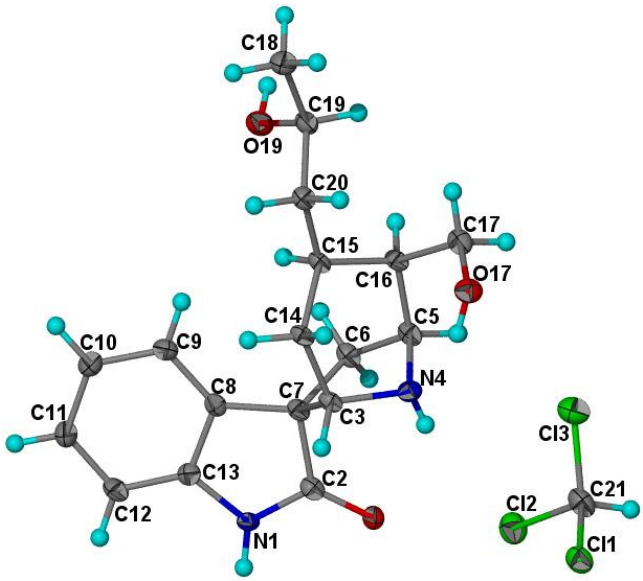

Figure 9.19. X-ray crystal structure of **143**.
[Flack parameter:[63] $x = -0.07(0.08)$;
Hooft parameter:[64] $y = -0.06(0.06)$].

Table 9.19. Crystal data and structure refinement parameters of (7*S*)-*N*(1)-demethylalstonoxine B (**143**)

Empirical formula	$C_{19}H_{25}N_2O_3Cl_3$
Molecular formula	$C_{18}H_{24}N_2O_3.CHCl_3$
Molecular weight, M_r	340.45
Melting point	110–112 ^oC
Temperature during diffraction experiment, T	100 K
X-ray source	Mo K_α
Crystal system	Orthorhombic
Space group	$P2_12_12_1$
a	9.7811(7) Å
b	12.2584(8) Å
c	17.0772(13) Å
α	90.00°
β	90.00°
γ	90.00°
Volume, V	2047.6(3) $Å^3$
No. of molecule per unit cell, Z	4
Density (calcd)	1.414 mg/mm^3
F(000)	912.0
Crystal size	0.36 × 0.26 × 0.16 mm
2θ range for data collection	4.1 to 52.88°
Index ranges	$-12 \leq h \leq 12$, $-15 \leq k \leq 15$, $-21 \leq l \leq 21$
Reflections collected	17212
Independent reflections	4207[R_{int} = 0.0998]
Data/restraints/parameters	4207/0/251
Goodness-of-fit on F^2	1.038
Final R indexes [$I \geq 2\sigma(I)$]	R_1 = 0.0487, wR_2 = 0.1142
Final R indexes [all data]	R_1 = 0.0672, wR_2 = 0.1253
Largest diff. peak/hole / e $Å^{-3}$	0.32/–0.40
Flack parameter, x	–0.07(0.08)
Hooft parameter, y	–0.06(0.06)

9.2.3.2 (7*S*)-Alstoumerine oxindole

(7*S*)-Alstoumerine oxindole (**144**) is a new oxindole of the sarpagine type alkaloid isolated from stem-bark extract of *Alstonia angustifolia*. As with alkaloid **143**, the NMR experimental results were insufficient to establish the relative stereochemistry of C-19. Since alkaloid **144** readily crystallized from CH_2Cl_2/hexanes solution, an X-ray diffraction analysis was carried out which reveals the structure and relative configuration of alkaloid **144**. From the crystal structure, it can be seen that a water molecule had been incorporated into the crystal lattice, and the water molecule formed hydrogen bond with the *N*-4 lone pair. The structure of **144** is shown in Figure 9.20, while the crystal data and structure refinement parameters are summarized in Table 9.20.

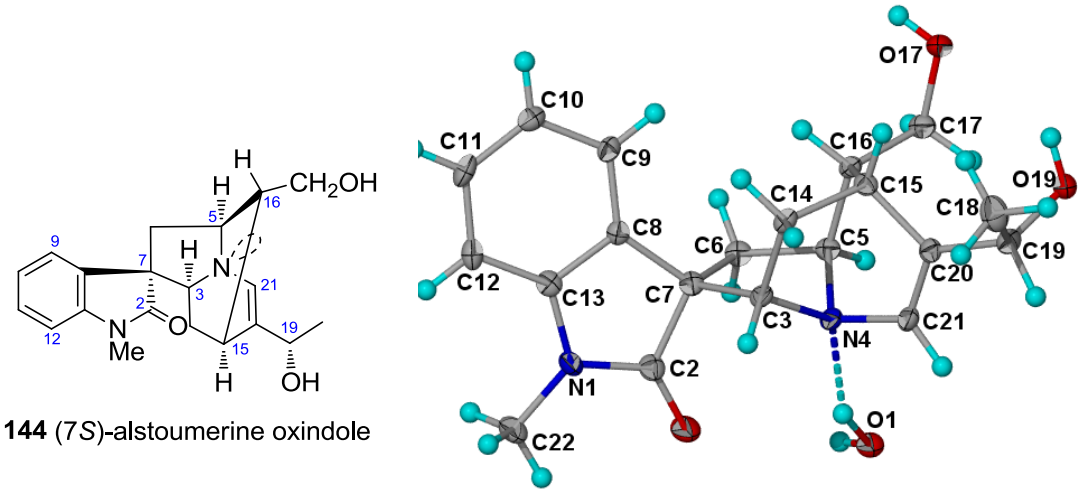

Figure 9.20. X-ray crystal structure of **144**.

Table 9.20. Crystal data and structure refinement parameters of (7*S*)-alstoumerine oxindole (**144**)

Empirical formula	$C_{20}H_{26}N_2O_4$
Molecular formula	$C_{20}H_{24}N_2O_3.H_2O$
Molecular weight, M_r	358.43
Melting point	> 160 °C dec
Temperature during diffraction experiment, T	100 K
X-ray source	Mo K_α
Crystal system	Orthorhombic
Space group	$P2_12_12$
a	11.5360(2) Å
b	19.2745(3) Å
c	8.11190(10) Å
α	90.00°
β	90.00°
γ	90.00°
Volume, V	1803.69(5) Å^3
No. of molecule per unit cell, Z	4
Density (calcd)	1.320 mg/mm^3
F(000)	768.0
Crystal size	0.22 × 0.16 × 0.05 mm
2θ range for data collection	4.12 to 52.78°
Index ranges	$-14 \leq h \leq 14$, $-23 \leq k \leq 24$, $-10 \leq l \leq 10$
Reflections collected	13706
Independent reflections	3699[R_{int} = 0.0618]
Data/restraints/parameters	3699/0/247
Goodness-of-fit on F^2	0.993
Final R indexes [$I \geq 2\sigma(I)$]	R_1 = 0.0444, wR_2 = 0.0815
Final R indexes [all data]	R_1 = 0.0670, wR_2 = 0.0912
Largest diff. peak/hole / e Å^{-3}	0.19/–0.19

9.2.4 Alkaloids from *Leuconotis griffithii*

9.2.4.1 Leuconodines B and E

The alkaloids leuconodines B (**68**) and E (**71**) are new leuconoxine-type alkaloids isolated from the stem-bark extract of *L.griffithii*.

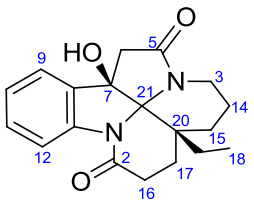

68 leuconodine B

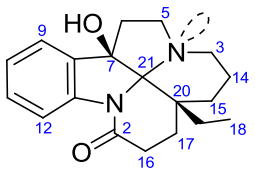

71 leuconodine E

Crystals of **68** were obtained from the slow evaporation of **68** in CH_2Cl_2/MeOH solution. From the crystal structure, it can be seen that a MeOH molecule has been incorporated into the crystal lattice. The structure of **68** is shown in Figure 9.21, while the crystal data and structure refinement parameters are summarized in Table 9.21.

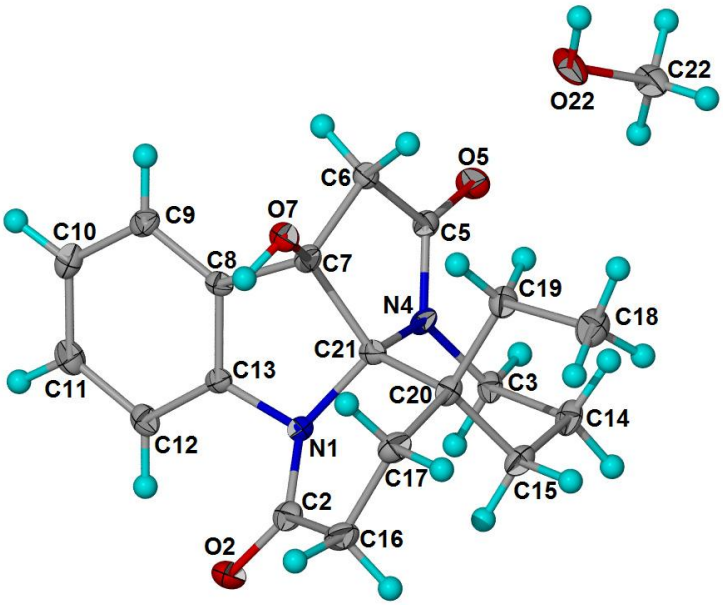

Figure 9.21. X-ray crystal structure of **68**.

Table 9.21. Crystal data and structure refinement parameters of leuconodine B (**68**)

Empirical formula	$C_{20}H_{26}N_2O_4$
Molecular formula	$C_{19}H_{22}N_2O_3.CH_3OH$
Molecular weight, M_r	358.43
Melting point	198–200 °C
Temperature during diffraction experiment, T	100 K
X-ray source	Mo K_α
Crystal system	Orthorhombic
Space group	$P2_12_12_1$
a	8.0382(5) Å
b	14.5281(9) Å
c	15.2187(8) Å
α	90.00°
β	90.00°
γ	90.00°
Volume, V	1777.24(18) Å^3
No. of molecule per unit cell, Z	4
Density (calcd)	1.340 mg/mm^3
F(000)	768.0
Crystal size	0.17 × 0.15 × 0.04 mm
2θ range for data collection	3.88 to 52.88°
Index ranges	$-10 \leq h \leq 10$, $-18 \leq k \leq 18$, $-18 \leq l \leq 18$
Reflections collected	12249
Independent reflections	2090[R_{int} = 0.1043]
Data/restraints/parameters	2090/0/240
Goodness-of-fit on F^2	1.008
Final R indexes [$I \geq 2\sigma(I)$]	R_1 = 0.0491, wR_2 = 0.0988
Final R indexes [all data]	R_1 = 0.0801, wR_2 = 0.1091
Largest diff. peak/hole / e Å^{-3}	0.29/–0.23

Crystals of **71** were obtained from the slow evaporation of **71** in CH_2Cl_2/MeOH solution. The structure of **71** is shown in Figure 9.22, while the crystal data and structure refinement parameters are summarized in Table 9.22.

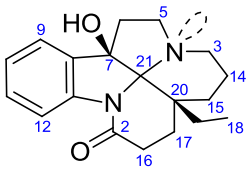

71 leuconodine E

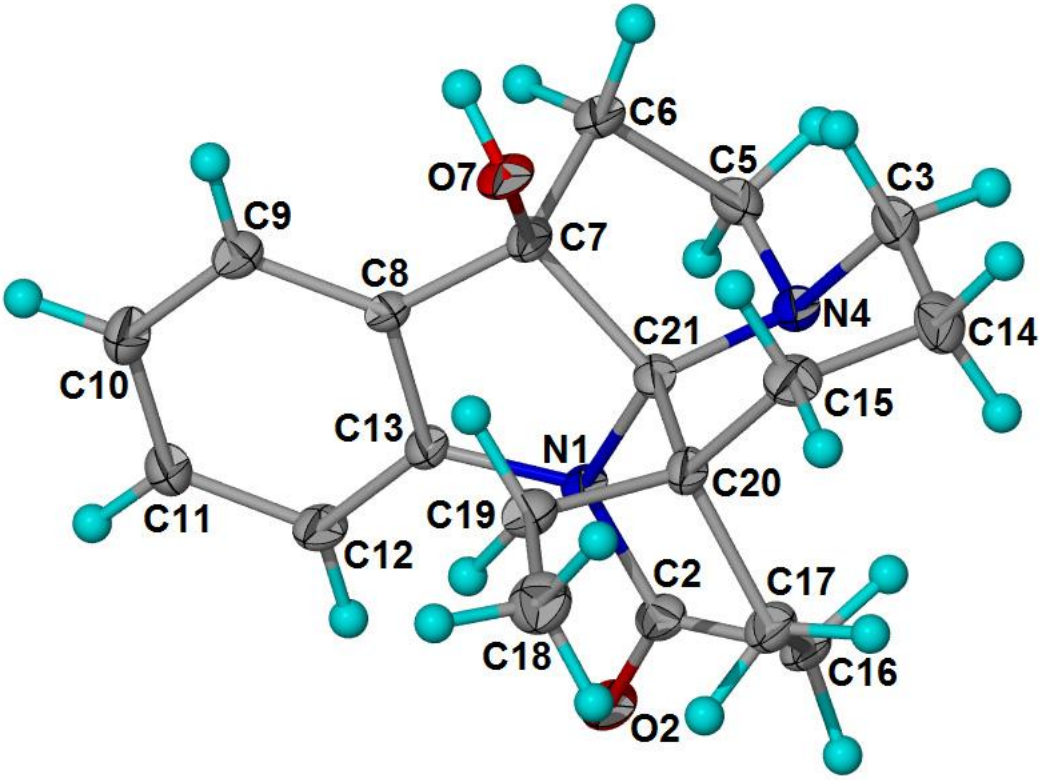

Figure 9.22. X-ray crystal structure of **71**.

Table 9.22. Crystal data and and structure refinement parameters of leuconodine E (**71**)

Empirical formula	$C_{19}H_{24}N_2O_2$
Molecular formula	$C_{19}H_{24}N_2O_2$
Molecular weight, M_r	312.40
Melting point	> 230 °C dec
Temperature during diffraction experiment, T	100 K
X-ray source	Mo K_α
Crystal system	Orthorhombic
Space group	$P2_12_12_1$
a	8.1326(7) Å
b	10.6116(9) Å
c	18.2366(17) Å
α	90.00°
β	90.00°
γ	90.00°
Volume, V	1573.8(2) Å^3
No. of molecule per unit cell, Z	4
Density (calcd)	1.318 mg/mm^3
F(000)	672.0
Crystal size	0.801 × 0.169 × 0.03
2θ range for data collection	4.44 to 46.72°
Index ranges	$-9 \leq h \leq 8$, $-11 \leq k \leq 11$, $-20 \leq l \leq 20$
Reflections collected	9956
Independent reflections	1332[R_{int} = 0.0872]
Data/restraints/parameters	1332/0/210
Goodness-of-fit on F^2	1.082
Final R indexes [$I \geq 2\sigma(I)$]	R_1 = 0.0403, wR_2 = 0.0858
Final R indexes [all data]	R_1 = 0.0654, wR_2 = 0.0966
Largest diff. peak/hole / e Å^{-3}	0.17/–0.25

9.2.4.2 *nor*-Rhazinicine

nor-Rhazinicine (**73**) is a new alkaloid isolated from the stem-bark extract of *Leuconotis griffithii*. Suitable crystals of **73** were obtained from the slow evaporation of **73** in CH_2Cl_2/MeOH solution. The structure of **73** is shown in Figure 9.23, while the crystal data and structure refinement parameters are summarized in Table 9.23.

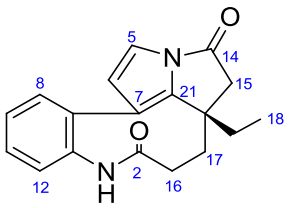

73 *nor*-rhazinicine

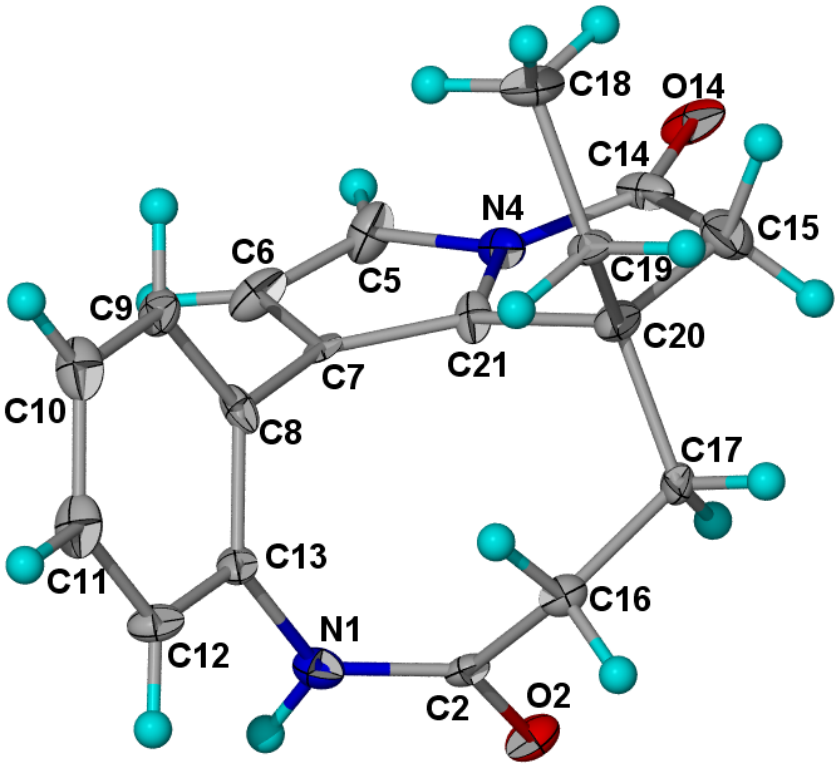

Figure 9.23. X-ray crystal structure of **73**.

Table 9.23. Crystal data and structure refinement parameters of *nor*-rhazinicine (**73**)

Empirical formula	$C_{18}H_{18}N_2O_2$
Molecular formula	$C_{18}H_{18}N_2O_2$
Molecular weight, M_r	294.34
Melting point	190–192 °C
Temperature during diffraction experiment, T	100 K
X-ray source	Mo K_α
Crystal system	Monoclinic
Space group	$P2_1$
a	13.646(3) Å
b	8.3619(17) Å
c	14.658(3) Å
α	90.00°
β	115.775(11)°
γ	90.00°
Volume, V	1506.2(5) Å^3
No. of molecule per unit cell, Z	4
Density (calcd)	1.298 mg/mm^3
F(000)	624.0
Crystal size	0.52 × 0.32 × 0.05
2θ range for data collection	3.08 to 60.26°
Index ranges	$-18 \leq h \leq 18$, $-11 \leq k \leq 7$, $-20 \leq l \leq 20$
Reflections collected	7175
Independent reflections	4095[R_{int} = 0.1347]
Data/restraints/parameters	4095/1/399
Goodness-of-fit on F^2	1.107
Final R indexes [$I \geq 2\sigma(I)$]	R_1 = 0.1262, wR_2 = 0.3258
Final R indexes [all data]	R_1 = 0.1574, wR_2 = 0.3522
Largest diff. peak/hole / e Å^{-3}	0.84/–0.74

CHAPTER TEN

Experimental

10.1 General

Melting points were determined on a Mel-Temp melting point apparatus and were uncorrected. Optical rotations were determined on a JASCO P-1020 digital polarimeter. IR spectra were recorded on a Perkin-Elmer Spectrum 400 spectrophotometer or on a Perkin-Elmer 1600 Series FT-IR spectrophotometer. UV spectra were obtained on a Shimadzu UV-3101PC. ESIMS and HRESIMS were obtained on an Agilent 6530 Q-TOF mass spectrometer. EIMS and HRLSIMS were obtained at Organic Mass Spectrometry, Central Science Laboratory, University of Tasmania, Tasmania, Australia. GC-EIMS was obtained on a Shimadzu GCMS-QP2010 Plus mass spectrometer. All air/moisture-sensitive reactions were carried out under N_2 in oven-dried glassware. THF was freshly distilled from Na/benzophenone under nitrogen while, CH_2Cl_2 and pyridine were distilled from CaH_2 under nitrogen. All other reagents were used without further purification.

10.2 NMR Spectroscopy

^{1}H, ^{13}C, and 2D NMR spectra were recorded at ^{1}H resonance frequency of either 400 MHz (JEOL JNM-LA 400, JNM-ECA 400, or Bruker Avance III 400 spectrometers) or 600 MHz (Bruker Avance III 600 spectrometer). The deuterium signals from $CDCl_3$, CD_2Cl_2, or THF-d_8 were used for the field frequency lock. All experiments were performed at room temperature (*ca*. 22 ^{o}C) unless otherwise stated. The chemical shifts were expressed in δ (ppm) downfield from TMS and all J values

were given in Hz. The multiplicity of each signal was denoted as follows: s - singlet, d - doublet, t - triplet, q - quartet, m - multiplet, br - broad.

10.3 Single Crystal X-ray Diffraction

X-ray diffraction analyses were carried out on a Bruker SMART APEX II CCD area detector system equipped with a graphite monochromator and a Mo K_α fine-focus sealed tube (λ = 0.71073 Å), or on an Agilent Technologies SuperNova Dual CCD area detector system equipped with mirror monochromator and a SuperNova (Cu K_α) X-ray source (λ = 1.50352 Å).

Suitable crystals were obtained mainly from slow evaporation in various solvent systems. The crystals were observed under a microscope with a polarizer attached. A single crystal was chosen based on the shape (does not contain deformity), size (more than 0.1 x 0.1 x 0.1 mm in dimension), and the ability to transmit and extinguish polarized light completely. The crystal was then fixed with an adhesive (perfluoropolyether oil) onto a glass fibre that is in turn glued into a 'copper pip' that fits into the well at the top of the goniometer head.

The goniometer head was then attached to the ϕ circle of the diffractometer. The crystal was optically adjusted so that its center does not move when it was rotated. A stream of N_2 gas cooled to 100 K was used for low temperature diffraction experiments. The diffraction experiment was carried out with full-sphere data collection (ω scan).

The structures were solved by direct methods (SHELXS-97) and refined with full-matrix least-squares on F^2 (SHELXL-97). All non-hydrogen atoms were refined anisotropically and all hydrogen atoms were placed in idealized positions and refined as riding atoms with the relative isotropic parameters. The absolute structures were

determined by refinement of the Flack parameter[63] and computation of the Hooft parameter.[64]

10.4 Chromatographic Methods

10.4.1 Normal phase chromatography

Thin layer chromatography was carried out using precoated 5 x 10 cm aluminium plates, 0.25 mm thickness, silica gel 60 F_{254} (Merck 5554). Column chromatography was performed using silica gel (Merck 9385, 230-400 Mesh ASTM). The ratio of silica gel to sample was approximately 30:1 for crude samples, and 100:1 for semi-pure fractions. The gel was made into a slurry with chloroform before it was packed onto a column and allowed to equilibrate for at least an hour before use. Centrifugal preparative TLC was carried out using a chromatotron (Harrison Research) with 1 mm thick plates 24 cm diameter of silica gel PF 254 (Merck 7749). The plate was prepared as follows. A long piece of cellophane tape was secured around the edge of the plate to form a mould. Silica gel (50 g) was added to about 100 ml of cold water and the slurry formed was poured onto the circular glass plate. The circular glass plate was rotated while the gel was being poured to obtain an even setting. The plate was then left to air dry for about an hour before being dried in an oven at 80 ^{o}C for about 12 hours. The sample was dissolved in a minimum volume of suitable solvent and loaded at the center of the plate while the plate was rotating to form a thin band. Elution was then carried out with the appropriate solvent system.

Some of the solvent systems used were Et_2O, Et_2O:hexanes, Et_2O:MeOH, CH_2Cl_2, CH_2Cl_2:MeOH, CH_2Cl_2:hexanes, CH_2Cl_2:MeOH, $CHCl_3$, $CHCl_3$:hexanes,

$CHCl_3$:MeOH, EtOAc:hexanes. In many instances, the solvents were saturated with NH_3 prior to use.

10.4.2 Gel permeation chromatography

Gel permeation chromatography was carried out using Sephadex G-75 (Aldrich). The gel was equilibrated (swelled) in excess MeOH at rt for 3 hours. It was then made into a slurry *via* stirring, poured into a column (100 x 3 cm), and allowed to equilibrate for at least a day. Samples were dissolved in a minimum amount of MeOH, filtered with nylon membrane (0.42 μm) prior to loading into the column. After the chromatography the column was regenerated by eluting with MeOH (three times the column volume).

10.4.3 Chiral phase high performance liquid chromatography

Chiral phase HPLC analysis and separation were performed using a system comprising a Waters 600 controller, a Waters 600 pump, and a Waters 2489 variable-wavelength absorbance detector. The column used was a Chiralpak AD-H (4.6 x 150 mm), Daicel, Japan, packed with amylose tris (3,5-dimethylphenylcarbamate) coated on 5 μm silica gel. The mobile phase used for the analysis and separation, was *n*-hexane/EtOH/diethylamine (DEA, 85:15:0.2), with a flow rate of 0.8 ml/min.

10.5 Dragendorff's Reagent

Solution A: 0.85 g of bismuth nitrate was dissolved in a mixture of 10 ml glacial acetic acid and 40 ml of distilled water.

Solution B: 8 g of potassium iodide was dissolved into 20 ml of distilled water.

A stock solution was prepared by mixing equal volumes of solutions A and B. Dragendorff's reagent was prepared by mixing 1 ml of stock solution with 2 ml of glacial acetic acid and 10 ml of distilled water. Orange spots on the developed TLC plates indicated the presence of alkaloids.

10.6 Chapter 2

10.6.1 Isolation and compound data of mersiphyllines A (37) and B (38)

The fractions containing alkaloids **37** and **38** obtained from the initial normal phase chromatography of the basic fraction from the leaf extract of *K. singapurensis* were pooled.[28] This pooled fraction was then further purified by repeated gel permeation chromatography (Sephadex G-75, MeOH as mobile phase), to give mersiphylline A (**37**) and mersiphylline B (**38**).

Mersiphylline A (37): colorless oil and subsequently as colorless block crystals from EtOH; mp 184–186 ^{o}C; $[\alpha]^{25}_{D}$ –59 (*c* 0.43, $CHCl_3$); UV (EtOH) λ_{max} (log ε) 219 (4.21), 245 (3.79), and 287 (3.16) nm; IR (dry film) ν_{max} 3463, 1746, and 1717 cm^{-1}; For ^{1}H and ^{13}C NMR data, see Table 2.1; EIMS *m/z* (rel. int.) 486 $[M]^+$ (43), 442 (100), 441 (88), 427 (37), 409 (29), 381 (48), 355 (22), 327 (20), 295 (15), 260 (10), 204 (26), and 158 (42); HREIMS *m/z* $[M]^+$ 486.1629 (calcd for $C_{24}H_{26}N_2O_9$, 486.1638).

Crystallographic data of mersiphylline A (**37**): crystal data and structure refinement parameters of **37** are summarized in Table 10.1.

Table 10.1. Crystal data and structure refinement parameters of mersiphylline A (**37**)

Empirical formula	$C_{26}H_{32}N_2O_{10}$
Molecular formula	$C_{24}H_{26}N_2O_9.C_2H_5OH$
Molecular weight, M_r	532.54
Melting point	184–186 ^oC
Temperature during diffraction experiment, T	100 K
X-ray source	Mo K_α
Crystal system	Orthorhombic
Space group	$P2_12_12_1$
a	10.8951(5) Å
b	14.6956(7) Å
c	15.0936(7) Å
α	90.00°
β	90.00°
γ	90.00°
Volume, V	2416.6(2) $Å^3$
No. of molecule per unit cell, Z	4
Density (calcd)	1.464 mg/mm^3
$F(000)$	1128
Crystal size	0.30 × 0.15 × 0.10 mm
2θ range for data collection	3.86 to 61°
Index ranges	$-15 \leq h \leq 5$, $-20 \leq k \leq 19$, $-20 \leq l \leq 19$
Reflections collected	13836
Independent reflections	3969[R_{int} = 0.0446]
Data/restraints/parameters	3969/0/348
Goodness-of-fit on F^2	1.026
Final R indexes [$I \geq 2\sigma(I)$]	R_1 = 0.0426, wR_2 = 0.0931
Final R indexes [all data]	R_1 = 0.0556, wR_2 = 0.0988
Largest diff. peak/hole / e $Å^{-3}$	0.347/–0.262

Mersiphylline B (38): colorless oil; $[\alpha]^{25}_{D}$ –58 (*c* 0.04, $CHCl_3$); UV (EtOH) λ_{max} (log ε) 212 (3.84), 245 (3.22), and 287 (2.90) nm; IR (dry film) ν_{max} 3427, 1744, and 1711 cm^{-1}; For ^1H and ^{13}C NMR data, see Table 2.1; EIMS *m*/*z* (rel. int.) 472 $[M]^+$ (73), 441 (18), 428 $[M – CO_2]^+$ (100), 427 $[M – CO_2H]^+$ (91), 413 (98), 395 (18), 381 (59), 367 (55), 351 (13), 335 (23), and 299 (21); HREIMS *m*/*z* 472.1836 $[M]^+$ (calcd for $C_{24}H_{28}N_2O_8$, 472.1846).

10.6.2 Esterification of mersiphylline A (38)

To a solution of **38** (11 mg, 0.023 mmol) in anhydrous benzene (4 ml) was added 113 μl of TMS-diazomethane (0.22 mmol, 2 M in hexanes). The solution was stirred at rt for 12 h and concentrated *in vacuo*. The crude mixture was purified *via* passage through a short pad of silica gel. The ^1H NMR spectrum of the crude product showed the absence of the characteristic deshielded COOH peak at *ca.* δ_H 16 ppm, indicating that the esterification reaction was complete.

10.6.3 Formation of the alkaloid-borane complex 40

BH_3-THF (28 μl, 1 M in THF) was added to **40** (7 mg, 0.0014 mmol) in THF at 0 ^oC and the mixture was stirred for 5 h, after which a further 28 μl (1 M in THF) BH_3.THF solution was added, and the mixture stirred for another 1 h at 0 ^oC. Removal of the solvent *in vacuo*, followed by centrifugal preparative TLC (SiO_2, 5% MeOH:Et_2O) gave **40** (6 mg, 84%; direct workup without H_2O or MeOH quenching gave the best yield of **40**) as a colorless oil: $[\alpha]^{25}_{D}$ –58 (*c* 0.04, $CHCl_3$); UV (EtOH) λ_{max} (log ε) 219 (4.78), 243 (4.24), and 289 (3.67) nm; IR (dry film) ν_{max} 3480 (OH), 2432, 2376, and 2285 (BH_2), 1748 (C=O, ester), 1704 (C=O, carbamate), and 1694 (C=O, borane ester) cm^{-1};

For ^{1}H and ^{13}C NMR data, see Table 2.1; EIMS *m/z* (rel. int.) 498 $[M]^+$ (35), 496 (16), 441 (100), 409 (33), 381 (49), 323 (25), 204 (18), 158 (26), and 44 (63); HREIMS *m/z* 498.1780 $[M]^+$ (calcd for $C_{24}H_{27}N_2O_9{}^{11}B$, 498.1804), *m/z* 496.1754 $[M - H]^+$ (calcd for $C_{24}H_{26}N_2O_9{}^{10}B$, 496.1762).

10.7 Chapter 3

10.7.1 Compound data of lirofolines A (44) and B (45)

Lirofoline A (44): colorless oil; $[\alpha]^{25}_{D}$ −41 (*c* 1.36, $CHCl_3$); UV (EtOH) λ_{max} (log ε) 216 (4.29), 258 (4.08), 280 (3.94), and 309 (3.96) nm; IR (dry film) ν_{max} 1651 (C=O) cm^{-1}; For ^1H and ^{13}C NMR data, see Table 3.1; EIMS *m/z* (rel int) 324 $[M]^+$ (100), 295 $[M - CHO \text{ or } M - CH_2CH_3]^+$ (20), 280 (56), 267 (10), 253 (20), 248 (19), 224 (9), 135 (37), and 122 (13); HREIMS found *m/z* 324.1837 $[M]^+$ (calcd for $C_{20}H_{24}N_2O_2$, 324.1838).

Lirofoline B (45): colorless oil; $[\alpha]^{25}_{D}$ −17 (*c* 0.08, $CHCl_3$); UV (EtOH) λ_{max} (log ε) 218 (4.31), 256 (4.09), 278 (3.92), and 308 (3.95) nm; IR (dry film) ν_{max} 3407 (OH) and 1651 (C=O) cm^{-1}; For ^1H and ^{13}C NMR data, see Table 3.1; FABMS *m/z* 355 $[M + H]^+$; HRFABMS found *m/z* 355.2018 $[M + H]^+$ (calcd for $C_{21}H_{26}N_2O_3$ + H, 355.2022).

10.7.2 Compound data of ibogaine (46)

The starting material for the transformation, ibogaine (**46**) was obtained from *T. corymbosa* and *T. divaricata* from previous alkaloid studies.[39,42]

Ibogaine (46): light yellowish oil; $[\alpha]^{25}_{D}$ +53 (*c* 0.10, $CHCl_3$); UV (EtOH) λ_{max} (log ε) 229 (4.48), 287 (4.24), and 296 (4.26) nm; IR (dry film) ν_{max} 3402 cm^{-1}; For ^1H NMR and ^{13}C NMR data, see Table 3.2; ESIMS *m/z* 311 $[M + H]^+$ ($C_{20}H_{26}N_2O$ + H).

10.7.3 Oxidation of ibogaine (46) to ibogaine *N*-oxide (50)

To a solution of **46** (50 mg, 0.18 mmol) in CH_2Cl_2 (10 ml) was added *m*-CPBA (37 mg, 0.22 mmol), and the mixture was stirred for 30 min at 0 ^oC. The mixture was quenched with 1 M Na_2CO_3 (10 ml), extracted with CH_2Cl_2 (3 x 20 ml), and the combined CH_2Cl_2 extracts were then washed with water, dried (Na_2SO_4), the solvent evaporated, and the residue purified by centrifugal preparative TLC (SiO_2, 25% MeOH:$CHCl_3$, NH_3-saturated) to give ibogaine *N*-oxide (**50**) (44 mg, 83%) as light yellowish oil; $[\alpha]^{25}_D$ −76 (*c* 0.16, $CHCl_3$); UV (EtOH) λ_{max} (log ε) 210 (4.00), 224 (3.98), 280 (3.58), 297 (3.50), and 307 (3.32) nm; IR (dry film) ν_{max} 3149 cm^{-1}, For ^1H and ^{13}C NMR data, see Table 3.2; ESIMS *m/z* 327 $[M + H]^+$; HRESIMS *m/z* 327.2080 $[M + H]^+$ (calcd for $C_{20}H_{26}N_2O_2 + H$, 327.2073).

10.7.4 Formation of alcohol 51 *via* Polonovski transformation

To a stirred solution of **50** (12 mg, 0.037 mmol) in 50 ml of CH_2Cl_2, was added acetic anhydride at −10 ^oC. After stirring for 15 min, the mixture was quenched with 10% NaOH (15 ml) and extracted with CH_2Cl_2 (3 x 20 ml). The combined organic phase was dried (Na_2SO_4), the solvent evaporated, and the residue was purified with a short pad of silica gel, eluting with CH_2Cl_2 to give alcohol **51** (8.2 mg, 70%). Only ^1H NMR and ESIMS were carried out on the alcohol, due to instability of **51**. Alcohol **51**: light yellowish oil; ^1H NMR (400 MHz, $CDCl_3$) δ 7.10 (1H, d, *J* = 8.9 Hz), 7.09 (1H, d, *J* = 2.3 Hz), 6.80 (1H, dd, *J* = 8.9, 2.3 Hz), 4.88 (1H, d, *J* = 11.4), 4.78 (1H, d, *J* = 11.4 Hz), 3.86 (3H, s), 3.94 (2H, s), 3.19 (1H, dt, *J* = 10, 3 Hz), 3.15 (1H, br dt, *J* = 12, 2.2 Hz), 2.79 (1H, dt, *J* = 10, 2 Hz), 2.74 (1H, br s), 2.07 (1H, br t, *J* = 12 Hz), 1.86 (1H, m), 1.76 (1H, m), 1.69 (1H, m), 1.58 (2H, m), 1.56 (1H, m), 1.52 (1H, m), 0.94 (3H, t, *J* =

7.3 Hz). ESIMS *m/z* 327 $[M + H]^+$; HRESIMS *m/z* $[M + H]^+$ 327.2077 (calcd for $C_{20}H_{26}N_2O_2$ + H, 327.2067).

10.7.5 Attempted oxidation of alcohol 51 to lirofoline A (44) *via* Dess-Martin periodinane (DMP) oxidation

A solution of the alcohol **51** (5 mg, 0.015 mmol) in CH_2Cl_2 (4 ml) was treated with DMP reagent (50 μl, 0.3 M in CH_2Cl_2) at rt. TLC of the reaction mixture showed no definitive products, although the starting material had been consumed.

10.7.6 Oxidation of alcohol 51 to lirofoline A *via* Ley oxidation

To a stirred suspension of the alcohol **51** (7 mg, 2.65 mmol), 4-methylmorpholine-*N*-oxide (542 mg, 46.3 mmol), and 4 Å molecular sieves (1.54 g, 500 mg/mmol) in CH_2Cl_2:MeCN 1:1 (5 ml) was added tetrapropylammonium perruthenate (TPAP, 54 mg, 0.154 mmol). The mixture was stirred for 20 h at rt, filtered through a pad of Celite, the solvent removed *in vacuo*, and the residue was purified by centrifugal preparative TLC (SiO_2, Et_2O, NH_3-saturated) to give lirofoline A (**44**) (2.1 mg, 30% yield). The spectroscopic (^1H and ^{13}C NMR, IR, UV) and other data ($[\alpha]_D$ and R_f of TLC in different solvent systems) of semisynthetic lirofoline A (**44**) were indistinguishable from those of the natural lirofoline A (**44**).[39]

10.8 Chapter 4

10.8.1 Isolation and compound data of leuconolam (54)

The fractions containing leuconolam (**54**), obtained from initial normal phase chromatography of the basic fraction from the stem-bark extract of *L. griffithii*, were pooled. This pooled fraction was then further purified by repeated normal phase chromatography, to give leuconolam (**54**).

Leuconolam (54): colorless block crystals from MeOH; mp 178–180 ^{o}C [lit[49] 263–264 ^{o}C]; $[\alpha]^{25}_{D}$ –303 (*c* 0.75, $CHCl_3$) [lit[49] $[\alpha]_D$ –28.3 (*c* 0.7 $CHCl_3$)]; UV (EtOH) λ_{max} (log ε) 205 (4.00), 220 (3.22), and 292 (3.96) nm; IR (dry film) ν_{max} 3263, 1683, and 1650 cm^{-1}; For ^{1}H and ^{13}C NMR data, see Tables 4.4 and 4.5, respectively; ESIMS *m/z* 327 $[M + H]^+$ ($C_{19}H_{22}N_2O_3$ + H).

Crystallographic data of alkaloid **54**: crystal data and structure refinement parameters of **54** are summarized in Table 10.2.

Table 10.2. Crystal data and structure refinement parameters of leuconolam (**54**)

Empirical formula	$C_{20}H_{26}N_2O_4$
Molecular formula	$C_{19}H_{22}N_2O_3.CH_3OH$
Molecular weight, M_r	358.43
Melting point	178–180 ^oC
Temperature during diffraction experiment, T	100 K
X-ray source	Mo K_α
Crystal system	Orthorhombic
Space group	$P2_12_12_1$
a	8.1821(6) Å
b	10.9066(8) Å
c	19.9093(15) Å
α	90.00°
β	90.00°
γ	90.00°
Volume, V	1776.7(2) $Å^3$
No. of molecule per unit cell, Z	4
Density (calcd)	1.340 mg/mm^3
Crystal size	0.43 × 0.32 × 0.25 mm
2θ range for data collection	4.1 to 61.78°
Index ranges	$-7 \leq h \leq 11$, $-11 \leq k \leq 12$, $-27 \leq l \leq 27$
Reflections collected	4213
Independent reflections	2363[R_{int} = 0.0529]
Data/restraints/parameters	2363/0/243
Goodness-of-fit on F^2	1.001
Final R indexes [$I \geq 2\sigma(I)$]	R_1 = 0.0389, wR_2 = 0.0961
Final R indexes [all data]	R_1 = 0.0433, wR_2 = 0.0991
Largest diff. peak/hole / e $Å^{-3}$	0.29/–0.24

10.8.2 Reaction of leuconolam (54) with NaHMDS

To a stirred solution of **54** (11.1 mg, 0.034 mmol) in THF (5 ml) was added dropwise NaHMDS (34 μl, 1 M) and the mixture was stirred at 0 ^{o}C. TLC analysis of the mixture over a period of 1–5 h showed only the presence of starting material.

10.8.3 Reaction of leuconolam (54) with NaOMe

To a solution of **54** (18 mg, 0.055 mmol) in MeOH (3 ml) was added a freshly prepared solution of Na (2.8 mg, 0.121 mmol) in 1 ml MeOH at 0 ^{o}C. TLC of the reaction mixture (in a period of 1–6 h) showed only the presence of **54**.

10.8.4 Reaction of leuconolam (54) with KOH/MeOH/EtOH

Leuconolam (**54**) (50 mg, 0.15 mmol) was dissolved in methanolic ethanol (9:1, 50 ml). Two pellets of KOH were then added and the solution was stirred at rt for 6 h, quenched with 5% HCl (20 ml), and basified with 10% $NaHCO_3$ (30 ml). The mixture was then extracted with CH_2Cl_2 (4 x 100 ml), washed with water, dried (Na_2SO_4), concentrated *in vacuo*, and the residue purified by centrifugal preparative TLC (SiO_2, 10% MeOH:Et_2O, NH_3-saturated) to give **74** (6 mg, 12%) and **76** (1.5 mg, 3%) and recovered **54** (10 mg, 20%).

Compound 74: colorless oil and subsequently as colorless block crystals from CCl_4/MeOH; mp 266–268 ^{o}C [lit[49] 175–177 ^{o}C]; $[\alpha]^{25}_{D}$ –198 (*c* 0.06, $CHCl_3$) [lit[49] $[\alpha]_D$ –14.3 (*c* 0.35, $CHCl_3$)]; UV (EtOH) λ_{max} (log ε) 210 (4.50), 253 (4.01), and 287 (3.38) nm; IR (dry film) ν_{max} 3226 and 1667 cm^{-1}; For ^{1}H and ^{13}C NMR data, see Table 4.1;

ESIMS *m/z* 327 $[M + H]^+$; HRESIMS *m/z* 327.1712 $[M + H]^+$ (calcd for $C_{19}H_{22}N_2O_3$ + H, 327.1703).

Crystallographic data of compound **74**: crystal data and structure refinement parameters of **74** are summarized in Table 10.3.

Table 10.3. Crystal data and structure refinement parameters of compound **74**

Empirical formula	$C_{19}H_{22}N_2O_3$
Molecular formula	$C_{19}H_{22}N_2O_3$
Molecular weight, M_r	326.39
Melting point	266–268 ^oC
Temperature during diffraction experiment, T	100 K
X-ray source	Mo K_α
Crystal system	Triclinic
Space group	$P1$
a	10.1848(2) Å
b	10.3617(2) Å
c	10.3845(2) Å
α	71.7420(10)°
β	67.3790(10)°
γ	60.6480(10)°
Volume, V	871.06(3) $Å^3$
No. of molecule per unit cell, Z	2
Density (calcd)	1.244 mg/mm^3
$F(000)$	348.0
Crystal size	0.62 × 0.21 × 0.10 mm
2θ range for data collection	4.3 to 55°
Index ranges	$-13 \leq h \leq 13$, $-13 \leq k \leq 13$, $-13 \leq l \leq 13$
Reflections collected	8035
Independent reflections	3993[R_{int} = 0.0509]
Data/restraints/parameters	3993/3/488
Goodness-of-fit on F^2	1.020
Final R indexes [$I \geq 2\sigma(I)$]	R_1 = 0.0486, wR_2 = 0.1257
Final R indexes [all data]	R_1 = 0.0531, wR_2 = 0.1287
Largest diff. peak/hole / e $Å^{-3}$	1.27/–0.27

Compound 76: colorless oil and subsequently as colorless block crystals from MeOH: mp 250–252 ^{o}C; $[\alpha]^{25}_{D}$ = –150 (*c* 0.01, $CHCl_3$); UV (EtOH) λ_{max} (log ε) 210 (4.46), 251 (4.22), and 306 (3.00) nm; IR (dry film) ν_{max} 3322, 1712, and 1681 cm^{-1}; For ^{1}H and ^{13}C NMR data, see Table 4.1; ESIMS *m/z* 327 $[M + H]^+$; HRESIMS *m/z* 327.1710 $[M + H]^+$ (calcd for $C_{19}H_{22}N_2O_3 + H$, 327.1703).

Crystallographic data of **76**: crystal data and structure refinement parameters of **76** are summarized in Table 10.4.

Table 10.4. Crystal data and structure refinement parameters of compound **76**

Empirical formula	$C_{19}H_{22}N_2O_3$
Molecular formula	$C_{19}H_{22}N_2O_3$
Molecular weight, M_r	326.39
Melting point	250–252 ^{o}C
Temperature during diffraction experiment, *T*	100 K
X-ray source	Mo K_α
Crystal system	Orthorhombic
Space group	$P2_12_12_1$
a	9.6652(5) Å
b	16.1799(9) Å
c	21.1959(11) Å
α	90.00°
β	90.00°
γ	90.00°
Volume, *V*	3314.7(3) Å^3
No. of molecule per unit cell, *Z*	8
Density (calcd)	1.308 mg/mm^3
F(000)	1392.0
Crystal size	0.31 × 0.27 × 0.15 mm
2θ range for data collection	3.16 to 61.26°
Index ranges	$-13 \le h \le 13$, $-23 \le k \le 22$, $-29 \le l \le 30$
Reflections collected	36904
Independent reflections	5465[R_{int} = 0.0352]
Data/restraints/parameters	5465/0/445
Goodness-of-fit on F^2	1.013
Final R indexes [$I \ge 2\sigma(I)$]	R_1 = 0.0356, wR_2 = 0.0877
Final R indexes [all data]	R_1 = 0.0409, wR_2 = 0.0905
Largest diff. peak/hole / e Å^{-3}	0.33/–0.20

10.8.5 Reaction of leuconolam (54) with 5% HCl

To a stirred solution of 5% HCl (5 ml) was added **54** (11 mg, 0.034 mmol). The mixture was stirred for 12 h at rt. The mixture was quenched with 10% Na_2CO_3 (10 ml), extracted with CH_2Cl_2 (3 x 10 ml), washed with water (3 x 20 ml), dried (Na_2SO_4), and concentrated *in vacuo*. TLC of the residue showed only the presence of **54** (8.9 mg, 81% recovery).

10.8.6 Reaction of leuconolam (54) with 5% HCl/CH_2Cl_2 in the presence of tetraethylammonium chloride (TEACl)

Leuconolam (**54**) (14.5 mg, 0.044 mmol) was added into a two-phase system comprising 5% HCl (5 ml), CH_2Cl_2 (5 ml), and TEACl (7 mg, 0.044 mmol). The mixture was stirred for 12 h at rt, quenched with 10% Na_2CO_3 (10 ml), and extracted with CH_2Cl_2 (3 x 5 ml). The combined organic extract was then washed with water (3 x 20 ml), dried (Na_2SO_4), concentrated *in vacuo*, and the residue purified by centrifugal preparative TLC (SiO_2, 5% MeOH:Et_2O, NH_3-saturated) to give 6,7-dehydroleuconoxine (**63**) (6.5 mg, 47%), amino lactam-lactone **78** (0.2 mg, 1.4%) and recovered **54** (5.1 mg, 35%).

6,7-Dehydroleuconoxine (63): colorless block crystals from CH_2Cl_2/hexanes; mp 164–168 ^{o}C; $[\alpha]^{25}_{D}$ +271 (*c* 0.11, $CHCl_3$); UV (EtOH) λ_{max} (log ε) 203 (4.32), 252 (4.33), and 350 (3.70) nm; IR (dry film) ν_{max} 1691, 1649, and 1595 cm^{-1}; For ^{1}H and ^{13}C NMR data, see Tables 4.4 and 4.5, respectively; ESIMS *m/z* 309 $[M + H]^+$; HRESIMS *m/z* 309.1590 $[M + H]^+$ (calcd for $C_{19}H_{20}N_2O_2$ + H, 309.1598); GC-EIMS

m/*z* (rel int) 308 $[M]^+$ (74), 279 $[M - CH_2CH_3]^+$ (100), 251 (58), 237 (20), 223 (28), 209 (15), 184 (10), 171 (18), 156 (32), 142 (8), and 129 (18).

Crystallographic data of **63**: crystal data and structure refinement parameters of **63** are summarized in Table 10.5.

Table 10.5. Crystal data and structure refinement parameters of 6,7-dehydroleuconoxine (**63**)

Empirical formula	$C_{19}H_{20}N_2O_2$
Molecular formula	$C_{19}H_{20}N_2O_2$
Molecular weight, M_r	308.38
Melting point	164–168 ^oC
Temperature during diffraction experiment, T	100 K
X-ray source	Mo K_α
Crystal system	Orthorhombic
Space group	$P2_12_12_1$
a	8.8855(4) Å
b	11.3940(5) Å
c	14.8635(7) Å
α	90°
β	90°
γ	90°
Volume, V	1504.80(12) $Å^3$
No. of molecule per unit cell, Z	4
Density (calcd)	1.3611 mg/mm^3
$F(000)$	656.3
Crystal size	0.48 × 0.34 × 0.26 mm
2θ range for data collection	4.5 to 61.2°
Index ranges	$0 \leq h \leq 12$, $0 \leq k \leq 15$, $0 \leq l \leq 21$
Reflections collected	2554
Independent reflections	2554[R_{int} = 0.0000]
Data/restraints/parameters	2554/0/208
Goodness-of-fit on F^2	1.042
Final R indexes [$I \geq 2\sigma(I)$]	R_1 = 0.0374, wR_2 = 0.0929
Final R indexes [all data]	R_1 = 0.0433, wR_2 = 0.0968
Largest diff. peak/hole / e $Å^{-3}$	0.29/–0.26

Amino lactam-lactone 78: yellowish oil and subsequently as yellowish block crystals from CH_2Cl_2/hexanes; mp 179–182 ^oC; $[\alpha]^{25}_D$ +116 (*c* 0.52, $CHCl_3$); UV (EtOH) λ_{max} (log ε) 212 (4.87), 240 (4.83), and 342 (4.01) nm; IR (dry film) ν_{max} 3483, 3397, 1743, and 1709 cm^{-1}; For ^1H and ^{13}C NMR data, see Table 4.6; EIMS *m/z* (rel. int.) 326 $[M]^+$ (100), 299 (5), 280 (10), 267 (12), 239 (20), 225 (5), 209 (7), and 185 (8); HREIMS *m/z* $[M]^+$ 326.1629 (calcd for $C_{19}H_{22}N_2O_3$, 326.1630).

Crystallographic data of **78**: crystal data and structure refinement parameters of **78** are summarized in Table 10.6.

Table 10.6. Crystal data and structure refinement parameters of compound **78**

Empirical formula	$C_{39}H_{46}N_4O_6Cl_2$
Molecular formula	$2C_{19}H_{22}N_2O_3.CH_2Cl_2$
Molecular weight, M_r	737.70
Melting point	179–182 ^oC
Temperature during diffraction experiment, *T*	100 K
X-ray source	Mo K_α
Crystal system	Monoclinic
Space group	$P2_1$
a	8.00860(10) Å
b	14.9302(3) Å
c	15.3044(3) Å
α	90.00°
β	94.6480(10)°
γ	90.00°
Volume, *V*	1823.93(6) $Å^3$
No. of molecule per unit cell, *Z*	2
Density (calcd)	1.447 mg/mm^3
Crystal size	0.63 × 0.17 × 0.04 mm
2θ range for data collection	3.64 to 61.02°
Index ranges	$-11 \le h \le 10$, $-20 \le k \le 21$, $-21 \le l \le 22$
Reflections collected	19605
Independent reflections	10151[R_{int} = 0.0318]
Data/restraints/parameters	10151/0/462
Goodness-of-fit on F^2	0.958
Final R indexes [$I \ge 2\sigma(I)$]	R_1 = 0.0460, wR_2 = 0.0998
Final R indexes [all data]	R_1 = 0.0724, wR_2 = 0.1134
Largest diff. peak/hole / e $Å^{-3}$	0.37/–0.41
Flack parameter, *x*	–0.06(0.06)
Hooft parameter, *y*	–0.02(0.03)

10.8.7 Reaction of leuconolam (54) with concentrated HCl in MeOH

Leuconolam (**54**) (12.9 mg, 0.040 mmol) was dissolved in a minimal amount of MeOH (*ca.* 0.1 ml). Concentrated HCl was then added dropwise (2 drops). The mixture was stirred for 16 h at rt, quenched with 10% Na_2CO_3 (10 ml), and extracted with CH_2Cl_2 (3 x 5 ml). The combined organic extract was then washed with water (3 x 20 ml), dried (Na_2SO_4), concentrated *in vacuo*, and the residue purified by centrifugal preparative TLC (SiO_2, 5% MeOH:Et_2O, NH_3-saturated) to give *O*-methylleuconolam (**77**) (8.6 mg, 63%) and recovered **73** (0.5 mg, 4%).

***O*-Methylleuconolam (77)**: colorless oil and subsequently as colorless block crystals from MeOH; mp 214–218 ^oC [lit[49] 155–156 ^oC]; $[\alpha]^{25}_D$ −240 (*c* 0.6, $CHCl_3$); UV (EtOH) λ_{max} (log ε) 238 (3.99) and 348 (3.03) nm; IR (dry film) ν_{max} 3477 and 1693 cm^{-1}; For ^1H and ^{13}C NMR data, see Table 4.3; ESIMS *m/z* 341 $[M + H]^+$ ($C_{20}H_{24}N_2O_3$ + H).

10.8.8 Reaction of leuconolam (54) with 10-camphorsulfonic acid (CSA) in anhydrous CH_2Cl_2

To a stirred solution of CSA (15 mg, 0.066 mmol) and CH_2Cl_2 (5 ml) was added leuconolam (**54**) (14.3 mg, 0.044 mmol). The mixture was stirred for 12 h at rt, quenched with 10% K_2CO_3 (10 ml), and extracted with CH_2Cl_2 (3 x 5 ml). The combined organic extract was then washed with water (3 x 10 ml), dried (Na_2SO_4), concentrated *in vacuo*, and the residue purified by centrifugal preparative TLC (SiO_2, 5% MeOH:Et_2O, NH_3-saturated) to give 6,7-dehydroleuconoxine (**63**) (8.2 mg, 62%), amino lactam-lactone **78** (0.1 mg, 2%) and recovered **54** (1.4 mg, 10%).

10.8.9 Reaction of leuconolam (54) with CSA in anhydrous CH_2Cl_2/MeOH

To a stirred solution of CSA (13.2 mg, 0.057 mmol) and CH_2Cl_2 (5 ml) was added leuconolam (**54**) (11.8 mg, 0.038 mmol). The mixture was stirred for 30 min and MeOH (6 μl, 0.152 mmol) then was added. The mixture was stirred for another 11 h at rt, quenched with 10% K_2CO_3 (10 ml), and extracted with CH_2Cl_2 (5 x 10 ml). The combined organic extract was then washed with water (3 x 10 ml), dried (Na_2SO_4), concentrated *in vacuo*, and the residue purified by centrifugal preparative TLC (SiO_2, 5% MeOH:Et_2O, NH_3-saturated) to give *O*-methylleuconolam (**77**) (6.6 mg, 54%) and 6,7-dehydroleuconoxine (**63**) (2.2 mg, 19%).

10.8.10 Reaction of leuconolam (54) with CSA in anhydrous MeOH

To a stirred solution of CSA (11.8 mg, 0.051 mmol) and MeOH (5 ml) was added leuconolam (**54**) (11 mg, 0.034 mmol). The mixture was stirred for 12 h at rt, quenched with 10% K_2CO_3 (10 ml), and extracted with CH_2Cl_2 (5 x 10 ml). The combined organic extract was then washed with water (3 x 10 ml), dried (Na_2SO_4), concentrated *in vacuo*, and the residue purified by centrifugal preparative TLC (SiO_2, 5% MeOH:Et_2O, NH_3-saturated) to give *O*-methylleuconolam (**77**) (10.9 mg, 94%), amino lactam-lactone **78** (0.1 mg, 2%) and recovered **54** (0.4 mg, 4%).

10.8.11 Reaction of leuconolam (54) with *p*-toluenesulfonic acid (PTSA) in anhydrous MeOH

To a stirred solultion of PTSA (9.5 mg, 0.056 mmol) and MeOH (5 ml) was added leuconolam (**54**) (12 mg, 0.037 mmol). The mixture was stirred for 12 h at rt, quenched

with 10% K_2CO_3 (10 ml) and extracted with CH_2Cl_2 (5 x 10 ml). The combined organic extract was then washed with water (3 x 10 ml), dried (Na_2SO_4), concentrated *in vacuo*, and the residue purified by centrifugal preparative TLC (SiO_2, 5% MeOH:Et_2O, NH_3-saturated) to give *O*-methylleuconolam (**77**) (11.8 mg, 94%), amino lactam-lactone **78** (0.1 mg, 0.8%), and recovered **54** (0.4 mg, 4%).

10.8.12 Reaction of leuconolam (54) with PTSA in anhydrous CH_2Cl_2

To a stirred solution of PTSA (8.6 mg, 0.05 mmol) and CH_2Cl_2 (5 ml) was added leuconolam (**54**) (11.7 mg, 0.036 mmol). The mixture was stirred for 15 h at rt, quenched with 10% Na_2CO_3 (10 ml), and extracted with CH_2Cl_2 (3 x 5 ml). The combined organic extract was then washed with water (3 x 10 ml), dried (Na_2SO_4), concentrated *in vacuo*, and the residue purified by centrifugal preparative TLC (SiO_2, Et_2O, NH_3-saturated) to give 6,7-dehydroleuconoxine (**63**) (0.6 mg, 5%), amino lactam-lactone **78** (5 mg, 42%) and recovered **54** (0.4 mg, 3%).

10.8.13 Reaction of 6,7-dehydroleuconoxine (63) with 5% HCl/CH_2Cl_2 in the presence of TEACl

6,7-Dehydroleuconoxine (**63**) (19.5 mg, 0.063 mmol) was added into a two-phase system comprising 5% HCl (5 ml), CH_2Cl_2 (5 ml), and TEACl (10 mg, 0.063 mmol). The mixture was stirred for 12 h at rt, quenched with 10% Na_2CO_3 (10 ml), and extracted with CH_2Cl_2 (3 x 5 ml). The combined organic extract was then washed with water (3 x 20 ml), dried (Na_2SO_4), concentrated *in vacuo*, and the residue purified by centrifugal preparative TLC (SiO_2, 5% MeOH:Et_2O, NH_3-saturated) to give leuconolam (**54**) (2.9 mg, 15%) and recovered 6,7-dehydroleuconoxine (**63**) (16.3 mg, 84%).

10.8.14 Reaction of 6,7-dehydroleuconoxine (63) with CSA in anhydrous CH_2Cl_2

To a stirred solution of CSA (11.8 mg, 0.051 mmol) and CH_2Cl_2 (5 ml) was added 6,7-dehydroleuconoxine (**63**) (11 mg, 0.034 mmol). TLC of the reaction mixture after 15 h showed traces of leuconolam (**54**) and amino lactam-lactone **78**, in addition to the starting material **63**.

10.8.15 Reaction of 6,7-dehydroleuconoxine (63) with PTSA in anhydrous CH_2Cl_2

To a stirred solution of PTSA (9.2 mg, 0.054 mmol) and CH_2Cl_2 (5 ml) was added 6,7-dehydroleuconoxine (**63**) (10.3 mg, 0.036 mmol). The mixture was stirred for 10 h at rt, quenched with 10% Na_2CO_3 (10 ml), and extracted with CH_2Cl_2 (3 x 5 ml). The combined organic extract was then washed with water (3 x 10 ml), dried (Na_2SO_4), concentrated *in vacuo*, and the residue purified by centrifugal preparative TLC (SiO_2, Et_2O, NH_3-saturated) to give amino lactam-lactone **78** (7.1 mg, 70%) and recovered **63** (0.3 mg, 1%).

10.8.16 Reaction of *O*-methylleuconolam (77) with PTSA in anhydrous CH_2Cl_2

To a stirred solution of PTSA (8 mg, 0.044 mmol) and CH_2Cl_2 (5 ml) was added *O*-methylleuconolam (**77**) (10 mg, 0.029 mmol). TLC of the mixture after 10 h showed traces of leuconolam (**54**) and amino lactam-lactone (**78**), in addition to the starting material **77**.

10.8.17 Hydrogenation of 6,7-dehydroleuconoxine (63)

6,7-Dehydroleuconoxine (**63**) (20 mg, 0.061 mmol) was dissolved in CH_2Cl_2 (5 ml) and then stirred over 10% Pd/C (12.4 mg) under a hydrogen atmosphere (hydrogen balloon) at rt for 1 h. The catalyst was removed by filtration over Celite. Evaporation of the solvent *in vacuo*, followed by chromatography of the resulting residue (SiO_2, 5% MeOH:Et_2O, NH_3-saturated) gave leuconoxine (**56**) (18.1 mg, 90%) as a colorless oil and subsequently as colorless block crystals from MeOH; mp 210–215 ^oC (lit[50] 238–242 ^oC); $[\alpha]^{25}_D$ –86 (*c* 0.68, $CHCl_3$) [lit[50] $[\alpha]^{25}_D$ –88 (*c* 1.2, MeOH)]; UV (EtOH) λ_{max} (log ε) 202 (4.42), 240 (3.82), and 270 (3.16) nm; IR (dry film) ν_{max} 1743 and 1709 cm^{-1}; For ^1H and ^{13}C NMR data, see Table 4.8; ESIMS *m/z* 311 $[M + H]^+$ ($C_{19}H_{22}N_2O_2$ + H).

10.8.18 Bromination of leuconolam (54)

Leuconolam (**54**) (11 mg, 0.034 mmol) was dissolved in $CHCl_3$ (4 ml), and Br_2 (2.6 μl, 0.051 mmol) was added dropwise at rt. After being stirred for 14 h, the mixture was quenched with 10% Na_2CO_3 (10 ml), extracted with $CHCl_3$ (3 x 5 ml), washed with water, dried (Na_2SO_4), the solvent removed *in vacuo*, and the residue purified by centrifugal preparative TLC (SiO_2, 5% MeOH:$CHCl_3$, NH_3-saturated) to give 6β,7β-dibromoleuconoxine (**82**) (13.7 mg, 86%) as white amorphous; mp 98–102 ^oC (lit[49] mp 109–110 ^oC); $[\alpha]^{25}_D$ –38 (*c* 0.62, $CHCl_3$) [lit[49] $[\alpha]^{25}_D$ –32 (*c* 0.5, $CHCl_3$)]; UV (EtOH) λ_{max} (log ε) 208 (4.32), 227 (4.22), and 292 (3.35) nm; IR (dry film) ν_{max} 1709 and 1691 cm^{-1}; For ^1H and ^{13}C NMR data, see Table 4.9; ESIMS *m/z* 467 $[M + H]^+$; HRESIMS *m/z* 466.9965 $[M + H]^+$ (calcd for $C_{19}H_{20}N_2O_2{}^{79}Br_2$ + H, 466.9964).

10.8.19 Bromination of 6,7-dehydroleuconoxine (63)

6,7-Dehydroleuconoxine (**63**) (7 mg, 0.021 mmol) was dissolved in $CHCl_3$ (4 ml), and Br_2 (1.2 μl, 0.032 mmol) was added dropwise at rt, and the mixture stirred for 13 h. The mixture was quenched with 10% Na_2CO_3 (10 ml), extracted with $CHCl_3$ (3 x 5 ml), washed with water, dried (Na_2SO_4), the solvent removed *in vacuo*, and the residue purified by centrifugal preparative TLC (SiO_2, 5% MeOH:$CHCl_3$, NH_3-saturated) to give 6β,7β-dibromoleuconoxine (**82**) (9.6 mg, 96%).

10.8.20 Debromination of 6β,7β-dibromoleuconoxine (82)

To a solution of 6β,7β-dibromoleuconoxine (**82**) (13 mg, 0.028 mmol) in AcOH (5 ml) was added freshly activated zinc (91 mg, 0.139 mmol). The mixture was stirred for 2 h, after which the mixture was poured into saturated Na_2CO_3 (30 ml), extracted with CH_2Cl_2 (3 x 20 ml), washed with water (3 x 20 ml), dried (Na_2SO_4), the solvent removed *in vacuo*, and the residue purified by centrifugal preparative TLC (SiO_2, 5% MeOH:$CHCl_3$, NH_3-saturated) to give 6,7-dehydroleuconoxine (**63**) (3.7 mg, 41%).

10.8.21 Reaction of 6,7-dehydroleuconoxine (63) with $BH_3.SMe_2$

$BH_3.SMe_2$ (75 μl, 1 M in THF) was added to 6,7-dehydroleuconoxine (**63**) (16 mg, 0.051 mmol) in THF (5 ml) and the mixture was stirred for 24 h at rt. The progress of the reaction was monitored by TLC and the reaction was quenched with NH_4Cl solution when >95% of the starting material had been consumed. The mixture was extracted with CH_2Cl_2 (3 x 10 ml), washed with water (3 x 20 ml), dried over Na_2SO_4, filtered, the solvent removed *in vacuo*, and the residue purified by centrifugal preparative TLC

(SiO_2, 5% MeOH:$CHCl_3$, NH_3-saturated) to give compounds **86** (5.6 mg, 37%) and **87** (1 mg, 6%).

Compound 86: yellowish oil and subsequently as yellowish needles from MeOH; mp 128–132 ^{o}C; $[\alpha]^{25}_{D}$ = +584 (*c* 0.35, $CHCl_3$); UV (EtOH) λ_{max} (log ε) 209 (3.65), 246 (3.86), and 388 (3.02) nm; IR (dry film) ν_{max} 1682 and 1641 cm^{-1}; For ^{1}H and ^{13}C NMR data, see Table 4.10; ESIMS *m/z* 295 $[M + H]^+$; HRESIMS *m/z* $[M + H]^+$ 295.1792 (calcd for $C_{19}H_{22}N_2O$ + H, 295.1805).

Crystallographic data of compound **86**: crystal data and structure refinement parameters of **86** are summarized in Table 10.7.

Table 10.7. Crystal data and structure refinement parameters of compound **86**

Empirical formula	$C_{19}H_{22}N_2O$
Molecular formula	$C_{19}H_{22}N_2O$
Molecular weight, M_r	294.39
Melting point	128–132 ^oC
Temperature during diffraction experiment, T	100 K
X-ray source	Mo K_α
Crystal system	Orthorhombic
Space group	$P2_12_12_1$
a	11.2107(6) Å
b	11.5443(6) Å
c	12.1199(7) Å
α	90.00°
β	90.00°
γ	90.00°
Volume, V	1568.55(15) $Å^3$
No. of molecule per unit cell, Z	4
Density (calcd)	1.247 mg/mm^3
$F(000)$	632.0
Crystal size	0.90 × 0.60 × 0.02 mm
2θ range for data collection	4.88 to 55°
Index ranges	$-14 \leq h \leq 14$, $-15 \leq k \leq 15$, $-15 \leq l \leq 14$
Reflections collected	14949
Independent reflections	2057[R_{int} = 0.0271]
Data/restraints/parameters	2057/0/200
Goodness-of-fit on F^2	1.029
Final R indexes [$I \geq 2\sigma(I)$]	R_1 = 0.0379, wR_2 = 0.0921
Final R indexes [all data]	R_1 = 0.0478, wR_2 = 0.0985
Largest diff. peak/hole / e $Å^{-3}$	0.14/–0.11

Compound 87: fluorescent yellowish oil and subsequently as fluorescent yellowish rods from CH_2Cl_2/hexanes; mp 198–200 ^oC; $[\alpha]^{25}_D$ = +667 (*c* 0.33, $CHCl_3$); UV (EtOH) λ_{max} (log ε) 209 (4.14), 245 (4.42), and 394 (3.64) nm; IR (dry film) ν_{max} 3343, 1666, and 1644 cm^{-1}; For ^1H and ^{13}C NMR data, see Table 4.10; ESIMS *m/z* 311 $[M + H]^+$; HRESIMS *m/z* $[M + H]^+$ 311.1750 (calcd for $C_{19}H_{22}N_2O_2$ + H, 311.1754).

Crystallographic data of compound **87**: crystal data and structure refinement parameters of compound **87** are summarized in Table 10.8.

Table 10.8. Crystal data and structure refinement parameters of compound **87**

Empirical formula	$C_{19}H_{24}N_2O_2$
Molecular formula	$C_{19}H_{24}N_2O_2$
Molecular weight, M_r	312.40
Melting point	128–132 ^oC
Temperature during diffraction experiment, *T*	100 K
X-ray source	Mo K_α
Crystal system	Trigonal
Space group	$P3_1$
a	11.4602(2) Å
b	11.4602(2) Å
c	10.0616(2) Å
α	90.00°
β	90.00°
γ	120.00°
Volume, *V*	1144.41(4) $Å^3$
No. of molecule per unit cell, *Z*	3
Density (calcd)	1.360 mg/mm^3
F(000)	504.0
Crystal size	0.7 × 0.2 × 0.2 mm
2θ range for data collection	4.1 to 54.9°
Index ranges	$-14 \le h \le 14$, $-14 \le k \le 14$, $-13 \le l \le 13$
Reflections collected	8827
Independent reflections	3344[R_{int} = 0.0480]
Data/restraints/parameters	3344/1/210
Goodness-of-fit on F^2	1.211
Final R indexes [$I \ge 2\sigma(I)$]	R_1 = 0.1315, wR_2 = 0.3662
Final R indexes [all data]	R_1 = 0.1326, wR_2 = 0.3669
Largest diff. peak/hole / e $Å^{-3}$	0.72/–0.72

10.8.22 Attempted enolate-mediated C-6 oxidation of leuconoxine (56)

A solution of **56** (11 mg, 0.035 mmol) in THF (5 ml) was added to a solution of lithium diisopropylamide (LDA, 27 μl, 2 M in THF) in THF (10 ml) at 0 ^{o}C and the resulting mixture was stirred for 30 min. Dry O_2 was then bubbled into the solution for 10 min. Na_2SO_3 solution (1 M, 2 ml) was added and the mixture extracted with CH_2Cl_2 (3 x 10 ml), dried (Na_2SO_4), and then concentrated *in vacuo*. The resulting residue was purified by centrifugal preparative TLC (SiO_2, 5% MeOH:Et_2O, NH_3-saturated) to afford compound **90** (2.4 mg, 21%) and recovered **56** (7.6 mg, 69%).

Compound 90: colorless oil, and subsequently as colorless needles from CH_2Cl_2/hexanes; mp 184–186 ^{o}C; $[\alpha]^{25}_{D}$ = –29 (*c* 0.16, $CHCl_3$); UV (EtOH) λ_{max} (log ε) 210 (4.10), 241 (3.88), and 274 (3.23) nm; IR (dry film) ν_{max} 3417 and 1675 cm^{-1}; For ^{1}H and ^{13}C NMR data, see Table 4.11; ESIMS *m/z* 327 $[M + H]^+$; HRESIMS *m/z* $[M + H]^+$ 327.1710 (calcd for $C_{19}H_{22}N_2O_3$ + H, 327.1703).

Crystallographic data of compound **90**: crystal data and structure refinement parameters of compound **90** are summarized in Table 10.9.

Table 10.9. Crystal data and structure refinement parameters of compound **90**

Empirical formula	$C_{19}H_{22}N_2O_3$
Molecular formula	$C_{19}H_{22}N_2O_3$
Molecular weight, M_r	326.39
Melting point	184–186 ^{o}C
Temperature during diffraction experiment, T	298 K
X-ray source	Mo K_α
Crystal system	Orthorhombic
Space group	$P2_12_12_1$
a	7.1721(4) Å
b	26.1619(13) Å
c	27.9882(15) Å
α	90.00°
β	90.00°
γ	90.00°
Volume, V	5251.6(5) Å^3
No. of molecule per unit cell, Z	12
Density (calcd)	1.238 mg/mm^3
F(000)	2088.0
Crystal size	0.68 × 0.08 × 0.02 mm
2θ range for data collection	4.26 to 41.8°
Index ranges	$0 \leq h \leq 7$, $0 \leq k \leq 26$, $0 \leq l \leq 28$
Reflections collected	3171
Independent reflections	3171[R_{int} = 0.0000]
Data/restraints/parameters	3171/0/656
Goodness-of-fit on F^2	0.920
Final R indexes [$I \geq 2\sigma(I)$]	R_1 = 0.0508, wR_2 = 0.1153
Final R indexes [all data]	R_1 = 0.0769, wR_2 = 0.1242
Largest diff. peak/hole / e Å^{-3}	0.38/–0.21

10.8.23 Reaction of leuconolam (54) with trifluoroacetic acid

To a stirred solution of **54** (11 mg, 0.034 mmol) and CH_2Cl_2 (5 ml) was added TFA (9.5 μl, 0.068 mmol). The mixture was stirred for 13 h at rt, quenched with 10% Na_2CO_3 (10 ml), and extracted with CH_2Cl_2 (3 x 5 ml). The combined organic extract was then washed with water (3 x 10 ml), dried (Na_2SO_4), concentrated *in vacuo*, and the residue purified by centrifugal preparative TLC (SiO_2, 5% MeOH:Et_2O, NH_3-saturated) to give 6,7-dehydroleuconoxine (**63**) (4.1 mg, 37%) and recovered leuconolam (**54**) (5.8 mg, 53%).

10.8.24 Reaction of leuconolam (54) with excess trifluoroacetic acid

To a stirred solution of **54** (13 mg, 0.04 mmol) and CH_2Cl_2 (5 ml) was added TFA (60 μl, 0.8 mmol). The mixture was stirred for 12 h at rt, quenched with 10% Na_2CO_3 (10 ml), and extracted with CH_2Cl_2 (3 x 5 ml). The combined organic extract was then washed with water (3 x 10 ml), dried (Na_2SO_4), concentrated *in vacuo*, and the residue purified by centrifugal preparative TLC (SiO_2, 5% MeOH:Et_2O, NH_3-saturated) to 6,7-dehydroleuconoxine (**63**) (3.9 mg, 30%), leuconodine A (**67**) (3.3 mg, 25%) and recovered **54** (1.2 mg, 9%).

Leuconodine A (67): colorless oil and subsequently as colorless block crystals from EtOH; mp 134–136 ^{o}C; $[\alpha]^{25}_{D}$ = –19 (*c* 0.03, $CHCl_3$); UV (EtOH) λ_{max} (log ε) 209 (4.16), 241 (3.89), and 277 (3.29) nm; IR (dry film) ν_{max} 3357 and 1676 cm^{-1}; For ^{1}H and ^{13}C NMR data, see Table 4.12; EIMS *m/z* (rel. int.) 326 $[M]^+$ (100), 309 (8), 298 (48), 283 (35), 252 (18), 237 (8), and 212 (17); HREIMS *m/z* 326.1633 $[M]^+$ (calcd for $C_{19}H_{22}N_2O_3$, 326.1630).

Crystallographic data of alkaloid **67**: crystal data and structure refinement parameters of alkaloid **67** are summarized in Table 10.10.

Table 10.10. Crystal data and structure refinement parameters of leuconodine A (**67**)

Empirical formula	$C_{21}H_{28}N_2O_4$
Molecular formula	$C_{19}H_{22}N_2O_3.C_2H_5OH$
Molecular weight, M_r	372.45
Melting point	134–137 ^oC
Temperature during diffraction experiment, T	100 K
X-ray source	Mo K_α
Crystal system	Orthorhombic
Space group	$P2_12_12_1$
a	7.3486(4) Å
b	15.0738(7) Å
c	16.6740(8) Å
α	90.00°
β	90.00°
γ	90.00°
Volume, V	1847.00(16) $Å^3$
No. of molecule per unit cell, Z	4
Density (calcd)	1.339 mg/mm^3
F(000)	1128
Crystal size	0.63 × 0.17 × 0.04 mm
2θ range for data collection	3.64 to 61.02°
Index ranges	$-10 \leq h \leq 10$, $-21 \leq k \leq 21$, $-22 \leq l \leq 22$
Reflections collected	19671
Independent reflections	3065[R_{int} = 0.1165]
Data/restraints/parameters	3065/0/248
Goodness-of-fit on F^2	1.066
Final R indexes [$I \geq 2\sigma(I)$]	R_1 = 0.0512, wR_2 = 0.1044
Final R indexes [all data]	R_1 = 0.1133, wR_2 = 0.1263
Largest diff. peak/hole / e $Å^{-3}$	0.26/–0.28

10.8.25 Oxidation of leuconodine A (67)

A solution of **67** (7 mg, 0.021 mmol) in CH_2Cl_2 (5 ml) was treated with the Dess-Martin periodinane reagent (82 μl, 0.3 M in CH_2Cl_2) and the mixture was stirred at rt for 30 min. Et_2O (25 ml) and NaOH (10 ml, 1.3 M) were then added and the mixture was stirred for another 15 minutes. The aqueous layer was removed and the organic layer was washed with 1.3 M NaOH (2 x 10 ml), dried with Na_2SO_4, the solvent removed *in vacuo*, and the residue purified by centrifugal preparative TLC (SiO_2, 5% MeOH:Et_2O, NH_3-saturated) to give leuconodine F (**72**) (5.3 mg, 76%) as colorless oil, and subsequently as colorless block crystals from MeOH: mp 246–250 ^{o}C; $[\alpha]^{25}_{D}$ = +94 (*c* 0.05, $CHCl_3$); UV (EtOH) λ_{max} (log ε) 202 (4.42), 234 (4.12), 251 (4.02) and 349 (3.10) nm; IR (dry film) ν_{max} 1715 and 1689 cm^{-1}; For ^{1}H and ^{13}C NMR data, see Table 4.12; ESIMS *m/z* $[M + H]^+$ 325; HRESIMS *m/z* 325.1453 $[M + H]^+$ (calcd for $C_{19}H_{20}N_2O_3$, 325.1547).

Crystallographic data of alkaloid **72**: crystal data and structure refinement parameters of alkaloid **72** are summarized in Table 10.11.

Table 10.11. Crystal data and structure refinement parameters of leuconodine F (**72**)

Empirical formula	$C_{19}H_{20}N_2O_3$
Molecular formula	$C_{19}H_{20}N_2O_3$
Molecular weight, M_r	324.37
Melting point	246–250 ^{o}C
Temperature during diffraction experiment, T	100 K
X-ray source	Mo K_α
Crystal system	Monoclinic
Space group	$P2_1$
a	9.7373(4) Å
b	7.3976(3) Å
c	11.4361(5) Å
α	90.00°
β	107.522(2)°
γ	90.00°
Volume, V	785.55(6) Å^3
No. of molecule per unit cell, Z	2
Density (calcd)	1.371 mg/mm^3
F(000)	344.0
Crystal size	0.64 × 0.09 × 0.03
2θ range for data collection	3.74 to 52.82°
Index ranges	$-12 \leq h \leq 12$, $-9 \leq k \leq 9$, $-14 \leq l \leq 14$
Reflections collected	5507
Independent reflections	1735[R_{int} = 0.0332]
Data/restraints/parameters	1735/1/218
Goodness-of-fit on F^2	1.048
Final R indexes [$I \geq 2\sigma(I)$]	R_1 = 0.0333, wR_2 = 0.0718
Final R indexes [all data]	R_1 = 0.0461, wR_2 = 0.0761
Largest diff. peak/hole / e Å^{-3}	0.20/–0.17

10.9 Chapter 5

10.9.1 Partial synthesis of alstolucine A (91)

10.9.1.1 Compound data of alstolucines A (91) and B (94)

Alstolucines A (**91**) and B (**94**) were isolated from the leaf extract of *Alstonia spatulata.*[74]

Alstolucine A (91): light yellowish oil; $[\alpha]^{25}_{D}$ –438 (*c* 0.12, $CHCl_3$); UV (EtOH) λ_{max} (log ε) 230 (3.32), 298 (3.26), and 328 (3.46) nm; IR (dry film) ν_{max} 3378, 1742, and 1683 cm^{-1}; For ^{1}H and ^{13}C NMR data, see Table 5.1; ESIMS *m/z* 413 $[M + H]^+$; HRESIMS *m/z* 413.2074 $[M + H]^+$ (calcd for $C_{23}H_{28}N_2O_5 + H$, 413.2071).

Alstolucine B (94): colorless block crystals from $CHCl_3$; mp >160 ^{o}C dec; $[\alpha]^{25}_{D}$ –515 (*c* 1.28, $CHCl_3$); UV (EtOH) λ_{max} (log ε) 232 (3.85), 295 (3.75), and 326 (3.91) nm; IR (dry film) ν_{max} 3361, 1704, and 1678 cm^{-1}; For ^{1}H and ^{13}C NMR data, see Table 5.1; ESIMS *m/z* 339 $[M + H]^+$; HRESIMS *m/z* 339.1714 $[M + H]^+$ (calcd for $C_{20}H_{22}N_2O_3 + H$, 339.1703).

Crystallographic data of alkaloid **94**: crystal data and structure refinement parameters of alkaloid **94** are summarized in Table 10.12.

Table 10.12. Crystal data and structure refinement parameters of alstolucine B (**94**)

Empirical formula	$C_{20}H_{22}N_2O_3$
Molecular formula	$C_{20}H_{22}N_2O_3$
Molecular weight, M_r	338.40
Melting point	>160 ^{o}C dec
Temperature during diffraction experiment, T	100 K
X-ray source	Mo K_α
Crystal system	Orthorhombic
Space group	$P2_12_12_1$
a	7.80370(10) Å
b	11.7086(2) Å
c	18.3534(3) Å
α	90.00°
β	90.00°
γ	90.00°
Volume, V	1676.96(5) Å^3
No. of molecule per unit cell, Z	4
Density (calcd)	1.340 mg/mm^3
F(000)	720.0
Crystal size	0.55 × 0.26 × 0.14 mm
2θ range for data collection	4.12 to 54.98°
Index ranges	$-10 \leq h \leq 10$, $-15 \leq k \leq 15$, $-23 \leq l \leq 23$
Reflections collected	15918
Independent reflections	2204 [R_{int} = 0.0365]
Data/restraints/parameters	2204/0/228
Goodness-of-fit on F^2	1.073
Final R indexes [$I \geq 2\sigma(I)$]	R_1 = 0.0350, wR_2 = 0.0917
Final R indexes [all data]	R_1 = 0.0384, wR_2 = 0.0941
Largest diff. peak/hole / e Å^{-3}	0.30/–0.34

10.9.1.2 Epimerization of (–)-alstolucine B (94) to compound 95

To a solution of the ketone **94** (12 mg, 0.035 mmol) in 1 ml of MeOH was added a freshly prepared solution of Na (1.2 mg, 0.053 mmol) in 1 ml MeOH at 0 ^{o}C. The mixture was allowed to stir at rt for 3 h. The solvent was evaporated *in vacuo*, and water (5 ml) was added. The product was extracted with CH_2Cl_2 (3 x 10 ml). The combined organic extract was dried (Na_2SO_4), filtered, and concentrated *in vacuo*, and the residue was purified by centrifugal preparative TLC (SiO_2, 5% MeOH:$CHCl_3$, NH_3-saturated) to afford the isomerized ketone **95** (4.2 mg, 35%), and recovered **94** (7.6 mg, 63%).

Compound 95: light yellowish oil; $[\alpha]^{25}_{D}$ –371 (*c* 0.35, $CHCl_3$); UV (EtOH) λ_{max} (log ε) 229 (3.32), 297 (3.21), and 328 (3.38) nm; IR (dry film) ν_{max} 3364, 1704, and 1678 cm^{-1}; For ^{1}H and ^{13}C NMR data, see Table 5.2; ESIMS *m/z* 339 $[M + H]^+$; HRESIMS *m/z* 339.1710 $[M + H]^+$ (calcd for $C_{20}H_{22}N_2O_3 + H$, 339.1703).

10.9.1.3 $NaBH_4$ reduction of compound 95

To a mixture of compound **95** (8 mg, 0.024 mmol) in 2 ml of MeOH at 0 ^{o}C was added $NaBH_4$ (1.6 mg, 0.041 mmol). The solution was stirred at rt for 1 h. Saturated $NaHCO_3$ (5 ml) solution was added, and the product was extracted with CH_2Cl_2 (3 x 10 ml). The combined organic extract was dried (Na_2SO_4), filtered, and concentrated *in vacuo*, and the residue was purified by centrifugal preparative TLC (SiO_2, 10% MeOH:Et_2O, NH_3-saturated) to afford *N*(4)-demethylalstogustine (**92**, 6.8 mg, 85%) and compound **93** (0.8 mg, 10%).

***N*(4)-Demethylalstogustine (92)**: light yellowish oil; $[\alpha]^{25}_{D}$ −399 (*c* 0.33, $CHCl_3$) [lit[76] $[\alpha]_D$ −442 (*c* 0.55, EtOH)]; UV (EtOH) λ_{max} (log ε) 228 (3.88), 298 (3.82), and 329 (3.98) nm; IR (dry film) ν_{max} 3373 and 1670 cm^{-1}; For ^1H and ^{13}C NMR data, see Table 5.2; ESIMS *m/z* 341 $[M + H]^+$; HRESIMS *m/z* 341.1866 $[M + H]^+$ (calcd for $C_{20}H_{24}N_2O_3$ + H, 341.1860).

Compound 93: light yellowish oil; $[\alpha]^{25}_{D}$ −361 (*c* 0.18, $CHCl_3$); UV (EtOH) λ_{max} (log ε) 226 (3.82), 298 (3.77), and 329 (3.94) nm; IR (dry film) ν_{max} 3370 and 1672 cm^{-1}; For ^1H and ^{13}C NMR data, see Table 5.2; ESIMS *m/z* 341 $[M + H]^+$; HRESIMS *m/z* 341.1867 $[M + H]^+$ (calcd for $C_{20}H_{24}N_2O_3$ + H, 341.1860).

10.9.1.4 *O*-Acylation of *N*(4)-demethylalstogustine (92)

To a stirred solution of **92** (6.5 mg, 0.019 mmol), CH_2Cl_2 (5 ml), and triethylamine (13 μl, 0.095 mmol), was added dropwise ethyl chloroformate (9 μl, 0.095 mmol), and the mixture was stirred for 30 min at rt. The mixture was quenched with saturated NH_4Cl (10 ml) and extracted with CH_2Cl_2 (3 x 10 ml). The combined organic extract was dried (Na_2SO_4), the solvent evaporated *in vacuo*, and the residue purified by centrifugal preparative TLC (SiO_2, 2% MeOH:$CHCl_3$, NH_3-saturated) to give the *O*-carboethoxy derivative, alstolucine A (**91**) (5.4 mg, 69%) as a light yellowish oil. The spectroscopic (^1H and ^{13}C NMR, IR, and UV) and other data ($[\alpha]_D$ and R_f of TLC in different solvent systems) of semisynthetic alstolucine A (**91**) were indistinguishable from those of the natural alstolucine A (**91**).[74]

10.9.2 Partial synthesis of (–)-eburnamaline (96)

10.9.2.1 Compound data of (–)-eburnamaline (96) and (+)-eburnamonine (98)

The alkaloid (–)-eburnamaline (**96**) was obtained the stem-bark extract of from *L. griffithii*.[81]

(–)-Eburnamaline (96): light yellowish oil; $[\alpha]^{25}_{D}$ –49 (*c* 0.21, $CHCl_3$); UV (EtOH) λ_{max} (log ε) 230 (3.76) and 280 (3.16) nm; IR (dry film) ν_{max} 3370 cm^{-1}; For ^{1}H and ^{13}C NMR data, see Table 5.3; EIMS *m/z* (rel. int.) *m/z* 312 $[M]^+$ (100), 294 (23), 283 (20), 265 (76), 242 (26), 224 (38), 208 (18), 196 (12), 180 (8), and 144 (5); HREIMS *m/z* 312.1827 (calcd for $C_{19}H_{24}N_2O_2$, 312.1838); ESIMS *m/z* 313 $[M + H]^+$; HRESIMS *m/z* 313.1926 $[M + H]^+$ (calcd for $C_{19}H_{24}N_2O_2$ + H, 313.1911).

The starting material for the partial synthesis of (–)-eburnamaline (**96**), (+)-eburnamonine (**98**) was obtained from the stem extract of *Kopsia larutensis*.[87]

(+)-Eburnamonine (98): colorless block crystals; mp 175–177 ^{o}C; $[\alpha]^{25}_{D}$ +108 (*c* 0.24, $CHCl_3$); UV (EtOH) λ_{max} (log ε) 207 (4.40), 246 (4.46), 270 (4.18), and 302 (3.91) nm; IR (dry film) ν_{max} 1716 (C=O, lactam) cm^{-1}; For ^{1}H and ^{13}C NMR data, see Table 5.3; ESIMS *m/z* $[M + H]^+$ 295 ($C_{19}H_{22}N_2O$ + H).

10.9.2.2 Oxidation of (+)-eburnamonine (98)

Method A. A solution of (+)-eburnamonine (**98**) (100 mg, 0.34 mmol) in THF (5 ml) was added to a solution of lithium diisopropylamide (LDA, 0.42 ml, 2 M in THF) in THF (10 mL) at 0 ^{o}C and the resulting mixture was stirred for 30 min. Dry O_2 was then bubbled into the solution for 10 min. Na_2SO_3 solution (1 M, 5 ml) was added and the mixture extracted with EtOAc (3 x 15 ml), dried (Na_2SO_4), and then concentrated *in vacuo*. The resulting residue was purified by centrifugal preparative TLC (SiO_2, 2% MeOH:$CHCl_3$, NH_3-saturated) to afford (+)-17β-hydroxyeburnamonine (**99**) (27.5 mg, 26%).

Method B. A solution of (+)-eburnamonine (**98**) (46 mg, 0.16 mmol) in THF (2 ml) was added to a solution of lithium diisopropylamide (LDA, 0.2 ml, 2 M in THF) in THF (2 ml) at 0 ^{o}C and the resulting mixture stirred for 30 min. A solution of (1*S*)-(+)-(10-camphorsulfonyl)oxaziridine (90 mg, 0.4 mmol) in THF (1 ml) was then added, and the mixture stirred for another 20 min. The reaction was quenched by addition of a saturated solution of NH_4Cl (2 ml), and the mixture poured into brine (10 ml) and extracted with CH_2Cl_2 (3 x 10 ml). The combined organic extracts were dried (Na_2SO_4), filtered, concentrated *in vacuo*, and the resulting residue was then purified by centrifugal preparative TLC (SiO_2, 2% MeOH:$CHCl_3$, NH_3-saturated) to afford (+)-17β-hydroxyeburnamonine (**99**) (40 mg, 83%).

(+)-17β-Hydroxyeburnamonine (99): light yellowish oil; $[\alpha]^{25}_{D}$ +126 (*c* 0.62, $CHCl_3$); UV (EtOH) λ_{max} (log ε) 229 (4.15) and 282 (3.56) nm; IR (dry film) ν_{max} 3382 and 1703 cm^{-1}; For ^{1}H and ^{13}C NMR data, see Table 5.4; ESIMS *m/z* 311 $[M + H]^+$; HRESIMS *m/z* $[M + H]^+$ 311.1760 (calcd for $C_{19}H_{23}N_2O_2$, 311.1760).

10.9.2.3 Reduction of (+)-17β-hydroxyeburnamonine (99)

To a solution of **99** (72 mg, 0.23 mmol) in THF (10 ml) at 0 ^{o}C was added $LiAlH_4$ (23 mg, 0.6 mmol) and the mixture was refluxed for 2 h. The mixture was cooled to 0 ^{o}C, following which, water (0.1 ml), then NaOH (3 M, 0.1 ml), and finally water (0.3 ml) was added. The mixture was stirred for 3 h at rt and then filtered through a pad of Celite. The filtrate was concentrated *in vacuo* and the resulting residue was purified by centrifugal preparative TLC (SiO_2, 5% MeOH:CH_2Cl_2, NH_3-saturated) to afford compounds **96** (39 mg, 54%) and **100** (28 mg, 39%). The spectroscopic (^{1}H and ^{13}C NMR, IR, and UV) and other data ($[\alpha]_D$ and R_f of TLC in different solvent systems) of semisynthetic (–)-eburnamaline (**96**) were indistinguishable from those of the natural (–)-eburnamaline (**96**).[80]

Compound **100**: white amorphous solid and subsequently as colorless crystals from CH_2Cl_2; mp 190–193 ^{o}C; $[\alpha]^{25}_D$ –44 (*c* 0.62, MeOH); UV (EtOH) λ_{max} (log ε) 229 (4.41) and 281 (3.82) nm; IR (dry film) ν_{max} 3448 cm^{-1}; For ^{1}H and ^{13}C NMR data, see Table 5.4; ESIMS *m/z* 313 $[M + H]^+$; HRESIMS *m/z* 313.1915 $[M + H]^+$ (calcd for $C_{19}H_{24}N_2O_2 + H$, 313.1916).

Crystallographic data of compound **100**: crystal data and structure refinement parameters of compound **100** are summarized in Table 10.13.

Table 10.13. Crystal data and structure refinement parameters of compound **100**

Empirical formula	$C_{41}H_{54}Cl_6N_4O_4$
Molecular formula	$2C_{19}H_{24}N_2O_2 .3CH_2Cl_2$
Molecular weight , M_r	879.58
Melting point	190–193 ^oC
Temperature during diffraction experiment, T	100 K
X-ray source	Mo K_α
Crystal system	Hexagonal
Space group	$P6_5$
a	20.6890(4) Å
b	20.6890(4) Å
c	17.1028(3) Å
α	90.00°
β	90.00°
γ	120.00°
Volume, V	6339.8(2) $Å^3$
No of molecule per unit cell, Z	15
Density (calcd)	2.051 mg/mm^3
F(000)	6930.0
Crystal size	0.38 × 0.08 × 0.07 mm
2θ range for data collection	2.28 to 52.78°
Index ranges	$-25 \leq h \leq 25$, $-24 \leq k \leq 25$, $-21 \leq l \leq 21$
Reflections collected	55539
Independent reflections	8656[R_{int} = 0.0947]
Data/restraints/parameters	8656/1/502
Goodness-of-fit on F^2	1.083
Final R indexes [$I \geq 2\sigma (I)$]	R_1 = 0.0526, wR_2 = 0.1224
Final R indexes [all data]	R_1 = 0.0735, wR_2 = 0.1369
Largest diff. peak/hole / e $Å^{-3}$	0.71/–0.34
Flack parameter, x	–0.07(0.06)

10.10 Chapter 6

10.10.1 Compound data of perhentidines A–C (101–103), perhentinine (104), and macralstonine (105)

The alkaloids perhentidines A–C (**101–103**), perhentinine (**104**) and macralstonine (**105**) were isolated from the stem-bark extracts of *Alstonia macrophylla* and *Alstonia angustifoia*.[89]

Perhentidine A (101): light yellowish oil; $[\alpha]^{25}_{D}$ –77 (*c* 0.40, $CHCl_3$); UV (EtOH) λ_{max} (log ε) 231 (4.69) and 286 (3.69) nm; IR (dry film) ν_{max} 3400, 1702, 1648, and 1617 cm^{-1}; For ^1H and ^{13}C NMR data, see Tables 6.1 and 6.2, respectively; ESIMS *m/z* 705 $[M + H]^+$; HRESIMS *m/z* 705.4010 $[M + H]^+$ (calcd for $C_{43}H_{52}N_4O_5$ + H, 705.4013).

Perhentidine B (102): light yellowish oil; $[\alpha]^{25}_{D}$ –38 (*c* 0.52, $CHCl_3$); UV (EtOH) λ_{max} (log ε) 234 (4.49) and 286 (3.81) nm; IR (dry film) ν_{max} 3392, 1707, 1653, and 1618 cm^{-1}; For ^1H and ^{13}C NMR data, see Tables 6.1 and 6.2, respectively; ESIMS *m/z* 705 $[M + H]^+$; HRLSIMS *m/z* 705.3993 $[M + H]^+$ (calcd for $C_{43}H_{52}N_4O_5$ + H, 705.4013).

Perhentidine C (103): light yellowish oil; $[\alpha]^{25}_{D}$ –73 (*c* 0.50, $CHCl_3$); UV (EtOH) λ_{max} (log ε) 230 (4.53) and 285 (3.93) nm; IR (dry film) ν_{max} 3387, 1703, 1651, and 1615 cm^{-1}; For ^1H and ^{13}C NMR data, see Tables 6.1 and 6.2, respectively; EIMS *m/z* (rel. int.) 686 $[M – H_2O]^+$ (100), 616 (6), 547 (5), 486 (42), 379 (27), 343 (12), 307 (15), 277 (5), 251 (19), 197 (99), 170 (21), and 70 (8); HRLSIMS *m/z* 705.4029 $[M + H]^+$ (calcd for $C_{43}H_{52}N_4O_5$ + H, 705.4013).

Perhentinine (104): light yellowish oil; $[\alpha]^{25}_{D}$ −61 (*c* 0.12, $CHCl_3$); UV (EtOH) λ_{max} (log ε) 231 (4.25) and 298 (3.45) nm; IR (dry film) ν_{max} 3400, 1701, 1651, and 1616 cm^{-1}; For ^{1}H and ^{13}C NMR data, see Tables 6.3 and 6.4, respectively; ESIMS *m/z* 705 $[M + H]^+$; HRESIMS *m/z* 705.4019 $[M + H]^+$ (calcd for $C_{43}H_{52}N_4O_5$ + H, 705.4013).

Macralstonine (105): colorless rectangular rod crystals from CH_2Cl_2/MeOH; mp 260−263 °C [lit[92] 279−280 °C]; $[\alpha]^{25}_{D}$ +23 (*c* 0.5, $CHCl_3$) [lit[92] +22 (*c* 2.0, $CHCl_3$)]; UV (EtOH) λ_{max} (log ε) 229 (4.47), 259 (2.94) and 294 (2.85) nm; IR (dry film) ν_{max} 3402, 1701, 1651, and 1616 cm^{-1}; (nujol) 3393, 1643, and 1619 cm^{-1}; ($CHCl_3$) ν_{max} 3683, 1706, 1649, and 1618 cm^{-1}; For ^{1}H and ^{13}C NMR data, see Tables 6.5 and 6.6, respectively; ESIMS *m/z* 705 $[M + H]^+$.

Crystallographic data of alkaloid **105**: crystal data and structure refinement parameters of alkaloid **105** are summarized in Table 10.14.

Table 10.14. Crystal data and structure refinement parameters of mactalstonine (**105**)

Empirical formula	$C_{43}H_{52}N_4O_5$
Molecular formula	$C_{43}H_{52}N_4O_5$
Molecular weight, M_r	704.89
Melting point	260–263 ^{o}C
Temperature during diffraction experiment, T	100 K
X-ray source	Cu K_α
Crystal system	Monoclinic
Space group	$C2$
a	30.173(4) Å
b	6.7184(6) Å
c	18.895(2) Å
α	90.00°
β	108.475(14)°
γ	90.00°
Volume, V	3632.9(7) Å^3
No. of molecule per unit cell, Z	4
Density (calcd)	1.289 mg/mm^3
F(000)	1512.0
Crystal size	0.20 x 0.10 x 0.02 mm
2θ range for data collection	6.18 to 134.94°
Index ranges	$-36 \leq h \leq 34$, $-8 \leq k \leq 7$, $-22 \leq l \leq 22$
Reflections collected	16346
Independent reflections	6280[R_{int} = 0.0528]
Data/restraints/parameters	6280/1/477
Goodness-of-fit on F^2	1.051
Final R indexes [$I \geq 2\sigma(I)$]	R_1 = 0.0720, wR_2 = 0.1869
Final R indexes [all data]	R_1 = 0.0947, wR_2 = 0.2054
Largest diff. peak/hole / e Å^{-3}	0.26/–0.27
Flack parameter	0.1(0.4)
Hooft parameter	–0.30(0.14)

10.10.2 General procedure for the acetylation of alkaloids 101–106

To a solution of the appropriate alkaloid (1.0 mmol), pyridine (3 equiv), and CH_2Cl_2, was added acetic anhydride (1.5 equiv), and the mixture was stirred at rt. The progress of the reaction was monitored by TLC. When the TLC showed *ca.* 95% completion, the reaction was quenched with 5% Na_2CO_3. The organic layer was washed with water, dried with Na_2SO_4, concentrated *in vacuo*, and the residue was purified by centrifugal preparative TLC (SiO_2, 2–5% MeOH:$CHCl_3$, NH_3-saturated) to give the corresponding *O*-acetyl derivatives.

***O*-Acetylperhentidine A (101a)**. Reaction of **101** (18.3 mg, 0.026 mmol) with acetic anhydride (3.7 μl, 0.039 mmol) in pyridine (6.3 μl, 0.079 mmol) and CH_2Cl_2 (2 ml) gave **101a** (9.1 mg, 47%): light yellowish oil; $[\alpha]^{25}_{D}$ –111 (*c* 0.45, $CHCl_3$,); UV (EtOH) λ_{max} (log ε) 210 (4.73), 230 (4.99), and 285 (4.30) nm; IR (neat) ν_{max} 1732, 1703, 1652, and 1620 cm^{-1}; For ^1H and ^{13}C NMR data, see Tables 6.7 and 6.8, respectively; ESIMS *m/z* 747 $[M + H]^+$; HRESIMS *m/z* 747.4122 $[M + H]^+$ (calcd for $C_{45}H_{54}N_4O_6$ + H, 747.4116).

***O*-Acetylperhentidine B (102a)**. Reaction of **102** (18.8 mg, 0.027 mmol) with acetic anhydride (3.9 μl, 0.04 mmol) in pyridine (6.4 μl, 0.081) and CH_2Cl_2 (2 ml) gave **102a** (8.5 mg, 43%): light yellowish oil; $[\alpha]^{25}_{D}$ –42.3 (*c* 0.43, $CHCl_3$,); UV (EtOH) λ_{max} (log ε) 210 (4.76), 230 (5.01), and 288 (4.32) nm; IR (neat) ν_{max} 1734, 1709, 1654, and 1619 cm^{-1}; For ^1H and ^{13}C NMR data, see Tables 6.7 and 6.8, respectively; ESIMS *m/z* 747 $[M + H]^+$; HRESIMS *m/z* 747.4109 $[M + H]^+$ (calcd for $C_{45}H_{54}N_4O_6$ + H, 747.4116).

***O*-Acetylperhentidine C (103a)**. Reaction of **103** (2.8 mg, 0.004 mmol) with acetic anhydride (0.6 μl, 0.006 mmol) in pyridine (1 μl, 0.012) and CH_2Cl_2 (1 ml) gave **103a** (2.2 mg, 74%): colorless oil; $[\alpha]_D$ −105 (*c* 0.11, $CHCl_3$); UV (EtOH) λ_{max} (log ε) 230 (4.70) and 285 (4.07) nm; IR (dry film) ν_{max} 1737, 1706, 1650, and 1618 cm^{-1}; For ^1H and ^{13}C NMR data, see Tables 6.7 and 6.8, respectively; ESIMS *m/z* 747 $[M + H]^+$; HRESIMS *m/z* 747.4118 $[M + H]^+$ (calcd for $C_{45}H_{54}N_4O_6$ + H, 747.4116).

***O*-Acetylperhentinine acetate (104a)**. Reaction of **104** (15.1 mg, 0.021 mmol) with acetic anhydride (3 μl, 0.032 mmol) in pyridine (5 μl, 0.063 mmol) and CH_2Cl_2 (2 ml) gave **104a** (8.2 mg, 52%): light yellowish oil; $[\alpha]^{25}_D$ −103 (*c* 0.35, $CHCl_3$,); UV (EtOH) λ_{max} (log ε) 210 (4.90), 230 (5.15), and 295 (4.41) nm; IR (neat) ν_{max} 1736, 1706, 1651, and 1618 cm^{-1}; For ^1H and ^{13}C NMR data, see Tables 6.3 and 6.4, respectively; ESIMS *m/z* 747 $[M + H]^+$; HRESIMS *m/z* 747.4123 $[M + H]^+$ (calcd for $C_{45}H_{54}N_4O_6$ + H, 747.4116).

***O*-Acetyl-*E*-*seco*macralstonine (106a)**. Reaction of **106** (16.8 mg, 0.024 mmol) with acetic anhydride (3.4 μl, 0.036 mmol) in pyridine (5.8 μl, 0.071 mmol) and CH_2Cl_2 (2 ml) gave **106a** (11 mg, 62%): light yellowish oil; $[\alpha]^{25}_D$ +34 (*c* 1.1, $CHCl_3$,); UV (EtOH) λ_{max} (log ε) 211 (4.72), 230 (5.00), and 297 (4.21) nm; IR (neat) ν_{max} 1732, 1715, 1651, and 1614 cm^{-1}; For ^1H and ^{13}C NMR data, see Tables 6.5 and 6.6, respectively; ESIMS *m/z* 747 $[M + H]^+$; HRESIMS *m/z* 747.4119 $[M + H]^+$ (calcd for $C_{45}H_{54}N_4O_6$ + H, 747.4116).

10.10.3 Conversion of perhentinine (104) to its dimethyl diiodide salt 104b

Iodomethane (0.5 ml, 8 mmol) was added to perhentinine (**104**) (16 mg, 0.02 mmol) and allowed to stand for 24 h at rt. Excess iodomethane was then removed under reduced pressure to furnish a yellowish residue which on recrystallization from hot MeOH, gave the corresponding dimethyl diiodide salt **104b** (14 mg, 62%): light yellowish block crystals; mp 228–230 ^{o}C; $[\alpha]^{25}_{D}$ –55 (*c* 0.05, MeOH); UV (EtOH) λ_{max} (log ε) 221 (5.83) and 295 (4.97) nm; ESIMS *m/z* 367 $[M]^{2+}$; HRESIMS *m/z* 367.2207 $[M]^{2+}$ (calcd for $C_{45}H_{58}N_4O_5$, 734.4396).

Crystallographic data of compound **104b**: crystal data and structure refinement parameters of compound **104b** are summarized in Table 10.15.

Table 10.14. Crystal data and structure refinement parameters of compound **104b**

Empirical formula	$C_{42}H_{54}N_4O_5I_2$
Molecular formula	$C_{42}H_{54}N_4O_5{}^{2+}I_2{}^{2-}$
Molecular weight, M_r	948.69
Melting point	228–230 ^{o}C
Temperature during diffraction experiment, T	100 K
X-ray source	Mo K_α
Crystal system	Orthorhombic
Space group	$P2_12_12_1$
a	14.5059(2) Å
b	14.8002(2) Å
c	22.4594(3) Å
α	90.00°
β	90.00°
γ	90.00°
Volume, V	4821.81(11) Å^3
No. of molecule per unit cell, Z	4
Density (calcd)	1.307 mg/mm^3
F(000)	1920.0
Crystal size	0.21 x 0.19 x 0.16 mm
2θ range for data collection	3.3 to 50°
Index ranges	$-17 \leq h \leq 17$, $-17 \leq k \leq 17$, $-26 \leq l \leq 26$
Reflections collected	37534
Independent reflections	8480[R_{int} = 0.0340]
Data/restraints/parameters	8480/0/585
Goodness-of-fit on F^2	1.590
Final R indexes [$I \geq 2\sigma(I)$]	R_1 = 0.0634, wR_2 = 0.1922
Final R indexes [all data]	R_1 = 0.0695, wR_2 = 0.1988
Largest diff. peak/hole / e Å^{-3}	3.10/–0.90
Flack parameter	0.04(0.03)
Hooft parameter	0.022(0.07)

10.11 Chapter 7

10.11.1 Compound data of scolaricine (114), lumutinine C (116), and alstoumerine (118)

The alkaloid scholaricine (**114**) was obtained from the leaf extract of *Alstonia angustiloba.*[104] Lumutinine C (**116**) was obtained from the bark extract of *Alstonia macrophylla*,[105] while alstoumerine (**118**) was obtained from the stem-bark extract of *Alstonia angustifolia*.[74]

Scholaricine (114): light yellowish oil and subsequently as colorless needles from $CHCl_3$; mp 176–180 ^oC [lit[102] >180 ^oC dec]; $[\alpha]^{25}_D$ –577 (*c* 0.56, $CHCl_3$) [lit[102] –200 ($CHCl_3$)]; UV (EtOH) λ_{max} (log ε) 213 (4.19), 237 (3.97), 286 (3.60), and 341 (3.94) nm; For ^1H and ^{13}C NMR data, see Table 7.2; ESIMS *m*/*z* 357 $[M + H]^+$.

Crystallographic data of alkaloid **114**: crystal data and structure refinement parameters of alkaloid **114** are summarized in Table 10.16.

Table 10.16. Crystal data and structure refinement parameters of scholaricine (**114**)

Empirical formula	$C_{44}H_{58}N_4O_{11}$
Molecular formula	$2C_{20}H_{24}N_2O_4.C_4H_8O_2.H_2O$
Molecular weight, M_r	818.94
Melting point	176–180 ^oC
Temperature during diffraction experiment, T	100 K
X-ray source	Mo K_α
Crystal system	Orthorhombic
Space group	$P2_12_12_1$
a	10.4901(3) Å
b	18.5736(5) Å
c	21.1075(5) Å
α	90.00°
β	90.00°
γ	90.00°
Volume, V	4112.56(19) $Å^3$
No. of molecule per unit cell, Z	4
Density (calcd)	1.326 mg/mm^3
$F(000)$	1760
Crystal size/mm^3	0.301 × 0.282 × 0.096
2θ range for data collection	2.92 to 50°
Index ranges	$-12 \leq h \leq 12$, $-22 \leq k \leq 22$, $-25 \leq l \leq 25$
Reflections collected	31934
Independent reflections	4055[R_{int} = 0.1005]
Data/restraints/parameters	4055/3/545
Goodness-of-fit on F^2	1.071
Final R indexes [$I \geq 2\sigma(I)$]	R_1 = 0.0592, wR_2 = 0.1509
Final R indexes [all data]	R_1 = 0.0839, wR_2 = 0.1641
Largest diff. peak/hole / e $Å^{-3}$	0.296/–0.634

Lumutinine C (116): light yellowish oil; $[\alpha]^{25}_{D}$ +84 (c 0.3, $CHCl_3$); UV (EtOH) λ_{max} (log ε) 208 (5.31), 228 (5.33), and 284 (4.78) nm; IR(dry film) ν_{max} 3360 cm^{-1}; For ^{1}H and ^{13}C NMR data, see Table 7.3; ESIMS *m/z* 661 $[M + H]^+$; HRESIMS *m/z* 661.3749 $[M + H]^+$ (calcd for $C_{41}H_{48}N_4O_4$+ H, 661.3748).

Alstoumerine (118): colorless block crystals from $CHCl_3$; mp 174–176 ^{o}C [lit[106] 170 ^{o}C]; $[\alpha]^{25}_{D}$ –30 (*c* 0.09, $CHCl_3$) [lit[106] –5.5 (*c* 2.0, $CHCl_3$)]; UV (EtOH) λ_{max} (log ε) 219 (3.89), 234 (3.93), 274 (3.73), 284 (3.77), and 293 (3.71) nm; For ^{1}H NMR and ^{13}C NMR data, see Table 7.4; ESIMS *m/z* 325 $[M + H]^+$.

Crystallographic data of alkaloid **118**: crystal data and structure refinement parameters of alkaloid **118** are summarized in Table 10.17.

Table 10.17. Crystal data and structure refinement parameters of alstoumerine (**118**)

Empirical formula	$C_{22}H_{26}Cl_6N_2O_2$
Molecular formula	$C_{20}H_{24}N_2O_2.2CHCl_3$
Molecular weight, M_r	563.15
Melting point	174–176 ˚C
Temperature during diffraction experiment, T	100(2)
X-ray source	Mo K_α
Crystal system	Orthorhombic
Space group	$P2_12_12_1$
a	10.3890(2) Å
b	10.4473(2) Å
c	23.0709(4) Å
α	90.00°
β	90.00°
γ	90.00°
Volume, V	2504.05(8) $Å^3$
No. of molecule per unit cell, Z	4
Density (calcd)	1.494 mg/mm^3
F(000)	1160
Crystal size	0.69 × 0.18 × 0.16
2θ range for data collection	4.28 to 60.96°
Index ranges	$-14 \leq h \leq 14$, $-14 \leq k \leq 14$, $-32 \leq l \leq 31$
Reflections collected	27532
Independent reflections	7322[R_{int} = 0.0389]
Data/restraints/parameters	7322/22/321
Goodness-of-fit on F^2	1.024
Final R indexes [$I \geq 2\sigma(I)$]	R_1 = 0.0397, wR_2 = 0.0827
Final R indexes [all data]	R_1 = 0.0493, wR_2 = 0.0867
Largest diff. peak/hole / e $Å^{-3}$	0.436/–0.326
Flack Parameter	0.01(0.04)
Hooft Parameter	0.01(0.04)

10.11.2 Determination of the C-19 configuration of alstoumerine (118) by Horeau's method

Alstoumerine (**118**) (45 mg, 0.145 mmol) was added to a solution of racemic 2-phenylbutyric anhydride (168 μl, 0.145 mmol) in anhydrous pyridine (1 ml). The resulting mixture was stirred for 20 h at rt. Water (3 ml) was then added and the mixture was allowed to stand for 30 min. The pH of the solution was adjusted to pH 9 by drop-wise addition of NaOH (0.1 M), after which the solution was extracted with CH_2Cl_2 (3 x 20 ml). The aqueous layer was acidified to pH 3 using 1.0 M HCl and extracted with CH_2Cl_2 (3 x 10 ml). Evaporation of the solvent from the organic phase gave the unreacted 2-phenylbutyric acid: $[\alpha]^{25}_{D}$ –3.1 (*c* 1.66, C_6H_6); $[\alpha]^{25}_{D}$ –3 (*c* 1.66, $CHCl_3$). The optical rotation of the unreacted 2-phenylbutyric acid was found to be negative (*R*), indicating the *S* configuration at C-19 in alstoumerine (**118b**). The determination was repeated several times to confirm that the correct result was obtained

10.12 Chapter 8

10.12.1 Compound data of andransinine (119)

(±)-Andransinine (**119**) was isolated first isolated from the leaf extract of *Alstonia* angustiloba,[123] and subsequently from the leaf extract of *Kopsia pauciflora*.[58]

(±)-Andransinine (119) from *A. angustiloba*: light orange block crystals from EtOAc, mp 212–214 °C; colorless needles from CH_2Cl_2/hexanes, mp 186–190 ^oC; colorless lath crystals from MeOH, mp 204–206 ^oC; $[\alpha]^{25}_D$ –8 (*c* 0.13, $CHCl_3$); UV (EtOH) λ_{max} (log ε) 223 (3.70) and 284 (3.08) nm; IR (dry film) ν_{max} 3378, 2885, 2840, and 1732 cm^{-1}; For ^1H and ^{13}C NMR data, see Table 8.3; ESIMS *m/z* 381 $[M + H]^+$; HRESIMS *m/z* 381.2178 $[M + H]^+$ (calcd for $C_{23}H_{28}N_2O_3$ + H, 381.2173).

(±)-Andransinine (119) from *K. pauciflora*: $[\alpha]^{25}_D$ 0 (*c* 0.18, $CHCl_3$); The melting points of crystals obtained from various solvent systems, UV, IR, ^1H and ^{13}C NMR, and HRESIMS data were similar to those of (±)-andransinine (**119**) obtained from *A. angustiloba*.

10.12.2 X-ray crystallographic analysis of (±)-andransinine (119)

Racemic conglomerate crystals of (±)-andransinine (**119**) were obtained from EtOAc solution. The crystal data and structure refinement parameters of **119** are shown in Table 8.4.

Racemic compound crystals of (±)-andransinine (**119**) were obtained from CH_2Cl_2/hexanes solution. The crystal data and structure refinement parameters are summarized in Table 10.18.

Table 10.18. Crystal data and structure refinement parameters of alkaloid **119** obtained from CH_2Cl_2/hexanes solution

Empirical formula	$C_{23}H_{28}N_2O_3$
Molecular formula	$C_{23}H_{28}N_2O_3$
Molecular weight, M_r	380.47
Melting point	186–190 ^oC
Temperature during diffraction experiment, T	100 K
X-ray source	Mo K_α
Crystal system	Monoclinic
Space group	$C2/c$
a	39.082(4) Å
b	8.5880(11) Å
c	24.128(3) Å
α	90.00°
β	105.802(7)°
γ	90.00°
Volume, V	7792.2(16) $Å^3$
No. of molecule per unit cell, Z	16
Density (calcd)	1.297 mg/mm^3
$F(000)$	3264.0
Crystal size	0.54 × 0.25 × 0.03 mm
2θ range for data collection	3.5 to 50°
Index ranges	$-46 \leq h \leq 46$, $-10 \leq k \leq 10$, $-27 \leq l \leq 28$
Reflections collected	29475
Independent reflections	6868[R_{int} = 0.2374]
Data/restraints/parameters	6868/0/509
Goodness-of-fit on F^2	0.766
Final R indexes [$I \geq 2\sigma(I)$]	R_1 = 0.0573, wR_2 = 0.0949
Final R indexes [all data]	R_1 = 0.1933, wR_2 = 0.1292
Largest diff. peak/hole / e $Å^{-3}$	0.24/–0.25

Racemic compound crystals of (±)-andransinine (**119**) were obtained from MeOH solution. The crystal data and structure refinement parameters are summarized in Table 10.19.

Table 10.19. Crystal data and structure refinement parameters of alkaloid **119** obtained from MeOH solution.

Empirical formula	$C_{24}H_{32}N_2O_4$
Molecular formula	$C_{23}H_{28}N_2O_3.CH_3OH$
Molecular weight, M_r	412.52
Melting point	204–206 ^oC
Temperature during diffraction experiment, T	100 K
X-ray source	Mo K_α
Crystal system	Orthorhombic
Space group	Pna2$_1$
a	8.6828(2) Å
b	21.4082(4) Å
c	11.2277(2) Å
α	90.00°
β	90.00°
γ	90.00°
Volume, V	2087.04(7) Å^3
No. of molecule per unit cell, Z	4
Density (calcd)	1.313 mg/mm^3
F(000)	888.0
Crystal size	0.84 × 0.36 × 0.24 mm
2θ range for data collection	3.8 to 55°
Index ranges	$-11 \leq h \leq 11$, $-27 \leq k \leq 27$, $-14 \leq l \leq 14$
Reflections collected	18902
Independent reflections	4796[R_{int} = 0.0263]
Data/restraints/parameters	4796/1/275
Goodness-of-fit on F^2	1.028
Final R indexes [$I \geq 2\sigma(I)$]	R_1 = 0.0352, wR_2 = 0.0908
Final R indexes [all data]	R_1 = 0.0372, wR_2 = 0.0923
Largest diff. peak/hole / e Å^{-3}	0.49/–0.34

10.12.3 X-ray diffraction and chiral phase HPLC analyses of a single crystal of andransinine (119) selected from the racemic conglomerate

Racemic conglomerate crystals of (±)-andransinine (**119**) were obtained from EtOAc solution. A crystal with substantial size (*ca.* 0.43 x 0.35 x 0.28 mm) was selected from the conglomerate. It was then cut into half (*ca.* 0.20 x 0.35 x 0.28 mm). This half crystal was subjected to an X-ray diffraction analysis, using Cu K_α radiation. The crystal data and structure refinement parameters are summarized in Table 10.20.

The remaining half of the andransinine (**119**) crystal (*ca.* 0.23 x 0.35 x 0.28 mm) was dissolved in a minimum amount of EtOH and subjected to chiral phase HPLC analysis, using a chiral column (Chiralpak AD-H, 4.6 mm x 150 mm, Daicel, Japan) with *n*-hexane/EtOH/DEA (85:15:0.2, flow rate 0.8 ml/min) as eluting solvent. A single peak was observed, corresponding to a retention time of 3 min 47 sec.

Table 10.20. Crystal data and structure refinement parameters of alkaloid **119** (half crystal)

Empirical formula	$C_{23}H_{28}N_2O_3$
Molecular formula	$C_{23}H_{28}N_2O_3$
Molecular weight, M_r	380.47
Melting point	212–214 °C
Temperature during diffraction experiment, T	100 K
X-ray source	Cu K_α
Crystal system	Monoclinic
Space group	$P2_1$
a	8.50960(10) Å
b	9.15380(10) Å
c	12.53330(10) Å
α	90.00°
β	96.0300(10)°
γ	90.00°
Volume, V	970.882(17) Å^3
No. of molecule per unit cell, Z	2
Density (calcd)	1.301 mg/mm^3
F(000)	408.0
Crystal size	0.20 × 0.15 × 0.10
2θ range for data collection	7.1 to 148.34°
Index ranges	$-10 \leq h \leq 10$, $-11 \leq k \leq 10$, $-15 \leq l \leq 15$
Reflections collected	7322
Independent reflections	3769[R_{int} = 0.0191]
Data/restraints/parameters	3769/1/255
Goodness-of-fit on F^2	1.047
Final R indexes [$I \geq 2\sigma(I)$]	R_1 = 0.0347, wR_2 = 0.0904
Final R indexes [all data]	R_1 = 0.0349, wR_2 = 0.0907
Largest diff. peak/hole / e Å^{-3}	0.21/–0.19
Flack parameter, x	–0.06(0.15)
Hooft parameter, y	–0.03(0.04)

10.12.4 Resolution of (±)-andransinine (119) by chiral phase HPLC followed by X-ray diffraction analyses of the resolved enantiomers

(±)-Andransinine (**119**) (9.1 mg) was dissolved in EtOH (1 ml) and resolved by means of chiral phase HPLC (100 injections, 10 μl each) using a chiral column (Chiralpak AD-H, 4.6 mm x 150 mm, Daicel, Japan) and eluting with *n*-hexane/EtOH/DEA (85:15:0.2, flow rate 0.8 ml/min) to yield two fractions: Fraction 1 (retention time 3 min 51 sec, 2.2 mg) and Fraction 2 (retention time 7 min 52 sec, 1.3 mg).

(+)-Andransinine (119a) from Fraction 1, colorless block crystal from EtOAc (ee > 99%); mp 212–214 °C; $[\alpha]^{25}_{D}$ +85 (*c* 0.10, $CHCl_3$); The UV, IR, ^{1}H and ^{13}C NMR data were identical to racemic **119**. The crystal data and structure refinement parameters, bond lengths, and bond angles are summarized in Table 10.21.

Table 10.21. Crystal data and structure refinement parameters of (+)-andransinine (**119a**)

Empirical formula	$C_{23}H_{28}N_2O_3$
Molecular formula	$C_{23}H_{28}N_2O_3$
Molecular weight, M_r	380.47
Melting point	212–214 °C
Temperature during diffraction experiment, T	100 K
X-ray source	Cu K_α
Crystal system	Monoclinic
Space group	$P2_1$
a	8.5069(2) Å
b	9.1472(2) Å
c	12.5299(3) Å
α	90.00°
β	96.035(2)°
γ	90.00°
Volume, V	969.60(4) Å^3
No. of molecule per unit cell, Z	2
Density (calcd)	1.3032 mg/mm^3
F(000)	409.3
Crystal size	0.20 × 0.15 × 0.10
2θ range for data collection	7.1 to 150.58°
Index ranges	$-9 \leq h \leq 10$, $-11 \leq k \leq 10$, $-15 \leq l \leq 10$
Reflections collected	9097
Independent reflections	3624[R_{int} = 0.0222]
Data/restraints/parameters	3624/0/254
Goodness-of-fit on F^2	1.023
Final R indexes [$I \geq 2\sigma(I)$]	R_1 = 0.0297, wR_2 = 0.0783
Final R indexes [all data]	R_1 = 0.0309, wR_2 = 0.0784
Largest diff. peak/hole / e Å^{-3}	0.17/–0.16
Flack parameter, x	–0.10(0.12)
Hooft parameter, y	–0.07(0.08)

(–)-Andransinine (119b) from Fraction 2, colorless block crystals from EtOAc (ee > 99%); mp 212–214 °C $[\alpha]^{25}_{D}$ –85 (*c* 0.07, $CHCl_3$); The UV, IR, ^1H and ^{13}C NMR data were identical to racemic **119**. The crystal data and structure refinement parameters are summarized in Table 10.22.

Table 10.22. Crystal data and structure refinement parameters of (–)-andransinine (**119b**)

Empirical formula	$C_{23}H_{28}N_2O_3$
Molecular formula	$C_{23}H_{28}N_2O_3$
Molecular weight, M_r	380.47
Melting point	212–214 °C
Temperature during diffraction experiment, T	100 K
X-ray source	Cu K_α
Crystal system	Monoclinic
Space group	$P2_1$
a	8.5089(2) Å
b	9.1505(2) Å
c	12.5241(2) Å
α	90.00°
β	96.049(2)°
γ	90.00°
Volume, V	969.71(4) Å^3
No. of molecule per unit cell, Z	2
Density (calcd)	1.3030 mg/mm^3
F(000)	409.3
Crystal size	0.20 × 0.15 × 0.10
2θ range for data collection	7.1 to 153.14°
Index ranges	$-10 \leq h \leq 10$, $-11 \leq k \leq 11$, $-15 \leq l \leq 15$
Reflections collected	9877
Independent reflections	3991[R_{int} = 0.0198]
Data/restraints/parameters	3624/0/254
Goodness-of-fit on F^2	1.023
Final R indexes [$I \geq 2\sigma(I)$]	R_1 = 0.0301, wR_2 = 0.0803
Final R indexes [all data]	R_1 = 0.0310, wR_2 = 0.0803
Largest diff. peak/hole / e Å^{-3}	0.21/–0.17
Flack parameter, x	–0.08(0.12)
Hooft parameter, y	0.04(0.06)

10.13 Chapter 9

10.13.1 Conversion of lumusidine A (125) to its dimethyl diiodide salt 125a

Iodomethane (0.5 ml) was added to lumusidine A (**125**) (4.2 mg, 0.006 mmol) and allowed to stand for 24 h at rt. Excess iodomethane was then removed under reduced pressure to furnish a yellowish residue that, on recrystallization from hot MeOH, gave the corresponding dimethyl diiodide salt **125a** (2.8 mg, 48%): light yellowish block crystals; mp >198 ^{o}C dec; ESIMS *m/z* 358 $[M]^{2+}$; HRESIMS *m/z* 358.2157 $[M]^{2+}$ (calcd for $C_{45}H_{56}N_4O_4$, 716.4302).

10.13.2 Conversion of lumusidine B (126) to its dimethyl diiodide salt 126a

Iodomethane (0.5 ml) was added to lumusidine A (**126**) (5.4 mg, 0.008 mmol) and allowed to stand for 24 h at rt. Excess iodomethane was then removed under reduced pressure to furnish a yellowish residue that, on recrystallization from MeOH, gave the corresponding dimethyl diiodide salt **126a** (3.2 mg, 40%): light yellowish block crystals; mp 230−234 °C; ESIMS *m/z* 367 $[M]^{2+}$; HRESIMS *m/z* 367.2207 $[M]^{2+}$ (calcd for $C_{45}H_{58}N_4O_5$, 734.4407).

10.13.3 Conversion of alkaloid 130 to its methyl iodide salt 130a

Iodomethane (0.5 ml) was added to alkaloid **130** (0.3 mg, 0.001 mmol) and allowed to stand for 24 h at rt. Excess iodomethane was then removed under reduced pressure to furnish a yellowish residue that, on recrystallization from MeOH, gave the corresponding dimethyl diiodide salt **130a** (0.1 mg, 23%): light yellowish block

crystals; mp 214–218 °C; ESIMS *m/z* 323 $[M]^+$; HRESIMS *m/z* 323.1758 $[M]^+$ (calcd for $C_{19}H_{20}N_2O_2$, 323.1760).

REFERENCES

1. Wink, M. In *Modern Alkaloids: Structure, Isolation, Synthesis and Biology*; Fattorusso, E. and Taglialatela-Scafati, O., Eds.; Wiley-VCH: Weinheim, 2008; Chapter 1, pp 3–24.
2. Roberts, M. F.; Wink, M. *Alkaloids – Biochemistry, Ecology and Medicinal Applications*; Plenum Press: New York, 1998.
3. Harborne, J. B. *Introduction to Ecological Biochemistry*, 4th ed.; Academic Press: London, 1993.
4. Teuscher, E. and Lindequist, U. *Biogene Gifte. Biologie-Chemie-Pharmakologie-Toxikologie*; Wissenschaftliche Verlagsgesellschaft: Stuttgart, 1998.
5. Wink, M. In *The Alkaloids: Chemistry and Pharmacology;* Cordell G. A., Ed.; Academic Press: San Diego, 1993; Vol. 43, pp 1–118.
6. *Herbivores: Their Interactions with Secondary Plant Metabolites: The Chemical Participants*; Rosenthal, G. A.; Berenbaum, M. R., Eds.; Academic Press: San Diego, 1991, Vol. 1.
7. *Herbivores: Their Interactions with Secondary Plant Metabolites: Ecological and Evolutionary Processes*; Rosenthal, G. A.; Berenbaum, M. R., Eds.; Academic Press: San Diego, 1992, Vol. 2.
8. *Annual Plant Reviews*; Wink, M., Ed.; Sheffield Academic Press: Sheffield, 1999; Vol 2.
9. Blum, M. S. *Chemical Defenses of Arthropods*; Academic Press, New York, 1981.
10. Cordell, G. A.; Quinn-Beattie, M. L.; Farnsworth, N. R. *Phytother. Res.* **2001**, *15*, 183–205.
11. *Dictionary of Alkaloids*; Buckingham, J.; Baggaley, K. H.; Roberts, A. D.; Szabó, L. F., Eds.; CRC Press: New York, 2010 and references cited therein.

12. Winterstein, E.; Trier, G. *Die Alkaloide eine Monographie der naturlichen Basen*, Borntrager: Berlin, 1910.

13. Pelletier, S. W. In *Alkaloids: Chemical and Biological Perspectives*; Pelletier, S. W., Ed.; Wiley: New York, 1983; Vol. 1.

14. Hesse, M. *Alkaloids: Nature's Curse or Blessing*; Wiley-VCG: Weinheim, 2002.

15. *Indole Alkaloids*; Atta-ur-Rahman; Basha, A. Eds.; Harwood Academic Publishers: Amsterdam, 1998, Vol. 2.

16. Kisakurek, M. V.; Leeuwenberg, A. J. M.; Hesse, M. In *Alkaloids: Chemical and Biological Perspectives*; Pelletier, S. W., Ed.; Wiley: New York, 1983, Vol. 1, pp 211–376.

17. Kisakurek, M. V.; Hesse, M. In *Indole and Biogenetically Related Alkaloids*; Phillipson, J. D. and Zenk, M. H., Eds.; Academic Press: London, 1980; pp 11–26.

18. Atta-ur-Rahman; Basha, A. In *Biosynthesis of Indole Alkaloids*; Clarendon Press: Oxford, 1983.

19. Danieli, B.; Plamisano, G. In *The Alkaloids - Chemistry and Pharmacology*; Brossi, A., Ed.; Academic Press: Orlando, 1986, Vol. 27.

20. Van Beek, T. A.; Verpoorte, R.; Baerheim, S. A.; Leeuwenberg, A. J. M.; Bisset, N. G. *J. Ethnopharmacol*. **1984**, *10*, 1–156 and references cited therein.

21. (a) Wenkert, E. *J. Am. Chem. Soc.* **1962**, *84*, 98–102. (b) Wenkert, E.; Wickberg, B. *J. Am. Chem. Soc.* **1965**, *87*, 1580–1589.

22. Scott, A. I. *Acc. Chem. Res.* **1970**, *3*, 151–157 and references cited therein.

23. Kam, T. S.; Subramaniam, G.; Lim, T. M. *Tetrahedron Lett.* **2001**, *42*, 5977–5980.

24. Subramaniam, G.; Choo, Y. M.; Hiraku, O.; Komiyama, K.; Kam, T. S. *Tetrahedron* **2008**, *64*, 1397–1408.

25. Kam, T. S.; Lim, K. H. In *The Alkaloids: Chemistry and Biology*; Cordell, G. A., Ed.; Academic Press: The Netherlands, 2008; Vol. 66, pp 1–111.

26. Kam, T. S.; Subramaniam, G. *Tetrahedron Lett.* **2004**, *45*, 3521–3524.

27. Subramaniam, G.; Kam, T. S.; Ng, S. W. *Acta Cryst*. **2003**, *E59*, o555–o557.

28. Low, Y. Y.; Subramanian, G.; Lim, K. H.; Wong, R. C. S.; Robinson, W. T.; Kam, T. S. *Tetrahedron* **2009**, *65*, 6873–6876.

29. (a) Rosen, W. E. *Tetrahedron Lett.* **1961**, *2*, 481–484. (b) Wenkert, E.; Guo, M.; Pestchanker, M. J.; Shi, Y. J.; Vankar, Y. D. *J. Org. Chem.* **1989**, *54*, 1166–1174.

30. Brown, H. C. In *Boranes in Organic Chemistry*; Cornell University Press: Ithaca, New York; 1972.

31. Nung, M. Y.; Chwang, S. P.; Brown, H. C.; Krishnamurthy, S.; Stocky, T. P. *J. Org. Chem.* **1973**, *38*, 2786–2792.

32. Brown, H. C.; Kramer, G. W.; Levy, A. B.; Midland, M. M. In *Organic Syntheses via Boranes*; John Wiley and Sons: New York; 1975.

33. Miller, N. E. *Inorg. Chem*. **1974**, *13*, 1459–1467.

34. Corey, E. J.; Bakshi, R. K.; Shibata, S. *J. Am. Chem. Soc*. **1987**, *109*, 5551–5553.

35. Leach, J. B.; Ungermann, C. B.; Onak, T. P. *J. Magn. Reson*. **1972**, *6*, 74–83.

36. Brown, H. C.; Heim, P.; Yoon, N. M. *J. Am. Chem. Soc*. **1970**, *92*, 1637–1646.

37. Brown, H. C.; Stocky, T. P. *J. Am. Chem. Soc*. **1977**, *99*, 8218–8266.

38. Wang, A. H. J.; Paul, I. C. *Acta Cryst*. **1977**, *B33*, 2977–2979.

39. Low, Y. Y.; Lim, K. H.; Choo, Y. M.; Pang, H. S.; Etoh, T.; Hayashi, M.; Komiyama, K.; Kam, T. S. *Tetrahedron Lett.* **2010**, *51*, 269–272.

40. Büchi, G.; Manning, R. E. *J. Am. Chem. Soc.* **1966**, *88*, 2532–2535.

41. (a) Langlois, N.; Gueritte, F.; Langlois, Y.; Potier, P. *J. Am. Chem. Soc.* **1976**, *98*, 7017–7024. (b) Langlois, N.; Gueritte, F.; Langlois, Y.; Potier, P. *Tetrahedron*

Lett. **1976**, *17*, 1487–1490. (c) Kutney, J. P.; Joshua, A. V.; Liao, P. H. *Heterocycles* **1977**, *6*, 297–304. (d) Honma, Y.; Ban, Y. *Heterocycles* **1977**, *6*, 291–296. (e) Kutney, J. P.; Joshua, A. V.; Liao, P. H.; Worth, B. R. *Can. J. Chem.* **1977**, *55*, 3235–3242. (f) Honma, Y.; Ban, Y. *Tetrahedron Lett.* **1978**, *19*, 155–158. (g) Andriamialisoa, R. Z.; Langlois, N.; Langlois, Y.; Potier, P.; Bladon, P. *Can. J. Chem.* **1979**, *57*, 2572–2577. (h) Mangeney, P.; Langlois, N.; Leroy, C.; Riche, C.; Langlois, Y. *J. Org. Chem.* **1982**, *47*, 4261–4264.

42. Lim, K. H. Biologically active indole and bisindole alkaloids from *Kopsia* and *Tabernaemontana*, Ph.D. Thesis, University of Malaya, Kuala Lumpur, December 2008.

43. Pang, H. S. Biologically active indole and bisindole alkaloids from *Tabernaemontana divaricata*. M.S. Thesis, University of Malaya, Kuala Lumpur, April 2004.

44. Lim, K. H.; Low, Y. Y.; Kam, T. S. *Tetrahedron Lett.* **2006**, *47*, 5037–5039, and reference cited therein.

45. (a) Dess, D. B.; Martin, J. C. *J. Org. Chem.* **1983**, *48*, 4155–4156. (b) Dess, D. B.; Martin, J. C. *J. Am. Chem. Soc.* **1991**, *113*, 7277–7287.

46. (a) Griffith, W. P.; Ley, S. V.; Whitcombe, G. P.; White, A. D. *J. Chem. Soc., Chem. Commun.* **1987**, 1625–1627. (b) Ley, S. V.; Norman, J.; Griffith, W. P.; Marsden, S. P. *Synthesis*, **1994**, 639–666.

47. Goh, S. H.; Mohd. Ali, A. R. *Tetrahedron Lett*. **1986**, *27*, 2501–2504.

48. Chen, W.; Mohd. Ali, A. R.; Goh, S. H.; Sinn, E.; Butcher, R. J. *Acta Cryst*. **1986**, *C42*, 349–351.

49. Goh, S. H.; Mohd. Ali, A. R.; Wong, W. H. *Tetrahedron* **1989**, *45*, 7899–7920.

50. Abe, F.; Yamauchi, T. *Phytochemistry* **1994**, *35*, 169–171.

51. Linde, H. H. A. *Helv. Chim. Acta* **1965**, *48*, 1822–1842.

52. Kam, T. S.; Tee, Y. M.; Subramaniam, G. *Nat. Prod. Lett.* **1998**, *12*, 307–310.

53. Kam, T. S.; Subramaniam, G.; Chen, W. *Phytochemistry* **1999**, *51*, 159–169.

54. Lim, K. H.; Kam, T. S. *Helv. Chim. Acta* **2007**, *90*, 31–35.

55. Kam, T. S.; Subramaniam, G.; Lim, K. H.; Choo, Y. M. *Tetrahedron Lett*. **2004**, *45*, 5995–5998.

56. (a) Magolan, J.; Carson, C. A.; Kerr, M. A. *Org. Lett.* **2008**, *10*, 1437–1440. (b) Biechy, A.; Zard, S. Z. *Org. Lett.* **2009**, *11*, 2800–2803. (c) Nakajima, R.; Ogino, T.; Yokoshima, S.; Fukuyama, T. *J. Am. Chem. Soc.* **2010**, *132*, 1236–1237. (d) Iwama, Y.; Okano, K.; Sugimoto, K.; Tokuyama, H. *Org. Lett.* **2012**, *14*, 2320–2322.

57. Anthoni, U.; Bock, K.; Chevolot, L.; Larsen, C.; Nielsen, P. H.; Christophersen, C. *J. Org. Chem.* **1987**, *52*, 5638–5639.

58. Gan, C. Y. Biologically active indole and bisindole alkaloids from *Leuconotis* and *Kopsia*. Ph.D. Thesis, University of Malaya, Kuala Lumpur, December 2012 (in preparation).

59. (a) Bernauer, K.; Englert, G.; Vetter, W.; Weiss, E. *Helv. Chim. Acta* **1969**, *52*, 1886–1905. (b) Oberhänsli, W. E. *Helv. Chim. Acta* **1969**, *52*, 1905–1911.

60. Sim, K. M. Alkaloids from *Holarrhena*, *Kopsia*, and *Tabernaemontana*. Ph.D. Thesis, University of Malaya, Kuala Lumpur, March 2001.

61. Banwell, M. G.; Edwards, A. J.; Jolliffe, K. A.; Smith, J. A.; Hamel, E.; Verdier-Pinard, P. *Org. Biomol. Chem.* **2003**, *1*, 296–305.

62. Banwell, M. G.; Beck, D. A. S.; Willis, A. C. *Arkivoc* **2006**, *iii*, 163–174.

63. (a) Flack, H. D. *Acta Cryst.* **1983**. *A39*, 876–881. (b) Flack, H. D.; Bernardinelli, G. *J. Appl. Cryst.* **2000**, *33*, 1143–1148.

64. (a) Hooft, R. W. W.; Straver, L. H.; Spek, A. L. *J. Appl. Cryst.* **2008**, *41*, 96–103. (b) Hooft, R. W. W.; Straver, L. H.; Spek, A. L. *J. Appl. Cryst.* **2010**, *43*, 665–668.

65. Décor, A.; Bellocq, D.; Thoison, O.; Lekieffre, N.; Chiaroni, A.; Ouazzani, J.; Cresteil, T.; Guéritte, F.; Baudoin, O. *Bioorg. Med. Chem.* **2006**, *14*, 1558–1564.

66. Feng, T.; Cai, X. H.; Liu, Y. P.; Li, Y.; Wang, Y. Y.; Luo, X. D. *J. Nat. Prod.* **2010**, *73*, 22–26.

67. (a) Anikin, V. F.; Veduta, V. V.; Merz, A. *Monatsh. Chem.* **1999**, *130*, 681–690. (b) Bellucci, G.; Chiappe, C.; Bianchini, R.; Lemmen, P.; Lenoir, D. *Tetrahedron* **1997**, *53*, 785–790.

68. Ruasse, M. F. *Adv. Phys. Org. Chem*. **1993**, *28*, 207–291. (b) Melloni, G.; Modena, G.; Tonellato, U. *Acc. Chem. Res.* **1981**, *14*, 227–233.

69. Herges, R.; Papafilippopoulos, A.; Hess, K.; Chiappe, C; Lenoir, D.; Detert, H. *Angew. Chem. Int. Ed.* **2005**, *44*, 1412–1416.

70. Braun, L. M.; Braun, R. A.; Crissman, H. R.; Opperman, M.; Adams, R. M. *J. Org. Chem.* **1982**, *36*, 2388–2389.

71. Brown, H. C.; Choi, Y. M.; Narasimhan, S. *J. Org. Chem.* **1982**, *47*, 3153–3163.

72. Hu, W. H.; Tsai, P. C.; Hsu, M. K.; Wang, J. J. *J. Org. Chem.* **2004**, *69*, 3983–3985.

73. Wasserman, H. H.; Lipshutz, B. H. *Tetrahedron Lett.* **1975**, *16*, 1731–1734.

74. Tan, S. J.; Low, Y. Y.; Choo, Y. M.; Abdullah, Z.; Etoh, T.; Hayashi, M.; Komiyama, K.; Kam, T. S. *J. Nat. Prod.* **2010**, *73*, 1891–1897.

75. Banerji, A.; Siddhanta, A. K. *Phytochemistry* **1981**, *20*, 540–542.

76. Hu, W. L.; Zhu, J. P.; Hesse, M. *Planta Med.* **1989**, *55*, 463–466.

77. Kuehne, M. E.; Xu, F.; Brook, C. S. *J. Org. Chem.* **1994**, *59*, 7803–7806.

78. Tan, S. J. Biologically active indole and bisindole alkaloids from *Alstonia*. Ph.D. Thesis, University of Malaya, Kuala Lumpur, December 2011.

79. Hu, W. L.; Zhu, J. P.; Prewo, R.; Hesse, M. *Phytochemistry* **1989**, 28, 1963–1966.

80. Gan, C. Y.; Low, Y. Y.; Etoh, T.; Hayashi, M.; Komiyama, K.; Kam, T. S. *J. Nat. Prod.* **2009**, *72*, 2098–2103.

81. Awang, K.; Pais, M.; Sévenet, T.; Schaller, H.; Nasir, A. M.; Hadi, A. H. A. *Phytochemistry* **1991**, *30*, 3164–3167.

82. Kam, T. S.; Tan, P. S.; Chen, W. *J. Nat. Prod.* **1993**, *33*, 921–924.

83. Kam, T. S.; Sim, K. M.; Lim, T. M. *Tetrahedron Lett.* **2001**, *42*, 4721–4723.

84. Bisset, N. G.; Das, B. C.; Parello, J. *Tetrahedron* **1973**, *29*, 4137–4148.

85. Lim, K. H.; Hiraku, O.; Komiyama, K.; Koyano, T.; Hayashi, M.; Kam, T. S. *J. Nat. Prod.* **2007**, *70*, 1302–1307.

86. Lim, K. H.; Kam, T. S. *Phytochemistry* **2008**, *69*, 558–561.

87. Kam, T. S.; Tan, P. S.; Chuah, C. H. *Phytochemistry* **1992**, *31*, 2936–2938.

88. Davis, F. A.; Haque, M. S.; Ulatowski, T. G.; Towson, J. C. *J. Org. Chem.* **1986**, *51*, 2402–2404.

89. Lim, S. H.; Low, Y. Y.; Tan, S. J.; Lim, K. H.; Thomas, N. F.; Kam, T. S. *J. Nat. Prod.* **2012**, *75*, 942–950.

90. Kam, T. S.; Choo, Y. M.; Komiyama, K. *Tetrahedron* **2004**, *60*, 3957–3966.

91. Sharp, T. M. *J. Chem. Soc.* **1934**, 1227–1232.

92. Kishi, T.; Hesse, M.; Vetter, W.; Gemenden, C. W.; Taylor, W. I.; Schmid, H. *Helv. Chim. Acta* **1966**, *49*, 946–964.

93. Keawpradub, N.; Houghton, P. J.; Eno-Amooquaye, E.; Burke, P. J. *Planta Med.* **1997**, *63*, 97–101.

94. Ghedira, K.; Zeches-Hanrot, M.; Richard, B.; Massiot, G.; Le Men-Olivier, L.; Sevenet, T.; Goh, S. H. *Phytochemistry* **1988**, *27*, 3955–3962.

95. Changwichit, K.; Khorana, N.; Suwanborirux, K.; Waranuch, N.; Limpeanchob, N.; Wisuitiprot, W.; Suphrom, N.; Ingkaninan, K. *Fitoterapia* **2011**, *82*, 798–804.

96. Koyama, K.; Hirasawa, Y.; Hosoya, T.; Teh, C. H.; Chan, K. L.; Morita, H. *Bioorg. Med. Chem.* **2010**, *18*, 4415–4421.

97. Hu, W. L.; Zhu, J. P.; Hesse, M. *Planta Med.* **1989**, *55*, 463–466.

98. Yamauchi, T.; Abe, F.; Chen, R. F.; Nonaka, G. I.; Santisuk, T.; Padolina, W. G. *Phytochemistry* **1990**, *29*, 3547–3552.

99. Kuehne, M. E.; Xu, F.; Brook, C. S. *J. Org. Chem.* **1994**, *59*, 7803–7806.

100. Gan, L. S.; Yang, S. P.; Wu, Y.; Ding, J.; Yue, J. M. *J. Nat. Prod.* **2006**, *69*, 18–22.

101. Keawpradub, N.; Takayama, H.; Aimi, N.; Sakai, S-I. *Phytochemistry* **1994**, *37*, 1745–1749.

102. Atta-ur-Rahman; Asif, M; Ghazala, M.; Fatima, J.; Alvi, K. A. *Phytochemistry* **1985**, *24*, 2771–2773.

103. Zeches, M.; Ravao, T.; Richard, B.; Massiot, G.; Le Men-Olivier, L.; Guilhem, J.; Pascard, C. *Tetrahedron Lett.* **1984**, *25*, 659–662.

104. Kam, T. S.; Choo, Y. M. *Helv. Chim. Acta* **2004**, *87*, 366–369.

105. Lim, S. H.; Tan, S. J.; Low, Y. Y.; Kam, T. S. *J. Nat. Prod.* **2011**, *74*, 2556–2562.

106. Atta-ur-Rahman; Abbas, S. A.; Nighat, F.; Ahmed, G.; Choudhary, M. I.; Alvi, K. A.; Habib-ur-Rehman; De Silva, K. T. D.; Arambewela, L. S. R. *J. Nat. Prod.* **1991**, *54*, 750–754.

107. Horeau, A.; Kagan, H. B. *Tetrahedron* **1964**, *20*, 2431–2441.

108. Kam, T. S.; Iek, I. H.; Choo, Y. M. *Phytochemistry* **1999**, *51*, 839–844.

109. Kam, T. S.; Choo, Y. M. *Phytochemistry* **2004**, *65*, 603–608.

110. Pinchon, T. M.; Nuzillard, J. M.; Richard, B.; Massiot, G.; Le Men-Olivier, L.; Sevenet, T. *Phytochemistry* **1990**, *29*, 3341–3344.

111. Clivio, P.; Richard, B.; Deverre, J. R.; Sevenet, T.; Zeches, M.; Le Men-Oliver, L. *Phytochemistry* **1991**, *30*, 3785–3792.

112. Jacques, J.; Collet, A.; Wilen, S. H. In *Enantiomers, Racemates and Resolutions*; Krieger Publishing Company: Malabar, FL, 1994.

113. Kelvin W. T. In *Baltimore Lectures on Molecular Dynamics and the Wave Theory of Light*, C. J. Clay: London, 1904; pp 602–642.

114. (a) Pasteur, L. *Ann. Chim. Phys.* **1848**, *24*, 442–459. (b) Pasteur, L. *Ann. Chim. Phys.* **1850**, *28*, 56–99.

115. *Crystal Structure Analysis: Principles and Practice*; Clegg, W., Ed.; Oxford University Press: New York, 2009.

116. *International Tables for Crystallography: Volume A (Space-group Symmetry)*, 5th ed.; Hahn, T., Ed.; Kluwer Academic Publishers: Dordrecht, 2002.

117. Thompson, A. L.; Watkin, D. J. *Tetrahedron: Asymmetry* **2009**, *20*, 712–717.

118. Moss, G. P. *Pure Appl. Chem.* **1996**, *68*, 2193–2222.

119. (a) Flack, H. D.; Bernardinelli, G. *Acta Cryst.* **1999**, *A55*, 908–915. (b) Flack, H. D. *Helv. Chim. Acta* **2003**, *86*, 905–921.

120. Barron, L. D. In *Chirality in Natural and Applied Scienc*e; Lough, W. J.; Wainer, I. W, Eds.; Oxford: Blackwell Publishing, 2002; pp 53–86.

121. Kan-Fan, C.; Massiot, G.; Ahond, A.; Das, B.C.; Husson, H.-P.; Potier, P.; Scott, A. I.; Wei, C.C. *J. Chem. Soc., Chem. Commun.* **1974**, 164–165.

122. Riche, C.; Pascard-Billy, C.; *Acta Cryst.* **1979**, *B35*, 666–669.

123. Ku, W. F.; Tan, S. J.; Low, Y. Y.; Komiyama, K.; Kam, T. S. *Phytochemistry* **2011**, *72*, 2212–2218.

124. (a) Pérez-Gracía, L.; Amabilino, D. A. *Chem. Soc. Rev.* **2002**, *31*, 342–356. (b) Pérez-Gracía, L.; Amabilino, D. A. *Chem. Soc. Rev.* **2007**, *36*, 941–967.

125. Yamamoto, C.; Okamoto, Y. In *Enantiomer Separation*, Toda, F. Ed.; Kluwer Academic Publisher: The Netherlands, 2004; pp 301–322.

126. Gan, C. Y.; Low, Y. Y.; Robinson, W. T.; Komiyama, K.; Kam, T. S. *Phytochemistry* **2010**, *71*, 1365–1370.

127. Lim, S. H.; Low Y. Y.; Subramaniam, G.; Abdullah Z.; Thomas N. F; Kam T. S., *Phytochemistry*, **2013**, 87, 148–156.

128. Kam, T. S.; Sim, K. M. *J. Nat. Prod.* **2002**, *65*, 669–672.

129. Yap, W. S.; Gan, C. Y.; Low, Y. Y.; Choo, Y. M.; Etoh, T.; Hayashi, M.; Komiyama, K.; Kam, T. S. *J. Nat. Prod.* **2011**, *74*, 1309–1312.

130. Yap, W. S. Biologically active alkaloids from *Kopsia*, M.S. Thesis, University of Malaya, Kuala Lumpur, December 2011.